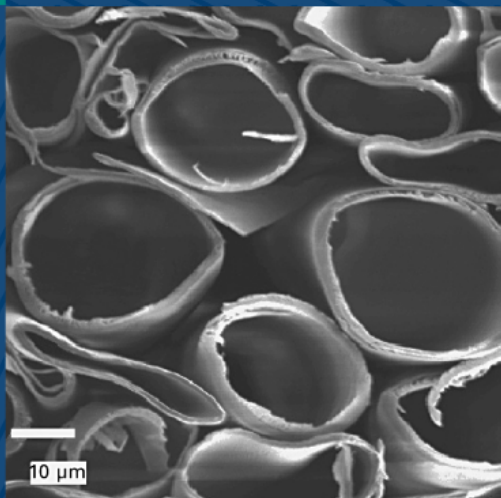


WOODHEAD PUBLISHING IN TEXTILES



# Handbook of textile fibre structure

Volume 2: Natural,  
regenerated, inorganic  
and specialist fibres

Edited by S. J. Eichhorn, J. W. S. Hearle,  
M. Jaffe and T. Kikutani



The Textile Institute

WP

# Handbook of textile fibre structure



## **The Textile Institute and Woodhead Publishing**

The Textile Institute is a unique organisation in textiles, clothing and footwear. Incorporated in England by a Royal Charter granted in 1925, the Institute has individual and corporate members in over 90 countries. The aim of the Institute is to facilitate learning, recognise achievement, reward excellence and disseminate information within the global textiles, clothing and footwear industries.

Historically, The Textile Institute has published books of interest to its members and the textile industry. To maintain this policy, the Institute has entered into partnership with Woodhead Publishing Limited to ensure that Institute members and the textile industry continue to have access to high calibre titles on textile science and technology.

Most Woodhead titles on textiles are now published in collaboration with The Textile Institute. Through this arrangement, the Institute provides an Editorial Board which advises Woodhead on appropriate titles for future publication and suggests possible editors and authors for these books. Each book published under this arrangement carries the Institute's logo.

Woodhead books published in collaboration with The Textile Institute are offered to Textile Institute members at a substantial discount. These books, together with those published by The Textile Institute that are still in print, are offered on the Woodhead website at [www.woodheadpublishing.com](http://www.woodheadpublishing.com). Textile Institute books still in print are also available directly from the Institute's website at [www.textileinstitutebooks.com](http://www.textileinstitutebooks.com).

A list of Woodhead books on textile science and technology, most of which have been published in collaboration with The Textile Institute, can be found on pages xv–xx.

Woodhead Publishing in Textiles: Number 88

# Handbook of textile fibre structure

Volume 2: Natural, regenerated,  
inorganic and specialist fibres

---

Edited by

S.J. Eichhorn, J.W.S. Hearle, M. Jaffe and  
T. Kikutani



The Textile Institute



CRC Press

Boca Raton Boston New York Washington, DC

WOODHEAD PUBLISHING LIMITED  
Oxford Cambridge New Delhi

Published by Woodhead Publishing Limited in association with The Textile Institute  
Woodhead Publishing Limited, Abington Hall, Granta Park, Great Abington,  
Cambridge CB21 6AH, UK  
www.woodheadpublishing.com

Woodhead Publishing India Private Limited, G-2, Vardaan House, 7/28 Ansari Road,  
Daryaganj, New Delhi – 110002, India

Published in North America by CRC Press LLC, 6000 Broken Sound Parkway, NW,  
Suite 300, Boca Raton, FL 33487, USA

First published 2009, Woodhead Publishing Limited and CRC Press LLC

© 2009, Woodhead Publishing Limited

The authors have asserted their moral rights.

This book contains information obtained from authentic and highly regarded sources. Reprinted material is quoted with permission, and sources are indicated. Reasonable efforts have been made to publish reliable data and information, but the authors and the publishers cannot assume responsibility for the validity of all materials. Neither the authors nor the publishers, nor anyone else associated with this publication, shall be liable for any loss, damage or liability directly or indirectly caused or alleged to be caused by this book.

Neither this book nor any part may be reproduced or transmitted in any form or by any means, electronic or mechanical, including photocopying, microfilming and recording, or by any information storage or retrieval system, without permission in writing from Woodhead Publishing Limited.

The consent of Woodhead Publishing Limited does not extend to copying for general distribution, for promotion, for creating new works, or for resale. Specific permission must be obtained in writing from Woodhead Publishing Limited for such copying.

Trademark notice: Product or corporate names may be trademarks or registered trademarks, and are used only for identification and explanation, without intent to infringe.

British Library Cataloguing in Publication Data

A catalogue record for this book is available from the British Library.

Library of Congress Cataloging in Publication Data

A catalog record for this book is available from the Library of Congress.

Woodhead Publishing ISBN 978-1-84569-730-3 (book)

Woodhead Publishing ISBN 978-1-84569-731-0 (e-book)

CRC Press ISBN 978-1-4398-2027-8

CRC Press order number N10129

The publishers' policy is to use permanent paper from mills that operate a sustainable forestry policy, and which has been manufactured from pulp which is processed using acid-free and elemental chlorine-free practices. Furthermore, the publishers ensure that the text paper and cover board used have met acceptable environmental accreditation standards.

Typeset by Replika Press Pvt Ltd

Printed by TJ International Limited, Padstow, Cornwall, UK

# Contents

---

*Contributor contact details* *xi*

## Part I Natural fibres

1	An introduction to cellulosic fibres D CIECHAŃSKA, E. WESOŁOWSKA and D WAWRO, Institute of Biopolymers and Chemical Fibres, Poland	3
1.1	Introduction	3
1.2	Organic and inorganic cellulose solvents	13
1.3	Chemical, physical and biochemical modification of cellulose structure	19
1.4	Overview of technologies for spinning cellulosic fibres	25
1.5	Cellulose-based composite fibres	36
1.6	Prospectives – nanocellulosic fibres	46
1.7	References	51
2	The structure of cotton and other plant fibres M P ANSELL, University of Bath, UK and L Y MWAIKAMBO, University of Dar es Salaam, Tanzania	62
2.1	Introduction	62
2.2	Categorization of plant fibres	63
2.3	Composition and structure of plant fibres	63
2.4	Structure of seed fibres: cotton, kapok and akund	77
2.5	Structure of bast fibre bundles: jute, kenaf, hemp and flax	81
2.6	Structure of leaf fibres: sisal and banana	84
2.7	Structure of fruit fibres: coir and oil palm empty fruit bunch	87
2.8	Conclusions	89
2.9	References and further reading	90

vi	Contents	
3	An introduction to protein fibres J W S HEARLE, University of Manchester, UK	95
3.1	Introduction	95
3.2	Protein structures	96
3.3	The diversity of protein fibres	99
3.4	Conclusion	105
3.5	References	106
4	The structure and properties of wool and hair fibres F-J WORTMANN, University of Manchester, UK	108
4.1	Introduction	108
4.2	Keratin fibres	109
4.3	Chemical composition	111
4.4	Fibre formation	115
4.5	Morphology	117
4.6	Molecular structures	121
4.7	Mechanical properties and models	125
4.8	Thermal transitions	128
4.9	Conclusions	138
4.10	Sources of further information and advice	138
4.11	References	139
5	The structure of silk F VOLLRATH, D PORTER and C DICKO, University of Oxford, UK	146
5.1	Introduction	146
5.2	Silk mechanics	147
5.3	Silk composition	152
5.4	Fine structure and morphology	154
5.5	Spider silk: lessons from nature	164
5.6	Silk fibre and its models	175
5.7	Influence of structure on properties	179
5.8	Artificial silks	184
5.9	Conclusions	188
5.10	Acknowledgements	189
5.11	Sources of further information	189
5.12	References	189
 <b>Part II Regenerated natural</b>		
6	The structure of man-made cellulosic fibres J GANSTER and H-P FINK, Fraunhofer-Institute for Applied Polymer Research, Germany	201
6.1	Introduction and spinning methods	201

6.2	Structural levels and general models	204
6.3	Rayon (viscose)-type fibres	209
6.4	Lyocell-type fibres	218
6.5	Cellulose acetate-based fibres	222
6.6	Future trends	228
6.7	References	229
7	Regenerated protein fibres: a preliminary review M M BROOKS, University of Southampton, UK	234
7.1	Introduction	234
7.2	First and second generation regenerated protein fibres	235
7.3	Third generation regenerated protein fibres	256
7.4	Summary	261
7.5	Notes	261
7.6	Acknowledgements	262
7.7	References	262
8	The structure of alginate, chitin and chitosan fibres B NIEKRASZEWICZ, Technical University of Lodz, Poland and A NIEKRASZEWICZ, Institute of Biopolymers and Chemical Fibres, Poland	266
8.1	Introduction	266
8.2	Alginate fibres	266
8.3	Chitin and chitosan fibres	281
8.4	Conclusions	298
8.5	Sources of further information and advice	298
8.6	Acknowledgements	299
8.7	References	299
<b>Part III Manufactured non-polymer fibres</b>		
9	The structure and properties of glass fibres F R JONES, University of Sheffield, UK and N T HUFF, Owens Corning Inc., USA	307
9.1	Introduction	307
9.2	The nature of glass	310
9.3	Fibre manufacture	322
9.4	Strength of glass fibres	326
9.5	Protection of fibres for strength retention	340
9.6	Summary	349
9.7	References	349

10	The structure of carbon fibres O PARIS, University of Leoben, Austria and Max Planck Institute of Colloids and Interfaces, Germany and H PETERLIK, University of Vienna, Austria	353
10.1	Introduction	353
10.2	Short historical overview	354
10.3	Types and production of carbon fibres	355
10.4	Fibre structure	357
10.5	Mechanical properties of carbon fibres and their structural origin	368
10.6	Open questions and future directions	372
10.7	Sources of further information and advice	372
10.8	Acknowledgements	373
10.9	References	373
11	Processing, structure and properties of ceramic fibers G MOTZ, University of Bayreuth, Germany and R K BORDIA, University of Washington, USA	378
11.1	Introduction	378
11.2	Processing, structure and properties of non-oxide fibers	379
11.3	Processing, structure and properties of oxide fibers	398
11.4	Comparison of ceramic fibers	404
11.5	Examples of current and anticipated applications	408
11.6	Research and development priorities	409
11.7	Summary and conclusions	410
11.8	Sources of further information and advice	411
11.9	Acknowledgements	414
11.10	References	414
12	Structure and properties of asbestos E J W WHITTALAR, formerly of Ferodo Ltd, UK	425
12.1	Introduction	425
12.2	Classification, occurrence and physical properties of asbestos	426
12.3	Amphibole asbestos	428
12.4	Chrysotile	435
12.5	Synthetic asbestos	448
12.6	References	449
13	Thermally and chemically resistant fibres: structure and properties J W S HEARLE, University of Manchester, UK	450
13.1	Introduction	450

13.2	Thermally resistant fibres	451
13.3	Chemically resistant fibres	454
13.4	Conclusion	456
13.5	References	457
14	Structure, properties and characteristics of optical fibres A ARGYROS, The University of Sydney, Australia	458
14.1	Introduction	458
14.2	Waveguide concepts	459
14.3	Fibre structure and optical properties	462
14.4	Types of optical fibres, materials and applications	467
14.5	New materials and material combinations in optical fibres	479
14.6	Conclusions	480
14.7	Sources of further information and advice	481
14.8	References	482
15	Production and applications of hollow fibers M T DEMEUSE, Celgard, LLC, USA	485
15.1	Introduction	485
15.2	Background	486
15.3	Types of fibers and general features	489
15.4	Polymers used	492
15.5	Structure–property relationships	495
15.6	Conclusions and recommendations	496
15.7	Sources of further information and advice	497
15.8	References	498
	<i>Index</i>	500





## Contributor contact details

---

(\* = main contact)

### Editors

Dr Stephen J. Eichhorn  
Materials Science Centre  
School of Materials  
Grosvenor Street  
University of Manchester  
Manchester M1 7HS  
UK

E-mail: [s.j.eichhorn@manchester.ac.uk](mailto:s.j.eichhorn@manchester.ac.uk)

John W. S. Hearle  
Emeritus Professor of Textile  
Technology  
University of Manchester  
UK  
and  
The Old Vicarage  
Mellor  
Stockport SK6 5LX  
UK

E-mail: [johnhearle@hearle.eclipse.co.uk](mailto:johnhearle@hearle.eclipse.co.uk)

Professor Mike Jaffe  
Department of Biomedical  
Engineering  
New Jersey Institute of Technology  
Medical Device Concept  
Laboratory  
111 Lock Street  
Newark, NJ 07103  
USA

Professor Takeshi Kikutani  
Graduate School of Science and  
Engineering  
Department of Organic and  
Polymeric Materials  
Tokyo Institute of Technology  
2-12-1-S8-32  
O-okayama  
Meguro-ku  
Tokyo 152-8552  
Japan

E-mail: [kikutani.t.aa@m.titech.ac.jp](mailto:kikutani.t.aa@m.titech.ac.jp)

## Chapter 1

Dr Danuta Ciechańska,\* Ewa  
Wesołowska and Dariusz Wawro  
Institute of Biopolymers and  
Chemical Fibres  
ul. M. Skłodowskiej-Curie 19/27  
90-570 Łódź  
Poland

E-mail: [dciechan@ibwch.lodz.pl](mailto:dciechan@ibwch.lodz.pl)

## Chapter 2

Dr Martin P. Ansell\*  
BRE Centre for Innovative  
Construction Materials  
Department of Mechanical  
Engineering  
University of Bath  
Bath BA2 7AY  
UK

E-mail: [M.P.Ansell@bath.ac.uk](mailto:M.P.Ansell@bath.ac.uk)

Dr Leonard Y. Mwaikambo  
Department of Engineering  
Materials  
University of Dar es Salaam  
P.O. Box 35131  
Dar es Salaam  
Tanzania

E-mail: [lyrmwaikambo@udsm.ac.tz](mailto:lyrmwaikambo@udsm.ac.tz)

## Chapters 3 and 13

John W. S. Hearle  
Emeritus Professor of Textile  
Technology  
University of Manchester  
UK  
and  
The Old Vicarage  
Mellor  
Stockport SK6 5LX  
UK

E-mail: [johnhearle@hearle.eclipse.co.uk](mailto:johnhearle@hearle.eclipse.co.uk)

## Chapter 4

Professor Franz-Josef Wortmann  
Textiles & Paper  
School of Materials  
University of Manchester  
Manchester M60 1QD  
UK

E-mail: [f-j.wortmann@manchester.ac.uk](mailto:f-j.wortmann@manchester.ac.uk)

## Chapter 5

Professor Fritz Vollrath\*, Dr David  
Porter and Cedric Dicko  
Department of Zoology  
University of Oxford  
South Parks Road  
Oxford OX1 3PS  
UK

E-mail: [fritz.vollrath@zoo.ox.ac.uk](mailto:fritz.vollrath@zoo.ox.ac.uk)

## Chapter 6

Dr Johannes Ganster\* and  
Professor Hans-Peter Fink  
Fraunhofer Institute for Applied  
Polymer Research  
Geiselbergstraße 69  
14476 Potsdam-Golm  
Germany

E-mail: ganster@iap.fraunhofer.de

## Chapter 7

Mary M. Brooks  
Textile Conservation Centre  
Winchester Campus  
University of Southampton  
Park Avenue  
Winchester SO23 8DL  
UK

E-mail: mmb1@soton.ac.uk

## Chapter 8

Dr B. Niekraszewicz\*  
Man-Made Fibres Department  
Technical University of Łódź  
ul. Zeromskiego 116  
Łódź 90-924  
Poland

E-mail: Barbara.Niekraszewicz@p.lodz.pl

Dr A. Niekraszewicz  
Institute of Biopolymers and  
Chemical Fibres  
ul. M.Skłodowskiej-Curie 19/27  
Łódź 90-570  
Poland

E-mail: biomater@ibwch.lodz.pl

## Chapter 9

Professor Frank Jones\*  
Department of Engineering  
Materials  
University of Sheffield  
Sheffield S1 3JD  
UK

E-mail: f.r.jones@sheffield.ac.uk

Dr Norman Tom Huff  
Owens Corning Inc.  
46500 Humbolt Drive  
Novi, MI 48377  
USA

E-mail: Tom.Huff@owenscorning.com

## Chapter 10

Professor Oskar Paris\*  
Institute of Physics  
University of Leoben  
Franz-Josef-Strasse  
18, A-8700 Leoben  
Austria

E-mail: oskar.paris@unileoben.ac.at

and  
Max Planck Institute of Colloids  
and Interfaces  
Department of Biomaterials  
Germany

Professor Herwig Peterlik  
Faculty of Physics  
University of Vienna  
Vienna  
Austria

E-mail: herwig.peterlik@univie.ac.at

## Chapter 11

Dr Günter Motz  
LST Keramische Werkstoffe  
University of Bayreuth  
95440 Bayreuth  
Germany

E-mail: [Guenter.Motz@uni-bayreuth.de](mailto:Guenter.Motz@uni-bayreuth.de)

Professor Rajendra K. Bordia\*  
Department of Materials Science  
and Engineering  
Box 352120  
University of Washington  
Seattle, WA 98195  
USA

E-mail: [bordia@u.washington.edu](mailto:bordia@u.washington.edu)

## Chapter 14

Dr Alex Argyros  
School of Physics  
Building A28  
The University of Sydney  
NSW 2006  
Australia

E-mail: [a.argyros@usyd.edu.au](mailto:a.argyros@usyd.edu.au)

## Chapter 15

Dr Mark T. DeMeuse  
Celgard, LLC, a Division of  
PolyPore, Inc.  
13800 South Lakes Drive  
Charlotte, NC 28273  
USA

E-mail: [kumquats88@aol.com](mailto:kumquats88@aol.com)

## Woodhead Publishing in Textiles

---

- 1 **Watson's textile design and colour Seventh edition**  
*Edited by Z. Grosicki*
- 2 **Watson's advanced textile design**  
*Edited by Z. Grosicki*
- 3 **Weaving Second edition**  
*P. R. Lord and M. H. Mohamed*
- 4 **Handbook of textile fibres Vol 1: Natural fibres**  
*J. Gordon Cook*
- 5 **Handbook of textile fibres Vol 2: Man-made fibres**  
*J. Gordon Cook*
- 6 **Recycling textile and plastic waste**  
*Edited by A. R. Horrocks*
- 7 **New fibers Second edition**  
*T. Hongu and G. O. Phillips*
- 8 **Atlas of fibre fracture and damage to textiles Second edition**  
*J. W. S. Hearle, B. Lomas and W. D. Cooke*
- 9 **Ecotextile '98**  
*Edited by A. R. Horrocks*
- 10 **Physical testing of textiles**  
*B. P. Saville*
- 11 **Geometric symmetry in patterns and tilings**  
*C. E. Horne*
- 12 **Handbook of technical textiles**  
*Edited by A. R. Horrocks and S. C. Anand*
- 13 **Textiles in automotive engineering**  
*W. Fung and J. M. Hardcastle*

- 14 **Handbook of textile design**  
*J. Wilson*
- 15 **High-performance fibres**  
*Edited by J. W. S. Hearle*
- 16 **Knitting technology Third edition**  
*D. J. Spencer*
- 17 **Medical textiles**  
*Edited by S. C. Anand*
- 18 **Regenerated cellulose fibres**  
*Edited by C. Woodings*
- 19 **Silk, mohair, cashmere and other luxury fibres**  
*Edited by R. R. Franck*
- 20 **Smart fibres, fabrics and clothing**  
*Edited by X. M. Tao*
- 21 **Yarn texturing technology**  
*J. W. S. Hearle, L. Hollick and D. K. Wilson*
- 22 **Encyclopedia of textile finishing**  
*H-K. Rouette*
- 23 **Coated and laminated textiles**  
*W. Fung*
- 24 **Fancy yarns**  
*R. H. Gong and R. M. Wright*
- 25 **Wool: Science and technology**  
*Edited by W. S. Simpson and G. Crawshaw*
- 26 **Dictionary of textile finishing**  
*H-K. Rouette*
- 27 **Environmental impact of textiles**  
*K. Slater*
- 28 **Handbook of yarn production**  
*P. R. Lord*
- 29 **Textile processing with enzymes**  
*Edited by A. Cavaco-Paulo and G. Gübitz*
- 30 **The China and Hong Kong denim industry**  
*Y. Li, L. Yao and K. W. Yeung*
- 31 **The World Trade Organization and international denim trading**  
*Y. Li, Y. Shen, L. Yao and E. Newton*

- 32 **Chemical finishing of textiles**  
*W. D. Schindler and P. J. Hauser*
- 33 **Clothing appearance and fit**  
*J. Fan, W. Yu and L. Hunter*
- 34 **Handbook of fibre rope technology**  
*H. A. McKenna, J. W. S. Hearle and N. O'Hear*
- 35 **Structure and mechanics of woven fabrics**  
*J. Hu*
- 36 **Synthetic fibres: nylon, polyester, acrylic, polyolefin**  
*Edited by J. E. McIntyre*
- 37 **Woollen and worsted woven fabric design**  
*E. G. Gilligan*
- 38 **Analytical electrochemistry in textiles**  
*P. Westbroek, G. Priniotakis and P. Kiekens*
- 39 **Bast and other plant fibres**  
*R. R. Franck*
- 40 **Chemical testing of textiles**  
*Edited by Q. Fan*
- 41 **Design and manufacture of textile composites**  
*Edited by A. C. Long*
- 42 **Effect of mechanical and physical properties on fabric hand**  
*Edited by Hassan M. Behery*
- 43 **New millennium fibers**  
*T. Hongu, M. Takigami and G. O. Phillips*
- 44 **Textiles for protection**  
*Edited by R. A. Scott*
- 45 **Textiles in sport**  
*Edited by R. Shishoo*
- 46 **Wearable electronics and photonics**  
*Edited by X. M. Tao*
- 47 **Biodegradable and sustainable fibres**  
*Edited by R. S. Blackburn*
- 48 **Medical textiles and biomaterials for healthcare**  
*Edited by S. C. Anand, M. Miraftab, S. Rajendran and J. F. Kennedy*
- 49 **Total colour management in textiles**  
*Edited by J. Xin*



- 50 **Recycling in textiles**  
*Edited by Y. Wang*
- 51 **Clothing biosensory engineering**  
*Y. Li and A. S. W. Wong*
- 52 **Biomechanical engineering of textiles and clothing**  
*Edited by Y. Li and D. X-Q. Dai*
- 53 **Digital printing of textiles**  
*Edited by H. Ujiie*
- 54 **Intelligent textiles and clothing**  
*Edited by H. Mattila*
- 55 **Innovation and technology of women's intimate apparel**  
*W. Yu, J. Fan, S. C. Harlock and S. P. Ng*
- 56 **Thermal and moisture transport in fibrous materials**  
*Edited by N. Pan and P. Gibson*
- 57 **Geosynthetics in civil engineering**  
*Edited by R. W. Sarsby*
- 58 **Handbook of nonwovens**  
*Edited by S. Russell*
- 59 **Cotton: Science and technology**  
*Edited by S. Gordon and Y-L. Hsieh*
- 60 **Ecotextiles**  
*Edited by M. MirafTAB and A. Horrocks*
- 61 **Composite forming technologies**  
*Edited by A. C. Long*
- 62 **Plasma technology for textiles**  
*Edited by R. Shishoo*
- 63 **Smart textiles for medicine and healthcare**  
*Edited by L. Van Langenhove*
- 64 **Sizing in clothing**  
*Edited by S. Ashdown*
- 65 **Shape memory polymers and textiles**  
*J. Hu*
- 66 **Environmental aspects of textile dyeing**  
*Edited by R. Christie*
- 67 **Nanofibers and nanotechnology in textiles**  
*Edited by P. Brown and K. Stevens*

- 68 **Physical properties of textile fibres Fourth edition**  
*W. E. Morton and J. W. S. Hearle*
- 69 **Advances in apparel production**  
*Edited by C. Fairhurst*
- 70 **Advances in fire retardant materials**  
*Edited by A. R. Horrocks and D. Price*
- 71 **Polyesters and polyamides**  
*Edited by B. L. Deopura, R. Alagirusamy, M. Joshi and B. S. Gupta*
- 72 **Advances in wool technology**  
*Edited by N. A. G. Johnson and I. Russell*
- 73 **Military textiles**  
*Edited by E. Wilusz*
- 74 **3-D fibrous assemblies: Properties, applications and modelling of three-dimensional textile structures**  
*J. Hu*
- 75 **Medical textiles 2007**  
*Edited by J. Kennedy, A. Anand, M. Miraftab and S. Rajendran*
- 76 **Fabric testing**  
*Edited by J. Hu*
- 77 **Biologically inspired textiles**  
*Edited by A. Abbott and M. Ellison*
- 78 **Friction in textiles**  
*Edited by B .S. Gupta*
- 79 **Textile advances in the automotive industry**  
*Edited by R. Shishoo*
- 80 **Structure and mechanics of textile fibre assemblies**  
*Edited by P. Schwartz*
- 81 **Engineering textiles: Integrating the design and manufacture of textile products**  
*Edited by Y. E. El-Mogahzy*
- 82 **Polyolefin fibres: Industrial and medical applications**  
*Edited by S. C. O. Ugbolue*
- 83 **Smart clothes and wearable technology**  
*Edited by J. McCann and D. Bryson*
- 84 **Identification of textile fibres**  
*Edited by M. Houck*

- 85 **Advanced textiles for wound care**  
*Edited by S. Rajendran*
- 86 **Fatigue failure of textile fibres**  
*Edited by M. MirafTAB*
- 87 **Advances in carpet technology**  
*Edited by K. Goswami*
- 88 **Handbook of textile fibre structure**  
*Edited by S. Eichhorn, J.W.S Hearle, M.Jaffe and T. Kikutani*
- 89 **Advances in knitting technology**  
*Edited by T. Dias*
- 90 **Smart textile coatings and laminates**  
*Edited by W.C. Smith*
- 91 **Tensile failure of fibres handbook**  
*Edited by A. Bunsell*
- 92 **Interior textiles: Design and developments**  
*Edited by T. Rowe*
- 93 **Textiles for cold weather apparel**  
*Edited by J. Williams*
- 94 **Modelling and predicting textile behaviour**  
*Edited by X. Chen*
- 95 **Textiles for construction**  
*Edited by G. Pohl*
- 96 **Engineering apparel fabrics and garments**  
*J. Fan and L. Hunter*

# An introduction to cellulosic fibres

---

D CIECHAŃSKA, E WESOŁOWSKA and D WAWRO,  
Institute of Biopolymers and Chemical Fibres, Poland

**Abstract:** Cellulosic fibres occupy an important position among raw materials for the textile industry. They are used in apparel, household fabrics and various non-woven fabrics. Textile fabrics, such as non-woven, knitted fabrics, may be made of cellulose alone or in combination with other synthetic fibres. Cellulosic fibre-based textile products include feminine hygiene products, absorbent products, household wipes, babies' wipes and diapers, pillowcases, surgical dressings and shoe linings. This chapter first reviews the nature and characteristics of cellulosic fibres. It next discusses cellulose solvents and preparation of solutions, then describes the methods of modification of cellulose pulp in order to increase its reactivity. A review of technologies of cellulosic fibre production, including cellulose-based composite fibres, is presented. Novel, prospective methods of cellulosic fibre manufacture are discussed.

**Key words:** cellulosic fibres, cellulose solvents, modification of pulp, composite fibres, fibre spinning.

## 1.1 Introduction

### 1.1.1 Occurrence and formation of cellulose

Cellulose is the most abundant polymer occurring in nature. It is the structural material in plants and also occurs in certain bacteria and some marine organisms. In cotton fibres, it is found in an almost pure form, except for absorbed water, but more commonly it is mixed with other substances. For example, dry wood consists of 40–55% cellulose, 15–35% lignin and 25–40% hemicelluloses. Probably the oldest use of cellulose is as firewood. Cellulose along with the other natural vegetable materials becomes converted to peat, coal, oil and natural gas, so that directly or indirectly it is the dominant source of energy. However, many thousands of years ago early mankind found that it was easy to extract fibres from the stems of plants and twist them together to make string. This technique can be demonstrated today by extracting fibres from wild nettles. With the current concerns about climate change, the importance of cellulose is recognized as a way of locking up carbon dioxide.

Cellulose is formed by biosynthesis through enzyme-catalysed reactions in living cells. In plants, light energy from the sun converts carbon dioxide from the air and water from the ground into glucose, which then undergoes

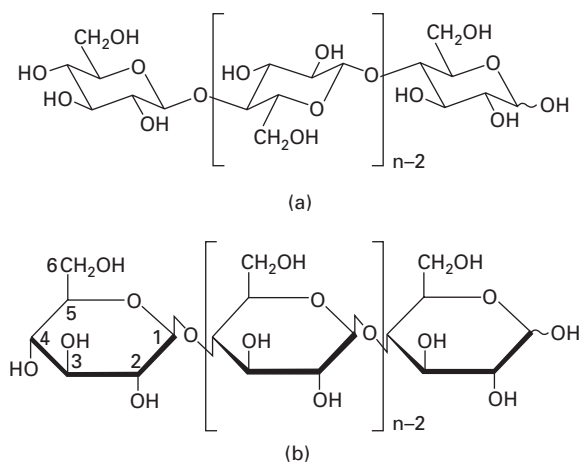
a condensation polymerization reaction with the elimination of water to form cellulose.

### 1.1.2 Cellulose chemistry

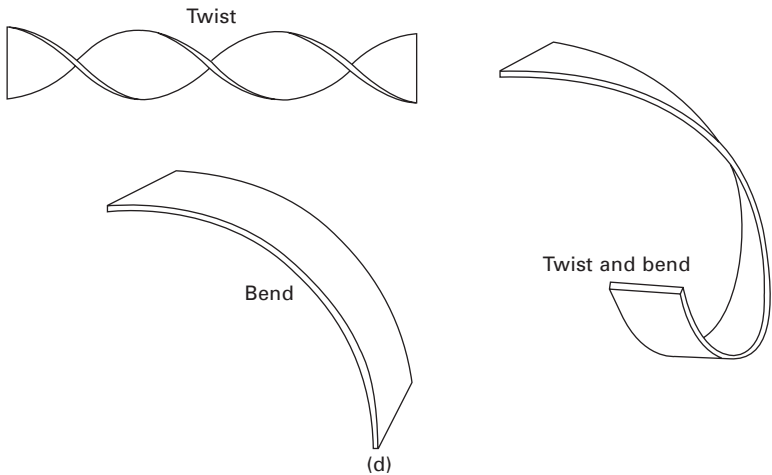
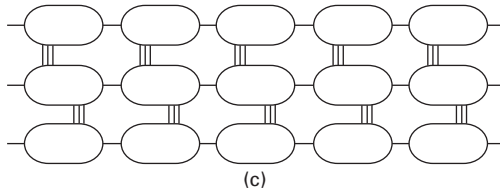
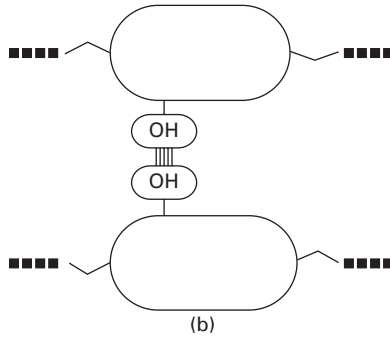
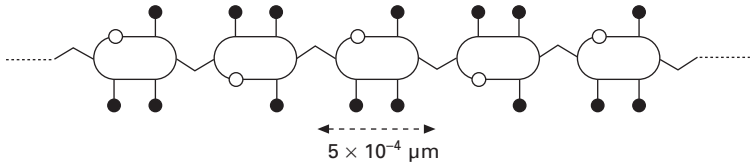
Glucose,  $C_6H_{12}O_6$ , has a ring structure of one oxygen  $-O-$  atom and five  $-CH-$  groups, four with pendant  $-OH$  groups and one with pendant  $-CH_2OH$ . When a molecule of  $H_2O$  is eliminated from two neighbouring  $-OH$  groups, a disaccharide such as sucrose is formed. For the formation of cellulose within plant cells, glucose molecules come to enzyme complexes and add on successively with the elimination of water to form the long polymer molecules. The chemical formula of cellulose is shown in Fig. 1.1 with an indication of its geometric form as well as a simple representation.

### 1.1.3 Physical structure

In order to understand the physical structure, important features of cellulose molecules are shown schematically in Fig. 1.2. The basic form is a sequence of six-membered rings with pendant  $-OH$  groups, Fig. 1.2(a), which can hydrogen bond, either individually, Fig. 1.2(b), or cooperatively, Fig. 1.2(c). In flexibility and conformations, the cellulose molecule is intermediate between the simple linear chains of polyolefins, nylons and polyesters such as polyethylene terephthalate and the stiffer, interactive chains of aramids, fully aromatic polyesters and PBO. In suitable circumstances, highly oriented, highly crystalline structures can be formed. However, because it is a ribbon-like molecule which can twist and bend in one plane, as indicated in Fig.



1.1 Chemical formula of cellulose, from Nevell and Zeronian [1].

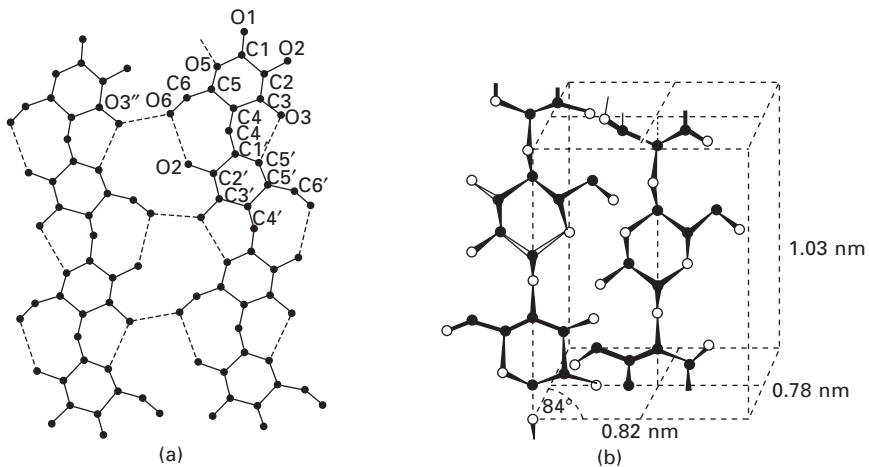


1.2 Schematic view of physical features of cellulose molecule: (a) the polymer; (b) crosslinking by hydrogen bonds; (c) crystal; (d) twisting and bending.

1.2(d), irregular conformations with distributed hydrogen bonds are found in amorphous regions of regenerated fibres. Because of chain breakage, it is difficult to obtain exact values for the molecular weight of natural cellulose. It is estimated that the chains contain about  $10^4$  glucose rings, giving a length of  $5 \mu\text{m}$  and a width of  $8 \times 10^{-4} \mu\text{m}$ . Dissolving cellulose to manufacture fibres reduces the molecular weight. Details of regular hydrogen bonding are shown in Fig. 1.3(a). There are still some uncertainties about the crystal lattices of cellulose, as reviewed by French [2], but a typical representation of the crystal lattice of cellulose I is shown in Fig. 1.3(b).

There are a number of active sites on the enzyme complexes so that about 30 cellulose chain molecules form together and can crystallize as fibrils. The crystalline form, Fig. 1.3(b), is known as cellulose I and has all the chains running in the same directions. The fibrils are then laid down in helical layers to form the cell walls of plants. Natural cellulose fibres have densities that are less than the crystal density. For this and other reasons, such as diffraction, spectroscopic, thermal and chemical data, they are often described as two-thirds crystalline. In another sense, they can be described as 100% crystalline, because they are composed of wholly crystalline fibrils. The measurement discrepancies result from imperfections in the way that the fibrils are packed together. In dry fibres, there is hydrogen bonding between the fibrils, but this reduces as water is absorbed with a consequent reduction in mechanical stiffness.

When cellulose is dissolved (or during swelling in caustic soda in mercerization), the parallel arrangement of molecules is lost. Recrystallization adopts a preferred cellulose II form with anti-parallel chains.



1.3 (a) Regular hydrogen bonding in cellulose, from French [2]. (b) Representation of crystal lattice of cellulose I, adapted from Meyer and Misch [3].

### 1.1.4 The variety of natural fibres

Table 1.1 is taken from the classification of textile fibres in *Textile Terms and Definitions* [4], which shows the three groups of natural cellulose fibres.

The seed fibres are single plant cells. Kapok, which has a limited use as a buoyant material, is a hollow fibre with a thin cell wall. In contrast to this, cotton was the most widely used fibre from around 1800 until near the end of the twentieth century. It is now second to polyester but far ahead of other textile fibres. It is grown through all the latitudes from the Mediterranean to Australia. The fibres grow out from the seeds in the cotton boll to form a primary wall, which is then filled in with a secondary wall. The helix angle is around 21°, but the helix alternates between right- and left-handed. At maturity, there is a small lumen at the centre of the fibre, which collapses on drying to give the convoluted form of cotton fibres.

Bast fibres stiffen the stems of plants. The leaf fibres stiffen long spiked leaves. Both bast and leaf fibres are multicellular. Helix angles of fibrils in the cells are less than in cotton, thus giving higher tensile moduli. Extraction of fibres from stems or leaves is by biological or chemical retting and mechanical action. The ultimate fibres (individual cells) are very small and usable fibres contain many ultimates. Flax is the high quality fibre from which linen is made. In medieval times, hemp was the dominant European fibre and it is now coming back into use. Ramie is used in high quality fabrics. Jute and kenaf are coarse fibres traditionally used in sacks, screens and matting. The leaf fibres are coarse and are mainly used in ropes and cords. Polypropylene has replaced the coarse plant fibres to a major extent.

Trees are the most abundant source of cellulose. Wood is a composite of many small cells. Although wood can be broken down into small fibres and can be dispersed in water to be reassembled as paper, it is not possible to extract these in a way that makes textile processing possible. The relevance

Table 1.1 Extract from the classification of textile fibres [4] which shows the three groups of natural cellulose fibres

Textile fibres			
Natural			Man-made
Animal (protein)	Vegetable (cellulose)		Mineral (asbestos)
↓	Seed	Bast	Leaf
	Cotton, kapok, etc.	Flax, hemp, jute, kenaf, ramie, etc.	Abaca or manila, henequen, phormium tenax, sisal, etc.
			↓
			↓



to textile fibre production is as the raw material for manufacturing artificial fibres.

### 1.1.5 Manufactured cellulose fibres

Manufactured cellulose fibres have a strong growth potential on the world market in competition with synthetic polymers. Their role will increase in sectors such as fibres, packaging materials, chemicals, medicine and hygienic products. Annually about 180 million tons of various cellulose pulps are consumed worldwide, most of it in paper and paperboard manufacture [5]. Only about 8 million tons a year of the raw material are being consumed in miscellaneous cellulose manufacturing which includes cellulose ethers and 3-D products.

According to the terminology established by the International Office for the Standardisation of Man-made Fibres – Bureau International pour la Standardisation des Fibres Artificielles (BISFA), the cellulosic man-made fibres obtained by transformation of natural polymers are classified as shown in Table 1.2 [6].

### 1.1.6 Acetate and triacetate fibres

The term acetate fibres relates to fibres made from cellulose acetate. The difference between acetate and triacetate fibres lies in the number of cellulose hydroxyl groups that are acetylated (Table 1.2). Cellulose acetate was the first man-made thermoplastic fibre.

These fibres are quite different from viscose and are characterized by high elongation at break and poor abrasion resistance, though resistance to pilling is very good, and they can be textured. The dry strength of the two types is similar, though triacetate fibres have higher strength in the wet state. The main end-uses for the filament yarns are in linings, dress wear and household furnishing. Staple acetate fibres are the major product used for cigarette filters. The biggest cigarette filter tow producer in Europe is Rhodia Acetow GmbH in Freiburg, Germany.

Triacetate fibres are used in sportswear, garments and woven fabrics that keep their shape. Due to their low moisture absorption, fabrics made from them are easily washed and dry very quickly. Fabrics made from blends of triacetate and wool are very popular, combining advantageous properties of both types of fibres: the warmth of wool and the drip-dry properties of triacetate [7].

### 1.1.7 Cupro fibres

According to BISFA [6] the term cupro relates to regenerated cellulosic fibres produced by the cuprammonium method. The cuprammonium process is very

Table 1.2 Generic classification of cellulosic fibres according to BISFA [6]

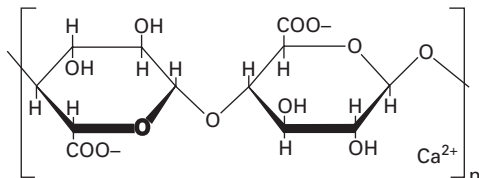
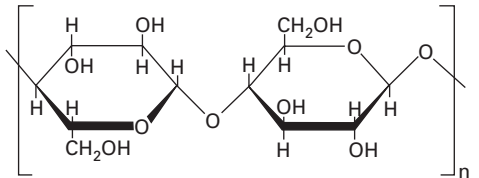
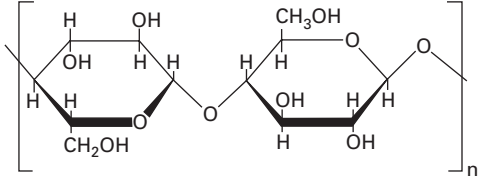
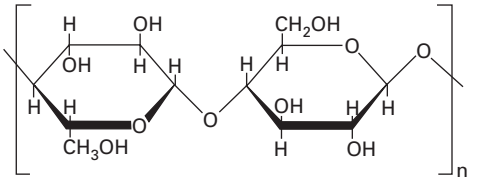
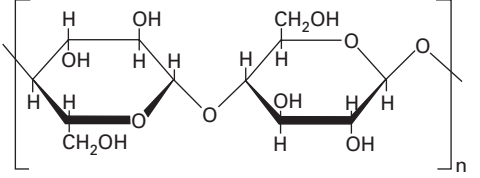
Generic name	Distinguishing attribute	Examples of chemical formulae
Acetate	Cellulose acetate fibre in which less than 92% but at least 74% of the hydroxyl groups are acetylated	<p>Secondary cellulose acetate</p> $\left[ \text{C}_6\text{H}_7\text{O}_2 - (\text{OX})_3 \right]_n$ <p>where X = H or CH<sub>3</sub>CO and the degree of esterification is at least 2.22 but less than 2.76</p>
Triacetate	Cellulose acetate fibre in which at least 92% of the hydroxyl groups are acetylated	<p>Cellulose triacetate</p> $\left[ \text{C}_6\text{H}_7\text{O}_2 - (\text{OX})_3 \right]_n$ <p>where X = H or CH<sub>3</sub>CO and the degree of esterification is between 2.76 and 3</p>
Alginate	Fibre obtained from the metal salts of alginic acid	<p>Calcium alginate:</p> 
Cupro	Cellulose fibre obtained by the cuprammonium process	<p>Cellulose:</p> 

Table 1.2 Cont'd

Generic name	Distinguishing attribute	Examples of chemical formulae
Lyocell	Cellulosic fibre obtained by an organic solvent spinning process. It is understood that: (1) an 'organic solvent' means essentially a mixture of organic chemicals and water, and (2) 'solvent spinning' means dissolving and spinning without the formation of a derivative	Cellulose: 
Modal	Cellulose fibre having a high breaking force $BF$ and a high wet modulus $B_w$ The breaking force $BF_c$ in the conditioned state and the wet modulus $F_w$ required to produce an elongation of 5% in its wet state are: $BF_c \geq 1.3 \sqrt{LD + 2LD}$ $F_w \geq 0.5 \sqrt{LD}$ where $LD$ is the mean linear density (mass per unit length) in decitex. $BF_c$ and $F_w$ are expressed in centinewtons	Cellulose: 
Viscose	Cellulose fibre obtained by the viscose process	Cellulose: 

similar to the viscose process. Cellulose is dissolved in a mixed solution of copper salts and ammonia, then the solution is pressed into a coagulation bath using a spinneret head where the cellulose is subjected to regeneration, giving a multifilament yarn. The raw materials in the cupro process can be wood pulp or cotton linters. Cupro fibres have a good drape and are easy to wash. The main application of these fibres is in forming multifilament yarns for woven fabrics and linings [8]. The process nowadays is exploited by only two companies, Bemberg (Italy) and Asahi (Kasei, Japan).

### 1.1.8 Lyocell fibres

A new generation of cellulosic fibres were invented in the 1980s. The process employs an organic solvent (*N*-methyl-morpholine *N*-oxide) to prepare a solution of cellulose from which fibres are spun by extrusion to a spinning bath. The name Lyocell is the generic name used by BISFA (International Office for the Standardisation of Man-made Fibres) [6] and the Federal Trade Commission (USA). Lenzing (Austria), a leader in that technology, is the sole producer in Europe selling the fibres under the brand name Tencel. The company operates Lyocell plants in Austria, Great Britain and the USA. Other producers are located in the Far East: Shanghai Shuanglu Chemical Fibre Co., Hanil and Hyosung in South Korea, and the Formosa Co. in Taiwan. Initially there were problems with high investment costs and difficulties in reusing the maximum amount of the expensive solvent. The problems were solved at the end of the 1980s and now more than 99% of the solvent is recovered after the spinning and recirculated to the process.

The physical and structural properties of Lyocell fibres differ from those of viscose fibres. They are characterized by higher strength, lower elongation, and a high degree of crystallinity and molecular orientation [9–11]. The outstanding strength of Lyocell fibres is the reason why they are an ideal candidate in yarn and fabric processing. Lyocell fibres combine the desired properties of viscose fibres (wearing comfort, water inhibition, biodegradability) with the excellent features of polyester fibres (high strength). Lyocell fibres are mostly used for apparel fabrics, especially outerwear. In technical sectors, due to their tendency to fibrillation, they can be applied to the manufacture of non-wovens, filters and special papers [12, 13].

### 1.1.9 Modal fibres

Modal and polynosic are names that are used for regenerated cellulose fibres with high tenacity and high wet modulus. Both types of fibres have the following properties:

- High wet modulus, i.e. resistance to extension in the wet state
- Higher ratio of wet to dry breaking tenacity

- High polymerization degree of cellulose
- Micro-fibrillar structure.

Such properties assure their dimensional stability in wet conditions, which is the most important feature from a practical point of view. High wet modulus fibres are resistant to stress and shrinkage, so keep their original shape. Blends of modal or polynosic fibres with other polymers such as flax, wool, polyester or polypropylene provide fabrics with improved properties, i.e. unchanged appearance, reduced shrinkage and better uniformity [8].

#### 1.1.10 Viscose fibres

The most popular cellulosic fibre is viscose, which is defined by BISFA as 'cellulose fibres obtained by the viscose process'. The viscose method dominates in the production of cellulose fibres with an approximately 80% share. The method had been invented at the beginning of the twentieth century, offering for nearly half a century the sole man-made fibres among textile raw materials. It was only after World War II that synthetic fibres began to rapidly penetrate the market, crowding viscose fibres out of their dominant position. In the viscose route, carbon disulphide ( $CS_2$ ) is used, causing water and air pollution with sulphur compounds, and the danger of fire and explosion. As an industrial poison, it is also a serious menace to operators. These factors resulted in many plant shut-downs and a decrease in production. Yet, despite all adversities, the viscose method survived. It has been greatly improved by the leading producers with respect to environmental pollution and work safety. Viscose fibres are a very versatile textile raw material that may be compared to natural fibres like cotton, wool, linen and silk. In textiles, they offer a high wearing comfort by being soft and cool. The prime attribute of viscose fibres is their hydrophilicity [14]. Additionally, the high water retention of viscose fibres is an advantage during wet processing and is connected with the quick liquid absorption of the end product. The disposal of biodegradable viscose fibres is easy. The fibre properties can be adjusted according to the needs of the customers. For example, fineness, length, wet strength and crimping can be easily controlled by varying the spinning conditions [15, 16]. They can be easily dyed and do not shrink during heating. Viscose fibres and their blends with other fibres are mostly used in the textile industry for clothes production, linings, furnishing fabrics and the manufacture of hygienic materials where high absorption properties are required.

#### 1.1.11 Alternative cellulosic fibres

Novel cellulosic fibres, alternative to viscose fibres, can be obtained from biomodified cellulose pulp using cellulolytic enzymes. Enzymatic modification of the cellulose structure causes an increase of cellulose reactivity and solubility

in alkali with controlled decrease of its molecular weight. The treated pulp is directly dissolved in aqueous sodium hydroxide solution and the fibres are spun using an acetic coagulation bath in a wet spinning method. At the beginning of the 1990s the process of manufacturing cellulosic fibres from enzyme-treated pulp, under the code name Celsol, was studied in cooperation between the Institute of Biopolymers and Chemical Fibres, the Tampere University of Technology (Finland) and the Technical University of Łódź (Poland) [17, 18]. Since then it has been further developed within the 6th European Framework Programme [19].

## 1.2 Organic and inorganic cellulose solvents

Cellulose pulp is one of the most important commodity raw materials. Annually about 180 million tons of various cellulose pulps are consumed worldwide, most of it in paper and paperboard products in the form of mechanical, chemo-mechanical or chemical pulp [5]. Application of cellulose to higher technology products such as fibres is limited because of its lack of solubility in cheap, common and non-toxic solvents. At present the problem of the dissolution of cellulose is one of the most important issues. Currently, methods for dissolving cellulose pulp used on an industrial scale are the viscose, cuprammonium and NMMO methods. In the first two methods certain toxic chemicals are required for derivatization and transferring cellulose into a soluble form [20–22]. Accordingly, regeneration is necessary to convert cellulose derivatives to regenerated cellulose. Moreover, both processes present real environmental hazards due to the emission of significant amounts of toxic by-products formed at the different stages of the process, which must be removed from effluents before their disposal. However, viscose fibres are still used in Europe and throughout the world in technical, textile and sanitary applications, despite the vehement expansion of polyester and polyamide in that direction; for example, viscose cord is a valuable material for the reinforcement of rubber, mainly in the production of automobile tyres. The special staple fibres called modal and polynosic (see Section 1.1.9) offer higher tenacity and improved wear properties. Viscose continuous yarn is available as multifilament in the count range of 50 to 660 dtex. High tenacity cord yarn produced by Cordenka (Germany) as a reinforcing material for high performance tyres, hoses, strapping and twines is made in the range of 1000 to 4000 dtex. Lenzing (Austria) is a world leader in the manufacture of cellulose fibres by the standard viscose process and a more ecological method based on organic solvents leading to Lyocell-type fibres [11]. In that process, cellulose is dissolved directly in NMMO at high temperature and the fibres are formed by extruding it into an aqueous solution of NMMO.

When analysing the possibility of obtaining cellulose solutions it is necessary to consider the effect of cellulose structure on its ability to dissolve.

However, the most essential factor that determines cellulose solubility is the presence of inter- and intramolecular hydrogen bonds. Treatment of cellulose I with various chemicals leads, depending on conditions, to obtaining a few polymorphic kinds of cellulose containing different amounts and quality of inter- and intramolecular hydrogen bonds, thus characterized by differing ability to dissolve. It is known that cellulose is characterized by structural polymorphism, i.e. the five crystallographic kinds (Cellulose I, II, III, IV and X) are associated with various parameters of the crystallographic network such as the crystallographic system (monoclinic, tetragonal) and dimensions of elementary cells [23]. Cellulose structures undergo transformation depending on the kind of solvent as well as on treatment conditions, mainly temperature [24, 25].

For many years the elaboration of new solvents for cellulose has been the focus of attention of world research centres. It is expected that as result of their application, novel methods of cellulose fibre manufacture will be proposed that are less inconvenient compared with the viscose process. Several articles have been devoted to systematizing the cellulose solvents. The classification of solvents proposed by Turbak *et al.* [26] is often cited by other scientists [27, 28].

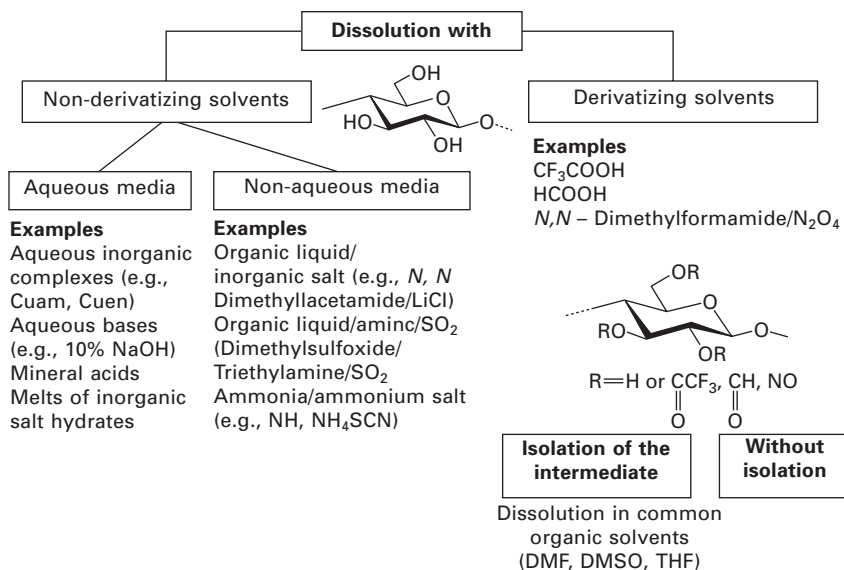
Generally, there are four groups of all known cellulose solvents:

- Cellulose as alkali (inorganic acids, ‘Lewis’ acids)
- Cellulose as acid (inorganic and organic alkalis)
- Cellulose complexes (inorganic and organic complexes)
- Cellulose derivatives (stable and unstable compounds).

According to reference 29 the cellulose solvents are divided into two groups, the so-called non-derivatizing and derivatizing solvents. The first group comprises systems that dissolve the polymer by intermolecular interactions only. The second relates to all the solvents where the dissolution process is combined with the formation of ‘unstable’ ether, ester or acetal derivatives. Both groups include aqueous and non-aqueous solvents. Figure 1.4 shows the classification of cellulose solvents [30].

Typical aqueous non-derivatizing solvents used for characterization and cellulose regeneration can be divided, depending on compound type, into the following sub-groups [30]:

- Transition metal complexes with amines or  $\text{NH}_3$  – cadoxen, cdtren, cooxen, cupren, cuam, cuen, nioxam, nioxen, nitren, zincoxen
- Transition metal complexes with tartaric acid – EWNN (FeTNa)
- Ammonium hydroxides – triton B (trimethylbenzyl ammonium hydroxide), TEOH (tetraethylammonium hydroxide), triton F (dimethyldibenzyl ammonium hydroxide), GuOH (guanidinum hydroxide)
- Alkali hydroxides – NaOH, LiOH.



#### 1.4 Classification of cellulose solvents [30].

Cuen, cuam and EWNN are commonly used as a solvents for cellulose characterization. The promising cellulose solvents, from an industrial point of view, are ZnCl<sub>2</sub> and NaOH, offering the possibility of obtaining concentrated spinning solutions for further processing into fibres.

Many patents describe how the most useful ZnCl<sub>2</sub> solutions for dissolving cellulose are aqueous solutions with 62–76% concentration of ZnCl<sub>2</sub>. In such solutions the cellulose can be dissolved in 5–12 wt% at 65–80°C [31–33]. Fibres from zinc chloride can be spun to acid [33] or alkaline coagulation bath [34]. The mechanical parameters of the fibres so obtained are similar to those of fibres produced by the viscose method and are characterized by a tenacity of 15–25 cN/tex and an elongation of 15–25%. The technological process in the manufacture of cellulose fibres based on zinc chloride solutions is less complicated than the viscose process, though it should be improved by increase of cellulose content, decrease of cellulose degradation during dissolving, and increase of spinning take-up [35].

The effect of aqueous NaOH solutions on cellulose has been a subject of interest for many years. Following very intensive investigation conducted by the Asahi Chemical Industry Co. in Japan, special consideration has been given to the possibility of obtaining spinnable solutions in aqueous NaOH. It has been found that cellulose is nearly completely soluble in 8–10 wt% of sodium hydroxide solution [36]. In order to increase cellulose reactivity and solubility in aqueous sodium hydroxide solution, the cellulose pulp should be subjected to special modification, for example by steam explosion



or biochemical methods using suitable enzymes [18, 36–38]. As a result of modification of cellulose an alkali-soluble pulp with average polymerization degree of 300–350 is produced. Alkaline solutions with a polymer content of 5–7 wt%, distinguished by suitable rheological behaviour, are useful for converting into a variety of shaped products.

It is well known from the literature that addition of zinc oxide or urea to NaOH solution plays a very important role in the cellulose dissolution process [39, 40]. Some publications indicate that NaOH/urea and NaOH/thiourea aqueous solutions can dissolve cellulose directly and quickly; these two solvent systems are expensive and almost non-toxic, and good cellulose fibres can be formed [41–43]. The properties of these cellulose solutions and the fibres obtained have been widely investigated. It has been found that the regular round cross-section of cellulose fibres spun from NaOH/thiourea aqueous solutions was similar to that of fibres of natural silk [44]. The mechanical properties of the fibres produced by the NaOH/urea or NaOH/thiourea methods are close to those of the fibres obtained by the NMMO process [45]. However, spinning solutions containing a higher cellulose content in these two solvents are unstable, which is a disadvantage for industrial production.

Recently a new NaOH/thiourea/urea aqueous solution has been identified as a more powerful cellulose solvent for preparing more stable spinning solutions containing higher concentrations of cellulose [46]. The mechanism of cellulose dissolution in this novel solvent was investigated by SEM, wide-angle X-ray diffraction (WAXD) and  $^{13}\text{C}$  NMR. The results imply that interactions between NaOH and urea, and between NaOH and thiourea, play an important role in improving the dissolution of cellulose. Moreover, NMR spectra of cellulose solutions show that the novel system is a direct solvent. During dissolution the structure of cellulose I changes to that of cellulose II, giving shaped products with cellulose structure II.

Mineral acids such as hydrochloric, sulphuric and phosphoric acids are characterized by their ability to dissolve cellulose. Turbak *et al.* [26] found that particularly phosphoric acid is an interesting solvent for cellulose. Thus observed the formation of liquid-crystalline solutions when cellulose was dissolved in phosphoric acid [47, 48]. It has long been known that production of liquid-crystal solutions is crucial for obtaining fibres with high mechanical properties. Boerstael *et al.* described the preparation of liquid-crystal spinning solutions of cellulose in anhydrous phosphoric acid [47]. Superphosphoric acid solvents were prepared by mixing two or more of the following components: orthophosphoric acid ( $\text{H}_3\text{PO}_4$ ), pyrophosphoric acid ( $\text{H}_4\text{P}_2\text{O}_7$ ), polyphosphoric acid ( $\text{H}_6\text{P}_4\text{O}_{13}$ ), phosphorus pentoxide ( $\text{P}_2\text{O}_5$ ) and water. The composition of the solvent was expressed in a  $\text{P}_2\text{O}_5$  concentration of approximately 74 wt%. The cellulose dissolution process proceeded very quickly, i.e. within a few minutes. Cellulose solutions in  $\text{P}_2\text{O}_5$ , having

different polymer content from 7.5 wt% up to 33 wt% were filtered, heated and extruded through a spinneret containing 1500 holes of 65  $\mu\text{m}$  diameter. Then fibres were subjected to drawing in an air gap and coagulation in a bath containing acetone. The mechanical properties of the fibres obtained were compared with those of fibres prepared by the viscose process, such as a textile yarn Enka<sup>®</sup> Viscose, Cordenka<sup>®</sup> 660 and 700 tyre yarns, and high-modulus Cordenka<sup>®</sup> EHM yarn. It has been found that fibres with a high tenacity of 1.70 GPa and a high modulus of 44 GPa can be prepared from liquid-crystal solutions of phosphoric acid. The mechanical properties of cellulose fibres prepared in this way were significantly higher than those of fibres produced by the conventional viscose process.

The second group of solvents are non-aqueous non-derivatizing solvents. Selected examples include unicomponent, bicomponent and tricomponent chemicals [30]:

- Unicomponent – *N*-ethylpyridinium chloride, *N*-methylmorpholine-*N*-oxide, triethylamine-*N*-oxide, *N*-methylpiperidine-*N*-oxide
- Bicomponent – DMSO/methylamine, DMSO/KSCN, DMSO/CaCl<sub>2</sub>, DMAc/LiCl, *N*-methylpyrrolidone/LiCl
- Tricomponent – NH<sub>3</sub>/NaCl/DMSO, ethylenediamine/NaI/*N,N*-dimethylformamide, diethylamine/SO<sub>2</sub>/DMSO.

DMAc/LiCl solvent is recognized as an excellent solvent for structural assessment of molecular weight distribution of cellulose [49–52].

Philipp *et al.* investigated cellulose solubility in different tricomponent systems containing polar solvent/sulphur compounds/amine such as acetonitrile/SO<sub>2</sub>/dimethylamine, DMSO/SO<sub>2</sub>/diethylamine and DMF/SOCl<sub>2</sub>/diethylamine, DMF/SOCl<sub>2</sub>/triethylamine [53–55]. It has been found that the best miscibility with cellulose occurs when the system contains SO<sub>2</sub>. In solvent systems containing SOCl<sub>2</sub> the area of miscibility with cellulose is significant lower. The study described was concerned only with the problem of cellulose solubility, not with polymer regeneration from these systems and cellulose fibre manufacture.

The most versatile solvent from this group is *N*-methylmorpholine-*N*-oxide (NMMO). This solvent is able to form a liquid-crystal solution as well as to dissolve cellulose relatively quickly under specific conditions, creating concentrated polymer solutions from which man-made cellulose fibres can be produced with outstanding mechanical properties [56–57]. Fibres based on aminooxide are characterized by high strength and stability but show a marked tendency to fibrillation in the wet state. Techniques are now being developed to reduce fibrillation and produce fibres with good washing stability [10, 58–62].

Recently there has been great interest in searching for alternative methods of cellulose dissolution, leading to derivatization and creation of sulphites,

nitrate or methyl derivatives. They are formed in a non-aqueous medium in which one of the components, the so-called 'active agent', binds with cellulose, while the second component is an organic solvent fulfilling assumed functions. Examples of derivatizing solvents and the derivatives formed are given in Table 1.3 [30]. The best known solvents of this group are  $N_2O_4$ /DMF and  $(CH_2O)_y$ /DMSO.

Studies on the dissolution of cellulose in  $N_2O_4$ /organic solvent systems were started in the 1940s [63] and have continued to the present [64–67]. It has been found that for  $N_2O_4$ /DMF solvent, cellulose solubility depends on the degree of polymerization (DP). Cellulose with DP = 1000 dissolves in amounts of up to about 3%; however, cellulose with DP = 400–500 dissolves in amounts of 6–8% and when DP = 300 it is possible to obtain spinning solutions with 10% of polymer content [68]. Similarly, cellulose solutions were prepared when  $CH_3CN$  or DMSO was applied as solvent.

The process of the dissolution of cellulose in a  $(CH_2O)_y$ /DMSO system was described for the first time in 1975 [69] and since then many more articles have been published [70–72]. The first spinning solutions from this system were prepared from cellulose with DP = 400–600 and were composed of 6 wt% cellulose, 6 wt% paraformaldehyde and 88 wt% solvent [73]. Mechanical properties (tenacity, elongation) of fibres spun to an aqueous coagulation bath containing 4%  $Na_2S$  were comparable to those of viscose fibres.

Many of the methods for dissolving cellulose described in this chapter include the use of different metal complexes or organic solvents. However, these methods are not applied industrially because of their use of toxic compounds, such as heavy metals, amines and multi-component solvent systems, which are very expensive and from which it is very difficult to recover solvent. Hence, these methods are disadvantageous from economic and environmental points of view.

The newest technologies offer ionic liquids (ILs) as very efficient solvents for various polysaccharides, including cellulose. Ionic liquid so-called 'green' solvents are defined as complex salts that melt at temperatures below 100°C, are 100% ions, are strongly polar, have no vapour pressure and are non-

*Table 1.3* Representative examples of derivatizing solvents and derivatives formed [30]

Solvent	Derivative
$N_2O_4$ /DMF	Cellulose nitrate
HCOOH/ $H_2SO_4$	Cellulose formate
$CF_3COOH$	Cellulose trifluoroacetate
$Cl_2CHCOOH$	Cellulose dichloroacetate
$(CH_2O)_y$ /DMSO	Methylcellulose
$CISi(CH_3)_3$ DMF	Trimethylsilylcellulose (TMSC)

flammable, electrically conductive and generally immiscible with organic compounds [74, 75].

Ionic liquids are able to dissolve biopolymers with a high degree of polymerization (DP) such as bacterial cellulose (BC) with DP up to 6500. Many of them can be recycled into the process indefinitely. Ionic liquids such as 1-*N*-butyl-3-methylimidazolium chloride ( $[\text{C}_4\text{mim}]^+\text{Cl}^-$ ), 1-*N*-ethyl-3-methylimidazolium chloride ( $[\text{C}_2\text{mim}]^+\text{Cl}^-$ ), 1-*N*-butyldimethylimidazolium chloride ( $[\text{C}_4\text{dmim}]^+\text{Cl}^-$ ) and 1-*N*-allyl-2,3-dimethylimidazolium bromide ( $[\text{Admim}]^+\text{Br}^-$ ) were investigated as solvents for the homogeneous acylation and carbanilation of the biopolymer cellulose [76].

Some aspects of the use of ILs in carbohydrate chemistry, in particular swelling, dissolution and functionalization of simple sugars, cyclodextrins, cellulose and its derivatives, starch and chitin/chitosan, have been discussed [77, 78]. Swatloski *et al.* studied various ILs including 1-*N*-butyl-3-methylimidazolium ( $[\text{C}_4\text{mim}]^+$ ) with different anions. It has been found that the chloride ion, as a small hydrogen bond acceptor, seems to be the most appropriate for cellulose dissolution. Unfortunately no information about the dissolution mechanism of cellulose in ILs is available up to now, though this is very important for polymer processing [79]. Recently, molten salt hydrates such as  $\text{LiX} \cdot n\text{H}_2\text{O}$  ( $\text{X} = \text{I}^-, \text{NO}_3^-, \text{CH}_3\text{COO}^-, \text{ClO}_4^-$ ) have been applied as efficient solvents for cellulose [80].

### 1.3 Chemical, physical and biochemical modification of cellulose structure

Practical application of cellulose pulp in chemical fibre technology requires suitable methods for modifying pulp in order to increase its reactivity and solubility in proper solvents such as, e.g., NaOH or NaOH/ZnO. The main goal of modification is to reduce inter- and intramolecular hydrogen bonds in order to decrease the degree of polymerization of cellulose; however, changes in the molecular, supermolecular and morphological structure of cellulose can also be observed [81–83]. The most common methods of cellulose pulp modification (activation) are alkalization, enzymatic modification, radiation treatment, steam explosion treatment and hydrothermic activation.

#### 1.3.1 Alkalization

Alkalization of cellulose is the oldest and commonest method for pulp degradation in the viscose process. The process is based on cellulose treatment with NaOH solution with concentration of 18–19 wt%. The goal of the process is to reduce intermolecular hydrogen bonds and to lower the polymerization degree of cellulose, leading to the formation of a new chemical compound – alkalicellulose. A visible change that occurs during alkalization is swelling

of the cellulose pulp. In the ripening process of alkalicellulose, degradation of the cellulose chain and lowering of its polymerization degree take place. However, the permissible fall of the polymerization degree is limited, because this parameter has a great impact on the tenacity of manufactured fibres.

In order to improve cellulose reactivity and swelling ability in sodium hydroxide solution, additives such as zinc oxide, urea and thiourea are introduced into NaOH solution [39, 40, 42, 45, 84–86]. Combination of these additives with NaOH solution, e.g. NaOH/thiourea/urea, can dissolve cellulose directly and quickly, and good cellulose fibres can be formed [46].

### 1.3.2 Enzymatic modification

Modern methods of modifying cellulose pulp include biotechnological methods with the use of cellulolytic enzymes. Enzymatic activation of chemical pulp is known from several patents and papers [18, 87–92]. The aim is to increase the reactivity and alkali solubility of treated pulp. Struszczyk and Nousiainen [89, 91] found that it is possible to apply enzyme-treated cellulose pulp for the preparation of aqueous alkaline cellulose spinning solution useful for fibre spinning. The biomodification process is based on the application of specific cellulolytic enzymes (cellulases) that hydrolyse the  $\beta$ -1,4 glucosidic bonds of cellulose. The cellulase components work synergistically as they degrade the cellulose molecules finally into glucose monomers and oligomers. Endoglucanases attack the middle of the glucan chains and markedly decrease the degree of polymerization of the cellulose. Exoglucanases or cellobiohydrolases attack the releasing glucan ends and remove cellobiose or glucose from the chain ends. Finally,  $\beta$ -glucosidases cut the cellobioses into glucose monomers [93, 94]. Most of the cellulolytic enzymes used for modifying hardwood and softwood dissolving pulps into directly alkaline soluble forms are produced by the fungi *Trichoderma reesei* or *Aspergillus niger* [94–98].

Qualitative and quantitative composition of the enzyme complex, as well as many structural features of the cellulose such as its polymerization degree, capillary system, crystallinity and ability to swell in aqueous solutions, have significant effects on the susceptibility of the cellulose to enzyme action [99]. Of essential importance in the enzymatic modification process is the distribution of the capillary system in the cellulose. Contact between the enzyme molecules and the surface of the cellulose particles is possible when the width of the cellulose capillaries significantly exceeds the dimensions of the enzyme molecule [100]. The ability to biomodify cellulose depends, to a large extent, on its structural features. Among many features that affect the rate of enzymatic modification, cellulose crystallinity is considered one of the most important. It has been postulated that the cellulolytic enzyme

degrades the more accessible amorphous regions of cellulose more readily than the less accessible crystalline regions [99, 101]. Moreover, it was found that susceptibility of the cellulose pulp to enzymes increases following preliminary mechanical treatment of the pulp [102]. The crystallinity of initial untreated, mechanically treated and enzymatically treated pulp, as measured by X-ray diffraction, is 66%, 55% and 56% respectively [103].

The mechanism of the increase of cellulose solubility in alkali is still under investigation. Researchers [97, 98, 104] have stated that enzymes decrease the degree of polymerization and the number of inter- and intramolecular hydrogen bonds of cellulose. It was found that the alkaline solubility of cellulose improved when the pulp was subjected to mechanical treatment prior to enzymatic treatment [102]. The enzymatically modified cellulose pulp was dissolved at low temperature in 9 wt% aqueous sodium hydroxide containing a small amount of zinc oxide. Zinc oxide is used to improve the solubility of the cellulose, decrease the solution viscosity, and increase the stability of the alkaline cellulose solution.

The enzymatic method of cellulose modification that produces alkali-soluble pulp is characterized by many advantages, such as the mild conditions of the process (enzymatic action takes place at 50°C and atmospheric pressure), the possibility of enzyme recirculation and the low environmental hazard [97, 105]. The method allows for elaboration and for developing a novel biotechnology-based process for converting cellulose into a variety of shaped bodies with high value.

### 1.3.3 Radiation treatment

Radiation treatment of cellulose was first described in the literature in 1952 [106]. It was noted that during treatment the cellulose underwent degradation and that such degraded cellulose could be used in the viscose process or for production derivatives (ethers, esters). Cellulose pulp was exposed to an electron beam with energy of 1.7 MeV in an electron accelerator. Interaction of electrons on the cellulose pulp influenced its polymerization degree as well as formation of new functional groups such as carbonyl, carboxyl and hemicellulose [107, 108].

Canadian company AECL (Atomic Energy of Canada Ltd) and Faserwerke Kelheim GmbH, Germany, elaborated the radiation method of cellulose modification, taking into consideration the possibility of improvement of economic aspects of the viscose process [106]. Treatment of cellulose pulp with  $\beta$ -radiation increases its reactivity and results in lower consumption of  $\text{CS}_2$  in the viscose process. The current consumption of  $\text{CS}_2$  in the viscose process when producing regenerated cellulosic items is around 28–36 wt% based on cellulose. As a result of radiation treatment, the consumption of  $\text{CS}_2$  in the pilot-scale production of regenerated cellulosic items can be

reduced by 20 wt%. The second, important advantage of this method is the possibility of reducing the amount of sodium hydroxide in the viscose solution to 5 wt%.

Exposure to high energy radiation, such as gamma rays, is a special way to activate cellulosic substrates by degradation [109]. Irradiation considerably changes the structure, reactivity, physico-chemical and mechanical properties of cellulose. At lower doses (below 10 kGy) crosslinking was observed [110], while irradiation of cellulose at higher doses results in degradation that leads to a decrease in DP and a decrease in crystallinity and crystal dimensions [111].

The effect of combining radiation and alkali treatments on cellulose properties was also studied [112, 113]. Cellulose powder was irradiated by Co-60 gamma rays in the dose range of 500–1500 kGy (10 kGy/h). Next the irradiated samples were treated with NaOH solution at room temperature. The experiments show that under the effect of irradiation and alkali treatment of cellulose there is a considerable degradation of the cellulose that is shown by the decrease in the degree of polymerization.

The manufacture of cellulose derivatives such as carboxymethylcellulose (CMC), cellulose carbamate (CC) and cellulose acetate (CA) from cellulose pulps irradiated with doses of 10 and 15 kGy has been investigated [114]. Positive results were achieved in the process of CC and CA manufacture. The action of ionizing radiation on cellulose increased its activity and facilitated formation of its esters: carbamate and acetate. Irradiation of the samples with doses of 10 and 15 kGy allowed researchers to obtain such values of the polymerization degree as were required for obtaining cellulose carbamate with excellent solubility in aqueous sodium hydroxide solution.

The radiation degradation of cellulose has become a relevant technical aspect of the manufacture of regenerated cellulose: the irradiation of pulp prior to viscose processing may result in reduced consumption of chemicals and time. Many authors promote electron treatment of wood pulp as a method for reducing the use of hazardous chemicals in the viscose process. Investigations with electron-treated pulp have been performed in several countries, including the USA, Canada, Mexico, Germany, the UK, Sweden, India and Taiwan [115–117].

#### 1.3.4 Steam-explosive treatment

The explosion pulping process is based on brief vapour-phase cooking at temperatures in the range of 180–250°C, followed by explosive decompression. The explosive method ('steam explosion') was invented by Mason in the early 1930s and was used for the utilization of wood chips and cellulose delignification. In this process, the wood chips were steam heated at a very high temperature, about 285°C, and at a pressure of 3.5 MPa for about 2



min. The pressure increased rapidly to about 7 MPa for about 5 s, and the chips exploded at atmospheric pressure into a pulp [118]. However, Kamide and coworkers noticed that this method can also be used for modification of cellulose, particularly to decrease the amount of intermolecular hydrogen bonds [36, 119, 120]. They investigated the effect of steam explosion conditions on the changes in morphology, degree of polymerization, solubility in aqueous alkali solution, and supermolecular structure of a softwood pulp. As a result of optimization of the method it was found that the most effective pressure is 2.9 MPa for a time of 30 s. Such modified cellulose was characterized by solubility in 9–10% aqueous sodium hydroxide solution with yield of 99 wt%. They also observed a decrease of polymerization degree, a decrease of the amorphous content of the samples in spite of an increase in solubility, and a breakdown in the intramolecular hydrogen bonds at the C<sub>3</sub> and C<sub>6</sub> positions. Studies carried out by Kamide allowed an explanation for the structural changes that occur in cellulose during treatment with superheated water vapour at high pressure. Yamashiki *et al.* [120] dissolved 50 g of steam-treated cellulose (DP = 331) in 950 g of 9.1 wt% aqueous NaOH solution precooled at 4°C and tried to use this solution for fibre spinning. The fibre were characterized by tenacity of 0.12 GPa and modulus of 9.45 GPa.

Similarly, Tanahashi *et al.* [121] studied the effects of steam explosion on the morphology and physical properties of wood and found that the amorphous cellulose becomes crystalline during the steaming process. Increased crystallinity of cellulose by promoting crystallization of the amorphous regions by steam explosion treatment was observed by other authors [122, 123]. The observations were confirmed by analyses using Raman spectral measurements and solid state NMR spectra. It is known that steam explosion pulp has higher porosity, higher specific surface area and higher hydrophilic character [124].

Steam explosion is a rapidly developing technology for the fractionation of biomass into its main components (cellulose, hemicellulose, lignin) and for the extraction of industrial polysaccharides [125, 126]. For last 10–15 years the steam explosion of lignocellulosic materials has been widely studied in order to increase the conversion yields of the polysaccharides into monosaccharides by enzymatic hydrolysis. Monosaccharides are finally used as starting material for fermentation products [127–129]. The method is also used for obtaining a high-purity chemical-free microcrystalline cellulose having a low degree of polymerization, which may be used in the pharmaceutical and nutritional industries [130].

Steam explosion may be an interesting alternative method of cellulose activation for dissolving cellulose and for the production of new textile fibres. The main advantage of modification by steam explosion is its ability to determine the essential features (polymerization degree, purity, etc.) of the end product by varying the process conditions.



### 1.3.5 Hydrothermic activation

Recently, special attention has been paid to another method of cellulose activation which is based on the heating of cellulose pulp suspension in water or methanol at 100–170°C under hyperbaric pressure [131]. The reaction in hot compressed water is the so-called hydrothermal activation. The cellulose after treatment is characterized by increased reactivity, which allows the manufacture of cellulose carbamate or viscose at lower CS<sub>2</sub> consumption. Such cellulose is also easily soluble in *N*-methylmorpholine-*N*-oxide (NMMO). It has been found that hydrothermal activation affects the solubility and molecular-weight distribution [132].

The method was known earlier but was used mainly for wood biomass decomposition, including waste wood, old paper and agricultural waste products [133]. Lignin, which contains many oxygen-based functional groups, can be an alternative source for the production of chemical compounds following its decomposition using hydrothermal treatment. Lignin subjected to activation in water at temperatures of 653–673 K and various pressures under an argon atmosphere produced three main products: catechol, phenol and *o*-cresol [134].

A US patent application [135] describes the method of degradation of polysaccharides (starch, guar gum, cellulose) by hydrothermal reaction performed in hot water at a pressure of 5–100 MPa and a temperature of 140–300°C, containing carbon dioxide being added by pressure application. A product obtained by the hydrolysis reaction is preferably a monosaccharide (such as glucose or galactose). Use of carbon dioxide in addition to hot water significantly improved the yield of a monosaccharide. Such a method allows the degradation of the food waste that contains a starch-containing agricultural product or wood and paper, into glucose or oligosaccharides.

The hydrothermal modification of cellulose was a research topic of the Institute of Biopolymers and Chemical Fibres, IBWCh, Poland, where the method of manufacture of cellulose carbamate based on hydrothermal treatment was elaborated. This innovation is protected by US patent [136]. For hydrothermal activation, the cellulose pulp was treated with water in the presence of catalysts for 0.5–10 h at 120–160°C under a pressure of up to 5 bar. The hydrothermal treatment of the cellulose produces activated pulp with controlled polydispersity of less than 2.7. The hydrothermal treatment of cellulose pulps was carried out in the presence of catalysts such as organic and/or inorganic acids, as well as inorganic or organic salts of inorganic and/or organic acids, which controlled the degradation and activation process. The controlled hydrothermal activation produces highly reactive cellulose pulp. Such pulp used for reaction with urea allows the production of cellulose carbamate characterized by good solubility in aqueous alkali solution as well as excellent spinnability for producing fibres, films and other products.

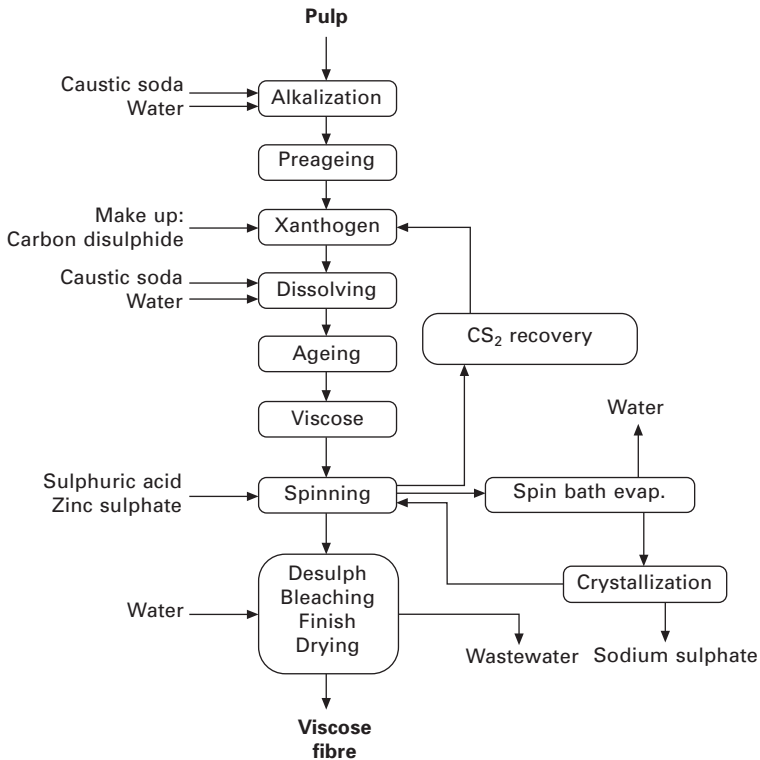
Further studies at IBWCh on the modification of cellulose pulp focused on the manufacture of cellulose directly soluble in sodium hydroxide solutions. The alkaline solutions were used for producing cellulosic fibres, foils, casings, beads, etc. The initial cellulose was hydrothermally treated with water at various temperatures and pressures, of about 100–200°C under a pressure of about 0.1–1.5 MPa [137]. The treated cellulose was directly dissolved in an aqueous solution of sodium hydroxide at a temperature of about 0°C. Alkaline cellulose solutions containing from about 5 wt% to about 10 wt% of polymer were converted into a variety of shaped articles. The process described is fully ecological without production of toxic and hazardous chemicals; cheap aqueous solvents are used instead of expensive organic solvents, and this method enables one to form stable solutions of cellulose without the necessity of preparing cellulose derivatives.

## 1.4 Overview of technologies for spinning cellulosic fibres

### 1.4.1 Viscose process

Cellulose pulp is one of the most important commodity raw materials. Annually about 118 million tons of various cellulose pulps are consumed worldwide, most of it in paper and paperboard manufacture [5]. About 8 million tons a year of the raw material is being consumed in the various cellulose manufacturing plants, including cellulose ethers and the 3-D products. Only 3 million tons are processed into fibres, which play an important role as raw material in the textile industry. Most commercial cellulose fibre manufacturing today utilizes the viscose process. It was invented at the dawn of the twentieth century and has remained in operation ever since. It is based on the derivatization of cellulose using carbon disulphite. The process has many steps to convert the solid pulp into soluble form. More detailed information can be found in references 20, 21, 138 and 139. An outline of the viscose process is illustrated in Fig. 1.5 [140].

The most critical step in the viscose process is xanthation, where alkali cellulose is reacted with carbon disulphide ( $\text{CS}_2$ ) to form sodium cellulose xanthate. Next, the sodium cellulose xanthate is dissolved into 5–8% aqueous sodium hydroxide to form yellow cellulose xanthate solution, so-called viscose. The solution is ripened for uniform distribution of xanthate groups in cellulose. After the ripening, the viscose dope is filtrated to remove undissolved particles and is deaerated to remove air bubbles. The viscose fibres are produced using a wet spinning method where the alkaline cellulose solution is extruded through a spinneret into a coagulation bath containing a mixture of acid and salts: sulphuric acid, sodium sulphate and zinc sulphate. In the coagulation bath the cellulose xanthate is converted into cellulose.



### 1.5 Flowsheets of the viscose process [140].

Before regeneration, the viscose fibres are stretched to orientate the cellulose molecule chains along the fibre axis. As a result of orientation the tenacity of the fibres increases and the elongation decreases [8].

By modifying the spinning conditions, the physical structure and form of the filament can be changed in many ways. Viscose fibres can be made with a symmetrical cross-section or a variety of cross-sectional shapes by extrusion through spinneret holes of suitable shape. By controlling the spinning conditions the viscose filaments can be spun in a form of skin-core structure in which the skin is thicker on one side of the filament than on the other side [8, 141–143]. The Lenzing Group has developed a high-absorbency fibre called Viscostar<sup>®</sup>, which is a viscose fibre with a star-shaped cross-section; it was designed to improve the absorbency of non-woven products, especially tampons [144].

Viscose fibres now available include fibres of widely different characteristics. Physical modifications of the regular viscose fibre range from changes in the form of the filament, e.g. hollow, shaped and surface-modified filaments, to changes in the fine structure as in the high tenacity rayons and high wet modulus (polynosic) rayons. Viscose fibres are used in the textile industry,

household fabrics and various non-woven fabrics. Textile fabrics may be woven of yarns made of viscose alone or in combination with other fibres such as polyester. Viscose fibre-based non-woven products include feminine hygiene products, absorbent products, baby wipes, computer disk liners, surgical swabs, etc.

According to the International Rayon and Synthetic Fibres Committee (CIRFS), the main viscose companies worldwide producing staple fibres are the Grasim and Aditya Birla Group (India) and Lenzing (Austria). In Europe the other staple producers are Sateri in Finland, Kelheim Fibres in Germany and Sniace in Spain, and filament producers are Enka and Cordenka in Germany, Bembercell in Italy, Glanzstoff in Austria and Svilosa in Bulgaria [145]. Table 1.4 shows the major sources of viscose production.

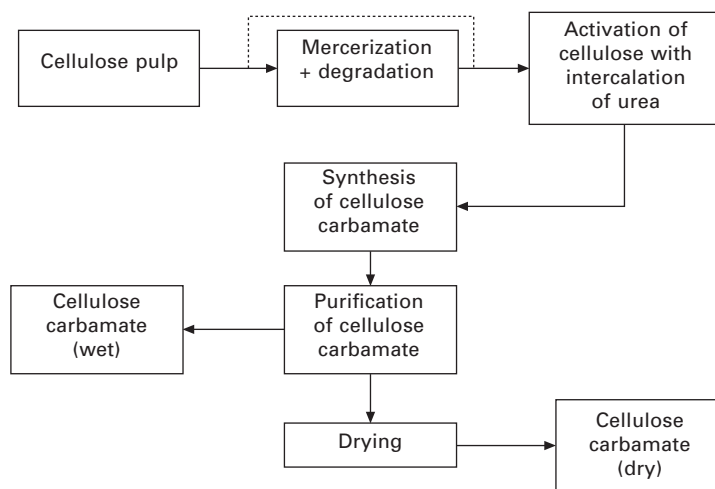
#### 1.4.2 Cellulose carbamate (CC) process

Other basic manufacturing techniques for the production of regenerated cellulosic fibres include the Carbamate process. Cellulose carbamate (CC) is the product of reaction between cellulose pulp and urea. Seventy years ago Hill and Jacobson found that such cellulose derivatives are soluble in aqueous sodium hydroxide solution and can be precipitated by acids as fibre or film [146]. Later this component was studied by many researchers [147–152]. In the 1980s a Finnish Company, Neste Oy, in cooperation with Kemira Oy developed a process for manufacturing CC and processing it into staple fibres under the trade name Cellca [153–155]. The process was based on activation of cellulose with liquid ammonia and electron beam irradiation. According to another patent (Zimmer AG, Germany) the reaction between cellulose and urea is performed in organic solvent as a liquid medium [156].

In the 1990s studies on elaboration of the method for manufacture of CC and spinning fibres were also conducted at the Institute of Biopolymers and Chemical Fibres, Poland [157–159]. The scheme of CC production is presented in Fig. 1.6 [160].

*Table 1.4* Viscose production [145]

Country	Total viscose filament and fibre (2005), tonnes
Europe	430,872
Brazil	40,055
China	1,180,000
CIS	41,020
India	295,421
Japan	35,796
Taiwan	114,455
Thailand	77,863



1.6 Scheme of CC production [160].

Table 1.5 Properties of cellulose fibres obtained from CC [160]

Property	Parameter
Titre (dtex)	1.5–2.0
Tenacity (cNtex)	12–22
Elongation (%)	16–22
Loop tenacity (cN/tex)	3.8–5.5
Nitrogen content (%)	0.3–0.5 fibres from regenerated cellulose 1.0–1.5 fibres from not decomposed CC

The combination of two stages of this process, i.e. mercerization and activation with intercalation of urea, allows one to obtain product with better dissolving properties. Chemical activation using gaseous acid anhydrides and organic or inorganic salts leads to changes in the structure and crystallinity of cellulose, resulting in homogeneous intercalation of urea. Cellulose carbamate is easily dissolved in 7–9 wt% of aqueous sodium hydroxide solution at temperatures below 0°C. The fibres were spun into a coagulation bath containing sulphuric acid; then in a regeneration bath containing about 4 wt% of NaOH the cellulose carbamate was regenerated in the form of fibres. The properties of the fibres obtained are presented in Table 1.5. Generally, the fibres spun from CC have analogous mechanical properties to standard viscose fibres.

The CarbaCell<sup>®</sup> technology, the special version of the carbamate process, was developed in Germany on an industrial scale by Zimmer AG in cooperation with the Fraunhofer Institute for Applied Polymer Research (Potsdam-Golm)

and the Institute for Textile Chemistry (Denkendorf) and is offered as an alternative method to the viscose process [161].

Cellulose carbamate solutions are well miscible with xanthate solutions [160]. It is possible to prepare the blended solutions by mixing the two separate CC and xanthate solutions or by introducing the CC solution to xanthate viscose immediately before spinning. The spinning process was performed in conditions typical of the viscose process. The mechanical properties of the blend fibres are listed in Table 1.6. The blend fibres are characterized by interesting properties. Compared to standard viscose fibres, the water retention value (WRV) and swelling coefficient (SC) in blend fibres were significantly increased, making them very useful for sanitary product applications.

### 1.4.3 Lyocell process

One of the main alternatives for the production of cellulose fibres is the NMMO process (*N*-methyl-morpholine-*N*-oxide), also called the Lyocell process, developed since the 1960s and commercialized in 1992 by Courtaulds in Mobile, Alabama, USA [11]. Earlier the research team of Franks and Varga [162–163], which was involved in studies on the manufacture of cellulose fibres based on amines, found that aqueous solutions of NMMO have excellent cellulose-dissolving properties and cellulose can be recovered from these solutions in the form of fibres by dilution with water.

The NMMO process consists of three steps [11]:

1. Production of homogeneous solution from cellulose pulp, NMMO and water, e.g. cellulose pulp with concentration of 13 wt% is dissolved in the *N*-methylmorpholine-*N*-oxide (67 wt%) containing approximately 20 wt% of water. The water is removed during dissolving.
2. The fibre forming process – the solution is filtered and passed through spinnerets to make the filaments, which are spun into water.
3. Recovery of NMMO from the regenerating and washing bath – NMMO solvent is recovered from this aqueous solution to 99.5% and reused.

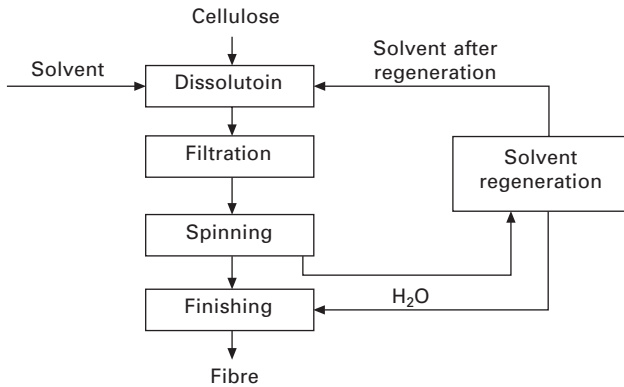
*Table 1.6* Some mechanical properties of CC–xanthate blend fibres [160]

Type of fibres	Content of CC in the spinning solution	Tenacity (cN/tex)	Loop (cN/tex)	Elongation (%)	WRV <sup>1</sup> (%)	SC <sup>2</sup> (%)
Viscose	0	23.2	6.9	18	92	99
Viscose/CC	15	20.9	6.1	21	100	112
Viscose/CC	30	19.0	6.1	25	128	134

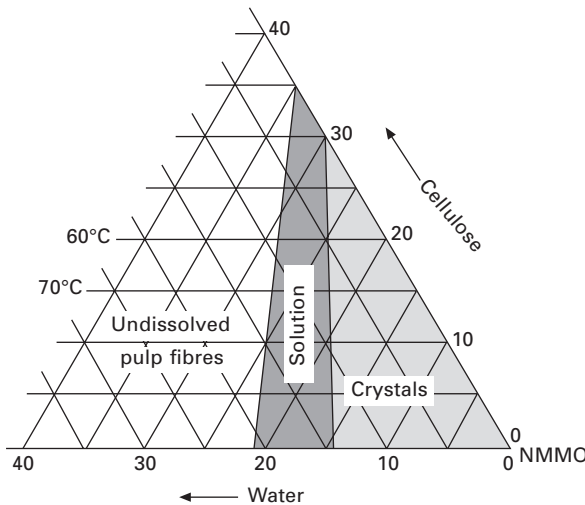
<sup>1</sup>Water retention value; <sup>2</sup>swelling coefficient.

The technology of cellulose fibres based on NMMO as a direct solvent of cellulose is presented in Fig. 1.7 [164]. It has been found that dissolution of cellulose in NMMO depends on the temperature and the content of water in the system, as illustrated in Fig. 1.8 [165].

The NMMO technology is fully ecological and environmentally friendly, with no effluents or gases emitted to the atmosphere. Lyocell fibres are characterized by high crystallinity, high orientation, low lateral hold between fibres, relatively large pore volume and high tenacity ranging from 35 to 42 cN/tex [166, 167]. They are an excellent raw material for the manufacture of



1.7 Flowsheet of cellulose fibre production by the NMMO process [164].



1.8 Phase diagram showing the effect of temperature and water content on the dissolution of cellulose in NMMO [165].

clothing, technical textiles and sanitary products. Table 1.7 shows the process parameters of Lyocell-type fibres, as compared with those of conventional viscose fibres [164].

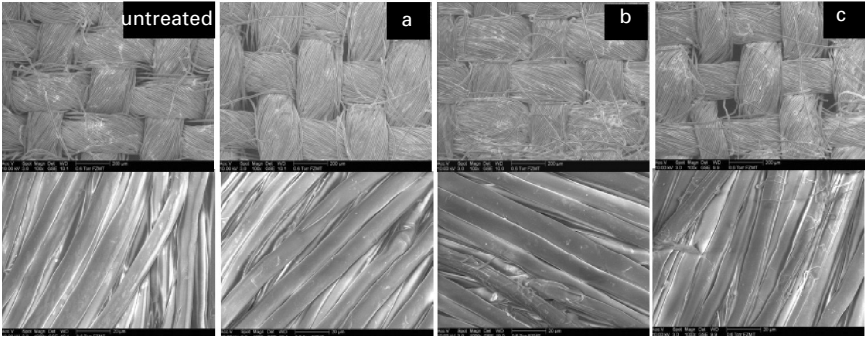
Despite many advantages, the NMMO process has not replaced the viscose process up to now. The main reason is the fibrillation of fibres manufactured by this method, which occurs with stress along the fibre axis in the wet state, imposing limitations on the use of the method in textile manufacture. However, such a tendency to fibrillation can be utilized in the technical textiles sector for manufacture of non-wovens, filters and special papers. Fibrillation improves filtration efficiency, air permeability, tear strength and opacity [168]. Although fibrillation could be used for creating attractive effects in the production of textiles, there is still a challenge to the product manufacturers to eliminate this problem [11]. Many research centres try to modify Lyocell fibres to eliminate their susceptibility to fibrillation. Modifications include enzymatic treatment, alkali and urea treatment and cross-linking [168–170]. Figures 1.9 and 1.10 show urea and alkali treatment of NMMO-type woven fabrics [170]. While the untreated fabrics show no fibrillation, by increasing the concentration of urea or alkali a very slight formation of microfibrils can be identified for both treatments.

Due to cross-linking, Courtaulds, Lenzing AG and Akzo-Nobel developed a Tencel A100 fibre with fibrillation reduced to a minimum [171]. Modification of the Lyocell-type fibres was also conducted by the Thuringian Institute of Textile and Plastics Research in Rudolstadt (Germany), resulting in production of fibres with bactericidal properties under the trade name Alceru Silver [172]. The Man-made Fibres Department at the Technical University

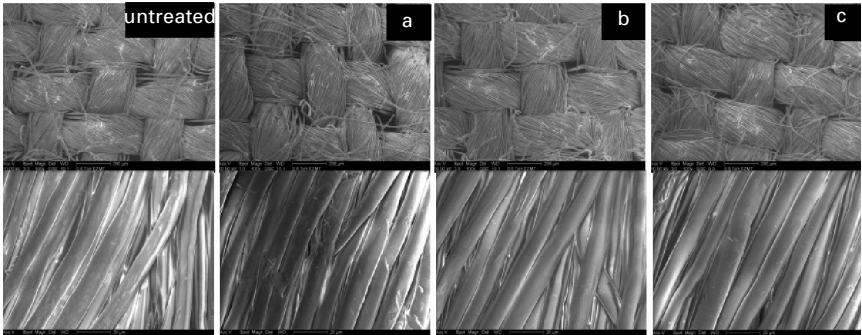
*Table 1.7* Comparison of process parameters of cellulose fibres produced by the viscose and NMMO processes [164]

No	Parameters	Values	
		Viscose process	NMMO process
1	Cellulose concentration in the spinning solution, %	7.5–9.5	12.0–25
2	Duration of fibre formation, h	35–48	2–4
3	Type of process	Periodic	Continuous
4	Fibre formation rate, m/min	12–90	60–300
5	Wastes	Toxic gases emitted to the atmosphere and salts discharged into sewage water	No gases or effluents
6	Energy consumption, %	100	35–40
7	Costs of system construction, %	30–35	100
8	Raw materials and product cycle	Open	Closed
9	Fibre properties	Low quality	High quality
10	Process characteristic	Fixed	Elastic





1.9 SEM images of untreated Lyocell-woven: (a) treated with urea 1.7M; (b) treated with urea 3.3M; (c) treated with urea 5M at magnification of 100× (upper) and 1000× (lower) [170].



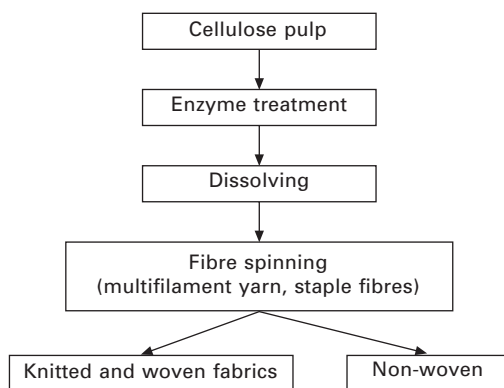
1.10 SEM images of untreated Lyocell-woven: (a) treated with NaOH 0.05M; (b) treated with NaOH 0.5M; (c) treated with NaOH 1.0M at magnification of 100× (upper) and 1000× (lower) [170].

of Łódź (Poland) studied the possibility of reducing the susceptibility of the fibres to fibrillation by modification of the fibre structure during the spinning process [164]. Modification was based on incorporating cationic, anionic or non-ionic surface-active modifiers into the spinning solution or the coagulating bath. Additionally, a low molecular weight polyethylene or high molecular weight poly(ethylene oxide) was also added to the spinning solution. The fibres obtained were characterized by different mechanical characteristics, moisture absorption and susceptibility to fibrillation, as well as a wide range of porosity [164].

Cellulose staple fibres of the Lyocell type are manufactured at three plants, in Mobile, Alabama (USA), Grimsby (England) and Heiligenkreuz (Austria); the total amount exceeds 120 000 tons per year (Table 1.8) [164].

*Table 1.8* Trade names of cellulose fibres produced by the NMMO process [164]

Company	Company location	Trade name of fibres	Form of fibres
Lenzing AG	Mobile, USA Grimsby, UK	Tencel	Staple fibres for clothing textiles
	Mobile, USA Grimsby, UK	Lyocell Courtaulds	Staple fibres for technical textiles
	Heiligenkreuz, Austria	Lyocell Lenzing	Staple fibres

*1.11* Scheme of cellulose fibre manufacture from enzyme-treated cellulose pulp [174].

#### 1.4.4 Celsol/Biocelsol process

Another environmentally friendly technology to produce cellulose fibres is based on biomodified cellulose pulp leading to direct cellulose solubilization in sodium hydroxide (NaOH)/water solutions. For several years, investigations have been conducted at the Institute of Biopolymers and Chemical Fibres (Poland) and Tampere University of Technology (Finland) aimed at elaborating a new concept for manufacturing cellulose fibres by directly dissolving enzyme-treated cellulose pulp in aqueous NaOH solutions to be used for fibre spinning (the Celsol/Biocelsol process) [87–90, 173].

Enzymatic modification of cellulose increases cellulose reactivity and solubility in aqueous sodium hydroxide solutions, which are distinguished by high stability and suitable rheological behaviour for preparation of different types of cellulose products such as fibres, film and fibrils. Figure 1.11 illustrates the scheme of the formation of fibres from biomodified cellulose pulp (the Celsol/Biocelsol process) [174].

In the Celsol/Biocelsol process, enzymes (cellulases) are used for modifying the cellulose, resulting in directly alkali-soluble cellulose. It has been found

that accessibility of the pulp to enzymes is increased by the use of suitable pre-treatment methods, particularly mechanical treatment [174, 175]. After that, the wet pulp is subjected to enzymes under controlled conditions consisting of controlled degradation of cellulose macromolecule chains with accompanying changes of its molecular, supermolecular and morphological structure. The enzymatic treatment of pulp causes, in comparison to the initial pulp, several changes as follows: decrease in the average polymerization degree and crystalline degree, reduction of hydrogen bonds, increase in intrinsic surface, and increase in solubility in aqueous sodium hydroxide.

After the treatment, the pulp is separated from the excess water, the enzymes are inactivated and the treated pulp is ready for the dissolution step. The enzymatically treated pulp is dissolved at low temperature into aqueous sodium hydroxide containing a small amount of zinc oxide. The solution is filtered to remove undissolved particles and deaerated to remove air bubbles. The alkaline cellulose solution is spun into the acidic coagulation bath in which the cellulose regenerates. Sulphuric acid and sodium sulphate in the spin bath cause the solidification of the cellulose molecules and their transition from the liquid state through the gel state into the solid state. After wet spinning, the cellulose fibres are washed, finished and dried.

Cellulases are produced as a multicomponent enzyme system by many moulds, and are comprised of several endoglucanases (EG), two or more cellobiohydrolases (CBH) and at least one  $\beta$ -glucosidase [176, 177]. The degrading effect of cellulase enzymes on cellulose has been studied for decades [91, 178–180].

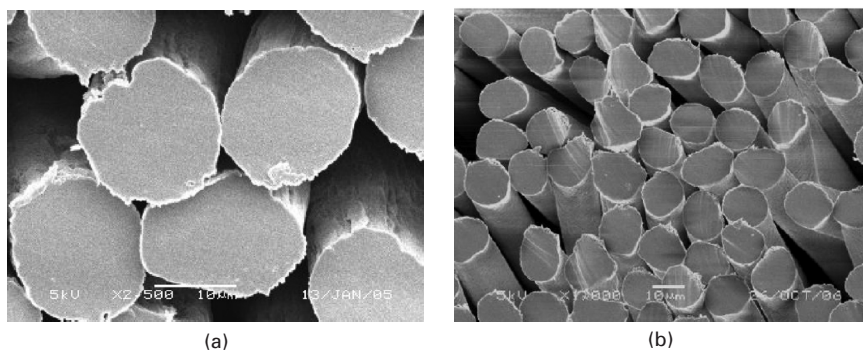
The well-known synergistic relationship between the actions of the components of the cellulase complex plays a crucial role in the cellulose degradation process. Two major modified strains of *Aspergillus niger* [175] and *Trichoderma reesei* [95] are the best producers of enzymes suitable for biomodification of cellulose pulp. It is also well known that direct contact between the enzymes and the substrate is a prerequisite to cellulose hydrolysis. Since cellulose is an insoluble and structurally complex substrate, this contact can be achieved by diffusion of the enzymes into the cellulose matrix.

From biomodified cellulose pulp the alkaline spinning solutions have been prepared. The effect of spinning conditions, the composition of the spinning bath, the draw ratio and the spinning speed on the mechanical properties of Celsol [181] and Biocelsol [182] fibres has been widely investigated. Both processes are very similar, though different raw pulps as well as different enzymatic treatment parameters have been used.

Some properties of regenerated cellulose fibres spun from alkali solutions of biomodified pulp are presented in Table 1.9. A SEM photo of the Biocelsol fibre cross-section is shown in Fig. 1.12. The fibres are characterised by an oval cross-section with little developed boundary line; they are regular and show no sticking.

*Table 1.9* Some mechanical properties of Celsol and Biocelsol fibres [181, 182]

Parameter	Celsol/Biocelsol fibres
Titre, dtex	1.4–5.8
Tenacity, cN/dtex	1.4–1.9
Elongation at break, %	11–19



1.12 (a, b) Typical cross-section of Biocelsol fibres [182].

A novel, environmentally friendly biotechnology-based method for converting cellulose into fibres was investigated and developed on a high laboratory scale. Biocelsol fibres can be used as a multifilament yarn and spun as such, as well as blended with other fibres, in weaving and knitting processes.

Suominen Nonwovens Ltd (Finland) produces viscose fibre-based hydroentangled non-wovens. Depending on the end use/product, Suominen are currently using viscose fibres in mixtures with synthetic fibres (polyester, polypropylene). The hydroentangled non-woven is applied to different wiping products used in baby care, personal care, household and industrial applications. Suominen has carried out successful trials in producing hydroentangled non-wovens based on Biocelsol and PET mixture fibres, as seen in Fig. 1.13. [183].

Spolsin, spol. s r.o. (Czech Republic) uses the viscose yarns for woven and knitted fabrics applications. Positive results have been achieved using Biocelsol yarns, as a substitution for viscose, for woven and knitted fabrics applications [183]. For the manufacture of woven fabrics, the Biocelsol multifilament yarns must be twisted or processed into sheath–core yarns to prevent damage during the weaving. The twisted and sheath–core yarns were woven into fabrics on a laboratory scale (Fig. 1.14). [182, 183].

Based on the results of these processing experiments, it can also be assumed that the yarns can be processed on an industrial scale. Moreover,



1.13 Hydroentangled non-woven sheet from Biocelsol and PET staple fibres made by Suominen Nonwovens Ltd [183].

the chemical behaviour of the Biocelsol fibres during the dyeing test was comparable with that of the viscose fibres.

## 1.5 Cellulose-based composite fibres

### 1.5.1 Cellulose blends with other polysaccharides (PS)

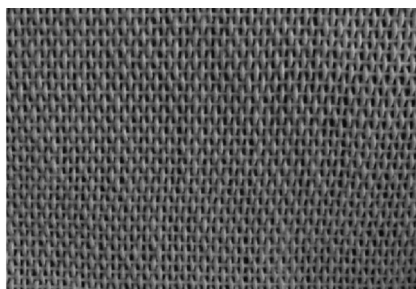
Considerable efforts have been devoted to the preparation of compatible blends of cellulose with other polysaccharides such as chitosan, starch and alginate. Chitosan, a co-polymer derived from the abundant natural polymer chitin, is composed of  $\beta$ -(1 $\rightarrow$ 4)-2-amino-2-deoxy-D-glucopyranose and  $\beta$ -(1 $\rightarrow$ 4)-2-acetamido-2-deoxy-D-glucopyranose units. Chitosan is a versatile biopolymer which displays a series of unique properties and therefore is used in different fields, including medicine, pharmacology and agriculture [184, 185]. The most important feature of this polymer is antimicrobial activity against a broad spectrum of bacteria [186–189]. Chitosan has the same  $\beta$ -(1 $\rightarrow$ 4)-glucopyranose units as cellulose, except that the 2-hydroxy is replaced by an acetamide group. The similarity of cellulose and chitosan structures suggests that both polymers can be blended sufficiently to form homogeneous composite films or membranes. There has been much progress in investigating of blends of chitosan with synthetic and natural polymers. It has been reported that modification of chitosan by blending with PEG or PVA may be an effective method of improving the hydrophilic properties of chitosan [190, 191]. Chitosan was also blended with several polymers such as polyamides, poly(acrylic acid), gelatin, silk fibroin and cellulose to change its mechanical properties [192–196]. Various studies (Raman and  $^{13}\text{C}$  NMR spectroscopy, X-ray analysis) have proved the presence of specific interactions between cellulose and chitosan molecules [196–198].



(a)



(b)



(c)

**1.14** Biocelsol end products: (a) sheath–core yarn; (b) fabric from twisted Biocelsol multifilament yarn; (c) woven fabric from sheath/core spun Biocelsol multifilament yarn [182–183].

Well known from the literature are various methods of preparation of chitin-chitosan/cellulose solutions that are useful for processing into composite chitin, chitosan and cellulose fibres, films or foams [199]. Chitin-chitosan can be mixed with cellulose directly or in steps of alkaline addition, xanthate formation or viscose formation. The chitin-chitosan/cellulose fibres or films have excellent antimicrobial activity and good biodegradability. Fibres can be blended and woven with natural fibres such as silk, cotton, flax or wool, regenerated fibres, man-made fibres, or synthetic fibres such as polyester, nylon and acrylic fibres. The chitin-chitosan/cellulose fibres are applicable to non-woven fabrics as well as textiles. Knitwear and textiles of chitin-chitosan/cellulose can be used for clothing such as socks, T-shirts, bedroom



commodities and medical materials such as like gauzes, bandages or plasters. The Omikenshi Company (Osaka, Japan) has established a commercial process to produce chitin/chitosan solution without using organic solvent and has commercialized production of fibres under the brand name of Crabyon by co-extruding with cellulose viscose. The fibres are sold by Swicofil AG Textile Services (Switzerland), the sales department of leading world textile raw material manufacturers. Because chitin/chitosan is built in part of Crabyon, its antimicrobial properties stay unchanged against washing or abrasion for a long time. Crabyon protects skin from drying because its moisture-retaining properties are better than those of cellulose fibres.

Other authors [200] have disclosed a process for preparing cellulose acetate/chitosan hollow fibres, including such steps as dissolving an appropriate amount of chitosan and cellulose acetate in formic acid, filtering the blend solution to remove insoluble or undissolved particles, degassing the blend solution to free any air bubbles followed by extruding the spinning solution into a coagulation bath to form fibres, and finally treating the chitosan/cellulose acetate blend fibres with a plasticizer which acts as a softening agent and for drying. The polymer blend solution comprises 2–4 wt% of chitosan and 10–30 wt% of cellulose acetate [200]. The fibres are prepared by a wet phase inversion method by extruding the blend solution through a spinneret in the form of a ring with different outer and inner diameters into a quenching bath of coagulation solution while a core quench liquid is delivered through the lumen of the fibres. The coagulation solution and the core quench liquid are also called the ‘external coagulant’ and ‘internal coagulant’, respectively. They can be composed of NaOH solution, ammonia solution, tripolyphosphate solution, water and mixtures thereof. Manufactured hollow fibres show a porous outer and inner surface with a larger pore size and characterized by very good mechanical properties. The tensile stress, elongation ratio and Young’s modulus at breakage of the blend fibres in the wet state were 22 MPa, 24% and 90 MPa respectively. Such fibres can be used in numerous applications, such as in the pharmaceutical industry as a membrane chromatography matrix to selectively separate proteins and enzymes, for recovery or removal of various toxic metal ions from water, wastewater or industrial effluents, and in medicine as blood or kidney dialysis membranes. Due to the high amount of chitosan (up to 25 wt%) in the fibers, they can adsorb some toxic macromolecules which are metabolized by human bodies and cannot be removed by conventional dialysis devices.

Starch and cellulose are two very similar polymers. Both are composed of the same glucose repeat units, but the glucose units in starch are connected by alpha linkages and oriented in the same direction while the glucose units in cellulose are connected by beta linkages and each unit is rotated 180° around the axis of the polymer backbone chain.

Intensive studies have been conducted into obtaining cellulose–starch fibrids and assessing their properties [201]. Fibrid formation consists first of separately obtaining polymer solution of starch and biomodified cellulose in aqueous sodium hydroxide solution and then mixing them together. The blend solution was injected through a nozzle into an acid coagulation bath where the polymer precipitated in the form of fibrids which were next carried out by the bath stream. Aqueous solutions of sulphuric acid of various concentrations, or solutions of sulphuric acid and sodium sulphate, were used for the coagulation baths. Selected properties of cellulose–starch fibrids are presented in Table 1.10.

On the basis of tests carried out, the influence of the starch content in the mixture, the coagulation bath content and the coagulation bath flow intensity on the properties (shape, dimensions and water retention value) of obtained fibrids was noted. Fibrids obtained from a solution of starch content 28 wt%, spun to 4 wt% of sulphuric acid solution at a flow intensity of 7.2 cm<sup>3</sup>/min were characterized by the smallest thickness (below 10 µm) and a length distribution in the range 300–800 µm. With increasing starch content in the mixture solution, it is necessary to increase the acid concentration and the salt content in the coagulation bath. From a solution containing 61 wt% of starch, fibrids were manufactured using a solution of sulphuric acid (150 g/dcm<sup>3</sup>) and sodium sulphate (80 g/dcm<sup>3</sup>) at a higher speed of the coagulation process. Fibrids of length 600–900 µm and diameter 10–20 µm were obtained. An increase of WRV fibrids with increase of the starch content in the blended solution was also observed.

Alginates are extracted from brown seaweeds. Chemically, they are linear copolymers composed of β-(1→4)-linked D-mannuronic acid and α-(1→4)-linked L-guluronic acid residues. Because of their interesting properties, including the ability to thicken solutions and gels and to form films, alginates, especially sodium alginate, are used in a variety of applications, mainly in the food industry as a coating to protect food from oxidation and oxygen/water permeability [202], in medicine as highly absorbent, biodegradable dressings [203, 204], and as membranes in the separation of aqueous–organic mixtures, for example, for dehydration of ethanol–water mixtures [205, 206]. The

Table 1.10 Selected properties of cellulose–starch fibrids [201]

Starch content in the polymer mixture, wt%	Secondary swelling factor WRV, %	Average fibrid thickness, µm	Average fibrid length, µm
28	306.5	<10	300–800
35	329.8	<10	800
83	631.9	50–100	600–900
61	599.5	10–20	600–900



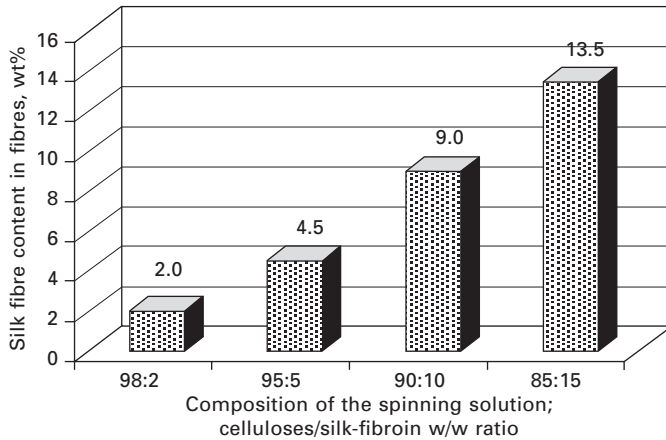
excellent pervaporation properties of alginate membranes is attributed mainly to their extraordinary selectivity to water in the sorption step. However, the presence of hydrophilic groups sometimes swells the membrane significantly, leading to its plasticization, which results in low selectivity. The blending of alginate with other polysaccharides, such as cellulose, could be a useful tool for the preparation of new alginate membranes with improved properties.

Blended fibrous membranes made from bacterial cellulose and alginate have been prepared in aqueous NaOH/urea [207]. The blend solution was coagulated in a 5 wt% CaCl<sub>2</sub> aqueous solution, and then treated with a 1% HCl solution. In order to achieve the developed nanoporous structure of the membrane, supercritical carbon dioxide drying was applied. The blend membrane containing 80% of bacterial cellulose and 20 wt% of alginate displayed a homogeneous structure and exhibited better water adsorption capacity and water vapour transmission rate. The average pore size of the blend membrane was 10.60 Å with a 19.50 m<sup>2</sup>/g surface area.

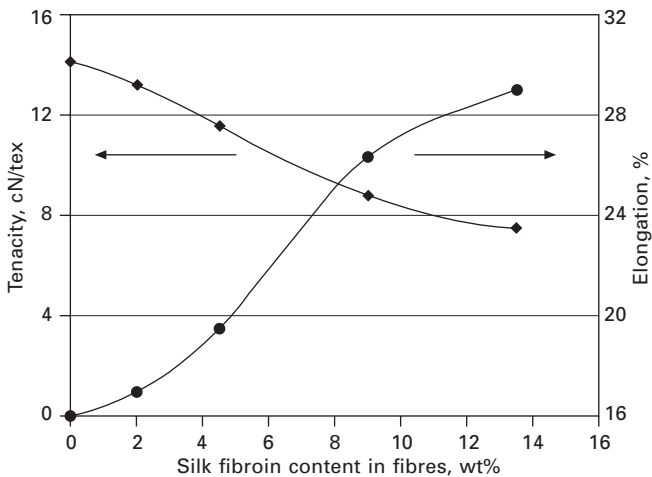
### 1.5.2 Cellulose blends with proteins

Cellulose creates excellent blends not only with polysaccharides but also with proteins. The Institute of Biopolymers and Chemical Fibres in cooperation with the National Institute of Agrobiological Science, Japan, has begun the preliminary scientific research into obtaining cellulose/silk-fibroin biomaterials in the form of fibres intended for manufacturing new-generation dressing materials [208]. Silk-fibroin is a fibrillar protein created by the larva of the *Bombyx mori* silkworm in the shape of a continuous filament, well known as natural silk, which is the basic structural material of the cocoons. The alkali solutions of biomodified cellulose (6.5 wt% of cellulose in 10 wt% of NaOH) and silk-fibroin (10 wt% of silk fibroin in 5 wt% of NaOH) were mixed at different ratios: 98:2, 95:5, 90:10 and 85:15. Fibre formation was achieved by the wet spinning method. An aqueous solution of H<sub>2</sub>SO<sub>4</sub> with addition of ammonium sulphate and sodium sulphate was used as the coagulation bath. Figure 1.15 shows the influence of the spinning solution composition on the silk-fibroin content in fibres.

The fibres obtained, with a silk-fibroin content within the range of 2% to 13.5%, were tested in order to assess their mechanical properties and their surface and cross-sections. Figure 1.16 presents the test results for the mechanical properties of cellulose/silk-fibroin fibres and cellulose fibres obtained under analogous conditions. The results obtained indicate that with increase in the silk-fibroin content, the fibres were characterized by a decrease in tenacity and an increase in the elongation at break. Cellulose/silk-fibroin fibres with the highest (13.5%) silk-fibroin content are characterized by relatively low tenacity and high elongation at break. Fibres with a silk-fibroin content from 2% to 9% are characterized by mechanical properties



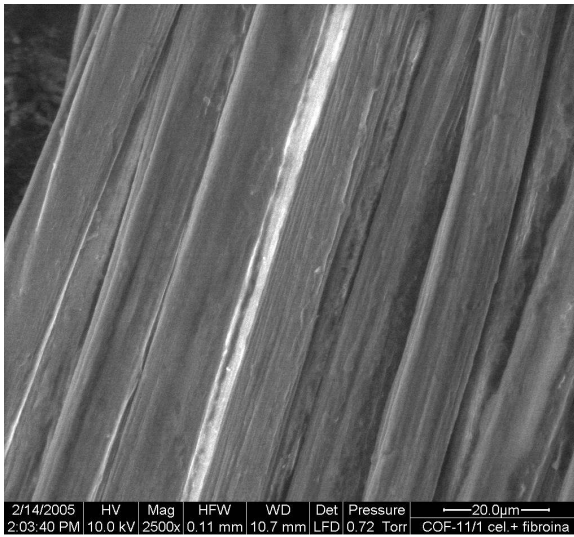
1.15 Dependence of silk-fibroin content in the fibres on the spinning solution composition. [208].



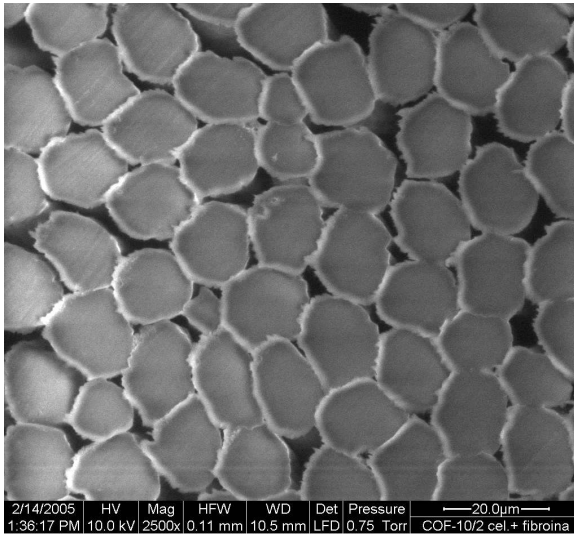
1.16 Influence of the silk-fibroin content in cellulose/silk-fibroin fibres on their mechanical properties: tenacity and elongation at break [208].

sufficient for their further processing into dressing materials. Figure 1.17 presents SEM photos of cellulose/silk-fibroin fibres, indicating that the fibres are characterized by a certain deformation of the cross-sectional shape in relation to a cylindrical cross-section, which reflects the weak coagulation properties of the ammonium sulphate for cellulose, though good for silk-fibroin. These investigations form the basis for more detailed future research on the manufacture of cellulose/silk fibroin blends.

Investigations have also been carried out on the manufacture of fibrous



(a)



(b)

1.17 (a, b) Photos from the scanning electron microscope (SEM) of cellulose/silk-fibroin [208].

composite materials based on biomodified cellulose and keratin obtained from chicken feathers [209]. Spinning solutions were prepared from these polymers, and after filtration and aeration they were used for the formation of fibres and fibrils. The investigations included the preparation of biomodified cellulose–keratin spinning solutions of different keratin content and estimation

of the composite fibre properties, as well as the sorption properties of the composites obtained. The mechanical properties of cellulose and cellulose–keratin fibres are presented in Table 1.11.

Introducing keratin into cellulose fibres lowered their mechanical properties, decreased the tenacity by a factor of nearly 2 and caused a significant decrease in elongation at break, but both parameters remained at a level which enables these fibres to be used for manufacturing composite fibrous materials. It was found that the modification of cellulose fibres with keratin changes their hygroscopicity, and values of the wetting angle. The cellulose–keratin fibres obtained are characterized by better sorption properties: higher hygroscopicity (45.9%) and smaller wetting degree (25°), compared to cellulose fibres for which the hygroscopicity is 40% and the wetting angle 27.3°. Improving the sorption properties of the biocomposites obtained creates opportunities to use them as hygienic fabrics.

Surfaces and cross-sections of the cellulose and cellulose–keratin fibres were evaluated by the SEM method. The photos are presented in Fig. 1.18. Evaluating the view of cellulose–keratin fibrous composite materials by the SEM method, differences in shape and surface between the two types of fibres were noted.

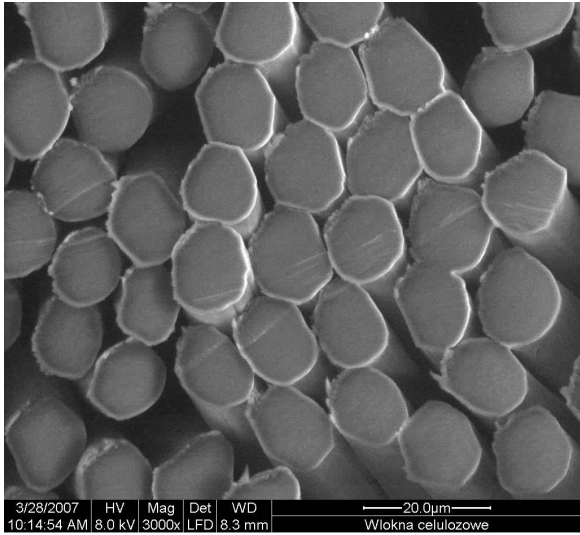
### 1.5.3 Cellulose blends with synthetics

Cellulose offers great potential and versatility when combined with plastics. By utilizing cellulose as a reinforcing material of thermoplastic polymers it is possible to create new materials with enhanced properties and superior performance. Plastics reinforced with cellulose and natural fibres have been widely investigated. By using different man-made cellulosic fibres (Rayon, Tencel, Viscose) and thermoplastic polymers such as polypropylene (PP), polyethylene (PE), high impact polystyrene (HIPS), poly(lactic acid) (PLA), and a thermoplastic elastomer (TPE) as the polymer matrix, a new class of fibres has been developed. Special attention has been paid to reinforcement

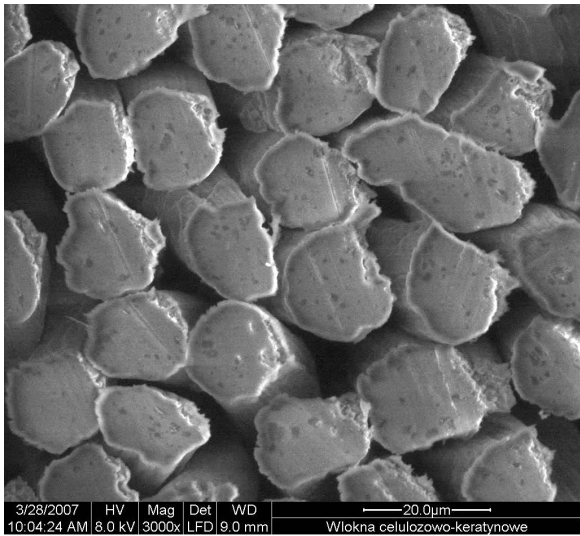
*Table 1.11* Mechanical properties of cellulose–keratin fibres [209]

Keratin content, %	0	2.6	3.0
Linear density, dtex	1.91	3.61	3.28
Coefficient of variation of linear density, %	3.04	3.19	3.45
Breaking force of fibres in conditioned state, cN	2.56	3.07	2.13
Coefficient of variation of breaking force in conditioned state, %	7.36	18.2	16.3
Tenacity in conditioned state, cN/tex	13.4	8.50	6.49
Elongation at break in conditioned state, %	32	22	16
Coefficient of variation of elongation at break in conditioned state, %	17.4	28.3	21.4

of PP in view of its applications in the automotive industry. The Rayon-PP composite was characterized by high strength and excellent impact behaviour as compared with glass fibre-reinforced PP. A fully biodegradable composite with excellent mechanical properties was obtained with Rayon reinforced PLA [210].

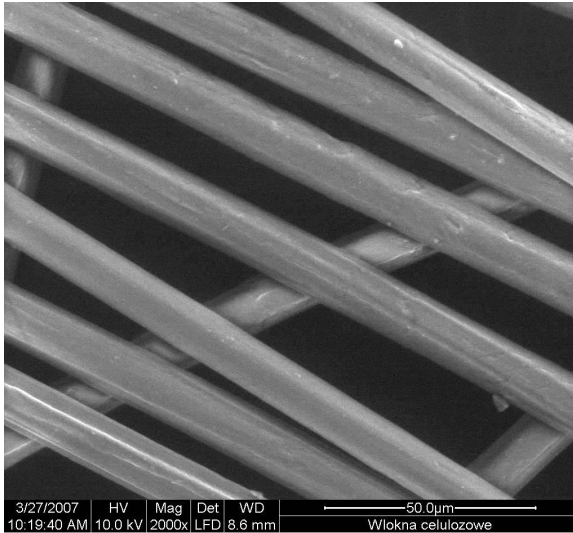


(a)

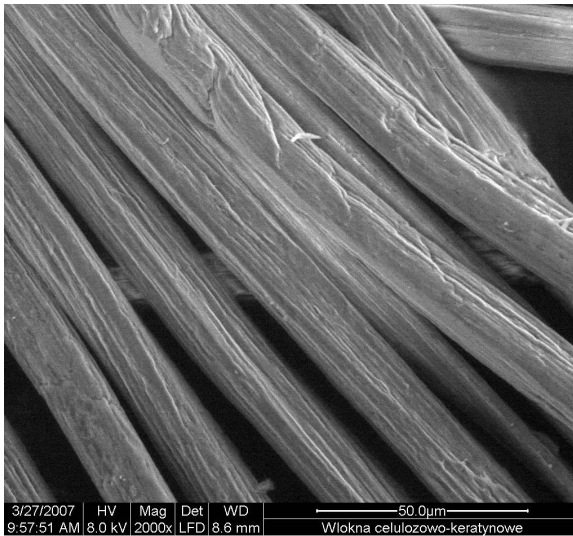


(b)

1.18 SEM photos of the fibre cross-sections and fibre surface: (a) and (c) cellulose fibres; (b) and (d) cellulose-keratin fibres [209].



(c)



(d)

### 1.18 Cont'd

The thermal and viscoelastic properties of polypropylene (PP)/cellulose microfibrils and PP/cellulose staple fibres were investigated by differential scanning calorimetry (DSC) and dynamic mechanical thermoanalysis (DMTA). It was found that the crystallization temperature and crystallinity of PP apparently increased in the presence of these fibres. The cellulose fibre surfaces act as nucleating agents for PP, resulting in the formation of



transcrystalline regions around the fibres. DMTA spectra of PP/cellulose composites show a significant increase in stiffness, improvement of the mechanical properties and a remarkable decrease of the damping values [211]. PP composites with cellulose microfibrils are characterized by unique properties such as high strength, formability, geometrical complexity at a very small scale, low density and abrasivity, biomedical compatibility and the possibility of recycling [212].

Blends of cellulose and polyurethane have improved properties and can be used as a biodegradable packaging material, for plastic shopping bags, silo sheets for the agricultural sector, hygiene articles, external wrappings for babies' nappies, transparent paper, copying films and decorative materials [213]. Investigations were also carried out on preparation of cellulose blends with poly(vinylpyrrolidone) [214], polyamides (PA66) [215, 216] and polyesters [217].

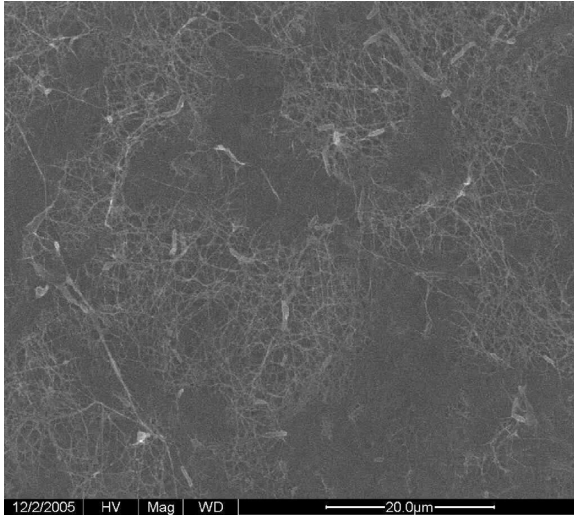
## 1.6 Prospectives – nanocellulosic fibres

Cellulose is the main component of the primary cell wall of green plants. For industrial use, cellulose is obtained mainly from wood pulp. However, the use of trees for the production of paper and construction materials continually depletes forest resources. Bacterial cellulose is the only alternative to plant cellulose because the biosynthesis process of bacterial cellulose takes only a few days, while trees need more than 30 years to achieve the full growth. In this respect, bacterial cellulose is the key material for the preservation of nature.

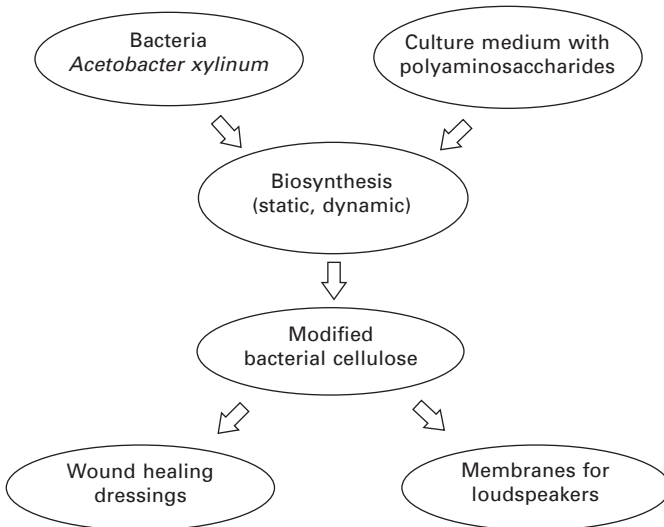
Bacterial cellulose is synthesized by the acetic bacteria *Acetobacter xylinum*. The fibrous structure of bacterial cellulose consists of a three-dimensional network of micro- and nanofibres containing glucan chains bound together by hydrogen bonds (Fig. 1.19) [218]. From the chemical point of view, bacterial cellulose is identical to that of plant origin and differs from the latter only in its supermolecular structure.

Properties of bacterial cellulose can be modified directly at the biosynthesis step, by addition of some modifiers into the culture medium. A method of bacterial cellulose modification using aminosaccharides, oligo-aminosaccharides and polyaminosaccharides such as chitosan and/or its derivatives, has been developed at the Institute of Biopolymers and Chemical Fibres, Łódź, Poland [219, 220].

Figure 1.20 presents the scheme of biosynthesis of modified bacterial cellulose (MBC) [221]. This novel biomaterial is characterized by many unique features, such as bacteriostatic activity against *Staphylococcus aureus* and *Escherichia coli* as well as bactericidal activity against *Escherichia coli*, biocompatibility, high water retention, biodegradability and non-allergenicity, which make it the ideal material for wound dressings. Tests of wound dressings



1.19 Bacterial cellulose fibrous network with bacteria cells [218].

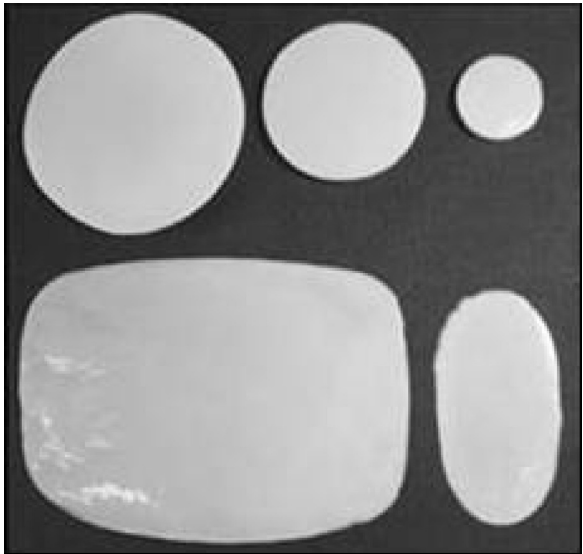


1.20 Scheme of biosynthesis of modified bacterial cellulose for medical articles and acoustic membranes [221].

based on modified bacterial cellulose, carried out on animals, showed good stimulation of factors accelerating the healing process, good conformability to the wound site and good protection against secondary infection. Modifying bacterial cellulose with chitosan during its biosynthesis results in a composite material with glucosamine and *N*-acetylglucosamine units incorporated into



the cellulose chain, which is characterized by a number of valuable features such as good mechanical properties in the wet state, high moisture-retention properties, release of mono- and oligosaccharides under lysozyme action, bacteriostatic activity against Gram-negative and Gram-positive bacteria, and bactericidal activity against Gram-positive bacteria. These features make modified bacterial cellulose an excellent dressing material for treating different kinds of wounds, burns and ulcers. Figure 1.21 presents a composite dressing



(a)



(b)

1.21 (a) Bacterial cellulose/chitosan composite pellicle; (b) modified bacterial cellulose in tubular form [218].

based on bacterial cellulose modified with chitosan in pellicle form and tubular form, which can be applied in medicine as vascular grafts [218].

Another interesting application of modified bacterial cellulose is in loudspeaker membranes [222–224]. Modified bacterial cellulose obtained during the biosynthesis process using the bacterial strain *Acetobacter xylinum* and a culture medium containing chitosan is characterized by high sonic velocity and high internal loss, which make it much more suitable for clearer and more detailed sound reproduction than conventional electroacoustic transducers.

Some parameters of loudspeakers with membranes made from modified bacterial cellulose are presented in Table 1.12 [224]. The application of modified bacterial cellulose to the manufacture of loudspeaker membranes allows the construction of a novel loudspeaker with unique parameters, including the mid-tweeter loudspeaker with a very wide sound transmission range from 520 Hz up to 22 kHz [224]. Loudspeakers with membranes made from MBC are shown in Fig. 1.22.

Recently, nanotechnology is revolutionizing the world of materials. Application of nanotechnology in the textile industry offers progress in developing a new generation of textile fibres with enhanced functionality and a wide range of applications. Electrospinning has been recognized as an efficient technique for the manufacture of polymer nanofibres. Various polymers have been successfully electrospun into ultrafine fibres in recent years. Most (about 90%) of all polymers used for fibres produced by the electrospinning technique are applied in solvent solution form. The process of manufacture of cellulose nanofibres based on NMMO solutions was developed at the Department of Man-Made Fibres of the Technical University of Łódź [225–227]. The scheme of cellulose nanofibre spinning is shown in Fig. 1.23 [164].

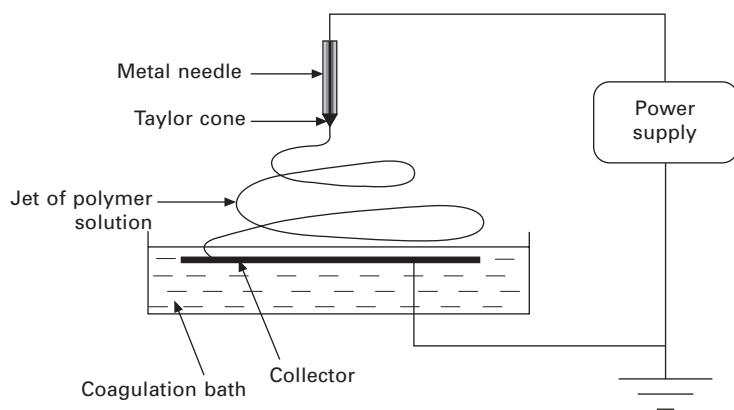
The properties of cellulose nanofibres depend on many factors such as polymer properties (molecular weight, polymer content in solution, etc.), solvent/solution properties (surface tension, electrical conductivity, etc.) and electrospinning conditions (voltage, temperature, distance between electrodes, etc.). Depending on the fibre spinning conditions, nanofibres can be prepared

*Table 1.12* Some parameters of loudspeakers with membranes made from MBC [224]

Parameter	Tweeter	Mid-range tweeter	Loudspeaker set
Frequency band (–3 dB)	1.4 kHz–22 kHz	520 Hz–22 kHz	78 Hz–22 kHz
Frequency band (–15 dB)	700 Hz–44 kHz	210 Hz–42 kHz	32 Hz–42 kHz
Impedance	8 Ω	8 Ω	8 Ω
Efficiency	91 dB	91.5 dB	90 dB



1.22 Dome loudspeakers (in the middle) equipped with membranes based on modified bacterial cellulose [224].



1.23 Scheme of apparatus for the formation of cellulose nanofibres [164].

in the form of single filaments, yarn or non-woven fabric with a variety of properties.

Recently, the usefulness of ionic liquids for cellulose dissolution and fibre spinning has been the subject of interest of many research centres. Typical solvents such as 1-*N*-butyl-3-methylimidazolium chloride (BMIMCl), 1-ethyl-3-methylimidazolium chloride (EMIMCl), BMIM-acetate and EMIM-acetate were used for the preparation of cellulose spinning solutions containing maximal usable polymer content. Spinning trials on cellulose fibres from these solutions were carried out using a dry-wet spinning method at TITK, Germany [228]. The fibres obtained were characterized by very good physico-mechanical properties: fibre tenacities and the values of the loop tenacities were 44–53 cN/tex and 22–33 cN/tex, respectively. The dissolution and processing of cellulose in ionic liquids was invented by Professor Robin Rogers and colleagues at the University of Alabama [229]. BASF has obtained an exclusive licence with the right to sublicense these and offer solutions of cellulose with different degrees of polymerization in EMIM acetate as a 5% solution under the trade name Cellionic™.

One of the challenges for the future is elaboration of the technology for obtaining thermoplastic cellulose. The research work should include the change of molecular and supermolecular cellulose structure in order to achieve thermoplastic material. Addition of low-molecular-weight components into the cellulose esterification process would enable to improve most of the elastic properties of composite materials. It is expected that thermoplastic cellulose could be useful for further processing by the melt-blown method.

## 1.7 References

1. Nevell T. P., Zeronian S. H., in *Cellulose Chemistry and its Applications*, editors Nevell T. P. and Zeronian S. H., Ellis Horwood, Chichester, UK, 1985, p. 15.
2. French A. D., in *Cellulose Chemistry and its Applications*, editors Nevell T. P. and Zeronian S. H., Ellis Horwood, Chichester, UK, 1985, p. 84.
3. Meyer K. H., Misch I., *Helv. Chim. Acta*, 20, 212, 1937.
4. Denton M. J., Daniels P. N., *Textile Terms and Definitions*, 11th edition, The Textile Institute, Manchester, UK, 2002.
5. Pulp and Paper Capacities Survey 2000–2001, FAO, Rome, 2001.
6. Bureau International pour la Standardisation des Fibres Artificielles (BISFA), 2006.
7. Choudhury A. K. R., *Textile Preparation and Dyeing*, Science Publishers, Enfield, NH, 2006.
8. Cook J. G., *Handbook of Textile Fibres: Vol II. Man-Made Fibres*, Woodhead Publishing, Cambridge, 1984.
9. Fink H. P., 'Strukturelle Aspekte neuer Cellulosenmaterialien', *Cellulosechemiker-Rundgespräch*, Baden-Baden, Germany, 23–26 June 1997.
10. Lenz J., Schurz J., Eichinger D., 'Properties and structure of Lyocell and viscose-type fibres in the swollen state', *Lenzinger Berichte* 74, 19–25, 1994.

11. *Chemical Fibres International* 47, 298–304, 1997.
12. Eichinger D., Lotz C., ‘Lenzing Lyocell – potential for technical textiles’, *Lenzinger Berichte* 75, 69–72, 1996.
13. Woodings C., ‘Lyocell fibres in spunlance nonwovens’, *Chemical Fibres International* 45, 390–394, 1995.
14. Münstermann U., Möschler W., Watzl A., ‘Hydroentanglement process’, in *Nonwoven Fabrics. Raw Materials, Manufacture, Applications, Characteristics, Testing Methods*, editors Albrecht W., Fuchs H. and Kittelmann W., Wiley-VCH, Weinheim, Germany, 2003, pp. 326–341.
15. Morton W. E., Hearle J. W. S., in *Physical Properties of Textile Fibres*, 3rd edition, Bookcraft, Midsomer Norton, UK, 1993, p. 725.
16. Albrecht W., ‘Fibrous material’, in *Nonwoven Fabrics. Raw Materials, Manufacture, Applications, Characteristics, Testing Methods*, editors Albrecht W., Fuchs H. and Kittelmann W., Wiley-VCH, Weinheim, Germany, 2003, pp. 15–85.
17. Matero M., Nousiainen P., Struszczyk H., Ciechańska D., Wawro D., East G., ‘Celsol – biotransformation of cellulose for fibre spinning’, in *The Chemistry and Processing of Wood and Plant Fibrous Materials*, editors Kennedy J. F., Phillips G. O. and Williams P. A., Woodhead Publishing, Cambridge, 1996.
18. Struszczyk H., Ciechańska D., Wawro D., Nousiainen P., Matero M., ‘Direct soluble cellulose of Celsol: Properties and behaviour’, in *Cellulose and Cellulose Derivatives: Physico-chemical Aspects and Industrial Applications*, editors Kennedy J. F., Phillips G. O., Williams P. A. and Piculell L. Woodhead Publishing, Cambridge, 1995, pp. 29–35.
19. EU FP6 Project, ‘Biotechnological process for manufacturing cellulosic products with added value (BIOCELSOL)’, Contract number NMP2-CT-2003-50 5567.
20. Cook J. G., *Handbook of Textile Fibres: Vol II. Man-Made Fibres*, 5th edition, Merrow, Watford, UK, 1993.
21. Dyer J., Daul G., ‘Rayon fibers’, in *Handbook of Fibre Science and Technology: Volume IV. Fibre Chemistry*, editors Lewin M. and Pearce E. M., Marcel Dekker, New York, 1985, pp. 909–999.
22. EP 807460, 1997.
23. Brandroup J., Immergut E. H., *Polymer Handbook*, V/117, John Wiley & Sons, New York, 1989.
24. Sarko A., Okano T., Nishimura H., *TAPPI Proceedings*, Boston, MA, 1983, p. 225.
25. Atalla R. A., Ellis J. D., *TAPPI Proceedings*, Boston, MA, 1983, p. 64.
26. Turbak E. A. F., Hammer R. B., Davies R. E., Herget H. L., *Chemtech* 10, 51, 1980.
27. Łaskiewicz B., ‘Wytwarzanie włókien celulozowych bez udziału dwusiarczku węgla’, (Manufacture of cellulose fibres without CS<sub>2</sub>), A.C.G.M. Lodart S.A., Łódź, 1997.
28. Przygocki W., *Włókna Chemiczne* 15, 135–147, 1989.
29. Dumitriu S., editor, *Polysaccharides: Structural Diversity and Functional Versatility*, 2nd edition, CRC Press, Boca Raton, FL, 2005.
30. Heinze T., Koschella A., ‘Solvents applied in the field of cellulose chemistry: a mini review’, *Polímeros* 15(2), 84–90, 2005.
31. US Pat. 4,899,149, 1991.
32. RU Pat. 147 6001, 1989.
33. JP. Pat. 58-1217, 1983.

34. Grinszpan D. D., *et al.*, *Chim. Volokna* 6, 6, 1988.
35. Grinszpan D. D., *et al.*, *Proceedings of Man-Made Fibres Symp.* Vol. 2, p. 7, Kalinin, 1990.
36. Kamide K., Okajima K., Matsui T., Kawasaka K., *Polym. J.* 16, 857, 1984.
37. PL Pat. 167 590, 1991
38. Nousiainen P., Matero M., Struszczyk H., East G., *Proceedings of Challenges in Cellulosic Man-Made Fibres, Viscose Chemistry Seminar*, Stockholm, 1994.
39. Na irina G. S., Kapierszlak Z. Z., Podolskaja L. W., *Chim. Wołokna* 4, 33, 1982.
40. Thomas T., *J. Am. Chem. Soc.* 75, 5347, 1953.
41. Ruan D., Zhang L., Zhou J., Jin H., Chen H., *Macromol. Biosci.* 4, 1105–1112, 2004.
42. Cai J., Zhang L., Zhou J., Li H., Chen H., Jin H., *Macromol. Rapid Commun.* 25, 1558–1562, 2004.
43. Chen X., Burger C., Fang D., Ruan D., Zhang L., Hsiao B. S., Chu B., *Polymer* 47, 2839–2848, 2006.
44. Ruan D., Zhang L., Zhou J., Jin H., Chen H., *Macromol. Biosci.* 4, 1105, 2005.
45. Pat. CN 03128386.1, 2005.
46. Huajin J., Chunxi Z., Lixia G., *Carbohydrate Polymers* 342 (6), 851–858, 2007.
47. Boerstol H., Maatman H., Westerink J. B., Koenders B. M., ‘Liquid crystalline solutions of cellulose in phosphoric acid’, *Polymer* 42, 7371, 2001.
48. US Pat. 5,938,971, 1999.
49. Ekmanis J. L., *Am. Lab. News* Jan/Feb, 10, 1987.
50. US Pat. 4,302,252, 1981.
51. Turbak A. F., ‘Newer cellulose solvent systems’, in *Wood and Agricultural Residues*, editor Soltes E. J., Academic Press, New York, 1983, pp. 87–99.
52. Strobin G., Ciechańska D., Wawro D., Boryniec S., Struszczyk H., Sobczak S., ‘Gel permeation chromatography of chemically, irradiated and enzymatically treated celluloses’, *Fibres and Textiles in Eastern Europe* 11, (4), 43, 2003.
53. Philipp B., Schleicher H., Wagenknecht W., *ACS Symposium Series*, 58, 278, 1977.
54. Philipp B., Schleicher H., Wagenknecht W., *Cell. Chem. Technol.* 9, 265, 1975.
55. Philipp B., Schleicher H., *Chem. Tech.* 7(11), 702, 1977.
56. GB Pat. 1,144,048, 1969.
57. US Pat. 4,246,221, 1979.
58. Chanzy H., Paillet M., Hagege R., ‘Spinning of cellulose from *N*-methylmorpholine *N*-oxide in the presence of additives’, *Polymer* 31, 400–405, 1990.
59. Coulsey H. A., Smith S. B., ‘The formation and structure of a new cellulosic fibre’, *Lenzinger Berichte* 75, 51–61, 1996.
60. Fink H. P., Weigel P., Purz H. J., Ganster J., ‘Structure formation of regenerated cellulose materials from NMMO solutions’, *Progress in Polymer Science*, 26 (9), 1473–1524, 2001.
61. Firgo H., Eibl M., Kalt W., Meister G., ‘Kritische Fragen zur Zukunft der NMMO-Technologie’, *Lenzinger Berichte* 74, 81–89, 1994.
62. Lenz J., Schurz J., Wrentschur E., ‘Comparative characterization of solvent spun cellulose and high wet modulus viscose fibres by their long periods’, *Acta Polym.* 43, 307–312, 1992.
63. Turbak A. F., Hammer R. B., Davies R. E., Partnoy R. A., *ACS Symposium Series* 58, 12, 1977.
64. US Pat. 4,056,675, 1977.

65. US Pat. 4,044,090, 1977.
66. Wagenknecht W., Nehls I., Philipp B., *Carbohydr. Res.* 237, 211, 1992.
67. Wagenknecht W., Nehls I., Philipp B., *Carbohydr. Res.* 240, 245, 1993.
68. Hammer R. B., Turbak A. F., *ACS Symposium Series* 58, 40, 1977.
69. Johnson D. C., Nicholson M. D., Haigh T. C., *Appl. Polym. Symposium* 28, 931, 1996.
70. Swenson H. A., *Appl. Polym. Symposium* 28, 945, 1996.
71. Seymour R. B., Johnson E. L., *J. Appl. Polym. Sci.* 20, 3425, 1976.
72. Baker T. J., Schroeder L. R., Johnson D. C., *Cellul. Chem. Technol.* 15, 311, 1981.
73. Hammer R. B., Turbak A. F., Davies R. E., Partnoy R. A., *ACS Symposium Series* 58, 71, 1977.
74. Wasserscheid P., Keim W., *Angew. Chem. Int. Ed.* 39, 3772, 2000.
75. Kasan B., Michels Ch., Meister F., 'Ionic liquids-new interesting solvents and shaping media for cellulose', *Alternative Cellulose Conference – TITK*, Rudolstadt, Germany, 5–7 September 2006.
76. Barthel S., Heinze T., *Green Chem.* 8, 301–306, 2006.
77. El Seoud Omar A., Koschella A., Fidale L. C., Dorn S., Heinze T., 'Applications of ionic liquids in carbohydrate chemistry: a window of opportunities', *Biomacromolecules* 8(9), 2629–2647, 2007.
78. Cuissinat C., Navard P., Heinze T., 'Swelling and dissolution of cellulose, Part V: Cellulose derivatives fibres in aqueous systems and ionic liquid', *Cellulose*, 15, (1), 2008.
79. Swatloski R. P., Spear S. K., Holbrey J. D., Rogers R. D., *J. Am. Chem. Soc.* 124, 4974, 2002.
80. Fischer S., Voigt W., Fischer K., *Cellulose* 6, 213, 1999.
81. Kennedy F., Phillips G. O., Williams P. A., eds, *Lignocellulosics: Science, Technology, Development and Use*, Ellis Horwood, New York, 1992.
82. Kennedy F., Phillips G. O., Williams P. A., ed, *Cellulose Sources and Exploitation: Industrial Utilization, Biotechnology and Physico-Chemical Properties*, Ellis Horwood, New York, 1990.
83. Kennedy F., Phillips G. O., Williams P. A., eds, *Cellulose and Cellulose Derivatives: Physico-Chemical Aspects and Industrial Applications*, Woodhead Publishing, Cambridge, 1995.
84. Ruan D., Zhang L., Zhou J., Jin H., Chen H., *Macromol. Biosci.* 4, 1105–1112, 2004.
85. Chen X., Burger C., Fang D., Ruan D., Zhang L., Hsiao B. S., Chu B., *Polymer*, 47, 2839–2848, 2006.
86. Ruan D., Zhang L., Zhou J., Jin H., Chen H., *Macromol. Biosci.* 4, 1105, 2005.
87. PL Pat. 167776, 1995.
88. PL Pat. 167519, 1995.
89. FI Pat. 107335, 2001.
90. Struszczyk H., Ciechańska D., Wawro D., *Fibres and Textiles in Eastern Europe* 3 (1), 47, 1995.
91. Struszczyk H., Wawro D., Ciechańska D., Nousiainen P., Dolk M., 'Direct dissolving cellulose: behaviour and properties', *Cellulose'91 Conference*, New Orleans, 1991.
92. Struszczyk H., Ciechańska D., Wawro D., 'Direct soluble cellulose of Celsol: properties and behaviour', *Cellucon'93*, Lund, Sweden, 1993.



93. Bhat M. K., Bhat S., 'Cellulose degrading enzymes and their potential industrial applications', *Biotechnology Advances* 15(3/4), 583–620, 1997.
94. Rahkamo L., Siika-aho M., Vehviläinen M., Dolk M., Viikari L., Nousiainen, P., Buchert J., 'Modification of hardwood dissolving pulp with purified *Trichoderma reesei* cellulases', *Cellulose* 3, 153–163, 1996.
95. Rahkamo L., Siika-aho M., Viikari L., Leppänen T., Bucher J., 'Effects of cellulases and hemicellulases on the alkaline solubility of dissolving pulps', *Holzforschung* 52, 630–634, 1998.
96. Rahkamo L., Vehviläinen M., Viikari L., Nousiainen P., Buchert J., 'Modification of dissolving pulp by hydrolysis with cellulase enzymes', Proc. ACS Symposium on Enzyme Applications in Fibres Processing, San Francisco, 13–17 April 1998, pp. 318–327.
97. Struszczyk H., Ciechańska D., 'Perspectives of enzymes for processing cellulose for new chemical fibres,' Proc. ACS Symposium on Enzyme Applications in Fibres Processing, San Francisco, 13–17 April 1998, pp. 306–317.
98. Vehviläinen M., Nousiainen P., Struszczyk H., Ciechańska D., Wawro D., East G., 'Celsol – biotransformation of cellulose for fibre spinning', *Proc. Tenth Anniversary International Cellucon Conference. The Chemistry and Processing of Wood and Plant Fibrous Materials*, 19–23 September 1994, Bangor, UK, pp. 1–8.
99. Fan L. T., Lee Y. H., Beardmore D. H., *Biotechnol. Bioeng.* 22, 177, 1980.
100. Fan L. T., Gharpuray M., Lee Y. H., *Cellulose Hydrolysis*, Springer-Verlag, Berlin, Heidelberg, 1987.
101. Fan L. T., Lee Y. H., Beardmore D. H., *Biotechnol. Bioeng.* 23, 419, 1981.
102. Matero M., Nousiainen P., Struszczyk H., Ciechańska D., Wawro D., East G., 'Celsol – biotransformation of cellulose for fibre spinning', *Cellucon'94 Conference*, Bangor, UK, 1994.
103. Rom M., Janicki J., Rabiej S., Slusarczyk C., Kwiatkowski R., Vehviläinen M., Nousiainen P., Siika-Aho M., Kallioinen A., Ciechańska D., Elg K., Franco T., 'Structure and properties of enzymatically modified cellulose pulp', *IXth International Conference on Frontiers of Polymers and Advanced Materials (ICFPAM): Book of Abstracts*, Cracow, Poland, 8–12 July 2007, editor Kajzar F., Tadeusz Ko ciuszko University of Technology, Institute of Natural Fibres, 2007, p. 269.
104. Cao Y., Tan H., 'Effects of cellulase on the modification of cellulose', *Carbohydr. Res.* 337, 1291–1296, 2002.
105. Bła ej A., Kosik M., *Cellulosics: Pulp, Fibre and Environmental Aspects*, Ellis Horwood, Chichester, UK, 1993, p. 355.
106. Rajagopal S., Stepanik T., *Proceedings: Enhancement of Cellulose Reactivity of Challenges in Cellulose Man-Made fibres, Viscose Chemistry Seminar*, Berol Nobel, Stockholm, 1994.
107. Dziędziela M., Rosiak J., *Cell. Chem. Technol.* 11, 261, 1977.
108. Erşow B. G., Iskaowa O. W., Matuszkina E. H., Samujłowa C. D., *Cell. Chem. Technol.* 21, 331, 1987.
109. Krässig H. A., *Cellulose Structure, Accessibility and Reactivity*, Gordon & Breach, Amsterdam, 1996, p. 216.
110. Pruzinec J., Kadlecik J., Varga S., Pivovarnicek F., 'Study of the effect of high-energy radiation on cellulose', *Radiochem. Radioanal. Letters* 49, 395, 1981.
111. Charlesby A., *Atomic Radiation and Polymers*, Pergamon Press, London, 1960, p. 361.
112. Takács E., Wojnárovits L., Földváry Cs., Hargittai P., Borsa J., *et al.*, 'Effect of



- combined gamma-irradiation and alkali treatment on cotton–cellulose’, *Radiation Physics and Chemistry* 57, 399–403, 2000.
113. Földváry Cs. M., Takács E., Wojnárovits L., ‘Effect of high-energy radiation and alkali treatment on the properties of cellulose’, *Radiation Physics and Chemistry* 67, 505–508, 2003.
  114. Iller E., Stupińska H., Starostka P., ‘Properties of cellulose derivatives produced from radiation – modified cellulose pulps’, *Radiation Physics and Chemistry* 76, 1189–1194, 2007.
  115. Dyer, J., Daul, G. C., ‘Rayon fibers’, in *Handbook of Fiber Chemistry*, editors Lewin M. and Pearce E. M., Marcel Dekker, New York, 1998, p. 738.
  116. Stepanik T. M., Rajagopal S., Ewing D., Whitehouse R., ‘Electron processing technology: a promising application of the viscose industry’, in *Proceedings of the 10th International Meeting on Radiation Processing (special issue)*, *Rad. Phys. Chem.* 52, 505–509, 1998.
  117. Stepanik T. M., Ewing D. E., Whitehouse R., ‘Electron treatment of wood pulp for the viscose process’, *Radiation Physics and Chemistry* 57, 377–379, 2000.
  118. US Pat. 1,655,618, 1928.
  119. Yamashiki T., Matsui T., Saitoh M., Okajima K., Kamide K., Sawada T., *Brit. Polym. J.* 22(2), 121, 1990.
  120. Yamashiki T., Matsui T., Saitoh M., Okajima K., Kamide K., Sawada T., *Brit. Polym. J.* 22(1), 73, 1990.
  121. Tanahashi M., Tamabuchi K., Goto T., Aoki T., Karina M., Higuchi T., ‘Characterization of steam-exploded wood. II. Chemical changes of wood components by steam explosion’. *Wood Research* 75, 1–12, 1988.
  122. Excoffier G., Peguy A., Rinaudo M., Vignon M. R., ‘Evolution of lignocellulosic components during steam explosion. Potential applications’, in *Proceedings of the International Workshop on Steam Explosion Techniques: Fundamentals and Industrial Applications*, 1988, pp. 83–95.
  123. Atalla R. H., ‘Structural transformations in celluloses’, in *Proceedings of the International Workshop on Steam Explosion Techniques: Fundamentals and Industrial Applications*, 1988, pp. 97–119.
  124. Donaldson L. A., Wong K. K. Y., Mackie K. L., *Wood Sci. Technol.* 22, 103, 1988.
  125. Dumitriu S., editor, *Polysaccharides: Structural Diversity and Functional Versatility*, 2nd edition, Marcel Dekker, New Delhi, 2004.
  126. *First World Conference on Biomass for Energy and Industry, Proceedings of the Conference*, Sevilla, Spain, June 2000.
  127. Saddler J. N., Brownell H. H., ‘Pretreatment of wood cellulosics to enhance enzymatic hydrolysis to glucose’, in *Proceedings of the International Symposium on Ethanol from Biomass*, Winnipeg, Canada, 13–15 October 1982.
  128. Barnett D., Dupeyre D., Excoffier G., Gagnaire D., Nava-Saucedo J. E., Vignon M. R., ‘Flash hydrolysis of aspen wood: characterization of water soluble compounds’, in *Energy from Biomass*, editors Strub A., Chartier P. and Schlessler G., Elsevier, London, 1982, pp. 889–893.
  129. Dekker R. F. H., Wallis A. F. A., ‘Enzymic saccharification of sugarcane bagasse pretreated by autohydrolysis-steam explosion’, *Biotechnol. Bioeng.* 25, 3027–3048, 1983.
  130. WO 060027, 1999.
  131. DD Pat. 298 789, 1993.

132. Michels Ch., Maron R., Taeger E., 'Characteristics of the amine oxide process developed at the Turing Institute of textiles and plastics', *Fibre Chemistry*, 28(1), 1996.
133. Mochidzuki K., Sakoda A., Suzuki M., 'Measurement of the hydrothermal reaction rate of cellulose using novel liquid-phase thermogravimetry', *Thermochimica Acta*, 348, 69–76, 2000.
134. Wahyudiono T., Kanetake M., Sasaki M., *Chem. Eng. Technol.* 30(8), 1113–1122, 2007.
135. US Pat. Appl. 20070267008, 2007.
136. US Pat. 5,906,926, 1999.
137. US Pat. 6,106,763, 2000.
138. McGarry W. J., Priest M. H., 'Viscose rayon tire yarn', in *Man-Made Fibres. Science and Technology. Volume 2*, editors Mark F. H., Atlas S. M. and Cernia E., Interscience, New York, London, Heidelberg, 1968, pp. 43–80.
139. Woodings C., *Regenerated Cellulose Fibres*, Woodhead Publishing, Cambridge, 2001.
140. Schmidbauer J., *Lenzinger Berichte* 75, 15–22, 1996.
141. Kato K., 'Procion dye staining for differentiation of skin and core of viscose rayon fibres', *Text. Res. J.* 29(8), 661–664, 1959.
142. Sisson W. A., 'The spinning of rayon as related to its structure and properties. *Text. Res. J.* 30(3), 153–170, 1960.
143. Rom M., Janicki J., Rabiej S., Slusarczyk C., Vehviläinen M., Nousiainen P., Ciechańska D., Wawro D., *Polymer Fibres Conference*, Manchester, UK, 12–14 July 2006.
144. Schmidbauer J., 'Viscostar® – a star-shaped viscose fiber for improved absorbency', Lenzing R&D, Austria.
145. CIRFS, Comité International de la Rayonne et des Fibres Synthétiques (The International Rayon and Synthetic Fibres Committee).
146. Hill J. W., Jacobson R. A., US Pat. 2,134,825, 1938.
147. Segal L., Eggerton F. V., *Text. Res. J.* 31, 460, 1961.
148. Hebeish A., Walay A., Abou Zeid N. Y., El-Alfy E. A., *Text. Res. J.* 48, 468, 1978.
149. Hebeish A., Abou Zeid N. Y., El-Alfy E. A., Walay A., *Cell. Chem. Technol.* 12, 671, 1978.
150. Hebeish A., El-Alfy E. A., Walay A., Abou Zeid N. Y., *J. Appl. Polym. Sci.* 25, 223, 1980.
151. Nozawa Y., Higashide F., *J. Appl. Polym. Sci.* 26, 2103, 1981
152. Ekman K., Eklund Y., Efors J., Hutunen J. L., Selin J. F., Turunen O. T., *Dissolving and Speciality Pulps Conference*, Boston, MA, 1983.
153. Meinander K., Eklund V., Fors J., Mandell L., Selin J. F., Turunen O. T., 'The Cella process', *Kemira News* 2, 8, 1987.
154. Ekman K., Eklund V., Fors J., Huttunen J. L., Selin J. F., Turunen O. T., *Cellulose Structure, Modification and Hydrolysis*, Wiley, New York, 1986, p. 131.
155. FI. Pat. 67562, 1984.
156. German Pat. Appl. DE 42 42 437 A1, 1992.
157. Struszczyk H., Urbanowski A., 'Polish cellulose carbamate: new effort for cellulosic man-made fibres manufacture', *Proceedings of Challenges in Cellulose Man-Made Fibres*, Stockholm, 1994.
158. PL Pat. 309718, 1995.

159. Struszczyk H., Urbanowski A., *Fibres and Textiles in Eastern Europe* 1, 28, 1993.
160. Urbanowski A., 'Cellulose carbamate: a new raw material for the manufacture of cellulosic fibres', *Chemical Fibers International* 46(4), 260, 1996.
161. Fink H. P., Ebeling H., Rihm R., 'Fibre formation from liquid crystalline solutions of cellulose carbamate in NMMO', *Proceedings of the 7th International Symposium Alternative Cellulose – Manufacturing, Forming, Properties*, Rudolstadt, Germany, 6–7 September 2006.
162. FR Pat. 2 423 559, 1978.
163. US Pat. 4,145,532, 1981.
164. Laszkiewicz B., Czarnecki P., Kulpinski P., Niekraszewicz B., Rubacha M., 'Three generations of the Lyocell type fibres', in *Proceedings of 7th International Symposium Alternative Cellulose – Manufacturing, Forming, Properties*, Rudolstadt, Germany, 6–7 September 2006.
165. Armstrong R. N., McCorsley C. C., Varga J. K., 'Spinnable solutions of cellulose in amine oxides', *Proceedings of the 5th International Dissolving Pulp Conference*, TAPPI, 1980.
166. Schurz J., *Lenzinger Berichte* 74, 37, 1994.
167. Rohrer C., Retzl P., Firgo H., *Lenzinger Berichte* 80, 75–81, 2001.
168. Öztürk H. B., 'Fibrillation and splitting tendency of Lyocell fibres', in *Proceedings of EPNOE Summer Course*, University of Innsbruck, Austria, 22–25 August, 2006.
169. Niekraszewicz B., 'Cellulose fibres with bioactive properties', in *Conference Proceedings Int. Text. Congress, AUTEX*, Terrassa, Spain, 18–20 October 2004, pp. 200–208.
170. Ehrhardt A., Bechtold T., 'Influence of alkali-urea treatment on physical properties of regenerated cellulosic fabrics', in *Proceedings of 7th International Symposium Alternative Cellulose – Manufacturing, Forming, Properties*, Rudolstadt, Germany, 6–7 September 2006.
171. Ward D., *Internat. Fiber J.* 16(3), 58, 2001.
172. Büttner R., Knobelsdorf C., Markwitz H., *43rd International Man-Made Fibres Congress*, Dornbirn, Austria, 2004
173. Ciechańska D., 'Investigation of cellulose bio-transformation', Ph. D. thesis, Technical University of Łódź, Poland, 1996.
174. Ciechańska D., Wawro D., Stepiewski W., Wesolowska E., Vehviläinen M., Nousiainen P., Kamppuri T., Hroch Z., Sandak, Janicki J., Włochowicz A., Rom M., Kovalainen A., 'Ecological method of manufacture of the cellulose fibres for advanced technical products', in *Edana Conference, Nonwovens Research Academy*, 29–30 March 2007, University of Leeds, UK.
175. Ciechańska D., Galas E., Struszczyk H., 'Biotransformation of cellulose', *Fibres and Textiles in Eastern Europe* 4(3–4), 148, 1996.
176. Ladish, M. R., Lin, K. W., Tsao, G. T., 'Process considerations in the enzymatic hydrolysis of biomass', *Enzyme Microb. Technol.* 5, 82–102, 1983.
177. Nevalainen, H., Penttilä, M., 'Molecular biology of cellulolytic fungi', in *The Mycota. II: Genetics and Biotechnology*, editor Kück U., Springer-Verlag, Berlin/Heidelberg, 1995, pp. 304–319.
178. Wood T. M., *Biochem. J.* 109, 217, 1968.
179. Reese E. T., in *Biological Transformation of Wood*, editor Liese W., Springer-Verlag, Berlin, 1975, pp. 165–181.
180. White A. R., in *Cellulose and Other Natural Polymer Systems*, editor Brown R.M., Plenum Press, New York, 1982, pp. 489–509.

181. Ciechańska D., Wawro D., Steplewski W., Kazimierczak J., Struszczyk H., 'Formation of fibres from bio-modified cellulose pulp', *Fibres and Textiles in Eastern Europe*, 13(6), 19, 2005.
182. 'Biotechnological process for manufacturing cellulosic products with added value (BIOCELSOL)', Publishable Final Activity Report, Project publication, 2007, <http://www.tut.fi/units/ms/teva/biocelsol/presentation.htm>.
183. 'Biotechnological process for manufacturing cellulosic products with added value (BIOCELSOL)', 2nd Publishable Executive Summary, Project publication, 2006, <http://www.tut.fi/units/ms/teva/biocelsol/presentation.htm>.
184. Maezaki Y., Tsuji K., Nakagava Y., Kawal Y., Akimoto M., Tsugita T., Takekawa W., Tereda A., Hara H., Mitsuoka T., 'Hypocholesterolemic effect of chitosan in adult males', *Biosci. Biotech. Biochem.* 57, 1439–1444, 1993.
185. Pospieszny H., Struszczyk H., Cajza M., 'Biological activity of *Aspergillus*-degraded chitosan', in *Chitin Enzymology*, Vol. 2, editor Muzzarelli R.A.A., Alec Edizioni, Grottamare, Italy, 1996, p. 385.
186. Hirano S., Nagano N., 'Effects of chitosan, pectic acid, lysozyme, and chitinase on the growth of several phytopathogens', *Agric. Biol. Chem.* 53, 3065–3066, 1989.
187. Muzzarelli R. A. A., Tarsi R., Filippini O., Giovanetti E., Biagini G., Varaldo P. E., 'Antimicrobial properties of *N*-carboxybutyl chitosan', *Antimicrobial Agents and Chemotherapy* 34, 2019–2023, 1990.
188. Domard A., Jaunieux Ch., Muzzarelli R. A. A., Roberts G., editors, *Advances in Chitin Science*, vol. I, Jacques André Publ., Lyon, France, 1996.
189. Struszczyk H., 'Some aspects of chitosan bioactivity', *Progress on Chemistry and Application of Chitin and its Derivatives*, vol. IV, 1998.
190. Kweon D. K., Kang D. W., 'Drug-release behavior of chitosan-g-poly(vinyl alcohol) copolymer matrix'. *J. Appl. Polym. Sci.* 74, 458–464, 1999.
191. Zhang M., Li X. H., Gong Y. D., Zhao N. M., Zhang X. F., 'Properties and biocompatibility of chitosan films modified by blending with PEG'. *Biomaterial* 23, 2641–2648, 2002.
192. Ratto J. A., Chen C. C., Blumstein R. B., 'Phase behavior study of chitosan/polyamide blends', *J. Appl. Polym. Sci.* 59, 1451–1461, 1996.
193. Lee J. W., Kim S. Y., Kim S. S., Lee Y. M., Lee K. H., Kim S. J., 'Synthesis and characteristics of interpenetrating polymer network hydrogel composed of chitosan and poly(acrylic acid)', *J. Appl. Polym. Sci.* 73, 113–120, 1999.
194. Arvanitoyannis I. S., Nakayama A., Aiba S. I., 'Chitosan and gelatin based edible films: state diagrams, mechanical and permeation properties', *Carbohydr. Polym.* 37, 371–382, 1998.
195. Park S. R., Lee K. Y., Ha W. S., Park S. Y., 'Structural changes and their effect on mechanical properties of silk fibroin/chitosan blends', *J. Appl. Polym. Sci.* 74, 2571–2575, 1999.
196. Isogai A., Atalla R. H., 'Preparation of cellulose–chitosan polymer blends', *Carbohydr. Polym.* 19, 25–28, 1992.
197. Hasegawa M., Isogai A., Onabe F., Usuda M., Atalla R. H., 'Characterization of cellulose–chitosan blend films', *J. Appl. Polym. Sci.* 45, 1873–1879, 1992.
198. Hasegawa M., Isogai A., Kuga S., Onabe F., 'Preparation of cellulose chitosan blend film using chloral dimethylformamide', *Polymer* 35, 983–987, 1994.
199. US Pat. 5,756,111, 1988.
200. WO 130117, 2006.

201. Józwicka J., Wawro D., Starostka P., Struszczyk H., Mikołajczyk W., 'Manufacturing possibilities and properties of cellulose-starch fibrils', *Fibres and Textiles in Eastern Europe* 9(4), 28–32, 2001.
202. Onsoyen E., 'Alginate: production, composition, physicochemical properties, physiological effects, safety, and food applications', in *Handbook of Dietary Fiber*, editors Cho S.S. and Dreher M.L., Marcel Dekker, New York, 2001.
203. Skjåk-Braek G., Espevik T., 'Application of alginate gels in biotechnology and biomedicine', *Carbohydrates in Europe*, 14, 19–25, 1996.
204. Thomas S., *Wound Management and Dressings*, Pharmaceutical Press, London, 1990.
205. Yeom C. K., Jegal J. G., Lee K. H., 'Characterization of relaxation phenomena and permeation behaviors in sodium alginate membrane during pervaporation separation of ethanol–water mixture', *J. Appl. Polym. Sci.* 62, 1561, 1996.
206. Huang R. Y. M., Pal R., Moon G. Y., 'Characteristics of sodium alginate membranes for the pervaporation dehydration of ethanol–water and isopropanol–water mixtures', *J. Membr. Sci.* 160, 101, 1999.
207. Phisalaphong M., Suwanmajo T., Tammarate P., 'Synthesis and characterization of bacterial cellulose/alginate blend membranes', *J. Appl. Polym. Sci.* 107, 3419–3424, 2007.
208. Strobin G., Wawro D., Stęplewski W., Ciechańska D., Józwicka J., Sobczak S., Haga A., 'Formation of cellulose/silk-fibroin blended fibres', *Fibres and Textiles in Eastern Europe* 14(4), 2006.
209. Wrzesniewska-Tosik K., Wawro D., Ratajska M., Stęplewski W., 'Novel biocomposites with feather keratin', *Fibres and Textiles in Eastern Europe* 15(5–6), 2007.
210. Fink H. P., 'Novel thermoplastic composites from commodity polymers and man-made cellulose fibers', *Macromol. Symp.* 244(1), 2006.
211. Amash A., Zugenmaier P., *Polymer Bulletin* 40 (2–3), 1998.
212. Panaitescu D. M., 'Polymer composites with cellulose microfibrils', *Polym. Eng. Sci.* 47(8), 2007.
213. US Pat. 5,166,232, 1992.
214. Masson J. F., Manley R. S. J., 'Miscible blends of cellulose and poly(vinylpyrrolidone)', *Macromolecules*, 24, 6670–6679, 1991.
215. Garcia-Ramirez M., Cavallé J. Y., Dupeyre D., Péguy A., 'Cellulose–polyamide 66 blends. Part I: Processing and characterization', *J. Polym. Sci., Polym. Phys.* 32, 1437–1448, 1994.
216. Garcia-Ramirez M., Cavallé J. Y., Dufresne A., Tékély P., 'Cellulose–polyamide 66 blends. Part II: Mechanical behavior', *J. Polym. Sci. Polym. Phys.* 33, 2109–2124, 1995.
217. Field N. D., Song S. S., 'Blends of poly(ethylene terephthalate) and cellulose', *J. Polym. Sci., Polym. Phys.* 22(1), 101–106, 1984.
218. Ciechańska D., Niekraszewicz A., Wesołowska E., 'Opportunities and challenges of polysaccharides (PS) in the biomedical field', *International Workshop on Biomacromolecules*, Stockholm, 1–4 June 2008.
219. PL Pat. 190961, 1998.
220. Ciechańska D., 'Multifunctional bacterial cellulose/chitosan composite materials for medical applications', *Fibres and Textiles in Eastern Europe* 12(4), 2004.
221. Ciechańska D., Struszczyk H., Guzińska K., Kazimierczak J., Wawro D., 'Progress in the new ecological methods for the manufacture and finishing of cellulose fibres, films and other products', *Conference Brugia*, 2002.

222. Polish Pat. Appl. P-342956, 2000.
223. PL Pat. 342957, 2000.
224. Ciechańska D., Struszczyk H., Kazimierczak J., Guzińska K., Pawlak M., Kozłowska E., Matusiak G., Dutkiewicz M., 'New electro-acoustic transducers based on modified bacterial cellulose', *Fibres and Textiles in Eastern Europe* 10(1), 2002.
225. Łaskiewicz B., Czarnecki P., Kulpinski P., Niekraszewicz B., Rubacha M., 'Nano-fibres – preparation, properties and application', Monography, Łódź, 2004.
226. EP 1 591 569 A1, 2004.
227. EP 1 601 824 B1, 2005.
228. Kosan B., Michel Ch., Meister F., 'Ionic liquids – new interesting solvents and shaping media for cellulose', *Proceedings of 7th International Symposium Alternative Cellulose – Manufacturing, Forming, Properties*, Rudolstadt, Germany, 6–7 September 2006.
229. WO 029.329, 2003.

## The structure of cotton and other plant fibres

---

M P ANSELL, University of Bath, UK and  
L Y MWAIKAMBO, University of Dar es Salaam, Tanzania

**Abstract:** The structure and properties of plant fibres are reviewed with emphasis on the deposition of cellulose microfibrils in the plant cell wall and the effect of microfibril angle on mechanical properties such as strength and stiffness. The worldwide production of cotton fibres for textile applications far exceeds that of other plant fibres, hence the structure of cotton is reviewed in detail. Plant fibre bundles such as sisal, hemp, jute and kenaf are finding new uses in structural applications in the automotive and construction industries and a significant proportion of the chapter is devoted to these industrial fibres. New developments in understanding structure–property relationships are continuously appearing in the literature and natural fibres have a strong part to play in a sustainable future.

**Key words:** plant fibre structure, cellulose microfibrils, microfibril angle (MFA), structure–property relationships, fibre bundles.

### 2.1 Introduction

In the years since the publication of the classic text *Fibre Structure* (Hearle and Peters, 1963) the literature on plant fibres has expanded rapidly, spurred on by the drive to better characterize the molecular structure of plant cell walls and the development of sustainable natural fibre composites for industrial applications. Bailey *et al.* (1963) devoted much of their chapter on vegetable fibres to the structure of cotton. The worldwide production of cotton fibres for textiles far exceeds that of other plant fibres, with a prediction that 23.6 m tonnes of cotton products will be manufactured in 2010 (Aksoy and Beghin, 2004). Hence it is essential to review key literature on the structure of cotton including advances in genetics. In recent years the excellent mechanical performance of plant fibres such as sisal, hemp, jute and kenaf has engendered considerable interest in their use for structural applications, including automotive panels (Suddell and Evans, 2002; Nishimura, 2006) and construction components (Riedel and Nickel, 1999). Flax, hemp and jute have been employed for clothing, domestic woven fabrics and ropes for thousands of years. Therefore a significant proportion of this chapter is devoted to these industrial fibres.

## 2.2 Categorization of plant fibres

Plant fibres composed of single cells are hollow and cylindrical and relatively short (up to 65 mm) with tapering ends. Cotton, kapok and akund, all seed fibres, are examples and the single cells are termed 'ultimate fibres'. The majority of plant fibres are multicellular, containing close-packed arrays of ultimate fibres rather like the longitudinal cells in wood, and these plant fibres should strictly be termed 'fibre bundles' (Farnfield, 1975; Vincent, 2000). Mechanical fibre bundles (i.e., with significant mechanical strength) are extracted from either plant stems (e.g., hemp, jute, flax, kenaf, ramie, also known as 'bast' fibre bundles), leaves (e.g., sisal, henequen, pineapple) or fruiting bodies (e.g., coir and palm empty fruit bunch) and are up to 300 mm in length. Once extracted from the plant and processed, fibre bundles are usually irregular in cross-section, with considerable variations in the number of ultimate cells often depending on the severity of the extraction process. Plant fibres are classified in terms of their fibre type, botanical name, family, origin and approximate level of production in Table 2.1.

## 2.3 Composition and structure of plant fibres

The chemical compositions of selected plant fibres are listed in Table 2.2 and the principal constituents are cellulose, hemicellulose, lignin and pectin. The fibres are represented in groups corresponding to their origin as seed (s), bast (b), leaf (l) or fruit (f) fibres. Plant fibres (termed lignocellulosic)

Table 2.1 Classification of plant fibres and approximate world annual production, modified from Mwaikambo (2006)

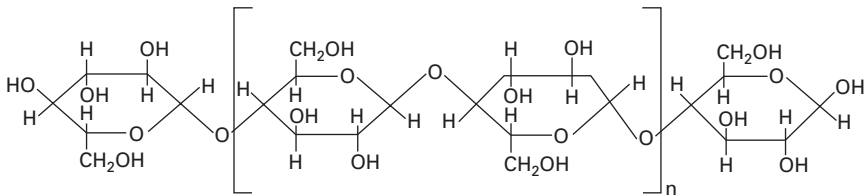
Plant fibre	Botanical name	Plant family	Fibre type	Production (10 <sup>3</sup> tonnes)
Cotton	<i>Gossypium</i> spp.	Malvaceae	Seed	19 010
Kapok	<i>Eriodendron anfractuosum</i>	Bombacaceae	Seed	123
Bagasse	<i>Saccharum officinarum</i> L.	Gramineae		
Bamboo	<i>Gigantochloa scortechinii</i> <i>Dendrocalamus apus</i>	Linaceae	Bast	10 000
Flax	<i>Linum usitatissimum</i>	Linaceae	Bast	830
Hemp	<i>Cannabis sativa</i> L.	Cannabaceae	Bast	214
Jute	<i>Corchorus capsularis</i>	Tiliaceae	Bast	2938
Kenaf	<i>Hibiscus cannabinus</i>	Malvaceae	Bast	970
Ramie	<i>Boehmeria nivea</i> Gaud	Urticaceae	Bast	100
Abaca	<i>Musa textilis</i>	Musaceae	Leaf	91
Banana	<i>Musa ulugurensis</i> Warb.	Musaceae	Leaf	200
Phormium	<i>Phormium tenax</i>	Agavaceae	Leaf	–
Pineapple	<i>Ananas cosmosus</i> Merr.	Bromliaceae	Leaf	–
Sisal	<i>Agave sisalana</i>	Agavaceae	Leaf	319
Coir	<i>Cocos nucifera</i> L.	Arecaceae	Fruit	315



Table 2.2 Chemical composition of selected plant fibres, modified from Mwaikambo (2006)

Plant fibre	Cellulose (%)	Hemicellulose (%)	Lignin (%)	Pectin (%)
Cotton <sup>s</sup>	82–96	2–6.4	0–5	<1–7
Kapok <sup>s</sup>	13	–	–	–
Flax <sup>b</sup>	60–81	14–20.6	2.2–5	1–4
Hemp <sup>b</sup>	70–92	18–22	3–5	1
Jute <sup>b</sup>	51–84	12–20	5–13	0.2
Kenaf <sup>b</sup>	44–87	22	15–19	2
Ramie <sup>b</sup>	68–76	13–15	0.6–1	2
Banana <sup>l</sup>	60–65	6–19	5–12	3–5
Pineapple <sup>l</sup>	70–82	16–19	5–12	2–3
Sisal <sup>l</sup>	43–78	10–24	4–12	0.8–2
Coir <sup>f</sup>	43–46	0.25	45–46	3–4
Oil palm EFB <sup>f</sup>	43–63	28–33	17–19	1

<sup>s</sup>Seed, <sup>b</sup>bast, <sup>l</sup>leaf and <sup>f</sup>fruit fibres.



2.1 Molecular structure of cellulose.

derive their physical stiffness from cellulose in the form of fibrous molecular bundles known as microfibrils arranged in lamellae in the plant cell wall around a hollow core (lumen). The other major constituents, hemicelluloses and lignin, bind to the stiff microfibrils and act as the matrix phase in a cellular biological composite.

### 2.3.1 Cellulose

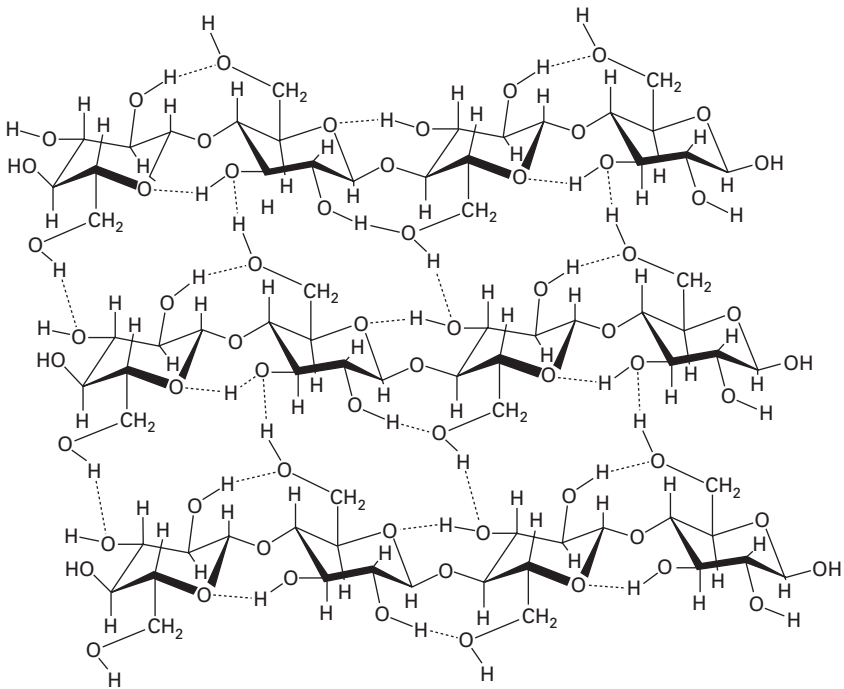
Table 2.2 demonstrates that cellulose is by far the major constituent of plant fibres but the precise composition of natural fibres depends on the method of analysis, the growth environment and geographical location of the plant, the level of maturity at the point of harvest and the position in the plant. Cellulose is a natural linear polymer (polysaccharide) with a molecular repeat unit comprised of a pair of D-anhydroglucose ring units joined by β-1→4 glycosidic oxygen linkages (Fig. 2.1) around which the molecular chain can bend and twist.

The rings are not flat but bent in a chair configuration and each successive unit is rotated through 180° with respect to the molecular axis. The molecule is unbranched and unfolded (Shenouda, 1979) and hydroxyl (-OH) groups

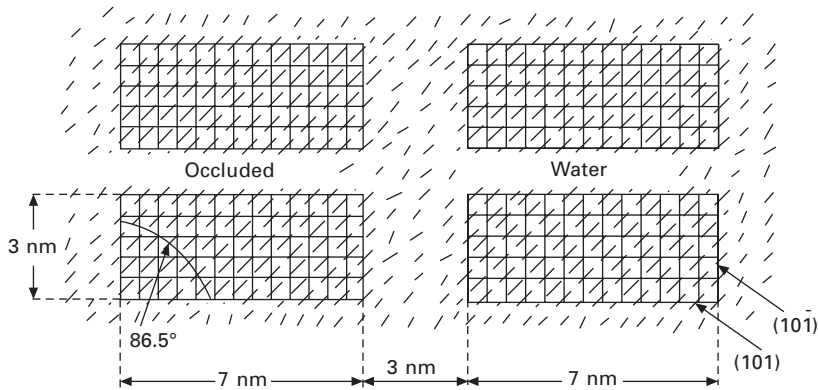
attached to the ring units can bond with hydroxymethyl ( $-\text{CH}_2\text{OH}$ ) groups on adjacent chains via hydrogen bonds to form microfibrils. Gardner and Blackwell (1974) proposed a hydrogen bonding network containing one inter-chain and also two intra-chain hydrogen bonds per cellulose unit. The linear conjoined structure is visualized in Fig. 2.2.

More recent studies of hydrogen bonding in native cellulose (Nishiyama *et al.*, 2002) using synchrotron and neutron diffraction data demonstrated that despite the high degree of crystallinity of cellulose crystals the inter-chain hydrogen bonds that keep cellulose chains aligned in sheets are inherently disorganized.

Frey-Wyssling (1954) described the fine structure of cellulose microfibrils in plant fibres such as ramie. He proposed that each microfibril contains four elementary fibrils (or micellar strands) in the form of flat filaments containing parallel arrays of anhydroglucose units. Each elementary fibril has dimensions in cross-section of 3 nm by 7 nm and the four elementary fibrils are surrounded by and separated by more randomly oriented paracrystalline cellulose molecules (Fig. 2.3), resulting in overall dimensions for each microfibril of approximately 9 nm by 20 nm.



2.2 Hydrogen bonding between cellulose chains (reproduced by permission of DoITPoMS Teaching and Learning Packages, University of Cambridge, <http://www.doitpoms.ac.uk/tlplib/wood/printall.php>).



2.3 Section through a microfibril comprised of four elementary fibrils, redrawn from Frey-Wyssling (1954).

Balashov and Preston (1955) reported on the dimensions of cellulose microfibrils from the alga *Valonia* and stated that microfibrils are flat ribbons varying in width from about 10 nm to about 35 nm and with a thickness to width ratio between 1/7 and 1/3. Evidence from electron diffraction measurements suggests that *Valonia* microfibrils are almost pure crystalline rods. The thickness of ramie, hemp, cotton, bacteria and tunicin (animal cellulose) microfibrils lies in the same range, but the internal structure of the cellulose microfibrils in these materials possesses a lower degree of crystallinity, conforming to Frey-Wyssling's model in Fig. 2.3 for ramie. The theoretical Young's modulus of cellulose microfibrils has been estimated to be as high as 250 GPa (Vincent, 1999) but the best theoretical and experimental estimates suggest values of 130–140 GPa (Eichhorn and Davies, 2006) which is the result of the less than perfect alignment of the molecules within microfibrils.

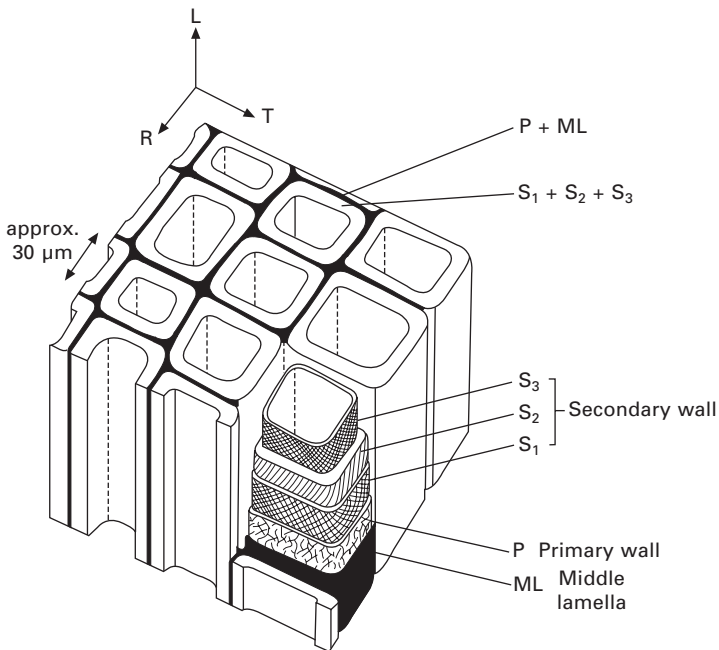
Nishino (2004) reviews the structure and properties of plant cellulose and states that microfibrils are of the order 5–30 nm in width and crystalline regions alternate with amorphous regions along the microfibril axis. Cellulose may exist in either  $I_{\alpha}$  (triclinic) form, typical of bacterial and algal cellulose, or  $I_{\beta}$  (monoclinic) form, typical of cellulose from plants and woods, the latter being more thermodynamically stable. However, plant cellulose may comprise both  $I_{\alpha}$  and  $I_{\beta}$  forms (Atalla and van der Hart, 1984) in varying ratios. In fact most algal cellulose contains some  $I_{\beta}$  content. From X-ray diffraction measurements of the stressed cellulose I lattice, Nishino and co-workers (1995) determined a crystal modulus of 138 GPa. The density of intra-molecular bonds in the plant cell wall plays a critical role in modifying the elastic modulus and calculations suggest reduced values of modulus between 60 and 75 MPa.

### 2.3.2 Effect of microfibril orientation on mechanical properties of plant fibres

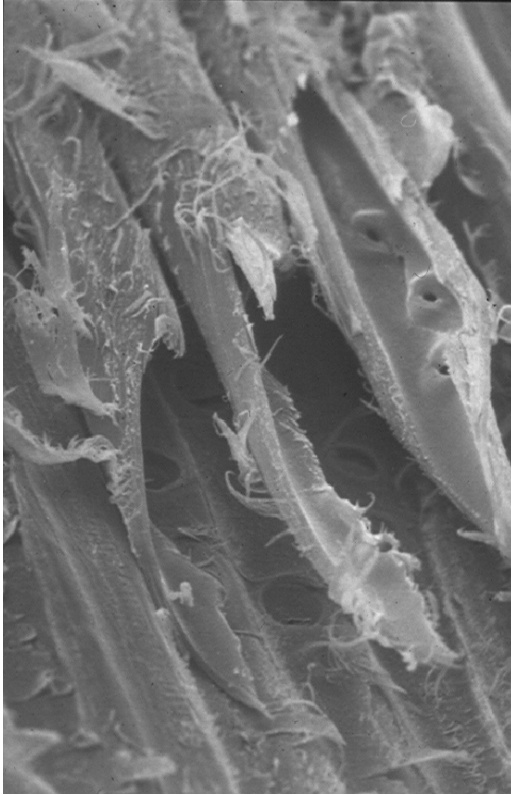
So how are cellulose microfibrils disposed in the plant cell wall? The structure of an ultimate cell (tracheid) in the earlywood of softwoods is visualized in Fig. 2.4. The structure comprises a close-packed array of ultimate cells which are closer to rectangular in section than circular and possess large lumens.

The structure of an individual earlywood cell is broken down into inter-lamellar, primary (P) wall and secondary (S) wall layers and microfibrils are drawn as solid lines. The primary wall contains randomly oriented microfibrils and the  $S_1$  and  $S_3$  layers contain cross-laminated sheaths of microfibrils. The  $S_2$  layer is unique in that the cellulose is disposed in a right-hand spiral and the thickness of this layer is much greater than that of the primary and other secondary wall layers (Dinwoodie, 2000). Hence the orientation of the microfibrils in the  $S_2$  layer will largely determine the mechanical properties of the wood. The location of spiral fractures in earlywood tracheids of Scots pine, fractured in tension, is determined by the orientation of the  $S_2$  layer (Fig. 2.5).

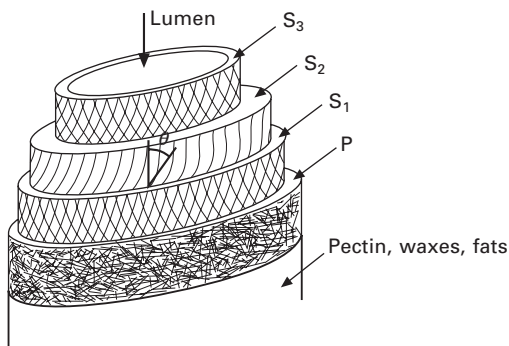
McLaughlin and Tait (1980), Aziz and Ansell (2004) and others visualize the general organization of microfibrils in the cell wall of plant fibres (Fig. 2.6).



2.4 The cellular structure of earlywood in softwoods.



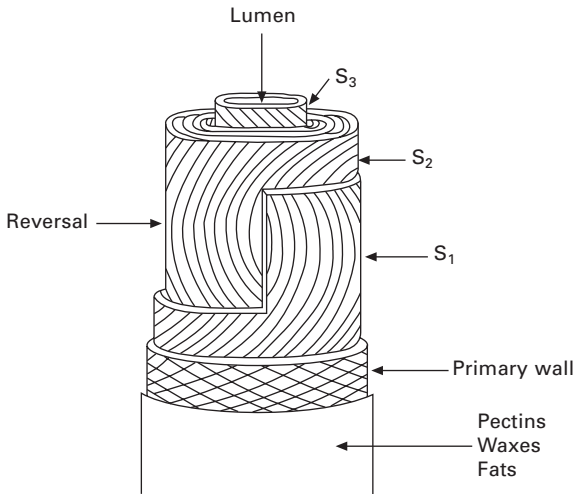
2.5 Fractured earlywood tracheids in Scots pine.



2.6 Generalized diagram of plant fibre ultimate cell (Aziz and Ansell, 2004).

In the same manner as wood, the  $S_2$  layer is thickest and the  $S_2$  microfibril angle controls mechanical properties along the fibre axis. Hence a small value for the microfibril angle (MFA) results in a high ultimate fibre modulus. The

MFA of cotton in the  $S_2$  layer is difficult to define as the microfibrils are observed to reverse their orientation within the cell wall. Morton and Hearle (1975) depict this reversal in a classic diagram, Fig. 2.7, which includes the disposition of the other cell wall layers. Khalili *et al.* (2001) and Barnett and Bonham (2004) review methods for measuring the MFA in plant cell walls. The methods are summarized in Table 2.3.



2.7 Cellular structure of cotton fibre (Morton and Hearle 1975).

Table 2.3 Methods for studying the orientation of microfibrils in the  $S_2$  layer of plant cell walls

Method	Authors
X-ray diffraction	Cave (1966) Meylan (1966) Evans <i>et al.</i> (1996) Cave and Robinson (1998)
Small angle X-ray scattering (SAXS)	Lichtenegger <i>et al.</i> (1998)
Polarized light microscopy	Preston (1934) Page (1969) Lawrence (1981)
Confocal microscopy	French <i>et al.</i> (2000)
Iodine precipitation	Bailey and Vestal (1937) Senft and Bendtsen (1985)
Inducement of cracks by UV irradiation	Huang (1995)
Measurement of pit aperture angles	Huang <i>et al.</i> (1998)
Soft rot fungi	Khalili <i>et al.</i> (2001)

The physical properties of ultimate plant fibres are compared in Table 2.4. Properties such as diameter, length and bulk density vary but in general it can be seen that bast and leaf fibres have the smallest MFAs and cotton (seed) and coir (fruit) fibres possess the highest MFAs. The mechanical properties of the ultimate fibres should depend on values of MFA. The tensile strength, Young's modulus and strain at failure of plant fibres are listed in Table 2.5.

Table 2.4 Physical properties of bast, leaf and seed fibres, modified from Mwaikambo (2006)

Plant fibre	Length of ultimates, $l$ (mm)	Diameter of ultimates, $d$ ( $\mu\text{m}$ )	Aspect ratio, $l/d$	Microfibril angle, $\theta$ ( $^\circ$ )	Density ( $\text{kg}\cdot\text{m}^{-3}$ )	Moisture content (eq.) (%)
Cotton <sup>s</sup>	20–64	11.5–17	2752	20–30	1550	8.5
Kapok <sup>s</sup>	8–32	15–35	724	–	311–384	10.9
Bamboo <sup>b</sup>	2.7	10–40	9259	–	1500	–
Flax <sup>b</sup>	27–36	17.8–21.6	1258	5	1400–1500	12
Hemp <sup>b</sup>	8.3–14	17–23	549	6.2	1400–1500	12
Jute <sup>b</sup>	1.9–3.2	15.9–20.7	157	8.1	1300–1500	12
Kenaf <sup>b</sup>	2–61	17.7–21.9	119	–	1220–1400	17
Ramie <sup>b</sup>	60–250	28.1–35	4639	–	1550	8.5
Abaca <sup>l</sup>	4.6–5.2	17–21.4	257	–	1500	14
Banana <sup>l</sup>	2–3.8	–	–	11–12	1300–1350	–
Pineapple <sup>l</sup>	–	20–80	–	6–14	1440–1560	–
Sisal <sup>l</sup>	1.8–3.1	18.3–23.7	115	10–22	1300–1500	11
Coir <sup>f</sup>	0.9–1.2	16.2–19.5	64	39–49	1150–1250	13

<sup>s</sup>Seed, <sup>b</sup>bast, <sup>l</sup>leaf and <sup>f</sup>fruit fibres.

Table 2.5 Mechanical properties of plant fibres, modified from Mwaikambo (2006)

Plant fibre	Tensile strength (MPa)	Specific strength (MPa)	Young's modulus (GPa)	Specific modulus (GPa)	Failure strain (%)
Cotton <sup>s</sup>	300–700	194–452	6–10	4–6.5	6–8
Kapok <sup>s</sup>	93.3	300	4	12.9	1.2
Bamboo <sup>b</sup>	575	383	27	18	–
Flax <sup>b</sup>	500–900	345–620	50–70	34–48	1.3–3.3
Hemp <sup>b</sup>	310–750	210–510	30–60	20–41	2–4
Jute <sup>b</sup>	200–450	140–320	20–55	14–39	2–3
Kenaf <sup>b</sup>	295–1191	–	22–60	–	–
Ramie <sup>b</sup>	915	590	23	15	3.7
Abaca <sup>l</sup>	12	–	41	–	3.4
Banana <sup>l</sup>	529–914	392–677	27–32	20–24	1–3
Pineapple <sup>l</sup>	413–1627	287–1130	60–82	42–57	0–1.6
Sisal <sup>l</sup>	80–840	55–580	9–22	6–15	2–14
Coir <sup>f</sup>	106–175	92–152	6	5.2	15–40

<sup>s</sup>Seed, <sup>b</sup>bast, <sup>l</sup>leaf and <sup>f</sup>fruit fibres.

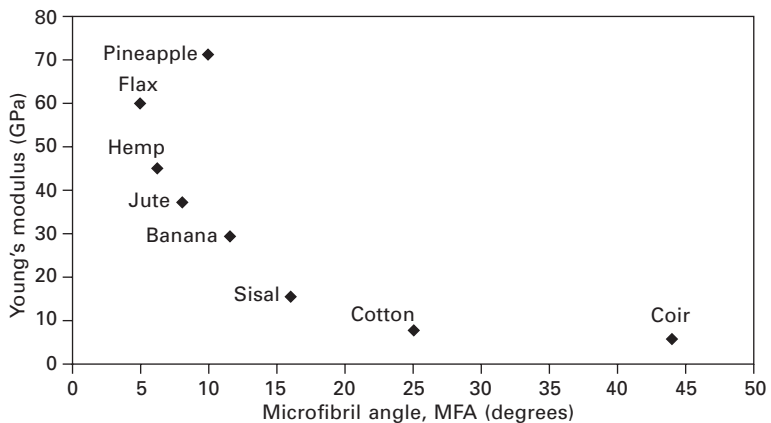
The specific tensile strength and Young's modulus (i.e. property divided by fibre specific gravity) are also listed in order to compare the properties per unit mass. In broad terms it may be seen that the fibres with the lowest microfibril angle (Table 2.4) and highest cellulose content (Table 2.2) possess the highest strengths and Young's moduli and the lowest strains at failure. McLaughlin and Tait (1980) and Mwaikambo and Ansell (2006a, 2006b) propose an equation for the axial Young's modulus,  $E_C$ , of plant fibres:

$$E_C = E_F \cos^2\theta \quad 2.1$$

where  $E_F$  is the Young's modulus of the microfibrils and  $\theta$  is the  $S_2$  layer filamentary winding angle (microfibril angle) defined with respect to the longitudinal fibre axis. In Fig. 2.8 average values of Young's modulus for ultimate fibres from Table 2.5 are plotted as a function of microfibril angle  $\theta$  from Table 2.4 and a clear trend is observed.

However, if the Young's modulus,  $E$ , is plotted versus  $\cos^2\theta$ , a linear relationship, which might have been expected from Eqn 2.1, is not observed, although  $E$  rises steeply with increasing  $\cos^2\theta$  (decreasing  $\theta$ ). Hearle (1967) proposed a modified form of Eqn 2.1 that fits data for cotton fibres. The model incorporates the Poisson effect and dimensional changes within the fibre cell wall.

In his classic book on cell wall mechanics of tracheids, Mark (1967) developed mechanical models, based on the properties of crystalline cellulose, for the wood cell wall. Cave (1968) also treated the plant cell wall as a two-phase fibre composite material and demonstrated good correlation between MFA and Young's modulus. The literature on cell wall mechanics has since



2.8 Young's modulus of plant fibres plotted versus microfibril angle (MFA).



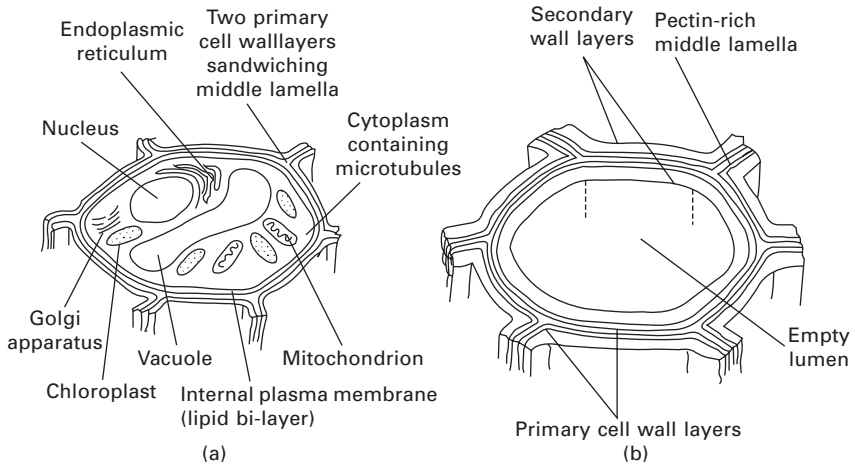
proliferated and Bruce (2003) reviewed key papers from the literature. In a publication of note, Hepworth and Bruce (2000) formulated a hierarchical model for potato tuber tissue and back-calculated the mechanical properties of cellulose ( $E = 130$  GPa) in the cell wall. They emphasized that the relationship between the molecular structure of cell wall polymers and their architecture influences not only elastic properties but also time-dependent viscoelastic behaviour, irreversible plastic behaviour and fracture of plant fibres. However, Vincent (1999) commented that irreversible plastic deformation in plant cell walls has yet to be demonstrated convincingly and that slow viscoelastic recovery is observed after apparent plastic deformation.

The mechanical properties of cotton and coir fibres are disadvantaged by their high MFA and are generally not selected for the reinforcement of natural fibre composites, whereas the lower MFAs of hemp, kenaf, sisal and jute are extensively exploited for plant fibre engineering composites. Needless to say, the excellent qualities of cotton fibres, spun into yarns and woven or knitted into flexible fibre assemblies (Hearle *et al.*, 1980) ensure their continuing application for clothing, where comfort, fineness and durability are essential factors.

### 2.3.3 The deposition of cellulose in plant cell walls

Stem cells in the vascular system of plants generate phloem and xylem cells with primary cell walls that differentiate into tracheary cells (e.g. wood tracheids) with the development of secondary cell walls. Differentiation involves cell wall thickening and stiffening (deposition of cellulose microfibrils encrusted with hemicelluloses and lignin), loss of the nucleus and finally cell death. The differences between the living plant cell and a differentiated tracheary cell are visualized in Fig. 2.9.

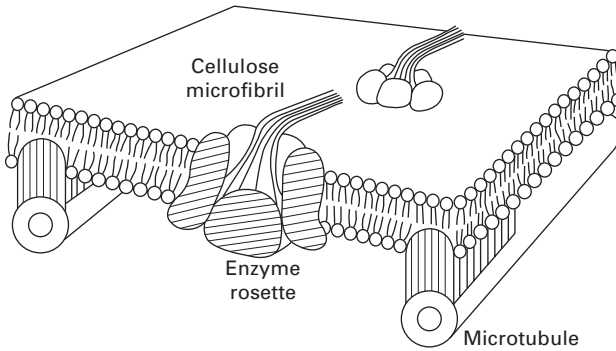
The living plant cell consists of a semi-permeable plasma membrane or plasmalemma, situated next to the primary cell wall, which envelops the liquid protoplast. The protoplast is divided into the cytoplasm and nucleoplasm (containing the nucleus or nuclei). The cytoplasm contains various types of organelle (analogous to organs in animals) including chloroplasts, mitochondria, ribosomes, the endoplasmic reticulum, Golgi apparatus and microtubules. Microtubules are associated with the production of new cell walls and are cylindrical in shape with a diameter of  $\sim 25$  nm as observed by Ledbetter and Porter (1963), who noted that the orientation of microtubules adjacent to the protoplast was the same as the orientation of cellulose microfibrils in the primary cell wall. Cellulose synthase enzyme complexes, bound into the cell membrane, are responsible for cellulose biosynthesis and according to Lerouxel *et al.* (2006) these synthases are 'the most prolific biomachines in nature'. Synthases are visible as 25–30 nm diameter rosettes in the electron microscope.



2.9 (a) Living plant cell with primary cell wall; (b) transformation to tracheary plant cell with secondary thickening.

The formation of cellulose microfibrils in the membranes of growing cells is described by Vincent (1999) and more recently by Doblin *et al.* (2002). Enzyme rosettes progress around the cell membrane, leaving behind them a trail of cellulose microfibrils approximately 5 nm in diameter containing approximately 40 molecular chains, which in turn combine into aggregated microfibrils up to 20 nm in diameter. In accordance with the Frey-Wyssling (1954) model, the cellulose microfibrils are not completely crystalline, as there are other sugars such as mannose and xylose which occupy gaps between molecular chains and the primary microfibrils. It is proposed that microfibrils organize themselves in the plant cell wall in the same manner as nematic or cholesteric liquid crystals (Neville, 1993). Because cellulose itself cannot form liquid crystals, it is reasoned that the microfibrils are surrounded by a sheath of hemicellulose which guides the process of self-assembly of aligned microfibrillar sheaths. The alignment of the microfibrils is further controlled by the orientation of microtubules in the cell cortex (Vincent, 1999), visualized in Fig. 2.10. Wasteneys (2004) suggests that microtubule organization may influence microfibril length and proposes that microtubules may modulate signalling pathways as plants respond to sensory inputs from the environment.

Emons and Mulder (2000) describe the spinning out of microfibrils from ~25 nm diameter rosettes in the plant cell wall. The microfibrils are organized into cell wall textures, including axial, transverse, crossed, helicoidal (staircase-like) and random textures, and cortical microtubules determine the orientation of the microfibrils in the growing plant cell wall. Emons and Mulder question the liquid crystal-like self-assembly process described by Vincent because of the size and mass of cellulose microfibrils putting them



2.10 Cellulose microfibrils formed from enzyme rosette and confined by microtubules within the cell wall (Vincent, 1999).

outside the colloidal domain. Instead they propose a geometrical model for the deposition of microfibrils which relates the deposition angle of microfibrils to the density of active synthases in the cell membrane, the distance between the microfibrils in a wall lamella and the geometry of the cell. The creation of cell wall texture is modelled mathematically and depends on the length of insertion domains for synthases, the insertion rate and the lifetime of the synthase.

In an extensive review Cosgrove (1997) describes the synthesis of cellulose microfibrils in the cell wall as a self-assembly process. Matrix polymers are secreted into the cell wall by the Golgi apparatus and integration with the microfibrils occurs. The expansion of the cell wall as it grows is the result of stress relaxation and creep in the flexible membrane mediated by proteins called expansins. This wall loosening is pH dependent and the expansins are able to disconnect the non-covalently bonded hemicelluloses, such as xyloglucans, from the cellulose, allowing the cell wall to expand driven by cell turgor. Cell wall loosening by expansins is further described by Cosgrove (2000) in a review paper. In future, genetics will play a major role in reengineering plant cell walls and will improve the understanding of plant cell wall growth and expansion.

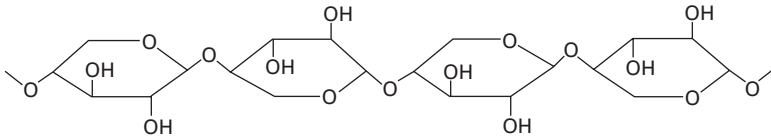
Exciting research on the epitaxial nanodeposition of cellulose I microfibrils onto fixed, nematic ordered substrates (Kondo *et al.*, 2002) demonstrates the advent of new methodologies for the design of functional nanomaterials.

### 2.3.4 Hemicellulose, lignin and pectins

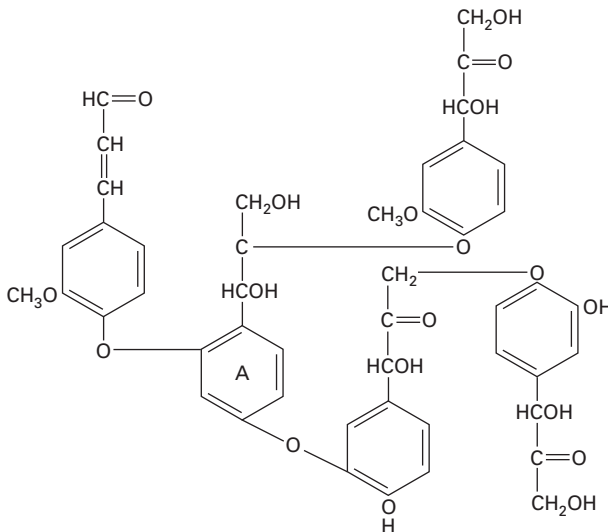
**Hemicelluloses** are linear or branched polymers and are essentially amorphous due to the many side groups attached to their heteropolysaccharide structures which contain sugar residues including xylans, mannans, arabinans and galactans (Heredia *et al.*, 1995). The second biggest constituent of plant fibres

is the hemicellulose  $\beta$ -1 $\rightarrow$ 4-D-xylan (Fig. 2.11) constructed from  $\beta$ -1 $\rightarrow$ 4-linked D-xylopyranosyl residues forming the linear backbone chain. The hemicelluloses are more closely associated with lignin than  $\alpha$ -cellulose and they constitute 30–40% of the dry weight of the plant cell wall. Hemicelluloses are much smaller molecules than cellulose, comprising of the order of 200 sugar units in contrast to 7500 to 15 000 sugar units in a cellulose molecule. Cell wall polysaccharides such as hemicelluloses are thought to assemble on the cellulose framework according to genetic evidence (Somerville *et al.*, 2004), so biogenesis of plant cells is driven by cellulose synthesis as described in Section 2.3.3 above.

**Lignin** is comprised of oxyphenolpropane units which form a 3-D polymer structure (Fig. 2.12), free-radical polymerized from cinnamyl alcohols. Reaction of lignin monomers with the lignin polymer may either extend the molecular chain or form crosslinks. In Fig. 2.12 the monomer unit labelled A has three functional groups linked to other monomer units and hence may form branches or crosslinks. Lignin and hemicellulose act as cementing phases for cellulose. Hence the structure of plant cell walls can be envisaged



2.11 Hemicellulose  $\beta$ -1  $\rightarrow$  4-D-xylan.

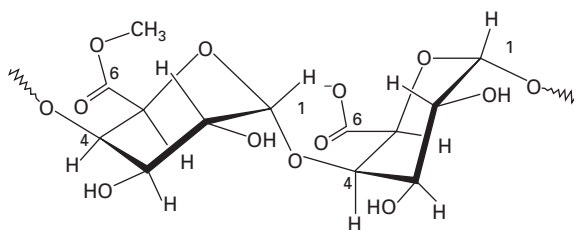


2.12 Example of a lignin polymer.

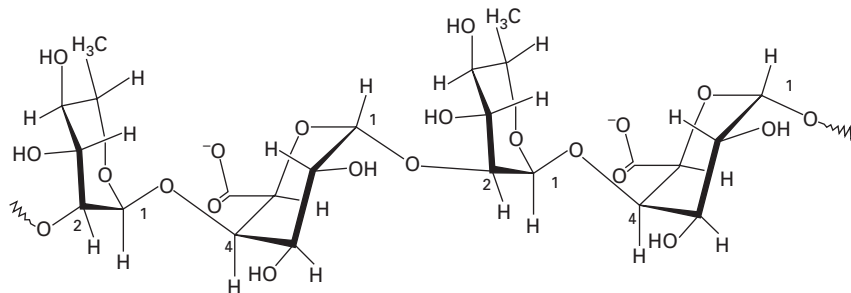
as a series of concentric layers of helically oriented cellulose microfibrils crosslinked by hemicellulose and lignin molecules. Unlike cellulose and hemicelluloses based on carbohydrate units, lignin performs the key role of repelling water and its glass transition temperature is reported to be 142°C by Thielemans *et al.* (2002).

**Pectins** occur in plant tissue and together with hemicelluloses and lignin form the cell wall ‘matrix’ for the cellulose microfibril ‘fibres’ in the manner of a synthetic composite. The pectins are concentrated in the middle lamellar and primary cell wall zones (Figs 2.6 and 2.7) as a space-filling hydrophilic gel (Cosgrove, 1997). The removal of pectins within fibre bundles such as those derived from flax and hemp is responsible for separating the bundles into ultimate fibres. Pectins are also located between microfibrils as a space-filling hydrophilic gel. Beleski-Carneiro *et al.* (2000) state that pectins are polymers comprised of polysaccharides mostly derived from partially methylated poly- $\alpha$ -(1 $\rightarrow$ 4)-galacturonic acid residues (Fig. 2.13) which are termed ‘smooth’. In addition there are ‘hairy’ zones along the molecular chain comprising alternating  $\alpha$ -(1 $\rightarrow$ 2)-L-rhamnosyl and  $\alpha$ -(1 $\rightarrow$ 4)-D-galacturonosyl sections containing branch points (Fig. 2.14) to which mostly neutral side chains of mainly L-arabinose and D-galactose are attached.

Pectins are extended and curved with a worm-like disposition and the ‘hairy’ regions are even more convoluted. They are commercially important because of their ability to form gels, for example in fruit preserves.



2.13 Poly- $\alpha$ -(1  $\rightarrow$  4)-galacturonic acid.



2.14 Alternating  $\alpha$ -(1  $\rightarrow$  2)-L-rhamnosyl and  $\alpha$ -(1  $\rightarrow$  4)-D galacturonosyl units.

## 2.4 Structure of seed fibres: cotton, kapok and akund

Cotton, kapok and akund are unicellular, elongated seed fibres. Cotton is by far the most commercially important of all plant fibres, used worldwide for the production of soft, breathable textiles. In contrast, the market for kapok and akund, mostly for fillings for mattresses and pillows and insulation products, is small and declining. Hence the majority of this section is devoted to cotton, which has been the subject of continuous intensive research into the morphological development of its cell wall and its genetic identity, leading to large-scale genetic modification to reduce heavy reliance on pesticides. The structure and properties of kapok and akund fibres are reviewed in Section 2.4.4.

### 2.4.1 Source and production of cotton fibres

Cotton plants (*Gossypium* sp.) are grown in tropical and sub-tropical regions of the world, including North and South America, Turkey, India and Africa between the latitudes of 40° south and 40° north. They are tetraploid which means that they contain four sets of chromosomes in the cell nucleus. Tetraploid plants grow tall and thrive in competition with other plants, especially when farmed in succession. Nearly all the cotton produced commercially is from the species *Gossypium hirsutum* and *Gossypium barbadense*, native to the Americas. Seeds are removed from the cotton boll (fibre plus seed cases) in the ginning process. Extracted fibres contain a very high proportion of cellulose (~95%) and there is less than 10% weight loss in the fibre extraction process. *Gossypium hirsutum* fibres range in length from 22 to 30 mm and are 11 to 22 µm in diameter. Hence their length is 1000 to 3000 times their diameter (Kim and Triplett, 2001). *Gossypium barbadense* fibres reach a length of over 60 mm and the length of a single cell is approximately 1200 times its diameter (Anderson and Kerr, 1938). After drying, the cylindrical fibres collapse into flat, twisted and kinked ribbons which can interlock when spun to form yarn which is the basis of cotton textiles. The commercial importance of cotton as a crop is reflected in the approximately 90 m bales ( $2 \times 10^{10}$  kg) that were harvested in 2001. The major cotton-producing nations planted 12% of their land with transgenic (genetically modified by recombinant DNA methods) cotton in 2001 (Kim and Triplett, 2001).

### 2.4.2 Development of cotton fibre morphology

Graves and Stewart (1988) describe cotton fibres as single elongated cells that develop from epidermal cells of the ovule (as the cells are not part of the vascular tissue they should strictly be termed trichomes). The differentiation of

epidermal cells into fibre cells occurs during an initiation phase approximately three days before anthesis, i.e. opening of the cotton flower. This phase is followed by initial primary cell wall elongation and the synthesis of secondary cell wall components, mainly cellulose, in a rapidly changing and dramatic manner over a period of approximately 40 days. As the cotton fibre grows, the cell wall takes up a larger proportion of its cross-sectional area and the size of the lumen decreases. The maturity ratio  $\theta$  is defined as the ratio of the cell wall area to the sectional area of the total cell.

Seagull (1992) followed changes in development of the cotton fibre cell wall *in vitro* at various days post-anthesis (DPA) by examining changes in microtubule arrays (see Section 2.3.3) and orientation of microfibrils. He noted three key points of development of the cell wall. The first change occurs at the transition from fibre initiation to elongation when microtubules reorient and order themselves. The second point is a transition between primary and secondary wall synthesis when shallow-pitched microtubule helices become steeply pitched. The third point is the four-fold increase in the number of microtubules early in secondary wall synthesis. The microtubules enforce order in the microfibrils, but the microfibrils also interact with each other, resulting in curving patterns of deposition and reversal of orientation of microfibrils. As the cell wall is predominantly comprised of cellulose molecules, hydrogen bonding between molecular chains influences the reversal of microfibrils in the cotton cell wall. Fifty or more reversals may occur in a single fibre. Kim and Triplett (2001) suggest that without these reversed zones the mature fibre would not twist when dried and it would not be possible to spin the fibres into yarns. However, spinnability may be a function of cellulose content. For example, akund and kapok fibre are difficult to spin because of their low cellulose content.

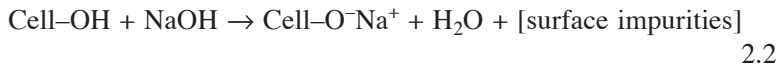
#### 2.4.3 Evidence for microstructure of cotton based on chemical modification

Evidence for the cell wall structure of cotton has been traditionally gained by chemical means, for example by treatment with acids or staining. Anderson and Kerr (1938) describe how pectins in the primary cell wall stain deeply with ruthenium red and the secondary cell wall remains colourless. The pectins are thought to mask the presence of cellulose in the primary cell wall, which may normally be detected by solubility in cuprammonia and a characteristic reaction with chlorozinc iodide or potassium triiodide and sulphuric acid. However, after removal of pectins with boiling dilute oxalic acid the cellulosic skeleton that remains may be dissolved in cuprammonia and the characteristic reactions confirm its presence. In addition X-ray diffraction confirms the presence of  $\beta$ -cellulose before and after chemical treatment. Staining the primary plant cell wall with Congo red or chlorozinc

iodide also renders cellulose microfibrils visible in the optical microscope (Anderson and Kerr, 1938).

The secondary cell wall contains a far higher proportion of cellulose than the primary cell wall. Swelling with suitable reagents, including cuprammonium solution, reveals the concentric nature of the lamellar secondary cell wall. The cellulose layers (or growth rings) vary in thickness (0.14–0.3  $\mu\text{m}$ ) depending on the time of day or stage of the growth season. Under conditions of constant temperature and illumination the growth rings disappear. If the temperature is varied artificially the development of growth rings may be controlled, so it can be concluded that the rings are the result of the daily cycle of variations in temperature and light experienced by the growing plant. Bailey *et al.* (1963) described the penetration of the wet cotton cell wall by the polymerization of methyl methacrylate causing the separation of microfibril lamellae which were found to be of the order of five microfibrils thick ( $\sim 1 \mu\text{m}$ ).

The practice of mercerizing cotton with strong solutions of caustic soda allows enhanced uptake of dyestuffs and controls texture. Impurities such as waxes and oils are removed and microfibrils become swollen and are revealed. The reaction of caustic soda is thought to proceed as follows:



Native cellulose I is converted to cellulose II at the fibre surface with a reduction in the length of crystallites and the degree of crystallinity and hence an increase in amorphous content. Transformation pathways between cellulose and Na-cellulose are proposed by Sarko *et al.* (1987). The microfibrillar structure becomes swollen and is ultimately disrupted at high caustic soda concentrations. Reactive sites are produced in the cell wall which will enhance moisture uptake or allow effective chemical bonding with adhesives in engineering composites. In order to stabilize the cell wall and reduce moisture uptake, alternative chemical treatments such as acetylation with acetic anhydride (Rowell, 1992) may be employed.

#### 2.4.4 Structure of kapok and akund fibres

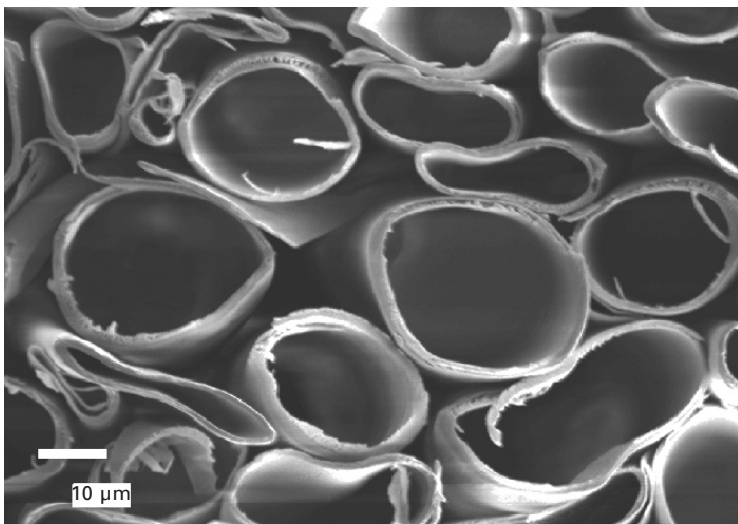
Kapok fibre is obtained from the seed pods of the tropical kapok tree (*Ceiba petandra*) which is a natural hybrid between Var. *caribaeae* and Var. *guineensis* (Purseglove, 1987). It is a native to West Africa, Mexico, the Central Americas and the Caribbean and has been introduced into India and the Far East. The unicellular fibre is very light and buoyant and is resistant to moisture uptake. Unlike cotton it does not collapse and twist on drying and has a low cellulose content, hence it cannot be easily spun together into yarn and woven. Bisanda and Mwaikambo (1997) report that a mixture of



kapok and cotton has been spun at a ratio of 2:3. The open kapok seed pod is brown in colour and the black seed is contained within the loose mass of white fibre. The major applications for the fibre are as down filling for mattresses, pillows, upholstery and toys and for thermal insulation.

A cross-section through a number of kapok fibres is presented in Fig. 2.15. The fibres, although slightly compressed together in this image, have not collapsed after drying and are thin-walled ( $\sim 2 \mu\text{m}$  thick) with a diameter of the order of  $22 \mu\text{m}$  and a length of approximately 20 mm. Similar seed fibres include dandelion and thistle fibres. The fibres possess low cellulose content (Table 2.2), apparent density (Table 2.3) and strength (Table 2.4). Khalili *et al.* (2000) used soft rot fungi to study the microstructure of the cell wall of *Ceiba pentandra* and observed two cell wall layers. The outer layer has microfibrils oriented transversely to the fibre axis, while microfibrils in the inner layer are oriented nearly parallel to the fibre axis. Evidence of these orientations is provided by Nilsson and Björdal (2008) who incubated kapok fibres with erosion or tunnelling bacteria.

Akund is a single-cell fibre (Kirby, 1963; Perry, 1975) obtained from *Calotropis procera* and *Calotropis gigantea*, members of the botanical family *Asclepiadaceae*. The fibre is sometimes referred to as vegetable floss or silk. It is fine, soft and lustrous, but very weak, and hence like kapok it is rarely used by itself as a textile fibre. Under the microscope the fibres appear similar to those of kapok but their base does not show the net-like thickenings seen in kapok. The average length ranges from 30 to 40 mm and the average diameter is around  $20 \mu\text{m}$ . Akund exhibits inferior buoyancy and



2.15 Cross-section through kapok fibres.

resistance to water absorption, thus it cannot be used as filler for products such as lifebelts.

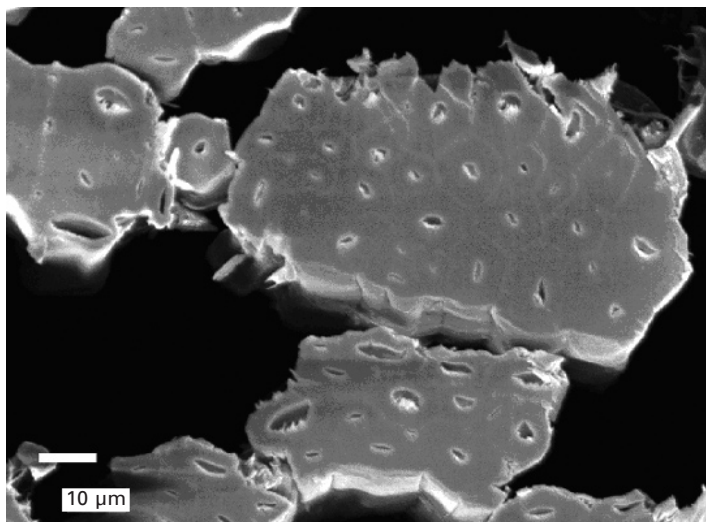
## 2.5 Structure of bast fibre bundles: jute, kenaf, hemp and flax

Bast fibres, also known as stem fibres, are derived from the stems or stalks of dicotyledonous plants (with two seed leaves). They are grown in temperate (e.g. hemp, flax and nettles), sub-tropical (e.g. jute) and tropical (e.g. kenaf) climates. To distinguish them from 'hard' leaf fibres they are often termed 'soft', which is a misnomer in terms of the mechanical properties for fibre bundles listed in Table 2.4. The term bast, or bark, is related to the phloem tissue of vascular plants but also to fibres found in the cortex and pericycle. Bast fibres are comprised of elongated, thick-walled ultimate fibres joined end to end and side by side axially along the stem. After harvesting, the bast fibres and bark (collectively the cortex) are removed from the stem by a mechanical decorticating process, based on a rotating wheel set with blunt knives which shears the fibres away from softer tissue, and the fibres are then washed and dried. The structures of four representative bast fibres with commercial importance are reviewed below.

### 2.5.1 Jute fibre

After cotton, jute is the most widely produced plant fibre, followed by flax and hemp, but it has a higher lignin content than flax and hemp (see Table 2.2). Jute is grown in hot (20–40°C) and humid (70–80% RH) climates in Bangladesh, India, China and Thailand where it reaches 2.5–3 m in height within a timescale of 4–6 months. The best area for growing the highest quality jute is the Bengal Delta. The variety *Corchorus capsularis* has a globular-shaped pod, while *Corchorus oliotorus* has cylindrical pods. The time of harvesting of plant fibres is critical in terms of maximizing quality (e.g. tenacity) and jute is harvested when approximately half of the crop is in pod. The fibre bundles are separated from the stem by the retting process, which takes place in low running water. Enzymes secreted by micro-organisms break down the non-cellulosic, interlamellar material between the ultimate fibres, which is rich in pectins (Sharma, 1987). The weight of dried fibre is in the range of 4.5–8% of the weight of the green plant. The resulting fibre bundles are irregular in shape with small lumens. A cross-section through typical fibre bundles is presented in Fig. 2.16. Ultimate fibres are 5–20 µm in diameter and the size of the bundles varies considerably.

Heyn (1966) prepared jute fibres (*Corchorus capsularis* L.) by swelling in water for several hours and an aqueous solution of uranyl acetate was used for staining the fibre. The uranyl acetate leaves the cellulose microfibrils

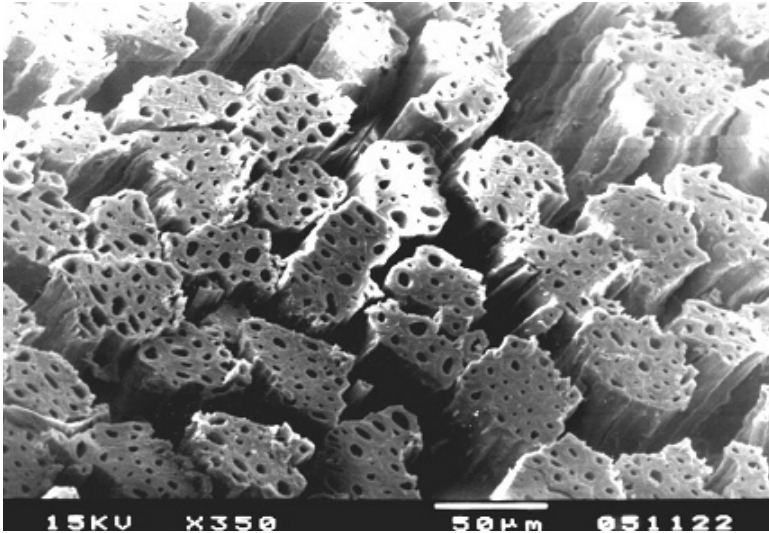


2.16 Cross-section through jute fibre bundles.

unstained on a stained background of amorphous phases (negative staining). Specimens were freeze-dried and sectioned for examination in the transmission electron microscope (TEM). The lateral width of the jute microfibrils was observed to be  $2.8 \pm 0.3$  nm, corresponding to dimensions determined by SAXS measurements. Heyn was able to observe amorphous zones in the microfibrils corresponding to less crystalline or tangled zones described by Nishino (2004) and many others.

### 2.5.2 Kenaf fibre

Kenaf (*Hibiscus cannabinus* L.) is related to cotton and is grown wild in Africa (Guinea hemp), and cultivated in Brazil, the Indian sub-continent, Cuba and south and south-west United States. The plant grows to about 5.5 m high in 4–5 months and fibre is concentrated in the lower part of the stem. The outer bast fibre comprises ~40% of the stalk's dry weight and the fibres are similar in quality to the best softwood fibres and are made into paper products (Sabharwal *et al.*, 1994). Either retting and hand stripping or mechanical separation is used to isolate the bast fibres into ~0.9 m lengths, with a pale, lustrous appearance and strength comparable to jute. Kenaf is used for paper-making, cordage and carpet-backing. The Toyota (Nishimura, 2006) and Proton car companies use kenaf as reinforcement for natural fibre composites. Kenaf fibre bundles are viewed in Fig. 2.17.



2.17 Kenaf fibre bundles.

### 2.5.3 Hemp fibre

Hemp (*Cannabis sativa*) is a centuries-old source of fibre for rope, sails and clothing and is grown in Russia, Eastern Europe and increasingly in Western Europe, including the UK. It is a tall leafy plant (1.5–4 m) with strong fibrous stalks and is best grown in well-drained soils. The outer portion of the hemp stem produces strong bast fibres with high cellulose content. Monoecious plants bearing male and female flowers produce better fibre than dioecious plants. The separation of bast fibres is achieved by dew retting in the field, which can be unreliable, so retting in water tanks is an alternative. The fibre bundles are 30–90 cm in length and 5–17  $\mu\text{m}$  in diameter. Ebskamp (2002) describes the processing of hemp and flax fibre bundles and proposes that fibre quality can be improved by controlled chemical or enzymatic treatment during retting and an improved understanding of the genes involved in cell wall metabolism. The use of cDNA microarrays to study secondary cell wall formation in hemp and flax has identified candidate genes which enhance mechanical properties of the fibre bundles or facilitate their extraction. Reduction of lignin levels could also improve the softness of the fibre and improve comfort in clothing.

### 2.5.4 Flax fibre

Flax is a field crop that can be grown and harvested within three months but the quality of the fibre is sensitive to being harvested too early, resulting in low yield, or too late, resulting in excessive lignification of the plant cell

wall and poor quality fibre. There are 15 to 40 fibre bundles in each stem and each bundle contains 12 to 40 ultimate fibres with thick walls and small lumens. Fibre bundles are separated by retting and decortication. Bos and Donald (1999) reviewed the cellular structure and mechanical properties of flax and studied the mechanical deformation of flax ultimate fibres using environmental scanning electron microscopy. They noted an  $S_2$  layer MFA of approximately  $10^\circ$ , brittle fracture in the primary cell wall and plastic deformation in the secondary cell wall.

## 2.6 Structure of leaf fibres: sisal and banana

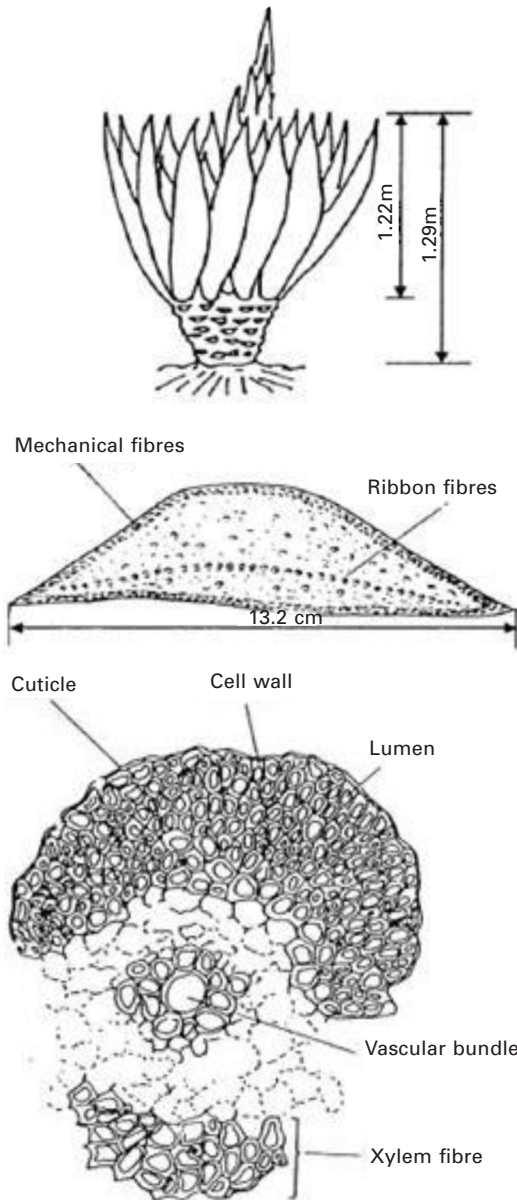
The mechanical properties of leaf fibre bundles depend on the orientation of microfibrils in the secondary cell wall. Leaf fibre bundles such as those from pineapple possess a high Young's modulus (60–82 GPa) and tensile strength (287–1130 MPa) for MFAs of 6–14°. Microfibrils are oriented along the schlerenchyma cells from the leaves of New Zealand flax (*Phormium tenax*) such that the cell wall has a Young's modulus of 70 GPa and tensile strength of 1 GPa (King and Vincent, 1996). The extraction and structure of two commercial leaf fibres are described below.

### 2.6.1 Sisal fibre

The world's sisal industries are located in tropical regions of Central and South America, Africa and Asia, especially in China. Sisal (*Agave sisalana*) was introduced into Tanzania from the Yucatan Peninsula in Mexico towards the end of the nineteenth century. The town of Sisal is located on the north coast of Mexico and the fibre is known locally as henequen (*Agave fourcroydes*). Since the 1960s the fibre has struggled to compete against synthetic fibres such as polypropylene. However, in the period 1999–2004 the world production of sisal increased by 12.7% to 252 900 tonnes. Sisal fibre is used for making ropes, as a reservoir for oil in the core of steel cables, for geotextiles and as reinforcement for cement ceiling tiles.

The sisal plant is a perennial succulent capable of producing approximately 185 leaves in its lifetime, arranged spirally around its thick stem, and each leaf contains about 1000 fibre bundles. The general form of the plant and section through the leaves is presented in Fig. 2.18 and the locations of the mechanical and ribbon fibres are indicated. The leaves are 61–122 cm long, 10–20 cm wide and 2.5–10 cm thick. Following decortication the leaves are dried, combed and sorted into grades. Long fibre bundles (>90 cm) are used for rope making and are ideal for the manufacture of fibre-based composites.

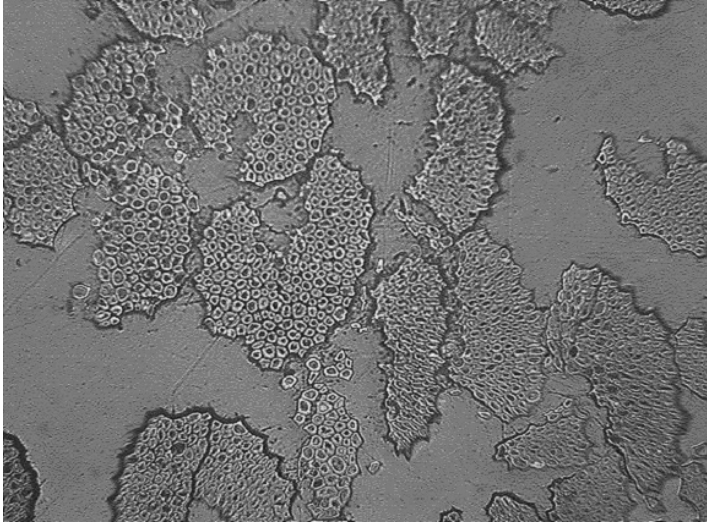
A cross-section of sisal fibre bundles mounted in resin and sectioned for optical microscopy (Fig. 2.19) demonstrates the typical variability of plant



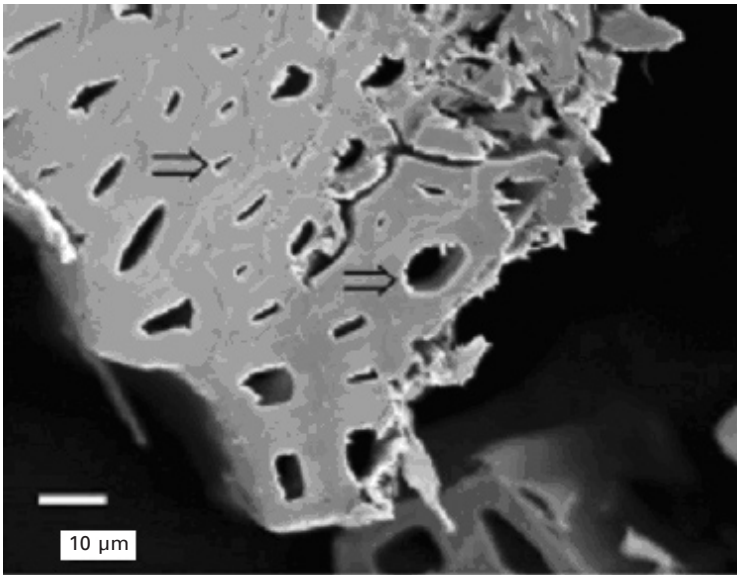
2.18 The sisal plant, section through a sisal leaf and section through a mechanical fibre (Bisanda, 1991).

fibres. Scanning electron microscopy of a fibre bundle cross-section (Fig. 2.20) reveals the irregularity of the fibre bundle and considerable variation in the size of the lumens (arrowed). A SEM image of a fibre bundle fractured in



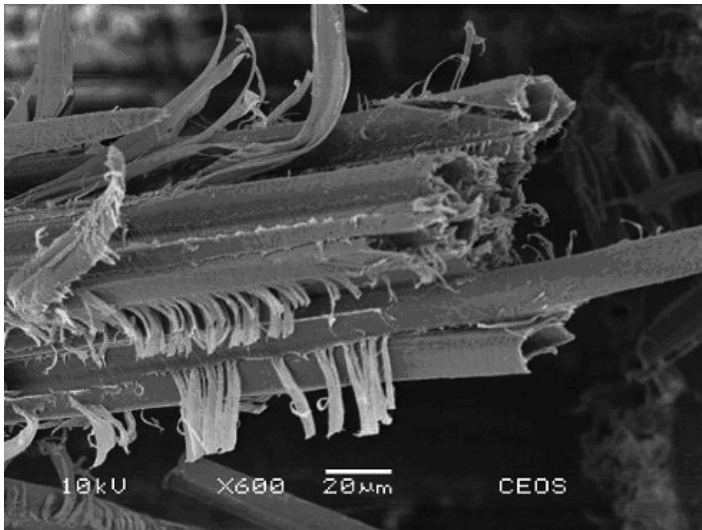


2.19 Cross-section of sisal fibre bundles (Towo and Ansell, 2008).



2.20 SEM image of cross-section through sisal fibre bundle (Mwaikambo and Ansell, 2006a).

tension (Fig. 2.21) reveals microstructural features of the cell wall. A helical cell wall fracture is seen at the top right of the image and microfibril sheaths have been pulled out of the ultimate cell walls.



2.21 Sisal fibre bundle fractured in tension (Towo, 2006).

### 2.6.2 Banana leaf fibre

The most cultivated banana plant is *Musa paradisiaca* L. var *Sapientum* or *Musa ulugurensis* Warb, although there are about 300 species in total. Leaves are up to 3 m long and 60 cm wide. The best fibres are produced just before the flowering stage when no fruit has formed. At this stage chunks of leaf are passed through a mangle to remove moisture and the fibre residues are dried and combed. If the leaves are left until after the fruit has ripened they are of inferior quality. Banana fibre has been used in Japan since the thirteenth century for the production of kimonos. Kulkarni *et al.* (1983) evaluated the mechanical properties of fibre bundles (diameter 50–250  $\mu\text{m}$ ) from banana leaves. Ultimate fibres with diameters in the range 18–30  $\mu\text{m}$  have cell wall thicknesses of about 1.25  $\mu\text{m}$ . The ultimate fibre lengths range from 2.7 to 5.5 mm, resulting in an aspect ratio of around 150. The MFA is of the order 11–12° and the mechanical properties are listed in Table 6.5. Strength is a function of the number of ultimate fibres in each bundle, the density of defects and strain rate; microfibrillar sheaths pull out of the cell wall at low strain rates.

## 2.7 Structure of fruit fibres: coir and oil palm empty fruit bunch

Fruit fibres generally perform a protective role and are characterized by high MFAs and coarse structure. The coconut and oil palm industries produce



very high volumes of fruit fibre so the structure, properties and application of these fibres are reviewed here.

### 2.7.1 Coir fibre

Coir is obtained from the fruit of the coconut palm (*Cocos nucifera*). The fibre-bearing tissue is located in the zone between the exocarp and the endocarp enveloping the kernel. The coconut palm is grown in the Indo-Malaysian region, in Central and South America and in West African countries. There are three types of fibre, namely the long and fine 'white' fibre, coarser brittle fibre and shorter staple 'mattress' fibre. The latter two are known as 'brown' fibres and are used for doormats and mattress filling. White fibre is suitable for making rope and fishing nets. Fibre bearing tissue is broken down into fibre bundles either by retting over a period of 3–9 months or by decortication. McLaughlin and Tait (1980) note that the microfibril angle of coir fibres lies in the range 30–35° and they fail at very high strains of 15–30%. They fail with the uncoiling of microfibrils in the cell walls of adjacent ultimate fibres. Martinschitz *et al.* (2008) characterized dry coir fibres using in-situ synchrotron radiation and noted an initial MFA of about 45° decreasing linearly under strain until failure to about 30° at 35% strain. Sreenivasan *et al.* (1996) examined the fine structure of coir fibres and used a high concentration of caustic soda to evaluate the spiral structure of microfibrils which have a MFA of about 40° in the as-received state. After swelling in water and stretching, the MFA can be reduced to 34° due to slight plasticization of the cell wall. After caustic soda treatment, which removes non-cellulosic material, followed by stretching, the MFA can be reduced to 10°. Kulkarni *et al.* (1983) comment that the coir ultimate fibres have diameters in the range 13–14 µm and cell wall thicknesses range from thin-walled (~1 µm) up to 8 µm.

### 2.7.2 Oil palm empty fruit bunch fibre

The oil palm (*Elaeis guineensis*) originated in the tropical forest of West Africa but is now exploited as a major oil crop by countries such as Malaysia and Indonesia. Fibrous materials left after milling include the oil palm empty fruit bunch (OPEFB), a coarse aggregate of fibrous material that protects the fruiting body. Each empty fruit bunch yields about 400 g of fibre. The fibres are traditionally used for stuffing mattresses but are currently being used as filler for thermoplastics in injection-moulded components in countries such as Malaysia.

Sreekala *et al.* (1997) evaluated the structure and properties of OPEFB fibre in the untreated state and following mercerization, silane treatment and acetylation. The cellulose content of the untreated fibre was found to be 65%

compared with 32–43% for coir. The untreated ultimate fibres were  $\sim 10 \mu\text{m}$  in diameter and the highly textured and grooved surface contains pores with an average diameter of  $0.07 \mu\text{m}$ . The microfibril angle of the OPEFB fibre was determined to be  $42^\circ$  by calculation. Law *et al.* (2007) examined the structure of OPEFB fibres and reported an average ultimate fibre diameter of  $19.1 \mu\text{m}$  and fibre bundle diameter of the order  $200\text{--}300 \mu\text{m}$  with a cellulose content of 62.9%. The surface of fibre bundles is pock-marked with numerous silica bodies and they propose that siliceous pathways link the bodies to the interior of the fibre bundle.

## 2.8 Conclusions

It is clear from the examination of the structure and properties of plant fibres that there are many similarities between seed, bast, leaf and fruit fibres in terms of their molecular constitution and the arrangement of cellulose microfibrils in a matrix of hemicelluloses, lignin, pectin and waxes. Single-cell seed fibres such as cotton and kapok differ from fibre bundles such as hemp and jute which comprise aggregations of ultimate fibres. The shape of fibre bundles depends on the extraction process, which may be mechanical, chemical or a combination of both. Plant fibres may often be spun and woven into fabrics, unlike wood tracheids, which have a similar structure to plant fibre ultimate cells. The structure and shape of microfibrils are well characterized as flat or flattish arrays of  $\beta$ -cellulose chains which spiral around the cell wall, but the processes of self-assembly of these secondary helical structures from primary cell walls is still a matter of debate and conjecture. However, microtubules play a major role in determining the orientation of microfibrils.

Cotton is a super-cell with very high cellulose content, and the orientation of microfibrils reverses in the cell wall lamellae so the microfibril angle (MFA) is variable. Most of the other plant fibres considered here have well-defined MFAs and there is a good correlation between low microfibril angles and high strength and stiffness. The Young's modulus of fibre bundles, for example flax ( $50\text{--}70 \text{ GPa}$ ) and pineapple ( $60\text{--}82 \text{ GPa}$ ), are remarkably high as a proportion of the Young's modulus of cellulose microfibrils ( $130\text{--}140 \text{ GPa}$ ) and significantly higher than values for wood tracheids ( $\sim 6\text{--}20 \text{ GPa}$ ). These high values of Young's modulus are a result of low MFAs and high cellulose content. As a result plant fibres are being exploited as reinforcement for sustainable engineering composites (Wambua *et al.*, 2003) as a substitute for E-glass which has a Young's modulus of  $73 \text{ GPa}$ . However, the very diverse range of applications for plant fibres in textiles will continue to be their major use. The literature on plant fibres is immense and ever expanding and new developments in understanding structure–property relationships are eagerly awaited.

## 2.9 References and further reading

- Aksoy, AM and Beghin, JC (eds) (2004), *Global Agricultural Trade and Developing Countries*, World Bank Trade and Development Series, Washington, DC.
- Anderson, DB and Kerr, T (1938), 'Growth and structure of cotton fiber', *Industrial and Engineering Chemistry*, **30**, 48–54.
- Atalla, RH and van der Hart, DL (1984), 'Native cellulose – a composite of two distinct crystalline forms', *Science*, **223**, 283–285.
- Aziz, SH and Ansell, MP (2004), 'Optimising the properties of green composites', Chapter 8 in *Green Composites – Polymer Composites and the Environment*, ed. Baillie, C, Woodhead Publishing, Cambridge, UK.
- Bailey, IW and Vestal, MR (1937), 'The orientation of cellulose in the secondary walls of tracheary cells', *Journal of the Arnold Arboretum*, **18**, 185–195.
- Bailey Jr, TLW, Tripp, VM and Moore, AT (1963), 'Cotton and other vegetable fibres', Chapter 12 in *Fibre Structure*, ed. Hearle, JWS and Peters, RH, Butterworth and the Textile Institute, Manchester, UK.
- Balashov, V and Preston, RD (1955), 'Fine structure of cellulose and other microfibrillar substances', *Nature*, **176**, 64–65.
- Barnett, JR and Bonham, VA (2004), 'Cellulose microfibril angle in the cell wall of wood fibres', *Biological Reviews*, **79**, 461–472.
- Beleski-Carneiro, EB, Alquini, Y and Reicher, F (2000), 'Pectins from the fruit of myrtaceae', in *Proceedings of the Third International Symposium on Natural Polymers and Composites*, ISNaPol/2000, São Pedro, Brazil, 14–17 May 2000, ed. Mattoso, LHC, Leão A and Frollini E, 162–170.
- Bisanda, ETN (1991) 'Sisal fibre reinforced composites', PhD thesis, University of Bath.
- Bisanda, ETN and Mwaikambo, LY (1997), 'The potential of kapok fibre as a replacement for cotton in textiles', *Journal of Agriculture, Science and Technology*, **1**, 66–71.
- Bos, HL and Donald, AM (1999), 'In situ ESEM study of the deformation of elementary flax fibres', *Journal of Materials Science*, **34**, 3029–3034.
- Bruce, DM (2003), 'Mathematical modelling of the cellular mechanics of plants', *Philosophical Transactions of the Royal Society of London B*, **358**, 1437–1444.
- Cave, ID (1966), 'X-ray measurement of microfibril angle', *Forest Products Journal*, **16**, 37–42.
- Cave, ID (1968), 'The anisotropic elasticity of the plant cell wall', *Wood Science and Technology*, **2**, 268–278.
- Cave, ID and Robinson, W (1998), 'Measuring microfibril angle distribution in the cell wall by means of X-ray diffraction', in *Microfibril Angle in Wood: Proceedings of the IAWA/IUFRO International Workshop on the Significance of Microfibril Angle to Wood Quality*, Westport, New Zealand, ed. Butterfield, BG, University of Canterbury Press, Christchurch, New Zealand, 108–115.
- Cosgrove, DJ (1997), 'Assembly and enlargement of the primary cell wall in plants', *Annual Review of Cell and Developmental Biology*, **13**, 171–201.
- Cosgrove, DJ (2000), 'Loosening of plant cell walls by expansins', *Nature*, **407**, 321–326.
- Dinwoodie, JM (2000), *Timber: Its Nature and Behaviour*, 2nd ed, E & FN Spon, London.
- Doblin, MS, Kurek, I, Jacob-Wilk, D and Delmer, DP (2002), 'Cellulose biosynthesis in plants: from genes to rosettes', *Plant and Cell Physiology*, **43**, 1407–1420.

- Ebskamp MJM (2002), 'Engineering flax and hemp for an alternative to cotton', *Trends in biotechnology*, **20**, 229–230.
- Eichhorn, SJ and Davies, GR (2006), 'Modelling the crystalline deformation of native and regenerated cellulose', *Cellulose*, **13**, 291–307.
- Emons, AMC and Mulder, BM (2000), 'How the deposition of cellulose microfibrils builds cell wall architecture', *Trends in Plant Science*, **5**, 35–40.
- Evans, R, Stuart, S and Vandertouw, J (1996), 'Microfibril angle scanning of increment cores by X-ray diffractometry', *Appita*, **96**, 879–882.
- FAO (2001), Data from the Economic and Social Department, Commodity and Trade Division, Food and Agriculture Organisation (FAO) of the United Nations.
- Farnfield, CA (1975), *Textile Terms and Definitions*, 7th edn, The Textile Institute, Manchester, UK.
- French, J Conn, AB Batchelor, WJ and Parker, IH (2000), 'The effect of fibre fibril angle on some handsheet mechanical properties', *Appita Journal*, **53**, 210–217.
- Frey-Wyssling, A (1954), 'The fine structure of cellulose microfibrils', *Science*, **119**, 80–82.
- Gardner, KH and Blackwell, J (1974), 'The structure of native cellulose', *Biopolymers*, **13**, 1975–2001.
- Graves, DA and Stewart, JM (1988), 'Chronology of the differentiation of cotton (*Gossypium hirsutum* L.) fiber cells', *Planta*, **175**, 254–258.
- Hearle, JWS (1967), 'The structural mechanics of fibres', *Journal of Polymer Science*, **20**, 215–251.
- Hearle, JWS and Peters, RH (eds) (1963), *Fibre Structure*, Butterworth and the Textile Institute, Manchester, UK.
- Hearle, JWS Thwaites, JJ and Amirbayat, J (eds) (1980), *Mechanics of Flexible Fibre Assemblies*, Nato Advanced Study Institutes Series, Series E: Applied Sciences – No. 38, Sijthoff and Noordhoff, Alphen aan den Rijn, The Netherlands.
- Hepworth, DG and Bruce, DM (2000), 'A method of calculating the mechanical properties of nanoscopic plant cell wall components from tissue properties', *Journal of Materials Science*, **35**, 5861–5865.
- Heredia, A Jiménez, A and Guillén, R (1995), 'Composition of plant cell walls', *Zeitschrift für Lebensmitteluntersuchung und – Forschung A*, **200**, 24–31.
- Heyn, ANJ (1966), 'The microcrystalline structure of cellulose in cell walls of cotton, ramie and jute fibres as revealed by negative staining of sections', *Journal of Cell Biology*, **29**, 181–197.
- Huang, CL (1995), 'Revealing fibril angle in wood sections by ultrasonic treatment', *Wood and Fibre*, **27**, 49–54.
- Huang, CL Kutscha, NP Leaf, GJ and Megraw, RA (1998), 'Comparison of microfibril angle measurement techniques', in *Microfibril Angle in Wood: Proceedings of the IAWA/IUFRO International Workshop on the Significance of Microfibril Angle to Wood Quality*, Westport, New Zealand, ed. Butterfield, BG, University of Canterbury Press, Christchurch, New Zealand, 177–205.
- Khalili, S Daniel, G and Nilsson, T (2000), 'Use of soft rot fungi for studies on the microstructure of kapok (*Ceiba petandra* (L.) Gaertn.) fibre cell walls', *Holzforschung*, **54**, 229–233.
- Khalili, S Nilsson, T and Daniel, G (2001), 'The use of soft rot fungi for determining the microfibrillar orientation in the S2 layer of pine tracheids', *Holz als Roh- und Werkstoff*, **58**, 439–447.

- Kim, JK and Triplett, BA (2001), 'Cotton fibre growth in planta and *in vitro*. Models for plant cell elongation and cell wall biogenesis', *Plant Physiology*, **127**, 1361–1366.
- King, MJ and Vincent, JFV (1996), 'Static and dynamic fracture properties of the leaf of New Zealand flax *Phormium tenax* (Phormiaceae: Monocotyledons)', *Proceedings of the Royal Society of London B*, **263**, 521–527.
- Kirby, RH (1963), *Vegetable Fibres*, Interscience Publishers, New York.
- Kondo, T Nojiri, M Hishikawa, Y Togawa, E Romanovicz, D and Brown Jr, RM (2002), 'Biodirected epitaxial nanodeposition of polymers on oriented macromolecular templates', *Proceedings of the National Academy of Sciences*, **99**, 14008–14013.
- Kulkarni, AG Satyanarayana, KG Rohatgi, PK and Vijayan, K (1983), 'Mechanical properties of banana fibres (*Musa sapientum*)', *Journal of Materials Science*, **18**, 2290–2296.
- Law, K-N Daud, WRW and Ghazali, A (2007), 'Morphological and chemical nature of fiber strands of oil palm empty-fruit bunch (OPEFB)', *BioResources*, **2**, 351–362.
- Lawrence, L (1981), 'A technique for measuring fibril angle using polarized light', *Wood and Fibre*, **13**, 13–16.
- Ledbetter, MC and Porter, KR (1963), 'A "microtubule" in plant cell fine structure', *Journal of Cell Biology*, **19**, 239–250.
- Lerouxel, O Cavalier, DM Liepman, AH and Keegstra, K (2006), 'Biosynthesis of plant cell wall polysaccharides – a complex process', *Current Opinion in Plant Biology*, **9**, 621–630.
- Lichtenegger, H Reiterer, A Tschegg, S and Fratzl, P (1998), 'Determination of spiral angles of elementary fibrils in the wood cell wall: comparison of small-angle X-ray scattering and wide-angle X-ray diffraction', in *Microfibril Angle in Wood: Proceedings of the IAWA/IUFRO International Workshop on the Significance of Microfibril Angle to Wood Quality*, Westport, New Zealand, ed. Butterfield, BG, University of Canterbury Press, Christchurch, New Zealand, 140–156.
- Mark, RE (1967), *Cell Wall Mechanics of Tracheids*, Yale University Press, New Haven, CT, and London.
- Martinschitz, KJ Boesecke, P Garvey, CJ Gindl, W and Keckes, J (2008), 'Changes in microfibril angle in cyclically deformed dry coir fibers studied by in-situ synchrotron X-ray diffraction', *Journal of Materials Science*, **43**, 350–356.
- McLaughlin, EC and Tait, RA (1980), 'Fracture mechanism of plant fibres', *Journal of Materials Science*, **15**, 89–95.
- Meylan, BA (1966), 'Measurement of microfibril angle by X-ray diffraction', *Forest Products Journal*, **17**, 51–58.
- Mohanty, AK Misra, M and Drzal, LT (2002), 'Sustainable biocomposites from renewable resources: opportunities and challenges in the green materials world', *Journal of Polymers and the Environment*, **10**(1–2), 19–26.
- Morton, WE and Hearle, JWS (1975), *An Introduction to Fibre Structure. Physical Properties of Textile Structures*, The Textile Institute, Heinemann, London.
- Mwaikambo, LY (2006), 'Review of the history, properties and application of plant fibres', *African Journal of Science and Technology*, **7**, 120–133.
- Mwaikambo, LY and Ansell, MP (2006a), 'Mechanical properties of alkali treated plant fibres and their potential as reinforcement materials. Part I. Hemp fibres', *Journal of Materials Science*, **8**, 2483–2496.
- Mwaikambo, LY and Ansell, MP (2006b), 'Mechanical properties of alkali treated plant fibres and their potential as reinforcement materials. Part II. Sisal fibres', *Journal of Materials Science*, **8**, 2497–2508.

- Neville, AC (1993), *Biology of Fibrous Composites: Development Beyond the Cell Membrane*, Cambridge University Press, Cambridge, UK.
- Nilsson, T and Björdal, B (2008), 'The use of kapok fibres for enrichment cultures of lignocellulose-degrading bacteria', *International Biodeterioration and Biodegradation*, **61**, 11–16.
- Nishimura, T (2006), 'Development of car components using kenaf and a new evolution in biomaterials', *Journal of the Society of Automotive Engineers of Japan*, **60**(1), 100–104.
- Nishino, T (2004), 'Natural fibre sources', Chapter 4 in *Green Composites – Polymer Composites and the Environment*, ed. Baillie, C, Woodhead Publishing, Cambridge, UK.
- Nishino, T Takano, K and Nakamae, K (1995), 'Elastic modulus of the crystalline regions of cellulose polymorphs', *Journal of Polymer Science, Part B, Polymer Physics*, **33**, 611–618.
- Nishiyama, Y Langan, P and Chanzy, H (2002), 'Crystal structure and hydrogen bonding system in cellulose I<sub>β</sub> from synchrotron X-ray and neutron fiber diffraction', *Journal of the American Chemical Society*, **124**, 9074–9082.
- Page, DH (1969), 'A method for determining the fibrillar angle in wood tracheids', *Microscopy Journal*, **90**, 137–143.
- Perry, DR (1975), *Identification of Textile Materials*, The Textile Institute, Manchester, UK.
- Preston, RD (1934), 'The organization of the cell wall of the conifer tracheid (Part III)', *Transactions of the Royal Society of London, Series B*, **224**, 131–171.
- Purseglove, JW (1987), *Tropical Crop Dicotyledons, Vols 1 and 2 combined*, Longman Group, London.
- Riedel, U and Nickel, J (1999), 'Natural fibre-reinforced biopolymers as construction materials – new discoveries', *Die Angewandte Makromolekulare Chemie* **272**, 34–40.
- Robson, J Hague, J Newman, G Jeronimidis, G and Ansell, MP (1993), 'Survey of natural materials for use in structural composites as reinforcement and matrices', Report No. EC/431/92 to DTI LINK Structural Composites Committee, January 1993.
- Rowell, RM (1992), 'Property enhancement of wood composites', in *Composite Applications – the Role of Matrix, Fibre and Interface*, ed. Rowell, RM, Vigo, T and Kinzig, B, VCH Publishers, New York.
- Sabharwal, S Aktar, K Blanchette, RA and Young, RA (1994), 'Biomechanical pulping of kenaf', *Tappi Journal*, **77**, 105–112.
- Sarko, A Nishimura, H and Okano, T (1987), 'Crystalline alkali–cellulose complexes as intermediates during mercerisation', in *The Structure of Cellulose: Characterisation of The Solid States*, ed. Atalla, RH, ACS Symposium Series 340, American Chemical Society, Washington DC, 169–177.
- Seagull, RW (1992), 'A quantitative electron microscopic study of changes in microtubule arrays and wall microfibril orientation during *in vitro* cotton fiber development', *Journal of Cell Science*, **101**, 561–577.
- Senft, JF and Bendtsen, BA (1985), 'Measuring microfibrillar angles using light microscopy', *Wood and Fibre*, **17**, 564–567.
- Sharma, HSS (1987), 'Studies on chemical and enzyme retting of flax on a semi-industrial scale and analysis of the effluents for their physico-chemical components', *International Biodeterioration*, **3**, 329–342.
- Shenouda, SG (1979), 'The structure of cotton cellulose', in *Applied Fibre Science Vol. 3*, ed. Happey, F, Academic Press, New York, 275–309.

- Somerville, C Bauer, S Brininstool, G Facette, M Hamann, T Milne, J Osborne, E Paredez, A Persson, S Raab, T Vorwerk, S and Youngs, H (2004), 'Toward a systems approach to understanding plant cell walls', *Science*, **306**, 2206–2211.
- Sreekala, MS Kumaran, MG and Thomas, S (1997), 'Oil palm fibers: Morphology, chemical composition, surface modification, and mechanical properties', *Journal of Applied Polymer Science*, **66**, 821–835.
- Sreenivasan, S Iyer, PB and Iyer, KRK (1996), 'Influence of delignification and alkali treatment on the fine structure of coir fibres (*Cocos nucifera*)', *Journal of Materials Science*, **31**, 721–726.
- Suddell, BC and Evans, WJ (2002), 'Natural fibre composites in automotive applications', Chapter 7 in *Natural Fibres, Biopolymers and their Biocomposites*, ed. Mohanty, AK, Misra, M and Drzal, AT, CRC Press, Boca Raton, FL.
- Thielemans, W Can, E Morye, SS and Wool, RP (2002), 'Novel application of lignin in composite materials', *Journal of Applied Polymer Science*, **83**, 323–331.
- Towo, AN (2006), 'Fatigue of natural fibre composites', PhD thesis, University of Bath.
- Towo AN and Ansell, MP (2008), Fatigue evaluation and dynamic mechanical thermal analysis of sisal fibre – thermosetting resin composites, *Composites Science and Technology*, **68**, 925–932.
- Vincent, JFV (1999), 'From cellulose to cell', *Journal of Experimental Biology*, **202**, 3263–3268.
- Vincent, JFV (2000), 'A unified nomenclature for plant fibres for industrial use', *Applied Composite Materials*, **7**, 269–271.
- Wambua, P Ivans, J and Verpoest, I (2003), 'Natural fibres: can they replace glass in fibre reinforced plastics?', *Composites Science and Technology*, **63**, 1259–1264.
- Wasteneys, GO (2004), 'Progress in understanding the role of microtubules in plant cell walls', *Current Opinion in Plant Biology*, **7**, 651–660.



**Abstract:** The chemistry of proteins is described. Diversity comes from the different side-groups in the constituent amino-acid residues. The three physical forms are  $\alpha$ -helical crystals, extended chain  $\beta$ -crystals and globular forms. The different structures in regenerated fibres, silks, wool and hair, and hagfish slime threads are described. These range from homogeneous amorphous forms to structures at many levels from the molecules to the whole fibre and influence the resulting fibre properties. The conclusion contrasts the lack of success in manufacturing fibres with the success of natural evolution. The possibilities of genetic engineering and biomimetics are mentioned.

**Key words:** protein chemistry, protein physical forms, regenerated protein fibres, silks, wool and hair, hagfish slime threads, genetic engineering and biomimetics.

### 3.1 Introduction

Proteins are the most prolific of biological materials. Their great diversity derives from the sequence of different side-groups on one position of a simple chemical repeat in the basic polymer molecule. An ‘alphabet’ of about 20 side-groups makes it possible to produce an enormous ‘dictionary’ of ‘words’ that are typically several hundred ‘letters’ in length. The ‘meanings’ of the ‘words’ with the different sequences of side-groups represent the different biological functions that proteins have in living organisms. Enzymes, blood, nerves, antibodies, muscle, tendons, etc., are all proteins. Natural protein fibres are a class of structural proteins, which also includes skin, nail, feathers and some horns.

It is now known that the code for protein synthesis is carried by the DNA in the chromosomes of living organisms. Each chromosome contains a number of genes with specific DNA sequences, which are based on a simpler ‘alphabet’ of four letters. The code is then transferred by messenger RNA to the sites of protein synthesis. The genes have evolved over millions of years to provide proteins with specific functions. However, equally important for fibres such as wool and hair is the triggering of production of different proteins as the fibre grows out of the follicle. For silks, the way in which the fibre is spun is as important as the protein composition in determining properties.

Protein fibres are structurally the most complex of fibres. In addition to the complexity along the polymer molecule, many are composed of a mixture



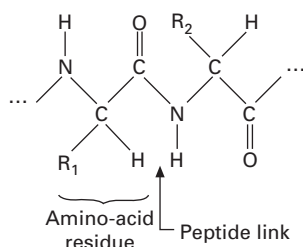
of proteins, in contrast to the single chemical compounds that dominate the composition of other fibres. On a coarser scale, multicellular fibres, such as wool and hair, have structural features at multiple levels.

## 3.2 Protein structures

### 3.2.1 Chemistry

Proteins are formed by the condensation of amino acids,  $\text{NH}_2\text{-CHR-COOH}$ , with the production of a peptide bond,  $\text{-NH-CO-}$ , and the elimination of  $\text{H}_2\text{O}$ . Two units of the polymer repeat are shown in Fig. 3.1. The diversity, due to what are described above by analogy as ‘letters’, comes from the different side-groups  $\text{-R}$ . The old set of comparative data in Table 3.1, which shows the diversity of the amino-acid residue composition in different protein fibres, gives the names of 18 amino acids with the formulae of the side-groups. A standard list now usually comprises 20 residues. In Table 3.1, the amides, asparagine and glutamine, are included with the corresponding aspartic and glutamic acids. There are other non-standard acids: Höcker (2000), quoting Lindley (1977) on the composition of Merino wool, lists 24 residues by including small amounts of other sulphur-containing residues: cysteine,  $\text{-CH}_2\text{-SH}$ ; cysteic acid,  $\text{-CH}_2\text{-SO}_3\text{H}$ ; thiocysteine,  $\text{-CH}_2\text{-S-SH}$ ; and lanthionine,  $\text{-CH}_2\text{-S-CH}_2\text{-}$ . Another table, quoted for Merino wool by Höcker (2002) from Crewther (1975), lists only 16 residues. In addition to glutamine and asparagines, the small amounts of histidine and tryptophan, which as shown in Table 3.1 occur in larger amounts in casein from milk, are omitted. The proportions listed in Table 3.1 should be regarded only as indicative values. The actual proportions vary with breed, diet and other factors. The two sets of data quoted by Höcker (2002) for Merino wool have differences of up to 20% in the amounts of some amino acids.

As indicated in Table 3.1, the amino-acid residues can be grouped in various chemical characteristics. This has an obvious influence on the chemical reactions of proteins. Structurally, proline is significant, because it forms a ring between adjacent  $\text{-N-}$  and  $\text{-CH-}$  groups, and so distorts the



3.1 Two units of a protein molecular repeat.

Table 3.1 Amino-acid residue content of three protein fibres, from Harris (1954)

Type	Side group	Amino acid	Proportion (g amino acid per 100 g protein) in:		
			Silk fibroin	Wool keratin	Casein
Inert	-H	Glycine	43.8	6.5	1.9
	-CH <sub>3</sub>	Alanine	26.4	4.1	3.5
	-CH(CH <sub>3</sub> ) <sub>2</sub>	Valine	3.2	5.5	6.02
	-CH <sub>2</sub> ·CH(CH <sub>3</sub> ) <sub>2</sub>	Leucine	0.8	9.7	10.55
	-CH(CH <sub>3</sub> )·CH <sub>2</sub> CH <sub>3</sub>	Isoleucine	1.37	-	5.27
	-CH <sub>2</sub> ·C <sub>6</sub> H <sub>5</sub>	Phenylalanine	1.5	1.6	6.46
Acidic	-CH <sub>2</sub> ·COOH	Aspartic acid	3.0	7.27	6.70
	-CH <sub>2</sub> ·CH <sub>2</sub> ·COOH	Glutamic acid	2.03	16.0	22.03
Basic	-CH <sub>2</sub> ·CH <sub>2</sub> ·CH <sub>2</sub> ·CH <sub>2</sub> ·NH <sub>2</sub>	Lysine	0.88	2.5	8.25
	-(CH <sub>2</sub> ) <sub>3</sub> ·NH·C(NH)NH <sub>2</sub>	Arginine	10.5	8.6	3.94
	$  \begin{array}{c}  \text{N:CH} \\    \\  \text{-CH}_2 \text{---} \text{C:CH} \text{---} \text{NH}  \end{array}  $	Histidine	0.47	0.7	3.24
Hydroxyl	-CH <sub>2</sub> OH	Serine	12.6	9.5	5.87
	-CH(OH)·CH <sub>3</sub>	Threonine	1.5	6.6	4.53
	-CH <sub>2</sub> ·C <sub>6</sub> H <sub>4</sub> OH	Tyrosine	10.6	6.1	6.28
Ring	$  \begin{array}{c}  \text{-CH}_2 \text{---} \\  \diagup \quad \diagdown \\  \text{CH}_2 \\  \diagdown \quad \diagup \\  \text{-CH}_2 \text{---}  \end{array}  $	Proline	1.5	7.2	10.54
Double	-CH <sub>2</sub> ·S·S·CH <sub>2</sub> -	Cystine	-	11.8	0.40
Miscellaneous	-CH <sub>2</sub> ·CH <sub>2</sub> ·S·CH <sub>3</sub>	Methionine	-	0.35	3.50
	$  \begin{array}{c}  \text{-CH}_2\text{-C} \\     \quad \diagup \\  \text{CH} \quad \text{---} \text{---} \\  \quad \quad \quad \diagdown \\  \quad \quad \quad \text{NH}  \end{array}  $	Tryptophan	-	0.7	1.37

form that the molecule can take up. The other important structural features are the crosslinks that can form between chains. Hydrogen bonding can occur between -CO and -NH groups in the main chain and between hydroxyl and amide side-groups. The presence of these groups accounts for the higher stiffness of dry fibres, in contrast to wet fibres where water molecules are absorbed between chains. Salt formation between acidic and basic groups will be affected by pH. Phenolic interactions can occur between the benzene rings in phenylalanine. Covalent amide bonds can form between -COOH and -NH<sub>2</sub>.

Cystine is by far the most important crosslink. Its presence in wool and hair and its absence from silk have a major influence on mechanical properties. When the protein is synthesised, cysteine, -CH<sub>2</sub>-SH, is the monomer, but it is subsequently oxidised to cystine, -CH<sub>2</sub>-S-S-CH<sub>2</sub>-, which gives a

disulphide link between chains. Reduction to cysteine and re-oxidation to cystine is a mechanism for setting wool and hair.

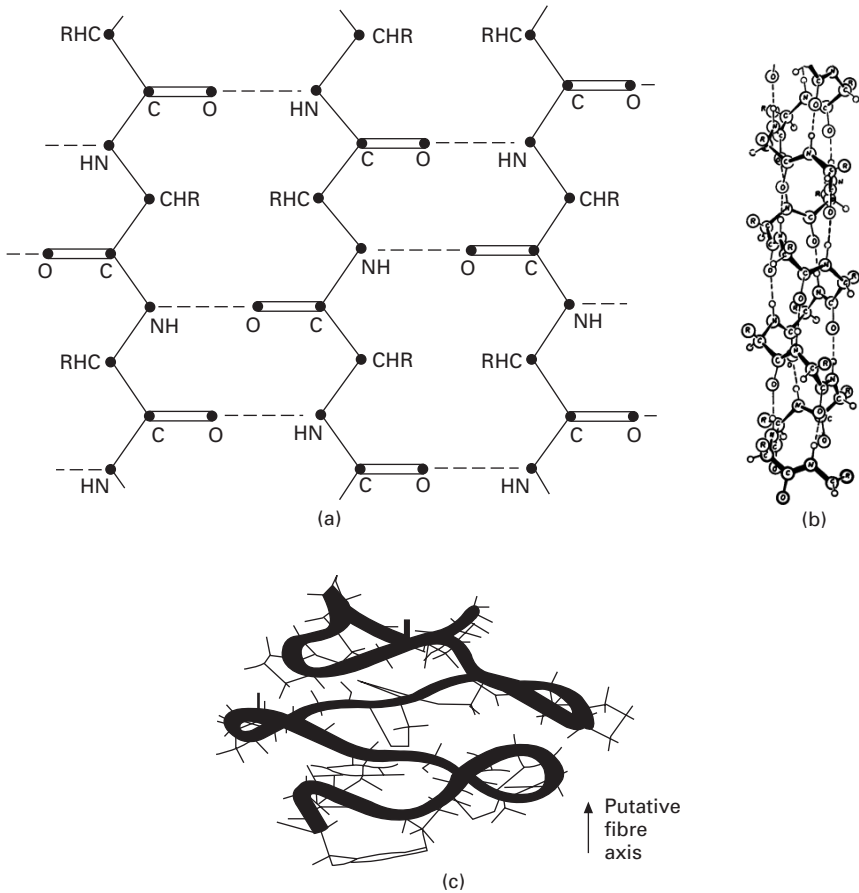
### 3.2.2 Physical forms

Proteins are commonly divided into crystalline and globular forms, but, as with the chemistry, the reality is complicated. X-ray diffraction studies of wool and silk from around 1930 onwards showed (1) that there was a mixture of crystalline and amorphous regions, and (2) that there were two different diffraction patterns, termed  $\alpha$  in wool and hair and  $\beta$  in silk. The  $\beta$ -form was resolved into a crystal structure with extended chains as shown in Fig. 3.2(a). The  $\alpha$ -form raised more problems. Astbury (see Howitt, 1949, 1953) found a spacing at 0.515 nm along the fibre axis and spacings at 0.98 and 2.7 nm across the axis. It was clear that the molecule was folded, and Astbury speculated on various ways in which the folding might occur between amino-acid residues, but he was unable to come up with a solution that fitted all the available information. It was not until Pauling broke the mind-set by realising that the geometric and chemical repeats did not need to coincide that the problem was resolved.

Some simple polypeptides, such as poly(glycine), crystallise as extended chains in  $\beta$ -sheets, as shown in Fig. 3.2(a). Others, such as poly(alanine), can form helical coils. In the structure proposed by Pauling *et al.* (1951) and shown in Fig. 3.2(b), there are 3.6 amino-acid residues in each turn, which has an axial repeat of 0.55 nm. These two basic forms are found in protein fibres. Owing to the presence of a variety of repeats, most with larger side-groups, the forms are distorted and the repeat lengths are reduced. Proline and cystine give bigger differences.

Globular proteins give the amorphous halo in X-ray diffraction. There is no repetitive crystal structure at the atomic level. However, in most if not all cases, this does not mean that the polymer has the random structure typical of rubbers and glassy plastics. Each globular protein molecule folds into a specific structure as it is formed, in order to minimise energy. Haemoglobin, which contains some helical segments among its folds, is a well-known example. A computer simulation of the folds in a GPGGSPGGY sequence, which gives elasticity to a spider drag-line, is shown in Fig. 3.2(c). Globular proteins can be regarded as quasi-crystalline, since they share with crystals a specifically defined structure.

In natural fibres, the distinction between crystalline and globular proteins is not so definitive. Various combinations can occur within protein molecules. Some proteins are block copolymers, which alternate crystallisable and non-crystallisable forms. In others, the regular helical sequences of the crystal structure may be interrupted by distortions due to sequences that do not fit into the regular lattice. Some have non-crystallisable terminal domains.



3.2 (a)  $\beta$ -sheet crystal structure. (b)  $\alpha$ -helix crystal structure. (c) An example of a globular form. Simulation of the GPGGSPGGY peptide unit in spider silk, from Hayashi *et al.* (1999). The amino acids and side-groups R are: G = glycine,  $-\text{H}$ ; P = proline,  $-\text{CH}_2-\text{CH}_2-\text{CH}_2-$ ; S = serine,  $-\text{CH}_2\text{OH}$ ; Y = tyrosine,  $-\text{CH}_2\text{C}_6\text{H}_6\text{OH}$ .

### 3.3 The diversity of protein fibres

#### 3.3.1 Fibre types

Protein fibres can be classified according to their mode of formation. In what follows, the different types will be reviewed in terms of increasing complexity of control of their formation. The structures range from simple homogeneous forms through increasing levels of structural differentiation in three classes of fibre, followed by a simplification in an unusual biological fibre.

### 3.3.2 Regenerated and other manufactured protein fibres

Following the success of the regenerated cellulosic fibres, viscose, acetate and other rayons, in the first quarter of the twentieth century, chemists turned their attention to the possibility of mimicking wool or silk by dissolving proteins and forming fibres by the established technologies of solution spinning. A variety of proteins were used in laboratory experiments and there was a small production of soya-bean fibre around 1940. In the 1950s, there was commercial production by major companies of fibres composed of casein from milk, zein from corn, and groundnut protein. Except possibly for some difference in a surface skin, these fibres have a homogeneous structure with no differentiation above the atomic level. Their X-ray diffraction patterns are circular haloes with no indication of crystallinity or orientation. When wet, the fibres are extremely weak but show good elastic recovery; when dry, they are stronger but still weaker than other fibres. They were used in applications with minimal mechanical demands, such as hat felts, and gave a pleasing softness in blends, but they eventually failed to be commercially viable.

Interest in regenerated protein fibres revived at the end of the twentieth century. For example, there is research in China on soya bean fibre. While a claim that this might replace cashmere is unlikely to succeed, this sort of regenerated protein fibres may find specialist uses, such as in the medical field. These fibres are made from globular proteins, so their amorphous structure is not surprising. What seemed to be a more promising line of research was the use of naturally crystalline proteins. Attempts to make fibres from solutions of proteins from waste wool were unsuccessful, although *Keratec* has found a market in cosmetics. This reflects the inability to mimic the many levels of structure in wool. Regeneration of silk using special solvents gives better properties (Xu *et al.*, 2005) but does not match the strength of natural silk. Just as regeneration of cellulose leads to a loss of the highly crystalline, oriented and chain-extended forms of natural fibres and leads to fringed micellar or fibrillar structures of crystalline and amorphous regions, so also it seems likely that regenerated silk has similar structures.

Spider silks are among the strongest of fibres and, unlike the synthetic high-strength fibres, have a high elastic extension, which gives superior toughness. The most ambitious, but ultimately unsuccessful, research into manufacturing protein fibres has been the attempt to mimic the production of spider silks. Genetic engineering has enabled spider silk proteins to be produced either by bacteria or in goat's milk, but it is now recognised that there is another step, namely fibre spinning, to give high performance, which is even more difficult to achieve. The fibres produced have low strengths. The critical problem is that the full extension of the polymer molecules along the fibre, which occurs in spider silk, is not maintained when the proteins go into solution and can fold and entangle in random forms.

### 3.3.3 Silks

Various moths, spiders and insects produce silk threads with a variety of protein compositions. The common feature is that the polymerisation and control of fibre formation are closely linked. Smith *et al.* (1985, 1987) showed that virgin polymerisation of polyethylene followed by fibre formation without allowing any chain folding led to high strengths, though the techno-economics did not compete with gel-spinning. Nature achieves the crystallisation of extended chain molecules without entanglements. Within the organism, the proteins are synthesised in glands and go into solution. They are then dragged through cell walls, which act as 'nano-spinnerets', into the duct and are assembled together as silk filaments, before being pushed or pulled out through a spigot into the air.

In principle, this could lead to the formation of a parallel assembly of fully extended chain molecules, similar to that suggested by Staudinger (1932), which is close to that found in gel-spun high-modulus polyethylene and liquid crystal aramid and PBO fibres. However, this would lead to a limiting extension of less than 5%. In order to achieve extensions from 50% to 500%, some chain folding occurs, as shown, for example, in Fig. 3.2(c). The important feature is that there is no entanglement. The topology is such that each chain is separate and parallel to its neighbours. Under tension, the chains can be pulled into the fully extended form, generating high strength. The system acts like a set of parallel strings of equal length and without entanglements, which are held at their ends and can take up wavy forms with the ends close together, but then be pulled out into a tight structure in a fully extended state. The difference is that whereas the strings show a sharp change from negligible resistance to a high resistance to extension, intermolecular forces in spider silks lead to a more gradual increase in tension.

As can be seen from Table 3.1, textile silk from the moth *Bombyx mori* has a much simpler protein composition than wool. There is no cystine to crosslink chains. About 80% consists of amino-acid residues with the three simplest side-groups,  $-H$ ,  $-CH_3$  and  $CH_2OH$ . Blocks containing a regular sequence of these three units, which crystallise in  $\beta$ -sheets with the form shown in Fig. 3.2(a). Tyrosine and other minor components of the block copolymer form amorphous regions. The structure is thus similar to the fringed micelle structure found in nylon, except that there is no chain folding at the ends of the crystals and no entanglement where the amorphous tie-molecules link the crystallites.

### 3.3.4 Wool and hair

Wool and other animal and human hairs have the most complex of fibre structures. They share a common pattern, but there are detailed differences

to some extent among different wools and more between different hairs. In what follows, the word *hair* is used to cover all hairs including wool.

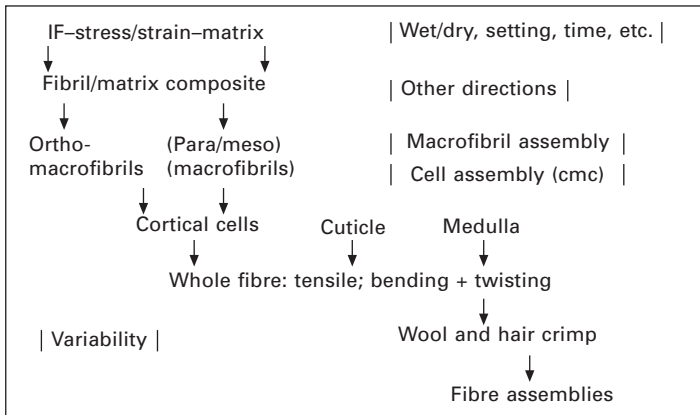
Hair, together with other natural structural materials, such as skin, nails and feathers, is usually described as made of *keratin*, but this covers a variety of chemical forms. A common feature of keratins is that they contain a sequence of chemical groups designated as NTD-1A(35)-L1-1B(101)-L12-2A(19)-L2-2B(121)-CTD. The 1A, 1B, 2A and 2B segments have constant numbers of amino-acid residues, as indicated, and crystallise in the  $\alpha$ -helical structure. There are differences in structure in different parts, for example, the 2B segments in hair contain cystine crosslinks, which must affect the mechanical and other properties. The terminal domains, NTD and CTD, and the links L1, L12 and L2 have different numbers in different keratins. Two keratins, type 1 acidic and type 2 basic, associate together in a twisted dimer. Four more levels of twisted pairs lead to an intermediate filament (IF), also referred to as a microfibril, of 32 molecules. The IFs are formed in a parallel assembly within elongated cortical cells at the first stage of growth from the follicle.

Further up the follicle, a family of globular proteins, termed keratin associated proteins (KAP), are laid down between the IFs. They constitute a matrix, which also contains the keratin NTDs and CTDs emerging from the IFs. Both the KAPs and the TDs contain cystine, which gives them a crosslinked structure with around 10 covalent bonds between network junctions.

The microfibrils associate as macrofibrils, which differ in form in the cells in the central cortex of hair. In the para-cortex, the microfibrils are all parallel to the fibre axis; in the ortho-cortex they are in a helical assembly. (There may also be a meso-cortex and a medulla.) If the ortho- and para-cortex are side-by-side, this leads to the crimp of hair due to differential expansion on drying; if they are symmetrically distributed, the hair is straight. Between the cells, there is a cell-membrane complex containing lipids. Surrounding the cortex there is a multi-layer cuticle. This consists of surface scales, which give a directional frictional effect and cause felting.

The many levels of structure in hair all contribute to the properties of the fibres. There is now sufficient knowledge to develop a computational total model of hair at least to a first approximation (Hearle, 2003). The computation would go through the sequence of levels shown in Fig. 3.3, starting with computational molecular modelling or an empirical input of microfibril and matrix properties and moving up the levels in terms of their structural mechanics. Such a model would be beneficial in research on hair, particularly for directing genetic engineering of improved fibres.

There are different explanations of the way in which the basic mechanical properties of hair are determined. In the model proposed by Chapman (1969), the microfibril/matrix composite is treated as a series of zones, which can



3.3 Levels of structure for mechanical modelling of wool and hair.

now be regarded as bounded at links where the TDs emerge into the matrix. The microfibrils extend first in a stiff region of deformation of the  $\alpha$ -helix. An  $\alpha \rightarrow \beta$  transition starts in one zone at 2% extension. The stress in the microfibril drops from a yield stress to the equilibrium stress for the transition and is taken up by extension of the matrix, which is treated as a fairly highly crosslinked rubber. The process continues at close to constant stress up to 30% extension, when all the zones have opened. The stress then increases as the matrix is further extended. In recovery the matrix stress–strain curve is followed down until all the  $\beta$ -forms have reverted to  $\alpha$ -helices. Other explanations of the stress–strain curve have been proposed, but there are strong arguments in favour of Chapman’s model (Hearle, 2000), though it could be refined in some details.

### 3.3.5 Hagfish slime threads

The fibres so far discussed are covered in detail in other chapters of this book. However, because of the interesting differences in formation, structure and properties, it is worth giving a brief account of another natural keratin fibre. Hagfish, which are long eel-like creatures, have gland cells on their surface (Spitzer and Koch, 1998). When the fish is disturbed a mixture of mucus and threads is emitted and forms a protective slime with mechanical properties described by Fudge *et al.* (2005). Entanglement would deter some predators but another mechanism is blocking of the gills of fish (Lim *et al.*, 2006).

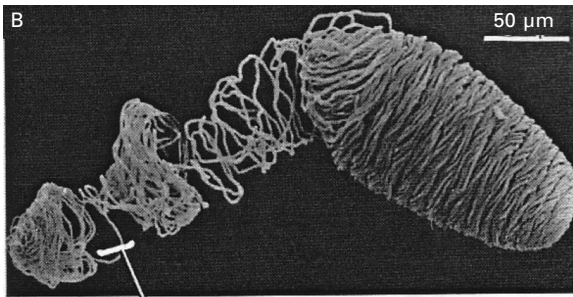
In contrast to the multicellular form of hair, hagfish slime threads (subsequently referred to as hagfish threads) are formed within single cells. As the keratin IFs are formed they assemble into fibres, which are 1–3  $\mu\text{m}$  in diameter and several centimetres long (Downing *et al.*, 1981, 1984). The



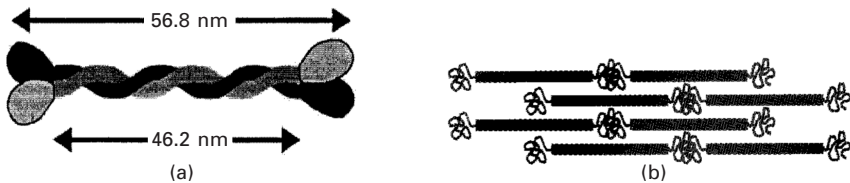
threads are laid down in a coiled bundle on the inside of a cell wall, as illustrated in Fig. 3.4. This mode of formation leads to a homogeneous fibre structure above the IF level.

In common with other IFs, the molecules associate from dimers to the full IFs with 32 chain molecules, but there are two important differences from hair. (1) There are no keratin-associated matrix proteins. A schematic diagram by Fudge and Gosline (2004), Fig. 3.5, shows central rods, which would be  $\alpha$ -helical, alternating with globular terminal domains (TDs). (2) Although the 1A-L1-1B-L12-2A-L2-2B sequences in the two keratins have the same numbers of residues, except for L12, the aminoacids are completely different, and the TDs contain no cystine to provide crosslinks (Koch *et al.*, 1994, 1995).

Measurements of mechanical properties of wet fibres are reported by Fudge *et al.* (2003) and related to an  $\alpha \rightarrow \beta$  transition. Although the fibre strength is comparable to that of wool, the break extension is over 200%. The stress-strain curve is divided into four regions. The extension is elastic up to 30% extension (zone I) and then becomes plastic with no recovery. The modulus continues to be low up to 80% extension (zone II), then increases steeply to 180% extension (zone III) before decreasing slightly up to break



3.4 The coil of hagfish thread, which is laid down inside the gland cell walls. From Koch *et al.* (1994).



3.5 Schematic views of hagfish thread IF structure, from Fudge and Gosline (2004). (a) The two keratins coiled together in the central rods of the dimer, with terminal domains at the ends. (b) Staggered series alternation of helical rods and globular TDs.

(zone IV). Different explanations for these unusual mechanical properties have been given by Fudge *et al.* (2003), model *F*, and Hearle (2008), model *H*. For zone I, *F* has elastic energy in TD conformations and *H* suggests deformation associated with crimp at some level of structure. Both models attribute zone II to an irreversible  $\alpha \rightarrow \beta$  transition. Unlike hair, there is no matrix under tension in parallel to reverse the transition. More research is needed to clarify the behaviour at the very low stresses in zones I and II. The experimental measurements are clearer at higher stresses and it is here that there is the main difference in interpretation. In *F*, the  $\alpha \rightarrow \beta$  transition continues in the central rods in zone III and then  $\beta$ -sheets slip and rupture in zone IV. For *H*, the deformation is attributed to plastic drawing of the TDs, regarded as quasi-crystalline assemblies. The stress–strain curve is qualitatively and quantitatively similar to that for the drawing of partially oriented polyester yarns.

In the dry state, an initial stiff region up to 2% extension is followed by a low modulus yield region and an increasing modulus above 80% extension and break at 120% extension. This is similar to the difference between wet and dry rayon and to the behaviour in drawing of glassy polymers.

### 3.4 Conclusion

A lesson to be learnt from the study of protein fibres is how successful evolution has been in developing structures that provide fibres with properties suited to purpose. Silks have a homogeneous structure of topologically parallel chains without entanglements in a mixture of axially oriented and less oriented segments. This leads to high strength and high elastic extension. In hair, a multicellular form with structural features at many levels gives performance functionality. Crimp leads to a bulky fleece in sheep, whereas a protective layer of straight fibres is more suited to some other animals. Elastic recovery when wet maintains the quality of the coat. The surface scales inhibit the movement of dirt to the skin. In contrast to this, a large plastic extension serves the needs of protection in hagfish threads. In wool, other hairs and silk, people have found many ways of using fibres for clothes and other purposes. Spider silks and hagfish threads are important for their scientific interest, though attempts are being made to ‘milk’ spiders to provide fibres with outstanding toughness for specialised uses.

The other lesson is how unsuccessful scientists and engineers have been in trying to manufacture protein fibres. The early attempts to regenerate globular proteins as fibres by solution spinning led to weak amorphous structures. Nor did regeneration of keratin from wool lead to useful fibres; unsurprisingly, the multilevel features were not reproduced. Slightly better results were found with silk, which has a homogeneous structure, as a starting material. A partially crystalline fibre was formed, but the parallel

arrangement of extended chains was lost. Strengths were less than that of natural silk and comparable to other fringed micelle fibres.

Genetic engineering, which has developed greatly over the last 25 years, offers more opportunities. It has been shown that the distribution of proteins in wool can be changed, though the resulting sheep, in which proteins from the cuticle appeared in the cortex, had poorer wool (Rogers, 2000). Extensive research in which structure–property relations guide the routes of genetic engineering would be needed to produce improved fibres. Computational molecular modelling at the nano-level would lead on to applied mechanics at coarser levels. Spider silk proteins can be produced in bulk by genetically engineered bacteria or goats, but spinning into fibres does not reproduce the ideal form of assembling chain molecules that occurs in spiders.

Imaginative research is need for successful routes to biomimetic engineering. Quoting Hearle, (2007), on spider silk proteins: ‘Blue-sky thinking envisages virgin polymerisation of appropriate amino-acids on enzyme complexes or catalysts, which must then be assembled in bundles (nano-filaments) in matched lengths. The bundles might be drawn through nano-spinnerets, after an operation analogous at a much smaller scale to the threading of yarn on a texturing machine. They would then be assembled in larger bundles (yarns) and wound up at a commercial speed. The critical requirement, after polymerisation, would be to avoid significant disarrangement of the molecular bundles.’ And for a route to mimic hagfish thread production with proteins genetically engineered for required functions: ‘Blue-sky thinking suggests that this might be achieved by artificial cell cultures. If the gland cells can be cultured, they would reproduce and form the internal coils of thread. Mature cells would move to the next production stage and be triggered to burst and release the thread. There would then be a need for a textile operation to collect the threads and assemble them into yarns, which could be wound up at a reasonable rate.’

### 3.5 References

- Chapman B M (1969), ‘A mechanical model for wool and other keratin fibres’, *Textile Res J*, 39, 1102–1109.
- Crewther W G (1975), ‘Primary structure and chemical properties of wool’, *Proc Int Wool Res Conf*, Aachen, I, 1–101.
- Downing S W, Spitzer R H, Salo W L, Downing S D, Saidel L J and Koch E A (1981), ‘Hagfish slime gland thread cells: organization, biochemical features, and length’, *Science*, 212, 326–327.
- Downing S W, Spitzer R H, Koch E A and Salo W L (1984), ‘The hagfish slime gland thread cell. I. A unique cellular system for the study of intermediate filaments and intermediate filament–microtubule interactions’, *J Cell Biol*, 98, 653–660.
- Fudge D S and Gosline J M (2004), ‘Molecular design of the  $\alpha$ -keratin composite: insights from a matrix-free model, hagfish slime threads’, *Proc Roy Soc London, B* 271, 291–299.

- Fudge D S, Gardner K H, Forsyth V T, Riekel C and Gosline J M (2003), 'The mechanical properties of hydrated intermediate filaments; insights from hagfish slime threads', *Biophys J*, 85, 2015–2027.
- Fudge D S, Levy N, Chiu S and Gosline J M (2005), 'Composition, morphology and mechanics of hagfish slime', *J Exptl Biol*, 208, 4613–4625.
- Harris M, editor (1954), *Handbook of Textile Fibers*, Washington DC, Harris Research Laboratories.
- Hayashi C Y, Shipley N H and Lewis R V (1999), 'Hypotheses that correlate the sequence, structure, and mechanical properties of spider silk proteins', *Int Biol Macromol*, 24, 271–275.
- Hearle J W S (2000), 'A critical review of the structural mechanics of wool and hair fibres', *Int J Biol Macromol*, 27, 123–138.
- Hearle J W S (2003), 'A total model for the structural mechanics of wool', *Wool Tech and Sheep Breeding*, 51, 95–117.
- Hearle J W S (2007), 'Protein fibres: structural mechanics and future opportunities', *J Mater Sci*, 42, 8010–8019.
- Hearle J W S (2008), 'An alternative model for the structural mechanics of hagfish slime threads', *Int J Biol Macromol*, 42, 420–428.
- Höcker H (2002), 'Fibre morphology', in Simpson W S and Crawshaw G H, editors, *Wool: Science and Technology*, Cambridge, UK, Woodhead Publishing.
- Howitt F O (1949, 1953), 'Protein fibres' in Preston J M, editor, *Fibre Science*, 1st and 2nd editions, Manchester, UK, The Textile Institute.
- Koch E A, Spitzer R H, Pithawalla R B and Parry D A D (1994), 'An unusual intermediate filament subunit from the cytoskeletal biopolymer released extracellularly into seawater by the primitive hagfish (*Eptatretus stouti*).', *J Cell Sci*, 107, 3133–3144.
- Koch E A, Spitzer R H, Pithawalla R B, Castillos F A and Parry D A D (1995), 'Hagfish biopolymer: a type I/type II homologue of epidermal keratin intermediate filaments', *Int J Biol Macromol*, 17, 283–292.
- Lim J, Fudge D S, Levy N and Gosline J M (2006), 'Hagfish slime exomechanics: testing the gill-blocking mechanism', *J Exptl Biol*, 209, 702–710.
- Lindley H (1977), 'The chemical composition and structure of wool', in Asquith R S, editor, *Chemistry of Natural Protein Fibres*, New York, Plenum Press, 147–192.
- Pauling L, Corey R B and Branson H R (1951), 'The structure of proteins: two hydrogen-bonded helical configurations of the polypeptide chain', *Proc Natl Acad Sci*, 37, 205–211. (Plus seven related papers by Pauling and Corey between pages 235 and 285.)
- Rogers G E (2000), 'Genetic engineering for novel fibres', *J Textile Inst*, 91, 24–41.
- Smith P, Chanzy H D and Rotzinger B P (1985), *Polymer Commun*, 26, 258.
- Smith P, Chanzy H D and Rotzinger B P (1987), *J Mater Sci*, 22, 523.
- Spitzer R H and Koch E A (1998), 'Hagfish skin and slime glands' in Jorgensen J M, Lomholt J P, Weber R E and Malte H, editors, *The Biology of Hagfishes*, London, Chapman & Hall.
- Staudinger H (1932), *Die Hochmolekularen Organischen Verbindungen*, Berlin, Springer-Verlag.
- Xu Y, Shao H, Zhang Y and Hu X (2005), 'Studies on spinning and rheological behaviors of regenerated silk fibroin/*N*-methylmorpholine-*N*-oxide·H<sub>2</sub>O solutions', *J Mater Sci*, 40, 5355–5358.

# The structure and properties of wool and hair fibres

---

F-J WORTMANN, University of Manchester, UK

**Abstract:** Wool and all other mammalian hairs are fibrous,  $\alpha$ -keratinous, nano-composite materials and as such part of a larger group of biological, functional materials, referred to as keratins. This chapter first reviews the chemical composition of  $\alpha$ -keratins as well as their morphological and molecular structures. Emphasis is next given to considerations of the mechanical properties of the primary structural components, namely the para-crystalline intermediate filaments and their associated, amorphous matrix. Third, the thermal transitions in these morphological components, that is, the glass and the denaturation transition, and their individual dependence on water content are considered in detail.

**Key words:** hair,  $\alpha$ -keratin, biological fibre/matrix composite, mechanical properties, thermal transitions.

## 4.1 Introduction

Wool and all other mammal hairs are  $\alpha$ -keratinous, composite materials and as such part of a larger group of biological, functional materials, referred to as keratins.

*Keratin* as a generic term is applied to resilient appendages of the integument, that is, the outer covering of higher vertebrates, such as hair, horn, nail, and feather, whose principal functions have been summarized by Fraser and MacRae (1980) as follows:

- Prevention of egress of tissue fluids
- Prevention of ingress of environmental fluids
- Prevention of ingress of micro-organisms, parasites and foreign matter
- Protection against mechanical injury and attack by predators
- Aggressive and defensive actions both within and between species
- Food gathering
- Temperature regulation
- Locomotion, including flight, climbing and floating.

Structurally, keratins have been classified on the basis of wide angle X-ray diffraction (WAXS) initiated by Astbury and Street (1931) and comprehensively reviewed by Fraser *et al.* (1972). Two principal types of patterns were identified, namely the  $\alpha$ -helical conformation for hard keratins of mammals, and the  $\beta$ -sheet structure for those of birds and reptiles, respectively.

The  $\alpha$ -keratins have traditionally further been subdivided into two groups (Mercer, 1961), namely, first the 'soft' (stratum corneum) and second the 'hard' keratins (hair, nail, etc.). This subdivision is based on differences in their chemical and physical properties, but further mainly in their protein composition and more particularly due to the amount of the amino acid *cystine* and thus the concentration of sulphur cross-links they contain (Giroud and Leblond, 1951).

Figure 4.1 shows rhinoceros horn (Fig. 4.1(a)) and part of a feather (Fig. 4.1(b)) as being representative for  $\alpha$ - and  $\beta$ -keratinous materials, respectively. It is interesting to note that rhinoceros horn, unlike those of other horned animals, consists only of  $\alpha$ -keratin and lacks a bony core. Figures 4.1(c) and (d) show typical WAXS patterns for  $\alpha$ - and  $\beta$ -keratin, while Figs 4.1(e) and (f) give different types of models for the respective single-strand  $\alpha$ -helical and multiple-strand  $\beta$ -structures.

As authors have reviewed and pointed out with more (Zahn, 1980) or less emphasis (Matoltsy, 1969; Swift, 1977), 'keratin' is thus not a material of clearly defined appearance and composition. The term and further descriptors, such as *hard* and *soft*, or  $\alpha$  and  $\beta$ , should thus be used in a generalized way and with due caution.

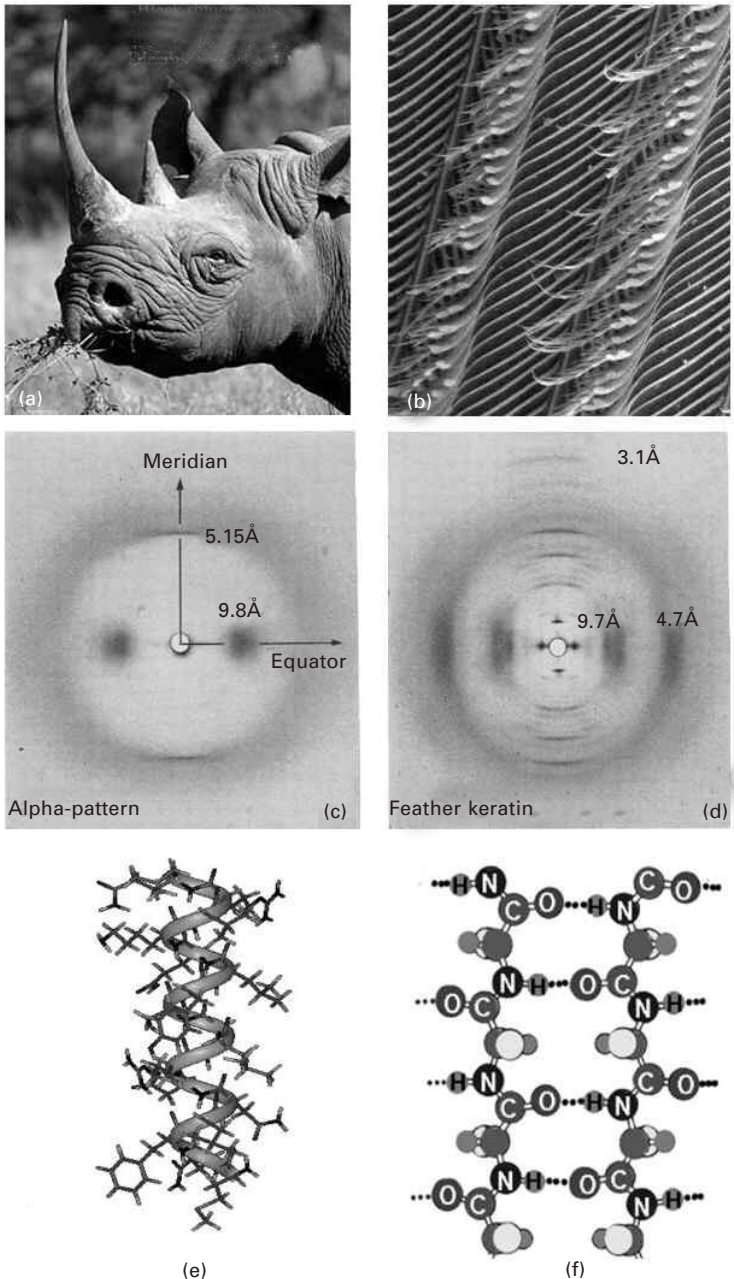
The present chapter is specifically concerned with hard,  $\alpha$ -keratins and with the fibres in that group.

## 4.2 Keratin fibres

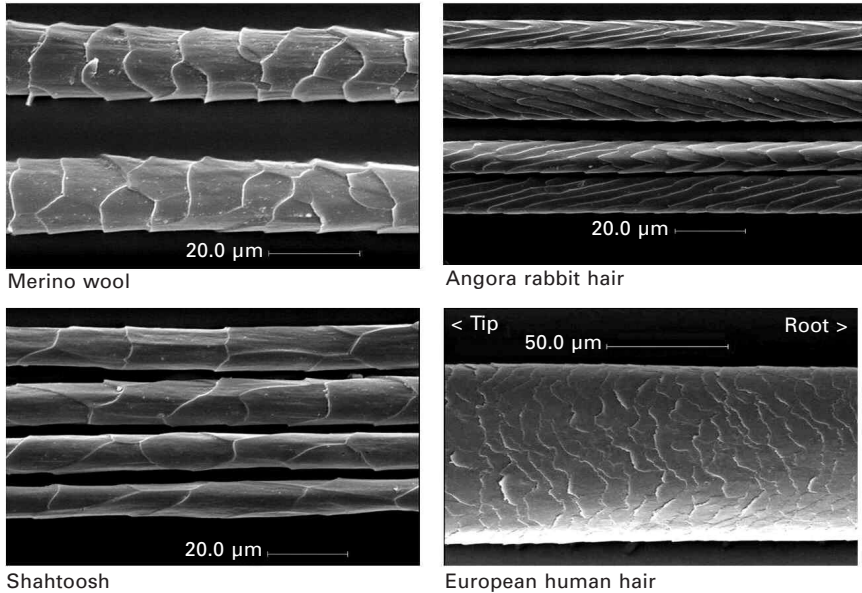
Although  $\alpha$ -keratinous fibres have an overall cylindrical form with an external overlapping scale pattern, they come in a wide variety of shapes and surface structures. Large differences are observed between species, as illustrated in Fig. 4.2, for such diverse fibres as sheep's (Merino) wool, angora rabbit hair, shahtoosh, and human hair, respectively. Differences are mainly observed for fibre diameter and the pattern presented by the surface scales (cuticle). The exposed scale edges point towards the fibre tip. This ensures low friction in the direction of the scales, that is away from the skin, and high friction against, thus providing an effective mechanism of expelling foreign matter and skin particles from the pelt or fleece as well as spreading sebum (wool grease). In a textile material, such as a yarn or a fabric, where fibre orientation is randomized, this directional friction effect facilitates the movement of fibres against each other during mechanical treatment and in the presence of water and auxiliaries, so that felting is induced (Makinson, 1979).

Differences in fibre appearance become increasingly subtle within a species but are still quite succinct when comparing fibres from a single animal and even along a single hair. These differences are of principal importance for the identification and discrimination of animal as well as human hair in





4.1 (a) Photo of a black rhinoceros, *Diceros bicorni michaeli* (adapted from Lewa, 2007); (b) part of a bird feather in an environmental scanning electron microscope (ESEM) (adapted from UoMN, 2006); (c) and (d) wide-Angle X-ray pattern of  $\alpha$ -helical and  $\beta$ -pleated sheet keratin, respectively (adapted from Fraser *et al.*, 1972); (e) molecular model for an  $\alpha$ -helical segment in  $\alpha$ -keratin (Nick, 1995) and (f) for a typical anti-parallel  $\beta$ -pleated sheet structure (adapted from Brooklyn College, 2008).



4.2 Various animal fibres (adapted from IWTO-58, 2000) of textile relevance and differing strongly in appearance, as well as European human hair in the scanning electron microscope (SEM). The exposed surface scale edges point towards the fibre tip.

Table 4.1 Elemental composition of wool fibres (water-free) (from Zahn *et al.*, 2003)

Element	Weight, %
Carbon	50.5
Hydrogen	6.8
Oxygen	22
Nitrogen	16.5
Sulphur	3.7
Ash	0.5

textile (IWTO-58, 2000; AATCC 20A, 2007) and forensic (Palenik, 1997) analyses, respectively.

### 4.3 Chemical composition

Wool, as the best investigated  $\alpha$ -keratin fibre (Fraser *et al.*, 1972; McLaren and Milligan, 1981; Zahn *et al.*, 2003), consists of carbon, hydrogen, oxygen, nitrogen and sulphur, in the proportions detailed in Table 4.1. Beyond the high sulphur content, which is characteristic for the  $\alpha$ -keratins, this composition is rather typical for proteins.



### 4.3.1 Proteins

Total hydrolysis of  $\alpha$ -keratin proteins, combining acid as well as enzymatic methods, yields 24 amino acids (Zahn *et al.*, 2003). The amino acids are classified by the composition of their side-chains into five groups, namely:

- ‘Acidic’ amino acids and their  $\omega$ -amides: aspartic acid, glutamic acid, asparagine, glutamine
- ‘Basic’ amino acids: arginine, lysine, histidine, tryptophan
- Amino acids with hydroxyl groups in the side-chain: *serine*, *threonine*, *tyrosine*
- Sulphur-containing amino acids: cysteine, thiocysteine, cysteic acid, cystine, lanthionine, methionine
- Amino acids without reactive, non-polar groups in the side-chain: glycine, alanine, valine, proline, leucine, isoleucine, phenylalanine.

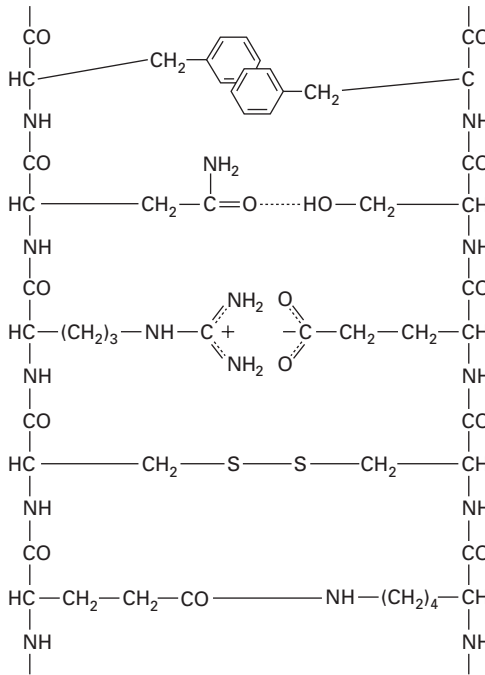
Systematic names and synonyms, structural and empirical formulas of the amino acids can be found in standard textbooks or Internet sources.

Typical concentrations of the amino acids in wool are given, e.g., by Zahn *et al.* (2003) and can furthermore be found in a wide variety of sources and for the various keratinous materials (e.g. Marshall and Gillespie, 1977; Marshall *et al.*, 1991; Robbins, 2002). The high amount of sulphur found in elemental analysis is due to the high concentration of the double amino acid cystine (460  $\mu\text{mol/g}$  in wool), which has two sulphur atoms forming a disulphide crosslink within and between protein chains. In wool, the proportions of acidic and basic groups are roughly the same (800–850  $\mu\text{mol/g}$ ). The total amount of amino acids with reactive side-chain groups is about 5400  $\mu\text{mol/g}$  compared to 3450  $\mu\text{mol/g}$  for the unreactive species. The sum of these two figures yields a good estimate of 8850  $\mu\text{mol/g}$  for the concentration of peptide groups in the protein chains of wool (Zahn *et al.*, 2003).

The side-chains account for about 50% of the protein material, interacting in various ways to stabilize its structure, as schematically shown in Fig. 4.3. From the top down, Fig. 4.3 shows first the interaction of two phenyl rings. In a similar way to the other apolar side-chains, they generate in water a hydrophobic effect, also referred to as apolar interaction, which is due to the aggregation of non-polar side-chains. The driving force for this effect is the reduction of the interface area of the side groups with, and thus the entropy gain of, the surrounding water molecules.

Second, a hydrogen bond is formed between an asparagine and a serine residue. Hydrogen bonds are generally formed in proteins between NH and C–OH groups as electron donors on the one hand and C=O and CO<sup>−</sup> groups as acceptors on the other. Hydrogen bonds play a central role for the stabilization of the  $\alpha$ -helical structures in keratin.

Third, a salt bridge is shown between an arginine and a glutamic acid



4.3 Structural formula of a fictive peptide chain to illustrate five important interactions between amino acid side-chains in keratins (Zahn *et al.*, 2003).

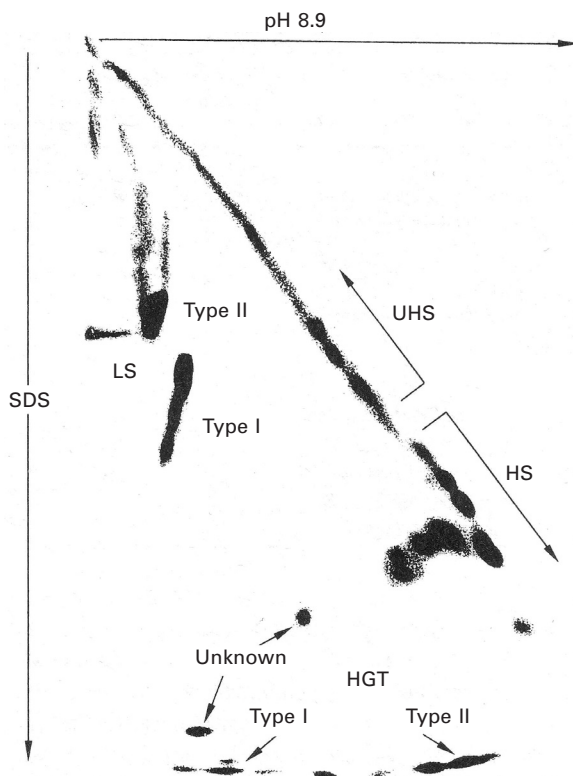
residue, which is generally formed through the electrostatic interaction between cationic and anionic side-chain groups.

Fourth, a disulphide bridge is shown between two cysteine residues. The disulphide bridge plays an important role in stabilizing keratinous materials, leading in particular to their relatively high wet strength, moderate swelling and insolubility.

Fifth, an isodipeptide bridge is formed by the reaction between glutamic acid and lysine. This second, though relatively rare, covalent bond is due to the isodipeptide  $N_\epsilon$ -( $\gamma$ -glutamyl) lysine, which provides an additional stabilizing effect in the cornified envelopes of cortex and cuticle cells (Zahn *et al.*, 2005).

Through heat and water, two further crosslinks (not shown) are formed by reactions between amino acids, namely, lanthionine through the two-step elimination of sulphur from cystine, and lysinoalanine (McLaren and Milligan, 1981).

Two-dimensional SDS-polyacrylamide gel electrophoresis (2D SDS-PAGE) enables the separation of the various proteins formed by the amino acids (see Fig. 4.4). The proteins are extracted from the fibres through exhaustive reduction of the sulphur crosslinks and carboxymethylation of the resulting



4.4 Separation of wool proteins after extraction from Merino wool by 2D SDS-PAGE (see text) according to charge (horizontal) and size (vertical). LS = low sulphur, HS = high sulphur, UHS = ultra high sulphur, HGT = high glycine-tyrosine (adapted by Zahn *et al.*, 2003, from Marshall, 1981).

thiol groups. Subsequently the proteins are separated according to charge and size (Marshall, 1981; Dowling *et al.*, 1986; Powell and Rogers, 1997; Zahn *et al.*, 2003). Figure 4.4 shows that the proteins fall essentially into two primary groups. These are the keratin intermediate filament (KIF) high molecular weight, low sulphur (LS) proteins on the one hand, and the keratin associated (KAP) proteins on the other. The latter in turn consist largely of the smaller, high sulphur (HS) and the high glycine-tyrosine (HGT) proteins. In each of the groups and subgroups a wide variety of individual protein species is observed (Haylett *et al.*, 1971; Höcker, 2002), as summarized in Table 4.2.

#### 4.3.2 Lipids

Wool (water free) consists mainly of proteins (*ca.* 97%). The remainder are lipids (*ca.* 2%) and about 1% mineral salts, nucleic acids and carbohydrates.

*Table 4.2* Primary protein fractions in Merino wool together with information on the contained protein families and some of their specific properties (Based on Haylett *et al.*, 1971; Powell and Rogers, 1997; Parry, 1997; Höcker, 2002; Zahn *et al.*, 2003)

Protein fraction	Fraction, %	Protein family	Number of residues	Properties
Low sulphur	58	5 acid Type I, KIF	392–416	
		5 basic Type II, KIF	479–506	
High sulphur	18	80–100 sulphur-rich KAP	94–211	16–24 mol% half-cystin
Ultra-high sulphur	8	3–15 ultra-high sulphur-rich KAP	168–197	33–37 mol% half-cystin
High gly/tyr	6	10 Type I gly/tyr-rich proteins	61–84	35–40 mol% gly and tyr
		5 Type II gly/tyr-rich proteins	ca. 80	60 mol% gly and tyr

gly = glycine, tyr = tyrosine.

The lipids are separated into an external and an internal fraction, respectively. The first group derives from wool grease and is almost completely removed through wool washing (scouring). Refined fractions of wool grease are known as lanolin, with widespread use in the cosmetic industry.

Internal lipids consist mainly of sterols (cholesterol, desmosterol), fatty acids (palmitic, stearic, oleic acid), and polar lipids, such as ceramides, cerebrosides (sphingolipids) and cholesterol sulphate (McLaren and Milligan, 1981; Zahn *et al.*, 2003). These lipids originate mainly from the cell membrane complex, as an integral part of the keratin fibre morphology (see Section 4.5). During cell apoptosis at the end of the keratinization process, lipids are trapped in various locations within the keratinous material.

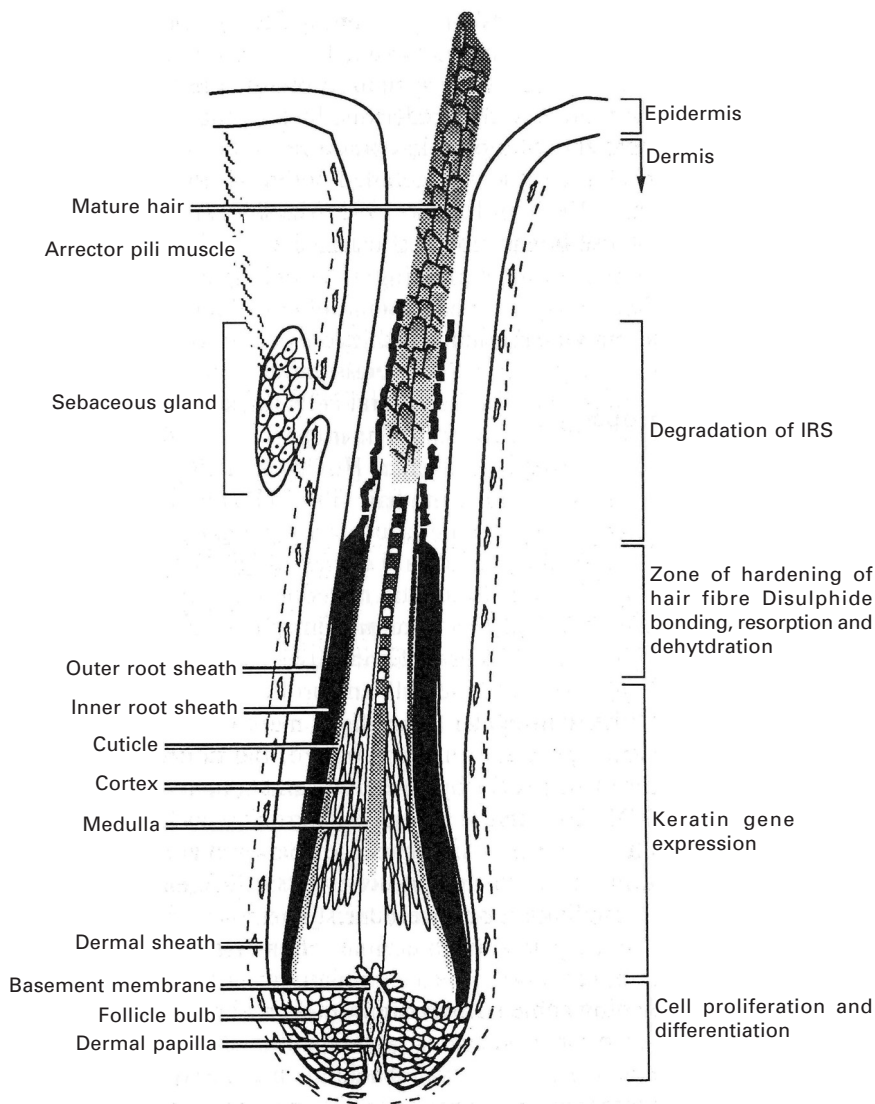
A characteristic of the structural lipids of the cuticle is the presence of a branched-chain C21 fatty acid, 18-methyleicosanoic acid, forming a substantial part of the lipids of the F-layer (see Section 4.5), and covalently bound through thioester bonds to the underlying proteins (Negri *et al.*, 1993; Zahn *et al.*, 2005).

#### 4.4 Fibre formation

Hairs grow from cavities (follicles) that extend from the surface of the skin through the epidermis into the dermis (Wollina, 1997). They are composed mainly of fibrous proteins, which characteristically contain cystin residues, forming intra- and intermolecular crosslinks. During hair growth a wide range of keratin proteins are laid down intracellularly in a defined sequence from which morphological fine structures develop until the cells (keratinocytes)

finally die in the terminal stages of keratin synthesis, when the sulphur crosslinks are formed.

Figure 4.5 from Powell and Rogers (1997) gives a detailed graphical representation of the various elements of the structure of the hair follicle



4.5 Schematic presentation of the hair follicle (Powell and Rogers, 1997) showing the major morphological components of the developing hair as well as the regions where the main events of cell proliferation, differentiation and keratinization take place (reproduced with permission).

and the main events during hair growth. Type I and Type II keratins (see Table 4.2), which form the IFs, are formed as first components just above the bulbus (Powell and Rogers, 1997). In higher regions of the follicle HS as well as HGT KAPs are formed, in varying amounts for the different cell types, *ortho*, *para* and *meso*, respectively. Gene expression studies (Langbein and Schweizer, 2005) confirm earlier results from elemental analysis by electron microscopy (Jones *et al.*, 1993) that proteins rich in sulphur are concentrated in para-cortical cells, while HGT proteins are preferentially found in the ortho-cortex. Finally, the UHS proteins of the cuticle are expressed. During travel towards the skin surface the cells move in different streams (Langbein and Schweizer, 2005), the cortical cells assuming a spindle shape while the outer cuticle cells become flat and rectangular to form the fibre surface, with overlapping scales (see Fig. 4.5).

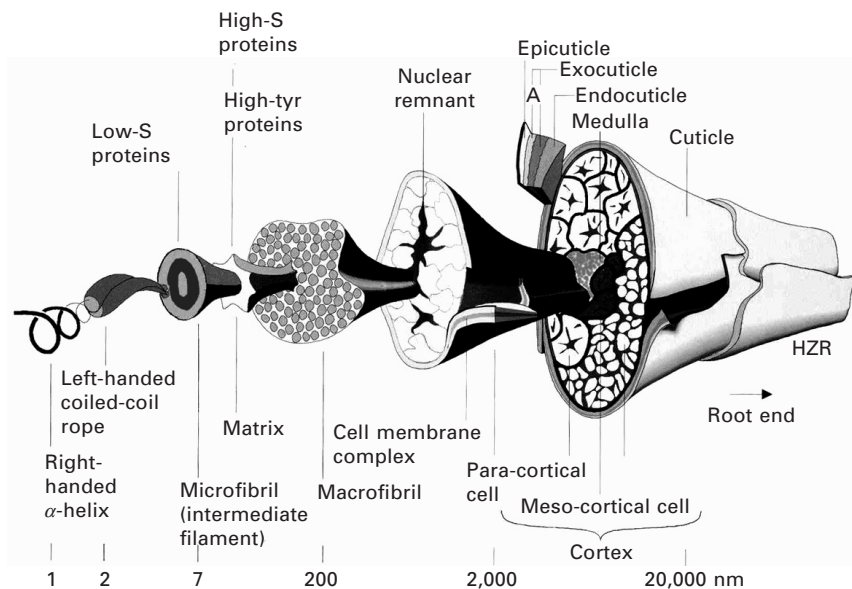
## 4.5 Morphology

Keratinous fibres such as wool and hair exhibit a complex biological composite structure, which is common to all mammalian  $\alpha$ -keratin fibres. Dobb *et al.* (1961) developed the first comprehensive and widely used graphical representation of the morphology of a wool fibre. This approach was further developed by Marshall *et al.* (1991), which is today the most widely used presentation concept for wool and hair (Feughelman, 1997; Schwan-Jonczk *et al.*, 1998). An alternative has been developed by Zahn *et al.* (1997) based on work by Eichner *et al.* (1985).

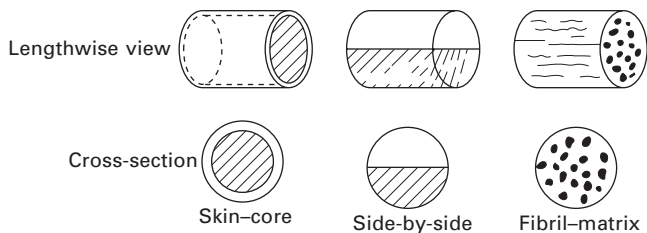
Figure 4.6 summarizes graphically the general structural features of an  $\alpha$ -keratinous fibre, as adapted by Feughelman (1997, 2002) from Marshall *et al.* (1991), which apply in close analogy to all  $\alpha$ -keratinous materials.

In order to assist the investigation and understanding of the physical and mechanical properties of such a complex fibre, Zahn *et al.* (1980) applied the structural principles for fibrous composites, as shown in Fig. 4.7, and arrived at a hierarchically structured morphology for an  $\alpha$ -keratin fibre, as given in Table 4.3.

On the first level, the fibre core is surrounded by the cuticle 'skin' as a protective sheath, which in the case of wool consists of a single layer of cuticle cells. The cells are nearly rectangular in shape and overlap like shingles on a roof, with the cell edges pointing towards the fibre tip. Their tilt angle away from the longitudinal fibre surface is about 2–3° (Bustard and Smith, 1990; Wortmann *et al.*, 2003). The cuticle cell dimensions are generally quoted as about 20–30  $\mu\text{m}$  (Höcker, 2002) for wool and about 50–70  $\mu\text{m}$  for human hair (Swift, 1997), where these dimensions seem to be roughly comparable with the overall fibre diameter, respectively. For wool the cells have longitudinally a wedge-shaped cross-section, which give the cells a height of the exposed edge of about 1  $\mu\text{m}$ . For other animal fibres



4.6 Graphical representation of the morphological structure of a Merino wool fibre at progressive magnifications from right to left (adapted by Feughelman, 1997, 2000, from Marshall *et al.*, 1991).



4.7 Structural principles of fibrous composites (adapted from Zahn *et al.*, 1980).

Table 4.3 Principal types of composite structures in  $\alpha$ -keratinous materials as shown in Fig. 4.7, progressing through various levels from the  $\mu\text{m}$ - to the nm-scale (see Fig. 4.6)

Level	Composite	Type	First component	Second Component
1	Fibre	Skin/core	Cuticle	Cortex
2	Cortex	Side-by-side	Ortho-cortex	Para-cortex
3	Cortex	Fibril/network	Cortical cells	Cell membranes
4	Cortical cell	Fibril/matrix	Macrofibrils	Intermacrofibrillar material
5	Macrofibrils	Fibril/matrix	Intermediate filaments (KIF)	Matrix (KAP)

the cross-section is more rectangular, leading to edge height around  $0.5\ \mu\text{m}$  and below. This difference in scale edge height is an important criterion for the microscopic differentiation of wool and other animal fibres (Wortmann and Arns, 1986; IWTO-58, 2000). Each cuticular cell has its distal edge on the fibre surface, while the opposite edge is in contact with the cortex. With the high degree of overlap of the cells, e.g. for human hair, presenting only about  $5\ \mu\text{m}$  of exposed length, the apparent thickness of the cuticle in the fibre cross-section may be up to 10 layers, thus providing effective protection for the underlying fibre core.

The individual cuticle cell consists of four different layers of amorphous proteins (Bradbury, 1973) laid down in parallel to the fibre axis, namely the epicuticle, the A-layer, the exo-cuticle and the endo-cuticle (Swift, 1997), which differ strongly in their cystine and isodipeptide content. The outermost surface of the cuticle cells, referred to as the F-layer, largely consists of a monolayer of 18-methyl eicosanoic acid (18-MEA) covalently bound to the underlying proteins of a highly resistant membrane through thioester linkages (Negri *et al.*, 1993). This composite structure of lipid layer and resistant membrane is the cuticular cell envelope (Zahn *et al.*, 2005) and is generally referred to as epicuticle. It can be delaminated from the underlying A-layer through the Allwoerden reaction with chlorine water (King and Bradbury, 1967). The volume fraction of the cuticle for wool is generally considered as being of the order of 10–15% (Swift, 1997; Höcker, 2002).

The fibre core is the cortex, which comprises about 90% of the fibre and consists of a compact arrangement of spindle-shaped, strongly interdigitated cortical cells (length *ca.*  $100\ \mu\text{m}$ , maximum diameter *ca.*  $5\ \mu\text{m}$ ) (Rogers, 1959). Depending on the type of keratin fibre, different types of cortical cells are observed, namely ortho-, para- and rarely meso-cells (Orwin *et al.*, 1984). Para-cells generally occupy a lower volume fraction (10–40%) compared to ortho-cells, but they show a higher degree of fine structural organization. Furthermore, they contain a larger amount of cystine and are thus higher crosslinked and tougher. In accordance with the chemical composition, higher elastic moduli have been determined for the para- (4.7 GPa) compared to the ortho-cortex (3.7 GPa;  $19^\circ\text{C}$ , 40% RH) (Caldwell and Bryson, 2005). The properties of meso-cells are somewhat between these two extremes.

In fine Merino wool, ortho- and para-cortical cells are laid down in a side-by-side arrangement (Level 2, see Table 4.3 and Fig. 4.7), which is generally considered to be the determining factor of fibre crimp (Cook and Fleischfresser, 1990). In other animal fibres neither the chemical distinction nor the segregation of the cell types in the cross-section is quite as apparent.

The interface between the cells, the cell membrane complex (CMC), is a continuous, layered phase of proteins, lipoproteins and adjacent membrane lipids. The fraction of the CMC has been estimated to be about 3% (Bradbury, 1973). As was observed quite early by light microscopy (Appleyard and



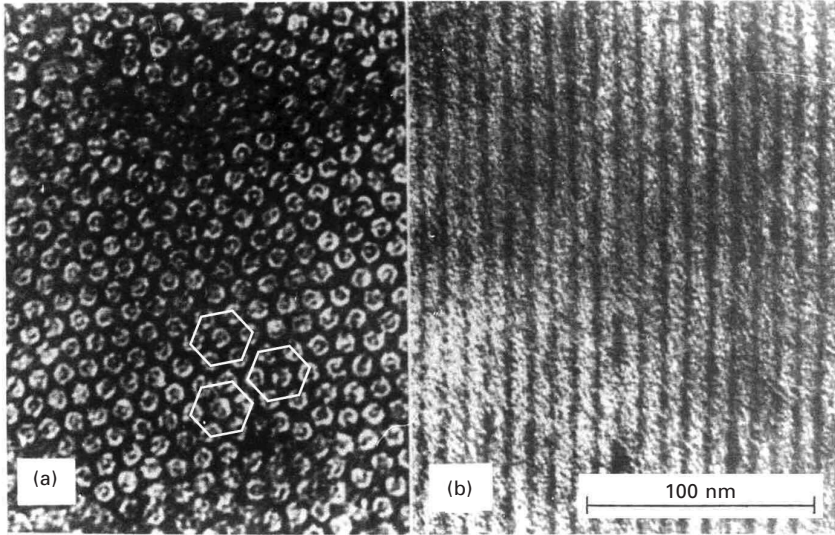
Dymoke, 1954), the CMC forms a continuous network around the cortical cells, thus formally qualifying this arrangement for the third level of structural differentiation (see Table 4.3) as a filament/matrix composite (see Fig. 8.7). The role of the CMC for the cohesion of the cortical cells becomes apparent when the CMC is chemically removed. The spindle cells are released and the fibre disintegrates (Woods, 1936; Bradbury, 1973).

However, due to the small fraction of CMC and the strong mechanical interaction of the cortical cells through interdigitation, the contributions of the CMC to most physical and mechanical properties of keratin fibres are generally considered to be negligible (Bradbury, 1973; Bendit and Feughelman, 1968; Zahn *et al.*, 2003).

In coarser wools, many animal fibres and certain types of human hair, a medulla is also observed. The medulla cells consist of empty vacuoles, which are separated from each other by a fine proteinaceous network. The cells may occur in relative isolation or in series, up to the point where they generate a continuous, hollow tube in the fibre centre, such as in angora rabbit hair (Wortmann *et al.*, 1989). In general, the fraction of medulla in individual fibre cross-sections is very variable and to some extent fibre type specific (Wildman, 1954).

A cortex cell contains around 5–20 macrofibrils with a diameter of 100–300 nm at the widest point (Rogers, 1959). Cytoplasmic and nuclear remnants form the intermacrofibrillar material, so that on the fourth level (see Table 4.3) again a fibril/matrix composite is formed.

The macrofibrils are composed of bundles of 500–800 intermediate filaments (KIF or just IF), traditionally also referred to as microfibrils. These are an impressive example of the self-organization of the low-sulphur, Type I and Type II IF-proteins, which are synthesized in the follicle at a very early stage of hair formation (see Section 4.4). The IFs have a diameter of about 8 nm and are spaced roughly 10 nm apart. The space between them is filled by material, traditionally referred to as matrix, which consists of keratin- or intermediate filament associated proteins (KAPs or IFAPs) of the sulphur-rich (HS) and the high-glycine–tyrosine (HGT) type (see Table 4.2). They represent about 40% of the fibre cross-section (Sikorski, 1975). Observations by transmission electron microscopy (Rogers, 1959; Filshie and Rogers, 1961; Powell and Rogers, 1997) have shown (see Fig. 4.8) that the IFs, namely in para-cortical cells, are arranged in highly ordered, hexagonal patterns in the cross-section, while being strictly parallel to the fibre axis. This makes this material on the fifth and final level of differentiation a nano-scaled filament/matrix composite according to the principles underlying Table 4.3. In ortho-cells the arrangement is less perfect; here a whorl-like pattern is observed (see Fig. 4.8).



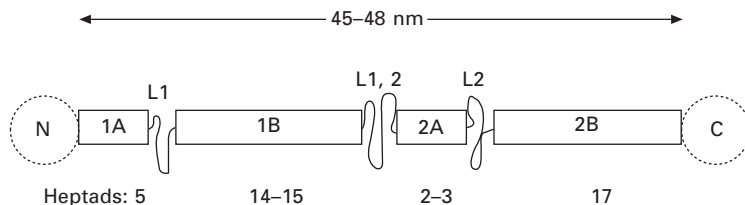
4.8 Electron micrograph of porcupine (*Hystrix cristata*) quill tip: (a) cross-section of the cortex, (b) longitudinal section of the cortex. The staining with heavy metals results in light staining of the low-sulphur IFs, while the surrounding high-sulphur proteins of the matrix are densely stained. The hexagonal arrangement of the IFs in the cross-section is indicated (adapted from Rogers, 1959; Filshie and Rogers, 1961).

## 4.6 Molecular structures

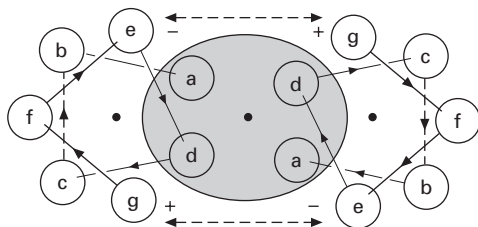
Intermediate filaments (IFs) are intracellular fibrous polymers, which are a prominent constituent of the cell's cytoskeleton. They are readily distinguished from actin microfilaments (6 nm) and microtubules (25 nm) through their size (10–12 nm). In mammals more than 67 genes encode proteins, which are able to self-assemble into IFs (Bernot and Coulombe, 2004; Langbein and Schweizer, 2005).

The primary structure of IF proteins, as a basis for the formation of the intermediate filaments, is comparatively conservative (Parry and Steinert, 1999) This is in contrast to the KAPs, for which the amount and composition are very variable within the group of hard  $\alpha$ -keratins (Bendit and Gillespie, 1978).

The monomeric unit of the IF, as shown schematically in Fig. 4.9, consists of a mainly  $\alpha$ -helical central rod with non-helical C- and N-terminal regions (Parry and Fraser, 1985; Dowling *et al.*, 1986). The central rod consists of approximately 40 amino acid heptads in right-handed,  $\alpha$ -helical sections with an overall length of  $\sim 47$  nm (Conway *et al.*, 1988). It is made up of two similar, 20–21 nm long, helical sections (1 and 2), connected by a non-helical linker (L1,2). The sections themselves again consist of shorter helical



4.9 Secondary structure of a typical  $\alpha$ -keratin monomer, namely the 8c-1 protein of the wool intermediate filament (see text). The C- and N-terminal ends of the protein are marked (Parry and Fraser, 1985; Dowling *et al.*, 1986).



4.10 Amino acids in the  $\alpha$ -helix are arranged according to a heptad sequence, denoted as a–g. The side-chains of residues a and d are apolar effecting the region of apolar interaction, as indicated by the grey oval. Residues e and g are negatively and positively charged, respectively, providing ionic interactions, represented by the broken arrows (adapted from Feughelman, 2002).

rods (A and B, respectively), linked by non-helical chain segments (L1, L2). The stability of various segments in the helical as well as the amorphous domains has been investigated by Molecular Dynamics (MD) simulation (Knopp *et al.*, 1996, 1997).

As the first step in the assembly of an IF, two different monomers, one acidic (Type I) and one basic (Type II), form a parallel, super-helical, left-handed, coiled-coil hetero-dimer, for which the structural integrity is ensured by the steric interaction of the side-groups of the helices (Dowling *et al.*, 1986; Fraser *et al.*, 1988, Parry and Steinert, 1999). The stability of the dimer association is ensured by ionic- and especially by apolar interactions. The latter are a consequence of the highly characteristic sequence motif of the amino acids in the helical segments. These follow the so-called heptad-rule (Parry and Fraser, 1985), so that cationic and anionic amino acids are in suitable positions for interactions between the monomers, and apolar amino acids are located in a band running along the segments, and providing the contact region of the monomers in the dimer, as shown in Fig. 4.10. This apolar region winds gradually around the axis of the helix in a left-handed manner. Ionic and apolar interactions are thus the primary driving and stabilization

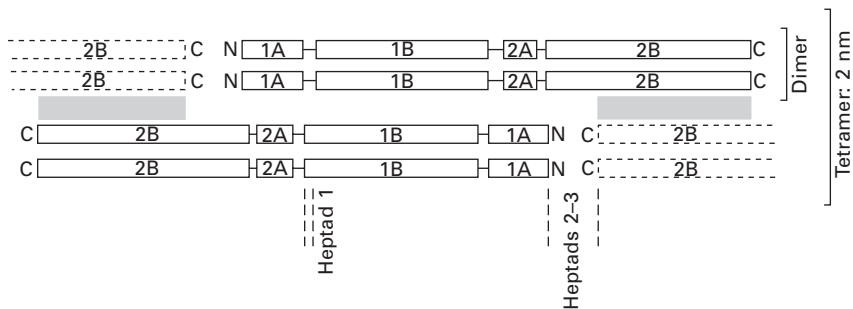
forces of the coiled-coil aggregate of two  $\alpha$ -helices. It is interesting to note that the 2B segment in the IF monomer shows a stagger with respect to the heptad rule close to its *N*-terminal end (Dowling *et al.*, 1986).

It is generally assumed (Parry and Steinert, 1999) that two dimers in antiparallel and staggered position form the tetramer, also referred to as protofilament, with a diameter of 2–3 nm. Though *in vitro* crosslinking studies indicated a number of possible arrangements (Steinert *et al.*, 1993), the structure, referred to as  $A_{22}$ , in which the 1B segments are arranged side-by-side and the 2B segments in a slight stagger of 2–3 heptads appears to be especially consistent with the mechanical and thermal properties of hair (Wortmann and Zahn, 1994; Wortmann *et al.*, 2006b).

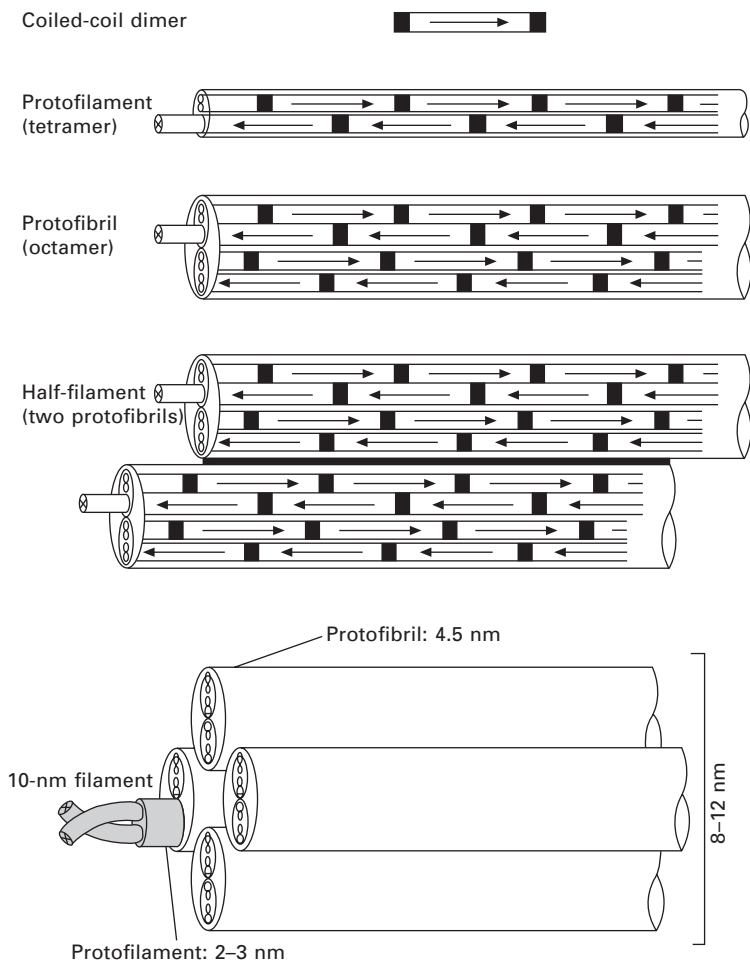
In this arrangement, shown in Fig. 4.11, the protofilament structure is stabilized by ionic interactions between the B segments, and especially by an overall number of six sulphur bonds between the 2B segments of different dimers, which are sterically possible by the shift of the dimers relative to each other by  $\sim 2$  heptads (Sparrow *et al.*, 1988). As a consequence  $\alpha$ -helical blocks are formed across the tetramer by the 1A, 2A and 1B segments, respectively.

Figure 4.12 summarizes from top to bottom the stepwise self-organization of the IF nano-structure, according to a  $2^n$  rule starting from the coiled-coil dimer. The protofilament (tetramer) doubles to form the protofibril (octamer), which again doubles to yield a half-filament, two of which finally yield the IF with a diameter of 8–12 nm and 32 KIF chains in the cross-section (Eichner *et al.*, 1985).

While models for ‘idealized IFs’ usually include these 32 monomers per filament cross-section, determinations of linear density show that this number can actually vary depending on the source and the type of IFs (Bernot and Coulombe, 2004). The actual arrangement of the tetramer and octamer is also



4.11 Arrangement of IF monomers in the tetrameric structure of the protofilament; The shaded areas indicate where disulphide bonds are formed between dimers (adapted from Sparrow *et al.*, 1988).



4.12 Hierarchical structure formation in the IF according to a 2-rule (adapted from Zahn *et al.*, 1997; Eichner *et al.*, 1985).

less well known than Fig. 4.11 would suggest (e.g. Feughelman *et al.*, 2005). The general arrangement can be expected to be of the ring or ring/core-type (see Fig. 4.6), as early investigations by transmission electron microscopy (TEM) have convincingly shown (Johnson and Sikorski, 1965).

The two basic principles of the self-organization of cytoplasmic IFs are first the parallel arrangement of two monomers in a dimer due to unspecific apolar and specific electrostatic interactions, and second the anti-parallel orientations of the dimers within a tetramer, which in turn leads to structurally apolar, mature IFs. While the first principle is well established, the second, though widely accepted (Bernot and Coulombe, 2004), is inconsistent with experimental evidence for keratin fibres, as reviewed by Feughelman *et al.*

(2003). Namely, the dielectric and piezo-electric properties of  $\alpha$ -keratin can only be explained if its  $\alpha$ -helical dipoles are synergistically aligned in the axial direction. This inconsistency shows a fundamental problem of our current understanding of the structure of the IF, at least in this context, which needs further investigation.

## 4.7 Mechanical properties and models

### 4.7.1 The two-phase model for $\alpha$ -keratins

The complex morphological and molecular structure of  $\alpha$ -keratins, shown for the example of wool in Fig. 4.6, echoes the construction principle of biological composite structures in general, namely to combine components with different properties in one material so as to maximize suitability for its purpose. Table 4.3 shows the stepwise differentiation of the morphological structure of wool into the most important two-phase structures, leading ultimately to the so-called two-phase model.

In view of their physical and mechanical properties and in agreement with microscopical evidence (Rogers, 1959), the dominant morphological components of wool and hair are partly  $\alpha$ -helical intermediate filaments (IF) embedded, with largely axial orientation, in an amorphous matrix (Feughelman, 1959, 1997).

The IF monomer contains  $\alpha$ -helical segments in series, which form larger aggregates in the superstructure of the IF, for which the term 'paracrystalline' (Hindeleh and Hosemann, 1991) seems to be appropriate. Rigorous simplification of the complex morphological structure (see Table 4.3 and Fig. 4.7) leads to a consideration of the cortex as effectively a nano-scaled, axially oriented filament/matrix composite.

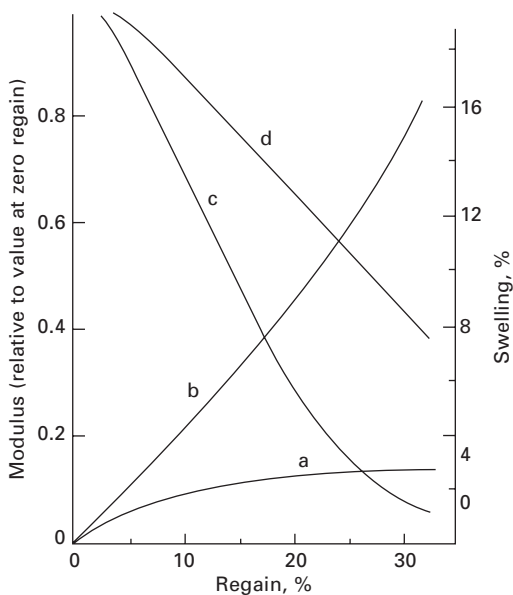
A specific contribution of the cuticle as the outer protective sheet to the mechanical properties of wool or hair is considered as being largely negligible (Feughelman and Haly, 1960; Bendit and Feughelman, 1968). The similarity of the stress/strain curves of wool and human hair, differing widely in the effective number of cuticle layers in the cross-section, has been used as an argument in support of this view (Wolfram and Lindemann, 1971).

If only the  $\alpha$ -helical central rod-like domains in the IFs are regarded as crystalline or rather para-crystalline, this phase accounts for 25–30% of the dry fibre (Bendit, 1968; Wortmann and Deutz, 1993). The other components make up the 'matrix' phase, which includes the cuticle, the cell membrane complex, the intermacrofibrillar material, the inter-filament material, and 40% of the IFs, i.e. the non-helical linkers and the ends of the IF monomers (Wortmann, 1992). This characteristic fibre structure leads to the marked differences between axial and lateral properties, as realized at a very early stage from the pronounced differences between axial and lateral swelling,

as well as between extensional and torsional properties (Onions, 1962).

Curves c and d in Fig. 4.13 show the swelling of wool fibres from dry to wet with increasing regain. In the follicle the keratin fibre is produced under wet conditions. Upon drying, the para-crystalline filaments will resist shrinkage so that on rewetting or swelling from the dry state the length change is rather small, 1–2%. Radial swelling is a property of the amorphous matrix only. The effect is a rather large difference of 16% between dry and wet and reflects the strong tendency of the matrix to absorb water. This stability of the  $\alpha$ -helical fraction in the IFs (Bendit and Feughelman, 1968; Feughelman, 1989) is an interesting phenomenon in view of the generally assumed sensitivity of the  $\alpha$ -helix against water, which in turn is attributed to the extensive hydrophobic interactions within the coiled-coil structure and the high degree of para-crystalline aggregation (see Section 4.6).

The tendency of keratin fibres to absorb and to be effectively plasticized by water is reflected in the decrease of the elastic modulus with humidity from dry to wet (see Fig. 4.13, Curve d). The effect is limited to a factor of 2.7 due to the humidity-invariant modulus of the filaments. Accordingly, the decrease is substantially more pronounced for torsion (Curve c), which is a property of the matrix only, with a factor of about 15 (Speakman, 1930; Bendit and Feughelman, 1968). Similar factors have been observed



4.13 Changes of swelling and moduli with regain for wool fibres: (a) length swelling; (b) radial swelling; (c) torsional modulus; (d) extensional modulus (Zahn *et al.*, 2003, adapted from Onions, 1962).

in extensional relaxation experiments of wool fibres, when separating the elastic and viscoelastic contributions of filaments and matrix, respectively (Wortmann and DeJong, 1985a)

The elastic and viscoelastic properties of wool fibres, as determined by the mechanical properties of IFs and matrix, largely determine crease resistance, dimensional stability, drape and handle of wool fabrics, while they are decisive factors for water wave formation and stability in human hair.

#### 4.7.2 Elastic moduli of specific morphological components

On stretching and relaxing wool fibres in the linear viscoelastic region ( $\epsilon < 0.8\%$ ), the behaviour of the crystalline phase is linearly elastic (Wortmann and DeJong, 1985b; Feughelman and Robinson, 1971) and that of the matrix phase is linearly viscoelastic. The matrix completely relaxes with a speed depending on relative humidity (Wortmann and DeJong, 1985a). The equilibrium modulus is independent of water regain and attributed to the helical fraction in the IFs. Taking into account the uncertainties for the fraction of helical material, its modulus  $E_{hx}$  is determined in the range of (Zahn *et al.*, 2003):

$$E_{hx} = 7.8\text{--}9.6 \text{ GPa}$$

The  $\alpha$ -helix is essentially stabilized by axial hydrogen bonds. It is thus not surprising that the estimated range for the modulus agrees well with the modulus of hydrogen-bonded, crystalline ice (ice I, 0°C:  $E = 10 \text{ GPa}$ ; Fletcher, 1970). A similar value was expected from low temperature modulus determinations of wool (Druhala and Feughelman, 1971, 1974). This agreement of the modulus values emphasizes the ideal arrangement and cooperation of the relatively short  $\alpha$ -helical segments in the microfibrillar para-crystal.

The limiting, elastic modulus of the dry (d) and wet (w) matrix  $E_m$  are calculated to be

$$E_m^d = 6.1\text{--}6.6 \text{ GPa}, E_m^w = 0.5 \text{ GPa}$$

$$E_m^d / E_m^w \approx 13$$

Under standard conditions (65% RH, 20°C) the matrix modulus is 3 GPa (Wortmann and DeJong, 1985a; Wortmann, 1992).

The dry/wet ratio of the moduli for the matrix is, as to be expected, in good agreement with the ratio of the corresponding torsional moduli ( $G_d/G_w \approx 15$ ) shown in Fig. 4.13, since in a filament/matrix composite the torsional behaviour is a property of the matrix.



The rather small difference between the moduli of crystalline helices and amorphous matrix in the dry state is attributed to the fact that under these conditions both components are stabilized by an array of hydrogen bonds. These are broken in the matrix under the influence of water, while they persist in the helical regions, due to the hydrophobic interactions and the high degree of aggregation.

The matrix in the two-phase model also includes the cuticle, which forms a distinctive, ring-like protective sheet around the fibre core, representing about 10% by weight of the fibre. Though the simplification appears to be well justified within a specific theoretical and experimental framework, various mechanical scenarios, such as in bending and torsion of human hair, where diameter-related effects gain relevance, can be envisaged where the cuticle would be expected to play a major role (Liu and Bryson, 2002).

Various approaches have been undertaken to determine the moduli of the various layers of the cuticle. Bryson and co-workers (Parbhu *et al.*, 1999), using nano-indentation, determined elastic moduli under ambient conditions of 19.8 GPa and 3.8 GPa for exo- and endo-cuticle, respectively. The latter value looks reasonable in view of the modulus range of the matrix in wool (see above), while the value of the exo-cuticle layer appears to be quite high. Both values are orders of magnitude higher than those measured by Gibson *et al.* (2001) for the surface of wool fibres ( $<10^{-3}$  GPa). In later work Bryson and co-workers (Caldwell and Bryson, 2005) determined elastic moduli for the cuticle in the range of 3 GPa for both layers of the cuticle, considering their initial high reading for the exo-cuticle as an artefact.

However, calculations by Stapels (2001) showed that the significantly lower cohesive bending set of human hair without cuticle, compared to native hair, can be explained if the modulus of the exo-cuticle is assumed to be of the order of 20 GPa. This observation gives support for the initial value given by Parbhu *et al.* (1999) and furthermore emphasizes the need to take specific care to appreciate, for a specific experimental situation, the limitations of the two-phase model for  $\alpha$ -keratinous materials.

Specific applications of structural composite theory to  $\alpha$ -keratins have been realized by Curiskis and Feughelman (1983) and more recently by Liu and Bryson (2002), and further extended to Molecular Dynamics (MD) simulations by Akkermans and Warren (2004).

## 4.8 Thermal transitions

The complex morphology of wool and hair fibres leads obviously to a wealth of facets of their structural and physical properties, a good number of which have been reviewed by Feughelman (1997). After detailed considerations of the interrelations between fibre morphology and structural models as well as component moduli, in what follows the various temperature- and

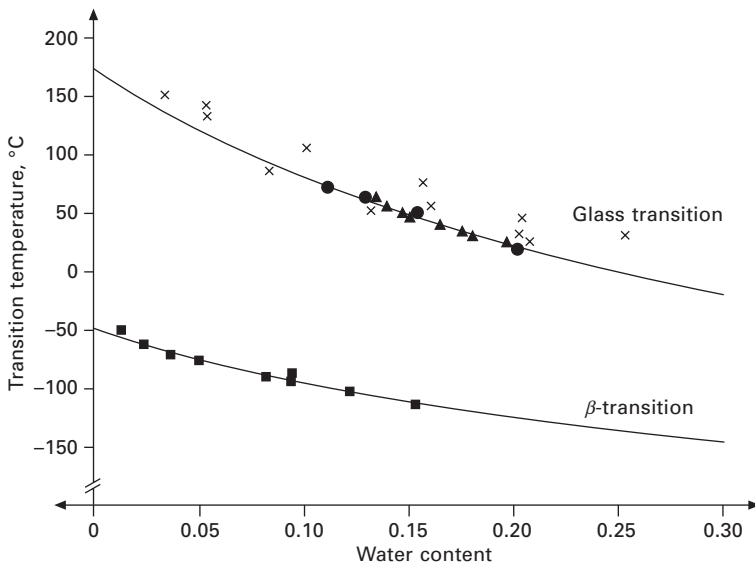
humidity-induced transitions of the  $\alpha$ -keratinous materials as viscoelastic, semi-crystalline, fibre/matrix composites are reviewed.

#### 4.8.1 The viscoelastic, $\alpha$ - and $\beta$ -transitions

Hard  $\alpha$ -keratins show those viscoelastic transitions which are characteristic for semi-crystalline polymers, such as a low temperature  $\beta$ - and a higher temperature  $\alpha$ -(glass) transition.

Druhala and Feughelman (1971, 1974) investigated the dynamic  $E$ -modulus of horse hair and rhino horn between  $-180^\circ\text{C}$  and room temperature for a wide range of water contents, finding distinct peaks in the  $\tan\delta$  values, signifying the  $\beta$ -transition temperature  $T_\beta$ , where the mobility even of short-chain segments or protein side-chains is frozen. The data are summarized in the lower curve of Fig. 4.14.

Since temperature and low molecular weight plasticizers have similar effects on the mobility of polymer chains, it is to be expected that also the glass transition temperature  $T_\alpha$  ( $\equiv T_G$ ) will depend on water content. Over 80 years ago King (1926) investigated the density and specific volume of wool at different water contents ( $25^\circ\text{C}$ ), yielding around a water weight fraction of 17.5% the turnover between the classical linear changes for polymers



4.14  $T_\beta$  values taken from Druhala and Feughelman (1971, 1974) (■) and values for  $T_G$  from Rosenbaum (1970) (▲), Wortmann *et al.* (1984) (●) and Phillips (1985) (×), as well as the analytical descriptions based on the Fox equation, plotted against water content.

above and below the glass transition. Rosenbaum (1970) investigated to what extent the Flory–Huggins equation for polymer solutions (Flory, 1953) could be applied for the description of the sorption isotherm of wool. The glass transition temperature was determined as the lower limiting temperature of applicability, beyond which the wool/water system transfers into the glassy state.

Wortmann *et al.* (1984) investigated the torsional recovery of wool fibres for various temperature/humidity combinations, combining their values with data from various other experiments. These investigations were followed up by Phillips (1985) and others (Huson, 1991; Kure *et al.*, 1997) using differential scanning calorimetry (DSC). The upper curve in Fig. 4.14 summarizes the results from Rosenbaum (1970), Wortmann *et al.* (1984) and Phillips (1985).

In the literature a number of approaches, differing in complexity (Gordon and Taylor, 1952; Couchman and Karasz, 1978), are described for the relation between glass transition temperature and plasticizer content. Analysis of the data (Wortmann *et al.*, 1984) shows, however, that wool as well as human hair (Wortmann *et al.*, 2006a) already follow well the simplest of these approaches, namely the Fox equation (Fox, 1956):

$$1/T_G = w_1/T_{G1} + w_2/T_{G2} \quad 4.1$$

where  $w$  is the weight fraction and the subscripts 1 and 2 refer to dry wool and pure water, respectively.

For wool the data could be well fitted to the data without any assumptions about the glass transition temperatures of the pure components, yielding through extrapolation (Wortmann *et al.*, 1984)  $T_{G1,wool} = 447$  K (174°C) and  $T_{G2,water} = 125$  K (–148°C). Considering the extrapolation range, the value for wool is in good agreement with torsional data by Menefee and Yee (1965) giving  $T_{G,wool} = 175$ °C. As discussed by Kalichevsky *et al.* (1992), for water there seems to be a general consensus that  $T_G$  falls into the region between 130–145 K, which is in good agreement with the extrapolated value obtained for the wool/water system. The line through the  $T_G$  data in Fig. 4.14 was determined on the basis of Equation 4.1 and the parameters given above. The visual assessment of the fit shows that the values of all three experimental approaches are equally well described by the Fox equation. Between ‘dry’ and ‘wet’ the glass transition temperature of wool changes by 180°C from 170–180°C to –5°C. At 65% RH with a water content of about 15% the glass transition temperature is around 50–60°C, so that under the conditions of normal climate wool is a semi-crystalline, glassy polymer. The  $T_\beta$  values in Fig. 4.14 can also be very well described by the application of the Fox equation (regression coefficient 99%), yielding  $T_{\beta,wool} = 224$  K (–49°C) and  $T_{\beta,water} = 63$  K (–210°C).

Looking at other keratin fibres, it is interesting to note that the glass

transition temperature of human hair (144°C) is 30°C lower than that of wool (174°C) (Wortmann *et al.*, 2006a). This result is rather unexpected, because hair is generally more hydrophobic in nature due to a higher fraction of high-glycine–tyrosine (HGT) proteins (Gillespie and Frenkel, 1972; Wortmann *et al.*, 1995). It is speculated that these proteins may induce a lower amount of hydrogen bonding in the matrix, stabilizing the glassy state, and may thus act as an ‘internal’ plasticizer (Wortmann *et al.*, 2006a).

The applicability of the Fox equation for  $T_{\alpha}$  as well as for  $T_{\beta}$  assumes a homogeneous distribution of water in the fibre. In view of the general two-phase structure of keratin fibres (neglecting the cuticle for the current argument) this is at first sight surprising, since the structure contains about 20–30% helical material, which does not absorb water. In nylon 6 as well as nylon 66, water sorption drops with the degree of crystallinity (Puffr and Sebenda, 1966). The same principle seems to apply for a variety of partly  $\alpha$ -helical proteins, such as lactoglobulin, zein and others (Breuer, 1972). Against this background Kure *et al.* (1997) and Pierlot (1999) applied for their work on wool a crystallinity-related bias to arrive at a value for the effective water content of the matrix.

The applicability of the Fox equation leads, however, to the conclusion that water realizes a pseudo-homogeneous distribution in the fibre, where similar relative amounts of water are adsorbed onto the surface of the helices as they are absorbed into the matrix. This conclusion is supported by investigations by Mellon *et al.* (1949) and Watt (1963), who showed that the sorption isotherm of wool remains largely unaffected when the helical fraction had been rendered amorphous. Stapels and Wortmann (2000) and Wortmann *et al.* (2006a) have shown that neither the water content nor the glass transition of human hair is affected by the thermal denaturation of the  $\alpha$ -helical structural component.

The humidity and temperature range between the  $\beta$ - and the  $\alpha$ -transition defines the range where the phenomenon of physical ageing (Struik, 1978) occurs, which plays an important role in the understanding of various aspects of the appearance retention of wool fabrics, such as wrinkling (Chapman, 1975a, 1975b; Wortmann and DeJong, 1985a), as well as for the stability of water waves in human hair, as an analogous phenomenon (Stapels, 2001).

#### 4.8.2 The denaturation transition

Using differential thermal analysis (DTA) and pressure-resistant sample containers, Ebert and Mueller (1965) and Ebert (1967) investigated the transition of wool fibres in various agents to study the phenomenon of supercontraction. For some of the conditions they applied, they observed multiple transitions at temperatures above approx. 100°C. The transition is due to the denaturation of the  $\alpha$ -helical material in keratin. Haly and

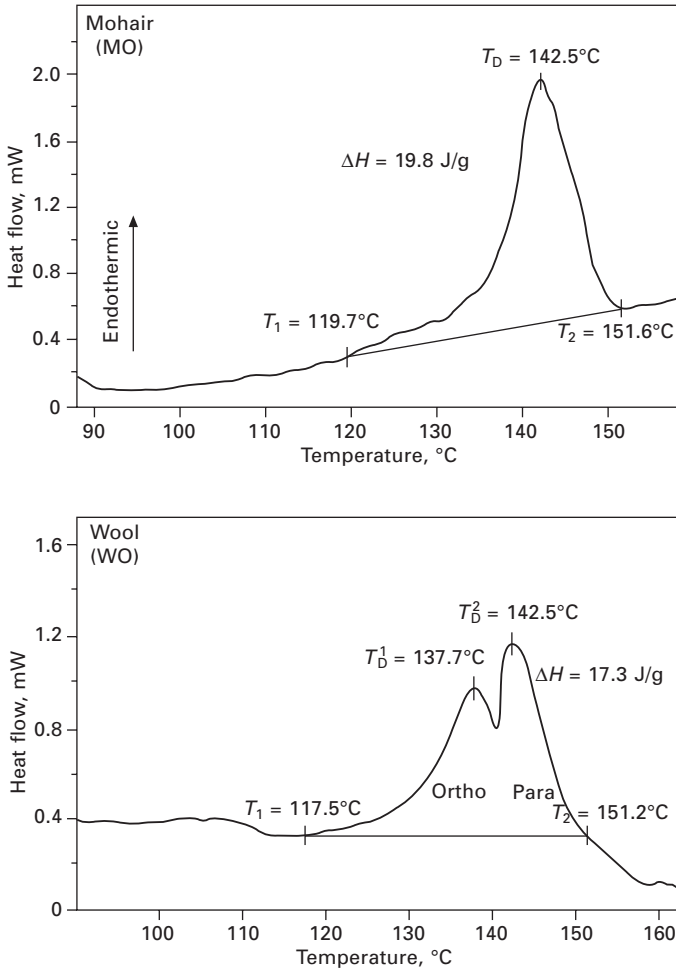
Snaith (1967) also used DTA to examine the performance of wool samples sealed into glass containers with various amounts of water. They observed a phase transition, often a doublet, which shifted with water content from approx. 230°C for dry wool to 140°C for wool in excess water. Spei (1990) reviewed his use of DSC to investigate the denaturation behaviour of various keratins in the dry state. Taking advantage of the shift of the peak to lower temperatures in water, Crighton and Hole (1985) developed a measurement cell for high pressure DTA to study the pronounced pressure dependence of the denaturation transition of keratins.

Wortmann and Deutz (1993) investigated the denaturation performance of various keratins in water by DSC, applying commercially available steel capsules, which gave safe access to temperatures of about 180°C, so that the denaturation transition temperatures as well as the enthalpies could be determined under conditions of equilibrium water vapour pressure. Denaturation temperatures are typically in the range of 110°C to 160°C, that is, well removed from pyrolysis conditions (Spei and Holzem, 1989; Monteiro *et al.*, 2005).

Figure 4.15 shows a typical DSC curve for mohair (hair of the Angora goat) and Merino (sheep) wool in water. As further materials, rhinoceros horn (RH), porcupine quill (PQ), finger nail (FN), echidna quill (EQ), European (EH) and African (AH) human hair were investigated (Wortmann and Deutz, 1993). Usually keratins show a single-peak structure for the denaturation, though double peaks were frequently observed for wool (Haly and Snaith, 1967; Spei and Holzem, 1989)

Investigating eight  $\alpha$ -keratins differing in their cystine content, the denaturation enthalpy in water was found to be largely material invariant at  $\Delta H = 17.1 \text{ J g}^{-1}$  dry keratin (Wortmann and Deutz, 1993). Assigning the enthalpy exclusively to the denaturation of the helical material leads to the conclusion that thus also the helix content for the materials is largely the same, estimated to be 25–30%, in accordance with literature data (Spei and Holzem, 1989). The large variation of the denaturation enthalpy that was observed by Spei and Holzem (1989) and Spei (1990) for a variety of keratins by ‘dry’ DSC could not be confirmed. This cannot be attributed to an effect of humidity, since Cao and Leroy (2005) showed for human hair that the denaturation enthalpy is not affected by the water content.

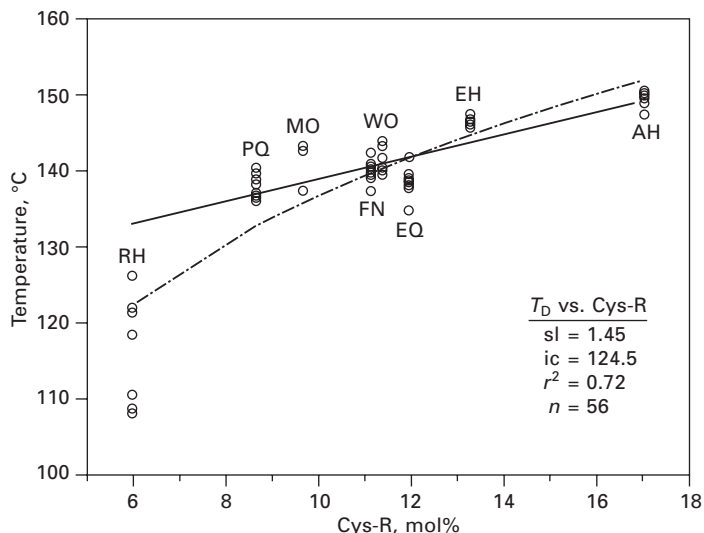
Feughelman (1989) reviewed the evidence originating from X-ray, infrared and mechanical experiments and showed that keratin fibres contain 25–30% crystalline,  $\alpha$ -helical material. Horikita *et al.* (1989) determined by X-ray diffraction techniques helix crystallinities between 24 and 31% for different wools, various goats and cameloid fibres, and for angora rabbit hair, without detecting any significant material specific variations. Cao and Billows (1999) more recently again conducted wide-angle X-ray diffraction experiments, finding somewhat lower values of 14–18% for Lincoln and Merino wool.



4.15 DSC traces for mohair (goat hair, MO) Merino (sheep) in water (Wortmann and Deutz, 1993).

The denaturation enthalpy reflects the progress of the helix–coil transition in the crystalline sections of the intermediate filaments, where the concentration of cystine is low and the location and distribution of the sulphur crosslinks are known to be material invariant (Sparrow *et al.*, 1988). Hence, the independence of  $\Delta H$  of the cystine content of the material (Wortmann and Deutz, 1993) is plausible, if not expected.

The cystine crosslinks are in fact mainly located outside the helical regions and in the matrix material. Accordingly, a significant positive and largely linear correlation was found between denaturation temperature and cystine content for various keratins, as shown in Fig. 4.16 and in accordance with



4.16 Regression analysis of the denaturation temperatures for single-peak endotherms, examining  $T_D$  vs. the content of cystine residues (Cys-R). Linear regression parameters apply for all data except rhino horn. The alternative, logarithmic regression, including all data, is given by the broken line (Wortmann and Deutz, 1993). For abbreviations see text.

literature observations (Crighton and Hole, 1985; Spei and Holzem, 1989). The differences in the denaturation temperatures for the various keratins can hence largely be attributed to differences in the matrix material, mainly related to its cystine and thus crosslink concentration. The matrix in this context comprises the non-helical parts of the IFs, the material between the IFs, and all other amorphous, morphological components.

When the helical sections in the intermediate filaments undergo the helix-coil transition a major shape change is the consequence, which also imposes a large deformation on the amorphous matrix in which they are embedded. The higher the amount and the viscosity of the matrix material, the more hindered the general shape change of the filaments will be, and the higher in consequence the denaturation temperature in a constant heating rate experiment. This kinetic control is reflected in the pronounced heating rate dependence of the denaturation temperature (Deutz *et al.*, 1991) which has to be seen in relation to the pronounced pressure dependence as observed by Crighton and Hole (1985). The shift of the DSC denaturation peak with heating rate is in fact different for the two peaks of the bimodal endotherm of Merino wool (Deutz *et al.*, 1991).

Furthermore, consideration of this model leads to the consequence that the double-peak structure in the endotherm, observed quite frequently for wool and less frequently for other materials, is related to the denaturation of the

helical fraction in intermediate filaments embedded in matrices of different cystine contents. The morphological components to satisfy this condition are readily identified as ortho- and para-cortical cells. The differences in cystine content between the two types of cells, being relative low in the ortho- and higher in the para-cells, lead to an estimate for the differences in denaturation temperatures between the cell types that is in satisfactory agreement with the experimental observation. This interpretation of the bi-model endotherm by Wortmann and Deutz (1998) confirmed the hypothesis, first put forward by Haly and Snaith (1967), Crighton and Hole (1985) and Crighton (1990).

Attributing the endotherm doublet to the ortho/para structure of certain keratins is in contrast to the older hypothesis by Spei and Holzem (1989), who attributed the second peak to the matrix (cystine decomposition). Spei's hypothesis was again taken up by Cao (1997) and finally comprehensively disproved by DSC investigations on separated ortho- and para-cortical cells from Merino wool by Wortmann and Deutz (1998).

Literature data indicate that a decrease of denaturation enthalpy, such as due to weathering of hair or wool (Schmidt and Wortmann, 1994), which is associated with damage to the  $\alpha$ -helical material, is not necessarily accompanied by a loss of X-ray crystallinity (Kanetaka *et al.*, 1993). Rather intriguing examples are mammoth (Gillespie, 1970) as well as mummy hair (Bertrand *et al.*, 2003), for which various analytical approaches indicate extensive damage to the intermediate filaments, while the overall structure of their  $\alpha$ -helical fraction, as seen by X-ray diffraction, appears largely unperturbed. Kuzuhara (2006, 2007) on the other hand, using Raman spectroscopy, showed protein denaturation in human hair from  $\alpha$ - to random form by oxidation and reduction. This scattered and somewhat anecdotal evidence is considered as being supportive in the context of DSC investigations for the 'native helix' hypothesis (Wortmann *et al.*, 2002, 2006b). This hypothesis maintains that the denaturation enthalpy relates in fact only to the amount of 'native'  $\alpha$ -helical material, which still shows a denaturation transition, rather than the total amount of  $\alpha$ -helical material in hair, which may already be chemically degraded to some extent.

The theory that the denaturation enthalpy is related to the amount of  $\alpha$ -helical material in keratin while the denaturation temperature reflects the thermal stability of the matrix has been successfully applied to interpret the effects of cosmetic treatments such as bleaching and perm-waving in the IFs and the matrix of human hair (Wortmann *et al.*, 2002), including kinetic aspects of the process (Wortmann *et al.*, 2006b, 2008). The specific role of the denaturation transition for the setting of wool fabrics has been elucidated in some detail by DeBoos (1987).

With the consideration from the model that the denaturation temperature of the helices is controlled by the viscosity of the surrounding matrix, it is not surprising that the denaturation temperature drops with the water content,

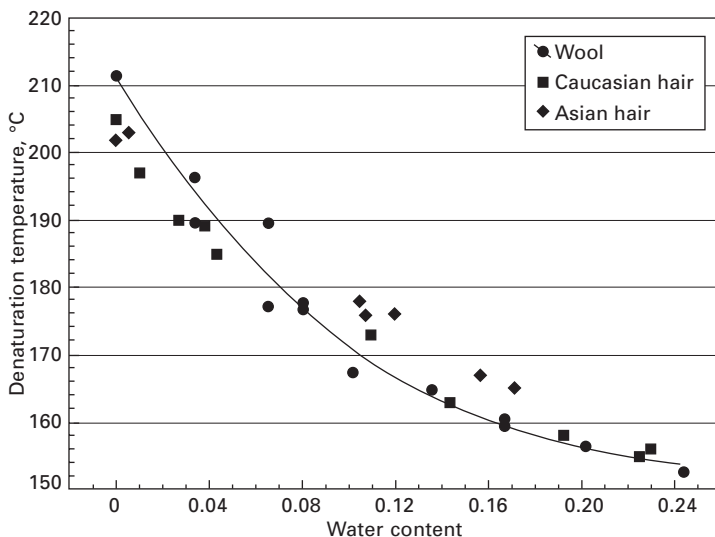


as shown by Haly and Snaith (1967) by DTA experiments on wool. Similar experiments have recently been conducted by Cao and Leroy (2005) on human hair, applying DSC. It is interesting to note that they showed that the denaturation enthalpy is not affected by a change of water content. The results obtained for the denaturation temperature by both groups of authors are summarized in Fig. 4.17.

The decrease of the denaturation temperature of the  $\alpha$ -helical material in keratin with water content cannot primarily be attributed to the plasticization of the matrix, since the denaturation temperatures at all water contents are well above the  $T_G$  of the matrix. The minimum difference between  $T_G$  and  $T_D$  is about  $40^\circ\text{C}$  for wool and  $70^\circ\text{C}$  for hair in the dry state. It is thus a genuine effect of water on the denaturation process of the helical material. The differences between the  $T_D$  data groups for wool and hair in Fig. 4.17 fall into the range expected from Fig. 4.16, due to the differences in cystine content and thus crosslink density of the matrix in both materials.

To interpret the water-induced depression of  $T_D$  for wool, Haly and Snaith (1967) applied the Flory theory of the melting point depression of polymer crystals by diluents (Flory, 1953), yielding in a form adapted to the current discussion:

$$1/T_D - 1/T_D^0 = (R/\Delta H_{hx}) (V_{hx}/V_1) (\Phi_1 - \chi\Phi_1^2) \quad 4.2$$



4.17 Denaturation temperatures for wool determined by DTA (Haly and Snaith, 1967) and for human hair by DSC (Cao and Leroy, 2005) up to the range of maximum water uptake of keratins. The solid line is the heuristic fit of the data for wool, approximating closely to any fit of the data applying the Flory equation (Equation 4.2).

where  $T_D$  is the denaturation temperature of the helical material in keratin with water and  $T_D^0$  that in the dry keratin, respectively;  $R$  is the gas constant ( $8.3143 \text{ J K}^{-1} \text{ mol}^{-1}$ );  $\Delta H_{\text{hx}}$  is the melting enthalpy per mole of helical material;  $V_{\text{hx}}$  is the molar volume of helical material and  $V_1$  the molar volume of water;  $\Phi_1$  is the volume fraction of water calculated from water content applying densities of  $1 \text{ g/cm}^3$  and  $1.31 \text{ g/cm}^3$  for water and keratin, respectively; and  $\chi$  is the helix/water interaction parameter. A similar form of the Flory equation is given by Cao and Leroy (2005).

To evaluate Equation 4.2 and in view of the data scatter in Fig. 4.17, all data for wool as well as for hair were combined up to the value of the maximum water content (<25%). They were submitted to a non-linear regression procedure (Wortmann, 2007), using the Levenberg–Marquardt approach to achieve minimization of the least-squared errors (Statistica, 2002), yielding (regression coefficient = 0.977,  $\pm 95\%$  confidence limits):

$$1/T_D^0 = 2.093 \cdot 10^{-3} \pm < 10^{-6}, \text{ giving } T_D^0 = 205^\circ\text{C}$$

$$(R/\Delta H_{\text{hx}})(V_{\text{hx}}/V_1) = 1.38 \cdot 10^{-3} \pm 0.25 \cdot 10^{-3}$$

$$\chi = 1.33 \pm 0.42$$

so that  $\chi$  lies with 95% probability between 0.91 and 1.75.

This value for the helix/water interaction parameter is in good agreement with the value of  $\chi \approx 1.1$  obtained from fitting, in the context of the Rosenbaum model (Rosenbaum, 1970), the Flory–Huggins equation to water sorption data for wool (Wortmann *et al.*, 2007). This result corroborates the theory of the effectively homogeneous distribution of water throughout the keratin structure (Wortmann, 2006a).

Calculating  $\Delta H_{\text{hx}}$  from these data yields an estimate of  $256 \text{ J g}^{-1}$ , based on the weighted mean of  $114 \text{ g mol}^{-1}$  for the amino acid residues in the low-sulphur protein fraction (Wortmann and Deutz, 1993; Marshall and Gillespie, 1977). With a value of  $\Delta H = 17.1 \text{ J g}^{-1}$  measured for keratins in water (Wortmann and Deutz, 1993) this would yield a very low degree of crystallinity of about 7%, which is lower by a factor of about four than the experimental expectation value of 25–30%.

Haly and Snaith (1967), making reference to Flory's (1953) lattice model, introduced a bias for the water volume fraction of  $1/4.7 = 0.21$ , which is the ratio  $V_1/V_{\text{hx}}$ . This approach implies that only about 20% of the water associated with the helical material is effective in the denaturation process. Cao and Leroy (2005) introduced a bias of similar size, equating this fraction of 'effective' water in a non-obvious way with the crystallinity of keratin and linking this to the hypothesis that all water taken up by a fibre resides exclusively in the matrix, as discussed above. With a bias of this size, Haly and Snaith (1967) as well as Cao and Leroy (2005) found good agreement with the experimental values for the denaturation enthalpy (Haly and Snaith,

1967), but also a very high value for the helix/water interaction parameter of  $\chi = 4.5$  (Cao and Leroy, 2005).

The author does not assume that this exceptional size of the interaction factor contributes to a deepened understanding of the helix/water interaction in keratins, but it rather suggests a serious gap in our understanding of the role of water for the denaturation transition, which merits further investigation, namely in view of the practical relevance of this process (DeBoos, 1987).

## 4.9 Conclusions

The science relating to  $\alpha$ -keratinous materials is a very mature field. Hair fibres are produced in follicles, which are easily accessible and suitable models for active organs of protein synthesis. Accordingly, comprehensive information is available on the proteins of material of specific relevance, such as wool and hair, their sequences, the sequence of their synthesis and deposition in the cause of hair formation. Numerous studies have also addressed the complex questions of self-organization, namely of the IF/matrix complex (Bernot and Coulombe, 2004). Though important aspects of the final structure of the IFs are still unclear, impressive progress has been made in understanding the structure of  $\alpha$ -keratins.

The progressive self-organization of the proteins during hair growth leads to a nano-scaled fibril/matrix composite with a protective skin with overall high performance characteristics with respect to its biological function. Against this background  $\alpha$ -keratins are potentially interesting models for biomimetic materials. To further this potential, and in this sharing the view of Hearle (2003, 2007), it would, however, be necessary to develop a total model for the structural mechanics of  $\alpha$ -keratinous materials (Bryson *et al.*, 2005). This would bring the understanding of the structure–property relationships at all levels of organization between micro- and nano-scales to a degree of sophistication comparable to that achieved for the biochemical aspects.

## 4.10 Sources of further information and advice

As pointed out above, the field of science that investigates the biological, chemical, physical and mechanical properties of  $\alpha$ -keratins in general and of specific fibres is very mature indeed. This applies especially for those fibres that are of textile (wool) or cosmetic (human hair) relevance. Accordingly, a very wide range of review articles and books are available and have been referenced in this article, covering the whole scope of fundamental as well as strongly applied topics, such as textile and cosmetic processing.

## 4.11 References

- AATCC 20A (2007), 'Fiber analysis: Quantitative', Standard Test Method, *AATCC Technical Manual 2008*, Research Triangle Park, NC, American Association of Textile Chemists and Colorists.
- Akkermans RLC, Warren PB (2004), 'Multiscale modelling of human hair', *Phil Trans Roy Soc London*, A362, 1783–1793.
- Appleyard HM, Dymoke CM (1954), 'Effect of ortho-chlorophenol on wool', *J Text Inst*, 45, T480–T481.
- Astbury WT, Street A (1931), 'X-ray studies of the structure of hair, wool and related fibres. I. General', *Phil Trans Roy Soc London*, A230, 75–101.
- Bendit EG (1968), 'Distribution of high- and low-sulfur fractions in alpha-keratin', *Text Res J*, 38, 15–21.
- Bendit EG, Feughelman M (1968), 'Keratin', *Encycl Polym Sci Tech*, 8, 1–44.
- Bendit EG, Gillespie JM (1978), 'The probable role and location of high-glycine-tyrosine proteins in the structure of keratins', *Biopolymers*, 17, 2743–2745.
- Bernot KM, Coulombe PA (2004), 'Intermediate filaments', *Encycl Biol Chem*, 458–462.
- Bertrand L, Doucet J, Dumas P, Simionovici A, Tsoucaris G, Walter P (2003), 'Microbeam synchrotron imaging of hairs from Ancient Egyptian mummies', *J Synchrotron Rad*, 10, 387–392.
- Bradbury J H (1973), 'Structure and chemistry of keratin fibers', *Adv Protein Chem*, 27, 111–211.
- Breuer MM (1972), 'The binding of small molecules to hair – I: The hydration of hair and the effect of water on the mechanical properties of hair', *J Soc Cosmet Chem*, 23, 447–470.
- Brooklyn College (2008), <http://academic.brooklyn.cuny.edu/biology/bio4fv/page/beta-pl.htm>
- Bryson WG, Wortmann FJ, Jones LN (2005), 'New directions for Merino wool fibre mechanical property modelling', *Proc 11th Int Wool Res Conf*, 105FWSA, Leeds, UK.
- Bustard HK, Smith RW (1990), 'Studies of factors affecting the light scattering by individual human hair fibers', *Int J Cosmet Sci*, 12, 121–133.
- Caldwell JP, Bryson WG (2005), 'Elastic moduli of the wool fiber cellular structure by atomic force microscopy', *Proc 11th Int Wool Conf*, 89FWS, Leeds, UK.
- Cao J (1997), 'Origin of the bimodal 'melting' endotherm of  $\alpha$ -form crystallites in wool keratin', *J Appl Polym Sci*, 63, 411–415.
- Cao J, Billows CA (1999), 'Crystallinity determination of native and stretched wool by X-ray diffraction', *Polymer Int*, 48, 1027–1033.
- Cao J, Leroy F (2005), 'Depression of the melting temperature by moisture for alpha-form crystallites in human hair keratin', *Biopolymers*, 77, 38–43.
- Chapman BM (1975a), 'The rheological behaviour of keratin during the ageing process', *Rheol Acta*, 14, 466–470.
- Chapman BM (1975b), 'The ageing of wool. Part I: Ageing at various temperatures', *J Text Inst*, 66, 339–342.
- Conway JF, Fraser RDB, MacRae TP, Parry DAD (1988), 'Protein chains in wool and epidermal keratin IF: Structural features and spatial arrangement', in Rogers GE, Reis PJ, Wards KA, Marshall RC, *The Biology of Wool and Hair*, London, Chapman & Hall, 127–144.

- Cook JR, Fleischfresser BE (1990), 'Crimping of wool fibers', *Text Res J*, 60, 77–85.
- Couchman PR, Karasz FE (1978), 'A classical thermodynamic discussion of the effect of composition on glass-transition temperatures', *Macromolecules*, 11, 117–119.
- Crighton JS (1990), 'The characterization of destabilized and stabilized wools', *Proc 8th Int Wool Text Res Conf*, I, 419–428, Christchurch, New Zealand.
- Crighton JS, Hole ER (1985), 'A study of wool in aqueous media by high pressure differential analysis', *Proc 7th Int Wool Text Res Conf*, I, 283–292, Tokyo.
- Curiskis JI, Feughelman M (1983), 'Finite element analysis of the composite fiber, alpha-keratin', *Text Res J*, 53, 271–274.
- De Boos AG (1987), 'The conflicting requirements of wool setting for the finisher and the tailor', *CSIRO Div Text Ind*, Rep. No. G61, Geelong, Australia.
- Deutz H, Wortmann FJ, Hoecker H (1991), 'Charakterisierung von Keratinen mittels Hochdruck-DSC', *Schriftenr Dtsch Woolf Inst*, 108, 327–338.
- Dobb MG, Johnston FR, Nott JA, Oster L, Sikorski J, Simpson WS (1961), 'Morphology of the cuticle layer in wool fibres and other animal hairs', *J Text Inst*, 52, T153–T170.
- Dowling LM, Crewther WG, Parry DAD (1986), 'Secondary structure of component 8c-1 of  $\alpha$ -keratin', *Biochem J*, 236, 705–712.
- Druhala M, Feughelman M (1971), 'Mechanical properties of keratin fibres between  $-196^{\circ}\text{C}$  and  $20^{\circ}\text{C}$ ', *Kolloid Z Z Polymere*, 248, 1032–1033.
- Druhala M, Feughelman M (1974), 'Dynamic mechanical loss in keratin at low temperatures', *Colloid Polym Sci*, 252, 381–391.
- Ebert G (1967), 'Anwendungsmöglichkeiten der Differentialkalorimetrie zur Untersuchung von Keratinfasern', *Melliand Textilber*, 48, 87–90.
- Ebert G, Mueller FH (1965), 'Calorimetric investigations on the heat of transition of wool during supercontraction', *Proc Int Wool Text Res Conf CIRTEL*, 4, 487–494, Paris.
- Eichner R, Rew P, Engel A, Aebi U (1985), 'Human epidermal keratin filaments: studies on their structure and assembly', *Ann NY Acad Sci*, 455, 381–402.
- Feughelman M (1959), 'A two-phase structure for keratin fibers', *Text Res J*, 29, 223–228.
- Feughelman M (1987), 'Keratins', *Encycl Polym Sci Eng*, 8, 566–600.
- Feughelman M (1989), 'A note on the water-impenetrable component of  $\alpha$ -keratin fibers', *Text Res J*, 59, 739–742.
- Feughelman M (1997), *Mechanical Properties and Structure of Alpha-keratin Fibres*, Sydney, Australia, UNSW Press.
- Feughelman M (2002), 'Natural protein fibres', *J Appl Polym Sci*, 83, 489–507.
- Feughelman M, Haly AR (1960), 'The mechanical properties of the ortho- and para-like components of Lincoln wool', *Text Res J*, 30, 897–900.
- Feughelman M, Robinson MS (1971), 'Some mechanical properties of wool fibers in the "Hookean" region from zero to 100% relative humidity', *Text Res J*, 41, 469–474.
- Feughelman M, Lyman D, Menefee E, Willis B (2003), 'The orientation of  $\alpha$ -helices in  $\alpha$ -keratin fibres', *Int J Biol Macromol*, 33, 149–152.
- Feughelman M, Willis B, James V (2005), 'The tetrameric structure of the intermediate filaments of alpha-keratin fibres', *Proc 11th Int Wool Res Conf*, Paper 65Fi, Leeds, UK.
- Filshie BK, Rogers GW (1961), 'The fine structure of  $\alpha$ -keratin', *J Molec Biol*, 3, 784–786.
- Fletcher NH (1970), *The Chemical Physics of Ice*, Cambridge, UK, Cambridge University Press.
- Flory PJ (1953), *Principles of Polymer Chemistry*, New York, Cornell University Press.

- Fox TG (1956), 'Influence of diluent and of copolymer composition on the glass temperature of a polymer system', *Bull Am Phys Soc*, 1, 123.
- Fraser RDB, MacRae TP (1980), 'Molecular structure and mechanical properties of keratins', in *The Mechanical Properties of Biological Materials, Symp Soc Exp Biol*, 34, 211–246, Cambridge, UK, Cambridge University Press.
- Fraser RDB, MacRae TP, Rogers GE (1972), *Keratins: Their Composition, Structure and Biosynthesis*, Springfield, IL, CC Thomas Publ.
- Fraser RDB, MacRae TP, Sparrow LG, Parry DAD (1988), 'Disulfide bonding in  $\alpha$ -keratin', *Int J Biol Macromol*, 10, 106–112.
- Gibson CT, Myhra S, Watson GS, Huson MG, Pham DK, Turner PS (2001), 'Effects of aqueous exposure on the mechanical properties of wool fibers – Analysis by atomic force microscopy', *Text Res J*, 71, 573–581.
- Gillespie JM (1970), 'Mammoth hair: stability of  $\alpha$ -keratin structure and constituent proteins', *Science*, 170, 1100–1102.
- Gillespie JM, Frenkel MJ (1972), 'The diversity of keratins', *Comp Biochem Physiol*, 47B, 339–346.
- Giroud A, Leblond CP (1951), 'The keratinisation of epidermis and its derivatives, especially the hair, as shown by X-ray diffraction and histochemical studies', *Ann New York Acad Sci*, 53, 613–626.
- Gordon M, Taylor JS (1952), 'Ideal copolymers and the second-order transitions of synthetic rubbers. I. Noncrystalline copolymers', *J Appl Chem*, 2, 493–500.
- Haly AR, Snaith JW (1967), 'Differential thermal analysis of wool – The phase transition endotherm under various conditions', *Text Res J*, 37, 898–907.
- Haylett T, Swart LS, Parris D, Joubert FJ (1971), 'Primary structure of some high-sulfur proteins of reduced wool', *Appl Polym Symp*, 18, 37–44.
- Hearle JWS (2003), 'A total model for the structural mechanics of wool', *Wool Tech Sheep Breed*, 51(1), 97–117.
- Hearle JWS (2007), 'Protein fibers: structural mechanics and future opportunities', *J Mater Sci*, 42(19), 8010–8019.
- Hindeleh AM, Hosemann R (1991), 'Microparacrystals: The intermediate stage between crystalline and amorphous', *J Mater Sci*, 26, 5127–5133.
- Höcker H (2002), 'Fiber morphology', in Simpson WS, Crawshaw GH, *Wool: Science and Technology*, Cambridge, UK, Woodhead Publishing, Chapter 3, 60–79.
- Horikita M, Fukuda M, Takaoko A, Kawai H (1989), 'Fundamental studies on the interaction between moisture and textiles. X: Moisture sorption properties of wool and hair fibers', *Sen-i Gakkaishi*, 45, 367–381.
- Huson MG (1991), 'DSC investigation of the physical ageing and deageing of wool', *Polym Int*, 26, 157–161.
- IWTO-58 (2000), 'Scanning electron microscopic analysis of speciality fibers and sheep's wool and their blends', *Standard Test Method of the International Wool Textile Organisation*, Ilkley, UK, The Woolmark Company.
- Johnson DJ, Sikorsky J (1965), 'Fine and ultrafine structure of keratin (V)', *Proc 3rd Int Wool Text Res Conf*, 1, 147–160, Paris.
- Jones LN, Kaplin IJ, Legge GJF (1993), 'Distributions of protein moieties in  $\alpha$ -keratin sections', *J Computer-Assisted Microsc*, 5, 85–89.
- Kalichevsky MT, Jaroszkiewicz EM, Blanshard JMV (1992), 'Glass transition of gluten. 1: Gluten and gluten–sugar mixtures', *Int J Biol Macromol*, 14, 257–266.
- Kanetaka S, Tomizawa K, Iyo H, Nakamura Y (1993), 'The effects of UV radiation on human hair concerning physical properties and fine structure of protein', *J Soc Cosmet Chem Jpn*, 27, 424–431.

- King AT (1926), 'Specific gravity of wool and its relation to swelling and sorption in water and other liquids', *J Text Inst*, 17, T53–T67.
- King NLR, Bradbury JH (1967), 'The chemical composition of wool, V: The epicuticle', *Aust J Chem*, 20, 2803–2807.
- Knopp B, Jung B, Wortmann FJ (1996), 'Comparison of two force fields in MD-simulations of  $\alpha$ -helical structures in keratins', *Macromol Theory Simul*, 5, 947–956.
- Knopp B, Jung B, Wortmann FJ (1997), 'Modelling of the transition temperature for the helical denaturation of  $\alpha$ -keratin intermediate filaments', *Macromol Theory Simul*, 6, 1–12.
- Kure JM, Pierlot AP, Russell IM, Shanks RA (1997), 'The glass transition of wool: An improved determination using DSC', *Text Res J*, 67, 18–22.
- Kuzuhara A (2006), 'Analysis of structural changes in bleached keratin fibers (black and white human hair) using Raman spectroscopy', *Biopolymers*, 81, 506–514.
- Kuzuhara A (2007), 'Analysis of structural changes in permanent waved human hair using Raman spectroscopy', *Biopolymers*, 85, 274–283.
- Langbein L, Schweizer J (2005), 'Keratins of the human hair follicle', *Int Rev Cytol*, 243, 1–78.
- Lewa Wildlife Conservance (2007), [www.lewa.org/black-rhino-facts.php](http://www.lewa.org/black-rhino-facts.php)
- Liu H, Bryson WG (2002), 'A three-component model of the wool fibre – Effects of morphology, elasticity and intermediate filament arrangement on fibre stiffness', *J Text Inst*, 93(1), 121–131.
- Makinson KR (1979), 'Shrinkproofing of wool', in *Fiber Science Series*, vol. 8, New York, Marcel Dekker.
- Marshall RC (1981), 'Analysis of the proteins from single wool fibres by two-dimensional electrophoresis', *Text Res J*, 51, 106–108.
- Marshall RC, Gillespie JM (1977), 'The keratin proteins of wool, horn and hoof from sheep', *Aust J Biol Sci*, 30, 389–400.
- Marshall RC, Orwin DFG, Gillespie JM (1991), 'Structure and biochemistry of mammalian hard keratin', *Electron Microsc Rev*, 4, 47–83.
- Matoltsy AG (1969), 'What is keratin?', in *Advances in Biology of Skin, Vol. 9: Hair Growth*, Oxford, UK, Pergamon Press, 559–569.
- Mclaren JA, Milligan B (1981), *Wool Science – The Chemical Reactivity of the Wool Fibres*, Marrickville, Australia, Science Press.
- Mellon EF, Korn AH, Hoover SR (1949), 'Water absorption of proteins. IV: Effect of physical structure', *J Amer Chem Soc*, 71, 2761–2764.
- Menefee E, Yee G (1965), 'Thermally induced structural changes in wool', *Text Res J*, 35, 801–812.
- Mercer EH (1961), *Keratin and Keratinisation*, Oxford, UK, Pergamon Press.
- Monteiro VF, Maciel AP, Longo E (2005), 'Thermal analysis of Caucasian human hair', *J Thermal Anal Calorim*, 79, 289–293.
- Negri AP, Cornell HJ, Rivett DE (1993), 'A model for the surface of keratin fibers', *Text Res J*, 63, 109–115.
- Nick B (1995), personal communication
- Onions WJ (1962), *Wool – An Introduction to its Properties, Varieties, Uses and Production*, London, E. Benn.
- Orwin DFG, Woods JL, Ranford SL (1984), 'Cortical cell types and their distribution in wool fibres', *Aust J Biol Sci*, 37, 237–255.
- Palenik S (1997), 'Forensic microscopy', *Europ. Microscopy Anal*, November, 5–7.
- Parbhu AN, Bryson WG, Lal R (1999), 'Disulfide bonds in the outer layer of keratin



- fibers confer higher mechanical rigidity: Correlative nano-indentation and elastic measurements with AFM', *Biochemistry*, 38, 11755–11761.
- Parry DAD (1997), 'Protein chains in hair and epidermal keratin IF: Structural features and spatial arrangements', in Jollès P, Zahn H, Höcker H, *Formation and Structure of Human Hair*, Basel, Switzerland, Birkhaeuser, 177–207.
- Parry DAD, Fraser RDB (1985), 'Intermediate filament structure: 1. Analysis of IF protein sequence data', *Int J Biol Macromol*, 7, 203–213.
- Parry DAD, Steinert PM (1999), 'Intermediate filaments: molecular architecture, assembly, dynamics and polymorphism', *Quarterly Rev Biophys*, 32, 99–187.
- Phillips DG (1985), 'Detecting a glass transition in wool by differential scanning calorimetry', *Text Res J*, 55, 171–174.
- Pierlot AP (1999), 'Water in wool', *Text Res J*, 69, 97–103.
- Powell BC, Rogers GE (1997), 'The role of keratin proteins and their genes in the growth, structure and properties of hair', in Jollès P, Zahn H, Höcker H, *Formation and Structure of Human Hair*, Basel, Switzerland, Birkhaeuser, 59–148.
- Puffr R, Sebenda J (1966), 'Structure and properties of polyamides. XXVII: Mechanism of water sorption in polyamides', *J Polym Sci*, C16, 79–93.
- Robbins CR (2002), *Chemical and Physical Behavior of Human Hair*, New York, Springer.
- Rogers GE (1959), 'Electron microscopy of wool', *J Ultrastruct Res*, 2, 309–330.
- Rosenbaum S (1970), 'Solution of water in polymers: the keratin–water isotherm', *J Polym Sci*, C31, 45–55.
- Schmidt H, Wortmann FJ (1994), 'High pressure differential scanning calorimetry and wet bundle tensile strength of weathered wool', *Text Res J*, 64, 690–695.
- Schwan-Joncck A, Lang G, Clausen T, Koehler J, Schuh W, Liebscher KD (1998), 'Hair preparations', in *Ullmann's Encyclopedia of Industrial Chemistry*, 6th edn, Weinheim, Germany, Wiley-VCH Verlag, 1–38.
- Sikorski J (1975), 'Structural studies of mammalian keratin', in Atkins EDT, Keller A, *Structure of Fibrous Biopolymers*, London, Butterworths, 271–287.
- Sparrow LG, Dowling LM, Loke VY, Strike PM (1988), 'Amino acid sequence of wool keratin IF proteins', in Rogers GE, Reis PJ, Wards KA, Marshall RC, *The Biology of Wool and Hair*, London, Chapman & Hall, 145–155.
- Speakman JB (1930), 'The adsorption of water by wool', *J Soc Chem Ind*, 49, 209T–213T.
- Spei M (1990), 'Die thermoanalytischen Methoden in der Keratinforschung und ihre Aussagekraft', *Melliand Textilber*, 71, 901–904.
- Spei M, Holzem R (1989), 'Thermoanalytical determination of the relative helix content of keratins', *Colloid Polym Sci*, 267, 549–551.
- Stapels M (2001), *Water waves in human hair – Investigation of the basic mechanics controlling formation and recovery*, PhD thesis D82, RWTH Aachen, Aachen, Germany, Verlagsgruppe Mainz.
- Stapels M, Wortmann FJ (2000), 'Determination of the humidity dependent glass transition temperature of human hair', *Proc 10th Int Wool Text Res Conf*, HH-5, 1–6, Aachen, Germany.
- Statistica (2002), StatSoft Inc., Tulsa, OK.
- Steinert PM, Marekov LN, Parry DAD (1993), 'Conservation of the structure of keratin intermediate filaments: molecular mechanism by which different keratin molecules integrate into pre-existing keratin intermediate filaments during differentiation', *Biochemistry*, 32, 10046–10056.



- Struik LCE (1978), *Physical Ageing in Amorphous Polymers and Other Materials*, Amsterdam, Elsevier.
- Swift JA (1977), 'The histology of keratin fibers', in Asquith RS, *Chemistry of Natural Protein Fibers*, London, John Wiley & Sons, 81–146.
- Swift JA (1997), *Fundamentals of Human Hair Science*, Weymouth, UK, Micelle Press.
- UoMN, University of Minnesota (2006), [www.charfac.umn.edu/gallery/feather.html](http://www.charfac.umn.edu/gallery/feather.html)
- Watt IC (1963), 'The sorption behavior of cystine-modified wool', *Text Res J*, 33, 631–638.
- Wildman AB (1954), *The Microscopy of Animal Fibres*, Leeds, UK, Wool Industries Research Association.
- Wolfram LJ, Lindemann MKO (1971), 'Some observations on the hair cuticle', *J Soc Cosmet Chem*, 22, 839–850.
- Wollina U (1997), 'Histochemistry of the human hair follicle', in Jollès P, Zahn H, Höcker H, *Formation and Structure of Human Hair*, Basel, Switzerland, Birkhaeuser, 31–58.
- Woods HJ (1936), 'The electrical orientation of wool cells', *Proc Leeds Phil Soc*, 3, 132–134.
- Wortmann FJ (1992), *Thermo- und hydroplastische Eigenschaften von Wollfasern*, Opladen, Germany, Westdeutscher Verlag.
- Wortmann FJ (2007), 'Temperature- and humidity-induced transitions in  $\alpha$ -keratinous materials', *Int J Sheep Wool Sci*, 55, Article 1.
- Wortmann FJ, Arns W (1986), 'Quantitative fiber mixture analysis by scanning electron microscopy. Part I: Blends of mohair and cashmere with sheep's wool', *Text Res J*, 56, 442–446.
- Wortmann FJ, DeJong S (1985a), 'Analysis of the humidity-time superposition for wool fibers', *Text Res J*, 55, 750–756.
- Wortmann FJ, DeJong S (1985b), 'Nonlinear viscoelastic behaviour of wool fibres in a single step relaxation test', *J Appl Polym Sci*, 30, 2195–2206.
- Wortmann F-J, Deutz H (1993), 'Characterizing keratins using high pressure differential scanning calorimetry', *J Appl Polym Sci*, 48, 137–150.
- Wortmann FJ, Deutz H (1998), 'Thermal analysis of ortho- and para-cortical cells isolated from wool fibers', *J Appl Polym Sci*, 68, 1991–1995.
- Wortmann FJ, Zahn H (1994), 'The stress/strain curve of  $\alpha$ -keratin fibers and the structure of the intermediate filament', *Text Res J*, 64, 737–743.
- Wortmann FJ, Rigby BJ, Phillips DG (1984), 'Glass transition temperature of wool as a function of regain', *Text Res J*, 54, 6–8.
- Wortmann FJ, Wortmann G, Arns W (1989), 'Quantitative fiber mixture analysis by scanning electron microscopy. Part II: Blends of wool with angora rabbit hair', *Text Res J*, 59, 73–80.
- Wortmann FJ, Wortmann G, Zahn H (1995), 'Extracting information from amino acid compositions of keratins using principal components analysis', *Text Res J*, 65, 669–675.
- Wortmann FJ, Springob C, Sendelbach G (2002), 'Investigations of cosmetically treated human hair by differential scanning calorimetry', *J Cosmet Sci*, 53, 219–228.
- Wortmann FJ, Schulze zur Wiesche E, Bierbaum A (2003), 'Analyzing the laser-light reflection from human hair fibers. I. Light components underlying the goniophotometric curves and fiber cuticle angles', *J Cosmet Sci*, 54, 301–316.
- Wortmann FJ, Stapels M, Elliott R, Chandra L (2006a), 'The effect of water on the glass transition of human hair', *Biopolymers*, 81, 371–375.

- Wortmann FJ, Popescu C, Sendelbach G (2006b), 'Nonisothermal denaturation kinetics of human hair and the effects of oxidation', *Biopolymers*, 83, 630–635.
- Wortmann FJ, Hullmann A, Popescu C (2007), 'Analysis of the wool–water sorption isotherm: an old problem revisited', *Proc Int Wool Text Org T&S Cttee*, Edinburgh.
- Wortmann FJ, Popescu C, Sendelbach G (2008), 'Effects of reduction on the denaturation kinetics of human hair', *Biopolymers*, 89, 600–605.
- Zahn H (1980), 'Wool is not keratin only', *Proc 6th Int Wool Text Res Conf*, Pretoria, South Africa.
- Zahn H (2002), 'Progress report on hair keratin research', *Int J Cosmet Sci*, 24, 163–169.
- Zahn H, Foehles J, Nienhaus M, Schwan A, Spei M (1980), 'Wool as a biological composite structure', *Ind Eng Chem Prod Res Div*, 19, 496–501.
- Zahn H, Wortmann FJ, Höcker H (1997), 'Chemie und Aufbau der Wolle', *Chemie in unserer Zeit*, 31(6), 280–290.
- Zahn H, Wortmann FJ, Wortmann G, Schaefer K, Hoffmann R, Finch R (2003), 'Wool', in *Ullmann's Encyclopedia of Industrial Chemistry*, 6th edn, Weinheim, Germany, Wiley-VCH Verlag, vol. 39, 525–555.
- Zahn H, Wortmann FJ, Höcker H (2005), 'Considerations on the occurrence of loricerin and involucrin in the cell envelope of wool cuticle cells', *Int J Sheep Wool Sci*, 53(1), paper 2.

---

F VOLLRATH, D PORTER and C DICKO,  
University of Oxford, UK

**Abstract:** A key feature of silk fibres is the carefully controlled assembly and directed growth that produce hierarchical structures at all length scales. The final result is a material of outstanding strength, functional flexibility and often with self-healing properties. Some salient results in silk research are reviewed to identify the fundamental ‘bio-principles’ that make silk a remarkable system to study. Specific aspects of silk diversity and versatility are presented.

**Keywords:** fibre, biomaterial, extrusion spinning, spider, silk worm.

## 5.1 Introduction

### 5.1.1 What is silk?

The word ‘silk’, primarily and in commercial parlance, defines fibres spun by larvae of the silk-moth *Bombyx mori*, which for commercial use are collected by unravelling the pupal cocoons (Asakura and Kaplan 1994; Lee 1999). However, other insects produce protein fibres with specific properties, such as the threads produced by many other moths and some butterflies (as larval safety-lines or pupal cocoons) or spun by caddis-flies (for underwater nets and ‘houses’), by bees and wasps (in their wax- and paper-works), by fleas (for cocoons) as well as by non-insects, mostly arachnids such as mites (in protective nets) and, especially, spiders, which use it for a wide range of purposes (Craig 1997, 2003). These lepidopteran, neuropteran, hymenopteran, siphonapteran, acarid and araneid silks share much of their biophysical and biochemical make-up, while at the same time displaying a range of interesting (and occasionally functionally important) differences. Notwithstanding the differences, the basic structural component of all major silks is the ‘nylon 2.2’ backbone of the macromolecule, while the basic functionality of all silks relies on the interaction between the amide groups of the backbone and the water molecules that surround it.

The silks of the lepidopteran moth *Bombyx mori* (the commercial silk worm) and a number of only very distantly related saturnid moths like *Antheraea* spp. (wild silks) are the mainstay of commercial silk production and consumption (at ca. 80 000 tons p.a.). Research on these silks tends to focus on commercial use and improvement of quality (Vollrath and Knight 2004). On the other hand, spider silks (and the silks of other arthropods) so far

are outside the commercial world, and consequently research focuses almost exclusively on gaining novel insights into the structure–property–function relationships of the constituent components of these materials (Vollrath and Porter 2006a, 2006b). Such research, basic for now, will become invaluable if and when the production of microbial and/or synthetic production of silk spinning feedstock becomes economically viable.

### 5.1.2 Aim of this review

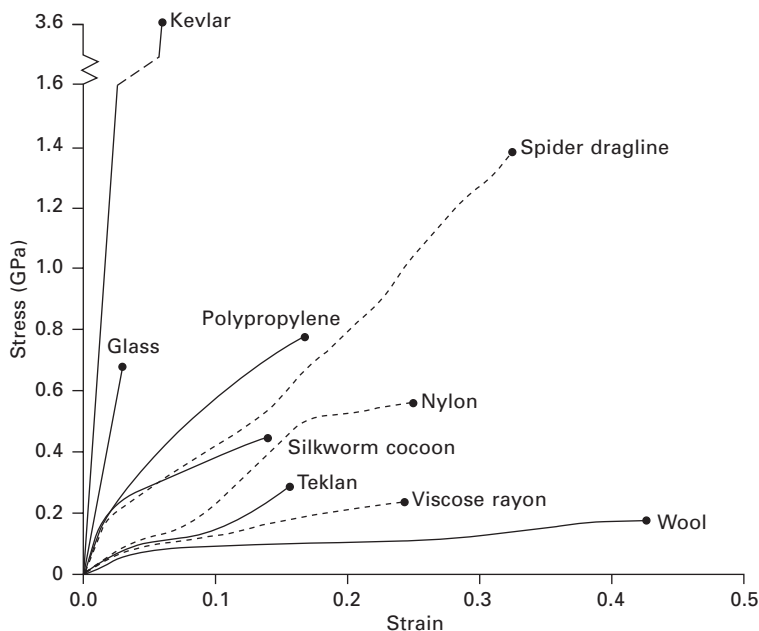
To understand the importance of these studies we need to briefly discuss silk biodiversity and experimental access to each type of fibre. The biological use of a silk, and the history of its evolution, with the forces of selection interacting with the resistance of tuning the material creating subsequent adaptations. For example, threads used for protective shelters (like in the silkworms) require resistance to drilling and biting but not (necessarily) elasticity, whereas the capture threads of spiders need exactly that: great elasticity because a web would just not function without it. This comparative approach coupled to state-of-the-art instrumental and theoretical analysis are presented and reviewed.

## 5.2 Silk mechanics

Natural silks are extremely fine, tough, strong and extensible even compared to standard polymers (see Fig. 5.1). A surprisingly diverse range of animals, all arthropods, generate a wide plethora of silks from a highly diverse number of production systems (Vollrath and Selden 2007). Some of these silk producers have only one type of gland while others have a veritable ‘battery’ of them, producing either the same kind or a wide range of very different types of silk filaments, fibres, ribbons, ‘cements’ or glues. Some animals, such as spiders, make silks throughout their life for a wide variety of purposes, while others, such as many insect larvae, make silk only rarely or indeed once, and in that case typically for a highly specific use (such as making a cocoon for pupation) (Foelix 1996). Accordingly, a single silk filament can range from a few nanometres in diameter to a few microns, and in length it can range from a few millimetres to over 1000 metres. In short, silk is not easily defined, nor is it easily placed in the context of protein extrusions.

### 5.2.1 Tensile properties

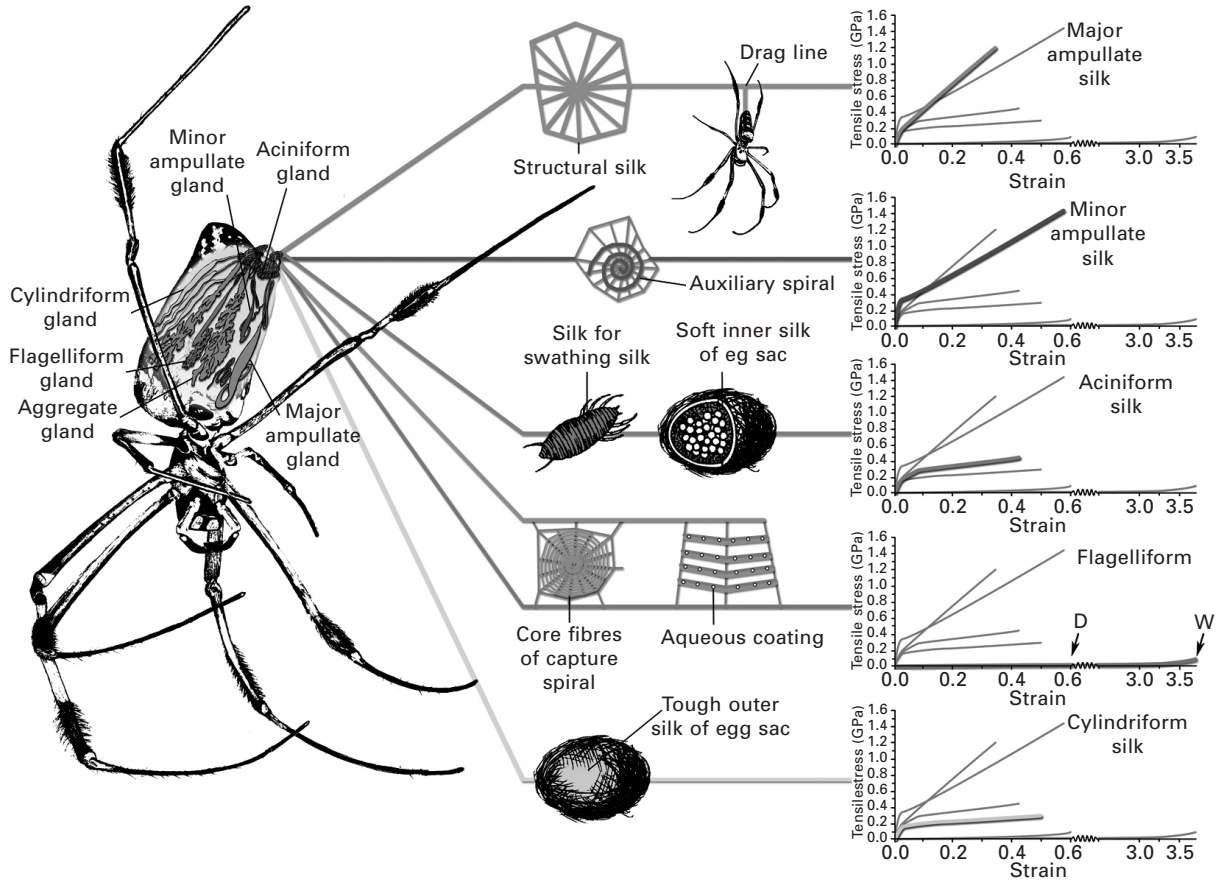
Among the animal taxa that produce silk, spiders stand out. Hence spider silks give perhaps the best image of the commercial potential of these interesting biopolymers. After all, spiders are the only animal order where all members rely heavily on the use of silk. And these animals rely on silk



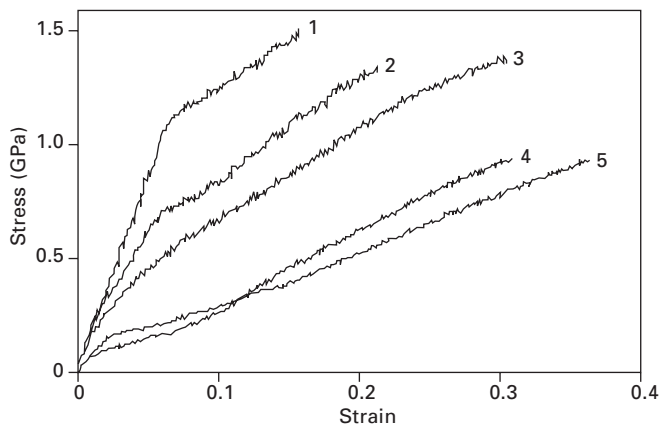
5.1 Comparative mechanical properties of some major polymer and biopolymer fibres. Modified from Wynne (1997).

in all walks of life, not only in one stadium and for only one or two very specific purposes. Moreover, all spiders produce more than one type of silk; some spiders, the orb-weavers for example, produce up to seven different types (Kovoor 1987), all with different material properties and for a wide range of different functions (see Fig. 5.2) (Kovoor 1990). Figure 5.3 shows variation of one type of silk (major ampullate or dragline) across species (Vollrath and Knight 2001).

In this dependence on the spinning conditions, silkworm silks resemble spider silks (see Section 5.5), which have led the way in recent silk studies principally because of one feature, experimental access. Spiders are much more amenable than silkworms to experimental manipulation, not least because the spider spinning from its abdomen cannot cut a thread if its feet are kept away, while a silkworm, spinning from its mouth, can easily bite through the thread. However, spider silks have another advantage over silkworm silks. The best of them (in terms of quality expressed in commercial, not biological, terms) are much 'better' than silkworm silks. For example, radius threads of *Nephila* show good extensibility, high tensile strength, large hysteresis and great toughness. For example (Vollrath *et al.* 2001), a radial/dragline thread drawn from the major ampullate (MAA) glands of mature female *Nephila edulis* (average weight  $527 \pm 103$  mg, mean  $\pm$  s.d.) at control spinning conditions (a drawing speed of  $20 \text{ mm s}^{-1}$  and a



5.2 Golden orb spider silk functions and associated mechanical properties. Modified from Vollrath and Porter (2006b).



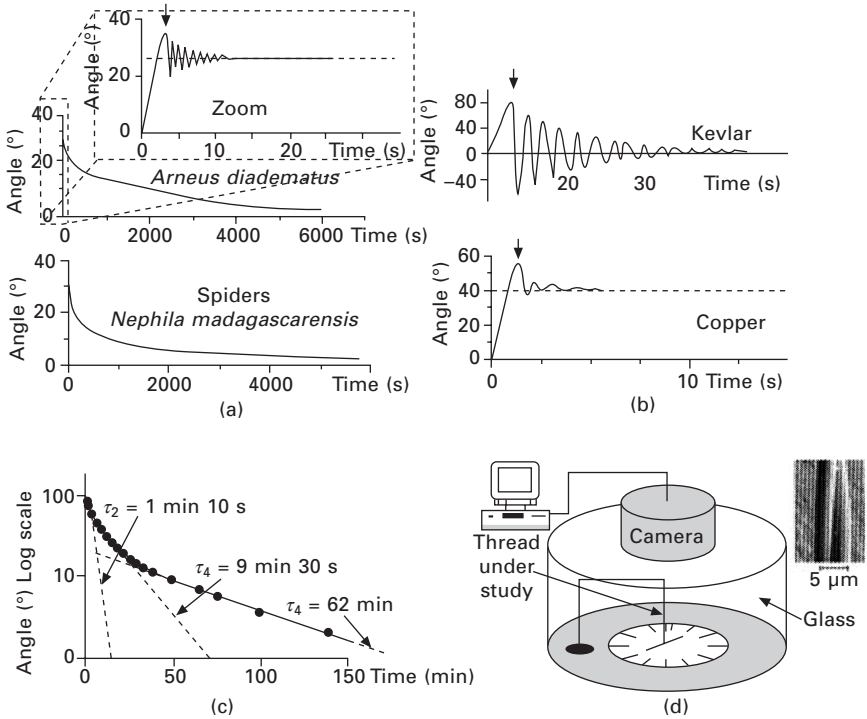
5.3 Mechanical properties across spider species. Stress–strain characteristics of dragline silk reeled from different web-building spiders: *Euprostheno* sp. (Pisauridae) (1), *Cyrtophora citricola* (Araneidae) (2), *Latrodectus mactans* (Theridiidae) (3), *Araneus diadematus* (Araneidae) (4) and *Nephila edulis* (Tetragnathidae) (5). The data (Vollrath and Knight 2001) were collected under comparable conditions by artificial reeling. They show that the silk of *Euprostheno* (1) is stiffer and requires more force to break it but is much less elastic and thus takes up less energy than the comparable silk of *Nephila* (5); the characteristics of the other species lie in between. We note also the differences in the initial moduli and yielding points.

IP Address: 129.132.211.108

temperature of 25°C) have an average silk diameter of  $3.35 \pm 0.63 \mu\text{m}$  with a normalised average breaking strain of  $0.39 \pm 0.08\%$ , a breaking stress of  $1.15 \pm 0.20 \text{ GPa}$ , an initial modulus of  $7.87 \pm 1.85 \text{ GPa}$ , a yield stress of  $0.153 \pm 0.058 \text{ GPa}$  and a breaking energy of  $165 \pm 28 \text{ kJ kg}^{-1}$ . These fibres had a moderate positive Poisson ratio with a linear thinning ratio of *ca.* 5% for each 10% of strain. Thus, MAA dragline silk from *Nephila* spiders has high initial modulus ( $\sim 14 \text{ GPa}$ ), good tensile strength ( $\sim 1.5 \text{ GPa}$ ) and high extensibility ( $\sim 40 \%$ ), which are all desirable features for a polymer fibre (Madsen *et al.* 1999). Moreover, this kind of silk also shows remarkable toughness at temperatures as low as even below  $-60^\circ\text{C}$ , as well as tough fracture behaviour even in liquid nitrogen (Yang *et al.* 2005). Even more unusual, the elongation to break decreases with increasing temperature and reaches a minimum around  $+70^\circ\text{C}$ . Strength and toughness of this silk begin to decrease around  $+100^\circ\text{C}$ , while the degradations temperature lies around  $370^\circ\text{C}$  (Yang *et al.* 2005). Thus, this benchmark MAA spider silk retains its exceptional mechanical properties over a temperature range from at least  $-66^\circ\text{C}$  (and probably down to liquid nitrogen temperatures) up to about  $+100^\circ\text{C}$ .

### 5.2.2 Torsional properties

A novel application of the torsional pendulum has been implemented by Emile *et al.* (2007). They use the high sensitivity of the technique to explore the viscoelastic behaviour of silks (Fig. 5.4). It is important to note that such techniques are less sensitive to flaws and ‘non-destructive’, and are a complementary approach to tensile testing. The authors explored the dynamics of the relaxation of the amino-acid polymers of the spider draglines and compared it to known synthetic polymers and metal. In a very elegant manner, the authors demonstrated the existence of the torsional self-shape-



5.4 Torsional behaviour of spider silks. Modified from Emile *et al.* (2007). (a) and (b) experimental torsion pendulum relaxation dynamics of four filaments: two spider dragline (diameter 2–3  $\mu\text{m}$ ) as well as Kevlar 29 (poly paraphenylene terephthalamide, 10  $\mu\text{m}$ ) thread and a copper wire (50  $\mu\text{m}$ ). Dotted line: new equilibrium position (c) torsional logarithm relaxation behaviour of a rubber resin adhesive system (RRAS) vs. the *Araneus diadematus* spider dragline. Black points: experimental measurements; line: theoretical fit; dotted straight lines: time constants associated with the different torsional levels of relaxation (d) experimental setup.



memory effect in different types of spider draglines, a thread that exhibits a behaviour different not only from man-made polymers or crystalline metallic threads but also from the common visco-elastic filaments.

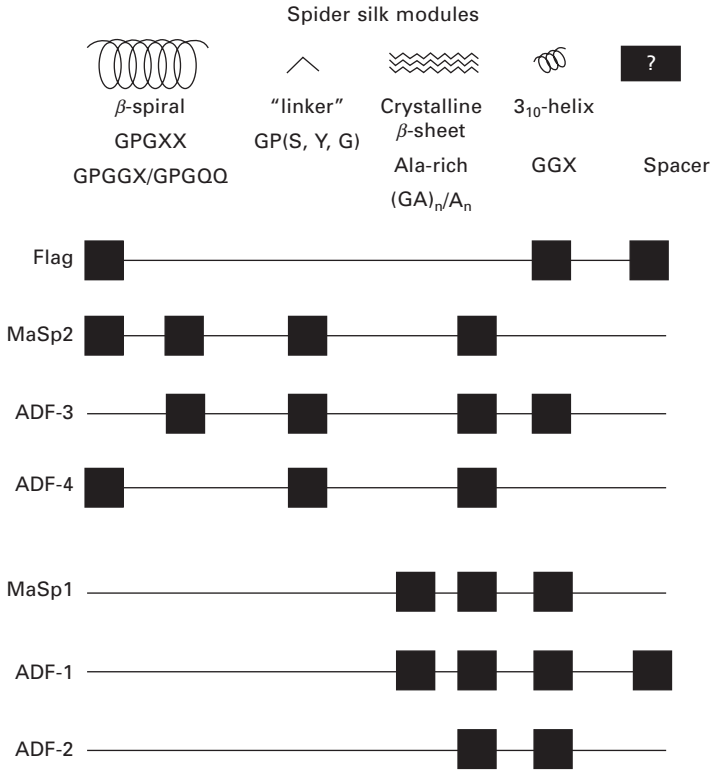
Fascinatingly, it appears that in the spider dragline threads, selection against twisting has led to the evolution of a self-shape-memory material. The authors interpret the self-repair in spider's silk filament to be based on reformations of non-covalent bonds that mainly include hydrogen bonds (Pauling *et al.* 1951) and van der Waals interactions. These would occur at different levels of the complex multilevel structure (Gosline *et al.* 1999b; Becker *et al.* 2003; Zhou and Zhang 2005) of a dragline silk. The so-called secondary structure, for instance a helix, represents the conformation of the primary amino-acid sequences. All domains in the dragline silk have a preferred secondary structure and are strongly oriented with the chains parallel to the fibre. The majority of the alanine residues are incorporated in regular  $\beta$ -sheets that form the microcrystalline domains and that also include part of the glycine residues. The remaining glycine-rich part forms the surrounding helical structures in a less crystalline matrix (van Beek *et al.* 2002). These secondary structures are mainly maintained by rather strong and highly directional hydrogen bonds. Structures in silk, beyond the secondary structure, include a larger tertiary structure with different folding patterns in the presence of hydrogen and van der Waals bonds. A quaternary fibrillar organisation in the silk includes the two main proteins organised in supramolecular helices and  $\beta$ -sheet where van der Waals interactions are ubiquitous.

### 5.2.3 Silk mechanics summary

The overview presented here shows not only the variety of silk functions, but also how silk can be used to provide insights into other important structural proteins at both a practical and a theoretical level. This leads us to conclude that silk can be considered as an ideal archetypal elastomeric protein. The range of mechanical properties that can be derived from silk-based proteins is enormous, from mineralised bone-like materials with a modulus of 20 GPa, through classical silks with a modulus of 2–10 GPa, down to viscid elastin-like rubbers with only 1 MPa. The outlined combination of experimental work with analytical modelling (see Section 5.7) shows the large range of mechanical properties that silk can assume with apparently small changes in chemical structure and processing. This makes silk an important analytical tool as well as an interesting biopolymer (Vollrath and Porter 2006a, 2006b)

## 5.3 Silk composition

The origin of the remarkable mechanical properties can be derived from knowledge of the composition and sequence of silk proteins (Fig. 5.5)



5.5 Genetic basis for silk structural strength. The spider silk genes share common amino acid motifs. These motifs are suggested to be structural modules. 'X' indicates a residue that may vary within or between proteins. MaSp1/MaSp2: Major ampullate spidroins 1/2 from *Nephila* sp. Flag: Flagelliform silk from *Nephila* sp. (capture thread). ADF: *Araneus diadematus* proteins. From Hayashi *et al.* (1999).

IP Address: 129.132.211.108

(Hayashi *et al.* 1999). The silks of neither spider nor silkworm, nor indeed any other animal, are simple single-protein biopolymers. The typical spider dragline silk originating in the Major Ampullate (MA or Ma) gland contains two major proteins, namely spidroin 1 and spidroin 2. The commercial *Bombyx* silks consist of three principal main proteins (Inoue *et al.* 2000a) in the fibre and five or six principal proteins in the coating (Michaille *et al.* 1986; Grzelak 1995). The spider and silkworm proteins (Kaplan and Lombardi 1990b; Hinman *et al.* 1992) are not small (*ca.* 350 kDa with an estimated 53–34 residues and 350 kDa with 59 residues (Sprague *et al.* 1979) respectively). The silks of caddis-flies (Trichoptera) or chironomid midges (Diptera), both aquatic insects, can be much larger (Case *et al.* 1994; Case and Smith 1994). A chironomid silk (of *C. tentans*) was found to consist of four rather similar, and all gigantic, silk proteins ranging from *ca.* 1000 kDa

to 15 000 kDa in addition to a fair number (six and rising) of much smaller proteins (40–200 kDa) (Case and Thornton 1999). Moreover, while spider and silkworm silks are biased towards residues with small side chains (i.e. ala, gly and ser), making up about 63% and 86% respectively) (Fournier 1979; Kaplan and Lombardi 1990a; Dicko *et al.* 2006), these are of lesser importance in midges and caddis-flies (about 30% and 40% respectively), while in these aqueous silks amino acids with polar residues and basic residues are more important (*ca.* 82% and 60% respectively) when compared with the dry silks of spiders and silkworms (*ca.* 35% and 23% respectively) (Case and Smith 1994).

Amino acid analyses tend to show that silks typically are very rich in glycine and alanine. Benchmark silks like those of *Bombyx mori* silkworms and *Nephila* spiders are cases in point (Bini *et al.* 2004; Dicko *et al.* 2006). Indeed, amino acids with short side chains predominate in almost all silks (Bini *et al.* 2004; Dicko *et al.* 2006). X-ray diffraction has, so far, already allowed the characterisation and grouping of many different silks from a wide range of taxa (Craig and Riekel 2002). Structurally these silks tend to all share more traits than differences; and it is typical of a ‘good’ silk to have a certain proportion of highly disordered, often coiled chains interspersed with highly ordered ‘crystallites’ of densely ‘pleated’ sheet structure, giving it a mixture of amorphous and block regions (Vollrath and Porter 2006b).

## 5.4 Fine structure and morphology

The silks of insects like the silkworm *Bombyx mori* have been mentioned several times in this chapter. In fact, far more is known about the biochemistry, molecular biology and genetics of the silkworm than of any spider. There are many similarities between insect silks and spider silks, e.g. the predominance of amino acids with short side chains or the occurrence of some sequence motifs, which can help to understand the general principles involved in the generation of their material properties. Yet, there are also major differences that have to be taken into account. Most insect silks are used as cocoons or protective webs in larval stages and originate in labial glands (Sehna and Akai 1990). In contrast, in almost all spider species the silk glands are situated in the so-called opisthosoma, the abdominal body segment of these animals (Foelix 1996). Apart from the different phylogenetic as well as ontogenetic origin of the glands, there are far more different gland types in spiders and they are usually not restricted to a certain developmental stage. The main difference lies in the usage of the silks and the subsequent adaptations of the material. Threads used for protective shelters, for instance, do not require elasticity whereas the capture threads of spider webs would just not function without it (Vollrath 2000a, 2000b). In this section, we present the variation found in silk fibre morphologies.

### 5.4.1 Spider silk morphology: *Nephila*

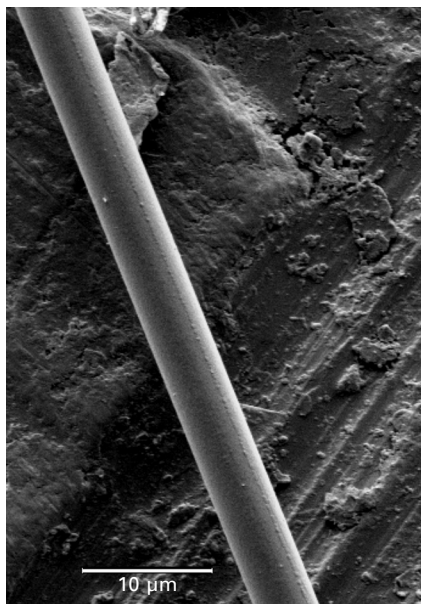
Most spider silks, like nearly all other silks, have some sort of hierarchical structure of the filament, which is partly a result of the mix (and layering) of the silk proteins and other components, and partly a result of the spinning process (Thiel *et al.* 1994). The fibres, however, appear relatively smooth and uniform under electron and light microscopy investigations. In Section 5.6 we will explore the nanoscale arrangement. Figure 5.6 shows typical *Nephila edulis* dragline silk. The fibres are characterised by a circular cross-section (sub-micron to 10–20  $\mu\text{m}$  in diameter). Interestingly, reeling the silk with the spider under anesthetic reveals the underlying fibrillar structure (Madsen and Vollrath 2000; Riekel *et al.* 2004). Another relevant observation is the fracture surface after failure giving a complex surface relief rather than a clean cleavage plan. This observation is in stark contrast with synthetic polymers (Perez-Riguero *et al.* 2001) and suggestive of a ductile failure.

### 5.4.2 Silkworm silk morphology: *Bombyx*

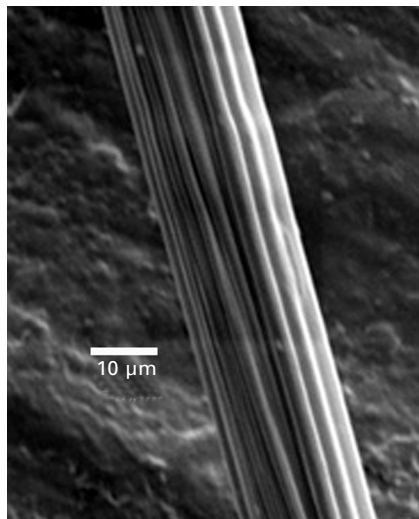
*Bombyx mori* silkworm silk (and there is only one type) shows a rather different morphology from that of any known spider silk fibre (Fig. 5.7). A silkworm thread does not represent the natural fibre *per se*, but a composite of core fibres covered by layers of coating. The core fibroin fibres are produced by the main part of the gland, while the coating sericin layers are produced in the middle and distal parts of the silk duct where they are layered on top of the passing liquid fibroin material, which is rapidly ‘hardening’ underneath the coating due to a combination of flow elongation, molecular alignment, pH shifts and shear-stressing. In this way, the extrusion process produces a layered fibroin–sericin thread (Figs 5.7a and 5.7b). In addition to fibrillar structure, akin to spider dragline (Figs 5.8 and 5.18), *Bombyx* fibres show a stacked-layer pattern (Putthanarat *et al.* 2000). The reasons for this arrangement are still unclear, and the present hypothesis attributes this pattern to the liquid crystalline formation of silk fibres. Typically, the fibril widths cover the range of 90–170 nm (similar numbers are found for *Nephila* silk). Their orientation is along the fibre axis, with 30–50% of fibril cross-overs at an angle of intersection between 30° and 50°. Similar behaviour is observed in *Nephila* silks (Vollrath *et al.* 1996). Differences, however, occur between the silks of *Bombyx mori* and *Nephila* sp. The next section describes these differences and their impact on silk mechanics.

### 5.4.3 Banding patterns vs. microvilli: crack deflection mechanisms?

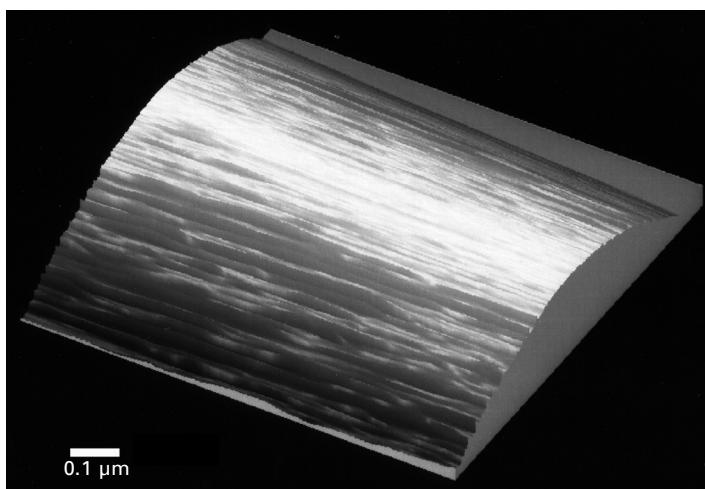
Silks are faced with tremendous mechanical challenges. For the animal, it is imperative that the materials hold to ensure protection against predators or



(a)



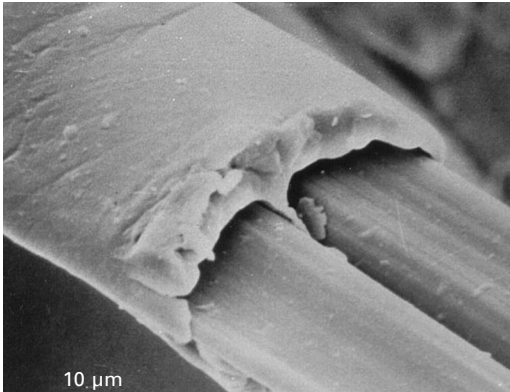
(b)



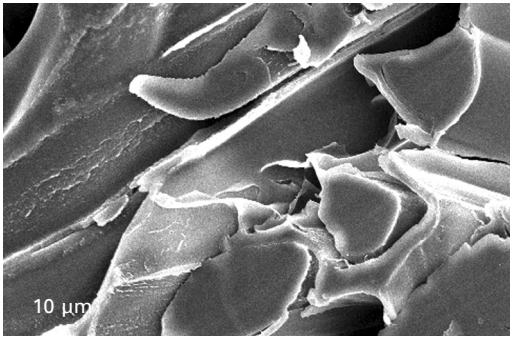
(c)

IP Address: 129.132.211.108

5.6 *Nephila* spider silk ultrastructural details. (a) *Nephila* dragline. (b) dragline of a *Nephila* produced under CO<sub>2</sub> anaesthetic (Madsen and Vollrath 2000). (c) AFM image of *Nephila* dragline surface.



(a)



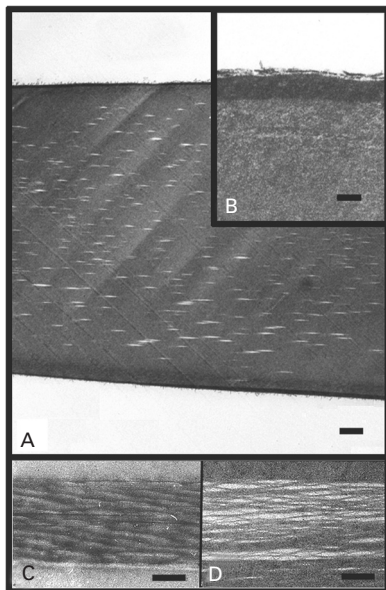
(b)

**5.7 *Bombyx mori* silk ultrastructural details.** (a) *Bombyx mori* undegummed silk bave. Within the bave, two brins and the sericin coating. SEM by G. Freddi. (b) *Bombyx mori* bave transverse section. Note the non-circular cross-sections.

IP Address: 129.132.211.108

capturing food. Thus, energy dissipation is critical. In a standard polymer, one would define a minimum crack size and design the polymers accordingly. In silks, energy dissipation is still unclear. We now know that the strength of a silk can be reduced to its nano-crystalline composition (Porter *et al.* 2005). More generally, it has been found that biological materials are insensitive to flaws at the nano-scale (Gao *et al.* 2003). This observation poses two interesting questions: first, is there a maximum rigid structure allowable in silks, beyond which crack propagation is damaging? And, second, how is variability in spinning conditions mitigated to ensure fibre performance? A detailed discussion of these issues is beyond the scope of this review. Instead we present two possible energy dissipation mechanisms found in the insect *Bombyx mori* and the spider *Nephila edulis*. Figure 5.8 shows longitudinal cross-sections of the two silk fibres. Two striking differences are observed: the insect silk section shows a banding pattern (Shen *et al.* 1998) and the





5.8 *Nephila* dragline thread fine structure. (a)–(d) SEM images of longitudinal sections of silk fibres showing skin-cool and microfibrillar structures (after Frische *et al.*, (1998).

IP Address: 129.132.211.108 spider silk has a much smoother structure with elongated cavities (Frische *et al.* 1998). Note that the chevron-like structure of the banding pattern might be an induced artefact due to the sectioning knife. The reasons, however, for such structures are unclear. Frische *et al.* (1998) found that the elongated cavities come from floating vesicles in the spinning dope that are later elongated during fibre formation. One can easily interpret such final structures as a crack deflector. The role of the banding pattern observed in *Bombyx* remains unclear.

#### 5.4.4 Silk diversity: comparative examples

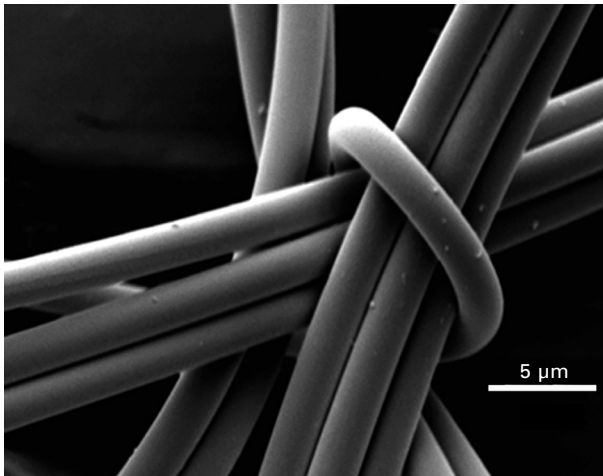
While all silks are multi-component materials, some silks are more complex than others. Among the more complex ones, the capture silks of the ecribellate and cribellate orb-weavers are perhaps the most advanced and astonishing composite materials (Figs 5.9c and 5.9d). They have evolved, independently, two very different ways to capture and hold prey insects and are excellent examples of the power of evolution when driven hard in a life–dinner arms race (between the fly and the spider, the former evolving to keep his life, the latter to have her dinner).

*Nephila*, like all other spiders, has more than one type of silk, each with specific properties that appear to be optimised to perform key functional roles

(Fig. 5.2). The principal web silk, the dragline, is produced by the major ampullate (MAA) gland. Minor ampullate (MIA) silk accompanies the MAA silk in the web, while flagelliform (FLG) silk forms the core filaments of the capture thread spiral. The capture thread filaments are coated by ‘silk’ from the aggregate (AGR) gland; this is not a solid filament, but an aqueous solution of hygroscopic peptides and sticky glycoproteins. Web threads are affixed to one another by a rapidly drying silk cement originating in the pyriform glands (PYR). The eggs are encased in very fine silk filaments from the tubuliform or cylindriform (CYL) glands as well as one type of aciniform (AC1) gland. Another type of aciniform gland (AC2) produces filaments for a multitude of other purposes such as strengthening the cement matrix. A detailed account of two capture mechanisms is given in the following section.

### Capture silks

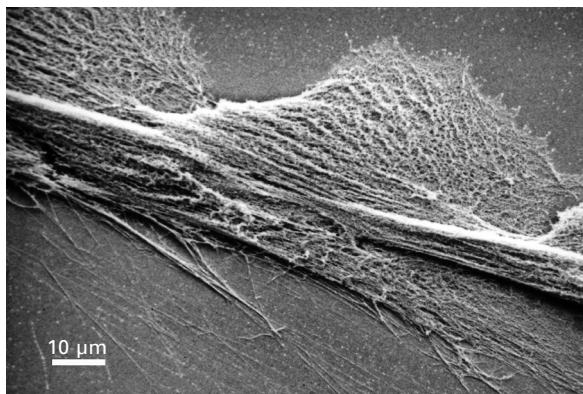
The sticky capture silks of the cribellate orb weaver *Nephila* and its kin are complex, albeit microscopic, mechanical windlass systems that make good use of the physics of biological micro-engineering (Fig 5.9c). In the ‘windlass’ silk (which operates in the wet state) the elasticity is provided



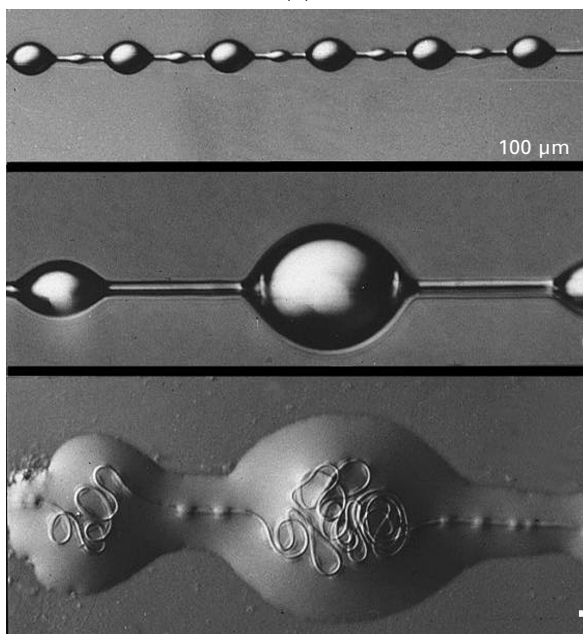
(a)

5.9 Spider silk structural diversity. (a) knot of *Nephila* dragline silk. (b) dry cribellate capture silk from *Uloborus* sp. Note the fine hackled threads that stick out by van der Waals forces. (c) viscid capture silk from *Araneus diadematus*. Sticky droplets harbouring a self-coiling micro-windlass mechanism. Adapted from Vollrath and Edmonds (1992). (d) the sticky glycoprotein ‘glue’ of the ecribellate orb-weavers.

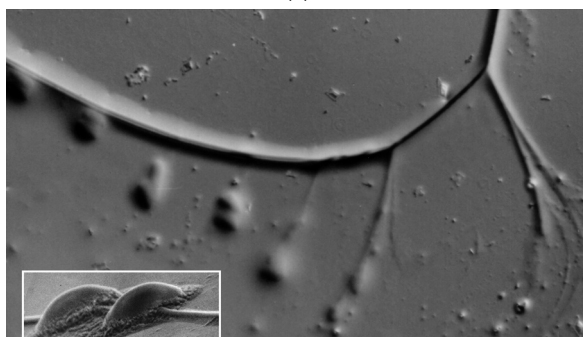




(b)



(c)



(d)

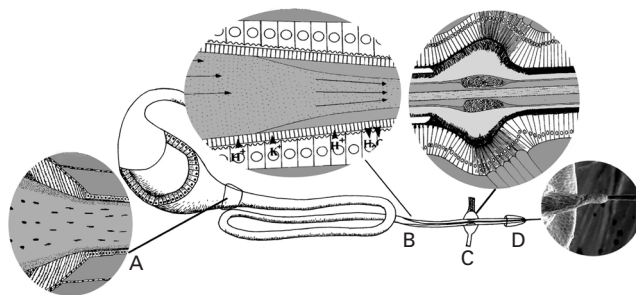
5.9 Cont'd

by a combination of surface tension of the aqueous coat and recoil of the plasticised silk fibre (Vollrath *et al.* 1990; Vollrath and Edmonds 1992), while adhesion is bestowed by a separate glycoprotein complex (Vollrath *et al.* 1990; Vollrath and Tillinghast 1991). These kinds of complex, micro-machine thread absorb energy by large extensibility (*ca.* 500%) of the wetted thread, which develops substantial force only after 100–200% extension, with the thread breaking suddenly at around 400–500% extension. Nevertheless, the engineering strength of such threads is in the order of  $1.5 \text{ GN m}^{-2}$  with a breaking energy of around  $160 \text{ J cm}^{-3}$  and is thus not far off from those of radial web threads and dragline threads ( $1.2 \text{ GN m}^{-2}$  and  $194 \text{ J cm}^{-3}$  respectively, measured for *Araneus diadematus* (Gosline *et al.* 1999a)).

The cribellate type of capture silk looks and functions rather differently. This silk-composite employs very fine filaments only a few nanometres in diameter. These nano-filaments originate, each separately, from an array of thousands of tiny, individual spigot ‘towers’. From here they are combed, by specific structures on the spider’s hind legs, into hackled bands of many threads onto supporting axial threads. These threads, in turn, are often crimped, and thus sprung. In this kind of silk, which operates only in the dry state, the hackled bands provide surprising elasticity as well as tremendous adhesion, which presumably functions largely by electrostatic forces (Opell 1993, 1995; Kohler and Vollrath 1995). The functional and developmental details of the two different elastic recoil mechanisms of the two types of capture silk micro-machines are interesting, albeit more from a composite than from a structural material point of view. Specifically the interaction of water and silk, so cleverly used by Nature in the droplet windlass system, takes full advantage of the high extensibility of wetted silks that derives largely from the high water content of the coat. However, water is important not only for these threads, but for many other types of thread as well, and the role of water as well as other solvents for understanding and manipulating the mechanical properties of spider silk cannot be understated. This can be of special interest if we aim to produce bio-engineered silks with specific properties.

### *Ribbon silk vs. cylindrical silk*

On a different note, dragine silks can present considerable diversity, comparing classical fibre from *Nephila* orb spiders to the ribbon silk from the *Loxosceles* spider suggests that these design features depend on a fundamental difference between the spinning mechanisms in *Loxosceles* and the orb web spiders (Knight and Vollrath 2002b). The major gland of orb web spiders, typified by that of *Nephila* spp., produces a cylindrical thread by a mechanism involving an internal draw-down starting well inside the distal part of the duct, followed by an external draw-down in the air after the spigot (Work 1977b;



5.10 A spider's extrusion spinning device. The spinning dope is stored as an aqueous solution in the lumen of the gland. On demand it flows through a tapering 'funnel' (A) into the body of the duct where it undergoes first flow elongation (B) and then transforms into the solid fibre. Before the exit through the spigot (D) it passes a ratchet clamp (C). Based on Vollrath and Knight (2001).

Vollrath and Knight 2001). In contrast, *Loxosceles* draws a highly flattened ribbon of silk directly from the spigot without an internal draw-down. To do this, the dope fed to the spigot must be highly fluid, in contrast to orb web spiders where the dope is thought to be largely solid by the time it reaches the spigot (Knight *et al.* 2000). Thus, differences between the structure of the MA gland in *Loxosceles* and orb web spiders may reflect differences in the spinning mechanism (see Fig. 5.10). This, in turn, probably reflects the different uses to which the two spiders put their MA silks: forming a retreat in *Loxosceles*, and extremely tough threads for major engineering works in orb web spiders. Given the antiquity of the Sicaridae to which *Loxosceles* belongs (Hormiga *et al.* 2000), the simplicity of the MA gland and of its spinning technology compared with that of orb web spiders may represent primitive features (Glatz 1973; Haupt and Kovoov 1993) derived from an ancestral spider and subsequently modified in orb web spinners.

#### 5.4.5 Supercontraction: water plasticisation

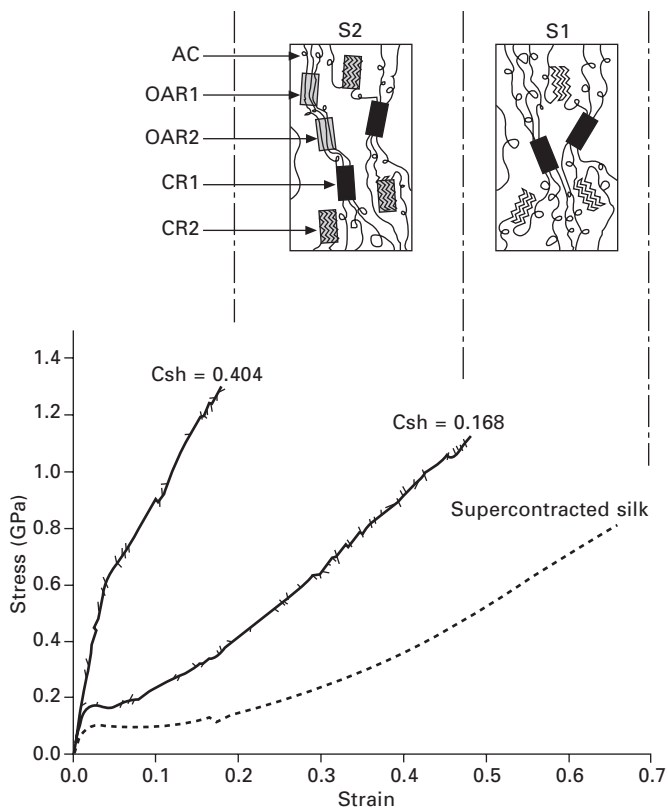
In the preceding section, we explored some examples of silk diversity. Part of the problem is to be able to decouple a circumstantial observation from a true feature required for fibre performance. In this section, we will present one such feature: supercontraction. Many spider silks contract in water and other small-molecular solvents. Some silks, like the MAA dragline threads *Araneus*, supercontract 50% in pure water, while other silks, such as the dragline silk of *Nephila*, require a stronger agent, such as 8 mol urea (Vollrath *et al.* 1996). The degree of supercontraction seems to be a function of the crystallinity of the material and can be used to study both the gross morphology of silks and their molecular structure (Liu *et al.* 2005a, 2005b,

2008). Note that *Bombyx mori* fibres do not supercontract and have a much higher crystalline content than *Nephila* dragline, for example.

The glass transition temperature of spider silk of about 75°C suggests that at room temperature the molecular chains are held in place by intermolecular hydrogen bonds. As these bonds are gradually destroyed by the actions of the solvents, the molecular chains begin to 'disorient', i.e. lose order. Thus, in essence, the contraction of spider silk in water results from the disorientation of the molecular chains (Work 1985; van Beek *et al.* 1999; Jelinski *et al.* 1999; Savage *et al.* 2004). The more hydrogen bonds are destroyed, the larger the shrinkage until finally, and in a strong solvent, the silk is totally dissolved (Shao and Vollrath 1999; Shao *et al.* 1999).

In a recent study Liu *et al.* (2005b) proposed a novel classification of supercontraction by introducing the concept of capacity to shrink (Csh). Csh is defined as the maximum longitudinal shrinkage of an unconstrained fibre in standard conditions, which is taken to be an indicator of molecular chain orientation (see Fig. 5.11). They propose that the value of Csh can be attributed to the degree of molecular orientation in the spider silk. This hypothesis fits well with the fact that, in artificial polymers, thermal shrinkage is determined by the orientation of the non-crystalline area at the specific temperature (Wu *et al.* 1996). Raman spectroscopy (Shao *et al.* 1999), X-ray diffraction (Grubb and Ji 1999), NMR (Eles and Michal 2004) and birefringence (Fornes *et al.* 1983) all suggest that supercontraction is driven by the recoverable disorientation of the molecular chains in the fibre's oriented amorphous region. Spider silk can be thought of as containing two main molecular 'phases', each with a possible range of 'states': amorphous (from disoriented to oriented) and crystalline (from poorly defined to well defined) (Simmons *et al.* 1996; Grubb and Jelinski 1997; Grubb and Ji 1999). Even under supercontraction, the well-defined crystalline region retains considerable order because solvent molecules cannot penetrate it (Simmons *et al.* 1996; Shao and Vollrath 1999), whereas at the same time the degree of orientation in the oriented amorphous, as well as the poorly defined crystalline, region decreases appreciably (Simmons *et al.* 1996; Grubb and Ji 1999). Spinning conditions would have little effect on the crystallites, but would greatly affect the alignment of the molecular chains in the amorphous region, thus altering the fraction of oriented amorphous region (see Fig. 5.11). This alone could explain the different capacities to shrink of the different fibres.

At the molecular level, it has been shown that, in water, silk with high birefringence shrinks less than silk with low birefringence, and we may assume that birefringence is positively correlated with degree of hydrogen bonding (Work 1977a). Thus, birefringence would also be positively correlated with molecular orientation and higher density, i.e. more so-called 'β-sheet crystal areas'; one might hypothesise that such very dense areas keep water molecules out, resulting in fewer broken hydrogen bonds and less shrinkage.



**5.11 Supercontraction and its relation to orientation in dragline silk.** The two states S1 and S2 and the stress–strain curves of their representative spider silks. In S1 the amorphous region is poorly oriented; in S2 the amorphous region is oriented to different extents. AC, amorphous molecular chains; OAR1, oriented amorphous region where weak polar solvents such as alcohols can penetrate; OAR2, oriented amorphous region where only strong polar solvents such as water can penetrate; CR1, crystalline region (well defined); CR2, crystalline region (poorly defined). The background of CR2 turns dark from S1 to S2, suggesting that the degree of orientation of this region increases. Adapted from Liu *et al.* (2005b).

## 5.5 Spider silk: lessons from nature

### 5.5.1 Beta silks

Silk have evolved to be some of Nature's most impressive composite materials (Craig 1997). Silk fibres (Denny 1980) and glues (Vollrath *et al.* 1990) are not only among the toughest polymers known, but they have a number of other characteristics that, although less well known, make them an interesting as well as an important object for research in the general areas of biopolymers

(Vollrath and Knight 2004), protein folding, biomimetics and the coevolution of behaviour, morphology and function (Vollrath 2000b).

Silk proteins (spidroins in spiders and fibroins in Lepidoptera insects) are assembled into well-defined nano-fibrillar architectures (Li *et al.* 1994; Vollrath *et al.* 1996; Eby *et al.* 1999; Inoue *et al.* 2000b, 2001; Putthanasarat, *et al.* 2000; Craig and Riekel 2002). Spidroins and fibroins are largely constructed from two chemically distinct repetitive motifs or 'blocks' (see Table 5.1 and Fig. 5.5), an insoluble crystalline block and a less soluble crystalline block (Hayashi *et al.* 1999; Hayashi and Lewis 2000; Fedic *et al.* 2002; Craig 2003). The crystalline blocks are composed of short side-chained amino acids in highly repetitive sequences that give rise to  $\beta$ -sheet structures. The formation of  $\beta$ -sheet structures is the hallmark of all silks.

Structural and sequence studies have highlighted two interesting prerequisites to fibre formation. Firstly, the animal must control the size and concentration of  $\beta$ -crystals (Iizuka 1965; Urs *et al.* 1993) to be able to extrude the silk without accidental aggregation and achieve good mechanical properties. Secondly, silk proteins (despite their large size and overall hydrophobicity) are processed in an aqueous environment at ambient temperature and pressure. This suggests an extremely tight control of conformation, solubility and transport of the protein(s) along the spinning pathway. In the following sections we break down the spinning process in its most important aspects.

### 5.5.2 Co-evolution of silk spinning and silk 'dope'

Silk fibre diversity is accompanied by a spinning diversity. In spiders and silk-spinning insects, the spinning apparatus is as important as the spinning dope. The evolution of silk has to take into account both these aspects, as well as the environmental pressures. Authors have tried to match the emergence of new silks and function to particular spinning innovation and evolutionary events (Bond and Opell 1998). In general, spider evolution and cladogenesis underpin the animal's ever-increasing investment in silk production in this interesting taxon, and allow us to correlate spider diversification and silk properties (Bond and Opell 1998; Craig 2003). Not surprisingly, the structure–function relationship in spider silks is coupled with drastic changes in the design of the animal's spinning apparatus (see Fig. 5.12). The aciniform glands (simple spherical or pear-shaped structures, see Table 5.1) are accepted candidates for the most ancestral spinning device, making protective silks to shelter eggs and to line burrows (Schultz 1987). More advanced ecological functions (such as capture webs) led to the emergence of more complex glands and silks. The major ampullate gland (dragline and orb-web radial threads) is a case in point, where composition, chemistry and processing together deliver a highly specialised silk with properties that excite even modern fibre manufacturers.

Table 5.1 Summary of typical silk origins, composition and sequences

Silk type	Function	Proteins	Amino acid (%) <sup>1</sup>	Predicted structure from sequence <sup>2</sup>	Structure in solution <sup>3</sup>	Conformational change in solution <sup>4</sup>	Fibre degree of crystallinity (%) <sup>5</sup>	Fibre extensibility (%) <sup>6</sup>
Ma	Dragline Radial threads	MASp 1 and 2 (?)	Gly (38), Ala (29), SSC (70), PC (21)	(GA) <sub>n</sub> /(A) <sub>n</sub> β-structure GPGGX/GPGQQ 'β-spiral' GGX 3 <sub>1</sub> helix n = 2–8	Low concentration: disorder/PPII High concentration: helical/molten globule	β-Sheet	15–30%	35%
Mi	Auxiliary threads	MISp 1 and 2 (?)	Gly (40), Ala (35), SSC (80), PC (19)	(GA) <sub>n</sub> /(A) <sub>n</sub> β-structure GGX 3 <sub>1</sub> helix n = 2–8 Spacer	Helix like	β-Sheet	?	> 35%
Flag	Sticky spiral threads	Flag	Gly (36), Pro (14), SSC (51), PC (27)	GPGGX 'β-spiral' GGX 3 <sub>1</sub> helix spacer	β-Spiral	β-Turns	None	> 200%
Cyl	Cocoon silks	TuSp1	Ser (20), Ala (27), SSC (56), PC (45)	(A) <sub>n</sub> , (S) <sub>n</sub> , (SA) <sub>n</sub> , (SQ) <sub>n</sub> , GX, n = 0–3	Helix like	β-Sheet and β-turn	?	25%
Acinous	Coating, prey wrapping	AcSp 1	Gly (8), Ala (9), ser (5), Pro (5), SSC (22), PC (50)	No specific repeats but ~200 amino acids iteration along sequence	Helix like	β-Sheet and β-turn	?	80%
Pyriiform	Attachment disk	?	Gly (10), Ala (11), Ser (10), Pro (10), SSC (31), PC (52)	?	Helix like	β-Sheet and β-turn	?	?



<i>Bombyx mori</i>	Cocoon	Heavy, Light chains fibroins and P25 (6-6-1)	Gly (43), Ala (30), Ser (12), SSC (85), PC (23)	(GAGAGS) <sub>5-15</sub> β-Sheet (GX) <sub>5-15</sub> β-turns/helices GAAS spacer	Low concentration H-fibroin: disorder/PPII/β-turn type II (Silk 1) High concentration helical	β-Sheet (silk II)	40–50%	10–20%
<i>Antheraea pernyi</i>	Cocoon	Heavy chain fibroin	Gly (27), Ala (43), Ser (11), SSC (81), PC (26)	(S <sub>1-2</sub> A <sub>11-13</sub> ), GX <sub>1-4</sub> GGX, GGGX	Disorder and helical structures	β-Sheet	40%	35%
<i>Galleria mellonella</i>	Cocoon	Heavy, light chains fibroins and P25	Gly (28), Ala (22), Ser (17), SSC (67), PC (26)	(S <sub>1-2</sub> A <sub>1-4</sub> ) <sub>1-2</sub> , GLGGLS, XGGXG GPX spacer	?	β-Sheet	?	80%

Ma: major ampullate, Mi: minor ampullate. Flag: flagelliform, Cyl: cylindrical. PPII: polyproline II.

Small side chains (SSC) = Glycine<sup>+</sup> alanine<sup>+</sup> serine, Polar chains (PC) = Aspartic acid<sup>+</sup> threonine<sup>+</sup> serine<sup>+</sup> glutamic acid<sup>+</sup> tyrosine<sup>+</sup> histidine<sup>+</sup> arginine

<sup>1</sup> Amino acid composition: Ma Mi, Flag and Cyl from (Dicko *et al.*, 2004c), Acinous and Pyriform from unpublished data, *Bombyx mori*, *Antheraea pernyi* and *Galleria mellonella* from sequences.

<sup>2</sup> Sequences and predicted secondary structures: Ma, Mi, Flag (Hayash *et al.*, 1999); Cylindrical (Garb & Hayashi, 2005); Tubuliform (Tian & Lewis, 2005); Aciniform (Hayashi *et al.*, 2004); *Bombyx mori* (Inoue *et al.*, 2000a; Zhou *et al.*, 2000); *Galleria mellonella* (Zurovec & Sehnal, 2002); *Antheraea pernyi* (Sezutsu & Yukuhiro, 2000).

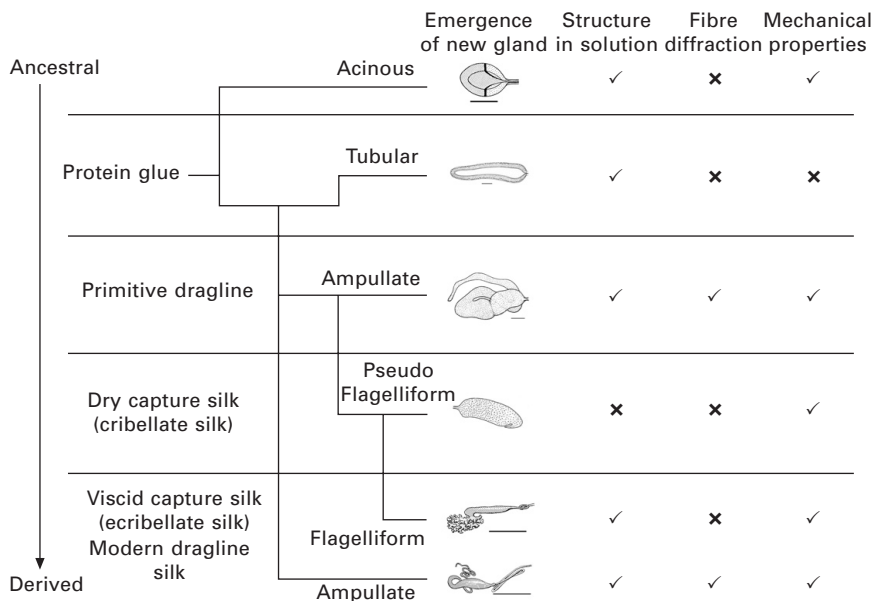
<sup>3</sup> Structure in solution: *Bombyx mori* (Iizuka & Yang, 1966; Yao *et al.*, 2004), Ma Mi, Flag and Cyl (Dicko *et al.*, 2004c), Acinous and Pyriform (see Fig. 5.8). *Antheraea pernyi* (Tsukada *et al.*, 1994). The helix like structure is loosely defined as a structure with a CD spectrum similar to myoglobin. β-spiral structure is defined as a super helical structure formed of 'straight' sections and β-turns.

<sup>4</sup> Conformational changes under denaturing conditions (see Fig. 5.8) and fibre formation.

<sup>5</sup> Degree of crystallinity: Ma (Riekel *et al.*, 1999); *Bombyx mori* and *Antheraea pernyi* (Iizuka, 1965).

<sup>6</sup> Fibres extensibility: Ma (Vollrath, 1999); Mi (Vollrath unpublished); Flag (Gosline *et al.*, 1999a); Cyl (Dicko *et al.*, 2004c); Acinous (Hayashi *et al.*, 2004); *Bombyx mori*, *Antheraea pernyi*, *Galleria mellonella* (Denny, 1980).





5.12 Evolution of silk glands, proteins and fibres. Composite evolutionary tree tracing the emergence of the different types of silk and their associated glands. On the other hand, known structural and mechanical data: (i) circular dichroism spectra of silk solution prior to spinning (Dicko *et al.* 2006); (ii) fibre X-ray diffraction pattern from Craig (2003); (iii) tensile tests.

IP Address: 129.132.211.108

Unlike most other silk-producing animals such as insects, spiders can produce up to nine different types of silks and have the ability to control key aspects of silk production over a wide range of conditions, (Vollrath and Knight 2001) controlling not only (i) silk protein composition and (ii) storage conditions but, crucially, also (iii) fibre extrusion conditions. The mechanisms by which spiders optimise and adjust silk properties and function are beginning to provide key information on structure–function relationships of silk proteins. Studies of the interplay between silks and spinning processes (Vollrath 2000a; Swanson *et al.* 2006) demonstrate a strong correlation between strength and relative elasticity with specific molecular architecture (Riekel *et al.* 2000; van Beek *et al.* 2002; Gosline *et al.* 2002). Numerous pitfalls await and over-interpretation is easily made. Figure 5.12 is an attempt to link a few of the structural data (silk structure in solution, X-ray diffraction of fibres and tensile tests) to a more classical evolutionary tree. An important point to make is that it is still possible to investigate such a tree because ancestral/non-specialist spiders are still available (e.g. mygalomorph). The complexity and intricacy of the relationships within the tree is daunting at first. But, in the next sections we will present some recent work where the identification

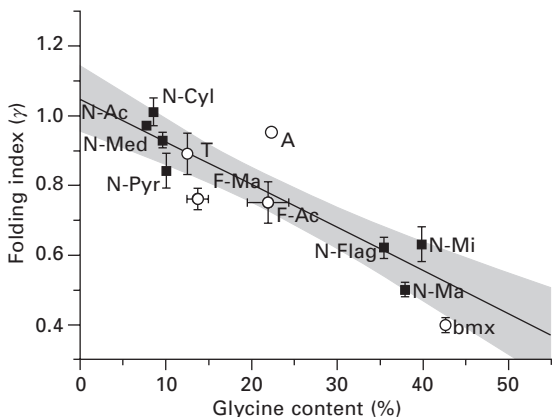
of key criteria and molecular markers has opened the way to a deeper understanding of silk evolution and structure–function relationships.

### 5.5.3 Silk processing: ‘dope’ structure, elastomericity and the role of glycine residues

Advances in molecular modelling of silk fibres are driving a major shift in our understanding of silk (Porter *et al.* 2005). Key features controlling the mechanical behaviour of the material are the ratios of the ordered and disordered fractions as well as the degree of hydration (Porter *et al.* 2005). Both parameters are interlinked and controlled by the animal during the extrusion process (Holland *et al.* 2006).

The ability of the ‘silk’ to implement small chemical changes by modifying hydrogen bonding sites during processing affects the properties of the bulk material significantly and has led to its status as an archetypal model elastomer (Vollrath and Porter 2006b). As such, it is interesting to examine the knowledge of silk proteins in solution in the light of the observations of Rauscher *et al.* (2006) that a fundamental requirement for elastomeric domains to remain disordered in solution is controlled by two major sequence determinants: proline and glycine content. This suggests that elastomeric assembly is, first, assisted by proline residues that conformationally restrict the main chain; and, second, helped by glycine residues that modify backbone hydration. Put together, the variation in proline and glycine content in elastomeric proteins and amyloids gives a composition threshold by which disorder is maintained and by which functional elastomericity becomes possible.

Interestingly, depending on the environment which they ‘inhabit’, glycine residues can promote either highly ordered or rather disordered structures (Chakrabarty *et al.* 1991; Serrano *et al.* 1992; Finkelstein and Ptitsyn 2002; Rauscher *et al.* 2006). This glycine ambivalence is based on an explicit approach of folding that properly accounts for the chemical nature of the backbone protein (Yang and Honig 1995a, 1995b; Yang *et al.* 1996; Uversky 2003; Kim and Conticello 2007). The important effects of hydration both during and after chain folding coupled with the ambivalent nature of glycine and its interplay with proline (maintaining disorder and promoting elastomeric properties) point towards silk proteins as ideal study models for detailed investigations into the structure–function relationship of natural elastomers. This novel view has resulted in a new classification of silk proteins structures in solution using circular dichroism (Dicko *et al.* 2008). In Fig. 5.13, the folding index (calculated from circular dichroism spectra) is plotted as a function of the glycine content in a selection of native silk protein extracts. The folding index is indicative of the amount of disorder present in each of the silks. A high folding index (above 0.6) indicates high folding into helical-like structures, whereas a low folding



5.13 Silk elastomericty and the role of glycine residues (Dicko *et al.* 2008). Inverse correlation between the folding index  $\gamma$  and glycine content. The regression was calculated solely using the *Nephila edulis* 7 glands (see Fig. 5.2) and analysed by a general linear model (GLM),  $n = 36$ ,  $F = 98.11$ ,  $p < 0.000$ , adjusted  $R_2 = 67\%$ . The grey area is the 95% confidence interval. The correlation was tested with T, A, F-Ma, F-Ac and bmx silks. Results: (i) the model quantitatively explained the structure function relationship found in the selected silks; and, (ii) to achieve specialisation and performance, silks require higher structural flexibility at the expense of reduced stability and increased conversion energy. Legend: *Nephila edulis* (Tetragnathidae) major ampullate (N-Ma), minor ampullate (N-Mi), flagelliform (N-Flag), cylindricform (N-Cyl), aciniform (N-Ac), pyriform (N-Pyr), median (N-Med); *Kukulkania hibernalis* (Filistatidae) major ampullate (F-Ma) and acinous (F-Ac); *Antrodiaetus unicolor* (Antrodiaetidae) single type glands (A), and *Aphonopelma chalcoldes* (Theraphosidae) acinous (T); *Bombyx mori* (Insecta: Bombycidae) (bmx).

IP Address: 129.132.211.108

index indicates more disordered structures. The conclusion found from this approach suggests that to promote silk specialisation and elastomericty the proteins must be maintained in a disordered state. The authors propose that glycine residues and the induced flexibility they provide allow for disorder to be maintained and controlled through specific chain hydration (Dicko *et al.* 2008). The second most important residue, proline, is discussed in the following section.

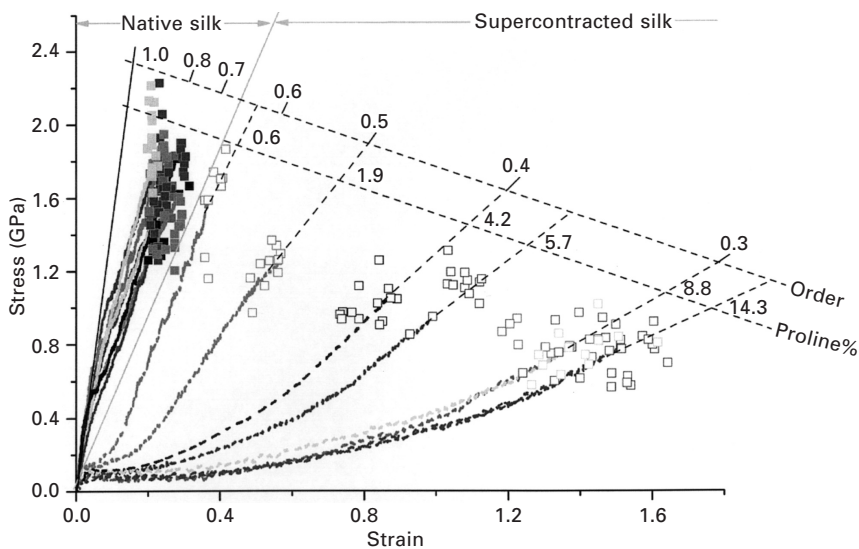
### 5.5.4 Silk processing: fibre formation and the role of proline residues

Interspecific differences in the mechanical and supercontraction properties are a well-established ‘window’ into silk structure–function relationships. Liu *et al.* (2008) attempted to add a deeper level of understanding on the

compositional level. Thus, the experiments they present, for the first time, demonstrate the quantitative relationships between the physical properties of spider major ampullate silks and their contents of a key amino acid: proline. These relationships, in combination with protein sequence data, support the hypothesis that the proline-related motif, that is, GPGXX, may be a key motif in silk (see Table 5.1 and Fig. 5.5). This motif possibly prevents tight packing and thus allows water molecules to access and disorient ordered glycine-rich motifs, which in turn leads to softening and to supercontraction. Furthermore, the initial modulus was found to decrease with increasing proline content. Liu *et al.* attribute this to a decreasing fraction of hydrogen bonds owing to proline's lack of one H-bond donor. Csh appears constant for proline-rich MA silks, probably due to a corresponding dense packing of proline and a limit of contraction in the molecular backbone. Because of their different capacities to shrink, supercontracted MA silks of different species display a variety of mechanical behaviours. Such findings, alongside a previous experimental study on the supercontraction phenomenon (Liu *et al.* 2005b), help us to better understand the link between mechanical properties and the structure of a spider MA silk. The results are summarised in Fig. 5.14.

The authors conclude that, for a given proline content (e.g., a species-specific MA composition), a fibre's physical properties would be determined largely by the degree of order locked into the final product by the processing conditions. Between silks of different species, on the other hand, both the chemical composition (the proportion of proline as proposed in this study) and the degree of order in the non-crystalline region (as determined by processing) would together determine the physical properties of the fibre. This conclusion must be true at least for those eight species of spiders we studied. Apparently, not all MaSp2 proteins of the MA silks in this study are identical in their domain architectures, and the crystal crosslink density of silks can vary depending on the largerscale sequence architecture of the dragline fibroins. It is possible that proline, alongside details in protein sequence (which cannot be identified by our comparative study), tunes the mechanical behaviour by changing the crystal crosslink density and hydrogen bonding network.

Taken together, a spider silk's properties are affected by the interplay of processing conditions and chemical composition. Processing conditions can adjust a spider silk's Csh in a certain range, while the proline content appears to determine in which range a silk's Csh can be adjusted. Mechanical properties are tuned by processing conditions, which mainly change the 'order' of molecular chains, while an important parameter, that is, initial modulus, is linked with proline content if the effect of 'order' is taken out. In the next section, we explore the geometry of the spinning pathway as well as two key processing parameters (reeling speed and temperature).



5.14 Structural order and supercontraction, and proline residues. Representative stress–strain curves of MAA silks from a range of species tested in either the native (solid line) or the supercontracted state (dashed line). Breaking points of all tested samples are shown as solid squares (native silk, 103 samples) or hollow squares (supercontracted silk, 93 samples). The reeling condition was tuned to produce native silk samples with a breaking strain of  $0.24 \pm 0.03$ . Each species is illustrated in a different shade of grey (from left to right), *Cyrtophora citricola*; *Latrodectus hesperus*; *Nephila edulis*; *Nephila senegalensis*; *Nuctenea sclopeteria*; *Argiope lobata*; *Argiope argentata*; *Araneus diadematus*. The proline content and ordered fraction (Porter *et al.* 2005) of supercontracted MA silks are marked. The straight black line defines the upper limit of native MA silk, where the ordered fraction is 1.0; the straight grey line roughly separates the stress–strain curves of native and supercontracted silks. Adapted from Liu *et al.* (2008).

### 5.5.5 Silk processing: dye geometry and processing variables

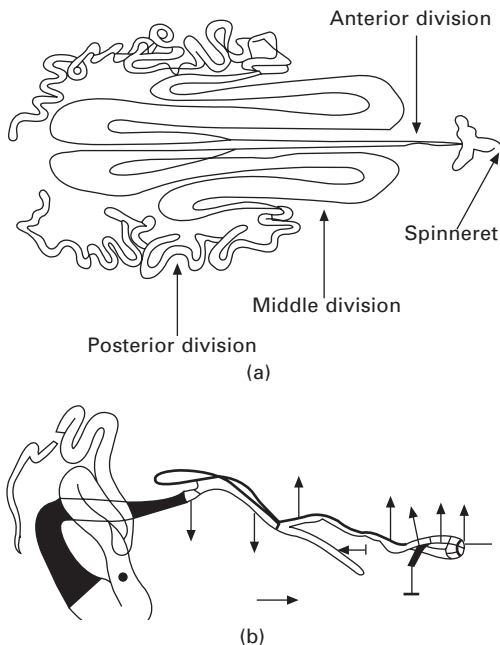
In the dragline silks, as in the capture silks, the different components and their interactions heavily depend on processing conditions during the natural extrusion and post-extrusion processes. Figure 5.15 shows the storage glands and spinning ducts from *Bombyx mori* and *Nephila edulis*. From the liquid feedstock in the gland, a silk converts into the solid thread inside the extrusion/spinning duct, a tapering tube of varying length and diameter (Figs 5.15c and 5.15d), which exits at a spigot (see Fig. 5.10a) (Knight and Vollrath 1999). The spider modifies the mechanical properties of its silk not only on a medium-term basis (e.g. in response to starvation) but also

in rapid response to immediate static and dynamic requirements of the web (Madsen *et al.* 1999). The animal must be able to do this not by changing the molecular structure (the feedstock dope is prepared well in advance of spinning) but by controlling molecular refolding and crosslinking during the extrusion process (Dicko *et al.* 2004a, 2006). Here, the feedstock is chemically modified by subtle pH alterations and the rate by which salts and water are pumped in and out of the duct as well as by the rate and ratio of flow elongation and the resulting shear forces (Vollrath and Knight 2001). All these factors have direct consequences on silk mechanics by affecting the degree and distribution of the different levels of order. The coating of a fibre will also have an effect (if nothing else, on the degree of water wetting possible). Finally, post-draw, whether inside the duct by the ratchet clamp mechanism (Vollrath and Knight 1999) or outside the duct by the action of pulling or scraping (Riekel *et al.* 2000), settles the silk's mechanical behaviour by locking the molecules into position. Many of these parameters and variables are affected by a centrally controlled production system (the spider's central nervous system) with considerable scope for feedback.

Two examples of dramatic consequences of processing variables are presented in Figs 5.16 and 5.17. The reeling speed is important not only for the animal's survival but also for the correct alignment and degree of crystallinity. Figure 5.16 shows a typical bell-shaped curve of the effect of reeling speed on breaking energy. An optimum is found at around 20 mm/s, which is the most natural spinning speed observed in the wild. Interestingly, temperature also affects the breaking energy, most likely by reducing conversion barriers. Another dramatic effect of reeling speed is found in *Bombyx* fibres. The animal spins his cocoon at a steady rhythm. Figure 5.17 shows that when the silk is forcibly reeled out of the worm, the quality (tensile property) increases dramatically to eventually be comparable to that of spider silk (Shao and Vollrath 2002).

### 5.5.6 Silk processing: the other influences

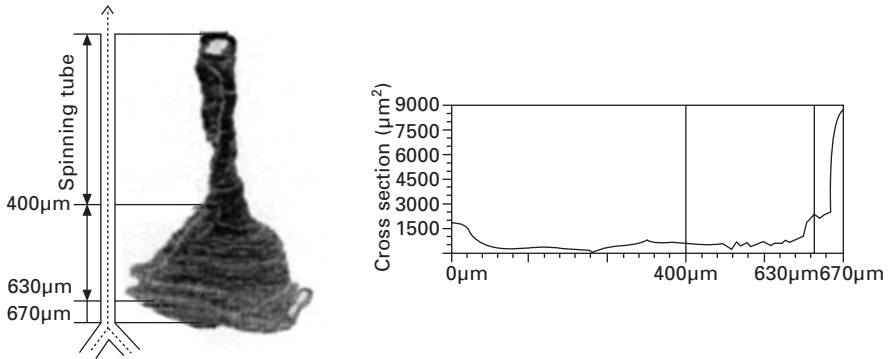
The wealth of articles on silk and its remarkable protein-based mechanical properties has somehow eclipsed the other components present in the gland extracts. Although predominantly protein-rich, the gland contains in varying amounts glyco-proteins (Vollrath and Tillinghast 1991), carbohydrates, lipids (Schulz 2001), small molecules (e.g. pigments, Holl and Henze 1988) and a wealth of ions, e.g. phosphates, calcium, potassium or sulphur (Knight and Vollrath 2001). The presence of all those compounds may be circumstantial. For example, silk glands can be considered as a dumping sac to remove toxins as well as retrieving water. Thus, compounds present in the silk may just happen to be there for no particular reasons. On the other hand, glyco-proteins and carbohydrates are thought to contribute to silk solubility by



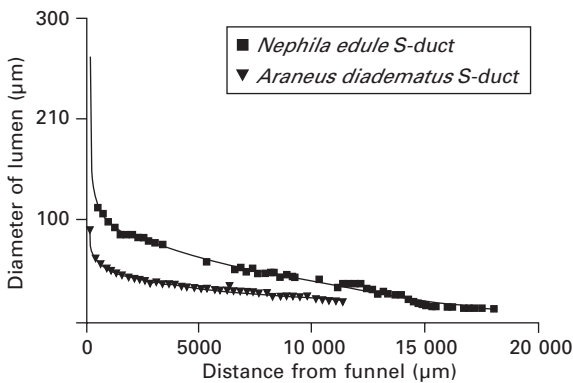
5.15 Spinning the fibres. *Bombyx mori* vs. spider ducts. (a) *Bombyx mori* silk gland, production and spinning from left to right. Right end is the spinneret. (b) *Nephila edulis* major ampullate spinning gland, production and spinning from left to right. (c) detail of the duct, spinning path, of *Samia cynthia ricini* silkworm (similar to *Bombyx mori*). Total length of the duct 670  $\mu\text{m}$ ; plotted is the change in cross-section along the duct. It shows a sharp drop in diameter from the base from 670 to 630  $\mu\text{m}$ , a shallow drop (hyperbolic profile) from 630 to 400  $\mu\text{m}$  and a constant cross-sectional area from 400  $\mu\text{m}$  to the exit spinneret. Total change of cross-sectional area 9000 to 1500  $\mu\text{m}^2$ . (d) plot of the diameter change along the spinning duct of *Nephila edulis* and *Araneus diadematus* spiders (duct length of 20 mm and 10 mm respectively). The spiders' ducts are hyperbolic die with diameter change of 100–300  $\mu\text{m}$  to 20–40  $\mu\text{m}$ . From Knight and Vollrath (1999) and Asakura *et al.* (2007).

balancing their hydrophobicity (Foo *et al.* 2006). The yellow pigmentation found in *Nephila* dragline is thought to help control the pH (Dicko *et al.* 2004a). While tanins in silkworm fibres are thought to contribute to the fibre's antibacterial defence system (Brunet and Coles 1974).

At the gene level, varying composition of silk protein polymorphs via gene splicing is also common (Craig and Riekel 2002). The animal uses a recombination of two genes (spidroin 1 and spidroin 2) to generate new silk protein constructs in response to its need.



(c)



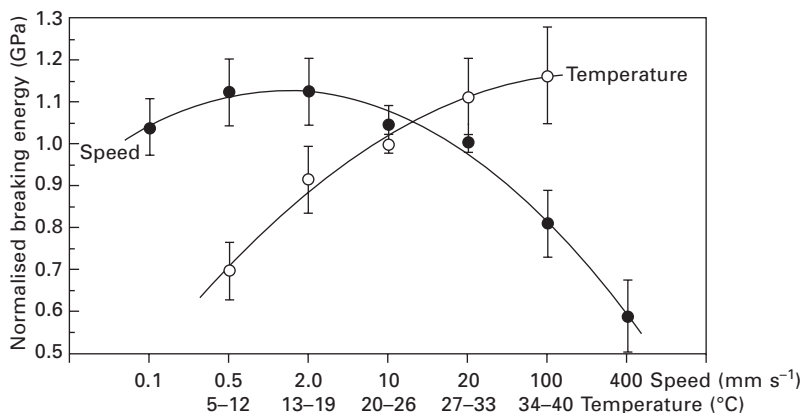
(d)

5.15 Cont'd

## 5.6 Silk fibre and its models

Remarkably, the overall mechanical properties (Denny 1980; Gosline *et al.* 1999a; Vollrath 2000b) of silks seem to depend less on the complex hierarchical organisation of silk on a microscopic level (Vollrath and Knight 1999; Inoue *et al.* 2000b; Knight and Vollrath 2002a) and more on the overall molecular structure (Gosline *et al.* 2002; Craig 2003; Fedic *et al.* 2003; Spenner *et al.* 2005) which by a complex spinning process (Vollrath and Knight 2001; Liu *et al.* 2005b) is formed into a material where nano-scale interactions predominate (Porter *et al.* 2005; Vollrath and Porter 2006b). From the early X-ray diffraction studies (Warwicker 1954; Marsh *et al.* 1955; Lucas *et al.* 1960; Rudall and Kenchington 1971) to the more modern spectroscopic results (Grubb and Jelinski 1997; Riekel *et al.* 1999; van Beek *et al.* 2000, 2002; Sirichaisit *et al.* 2003; Rousseau *et al.* 2004; Papadopoulos *et al.* 2007), the identification of the different conformations present in silk fibres and their



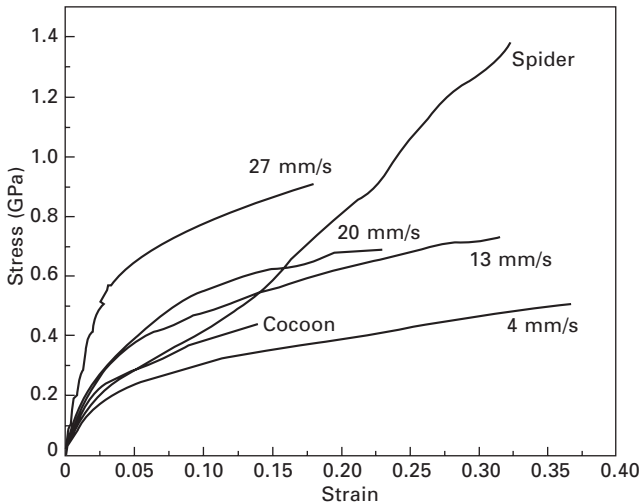


5.16 Processing variables: reeling speed and temperature. The effect of spinning conditions on the breaking stress of dragline silk spun by *Nephila edulis*. The black circles give the effects of modifying reeling speed and the white circles those of modifying body temperature. The average breaking energy for the sample threads at control conditions was  $165 \pm 30 \text{ kJ kg}^{-1}$ . In the graph, breaking stress is used rather than breaking force because the differences between individual spiders (as well as silk reeling speed and body temperature) affect the diameter of the silk thread, which in turn influences the force needed to break the thread. The control temperature was  $25^\circ\text{C}$  when the reeling speed was varied, and the control speed was set to  $20 \text{ mm s}^{-1}$  when the body temperature was varied, with the average natural spinning conditions for this species taken to match the control conditions. Adapted from Vollrath and Knight (2001).

IP Address: 129.132.211.108

role in determining the mechanical properties of silks have highlighted the presence of three major types of silks: (i) the rarely observed  $\beta$ -silk (Hepburn *et al.* 1979; Sutherland *et al.*, 2006), (ii) the cross- $\beta$  silks (Geddes *et al.* 1968); and (iii) the commonly observed co-linear (i.e. with strands parallel to the fibre axis)  $\beta$ -silks (Rudall and Kenchington 1971; Craig 1997). Interestingly  $\beta$ -silks and cross- $\beta$  silks have been reported to undergo, upon post-processing (i.e. stretching), a transition to the co-linear  $\beta$  structure.

Figure 5.18 summarises the most salient models of *Nephila* fibres and how they arise in time. Starting from the left are the first X-ray diffraction patterns measured by Kratky *et al.* in 1956 (Kratky 1956). Although these were from *Bombyx* fibres, *Nephila* spider dragline does not vary greatly in its diffraction pattern. Typically it was found and later confirmed that silk consists of, simply put, disordered regions interspersed with regions of order. The ordered regions can be either of high and permanent order (i.e. consist of crystalline blocks) or of medium and transient order (i.e. consist of molecular patterns that more readily unfold or refold). The crystalline



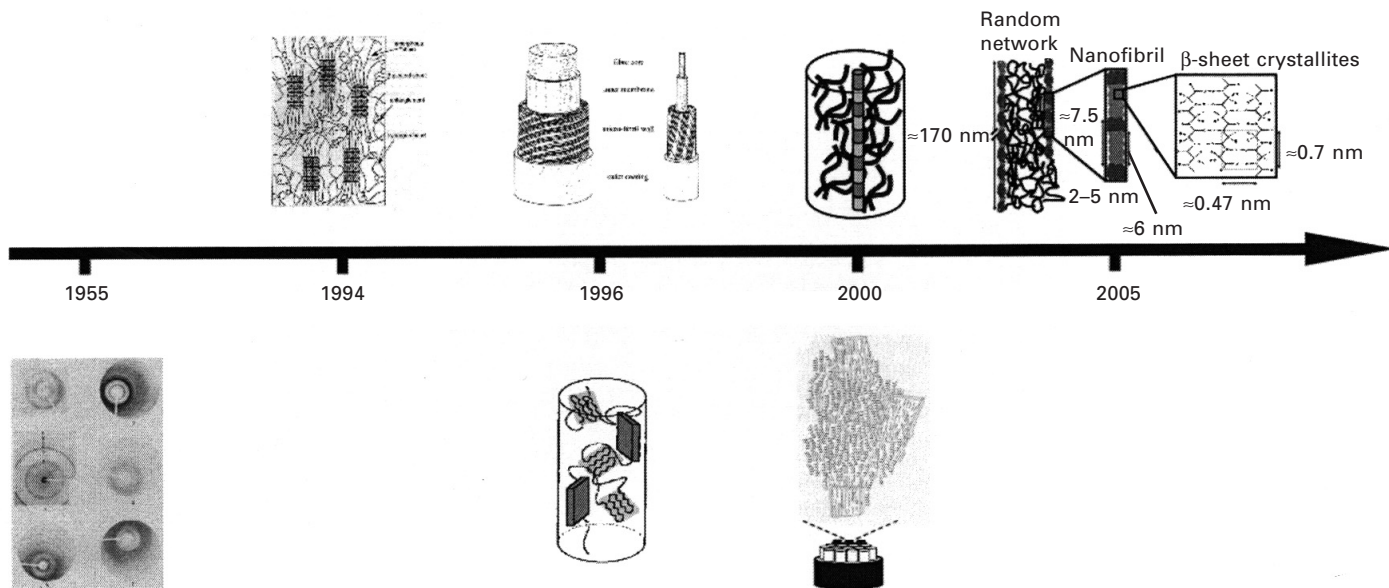
5.17 Reeling speed improves *Bombyx mori* silk fibres. Comparison of silks drawn at different speeds from the silkworm *Bombyx mori*. Stress-strain curves of washed and degummed single-filament silkworm silk (motor-reeled at 25°C at the indicated speeds), *Nephila* spider dragline silk (20 mm/s at 25°C) and standard, degummed commercial silk from a cocoon spun by the animal in the natural 'figure of eight' at speeds oscillating between 4 and 15 mm/s at 20°C. The area under the stress-strain curve represents the energy that a fibre can take up before breaking, and thus indicates its toughness. Adapted from Shao and Vollrath (2002).

IP Address: 129.132.211.108

blocks or domains contain  $\beta$ -pleated sheets oriented anti-parallel to the fibre axis. Crystallite size is in the nano-scale region, e.g.  $7 \times 5 \times 2$  nm (Riekell *et al.* 2000), with important implications on material properties (Vollrath and Porter 2006b). The degree of order, not necessarily identical to the degree of crystallinity, of *Nephila* MA fibres is in the region of 30–50% (Gosline *et al.* 1986) and is highly dependent on the conditions under which a fibre was spun (Liu *et al.* 2005a, 2005b, 2008).

The  $\beta$ -pleated sheets consist primarily of long stretches of poly-alanine motives. In *Nephila clavipes* MA silk, about 80% of the alanine is incorporated in this way, with about half of it residing densely packed in a highly orientated fraction. The other fraction is packed less densely, it is less well orientated and is, moreover, suspected to contain the GAG motifs flanking the highly orientated fraction (Simmons *et al.* 1996). The degree of integration of glycine (G) rich sequence motifs into the ordered regions, particularly the inclusion of GGX motifs, is still unresolved (Thiel *et al.* 1995; Kümmerlen *et al.* 1996; Michal and Jelinski 1998).

The following models show the increase of information regarding the interphase region between the crystalline  $\beta$ -sheets and amorphous regions.



5.18 Orientation and structural models. Timeline of silk models, from left to right. 1955, first X-ray diffraction pattern of *Bombyx* silk (Kratky 1956). 1994, Termonia model (Termonia 1994). 1996, upper part, Vollrath model (Vollrath *et al.* 1996); lower part Jelinsky and Grubb NMR model (Jelinski 1996). 2000/2002, upper part, Riekel X-ray diffraction model (Riekel *et al.* 2000); lower part, van Beek NMR model (van Beek *et al.* 2002). 2005, Sapede neutron diffraction model (Sapede *et al.* 2005) and Porter predictive modelling (Porter *et al.* 2005).

Interspaced are two models that attempt to explain silk mechanical behaviour based on ultrastructural knowledge. The first model by Termonia (1994), though ground-breaking at the time, failed to explain the complex behaviour of silk proteins. It was only in 2005 that a more physically realistic model was proposed (Porter *et al.* 2005). This model is further explored in Section 5.7.

The novel view on silk and its model, viewed from neutron diffraction (Sapede *et al.* 2005) includes water molecules and their dynamics. This new step is critical to understanding silk deformation mechanics, with water playing such an important role in plasticisation as well as toughening mechanisms (Vollrath and Porter 2006b; Porter and Vollrath 2008).

## 5.7 Influence of structure on properties

From the preceding discussion on the complex hierarchy of structure in silks, the key structural elements that determine the bulk physical properties of any given silk fibre must now be identified and transformed into a quantitative set of structure–property relations that includes most of the very large number of different types of silk. Early models for silk, such as that of Termonia, consider silk as a semicrystalline polymer, composed of ‘hard’ crystal domains that act like a distribution of crosslink sites in a ‘soft’ rubber matrix (Termonia 1994). While providing a relatively simple physical model that embodies the main features of silk as a semicrystalline polymer, a more general model is required to quantify the role of each of the structural features in silk, and how they combine to give such a large range of mechanical properties. Without understanding what differentiates a natural silk from conventional semicrystalline polymers or even regenerated silk, it is unlikely that synthetic analogues of silk will be developed.

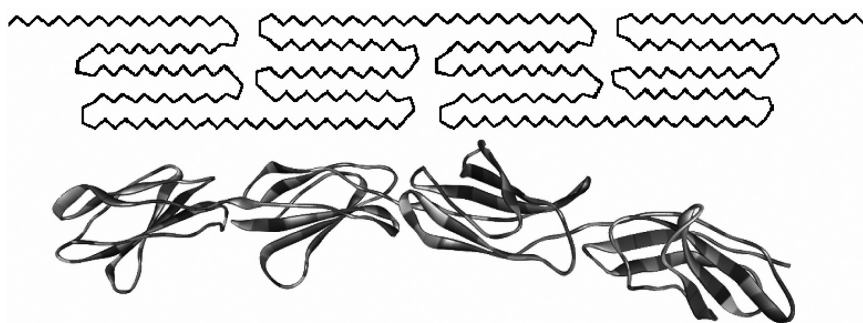
Here, we give a brief summary of recent models for silk properties that are based upon the biological principle of efficient management of energy for survival (Vollrath and Porter 2006b; Porter and Vollrath 2008). Each biological function requires a specific combination of stiffness, strength and toughness in a silk fibre. For example, dragline silks that support the weight of a spider or provide the structural scaffold of a web require stiffness and strength, while capture threads must absorb a considerable amount of kinetic energy and bind the prey of the spider. Cocoon silks must defend the insects or eggs against a wide range of penetration threats, which require a subtle combination of strength and durability. These key factors of stiffness, strength, and toughness can be expressed in terms of storage and dissipation of mechanical energy of deformation in a material, which can then be traced right back to mechanisms at the molecular and nanometre scales of structural morphology.

### 5.7.1 Order–disorder, water and nanostructures

Since silks are so diverse in their functions and structure, any model must use very general parameters that embody and quantify the effects that any specific combination of molecular structural features that has evolved can provide. This is particularly important, since analytical techniques such as X-ray scattering or NMR do not provide an unequivocal measure of structural features at the macromolecular and nanometre scales. The three main effects are the fractions of ordered (crystal) and disordered (glass and rubber) sites, the water fraction, and the nanoscale morphology for the structural domains.

A key structural feature that differentiates many silks from synthetic polymers can be suggested to be the nanoscale ‘string of beads’ morphology shown in Fig. 5.19, which shows a fibroin structure taken from the Swiss Protein Database and a graphical simplification. Viney *et al.* (1994) suggested that silk molecules assemble into lines of macromolecular balls that behave like liquid crystals in solution to facilitate the flow of the dope during spinning. However, the size, connectivity and orientation of the structural domains that are inferred from analysis and the combination of physical properties suggest a nanofibril structure that consists of domains (beads) of a hairpin folded polymer chain with lengths of the order of 4 nm and dry diameters of about 2 nm. The dry diameter comes from the removal of water from more symmetrical domains in the hydrated state in solution that are optimised for their flow profile.

The ‘string of beads’ nanofibril morphology in Fig. 5.19 is important for a number of physical properties. First, this liquid-crystal form facilitates the flow of the silk dope during solution spinning, which has been observed directly (Holland *et al.* 2006, 2007). Second, the nanometre size of the beads functions very much like nanoscale grains in a super-strong metal, where fracture mechanics suggests that failure strength has an approximately inverse



5.19 Nanofibril ‘string of bead’ structure. Adapted from Vollrath and Porter (2006a).

square-root relation with size of the main structural features (Porter *et al.* 2005; Porter and Vollrath 2008). As a rough guide, a silk with a modulus of 10 GPa and a domain size of 4 nm with a surface energy of  $0.15 \text{ J m}^{-2}$  would be expected to have strength of about 1.7 GPa, which is in good agreement with observation. Third, surprisingly isotropic mechanical properties are found in silks even though their optical birefringence suggests that they are highly oriented. This confusion is easily resolved by the bead morphology, since each bead consists of highly oriented segments of a polymer chain in the fibre axis, but this orientation consists of many short folded segments that have little mechanical connectivity. Thus, the nanometre scale of natural silk nanofibril morphological domains could be a key differentiator over synthetic polymers, or even regenerated silk, where aggressive solvent processing tends to remove these nanostructural features.

Since silks (and proteins in general) can take so many different crystallographic forms, a very pragmatic option is simply to look at the fraction of ordered and disordered states (Porter *et al.* 2005). Ordered states can be loosely identified with the different crystal forms of proteins, and more precisely as the fraction of peptide segments that have both hydrogen bonds in the amide group bonded to another amide group. This automatically implies some degree of alignment between parallel molecular chains. Disordered states have only one hydrogen bond of the amide group linked to another adjacent amide group, which implies misalignment of macromolecular chains. Disordered states can be either glassy or rubberlike, depending mainly on the fraction of water in the disordered domains, which reduces the glass transition temperature from the dry reference value of about  $200^\circ\text{C}$ . The size of the ordered and disordered domains is deliberately kept open at this stage, but the strength and toughness of silk fibres does imply an ability to share energy between the different forms at a nanometre scale. Also, the ‘string of beads’ morphology allows an assumption that mechanical properties are relatively isotropic, to a good first approximation.

IP Address: 129.132.211.108

### 5.7.2 Mechanical predictive and interpretative model

The main distinguishing features of ordered and disordered states are that ordered states tend to be quite rigid due to the strong hydrogen bonding, but disordered states are relatively mobile and allow low-temperature dynamic relaxations that dissipate mechanical energy and give toughness. This simple classification allows the energy management principle to be translated directly into a molecular-level model for mechanical properties, and the key step is to quantify the fraction of mechanical energy that is dissipated in the disordered fraction during deformation.

The model starts by calculating a reference pure elastic modulus for the polymer, which is the bulk modulus,  $B$ , that is determined by the cohesive

binding energy,  $E_{\text{coh}}$ , between peptide segments with a volume,  $V$ , in adjacent protein chains:

$$B \approx 18 \frac{E_{\text{coh}}}{V}$$

For example, the cohesive energy of an average peptide segment of a *Nephila* dragline silk is about 45 J/mol with a volume of  $52 \times 10^{-6} \text{ m}^3/\text{mol}$  using group additivity tables, which suggests a reference value of 15 GPa for the elastic modulus. This elastic modulus is then reduced in magnitude by the energy dissipated in the disordered fraction due to the loss tangent,  $\tan\delta$ , associated with low-temperature relaxations.

In many silks, the main low-temperature peak in loss tangent occurs at about  $-70^\circ\text{C}$  and has been attributed to side-chain mobility of the side-chain fragment of a peptide segment. The area under this loss peak,  $\tan\Delta \approx 19$ , can be quantified as a local transition event that is scaled in the disordered fraction,  $f_d$ , and then taken to have a normal distribution around the peak position to give an approximate height and width of the peak.

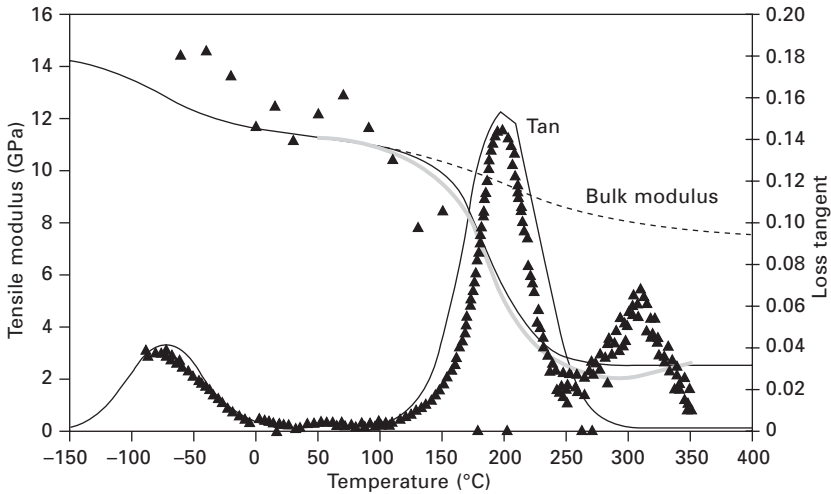
The transformation of the reference modulus,  $B$ , into an actual tensile modulus,  $Y$ , is then done using the equation

$$Y = B \exp \left( - \frac{f_d \int_0^T \tan \delta \, dT}{A B} \right)$$

where  $A \approx 1.5 \text{ kPa}^{-1}$  is a structural factor in segment dimensions that can be calculated easily from the molecular structure. For example, a disordered fraction of 0.33 in a typical dry *Nephila* spider dragline silk suggests a tensile modulus of 11 GPa, which reduces with greater fractions of disorder.

A similar calculation can be done for the modulus above the glass transition of the disordered fraction at about  $200^\circ\text{C}$ , which includes loss through the glass transition zone and shows that the modulus reduces to a lower limit of about 10 MPa for fully disordered material, with a value of about 2 GPa for the typical dragline silk given above. Figure 5.20 shows more detailed calculations of the dynamic mechanical properties of a generic silk in the form of modulus and loss tangent as a function of temperature.

The next step in predicting mechanical properties is to transform the modulus temperature curves of Fig. 5.20 to stress–strain plots through to failure. At the simplest level, this is done by using temperature as a dummy variable to calculate strain,  $\epsilon$ , and stress,  $\sigma$ , in a self-consistent form using the linear coefficient of thermal expansion,  $\beta \approx 0.0001 \text{ K}^{-1}$ , which can be calculated using structure–property relations (Porter 2002):



5.20 Property plot: DMA. Adapted from Vollrath and Porter (2006a).

$$\epsilon = \int_T^{T_e} \beta \, dT, \quad \sigma = \int_T^{T_e} \beta E \, dT$$

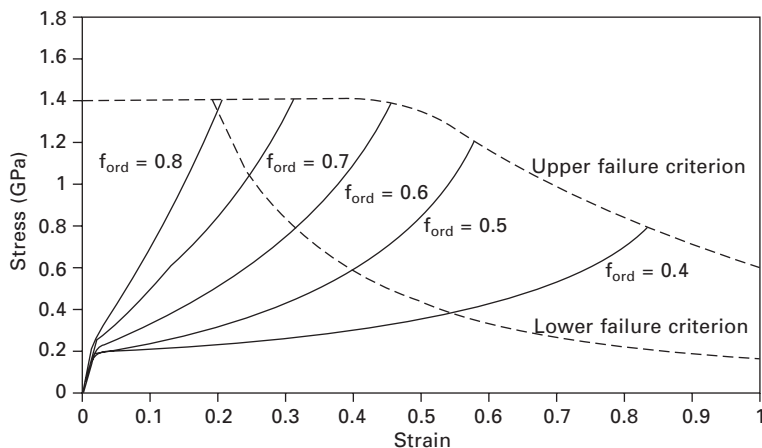
IP Address: 129.132.211.108

The yield point corresponds thermodynamically to the glass transition condition at a model elastic strain of about 2%, so the post-yield modulus corresponds to the modulus above the glass transition temperature. The strain hardening above the yield point in many silks is due to the gradual transformation of rubberlike states back to either crystal or glassy states of matter as mechanical energy forces the interacting molecular segments back together under higher strains. Generally, lower fractions of disorder absorb this strain energy faster and show hardening at lower strains.

This strain-hardening behaviour also has a direct influence on failure conditions in silk, since the material becomes brittle when all the rubberlike states have been transformed back to rigid crystal or glassy states. The failure stress and strain (if below the fracture mechanics limit of about 1.7 GPa) occur at the point where all the rubberlike states are lost. This is very much like the strain hardening and failure of conventional rubbers. Figure 5.21 shows the results of model calculations of stress–strain to failure for generic silks with different fractions of disorder, which shows all the main features associated with mechanical properties of dry silk fibres.

Finally, water plays an important role in controlling the mechanical properties of silks, and most other biological materials. The main effect of water is to soften the disordered fraction, since it is unable to destabilise the strong hydrogen bonding in the ordered states. One dramatic effect is





5.21 Property plot: mechanical envelope of properties. Adapted from Vollrath and Porter (2006a).

to induce supercontraction of about 50% shrinkage in some spider dragline silks as water attacks the proline segments that have been frozen into a metastable oriented structure by the ordered sites all around them, but relax to a disordered state as soon as water relaxes these local constraints (Liu *et al.* 2008). More generally, water reduces the  $T_g$  of the disordered fraction, and a  $T_g$  value of 300 K is reached at a water weight fraction of about 25% or 80% humidity (Porter and Vollrath 2008). Under these conditions, silk becomes much softer, as discussed above for temperatures above  $T_g$ .

The combination of water content and fraction of ordered and disordered states is a very powerful control mechanism for mechanical properties, such that silks (and proteins in general) can have a massive range of mechanical properties, from an upper limiting modulus value of about 20 GPa in a highly ordered dragline silk to the properties of a reinforced rubber with a modulus of the order of MPa in a highly hydrated disordered silk. Using the models outlined here, it is possible to understand and calculate the properties of a silk with a prescribed structure and composition, which will be a great asset in attempts to mimic silk as a synthetic engineering or biomedical fibre.

## 5.8 Artificial silks

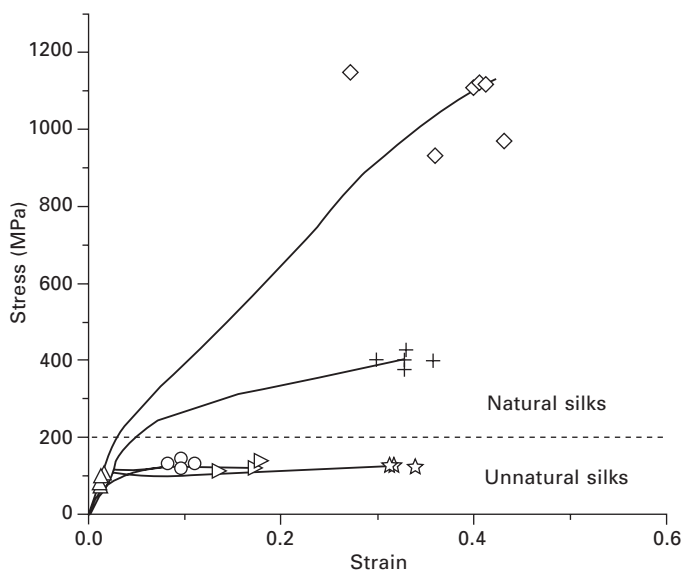
Silks are biopolymers with a wide range of interesting mechanical properties (Vollrath 2000b; Vollrath and Knight 2001). If these silks could be manufactured in quantity and quality and with comparably cheap and environmentally friendly production methods (Fahnestock *et al.* 2000; Fahnestock 2005), they could indeed become interesting alternative fibres to low-tech materials such

as nylon or cotton (which are cheap, but environmentally costly) or hi-tech materials such as Kevlar or Twaron (which are expensive and environmentally costly). The worldwide production of synthetic fibres exceeds several million tons per year and requires an equal amount of fossil carbohydrates; the consumption of energy is not even considered. Although decay of deposited synthetics is slow, in the end the degradation of these fibres will add to the overall balance of the greenhouse gas carbon dioxide. Recombinant spider silk, on the other hand, can be generated from sustainable resources and could be recycled since it is made of proteins and therefore fully degradable (Fahnestock *et al.* 2000). Thus, even the replacement of low-tech fibres would be beneficial by lowering carbon dioxide output and saving valuable resources. However, the key to low-tech applications lies in the capabilities to find cheap and efficient production methods to deliver the huge amount of material that is demanded.

Initially, artificial dragline-type spider silk will probably find use in medicine (Vollrath *et al.* 2002; Altman *et al.* 2003), partly because of the traditionally high return on investment in this field, partly because spider silks already have a long tradition as *ad hoc* emergency plaster. However, there would also be a potential future in other markets; it is likely that techno-silks, in addition to replacing some now traditional man-made fibres, might find a use in novel applications. Magnetic silk–fibre composites, for example, can be made by binding colloidal magnetite ( $\text{Fe}_3\text{O}_4$ ) nanoparticles to threads of dragline spider silk (Mayes *et al.* 1998). Such mineralised fibres retain their high strength and elasticity but can be oriented by an external magnetic field. Finally, artificial silks could find profitable employment in lightweight composites where their toughness and good thermal stability might be rather desirable.

### 5.8.1 Regenerated silks

An interesting idea to tailor silk fibre properties is to reuse silk proteins gathered from native silks and modify them to form new biomaterials. This process, often referred to as ‘regeneration’, consists in dissolving silk fibres (commonly silkworm silk cocoons) in chaotropic salt solutions to produce soluble silk proteins (Yamada *et al.* 2001). Alternatively, organic solvents can be used. Although very successful in its approach to providing large quantities of silk protein feedstock, the quality and polydispersity of the proteins are far from those of the native ones. Various tricks can be applied to crosslink or chemically modify regenerated silk in order to produce ‘silk’ fibres, films or porous structures. Figure 5.22 shows a typical graph comparing mechanical properties from a regenerated fibre and a native fibre. The gap between the two groups highlights the remarkable feat of spiders and insects in producing high-performance fibres. It has been a problem

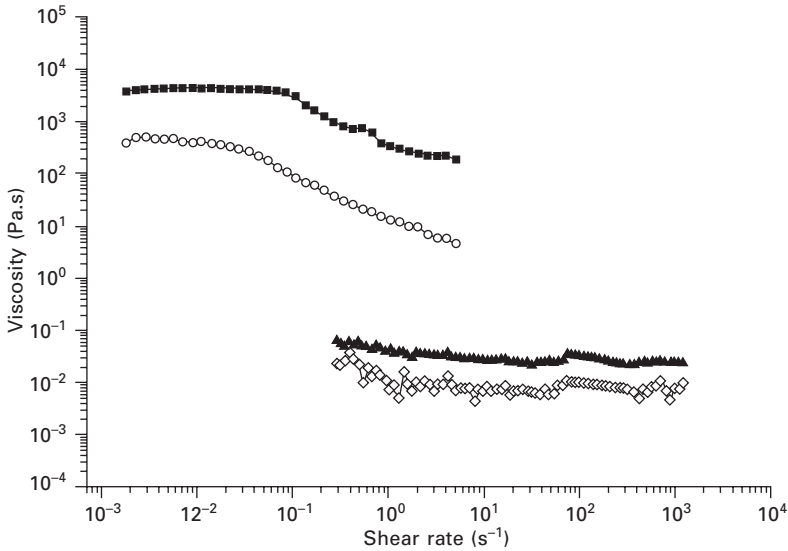


5.22 Regenerated silk mechanical properties. Natural and reconstituted silks have substantially different material properties. A representative sample drawn from the current published literature of the mechanical properties of silk fibres created by a variety of different reconstitution/respinning techniques (whose stress has been reported in Pa). Lines represent exemplar stress–strain curves, while points represent sample variation from that experiment. Natural silk: spider (*Nephila edulis*) major ampullate (diamonds) and silkworm (*Bombyx mori*) cocoon (crosses) have breaking stresses much higher than silks prepared from reconstituted spider silk spun in water (right-facing triangles) and reconstituted silkworm silk spun in water (circles) or spun in solvent with different spinning conditions (triangles and stars). Adapted from Holland *et al.* (2007).

IP Address: 129.132.211.108

screening for the right preparation method or fibre making method. This is simply because tensile testing was the preferred method of comparison. Recently, however, a thorough and detailed use of rheology showed that one could readily quantify the differences between regenerated silks and native silks (Holland *et al.* 2006).

Figure 5.23 shows a typical viscosity measurement over a range of shear rates. The data compares a native silk extract to a regenerated silk. The test sensitivity to silk preparation further emphasises the key role played by rheological tests (Holland *et al.* 2007). Furthermore (data not shown), over the range of all concentrations tested, natural silk dope consistently exhibited a zero shear viscosity and power law shear-thinning typical of a molten polymer, with higher concentrations representing higher overall



**5.23 Regenerated silk rheological properties.** Representative viscosity measurements of natural and reconstituted silkworm dope. Dry weight concentrations of natural dope are 18.6% weight/volume (squares) and 4.6% (circles), and of reconstituted dope 18.5% (triangles) and 4.5% (diamonds). For each concentration the same sample is represented in both graphs for consistency. Adapted from Holland *et al.* (2007).

viscosities. When compared on the same scale, reconstituted silks behaved like Newtonian fluids with significantly lower viscosities, in agreement with previous findings (Chen *et al.* 2001). The different concentrations of reconstituted silk dope that were tested had only slightly different rheologies, which suggests that for this material there is a direct, positive link between amount of material and viscosity. Taken together, these data (Holland *et al.* 2007) indicate that, despite the origin of the reconstituted molecules from native silk, the reconstitution process did substantially alter the integrity of the silk molecules. This alteration must have been sufficiently invasive to render the reconstituted molecules unable to respond to shear in the same way as their native predecessors.

## 5.8.2 Genetically engineered silks

In order to find an efficient way to produce spider silk proteins, a number of researchers and companies have attempted to express the relevant genes in a range of organisms that are relatively easily and cheaply cultured. This has included transgenic plants (e.g. potato tubers) and mammals (e.g. goat's milk), which could provide substantial harvests in agricultural production

systems (Arcidiacono *et al.* 1998; Scheller *et al.* 2001; Hueimmerich *et al.* 2004; Karatzas *et al.* 2005). These more 'advanced' but not necessarily more productive systems were used in addition to the more typical fermentation systems where spider silk genes were expressed in microorganisms such as *E. coli* and *Pichia pastoris* (O'Brien *et al.* 1998). Other host systems like MAC-T or BHK mammal cell lines were also used, but due to the high costs these were more of scientific interest (Lazaris *et al.* 2002). Commercially more interesting could be the use of specialist spider or insect cell lines. Products of sizes up to 150 kDa were successfully expressed in these systems and the applied gene cassette models are capable of extending the product size at will. However, it remains unclear whether the natural protein size is a requirement for the fibre quality and, aside from molecular size, whether the heterogeneity observed in the sequence repeats might also be important.

It is, of course, very much hoped that one or several of these production systems will be able, in the not too distant future, to supply sufficient amounts of raw materials to allow spinning silk-like fibres at a commercial scale. However, we must not forget the parallel development of appropriate 'spinning' extruders. Once a good and reliable expression system is up and running then we can test and optimise both the artificial spinning dopes and the spinning methods. Only by tuning both to act in synergy will we be able to manufacture fibres to match the spider's threads and their millions of years of co-evolution of feedstocks and extrusion systems. While such a biotechnological approach in itself poses a range of problems, both with the transfer of genes as well as with the expression and extraction of the relevant proteins, it emerges that the exceptional properties of a silk do not depend solely on the unique nature of the silk precursor feedstock. There is now strong evidence that a spider's (as well as a silkworm's) spinning mechanism may be no less important in determining a filament's material properties than the feedstock polymer (e.g. Vollrath and Knight 2001; Dicko *et al.* 2006).

IP Address: 129.132.211.108

## 5.9 Conclusions

The Napoleonic industry of using spider silk (i.e. from the golden silk spider *Nephila madagascariensis*) to spin gloves was of limited success, mainly because of the cannibalistic nature of the spiders. But spider silks before and since were seen as exemplary fibres for applications that required of their materials both thinness and toughness. Until very recently, the cross-hairs in optical instruments were made of spider silks (e.g. from the garden cross spider *Araneus diadematus*) not least because this silk is fine and of even diameter along its length. In today's public belief spider silk is often associated with bullet-proof vests. However, the ways in which a flak-jacket and a spider's web handle kinetic energy are rather different, and not interchangeable;

the toughness of a web silk relies on its extensibility, that of a flak jacket emphatically not. However, spider silks (and their analogues) seem to be finding a ready market in biomedical applications. First and foremost, most spider silks seem to be biocompatible (Meinel *et al.* 2005) over appropriate timescales as well as tough and readily decorated with interesting compounds. Consequently, today a major effort is being invested in developing spider and spider-like silks for this application (Vollrath and Porter 2006b). While it is one thing to use existing silks, with or without chemical modifications, it is another altogether to produce silks biosynthetically (i.e. using other organisms to express the silk proteins) or fully synthetically (using artificial sequencing).

## 5.10 Acknowledgements

For funding we thank the British EPSRC (grant GR/NO1538/01) and BBSRC (S12778), the European Commission (grants G5RD-CT-2002-00738 and MTKD-CT-2004-014533) and the AFSOR of the USA (grant F49620-03-1-0111). The CD is supported by St Edmund Hall, Oxford Junior Research Fellowship and EPSRC Life Science Interface Fellowship.

## 5.11 Sources of further information

<http://www.arachnology.org/Arachnology/Arachnology.html>

Craig, C. L. (2003). *Spider Webs and Silks*. New York, Oxford university Press.

Foelix, R. F. (1996). *Biology of Spiders* (2nd edition). New York, Oxford University Press.

The Oxford Silk Group, [www.oxfordsilkgroup.com](http://www.oxfordsilkgroup.com)

Vollrath, F. and D. P. Knight, (2001). 'Liquid crystalline spinning of spider silk'. *Nature*, **410**(6828): 541–548.

## 5.12 References

Altman, G. H., Diaz, F. *et al.* (2003). 'Silk-based biomaterials'. *Biomaterials* **24**(3): 401–416.

Asakura, T., Yao, J. *et al.* (2007). 'Structure of the spinning apparatus of a wild silkworm *Samia cynthia ricini* and molecular dynamics calculation on the structural change of the silk fibroin'. *Polymer* **48**(7): 2064–2070.

Arcidiacono, S., Mello, C. *et al.* (1998). 'Purification and characterization of recombinant spider silk expressed in *Escherichia coli*'. *Applied Microbiology and Biotechnology* **49**(1): 31–38.

Asakura, T. and Kaplan, D. L. (1994). 'Silk production and processing'. In *Encyclopedia of Agricultural Science*, ed. C. J. Arntzen and E. M. Ritter. London, Academic Press. Vol. 4: 1–11.

- Becker, N., Oroudjev, E. *et al.* (2003). 'Molecular nanosprings in spider capture-silk threads'. *Nature Materials* **2**: 278.
- Bini, E., Knight, D. P. *et al.* (2004). 'Mapping domain structures in silks from insects and spiders related to protein assembly'. *Journal of Molecular Biology* **335**(1): 27–40.
- Bond, J. E. and Opell, B. D. (1998). 'Testing adaptive radiation and key innovation hypotheses in spiders'. *Evolution* **52**(2): 403–414.
- Brunet, P. C. J. and Coles, B. C. (1974). 'Tanned silks'. *Proceedings of the Royal Society of London Series B – Biological Sciences* **187**(1087): 133–170.
- Case, S. T. and Smith, S. V. (1994). 'Synthetic and recombinant domains from a midge's giant silk protein: role for disulfide bonds'. In *Silk Polymers: Materials Science and Biotechnology*, ed. D. Kaplan, W. W. Wade, B. Farmer and C. Viney. Washington, DC, American Chemical Society. Symposium series **544**: 91–97.
- Case, S. T. and Thornton, J. R. (1999). 'High molecular mass complexes of aquatic silk proteins'. *International Journal of Biological Macromolecules* **24**(2–3): 89–101.
- Case, S. T., Powers, J. *et al.* (1994). 'Silk and silk proteins from two aquatic insects'. In *Silk Polymers: Materials Science and Biotechnology*, ed. D. Kaplan, W. W. Wade, B. Farmer and C. Viney. Washington, DC, American Chemical Society. Symposium series **544**: 80–90.
- Chakrabartty, A., Schellman, J. A. *et al.* (1991). 'Large differences in the helix propensities of alanine and glycine'. *Nature* **351**(6327): 586–588.
- Chen, X., Knight, D. P. *et al.* (2001). 'Regenerated Bombyx silk solutions studied with rheometry and FTIR'. *Polymer* **42**(25): 9969–9974.
- Craig, C. (1997). 'Evolution of arthropod silks'. *Annual Reviews of Entomology* **42**: 231–267.
- Craig, C. L. (2003). *Spider Webs and Silks: Tracing Evolution from Molecules to Genes to Phenotypes*. New York, Oxford University Press.
- Craig, C. L. and Riekel, C. (2002). 'Comparative architecture of silks, fibrous proteins and their encoding genes in insects and spiders'. *Comparative Biochemistry and Physiology B. Biochemistry and Molecular Biology* **133**(4): 493–507.
- Denny, M. W. (1980). 'Silks – their properties and functions'. In *The Mechanical Properties of Biological Materials*, ed. J. F. V. Vincent and J. D. Currey. Cambridge, UK, *Soc. Exp. Biol. Symp.* 34, Cambridge University Press, Vol. 34: 245–271.
- Dicko, C., Kenney, J. M. *et al.* (2004a). 'Transition to a beta-sheet-rich structure in spidroin *in vitro*: the effects of pH and cations'. *Biochemistry* **43**(44): 14080–14087.
- Dicko, C., Knight, D. *et al.* (2004b). 'Structural conformation of spidroin in solution: a synchrotron radiation circular dichroism study'. *Biomacromolecules* **5**(3): 758–767.
- Dicko, C., Knight, D. *et al.* (2004c). 'Major and minor ampullate, flagelliform and cylindrical glands secondary structures. Concentration and temperature effects'. *Biomacromolecules* **5**(6): 2105–2115.
- Dicko, C., Kenney, J. *et al.* (2006). 'Beta-silks: enhancing and controlling aggregation'. *Advances in Protein Chemistry*, **73**: 17–53.
- Dicko, C., Porter, D. *et al.* (2008). 'Structural disorder in silk proteins reveals the emergence of elastomericity'. *Biomacromolecules* **9**(1): 216–221.
- Eby, R. K., Putthanarat, S. *et al.* (1999). 'The nanofibrillar morphology of silks'. *Abstracts of Papers of the American Chemical Society* **217**: 069-BTEC.
- Eles, P. T. and Michal, C. A. (2004). 'Strain dependent local phase transitions observed during controlled supercontraction reveal mechanisms in spider silk'. *Macromolecules* **37**(4): 1342–1345.
- Emile, O., Le Floch, A. *et al.* (2007). 'Time-resolved torsional relation of spider draglines by an optical technique'. *Physical Review Letters* **98**(16): 167–402(4).

- Fahnestock, S. R. (2005). 'Fibrous proteins from recombinant microorganisms'. In *Biotechnology of Biopolymers; from Synthesis to Patents*, Vol. 2, ed. A. Steinbuechel and Y. Doi. Weinheim, Germany, Wiley-VCH, Vol. 2: 895–927.
- Fahnestock, S. R., Yao, Z. *et al.* (2000). 'Microbial production of spider silk proteins'. *Reviews in Molecular Biotechnology* **74**: 105–119.
- Fedic, R., Zurovec, M. *et al.* (2002). 'The silk of lepidoptera'. *Journal of Insect Biotechnology and Sericology* **71**: 1–15.
- Fedic, R., Zurovec, M. *et al.* (2003). 'Correlation between fibroin amino acid sequence and physical silk properties'. *Journal of Biological Chemistry* **278**(37): 35255–35264.
- Finkelstein, A. V. and Ptitsyn, O. B. (2002). *Protein Physics*, London and San Diego, CA, Academic Press.
- Foelix, R. F. (1996). *Biology of Spiders* (2nd edition). New York, Oxford University Press.
- Foo, C. W. P., Bini, E. *et al.* (2006). 'Role of pH and charge on silk protein assembly in insects and spiders'. *Applied Physics A: Materials Science & Processing* **82**(2): 223–233.
- Fornes, R. E., Work, R. W. *et al.* (1983). 'Molecular-orientation of spider silks in the natural and supercontracted states'. *Journal of Polymer Science Part B – Polymer Physics* **21**(7): 1163–1172.
- Fournier, A. (1979). 'Quantitative data on the *Bombyx mori* L. silkworm: a review'. *Biochimie* **61**: 283–320.
- Frische, S., Maunsbach, A. B. *et al.* (1998). 'Elongate cavities and skin-core structure in *Nephila* spider silk observed by electron microscopy'. *Journal of Microscopy–Oxford* **189**: 64–70.
- Gao, H., Ji, B. *et al.* (2003). 'Materials become insensitive to flaws at nanoscale: lessons from nature'. *Proceedings of the National Academy of Sciences* **100**(10): 5597–5600.
- Garb, J. E. and Hayashi, C. Y. (2005). 'Modular evolution of egg case silk genes across orb-weaving spider superfamilies'. *Proceedings of the National Academy of Sciences of the United States of America* **102**(32): 11379–11384.
- Geddes, A. J., Parker, K. D. *et al.* (1968). 'Cross- $\beta$  conformation in proteins'. *Journal of Molecular Biology* **32**(2): 343–344.
- Glatz, L. (1973). 'Der Spinnapparat der Orthognatha (Arachnida, Araneae)'. *Zeitschrift für Morphologie der Tiere* **75**: 1–50.
- Gosline, J. M., DeMont, M. E. *et al.* (1986). 'The structure and properties of spider silk'. *Endeavour* **10**(1): 31–43.
- Gosline, J. M., Guerette, P. A. *et al.* (1999a). 'The mechanical design of spider silks: from fibroin sequence to mechanical function'. *Journal of Experimental Biology* **202**(23): 3295–3303.
- Gosline, J., Guerette, P. *et al.* (1999b). 'Molecular and mechanical design of spider's silks'. *Comparative Biochemistry and Physiology A – Molecular & Integrative Physiology* **124**(suppl): S34.
- Gosline, J., Lillie, M. *et al.* (2002). 'Elastic proteins: biological roles and mechanical properties'. *Philosophical Transactions of the Royal Society of London Series B–Biological Sciences* **357**(1418): 121–132.
- Grubb, D. T. and Jelinski, L. W. (1997). 'Fiber morphology of spider silk: the effects of tensile deformation'. *Macromolecules* **30**(10): 2860–2867.
- Grubb, D. T. and Ji G. D. (1999). 'Molecular chain orientation in supercontracted and re-extended spider silk'. *International Journal of Biological Macromolecules* **24**(2–3): 203–210.



- Grzelak, K. (1995). 'Control of expression of silk protein genes'. *Comparative Biochemistry and Physiology* **110**(4): 671–681.
- Haupt, J. and Kovoov, J. (1993). 'Silk-gland system and silk production in Mesothelae (Araneae)'. *Annales des Sciences Naturelles, Zoologie et Biologie Animale* **14**(2): 35–48.
- Hayashi, C. Y. and Lewis, R. V. (2000). 'Molecular architecture and evolution of a modular spider silk protein gene'. *Science* **287**(5457): 1477–1479.
- Hayashi, C. Y., Shipley, N. H. *et al.* (1999). 'Hypotheses that correlate the sequence, structure, and mechanical properties of spider silk proteins'. *International Journal of Biological Macromolecules* **24**(2–3): 271–275.
- Hayashi, C. Y., Blackledge, T. A. *et al.* (2004). 'Molecular and Mechanical Characterization of Aciniform Silk: Uniformity of iterated sequence modules in a novel member of the spider silk fibroin gene family'. *Molecular Biology and Evolution* **21**(10): 1950–1959.
- Hepburn, H. R., Chandler, H. D. *et al.* (1979). 'Extensometric properties of insect fibroins: the green lacewing cross- $\beta$ , honeybee  $\alpha$ -helical and greater wax-moth parallel- $\beta$  conformations'. *Insect Biochemistry* **9**: 69–77.
- Hinman, M. B., Dong, Z. *et al.* (1992). 'Unusual structural features in spider dragline silk'. *Molecular Biology of the Cell* **3**: A113–A113.
- Holl, A. and Henze M. (1988). 'Spider pigments – their distribution, biochemistry and functions'. *Pigment Cell Research* **1**(4): 293–294.
- Holland, C. A., Terry, A. E. *et al.* (2006). 'Comparing the rheology of native spider and silkworm spinning dope'. *Nature Materials* **5**: 870–874.
- Holland, C., Terry, A. E. *et al.* (2007). 'Natural and unnatural silks'. *Polymer* **48**(12): 3388–3392.
- Hormiga, G., Scharff, N. *et al.* (2000). 'The phylogenetic basis of sexual size dimorphism in orb-weaving spiders (Araneae, Orbiculariae)'. *Systematic Biology* **49**: 435–462.
- Huemmerich, D., Scheibel, T. *et al.* (2004). 'Novel assembly properties of recombinant spider dragline silk proteins'. *Current Biology* **14**(22): 2070–2074.
- Iizuka, E. (1965). 'Degree of crystallinity and modulus relationships of silk thread from cocoons of *Bombyx mori* and other moths'. *Biorheology* **3**: 1–8.
- Iizuka, E. and Yang, J. T. (1966). 'Optical rotatory dispersion and circular dichroism of the beta-form of silk fibroin in solution'. *Proceedings of the National Academy of Sciences of the United States of America* **55**(5): 1175–1182.
- Inoue, S., Tanaka, K. *et al.* (2000a). 'Silk fibroin of *Bombyx mori* is secreted, assembling a high molecular mass elementary unit consisting of H-chain, L-chain, and P25, with a 6:6:1 molar ratio'. *Journal of Biological Chemistry* **275**(51): 40517–40528.
- Inoue, S. I., Magoshi, J. *et al.* (2000b). 'Atomic force microscopy: *Bombyx mori* silk fibroin molecules and their higher order structure'. *Journal of Polymer Science Part B – Polymer Physics* **38**(11): 1436–1439.
- Inoue, S., Kobayashi, M. *et al.* (2001). 'Atomic force microscopy on fibroin molecules and its aggregates'. *Abstracts of Papers of the American Chemical Society* **221**: 261–PMSE.
- Jelinski (1996). 'Molecular orientation and two-component nature of the crystalline fraction of spider dragline silk'. *Science* **271**: 84–87.
- Jelinski, L. W., Blye, A. *et al.* (1999). 'Orientation, structure, wet-spinning, and molecular basis for supercontraction of spider dragline silk'. *International Journal of Biological Macromolecules* **24**(2–3): 197–201.
- Kaplan, D. L. and Lombardi, S. J. (1990a). 'The amino acid composition of major

- ampullate gland silk (dragline) of *Nephila clavipes* (Araneae, Tetragnathidae). *Journal of Arachnology* **18**: 297–306.
- Kaplan, D. L. and Lombardi, S. J. (1990b). 'Isolation, cloning, and physiochemical characterization of spider silk from the golden orb-weaver, *Nephila clavipes*'. *Polymer Preprints* **31**: 195–196.
- Karatzas, C. N., Chretien, N. *et al.* (2005). 'High-toughness spider silk fibers spun from soluble recombinant silk produced in mammalian cells'. In *Biotechnology of Biopolymers; from Synthesis to Patents*, Vol. 2 ed. A. Steinbuchel and Y. Doi, Weinheim, Germany, Wiley-VCH. Vol. 2: 945–965.
- Kim, W. and Conticello, V. P. (2007). 'Protein engineering methods for investigation of structure–function relationships in protein-based elastomeric materials'. *Polymer Reviews* **47**(1): 93–119.
- Knight, D. P. and Vollrath, F. (1999). 'Liquid crystals and flow elongation in a spider's silk production line'. *Proceedings of the Royal Society of London Series B – Biological Sciences* **266**(1418): 519–523.
- Knight, D. P. and Vollrath, F. (2001). 'Changes in element composition along the spinning duct in a *Nephila* spider'. *Naturwissenschaften* **88**(4): 179–182.
- Knight, D. P. and Vollrath, F. (2002a). 'Biological liquid crystal elastomers'. *Philosophical Transactions of the Royal Society of London Series B – Biological Sciences* **357**(1418): 155–163.
- Knight, D. P. and Vollrath, F. (2002b). 'Spinning an elastic ribbon of spider silk'. *Philosophical Transactions of the Royal Society of London Series B – Biological Sciences* **357**(1418): 219–227.
- Knight, D. P., Knight, M. M. *et al.* (2000). 'Beta transition and stress-induced phase separation in the spinning of spider dragline silk'. *International Journal of Biological Macromolecules* **27**(3): 205–210.
- Kohler, T. and Vollrath, F. (1995). 'Thread biomechanics in the 2 orb-weaving spiders *araneus diadematus* (Araneae, Araneidae) and *Uloborus walckenaerius* (Araneae, Uloboridae)'. *Journal of Experimental Zoology* **271**(1): 1–17.
- Kovoor, J. (1987). 'Comparative structure and histochemistry of silk-producing organs in Arachnids'. In *Ecophysiology of Spiders*, ed. W. Nentwig, Berlin-Heidelberg-New York, Springer: 160–186.
- Kovoor, J. (1990). 'The silk-gland system in some Tetragnathinae (Araneae: Araneidae): comparative anatomy and histochemistry'. *Acta Zoologica Fennica* **190**: 215–222.
- Kratky, O. (1956). 'An X-ray investigation of silk fibroin'. *Transactions of the American Microscopical Society* **52**: 558–570.
- Kummerlen, J., van Beek, J. D. *et al.* (1996). 'Local structure in spider dragline silk investigated by two-dimensional spin-diffusion nuclear magnetic resonance'. *Macromolecules* **29**(8): 2920–2928.
- Lazaris, A., Arcidiacono, S. *et al.* (2002). 'Spider silk fibers spun from soluble recombinant silk produced in mammalian cells'. *Science* **295**(5554): 472–476.
- Lee, Y.-W. (1999). 'Silk reeling and testing manual'. FAO Agricultural Services bulletin no. 136, from <http://www.fao.org/docrep/x2099E/x2099e00.htm#con>.
- Li, S. F. Y., McGhie, A. J. *et al.* (1994). 'Comparative study of the internal structures of kevlar and spider silk by atomic-force microscopy'. *Journal of Vacuum Science & Technology A – Vacuum Surfaces and Films* **12**(4): 1891–1894.
- Liu, Y., Shao, Z. Z. *et al.* (2005a). 'Extended wet-spinning can modify spider silk properties'. *Chemical Communications* **19**: 2489–2491.
- Liu, Y., Shao, Z. Z. *et al.* (2005b). 'Relationships between supercontraction and mechanical properties of spider silk'. *Nature Materials* **4**(12): 901–905.

- Liu, Y., Sponner, A. *et al.* (2008). 'Proline and processing of spider silks'. *Biomacromolecules* **9**(1): 116–121.
- Lucas, F., Shaw, J. T. B. *et al.* (1960). 'Comparative studies of fibroins. I. The amino acid composition of various fibroins and its significance in relation to their crystal structure and taxonomy'. *Journal of Molecular Evolution* **2**: 339–349.
- Madsen, B. and Vollrath, F. (2000). 'Mechanics and morphology of silk drawn from anesthetized spiders'. *Naturwissenschaften* **87**(3): 148–153.
- Madsen, B., Shao, Z. Z. *et al.* (1999). 'Variability in the mechanical properties of spider silks on three levels: interspecific, intraspecific and intraindividual'. *International Journal of Biological Macromolecules* **24**(2–3): 301–306.
- Marsh, R. E., Corey, R. B. *et al.* (1955). 'An investigation of the structure of silk fibroin'. *Biochimica et Biophysica Acta* **16**: 1–34.
- Mayes, E. L., Vollrath, F. *et al.* (1998). 'Fabrication of magnetic spider silk and other silk-fiber composites using inorganic nanoparticles'. *Advanced Materials* **10**(10): 801–805.
- Meinel, L., Hofmann, S. *et al.* (2005). 'The inflammatory responses to silk films *in vitro* and *in vivo*'. *Biomaterials* **26**(2): 147–155.
- Michaille, J., Couble, P. *et al.* (1986). 'A single gene produces multiple sericin messenger-RNAs in the silk gland of *Bombyx mori*'. *Biochimie* **68**(10–1): 1165–1173.
- Michal, C. A. and Jelinski, L. W. (1998). 'Rotational-echo double-resonance in complex biopolymers: A study of *Nephila clavipes* dragline silk'. *Journal of Biomolecular NMR* **12**(2): 231–241.
- O'Brien, J. P., Fahnestock, S. R. *et al.* (1998). 'Nylons from nature: Synthetic analogs to spider silk'. *Advanced Materials* **10**(15): 1185–1195.
- Opell, B. D. (1993). 'What forces are responsible for the stickiness of spider cribellar threads?'. *Journal of Experimental Zoology* **265**(5): 469–476.
- Opell, B. D. (1995). 'Do static electric forces contribute to the stickiness of a spider's cribellar prey capture threads?'. *Journal of Experimental Zoology* **273**(3): 186–189.
- Opell, B. D. (1997). 'A comparison of capture thread and architectural features of deinopoid and araneoid orb-webs'. *Journal of Arachnology* **25**(3): 295–306.
- Papadopoulos, P., Sölter, J. *et al.* (2007). 'Structure–property relationships in major ampullate spider silk as deduced from polarized FTIR spectroscopy'. *European Physical Journal E – Soft Matter* **24**(2): 193–199.
- Pauling, L., Corey, R. B. *et al.* (1951). 'The structure of proteins: Two hydrogen-bonded helical configurations of the polypeptide chain'. *Proceedings of the National Academy of Sciences* **37**: 205–211.
- Perez-Riguero, J., Elices, M. *et al.* (2001). 'Tensile properties of *Argiope trifasciata* drag line silk obtained from the spider's web'. *Journal of Applied Polymer Science* **82**(9): 2245–2251.
- Porter, D. (2002). 'Modelling of structural materials'. *International Materials Reviews* **47**(5): 1–9.
- Porter, D. and Vollrath, F. (2008). 'The role of kinetics of water and amide bonding in protein stability'. *Soft Matter* **4**(2): 328–336.
- Porter, D., Vollrath, F. *et al.* (2005). 'Predicting the mechanical properties of spider silk as a model nanostructured polymer'. *European Physical Journal E* **16**(2): 199–206.
- Putthanarat, S., Stribeck, N. *et al.* (2000). 'Investigation of the nanofibrils of silk fibers'. *Polymer* **41**(21): 7735–7747.
- Rauscher, S., Baud, S. *et al.* (2006). 'Proline and glycine control protein self-organization into elastomeric or amyloid fibrils'. *Structure* **14**(11): 1667–1676.

- Riekkel, C., Branden, C. *et al.* (1999). 'Aspects of X-ray diffraction on single spider fibers'. *International Journal of Biological Macromolecules* **24**(2–3): 179–186.
- Riekkel, C., Madsen, B. *et al.* (2000). 'X-ray diffraction on spider silk during controlled extrusion under a synchrotron radiation X-ray beam'. *Biomacromolecules* **1**(4): 622–626.
- Riekkel, C., Rossle, M. *et al.* (2004). 'Influence of CO<sub>2</sub> on the micro-structural properties of spider dragline silk: X-ray microdiffraction results'. *Naturwissenschaften* **91**(1): 30–33.
- Rousseau, M. E., Lefevre, T. *et al.* (2004). 'Study of protein conformation and orientation in silkworm and spider silk fibers using Raman microspectroscopy'. *Biomacromolecules* **5**(6): 2247–2257.
- Rudall, K. and Kenchington, W. (1971). 'Arthropod silks: the problem of fibrous proteins in animal tissues'. *Annual Reviews of Entomology* **16**: 73–97.
- Sapede, D., Seydel, T. *et al.* (2005). 'Nanofibrillar structure and molecular mobility in spider dragline silk'. *Macromolecules* **38**(20): 8447–8453.
- Savage, K. N., Guerette, P. A. *et al.* (2004). 'Supercontraction stress in spider webs'. *Biomacromolecules* **5**(3): 675–679.
- Scheller, J., Gührs, K.-H. *et al.* (2001). 'Production of spider silk proteins in tobacco and potato'. *Nature Biotechnology* **19**: 573–577.
- Schultz, J. W. (1987). 'The origin of the spinning apparatus in spiders'. *Biological Review* **62**: 89–113.
- Schulz, S. (2001). 'Composition of the silk lipids of the spider *Nephila clavipes*'. *Lipids* **36**(6): 637–647.
- Sehnal, F. and Akai, H. (1990). 'Insect silk glands: their types, development and function, and effects of environmental factors and morphogenetic hormones on them'. *International Journal of Insect Morphology and Embryology* **19**(2): 79–132.
- Serrano, L., Neira, J. L. *et al.* (1992). 'Effect of alanine versus glycine in alpha-helices on protein stability'. *Nature* **356**(6368): 453–455.
- Sezutsu, H. and Yukuhiro, K. (2000). 'Dynamic rearrangement within the antheraea pernyi silk fibroin gene is associated with four types of repetitive units'. *Journal of Molecular Evolution* **51**(4): 329–338.
- Shao, Z. Z. and Vollrath, F. (1999). 'The effect of solvents on the contraction and mechanical properties of spider silk'. *Polymer* **40**(7): 1799–1806.
- Shao, Z. Z. and Vollrath, F. (2002). 'Materials: surprising strength of silkworm silk'. *Nature* **418**(6899): 741.
- Shao, Z. Z., Young, R. J. *et al.* (1999). 'The effect of solvents on spider silk studied by mechanical testing and single-fibre Raman spectroscopy'. *International Journal of Biological Macromolecules* **24**(2–3): 295–300.
- Shen, Y., Johnson, M. A. *et al.* (1998). 'Microstructural characterization of *Bombyx mori* silk fibers'. *Macromolecules* **31**(25): 8857–8864.
- Simmons, A. H., Michal, C. A. *et al.* (1996). 'Molecular orientation and two-component nature of the crystalline fraction of spider dragline silk'. *Science* **271**(5245): 84–87.
- Sirichaisit, J., Brookes, V. L. *et al.* (2003). 'Analysis of structure/property relationships in silkworm (*Bombyx mori*) and spider dragline (*Nephila edulis*) silks using Raman spectroscopy'. *Biomacromolecules* **4**(2): 387–394.
- Sponner, A., Unger, E. *et al.* (2005). 'Differential polymerization of the two main protein components of dragline silk during fibre spinning'. *Nature Materials* **4**(10): 772–775.
- Sprague, K. U. R., Mark B. *et al.* (1979). 'Alleles of the fibroin gene coding for proteins of different length'. *Cell* **17**: 407–413.

- Sutherland, T. D., Campbell, T. M. *et al.* (2006). 'A highly divergent gene duster in honey bees encodes a novel silk' *Genome Res.* 1414–1421.
- Swanson, B. O., Hayashi, C. Y. *et al.* (2006). 'Variation in the material properties of spider dragline silk across species'. *Applied Physics A: Materials Science and Processing* **82**(2): 213–218.
- Termonia, Y. (1994). 'Molecular modeling of spider silk elasticity'. *Macromolecules* **27**(25): 7378–7381.
- Thiel, B. L., Kunkel, D. D. *et al.* (1994). 'Physical and chemical microstructure of spider dragline – a study by analytical transmission electron-microscopy'. *Biopolymers* **34**(8): 1089–1097.
- Thiel, B. L., Kunkel, D. *et al.* (1995). 'Physical and chemical microstructure of spider dragline: A study by analytical transmission electron microscopy'. *Biopolymers* **34**(8): 1089–1097.
- Tian, M. and Lewis, R. V. (2005). 'Molecular characterization and evolutionary study of spider tubuliform (eggcase) silk protein'. *Biochemistry* **44**(22): 8006–8012.
- Tsukada, M., Gotoh, Y. *et al.* (1994). 'Structural-changes of silk fibroin membranes induced by immersion in methanol aqueous-solutions'. *Journal of Polymer Science Part B-Polymer Physics* **32**(5): 961–968.
- Urs, R. G. K., Subramanya, G. *et al.* (1993). 'Crystal size and minimum enthalpy of various races of silk fibers'. *Textile Research Journal* **63**(10): 610–613.
- Uversky, V. N. (2003). 'Protein folding revisited. A polypeptide chain at the folding–misfolding–nonfolding cross-roads: which way to go?'. *Cellular and Molecular Life Sciences* **60**(9): 1852–1871.
- van Beek, J. D., Kummerlen, J. *et al.* (1999). 'Supercontracted spider dragline silk: a solid-state NMR study of the local structure.' *International Journal of Biological Macromolecules* **24**(2–3): 173–178.
- van Beek, J. D., Beaulieu, L. *et al.* (2000). 'Solid-state NMR determination of the secondary structure of *Samia cynthia ricini* silk'. *Nature* **405**(6790): 1077–1079.
- van Beek, J. D., Hess, S. *et al.* (2002). 'The molecular structure of spider dragline silk: Folding and orientation of the protein backbone'. *Proceedings of the National Academy of Sciences of the USA* **99**(16): 10266–10271.
- Viney, C., Huber, A. E. *et al.* (1994). Optical characterization of silk secretions and fibers. *Silk Polymers: Materials Science and Biotechnology* **544**: 120–136.
- Vollrath, F. (1999). 'Biology of spider silk.' *International Journal of Biological Macromolecules* **24**(2–3): 81–88.
- Vollrath, F. (2000a). 'Coevolution of behaviour and material in the spider's web'. In *Biomechanics in Animal Behaviour*, ed. P. Domenici. Oxford, UK, Bios.
- Vollrath, F. (2000b). 'Strength and structure of spiders' silks'. *Reviews in Molecular Biotechnology* **74**: 67–83.
- Vollrath, F. and Edmonds, D. T. (1992). 'The contribution of atmospheric water vapour to the formation and efficiency of a spider's capture web'. *Proceedings of the Royal Society of London* **248**: 145–148.
- Vollrath, F. and Knight, D. P. (1999). 'Structure and function of the silk production pathway in the spider *Nephila edulis*'. *International Journal of Biological Macromolecules* **24**(2–3): 243–249.
- Vollrath, F. and Knight, D. P. (2001). 'Liquid crystalline spinning of spider silk'. *Nature* **410**(6828): 541–548.
- Vollrath, F. and Knight, D. (2004). 'Biology and technology of silk production'. In *Biotechnology of Biopolymers: from Synthesis to Patents*, Vol. 2, ed. A. Steinbuechel and Y. Doi. Weinheim, Germany, Wiley-VCH. Vol. 2, 873–894.

- Vollrath, F. and Porter, D. (2006a). 'Spider silk as a model biomaterial'. *Applied Physics A: Materials Science & Processing* **82**(2): 205–212.
- Vollrath, F. and Porter, D. (2006b). 'Spider silk as an archetypal protein elastomer'. *Soft Matter* **2**: 377–385.
- Vollrath, F. and Selden, P. (2007). 'The role of behavior in the evolution of spiders, silks, and webs'. *Annual Review of Ecology, Evolution, and Systematics* **38**(1): 819–846.
- Vollrath, F. and Tillinghast, E. K. (1991). 'Glycoprotein glue beneath a spider web's aqueous coat'. *Naturwissenschaften* **78**(12): 557–559.
- Sutherland, T. D., Campbell, T. M. *et al.* (2006). 'A highly divergent gene duster in honey bees encodes a novel silk'. *Genome Res.* 1414–1421.
- Vollrath, F., Fairbrother, W. J. *et al.* (1990). 'Compounds in the droplets of the orb spider's viscid spiral'. *Nature* **345**(6275): 526–528.
- Vollrath, F., Holtet, T. *et al.* (1996). 'Structural organization of spider silk'. *Proceedings of the Royal Society of London Series B – Biological Sciences* **263**(1367): 147–151.
- Vollrath, F., Madsen, B. *et al.* (2001). 'The effect of spinning conditions on the mechanics of a spider's dragline silk'. *Proceedings of the Royal Society of London Series B – Biological Sciences* **268**(1483): 2339–2346.
- Vollrath, F., Barth, P. *et al.* (2002). 'Local tolerance to spider silks and protein polymers *in vivo*'. *In Vivo* **16**(4): 229–234.
- Warwicker, J. O. (1954). 'The crystal structure of silk fibroin'. *Acta Crystallographica* **7**: 565–573.
- Work, R. W. (1977a). 'Dimensions, birefringences and force–elongation behaviour of major and minor ampullate silk fibres from orb web spinning spiders – The effects of wetting on these properties'. *Textile Research Journal* **47**: 650–662.
- Work, R. W. (1977b). 'Mechanisms of major ampullate silk fibre formation by orb-web spinning spiders'. *Transactions of the American Microscopical Society* **96**: 170–189.
- Work, R. W. (1985). 'Viscoelastic behavior and wet supercontraction of major ampullate silk fibers of certain orb-web-building spiders (Araneae)'. *Journal of Experimental Biology* **118**: 379–404.
- Wu, G., Jiang, J. D. *et al.* (1996). 'Oriented noncrystalline structure in PET fibers prepared with threadline modification process'. *Journal of Polymer Science Part B – Polymer Physics* **34**(12): 2035–2047.
- Wynne, A. (1997). *Textiles* Oxford, Macmillan Education, Oxford, UK.
- Yamada, H., Nakao, H. *et al.* (2001). 'Preparation of undegraded native molecular fibroin solution from silkworm cocoons'. *Materials Science & Engineering C – Biomimetic Materials Sensors and Systems* **14**(1–2): 41–46.
- Yang, A. S. and Honig, B. (1995a). 'Free energy determinants of secondary structure formation: I. Alpha-helices'. *Journal of Molecular Biology* **252**(3): 351–365.
- Yang, A. S. and Honig, B. (1995b). 'Free energy determinants of secondary structure formation: II. Antiparallel beta-sheets'. *Journal of Molecular Biology* **252**(3): 366–376.
- Yang, A. S., Hitz, B. *et al.* (1996). 'Free energy determinants of secondary structure formation: III. Beta-turns and their role in protein folding'. *Journal of Molecular Biology* **259**(4): 873–882.
- Yang, Y., Chen, X. *et al.* (2005). 'Toughness of spider silk at high and low temperatures'. *Advanced Materials* **17**(1): 84–88.
- Yao, J. M., Nakazawa, Y. *et al.* (2004). 'Structures of *Bombyx mori* and *Samia cynthia ricini* silk fibroins studied with solid-state NMR'. *Biomacromolecules* **5**: 680–688.

- Zhou, H. and Zhang, Y. (2005). 'Hierarchical chain model of spider capture silk elasticity'. *Physical Review Letters* **94**(2): 028104-4.
- Zhou, C.-Z., Confalonieri, F. *et al.* (2000). 'Fine organization of *Bombyx mori* fibroin heavy chain gene'. *Nucleic Acids Research* **28**(12): 2413–2419.
- Zurovec, M. and Sehnal, F. (2002). 'Unique molecular architecture of silk fibroin in the waxmoth, *Galleria mellonella*'. *Journal of Biological Chemistry* **277**(25): 22639–22647.



## The structure of man-made cellulosic fibres

J GANSTER and H-P FINK, Fraunhofer-Institute for  
Applied Polymer Research, Germany

**Abstract:** After a short introduction to cellulose fibre spinning methods, general aspects of cellulose man-made fibre structure at various levels of molecular organisation are outlined. In subsequent sections, the fibre structures of viscose, Lyocell and cellulose acetate fibres are studied in more detail. The main body of data given is obtained from scanning and transmission electron microscopy, wide and small angle X-ray scattering, and birefringence. Some market figures are provided for the most important fibre types. New developments are covered in a short final section.

**Key words:** cellulose man-made fibre, viscose, Lyocell, fibre structure, cellulose acetate.

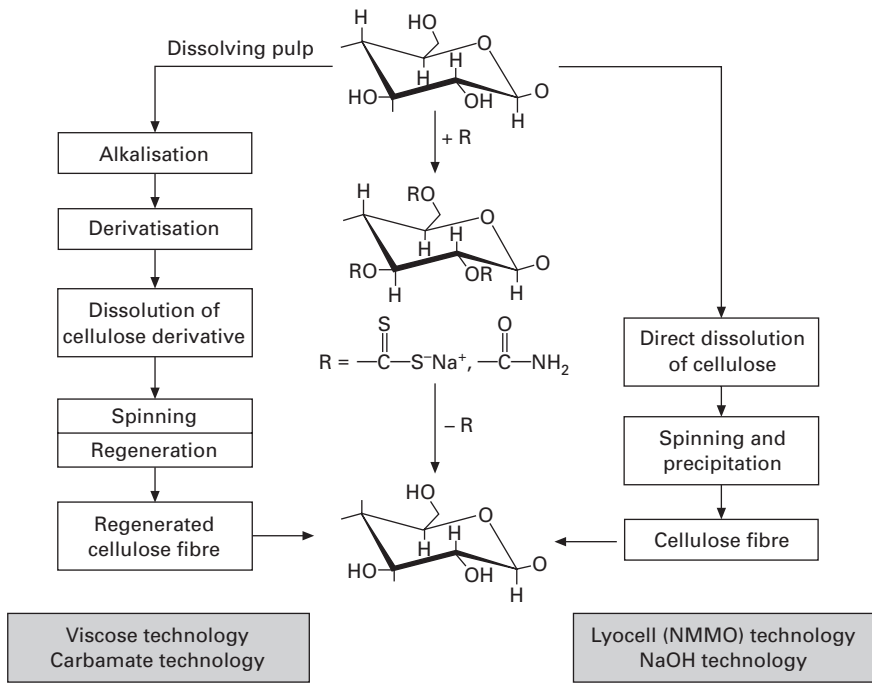
### 6.1 Introduction and spinning methods

Cellulose is the most abundantly biosynthesized polymer in nature, reaching production rates of about  $1.5 \times 10^{12}$  tons per year (Klemm *et al.* 2005). In combination with lignin and hemicelluloses it serves as the structural component in the cell wall of annual plants and trees, providing stiffness and strength. In particular pure form and high crystallinity, cellulose is synthesised by certain bacteria (e.g. *Acetobacter xylinus*) and occurs in certain algae as well (e.g. *Valonia ventricosa*).

For processing of cellulose, wood pulp is the most important material source which is mainly used for the production of paper and cardboard. A minor part, roughly 2%, corresponding to about 3 million tons per year of special-grade pulp with cellulose content higher than 93%, so-called dissolving pulp, goes into the production of fibres, films and cellulose esters and ethers. For the shaping of cellulose in general and for fibre production in particular, special methods have to be employed, since cellulose with its extended hydrogen bond network (see Section 6.2) is neither meltable nor soluble in the common organic solvents, let alone water. A detailed account of regenerated (spun) cellulose fibres is given in the book edited by Woodings (2001a).

For fibre production, two major processing principles are industrially implemented nowadays (Fig. 6.1): derivative methods and direct methods. In the former a cellulose derivative is produced after activation of cellulose,





6.1 Processing principles for cellulose fibre spinning. Left: derivative methods; right: direct methods.

dissolved and spun into a coagulation bath where the pure cellulose is regenerated. In the latter special solvent systems are employed without chemical alteration of the cellulose chains.

### 6.1.1 Derivative methods

Being more than 100 years old, the viscose process (Götze 1967) is still dominating in cellulose fibre production with an annual output of more than 2 million tons. For this wet-spinning process cellulose xanthogenate is produced by adding liquid carbon disulfide to pressed alkali pre-treated cellulose. This derivative is soluble in alkali and forms the so-called viscose, a viscous liquid resembling honey in both colour and consistency. After a certain period of ripening, the viscose is spun into an acidic coagulation bath where the xanthate groups are cleaved off the polymeric chains and the pure cellulose is regenerated in fibre form, called rayon, viscose rayon or viscose fibre. Depending on how the actual process is conducted, fibre qualities range from textile (filament and staple) to technical grades (rayon tyre cord yarn).

Another derivative method using urea instead of carbon disulfide has

IP Address: 129.132.211.108

been developed to commercial maturity, the CarbaCell process (Voges *et al.* 2000). Environmental benefits in avoiding carbon disulfide altogether are combined with the perpetuation of the viscose wet-spinning technology.

The manufacture of cellulose acetate fibres (e.g. Rustemeyer 2004) can be subsumed under the derivative methods, although acetate production and fibre spinning are separate industrial processes in this case. Cellulose acetate (CA) is produced by acetylation with acetic acid and acetic anhydride with sulfuric acid as catalyst. Cellulose triacetate (CTA) is obtained, which is partly saponified to get the desired degree of substitution (DS) of 2.4 to 2.5. Fibres are spun from CA for textile applications and filter tow (cigarette filters) from acetone in a dry-spinning process. A special type of highly oriented pure cellulose fibre, called Fortisan, was produced by steam drawing of CA fibres with subsequent saponification with caustic soda or sodium acetate (Sprague and Noether 1961).

### 6.1.2 Direct methods

Although cellulose is not soluble in the common organic solvents, a series of special solvents has been discovered in the long history of cellulose research (see Heinze and Liebert 1998, and Ganster and Fink 1999 for an overview). Only some of them have been used to spin cellulose fibres via a direct method.

The most important direct method that is industrially utilised is the NMMO or Lyocell process (see, e.g., Coulsey and Smith 1996, Fink *et al.* 2001), where an *N*-methylmorpholine-*N*-oxide/water mixture (Chanzy *et al.* 1979) is used at elevated temperatures as the solvent. Fibre spinning from the cellulose–NMMO–water system is performed via a dry-jet/wet-spinning process with an air gap between nozzle and aqueous precipitation bath. Remarkably, the shaping of the dope in the nozzle and the air gap can be considered like a melt-spinning process (Liu *et al.* 2001), hence, appropriate procedures like film-blowing and melt-blown non-wovens technologies were developed on the basis of the Lyocell process (Fink *et al.* 2001, Ebeling *et al.* 2006).

Other direct methods developed are the copper ammonia technology (cupro silk, see, e.g., Nishiyama 1997) still in production, the Celsol process (Vehviläinen and Nousiainen 1997) with sodium hydroxide and the use of DMAc/LiCl (Bianchi *et al.* 1989) as well as phosphoric acid (Boerstoel *et al.* 2001) as solvents.

More recently, ionic liquids as solvents for cellulose have been investigated (Laus *et al.* 2005, Hermanutz *et al.* 2008, Kosan *et al.* 2008). Results are promising, first of all with the prospect of higher concentrations in the spinning dope (almost 20% reported in Kosan *et al.* 2008).

## 6.2 Structural levels and general models

### 6.2.1 Single chain

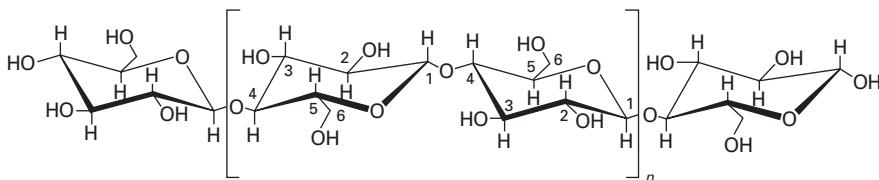
On the very basic, i.e. the configurational, level of covalent bonds, cellulose is a linear polysaccharide consisting of anhydroglucose units (AGUs) in the the  ${}^4C_1$  chair conformation linked through  $\beta(1 \rightarrow 4)$  glycosidic bonds such that, in contrast to amylose in starch which is  $\alpha(1 \rightarrow 4)$  linked, a rather straight chain conformation is easily generated (see Fig. 6.2). The number of AGUs constituting a chain is called the degree of polymerisation (DP). In wood pulps, typical values range from 300 to 1700 (Klemm *et al.* 2005), while viscose fibres have DPs in the range from 300 to 500 and NMMO fibres above that, a typical value being 600 (Fink *et al.* 2001).

Going from the single chain to the bulk solid state, cellulose turns out to be a partially crystalline polymer (see below). This holds true both for naturally occurring and for man-made (spun), i.e. regenerated, cellulose. However, at this structural level, where the chain conformations in conjunction with inter-chain interactions play the decisive role, marked differences between native and processed cellulose crystal structures are found.

### 6.2.2 Crystal structures – cellulose

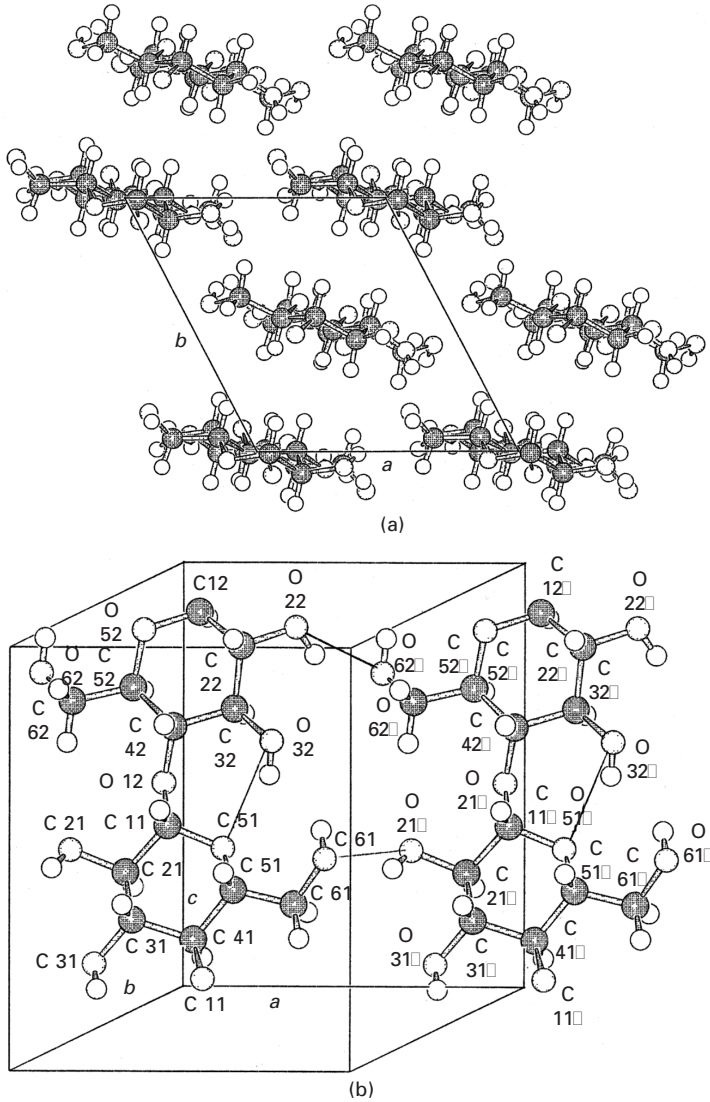
As is widely accepted nowadays, biosynthesised cellulose crystallises either in the triclinic  $I_\alpha$  form or in the monoclinic space group  $P2_1$ , the  $I_\beta$  form (see Zugenmaier 2008 for a detailed discussion and an outline of the historical development of X-ray models for native cellulose). The standard crystalline polymorph for both mercerised (alkali treated) and regenerated (spun) cellulose is called cellulose II, a monoclinic form of space group  $P2_1$  which is remarkably different from native cellulose crystals (see below).

Classical models of cellulose II date back to 1929, where Andress investigated the X-ray diagram of mercerised cellulose and determined the unit cell dimensions (Andress, 1929). Later, Kolpak and Blackwell (1976) and Stipanovic and Sarko (1976) used X-ray scattering and model calculations to determine the non-hydrogen atomic positions in the unit cell. More recently, those models were refined by Langan *et al.* (1999, 2001, 2005) with neutron and high-resolution synchrotron X-ray scattering. In contrast to the 1976

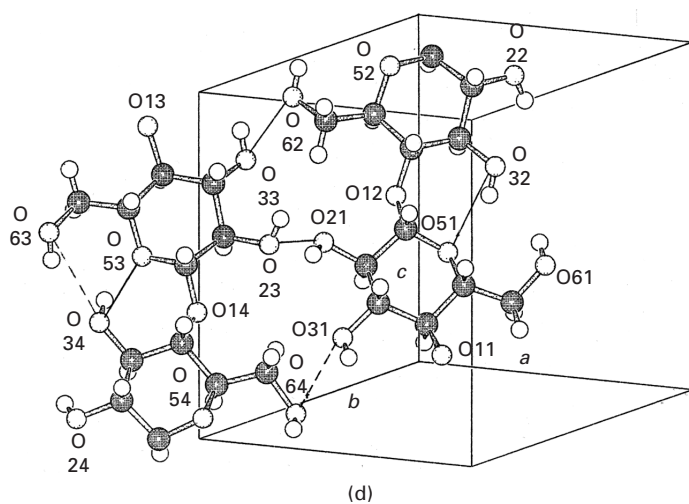
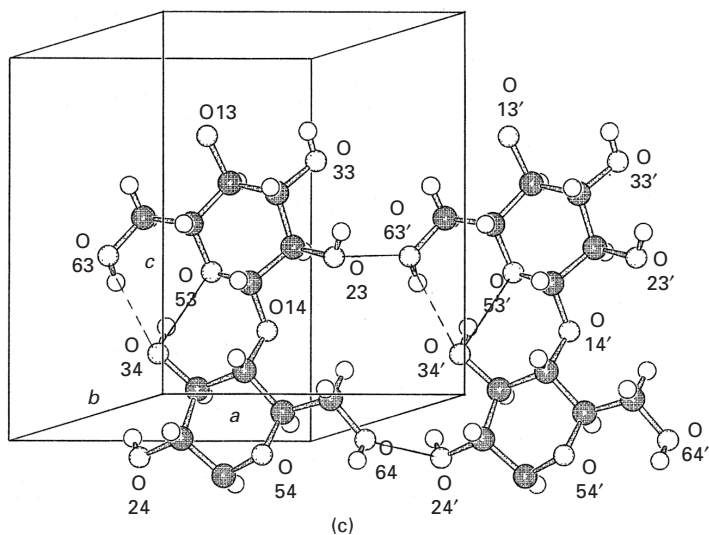


6.2 Chemical structure of cellulose chain with atom numbering.

models, the authors propose a different hydrogen bonding scheme and report, for the first time, a complete set of atomic coordinates including hydrogen atoms (Langan *et al.* 1999). In Fig. 6.3, the crystal structure according to Langan *et al.* (2001) is depicted by a projection onto the  $a$ - $b$  plane which is perpendicular to the chain axes (Fig. 6.3a) and three drawings show the



6.3 Crystal structure of cellulose II (Langan *et al.* 2001) reproduced from Zugenmaier (2008): (a) projection onto the  $a$ - $b$  plane; (b) (010) sheet through the origin; (c) (010) sheet through the centre; (d) (110) sheet.



## 6.3 Cont'd

molecules in the (010) sheet through the origin (Fig. 6.3b), the centre (c), and in the (110) sheet (d) of the unit cell as visualised by Zugenmaier (2001). A well-developed hydrogen bond system with both intra and inter-chain bonds is seen, as indicated by the narrow lines drawn between one oxygen and the other oxygen hosting the hydrogen in question.

One of the most striking differences of this crystal structure from native cellulose crystals is the chain orientation. While in cellulose  $I_\alpha$  or  $I_\beta$  all the chains have the same parallel direction, corner (origin) and centre chains in the cellulose II unit cell have anti-parallel directions, i.e. point in or out of

the paper plane in Fig. 6.3a. In Fig. 6.3b, both chains point downwards, if one counts the direction from C1 to C4, while in Fig. 6.3c the direction is upwards, and it is mixed in Fig. 6.3d. This poses some difficulties in explaining the solid state phase transition after swelling by alkali from native cellulose to cellulose II such that an inter-diffusion model was proposed between cellulose chains from adjacent native cellulose crystallites of opposite orientation (Okano and Sarko 1985). An alternative model based on a non-uniform fringed fibrillar morphology in connection with a conformation transition from bent to bent and twisted single chain conformations has been proposed by Hayashi *et al.* (see model discussions in Fink and Philipp (1985)).

Other cellulose polymorphs (III and IV) are described in the literature (see Zugenmaier 2008 and references therein) but are rarely encountered in practice since they are formed only after special treatment (dry liquid ammonia and heat treatment at 260°C, respectively).

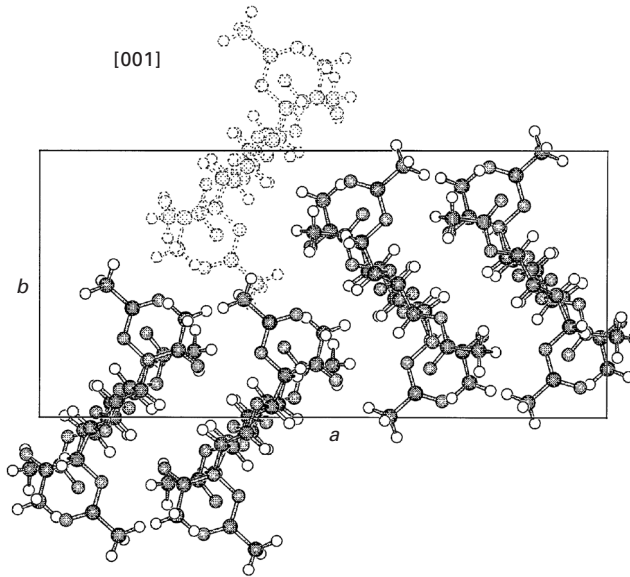
### 6.2.3 Crystal structures – cellulose acetate

Cellulose acetate crystallises best when all hydroxyl groups at positions 2, 3 and 6 (Fig. 6.2) are substituted by acetyl (COCH<sub>3</sub>) groups, i.e. when the degree of substitution (DS) is 3 (44.8% acetyl content). The derivative is then called cellulose triacetate (CTA) or primary CA. There are two crystalline polymorphs, CTA I originating from native cellulose, and CTA II obtained from cellulose II or by complete dissolution of native cellulose I. Again, an anti-parallel chain arrangement is observed for the CTA II crystal structure. Starting from a CTA II crystal structure proposed by Roche *et al.* (1978), Zugenmaier (2008) published the atomic coordinates of a refined orthorhombic model also having the space group  $P2_12_12_1$ . The  $a$ - $b$  projection of this model perpendicular to the chain direction is shown in Fig. 6.4. The two parallel chains on the  $a$ -axis are transformed by the symmetry operations to their anti-parallel counterparts shown on the right side of the unit cell. Hydrogen bonds are no longer formed since all hydroxyl groups are substituted by acetyl moieties and CTA is thermoplastic with a melting temperature of 307°C (Zugenmaier 2004).

Fibres are spun from partially saponified CTA called secondary or two and a half acetate having a DS of around 2.5 (acetyl content around 40%) and a random substituent distribution. Crystallisation is hampered due to the molecular irregularity such that no particular crystal structures have to be determined.

### 6.2.4 Partially crystalline structure

In general, man-made cellulosic fibres are considered partially crystalline with various degrees of crystallinity, crystallite dimensions and appreciable



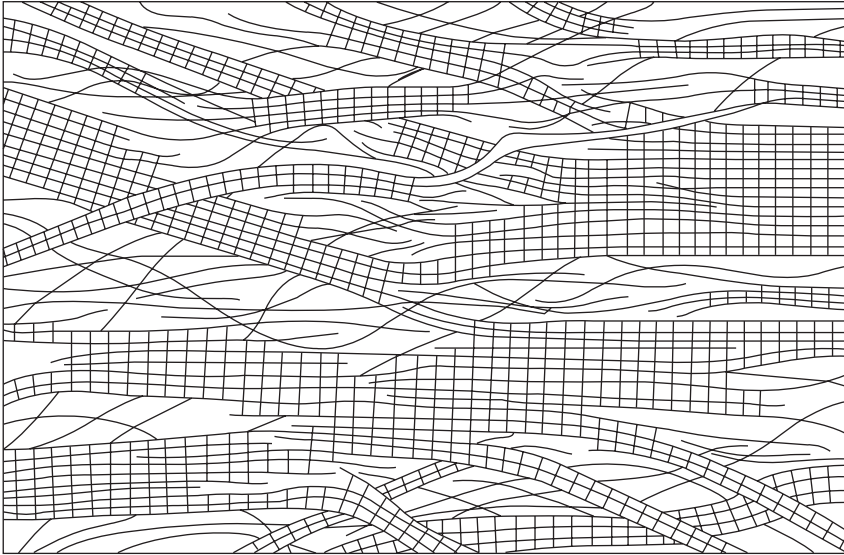
6.4 Crystal structure of cellulose triacetate according to Zugenmaier (2008), projection onto the  $a$ - $b$  plane (with kind permission of Springer Science and Business Media).

non-crystalline fractions. In contrast to many synthetic polymers, a spherulitic morphology is not observed.

A detailed theoretical approach to fibre properties, taking into account the morphological features of partial crystallinity with its application to selected cellulose spun fibres has been provided by Hearle (Hearle 2001). Three basic morphologies are defined: a lamellar structure with crystallites extending in the lateral direction forming lamellae perpendicular to the fibre direction, a micellar structure with broken-up lamellae and somewhat increased dimensions in the fibre direction, and a fibrillar structure with elongated crystallites in the fibre direction. In all cases, chain axes are more or less parallel to the fibre axis. The third type, in connection with fringe molecules connecting the crystallites, seems to be the most appropriate model for the morphological structure of most cellulose spun fibres (Hearle 1958, Schurz 1980, Fink and Walenta 1994) and is called the fringed fibrillar model as visualised in Fig. 6.5. However, there is a continuous transition between the fibrillar and micellar morphologies with decreasing fibril length such that viscose in contrast to modal fibres tend to have a micellar character (Hearle 1967).

In the following, crystallinities, crystallite dimensions and molecular orientations are discussed, which will further elucidate the given model concepts.





6.5 Fringed fibrillar model of cellulose according to Fink and Walenta (1994).

### 6.3 Rayon (viscose)-type fibres

Worldwide, the majority of viscose fibres are produced as staple fibre for textile and non-woven applications. In 2006 the world production was 2.168 million tons (Koslowski 2008). Filament yarns from the viscose process for textile and technical applications reached 363 000 tons in 2006 (Koslowski 2008) with an estimated share of technical yarns of 20% (based on data for 2005: Chemical Fibers International 2006).

Owing to the versatility of the viscose process, the products range from textile fibres with typical tenacities of around 25 cN/tex (375 MPa; see, e.g., Adusumalli *et al.* 2006) over technical yarns with 55 cN/tex or 825 MPa (rayon tyre cord yarn, e.g. Ganster *et al.* 2008) to specialities with extremely high moduli (2100 cN/tex (31.5 GPa), Cordenka EHM, e.g. Eichhorn *et al.* 2001) which are, however, no longer produced. Modal and polynosic, which figure in Table 6.1, are special viscose fibres with high wet modulus (HWM). Despite this broad property range, which is mainly due to changes in molecular orientation, a set of morphological features typical for viscose fibres can be highlighted.

#### 6.3.1 Cross-section, morphology and pore structure

Cross-sectional morphology is determined here and in what follows by transmission electron microscopy (TEM) with a Philips TEM CM 200 at



Table 6.1 Mechanical properties and X-ray crystallinities (WAXS- $x_c$ ) of various cellulose spun fibres (data extracted from Röder *et al.* 2006)

Sample no.	Titre (dtex)	Tenacity (cN/tex)	(MPa)	Elongation (%)	WAXS- $x_c$ (%)	Fibre type		
3	1.03	42.6	640	11.4	40	Lyocell	Filament	Exp.
8	1.30	24.0	360	6.0	47	Lyocell	Staple	Exp.
9	1.30	36.0	540	13.0	44	Lyocell	Staple	Comm.
12	1.32	42.8	640	15.5	27	Modal	Staple	Comm.
15	1.43	27.3	410	13.7	25	Polynosic	Staple	Comm.
17	1.50	23.4	350	17.4	26	Viscose	Staple	Comm.
19	1.36	29.1	435	15.8	30	Viscose	Staple	Comm.
23	1.89	52.3	785	15.1	24	Viscose	Filament	Comm.
26	2.52	22.3	335	24.3	29	Cupro	Filament	Comm.
27	3.32	17.0	255	7.8	38	Celsol	Filament	Exp.
28	2.85	19.8	300	7.7	46	Carbamate	Filament	Exp.
29	0.68	23.9	360	3.2	47	Fortisan	Filament	Exp.

Shaded area represents data for fibres spun by the viscose process although not all the fibres are called viscose.

120 kV from ultra-thin cross-sections (approx. 60 nm) prepared with an ultra-microtome Leica Ultracut S after initial embedding in a polymethyl methacrylate matrix (Purz and Schulz 1979).

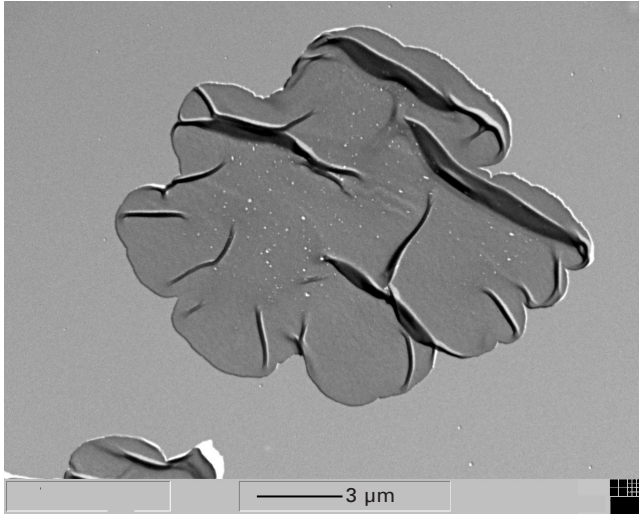
A typical cross-section for a viscose fibre spun in our laboratory is shown in Fig. 6.6a. Clearly seen is the lobular outer shape of the viscose fibre and the core–skin morphology with a porous and less dense core section and a well-developed and dense skin region of 1 to 2  $\mu\text{m}$  thickness. In Figs 6.6b and c, the inner and outer regions, respectively, of the fibre from Fig. 6.6a are shown with higher magnification. In contrast to the skin region, voids are present in the core with dimensions of around 100 nm diameter. In both regions pores in the order of 10 to 15 nm are visible. The longitudinal cut of a commercial viscose fibre with high wet modulus as shown in Fig. 6.6d also clearly displays the skin–core morphology. Obviously, the voids have a spindle-like shape in the direction of the fibre axis. (The creases visible in the figures are artefacts from the microtome cut.) Similar results have been found by other authors, notably by Abu-Rous *et al.* (2006), who also investigated Lyocell and modal fibres by TEM.

Note that other cross-sectional shapes can be generated by the use of non-circular spin holes, by hollow fibre spinning, or by injecting a gas or a gas-forming medium into the viscose to produce inflated fibres (Woodings 2001b). Moreover, all-skin morphologies for tyre yarn can be realised by adding dimethylamine or dimethylformamide to the viscose and/or spinbath (Woodings 2001b).

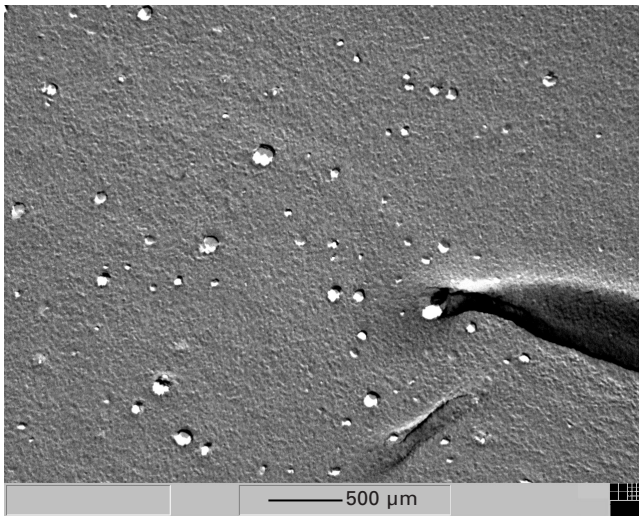
Scanning electron micrographs (SEM) of cross-sectional surfaces, cryo-fractured at liquid nitrogen temperature, were taken after sputtering with

4 nm platinum with a JEOL JSM 6330 F at 5 kV acceleration voltage and low probe current here and in what follows.

In Fig. 6.7 cryo-fracture micrographs are shown for viscose fibres from different starting pulps. Again the lobular fibre morphology is recognised. The first fibre fractures in a blunt manner while in Fig. 6.7b a rather step-wise fracture morphology is observed. Some inner detail is revealed which

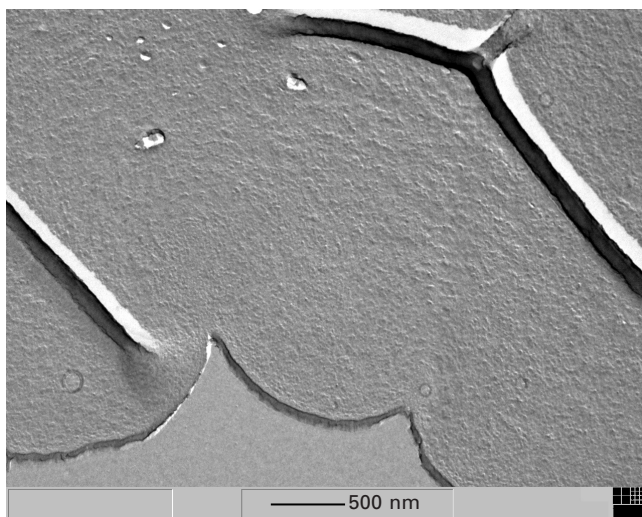


(a)



(b)

6.6 TEM micrographs of viscose fibre cross-sections: (a) lobular outer shape and skin-core structure; (b) zoom into inner region; (c) zoom into outer region; (d) longitudinal cut.



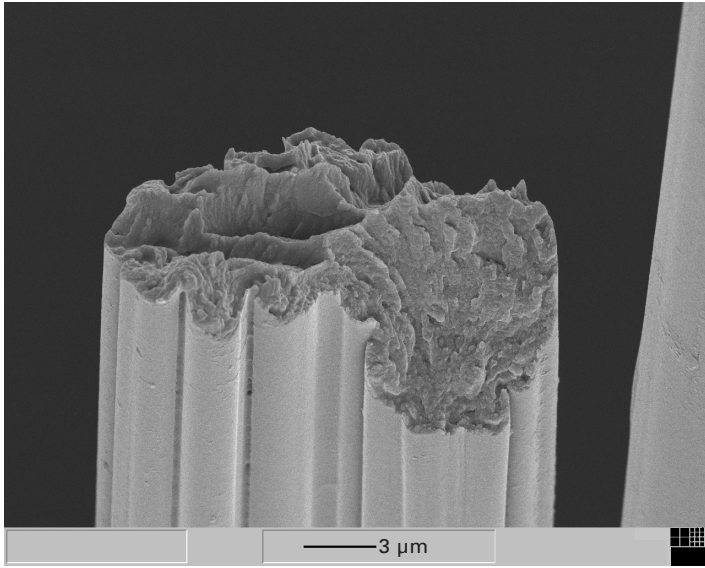
(c)



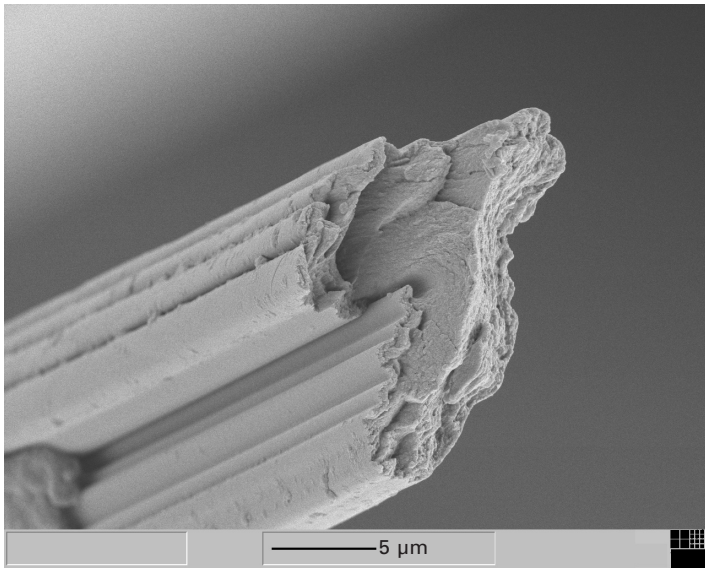
(d)

IP Address: 129.132.211.108

6.6 Cont'd



(a)

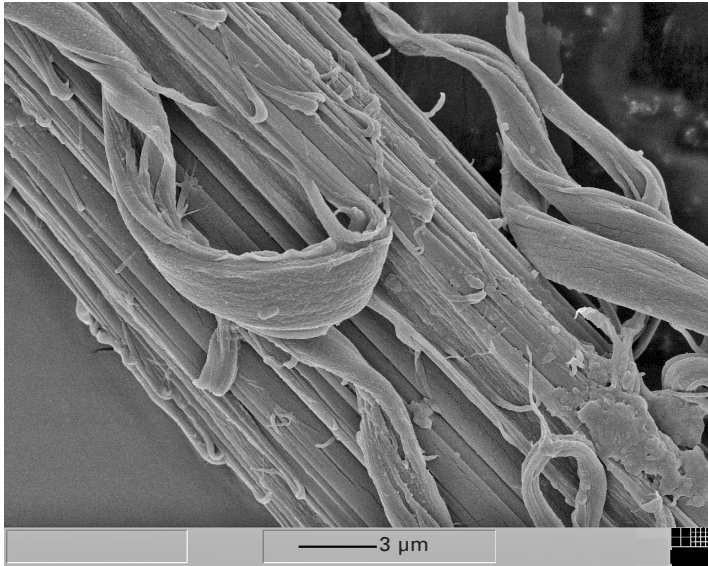


(b)

6.7 SEM micrographs of cryo-fracture surfaces of viscose fibres: (a) blunt fracture; (b) step-wise fracture.

becomes clearer when the single fibres (filaments) are subjected to a wet abrasion treatment with a rotating moist grinding rod. This test was used for quantifying the strong wet fibrillation tendency of Lyocell-type fibres of the first generation (Fink *et al.* 2001).





6.8 SEM micrograph of viscose fibre after wet abrasion treatment.

In Fig. 6.8, an SEM micrograph is presented of a viscose fibre treated in the manner described above. The oriented fibrillar morphology in accord with Fig. 6.5 is exposed by the mechanical destruction of inter-fibril linkages. However, the abrasion time to reach such a state is at least one order of magnitude higher than for Lyocell-type fibres of the first generation (*cf.* Fig. 6.12).

### 6.3.2 Crystallinity, crystallite dimensions and orientation

Crystallinities for viscose and other spun cellulose fibres as determined by wide angle X-ray scattering (WAXS) are presented in Table 6.1 as an excerpt from Table 1 in Röder *et al.* (2006). The X-ray method employed (Fink *et al.*, 1985) is based upon the work of Ruland (1961) and Vonk (1973) and uses isotropised samples and the scattering intensity of the complete measured angular range. By this method crystallites smaller than 2 to 3 nm are not included in the WAXS crystallinity (Ruland 1961). Besides crystallinity  $x_c$ , this method provides a lattice distortion measure  $k$  (disorder parameter).

Obviously, the fibres spun by whatever variant of the viscose process (shaded lines) have the lowest crystallinities in the whole table (except for Cupro), i.e. as compared to direct methods or saponified CA (Fortisan). Moreover, no correlation between crystallinity and tenacity is found. Even the viscose fibre with lowest tenacity of 23.4 cN/tex (no. 17) has a higher

crystallinity of 26% than the fibre with the highest strength of 52.3 cN/tex with a crystallinity of 24%. (no. 23).

Crystallinities of various spun cellulose fibres were also determined with WAXS by Lenz *et al.* (1988). Their values confirm the higher crystallinity in Lyocell compared to viscose fibres but are in general considerably higher than those given above. This is certainly due to the fact that Lenz *et al.* do not isotropise their samples and use only selected meridional fibre reflections for crystallinity evaluation, thus biasing the average towards higher crystallinity.

Crystallinity values for a series of spun cellulose fibres have been determined by  $^{13}\text{C}$ -CP-MAS solid state NMR by Ibbett *et al.* (2007). The authors claim a three-phase model of crystalline ordered, partially ordered and fully disordered regions with corresponding peak positions in the C4 region between 92 and 80 ppm and use a peak-fitting procedure to determine the mole fractions of the phases. A restructured excerpt of their Table 1 is presented here as Table 6.2. The crystalline fraction alone does not fit the findings from X-ray scattering in Table 6.1. However, the sum of crystalline and partially ordered fraction (ordered fraction) gives reasonable agreement with the values in Table 6.1. On the other hand, the well-established fact that  $^{13}\text{C}$ -CP/MAS-NMR spectroscopy reflects both the crystallinity and the crystallite dimensions of a cellulose sample (Newman 1999, Fink *et al.* 2004) should be taken into account in the discussion of NMR results.

Crystallite dimensions  $D_{(hkl)}$  perpendicular to the  $(hkl)$  lattice planes can be determined by WAXS from the half-width of the corresponding interference peak according to the classical Scherrer equation (e.g. Klug and Alexander 1974). An improved single-line method based on the micro-strain concept (Hofmann and Walenta 1987) has been applied to cellulose II by Hofmann *et al.* (1989) (see also Fink *et al.* 1995). Generally for cellulose II, it is difficult to separate an interference coming from lattice planes perpendicular to the

Table 6.2 Crystalline and partially ordered fraction of various cellulose spun fibres from  $^{13}\text{C}$ -CP/MAS-NMR (data from Ibbett *et al.* 2007)

Fibre type	Crystalline fraction (%)	Partially ordered fraction (%)	Ordered fraction (sum) (%)
Lyocell	17	26	43
Modal	13	16	29
Polynosic	9	12	21
Viscose	13	13	26
Tyre cord	9	8	17
Cupro	14	18	32
Fortisan	33	25	58

Shaded area represents data for fibres spun by the viscose process although not all the fibres are called viscose.

chain axis in an isotropised sample. From oriented samples, Haase *et al.* (1973) obtained a value of 11.2 nm for the crystallite dimension in the chain direction of a viscose fibre called Tufcel. This is in accord with findings by Rihm (2003), who determined 9.8 nm and 9.7 nm for viscose and tyre cord yarn, respectively.

Results for lateral dimensions from isotropised fibre samples of Table 6.1 are shown in Table 6.3 together with a calculated approximate measure for the crystallite area  $A = D_{(1-10)} D_{(110)}$  perpendicular to the chain axis (Patil *et al.* 1962). Obviously,  $D_{(hkl)}$  values tend to be generally higher for viscose than for Lyocell, while disorder parameters tend to be lower.

In polymeric fibres, chain orientation is the most crucial parameter for the mechanical properties such as modulus and strength. Due to the strong covalent bonds in the chain direction and the minor lateral interactions, only molecules with a high orientation in the fibre direction contribute significantly to high moduli and tenacities. Even for cellulose, where lateral hydrogen bonds impart a stronger interaction than ordinary van der Waals forces, the anisotropy is considerable. Molecular modelling of cellulose II at room temperature has shown that even for the crystalline state with a well-defined hydrogen bond network the two lateral moduli are roughly four and six times smaller, respectively, than the modulus in the chain direction (Ganster and Blackwell 1996). Therefore, a high chain orientation in the fibre direction, in particular in the non-crystalline regions where the hydrogen bond network is not as well developed, is required for high tensile properties.

Crystalline orientation is usually quantified by the Hermans factor  $f_c$  and is measured by X-ray diffraction using the second moment of the azimuthal

**Table 6.3** Tenacity, lattice distortion parameter  $k$ , crystallite dimensions  $D_{(hkl)}$  and cross-section  $A$  for the fibres of Table 6.1 from X-ray diffraction

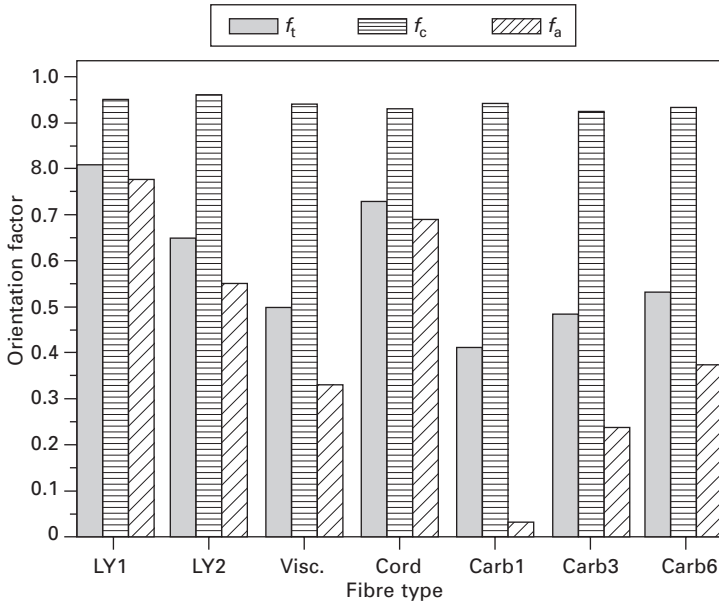
Sample no.	Tenacity (cN/tex)	$k$ ( $10^{-2} \text{ nm}^{-2}$ )	$D_{(1-10)}$ (nm)	$D_{(110)}$ (nm)	$D_{(020)}$ (nm)	$A$ ( $\text{nm}^2$ )	Fibre type
3	42.6	1.8	3.9	4.3	4.2	16.4	Lyocell
8	24.0	2.1	4.2	4.2	3.9	17.6	Lyocell
9	36.0	1.8	4.2	4.3	4.3	18.1	Lyocell
12	42.8	1.4	5.3	4.2	4.6	22.3	Modal
15	27.3	1.4	5.2	3.9	4.3	20.3	Polynosic
17	23.4	1.3	5.3	4.6	3.9	24.4	Viscose
19	29.1	1.4	5.6	4.2	4.5	23.5	Viscose
23	52.3	1.5	–	3.6	4.7	–	Viscose
26	22.3	1.5	5.7	4.9	5.4	27.9	Cupro
27	17.0	1.8	4.2	4.7	4.3	19.7	Celsol
28	19.8	2.1	3.9	5.1	4.3	19.9	Carbamate
29	23.9	1.5	6.1	5.0	5.6	30.5	Fortisan

Shaded area represents data for fibres spun by the viscose process although not all the fibres are called viscose.

intensity distribution of a certain interference while total orientation is measured by birefringence (see, e.g., Alexander 1969). From an average weighted with crystallinity, the amorphous (non-crystalline) chain orientation can be obtained.

Our results for various cellulose spun fibres are shown in Fig. 6.9. The meridional reflection (004) was used for the moment calculation of crystalline orientation. For calculating the total and amorphous orientation factors, a maximum crystalline and amorphous birefringence of 0.062 and 0.056, respectively, were assumed. The decisive role of amorphous orientation is seen. All the fibres have very similar crystalline orientation factors; however, the total and thence the amorphous orientation differ widely. For the two viscose fibres, the tyre cord yarn (Cord) with its high tenacity and modulus has a considerably higher amorphous orientation than the textile viscose fibre (Visc.). The development of carbamate fibres started out with low amorphous orientation (Carb1) and ended (Carb6) with an amorphous orientation comparable to viscose fibres.

Much lower and much more varying crystalline orientation factors were found by Lenz *et al.* (1993) for modal, viscose, NMMO, polynosic, carbamate and LiCl/DMAc fibres. They also used WAXS as the technique but evaluated two lateral reflections on the equator of the scattering pattern, the second



6.9 Total ( $f_t$ ), crystalline ( $f_c$ ) and amorphous ( $f_a$ ) orientation factors for Lyocell (LY1, LY2), viscose (Visc., Cord) and carbamate (Carb1, Carb3, Carb6) cellulose fibres.



of which, i.e. (10-1), is overlapping with (002) (in their nomenclature) and thus broadening the distribution.

It must be kept in mind that all the values given are averages over the whole fibre, i.e. over skin and core regions. An attempt to differentiate between skin and core with X-ray microbeam and electron diffraction of longitudinal fibre cuts has been reported by Müller *et al.* (2000). The authors find a far better crystallite alignment in the skin region (certainly due to higher shear forces there in the spinneret) and no significant differences in crystallinity and lateral crystallite size. Better chain orientation in the skin layer was corroborated by Eichhorn *et al.* (2003) with synchrotron X-ray diffraction with a 3  $\mu\text{m}$  spot size using an equatorial interference, i.e. lateral lattice planes.

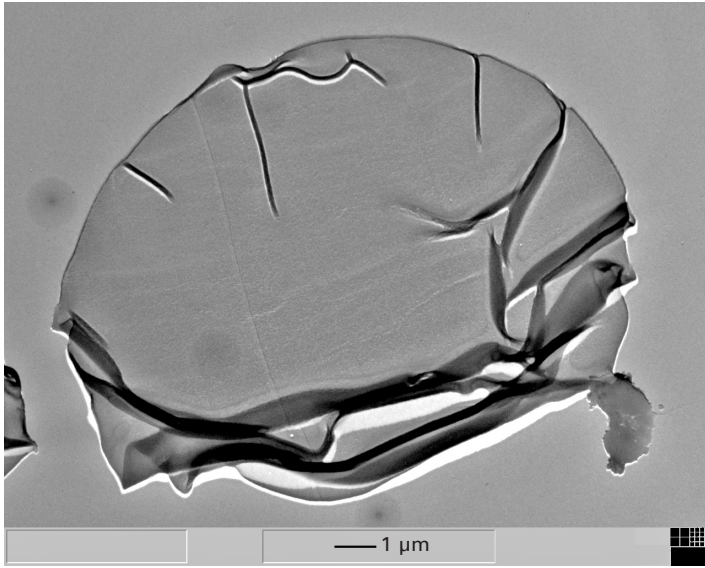
## 6.4 Lyocell-type fibres

Being the most important direct method, the Lyocell process is practically solely used by Lenzing AG to spin staple fibres, with an estimated fibre production of 115 000–120 000 tonnes in 2006 (Kosłowski 2008). The first fully commercial-scale line was put into operation in 1997 and since then steady growth and improvement of properties, e.g. by crosslinking to avoid wet fibrillation, has occurred (Ward 2001). A recent update on Lyocell fibre properties from the textile viewpoint can be found in Firgo *et al.* (2006).

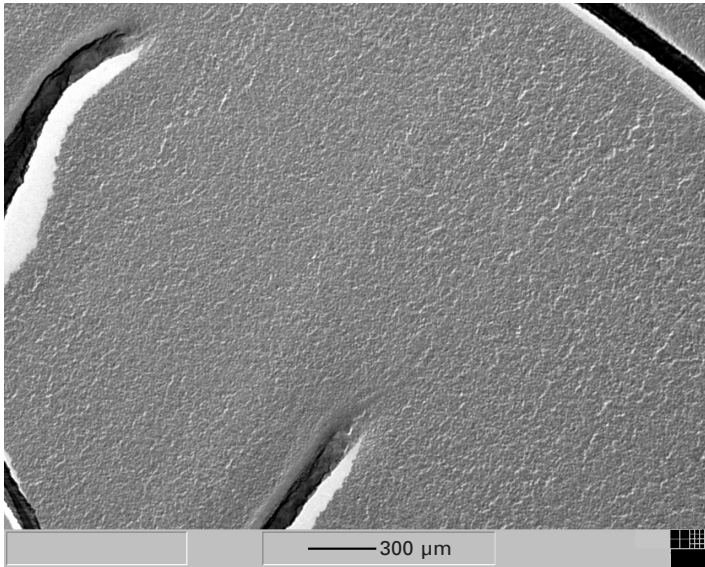
### 6.4.1 Cross-section, morphology and pore structure

A typical cross-section for a Lyocell fibre is shown in Fig. 6.10a. In contrast to viscose fibres, a widely circular cross-section, no lobulation and no visible skin–core morphology is observed. The magnified view (Fig. 6.10b) of the inner region is very similar to the morphology of the skin region in the viscose fibre. A more detailed analysis of the pore structure in Lyocell fibres has been performed by Abu-Rous *et al.* (2006). They used an  $\text{OsO}_4$  staining technique and observed nano-pores in the bulk with a slight gradient in pore density and a very porous skin layer.

The overall void structure in NMMO-type fibres (Tencel, Courtaulds) fibres was analysed using small-angle X-ray scattering with synchrotron radiation by Crawshaw and Cameron (2000) in both the wet and dried, as well the as rewetted and redried, states. An extensive network of small pores with average length 11 nm and lateral dimensions of approx. 0.3 nm and 36 nm were detected in the wet state. Upon drying, the overall pore volume is drastically reduced but the average size of a single pore is increased to  $270 \times 5 \times 34 \text{ nm}^3$ . Successive drying and rewetting decreases void length and volume fraction, and the authors compared that behaviour to the so-called hornification in native cellulose.



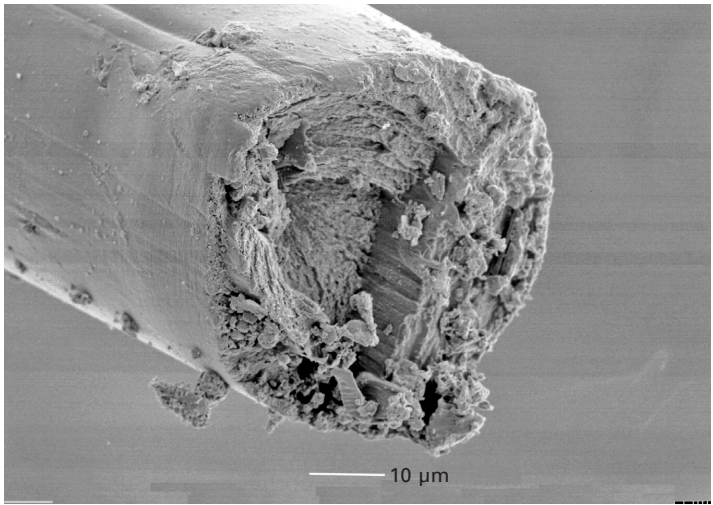
(a)



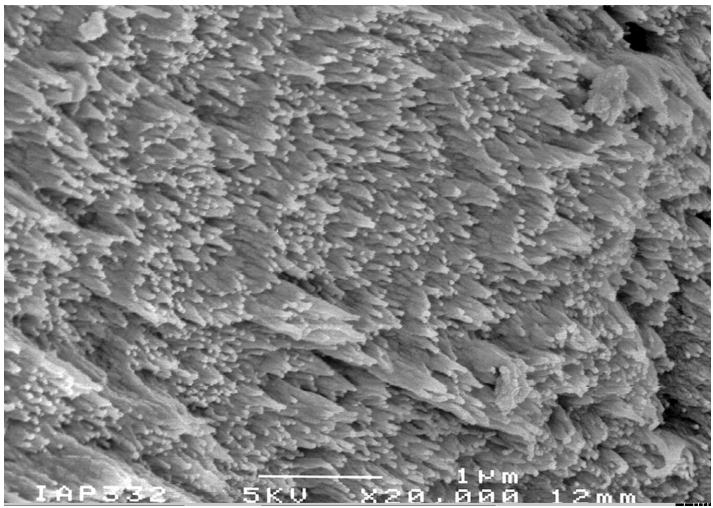
(b)

6.10 TEM micrographs of Lyocell fibre cross-sections: (a) overall shape; (b) zoom into inner region.

Cryo-fracture micrographs taken with SEM are displayed in Fig. 6.11. The fracture morphology is different from that for viscose fibres and appears with sharper features. A zoom into the fracture surface as in Fig. 6.11b shows a fibrillar structure which results in the damaged fibre structure seen in



(a)



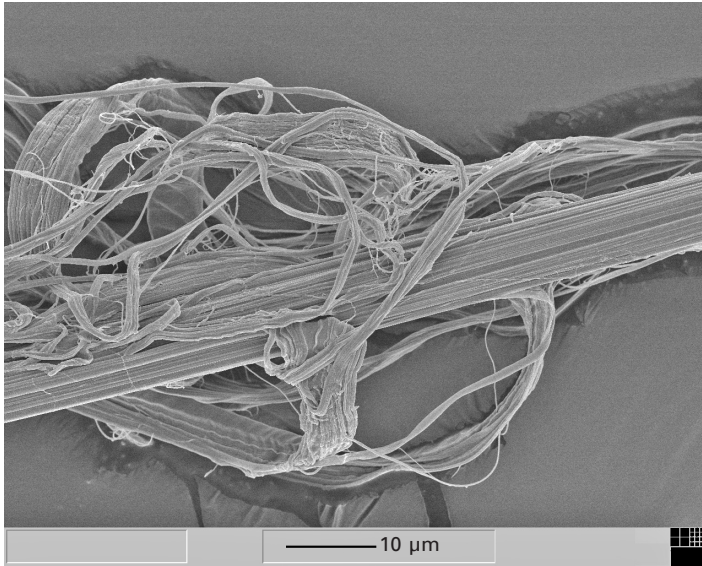
(b)

6.11 SEM micrographs of cryo-fracture surfaces of Lyocell fibres: (a) overall view; (b) zoom into fibrillar structure.

Fig. 6.12. As for Fig. 6.8, a wet abrasion treatment has been performed and, in comparison to the viscose case, finer fibrils are revealed.

#### 6.4.2 Crystallinity, crystallite dimensions and orientation

In Tables 6.1 and 6.2 for crystallinity and crystal size, respectively, Lyocell-type fibres have already been included. Crystallinities are generally higher



6.12 SEM micrograph of Lyocell fibre after wet abrasion treatment.

than for viscose fibres and seem to be inversely correlated with tenacity. Crystallite sizes perpendicular to the (1-10) planes and lateral crystallite areas are lower than for viscose fibres and the crystallites are less perfect since the  $k$ -factor is higher. For the crystallite dimension in the chain direction, Rihm (2003) finds 17.5 nm for an anisotropic Lyocell fibre sample. Thus, in Lyocell fibres the crystallites are considerably longer and slightly thinner than in viscose fibres. Moreover, using the crystallite areas and crystallinities from Tables 6.1 and 6.3 together with the mentioned crystallite lengths, the number of crystallites in Lyocell fibre no. 9 is 25% greater than the number of crystallites in viscose fibre no. 26, both taken as typical examples.

Combining SAXS and WAXS results, Lenz *et al.* (1992), provide a model of the so-called elementary fibril in Lyocell and modal fibres with crystallinities in the chain direction of 90% and 50–60%, respectively. In both cases, fibril thickness is 8 nm, while the lengths of the crystalline and amorphous regions are 16 nm and 8 nm in the Modal, and 21 nm and 2 nm in the Lyocell case.

As to chain orientation in Lyocell fibres, the two entries LY1 and LY2 in Fig. 6.9 represent Lyocell fibres of the first and second generations, respectively. Struggling with the wet fibrillation tendency of first Lyocell fibres, it became clear that amorphous chain orientation had to be reduced in order to improve the lateral connection between the fibrils. That was accomplished as seen in the figure. Total orientation factors from birefringence for four different Lyocell fibres, a viscose fibre and an experimental high modulus/high strength



fibre spun from phosphoric acid are reported by Gindl *et al.* (2008). Values are in the range of Fig. 6.9 and a systematic increase in modulus and strength is found with increased birefringence and reduction in diameter.

A systematic study of overall fibre orientation by birefringence and strain-induced Raman band shift as well as properties of NMMO fibres spun with six different draw ratios (from 0.7 to 8.9) was performed by Kong and Eichhorn (2005). Except for draw ratio 6, a monotonous increase in birefringence is seen. From the values reported, total orientation factors can be calculated to be in the range from 0.28 to 0.9, i.e. covering the values displayed in Fig. 6.9.

Quite recently, the crystalline and amorphous orientation of a Lyocell fibre (titre 13.55 dtex) as a function of strain up to 8% was investigated by Gindl *et al.* (2007). They used synchrotron radiation to determine the crystallite orientation  $f_c$  from the compound peak (110)/(020) (indexing according to Kolpak and Blackwell 1976) and found an  $f_c$  of 0.73 for the unstrained fibre. This is low compared to the values from Fig. 6.9 and is certainly due to the use of the equatorial double peak (110)/(020) instead of the meridional (004) reflection. Straining the fibre to 8%,  $f_c$  increases only slightly, while amorphous orientation measured from birefringence increases from 0.48 to 0.65. This is in full accord with Fig. 6.9 from which it can be concluded that amorphous (non-crystalline) in contrast to crystalline orientation is the crucial parameter for fibre development.

Recently, crystal orientation and crystal reorientation under tensile load in the NMMO fibres from Kong and Eichhorn (2005), was studied by synchrotron radiation with a beam size of 500 nm (Kong *et al.* 2007). Utilising the high spatial resolution, higher orientation was found in the skin than in the core region for all draw ratios due to higher shear forces near the fibre surface in the spinneret.

## 6.5 Cellulose acetate-based fibres

The world production of cellulose acetate filament yarn and acetate filter tow in 2006 was 70 000 tonnes and 680 000 tonnes, respectively (Koslowski 2008). Yarns are used in textile applications and filter tow mainly for cigarette filters. More details on application can be found on the Global Acetate Manufacturers' Association (GAMA) website (GAMA, 2008). A recent Macromolecular Symposium was devoted to properties and applications (Rustemeyer 2004). Currently produced acetate fibres have tenacities around 13 cN/tex, elongations at break over 20% and moduli around 340 cN/tex (own measurements, unpublished results). In general, cellulose acetate fibres are far less thoroughly studied than regenerated cellulose fibres, so that the information given here rests heavily upon our own investigations.

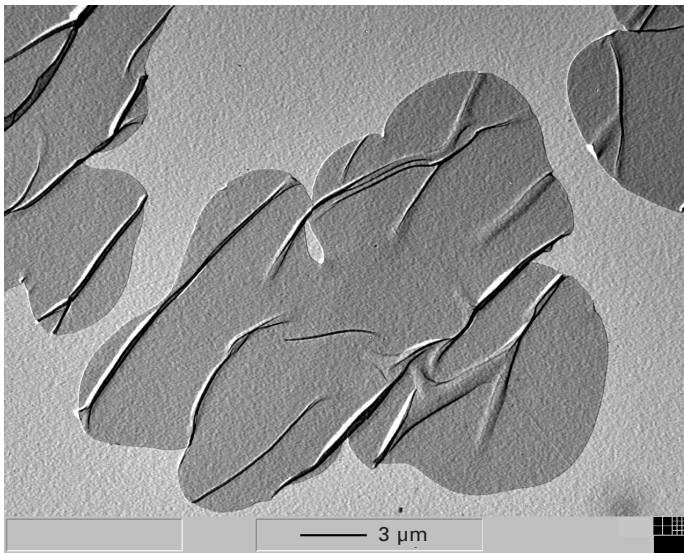
A pure cellulose fibre obtained by saponification of CA fibres which, however, has been out of production for decades is called Fortisan and will be covered in part in this section.

### 6.5.1 Cross-section, morphology and pore structure

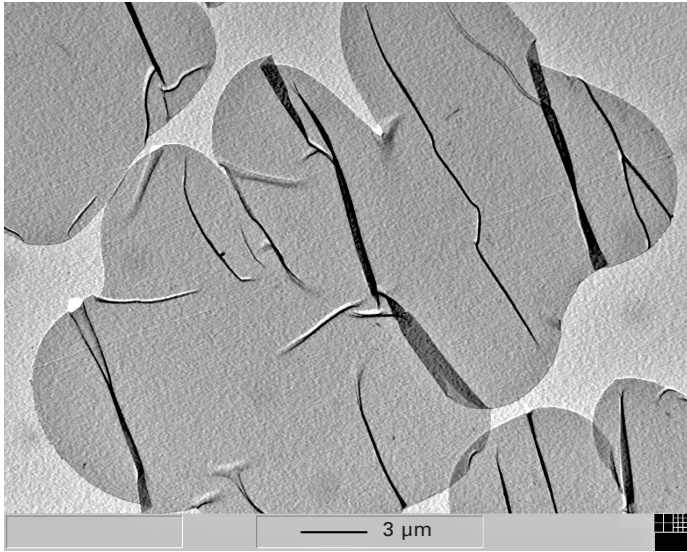
Typical cross-sections of three commercial CA filaments are shown in Fig. 6.13. The shape with its lobular circumference resembles that of viscose fibres. A skin-core structure with a coarser core region and a denser skin is present also here, as seen from the micrographs of the inner and outer regions of the fibre from Fig. 6.13 presented in Figs 6.14a and 6.14b, respectively. The differences are not as pronounced as for the viscose fibres from Fig. 6.6. Cryo-fracture micrographs taken with SEM from the respective fibres of Fig. 6.13 are displayed in Fig. 6.15. Compared to viscose and Lyocell, the acetate fracture surfaces have a smoother and less ragged appearance.

### 6.5.2 Crystallinity, crystallite dimensions and orientation

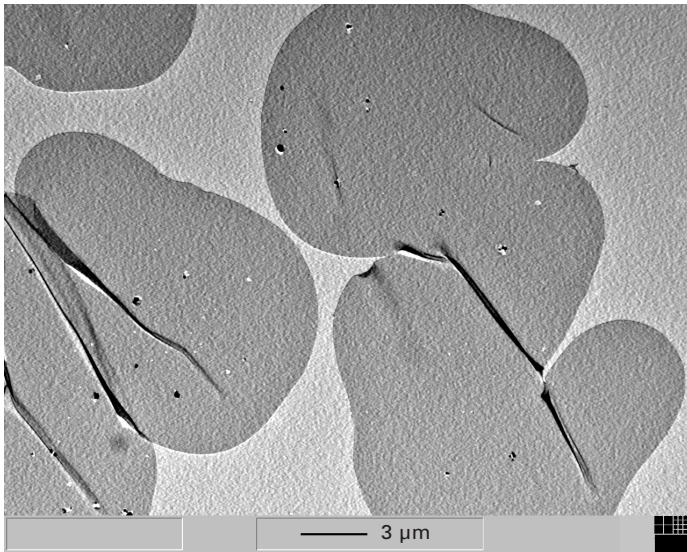
Crystallinities of CA fibres spun in our laboratory and determined by the above-mentioned Ruland–Vonk method were between 13 and 15% with



6.13 TEM micrographs of three different commercial cellulose acetate fibre cross-sections.



(b)



(c)

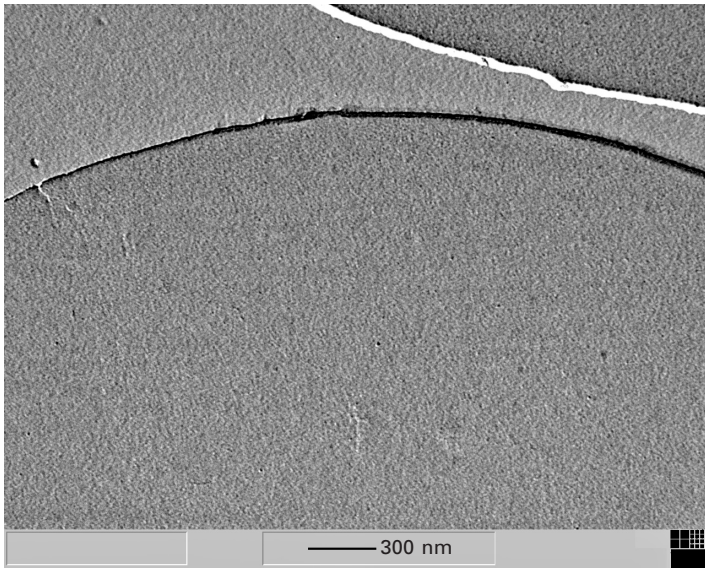
IP Address: 129.132.211.108

6.13 Cont'd

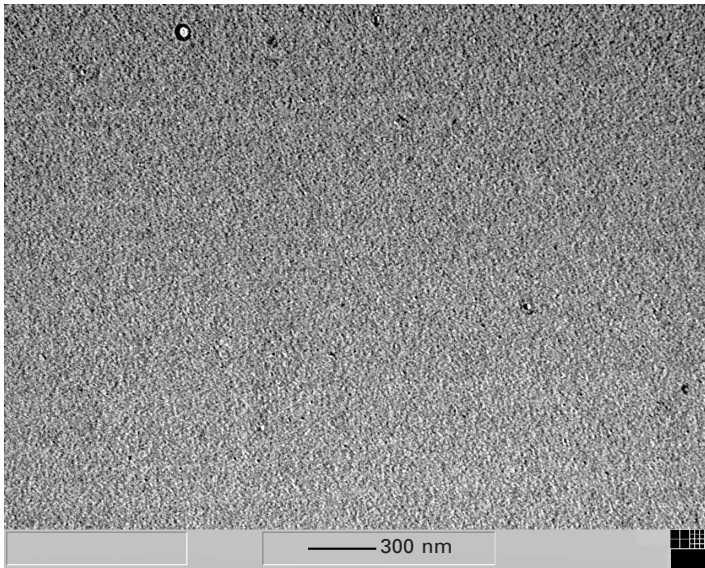
disorder parameters  $k$  in the range of 1.8 to 2.2. In contrast, the saponified Fortisan fibre has a crystallinity as high as 47% (Table 6.1).

Due to the low crystallinities even compared to the viscose fibres from Table 6.1, no crystallite dimensions could be determined for the CA fibres.





(a)



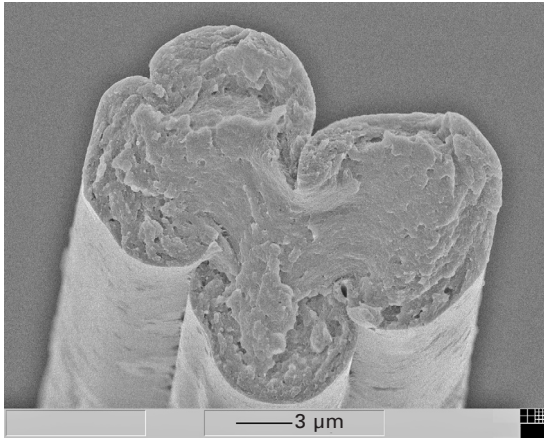
(b)

6.14 TEM micrographs of (a) inner and (b) outer regions of the fibre from Fig. 6.13a.

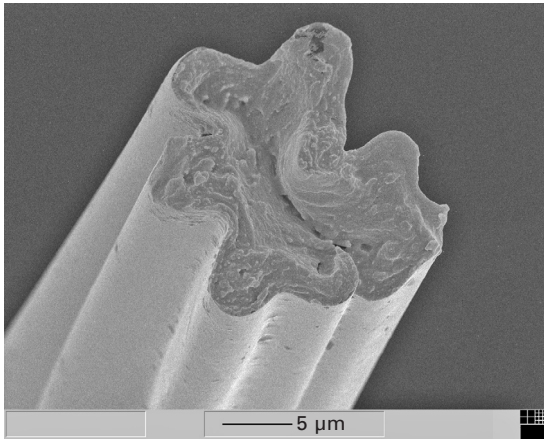
For Fortisan large crystallites with the highest lateral area of  $30.5 \text{ nm}^2$  of all the fibres in Table 6.3 are detected.

Chain orientation can be qualitatively assessed by wide-angle X-ray fibre patterns as shown in Fig. 6.16. It is clear from the X-ray diagrams that CA

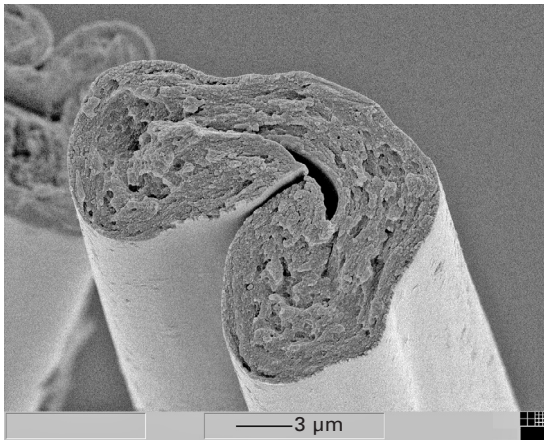




(a)



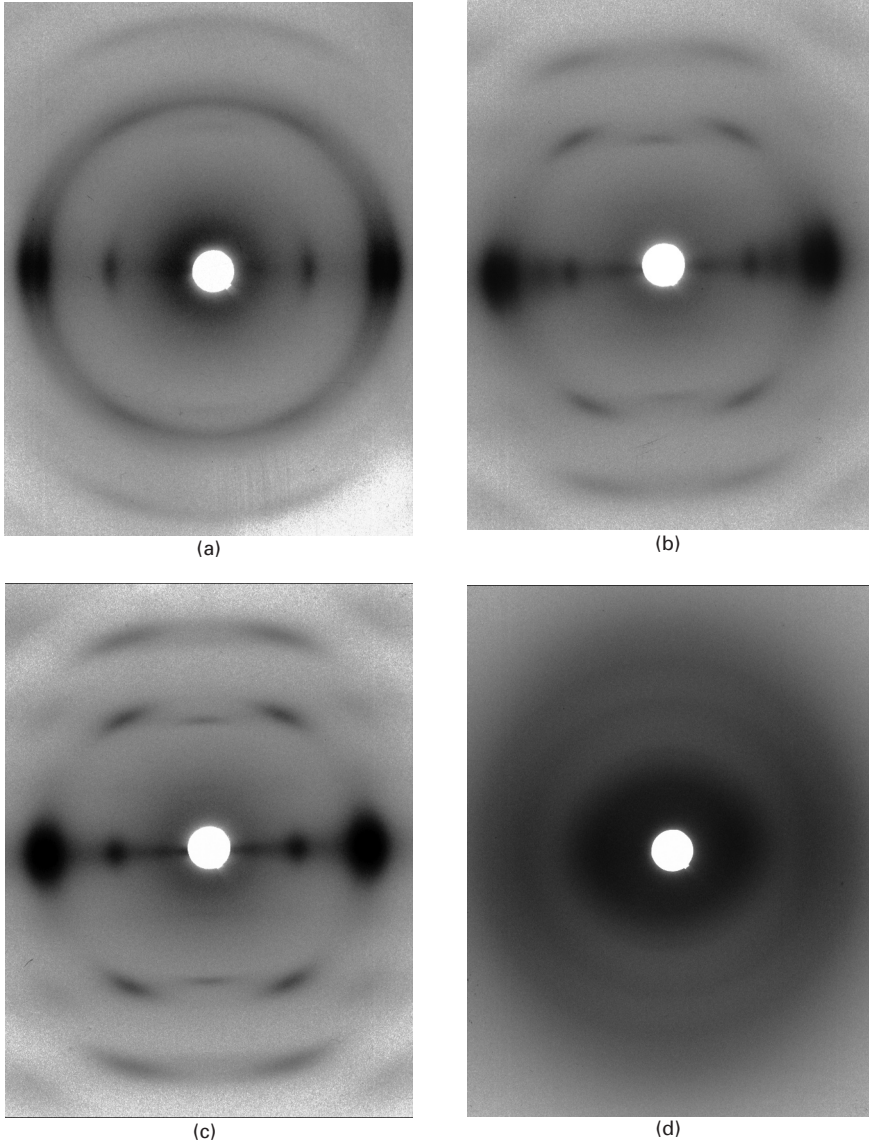
(b)



(c)

IP Address: 129.132.211.108

6.15 SEM micrographs of cryo-fracture surfaces of the fibres shown in Fig. 6.13.



IP Address: 129.132.211.108

6.16 X-ray flat film photographs of (a) viscose, (b) cellulose tyre cord yarn, (c) Lyocell, and (d) cellulose acetate fibres.

fibres are very different with their weak crystalline reflections as well as their complete amorphous halo which have only minor increased intensity in the equator region. This means weak anisotropy and a very low degree of chain orientation for the existing CA fibres.

## 6.6 Future trends

Although more than 100 years old, the viscose process is the subject of some recent investigations, though more from an industrial optimisation point of view. One obvious approach, for instance, is the use of less expensive pulps for fibre manufacture (Fink *et al.* 2008). A series of pulps has been tested and fibre properties reached levels of conventional fibres spun from dissolving pulps, whereas filtration processes are yet to be optimised in order to permit an industrial process.

As disclosed in a series of patents by Weyerhaeuser (e.g. Luo *et al.* 2001), high hemicellulose pulps have also been used to spin fibres with the Lyocell process (Zhang *et al.* 2008). The latter authors claim that spinning at higher concentrations is possible and that improved mechanical properties, increased fibrillation resistance, as well as better dyeing properties are obtained. They find a slightly lower crystallinity (50% vs. 52%) and a slightly higher crystalline orientation (0.827 vs. 0.818).

An exceptionally stiff and strong cellulose fibre spun from an anisotropic solution in phosphoric acid is described by Northolt *et al.* (2001). The authors report a strength of 1.3 GPa, a modulus of 45 GPa and a tensile elongation as low as 4.6%. Crystallite dimensions from X-ray scattering of the lateral (1–10) and the (004) chain reflections are found to be 3.9 nm and 17.8 nm, respectively. Compared to textile viscose (2.9 nm) and Cordenka 700 tyre cord yarn (3.7 nm) the lateral dimensions do not change much, though crystalline length is increased considerably (9 nm for viscose and 9.6 nm for tyre cord). From radial cracking and electron diffraction studies on a particular phosphoric acid spun fibre, they conclude a radial texture of the (110) lattice planes to be present in the fibre.

More recently, Fink *et al.* (2006) reported on cellulose fibres spun from highly concentrated anisotropic solutions of cellulose carbamate in NMMO via a dry jet-wet process. Resulting fibres show extraordinary high tenacities (up to 65 cN/tex, i.e. 975 MPa) and moduli (3300 cN/tex, i.e. 49.5 GPa) at high drawing ratios. Compared to former attempts at liquid crystalline solution spinning, the carbamate–NMMO system has the strong advantage of being based on existing technologies.

Cellulose filaments spun from an aqueous NaOH/urea solution prepared at reduced temperatures (precooled to  $-12^{\circ}\text{C}$ ) have been developed in view of setting up an alternative industrial process in the group of L. Zhang (Chen *et al.* 2006, Cai *et al.* 2007). Advantages of the new process are described as low cost, simplicity, reduced environmental impact and shorter production cycle. Tensile properties with maximum strength of 18 cN/tex (270 MPa) at an elongation of 13% do not yet reach typical textile viscose values (23 cN/tex, i.e. 345 MPa with 17% elongation) and an increase of cellulose concentration to 8% is anticipated. In terms of structure, round cross-sections

similar to those of Lyocell fibres are found along with higher crystallinity and lower crystalline orientation as compared to textile viscose fibres. Like viscose, the new fibres display a clear SAXS pattern generated by needle-shaped voids or a fibrillar structure aligned parallel to the fibre direction. However, the pattern is much enlarged compared to viscose, indicating the smaller dimensions of the voids or lamellar arrangements.

Electrospinning of cellulose to sub-micron scales from LiCl/DMAc and NMMO solutions has been reported by Kim *et al.* (2006). The authors find cellulose II crystallinity in fibres spun from NMMO and amorphous X-ray diffraction patterns in case of LiCl/DMAc.

Novel cellulose melt-blown non-wovens using the Lyocell process are described in Ebeling *et al.* (2006). Microfibre mats are obtained with fibres of circular to oval shape displaying a distinct skin-core structure in the TEM micrographs. Voids are present in both regions with dimensions in the range of 10–50 nm for weak coagulation and 30–130 nm for intensive coagulation with a tendency to larger pores in the core region.

As a new development, spinning cellulose and cellulose derivatives from ionic liquids must be mentioned (*cf.* Section 6.1.2). However, to the authors' knowledge, structural data such as given above for these kinds of fibres are not yet available in the open scientific literature.

## 6.7 References

- Abu-Rous, M., Ingolic, E., Schuster, K.C. 2006, 'Visualisation of the fibrillar and pore morphology of cellulosic fibres applying transmission electron microscopy', *Cellulose*, vol. 13, pp. 411–419.
- Adusumalli, R.-B., Müller, U., Weber, H., Röder, Th., Sixta, H., Gindl, W. 2006, 'Tensile testing of single regenerated cellulose fibres', *Macromol. Symp.*, vol. 244, pp. 83–88.
- Alexander, L.E. 1969, 'X-ray diffraction methods in polymer science', *Preferred Orientation in Polymers* in Wiley, New York, pp. 200–279.
- Andress, K.R. 1929, 'Das Röntgendiagramm der mercerisierten Cellulose', *Z. Phys. Chem. B*, vol. 4, pp. 190–206.
- Bianchi, E., Ciferri, A., Conio, G., Tealdi, A. 1989, 'Fiber formation from liquid-crystalline precursors. II. Cellulose in *N,N*-dimethylacetamide-lithium chloride', *J. Polym. Sci. B. Polym. Phys.*, vol. 27, pp. 1477–1484.
- Boerstoel, H., Maatman, H., Westerink, J.B., Koenders, B.M. 2001, 'Liquid crystalline solutions of cellulose in phosphoric acid', *Polymer*, vol. 42, pp. 7371–7379.
- Cai, J., Zhang, L., Thou, J., Qi, H., Chen, H., Kondo, T., Chen, X., Chu, B. 2007, 'Multifilament fibers based on dissolution of cellulose in NaOH/urea aqueous solution: structure and properties', *Adv. Mater.*, vol. 19, pp. 821–825.
- Chanzy, H., Dube, M., Marchessault, R.H. 1979, 'Crystallization of cellulose with *N*-methylmorpholine *N*-oxide'. A new method of texturing cellulose', *J. Polym. Sci. Lett. Ed.*, vol. 17, pp. 219–226.
- Chemical Fibers International*, 2006, vol. 56, issue 4, p. 202.

- Chen, X., Burger, Ch., Fang, D., Ruan, D., Zhang, L., Hsiao, B., Chu, B., 2006, 'X-ray studies of regenerated cellulose fibres wet spun from cotton linter pulp in NaOH/thiourea aqueous solutions', *Polymer*, vol. 47, pp. 2839–2848.
- Coulsey, H.A., Smith, S.B. 1996, 'The formation and structure of a new cellulosic fibre', *Lenzinger Berichte*, vol. 75, pp. 51–61.
- Crawshaw, J., Cameron R.E. 2000, 'A small angle X-ray scattering study of pore structure in Tencel cellulose fibres and the effects of physical treatments', *Polymer*, vol. 41, pp. 4691–4698.
- Ebeling, H., Fink, H.-P., Luo, M., Geus, H.-G. 2006, 'Cellulose meltblown nonwovens using the Lyocell-process', *Lenzinger Berichte*, vol. 86, pp. 124–131.
- Eichhorn, S.J., Sirichaisit, J., Young, R.J. 2001, 'Deformation mechanisms in cellulose fibres, paper and wood', *J. Mater. Sci.*, vol. 36, pp. 3129–3135.
- Eichhorn, S.J., Young, R.J., Davies, R.J., Riekel, C. 2003, 'Characterisation of the microstructure and deformation of high modulus cellulose fibres', *Polymer*, vol. 44, pp. 5901–5908.
- Fink, H.-P., Philipp, B. 1985, 'Models of cellulose physical structure from the viewpoint of the cellulose I to cellulose II transition', *J. Appl. Polym. Sci.*, vol. 30, pp. 3779–3790.
- Fink, H.-P., Walenta, E. 1994, 'Röntgenbeugungsuntersuchungen zur übermolekularen Struktur von Cellulose im Verarbeitungsprozess', *Das Papier*, vol. 48, pp. 739–748.
- Fink, H.-P., Fanter, D., Philipp, B. 1985, 'Wide angle X-ray study of the supermolecular structure at the cellulose I–cellulose II phase transition', *Acta Polym.*, vol 36, pp. 1–8.
- Fink, H.-P., Ganster, J., Fraatz, J., Nywlt, M. 1994, 'Relations between structure and mechanical properties of cellulosic man-made fibres', in *Proceedings of the Akzo-Nobel Viscose Chemistry Seminar – Challenges in Cellulosic Man-made Fibres*, Stockholm, 30 May – 3 June.
- Fink, H.-P., Hofmann, D., Philipp, B. 1995, 'Some aspects of lateral chain order in celluloses from X-ray scattering', *Cellulose*, vol. 2, pp. 51–790.
- Fink, H.-P., Weigel, P., Purz, H.J., Ganster, J. 2001, 'Structure formation of regenerated cellulose materials from NMMO-solutions', *Prog. Polym. Sci.*, vol. 26, pp. 1473–1524.
- Fink, H.-P., Weigel, P., Ganster, J., Rihm, R., Puls, J., Sixta, H., Parajo, J.C. 2004, 'Evaluation of new organosolv dissolving pulps. Part II: Structure and NMMO processability of the pulps', *Cellulose*, vol. 11, pp. 85–98.
- Fink, H.-P., Ebeling, H., Rihm, R. 2006, 'Fibre formation from liquid crystalline solutions of cellulose carbamate in *N*-methylmorpholine-*N*-oxide', *Proceedings of the 7th International Symposium 'Alternative Cellulose – Manufacturing, Forming, Properties'*, Rudolstadt, Germany, 6–7 September.
- Fink, H.-P., Ebeling, H., Fischer, K. 2008, 'Grundlagen für einen modifizierten Viskoseprozess unter Verwendung heimischer Rohstoffe', Project FKZ 22016703 sponsored by 'Fachagentur für Nachwachsende Rohstoffe', Federal Ministry BMELV, Germany.
- Firgo, H., Schuster, K.C., Suchomel, F., Männer, J., Burrow, T., Abu-Rous, M. 2006, 'The functional properties of Tencel – a current update', *Lenzinger Berichte*, vol. 85, pp. 22–30.
- GAMA website <http://www.acetateworld.com/>
- Ganster, J., Blackwell, J. 1996, 'NpH-MD-simulations of the elastic moduli of cellulose II at room temperature', *J. Mol. Mod.*, vol. 2, pp. 278–285.



- Ganster, J., Fink, H.P. 1999, 'Physical constants of cellulose', in *Polymer Handbook*, ed. E.H. Immergut, E.A. Grulke, 4th edition, John Wiley and Sons, New York, sect. V, pp. 135–157.
- Ganster, J., Fink, H.-P., Uihlein, K., Zimmerer, B. 2008, 'Cellulose man-made fibre reinforced polypropylene – correlations between fibre and composite properties', *Cellulose*, vol. 15, pp. 561–569.
- Gindl, W., Reifferscheid, M., Martinschitz, K.J., Boesecke, P., Keckes, J. 2007, 'Reorientation of crystalline and noncrystalline regions in regenerated cellulose fibres and films tested in uniaxial tension', *J. Polym. Sci. B: Polym. Phys.*, vol. 46, pp. 297–304.
- Gindl, W., Reifferscheid, M., Adusumalli, R.-B., Weber, H., Röder, Th., Sixta, H., Schöberl, T. 2008, 'Anisotropy of the modulus of elasticity in regenerated cellulose fibres related to molecular orientation', *Polymer*, vol. 49, pp. 792–799.
- Götze, K. 1967, *Chemiefasern nach dem Viskoseverfahren*, Springer, Berlin.
- Haase, J., Hosemann, R., Renwanz, B. 1973, 'Parakristalline Gitterstörungen in Kettenrichtung von Cellulose I und II', *Kolloid-Z. u. Z. Polymere*, vol. 251, pp. 871–875.
- Hearle, J.W.S. 1958, 'A fringed fibril theory of structure of crystalline polymers', *J. Polym. Sci.*, vol. 28, pp. 432–435.
- Hearle, J.W.S. 1967, 'Structural mechanics of fibres', *J. Polym. Sci. C*, vol. 20, pp. 215–251.
- Hearle, J.W.S. 2001, 'Physical structure and fibre properties', in *Regenerated Cellulose Fibres*, Woodhead Publishing, Cambridge, pp. 199–234.
- Heinze, Th., Liebert, T. 1998, 'Organic solvents and sophisticated derivatives of cellulose – promising tool in cellulose chemistry', *Cell. Chem. Technol.*, vol. 32, pp. 3–18.
- Hermanutz, F., Gähr, F., Uerdingen, E., Meister, F., Kosan, B. 2008, 'New developments in dissolving and processing of cellulose in ionic liquids', *Macromol. Symp.*, vol. 262, pp. 23–27.
- Hofmann, D., Walenta, E. 1987, 'An improved single line method for the wide angle X-ray scattering profile analysis of polymers', *Polymer*, vol. 28, pp. 1271–1276.
- Hofmann, D., Fink, H.-P., Philipp, B. 1989, 'Lateral crystallite size and lattice distortions in cellulose II samples of different origin', *Polymer*, vol. 30, pp. 237–241.
- Ibbett, R.N., Domvoglou, D., Fasching, M. 2007, 'Characterisation of the supermolecular structure of chemically and physically modified regenerated cellulosic fibres by means of carbon-13 solid state NMR', *Polymer*, vol. 48, pp. 1287–1296.
- Kim, Ch.-W., Kim, D.-S., Kang, S.-Y., Marquez, M., Joo, Y.L. 2006, 'Structural studies of electrospun cellulose nanofibers', *Polymer*, vol. 47, pp. 5097–5107.
- Klemm, D., Heublein, B., Fink, H.-P., Bohn, A. 2005, 'Cellulose: fascinating biopolymer and sustainable raw material', *Angew. Chem. Int. Ed.*, vol. 44, pp. 2–37.
- Klug, H.-P., Alexander, L.E. 1974, *X-ray diffraction procedures for polycrystalline and amorphous Materials*, John Wiley & Sons, pp. 687–690.
- Kolpak, F.J., Blackwell, J. 1976, 'Determination of the structure of cellulose II', *Macromolecules*, vol. 9, no. 2, pp. 273–278.
- Kong, K., Eichhorn, S.J. 2005, 'Crystalline and amorphous deformation of process controlled cellulose-II fibres', *Polymer*, vol. 46, pp. 6380–6390.
- Kong, K., Davies, R.J., McDonald, M.A., Young, R.J., Wilding, M.A., Ibbett, R.N., Eichhorn, S.J. 2007, 'Influence of domain orientation on the mechanical properties of regenerated cellulose fibres', *Biomacromolecules*, vol. 8, pp. 624–630.
- Kosan, B., Michels, Ch., Meister, F. 2008, 'Dissolution and forming of cellulose with ionic liquids', *Cellulose*, vol. 15, pp. 59–66.

- Koslowski, H.-J. 2008, personal communication from 'Fiber Organon', Fiber Economics Bureau, June 2007.
- Langan, P., Nishiyama, Y., Chanzy, H. 1999, 'A revised structure and hydrogen-bonding system in cellulose II from a neutron fiber diffraction analysis', *J. Am. Chem. Soc.*, vol 121, no. 43, pp. 9940–9946.
- Langan, P., Nishiyama, Y., Chanzy, H. 2001, 'X-ray structure of mercerized cellulose II at 1 Å resolution', *Biomacromolecules*, vol. 2, no. 2, pp. 410–416.
- Langan, P., Sukumar, N., Nishiyama, Y., Chanzy, H. 2005, 'Synchrotron X-ray structures of cellulose I $\beta$  and regenerated cellulose II at ambient temperature and 100 K', *Cellulose*, vol. 12, pp. 551–562.
- Laus, G., Bentivoglio, G., Schottenberger, H., Kahlenberg, V., Kopacka, H., Röder, Th., Sixta, H. 2005, 'Ionic liquids: current developments, potential and drawbacks for industrial applications', *Lenzinger Berichte*, vol. 84, pp. 71–85.
- Lenz, J., Schurz, J., Wrentschur, E. 1988, 'The fibrillar structure of cellulosic man-made fibres spun from different solvent systems', *J. Appl. Polym. Sci.*, vol 35, pp. 1987–2000.
- Lenz, J., Schurz, J., Wrentschur, E. 1992, 'Comparative characterisation of solvent spun cellulose and high wet modulus viscose fibres by their long periods', *Acta Polym.*, vol. 43, pp. 307–312.
- Lenz, J., Schurz, J., Wrentschur, E. 1993, 'Properties and structure of solvent-spun and viscose-type fibres in the swollen state', *Colloid and Polym. Sci.*, vol. 271, pp. 460–468.
- Liu, R-G., Shen, Y-Y., Shao, H-L., Wu, Ch-X., Hu, X-Ch. 2001, 'An analysis of Lyocell fiber formation as a melt-spinning process', *Cellulose*, vol. 8, pp. 13–21.
- Luo, M., Roscelli, V.A., Camarena, S., Neogi, A.N., Yancey, M.J., Gaddis, P.G., 2001, 'Process for melt blowing continuous Lyocell fibers', US Patent 6,306,334 B1.
- Müller, M., Riekkel, C., Vuong, R., Chanzy, H. 2000, 'Skin/core micro-structure in viscose rayon fibres analysed by X-ray microbeam and electron diffraction mapping', *Polymer*, vol. 41, pp. 2627–2632.
- Newman, R.H. 1999, 'Estimation of the lateral dimensions of cellulose crystallites using  $^{13}\text{C}$  NMR signal strengths', *Solid State Nuclear Magnetic Resonance*, vol. 15, pp. 21–29.
- Nishiyama K. 1997, in *Cellulosic Man-made Fibres, Proceedings of the Singapore Viscose Chemistry's Seminar*, Akzo-Nobel, 22–24 April.
- Northolt, M.G., Boerstael, H., Maatman, H., Huisman, R., Veurink, J., Elzerman, H. 2001, 'The structure and properties of cellulose fibres spun from an anisotropic phosphoric acid solution', *Polymer*, vol. 42, pp. 824–826.
- Okano, T., Sarko, A. 1985, 'Mercerisation of cellulose. II. Alkali-cellulose intermediates and a possible mercerisation mechanism', *J. Appl. Polym. Sci.*, vol. 30, pp. 325–332.
- Patil, N.B., Dweltz, N.E., Radhakrishnan, T. 1962, 'X-ray measurements of crystallinity and crystallite size in swollen and hydrolyzed cottons', *Textile Res. J.*, vol. 32, pp. 460–471.
- Purz, H.J., Schulz, E. 1979, 'Die Elektronenmikroskopie in der Polymerforschung', *Acta Polym.*, vol. 30, pp. 377–390.
- Rihm, R. 2003, 'Röntgen-Strukturuntersuchungen an Cellulose regeneratfasern', PhD Thesis, Technical University Berlin, [http://edocs.tu-berlin.de/diss/2003/rihm\\_rainer.pdf](http://edocs.tu-berlin.de/diss/2003/rihm_rainer.pdf)
- Roche, E., Chanzy, H., Boudeulle, M., Marchessault, R.H., Sundararajan, P. 1978, 'Three-dimensional crystalline structure of cellulose triacetate II', *Macromolecules*, vol. 11, pp. 86–94.



- Röder, Th., Moosbauer, J., Fasching, M., Bohn, A., Fink, H.-P., Baldinger, Th., Sixta, H. 2006, 'Crystallinity determination of man-made cellulose fibres – comparison of analytical methods', *Lenzinger Berichte*, vol. 86, pp. 132–136.
- Ruland, W. 1961, 'X-ray determination of crystallinity and diffuse disorder scattering', *Acta Cryst.*, vol. 14, pp. 1180–1185.
- Rustemeyer, P. 2004, 'Cellulose acetates: properties and applications', *Macromol. Symp.*, vol. 208, Wiley, ISBN 3–527–31041-x.
- Schurz, J. 1980, 'Die Struktur der Cellulose', *Lenzinger Berichte*, vol. 49, pp. 15–24.
- Sprague, B.S., Noether, H.D. 1961, 'The relationship of fine structure to mechanical properties of stretched saponified acetate fibres', *Text. Res. J.*, vol. 31, pp. 858–865.
- Stipanovic, A.J., Sarko, A. 1976, 'Packing analysis of carbohydrates and polysaccharides. 6. Molecular and crystal structure of regenerated cellulose II', *Macromolecules*, vol. 8, no. 5, pp. 851–857.
- Vehviläinen, M., Nousiainen, P. 1997, in *Proceedings of the Singapore Viscose Chemistry's Seminar*, Akzo-Nobel, 22–24 April.
- Voges, M., Brück, M., Fink, H.-P., Gensrich, J. 2000, 'The CarbaCell process – an environmentally friendly alternative for cellulose man-made fibre production', in *Proceedings of the Akzo-Nobel Cellulosic Man-made Fibre Seminar*, Stenungsund, 13–15 June.
- Vonk, C.G. 1973, 'Computerisation of Ruland's X-ray method for determination of crystallinity in polymers', *J. Appl. Cryst.*, vol. 6, pp. 148–152.
- Ward, D. 2001, 'Lyocell fibers make slow but steady progress', *Int. Fiber J.*, vol. 16, no. 3.
- Woodings, C. 2001a, *Regenerated Cellulose Fibres*, Woodhead Publishing, Cambridge.
- Woodings, C. 2001b, 'Applications development', in *Regenerated Cellulose Fibres*, Woodhead Publishing, Cambridge pp. 235–272.
- Zhang, H., Zhang, H., Tong, M., Shao, H., Hu, X. 2008, 'Comparison of the structures and properties of Lyocell fibers from high hemicellulose pulp and high  $\alpha$ -cellulose pulp', *J. Appl. Polym. Sci.*, vol. 107, 636–641.
- Zugenmaier, P. 2001, 'Conformation and packing of various crystalline cellulose fibers', *Prog. Polym. Sci.*, vol. 26, pp. 1341–1417.
- Zugenmaier, P. 2004, Characterisation and physical properties of cellulose acetates', *Macromol. Symp.*, vol. 2008, pp. 81–166.
- Zugenmaier, P. 2008, *Crystalline Cellulose and Derivatives – Characterisation and Structures*, Springer, Berlin.

# Regenerated protein fibres: a preliminary review

M M BROOKS, University of Southampton, UK

**Abstract:** This chapter describes the structure and characteristics of regenerated protein fibres, sometimes called azlons, a group of fibres which were first developed in the late nineteenth and early twentieth centuries, actually produced in the mid-twentieth century but then rapidly forgotten and only returned to the market in the late twentieth and early twenty-first centuries. These are man-made fibres produced from either animal or vegetable non-fibrous proteins which have been reconfigured to take up a fibrous form to emulate the natural protein fibres wool or silk. Production methods are described and the available evidence for their structure and behavioural characteristics is reviewed.

**Key words:** regenerated protein fibres, azlon fibres, regenerated protein fibre production, fibre characteristics, fibre behaviours.

## 7.1 Introduction

This chapter describes the structure and characteristics of regenerated protein fibres, a group of fibres which were first developed in the late nineteenth and early twentieth centuries, actually produced in the mid-twentieth century but then rapidly forgotten and only returned to the market in the late twentieth and early twenty-first centuries. Regenerated protein fibres, sometimes called azlons, are man-made fibres produced from either animal or vegetable non-fibrous proteins which have been reconfigured to take up a fibrous form to emulate the natural protein fibres wool or silk. They are defined in the USA *Textile Fiber Products Identification Act* (1958) as manufactured fibres ‘in which the fiber-forming substance is composed of any regenerated, naturally occurring proteins’.

Three generations of these regenerated protein fibres may be identified. The first were developed at the turn of the nineteenth and in the early twentieth centuries, the second in the mid-twentieth century and the third in the late twentieth and early twenty-first centuries. Each generation was developed in response to contemporaneous economic and social factors, but as the technology used for the first and second generations has close similarities (these will be discussed together) while the technologically different third generation fibres will be discussed separately. The relative paucity of surviving examples of these fibres means that analysis of second generation regenerated protein fibres is heavily dependent upon contemporaneous textual

evidence and that of first generation is totally dependent upon this. More detailed data is becoming available about the third generation fibres which are now available commercially. However, much of the evidence from all three generations comes from manufacturers and promoters and must be treated with caution without corroborative evidence drawn from artefacts.

## 7.2 First and second generation regenerated protein fibres

### 7.2.1 Development

The first generation fibres developed in the late nineteenth and early twentieth centuries were intended as substitutes for silk or for the substitute silks made from regenerated cellulose, commonly known as rayons. Protein sources explored included milk casein, gelatine, blood, egg albumen and vegetable albumen. Interest in these fibres seemed to have died away until the mid-1930s when the opposing forces of surplus (such as excess milk by-products) and actual or perceived lack of natural fibre (in the form of threatened wool imports and increased military demand) encouraged renewed interest. The search for a substitute for wool became dominant. At a time when synthetic fibres were in their infancy, wool was of vital military importance. As an American contemporary noted:

At the opening of the war, wool caused perhaps more concern than any other fiber. This was because it is a vital necessity in war – almost as precious as ammunition. Within a month after Pearl Harbor, the War Production Board brought pressure on mills to blend wool with other fibers in civilian goods ... Every ounce of this valuable fiber is needed for our men in the front lines ... Warm clothes may become as essential as either food or guns ... Textile fibers from the redwoods and from yuccas are being studied. Fibers from milk casein, from soybeans and many other sources are making their appearance. (O'Brian, 1942: 513)

Military textile requirements had the effect of restricting supplies available for the civilian market as the needs of the forces escalated and those fibres which were available for the domestic market were of lower quality. A 1944 survey undertaken by the American Bureau of Human Nutrition and Home Economics showed 'how essential fabrics were downgraded during the war' (Morrison and Fletcher, 1946: 21). An urgent search for substitute fibres was supported by American and European governments and industry. An extraordinary range of animal and vegetable protein sources, including blood, castor oil seeds, collagen, egg white, chicken feathers, fish albumen, gelatine, hair, hemp seed, hooves, horn, milk casein, soya beans, sunflower seeds, peanuts, corn (maize) zein as well as silk and wool waste were explored

for their potential to form fibres to blend with, bulk out or substitute for wool. This range indicates both the scope of the research – and possibly the randomness of some of the experimentation – in Europe, America and Japan. Only a few of these fibres reached commercial production.

Table 7.1 summarises what is so far known about the production dates, trade names and manufacturers of these first and second generation regenerated protein fibres. These included the milk fibres *Aralac* (USA) and *Lanital* (Italy) and its variants, the peanut fibres *Ardil* (UK) and *Sarelon* (USA) and the corn fibre *Vicara* (USA). Extensive research into the potential of fibres made from soya bean protein by Henry Ford and the Drackett Company does not seem to have resulted in a trademarked fibre, although a soya bean fibre was produced and used in hat felts (Brooks, 2005). Owing to persistent difficulties with the performance of regenerated protein fibres, particularly their wet strength, they were often blended with natural, man-made or synthetic fibres. However, technical and economic problems meant that the azlon fibres could not compete effectively – or economically – with either natural fibres or the newly developed synthetic fibres. They failed to become mainstream fibres and, despite the extensive time, energy, investment and promotion lavished upon them, were largely forgotten by both manufacturers and consumers (Brooks, 2007).

### 7.2.2 Surviving examples

Although some of the first generation azlon fibres were produced commercially, no surviving samples have yet been located (Brooks, 2006). Some surviving examples of the second generation fibres have been located. The vast majority are small fibre or tow samples, many of which are in the University of Leeds International Textile Archive, which holds the important collection of azlon fibres made by Ralph Marsden, an ICI employee (Walsh, 1987). Other significant holdings are in the Whitworth Museum, Manchester and the Smithsonian Institute, Washington, DC. These include samples of woven fabric swatches in both solid colours and printed designs.

### 7.2.3 Production

Production methods used for first and second generation fibres differ greatly from those developed for the third generation fibres, with a consequent impact on their respective fibre structures and properties. The following discussion of manufacturing processes therefore describes the first and second generation fibres together as their production methods have many similarities, while production methods for third generation fibres are discussed separately.

Proteins are more complex than cellulose and thus more difficult to use as a regenerated fibre source than cellulose. Wormell, a leading mid-twentieth

*Table 7.1* Production dates, trade names and manufacturers of first and second generation animal and vegetable regenerated protein fibres

Date	Fibre source	Trade names	Manufacturer
1894	Gelatin (slaughter-house waste)	Vanduara	1894 Adam Millar, Scotland Vanduara Company
1904– 1909	Milk	'casein sellwolle'	Frederick Todtenhaupt, Deutsche Kunstseidenfabrik, Germany
1930s/ 1940s		<i> Lanital</i> <i> Merinova</i>	SNIA Viscosa (Società Nazionale Industria Applicazioni), Italy, and Leumann (possibly Leumann Nobilitazioni Tessili), Italy
		<i> Caslen</i>	1949 Rubberset Co Casein fibre as replacement for horsehair
		No known trade name	Les Textiles Nouveaux, Belgium
		<i> Cargan</i>	Belgium
		<i> Casolana</i>	The Netherlands
		<i> Lactofil</i>	The Netherlands
		<i> Tiolan/Thiolan</i>	VEB Thuringisches Kunstfaserwerk 'Wilhelm Pieck', Germany
		<i> Thiozell</i>	Lódzkie Zakłady Włókien Sztucznych, Poland
		<i> Silkool</i>	1938 Kanebo, Japan
		<i> Fibrolane A, B, BX</i>	Courtaulds, UK
		<i> Lactron</i>	Unknown manufacturer
		<i> Aralac and Aralac R-53</i>	1939/1942–1948 Atlantic Research Associates, USA
1940s?	Chicken feathers	No known trade name	USA, manufacturer unknown; possibly United States Rubber Co.
1940s	Egg white	<i> Zealon</i>	Technical fibre only; Northern Regional Laboratory, USA
1948– 1957	Corn (maize)	<i> Vicara</i>	Virginia-Carolina Chemical Corp., Richmond, VA, USA
		<i> Zycon</i> used with animal fibres in hat felts	Virginia-Carolina Chemical Corp., Richmond, VA, USA
1935– 1957	Peanuts (groundnuts)	<i> Ardil</i>	Imperial Chemical Industries (ICI), UK
		<i> Fibrolane C</i> <i> Sarelon</i>	Courtaulds, UK US Department of Agriculture
1939– 1946?	Soya beans	No known trade name No known trade name	Ford Motor Company, USA Drackett Products Company

IP Address: 129.132.211.108

century British researcher, noted that unlike 'cellulosic fibres [which] are regenerated immediately on coagulation ... protein filaments have to be cross-linked if fibrous products are to be obtained' (1954: 19). Briefly, the process required the isolation of the protein from the source material, then

its solubilisation so it could be extruded into a coagulating bath followed by various after-treatments so that the fibres thus formed could be stabilised by creating cross-linkages. In practice, this was a delicate process which required careful management and considerable understanding (or intuition in the case of the earlier researchers) into the nature of the processes of protein denaturation and fibre formation.

Five main production stages can be identified, normally including the following:

1. Separation of the protein

If the protein was not in a readily accessible form, the first stage was to render the source protein into a suitable form for producing a fibre. In the case of milk or peanuts, this required the removal of fats and oils from the source protein, leaving a solid curd which had to be washed and dried and was then often ground into granules. The preparation of this curd was a delicate process. One of the reasons for the relative success of Ferretti's Italian milk fibre as opposed to that of Todtenhaupt's German fibre was the former's insistence on the type and quality of the casein curd used (Wormell, 1954: xv).

2. Solubilisation

This was required in order to produce a spinning solution. For proteins such as gelatine, this was the first stage and was relatively straightforward. Once obtained from slaughterhouse waste, the gelatine was dissolved in either hot water and potash or glacial acetic acid. If the protein took the form of curd or granules, this needed to be dissolved in a suitable solvent to form a 'spinning' solution with a high solids content. This solution was usually allowed to mature to improve viscosity, although careful control of oxidation and bacterial activity was vital during this process. Lundgren and O'Connell (1944: 372) used a synthetic detergent to create a viscous solution.

3. Extrusion

The ripened solution was then forced through spinnerets, usually into a coagulation bath, resulting in the formation of fibres, a process described contemporaneously as 'spinning'. These baths were usually salt and acid baths, such as sodium, aluminium or magnesium sulphate and sulphuric acid. The osmotic pressure created by the salt caused the diameter of the newly extruded filaments to shrink, thus strengthening them and minimising their tendency to clump together.

4. Insolubilisation (often called 'hardening')

The aim of the insolubilisation treatment was to encourage the formation of networks between protein chains with sufficient cross-links to improve the wet strength of the resulting fibre, but not with too many, which would result in an over-rigid structure (Wormell, 1954: 90). Acid baths

of formaldehyde were often used and the filaments could be stretched at the same time in an attempt to improve the parallel orientation of the molecules to the fibre length, resulting in better wet and dry strength. Lack of strength in the hot baths required for processing such as dyeing was a persistent problem. A delicate balance of acidity level and temperature was required to improve resistance to boiling water without damaging the fibre's physical appearance or properties. Acetylation, sometimes using acetic anhydride at temperatures of 80°C or above, could be used to improve colour, handle and dyeing performance (Traill, 1951: 268). An alternative method was to expose newly formed fibres to formaldehyde vapours.

#### 5. Washing, cutting and further production processes

The resulting tow was washed and dried and could then be cut into staple lengths. Further processing could be undertaken using standard textile techniques and machinery.

It should be remembered that certain processes could be carried out simultaneously or in a different order. For example, insolubilisation could be achieved by mixing the requisite chemicals into the liquid protein before extrusion, adding them to the coagulating bath or introducing them as an after-treatment in either a chemical bath or vapour.

### 7.2.4 Identification

The first step in understanding the fibre characteristics of the surviving first and second generation regenerated protein fibres is identifying those fibres which may have survived. This can be difficult as the makers were, obviously, striving to replicate the chemical content of silk or wool and physical structure as closely as possible. For example, Millar was aiming to use protein derived from blood or egg albumen, milk casein or vegetable albumen in combination with metallic compounds to produce fibres which were chemically and physically comparable in flexibility, elasticity and tensile strength to silk, wool and hair (BP patent 6,700 1898/1899). Furthermore, regenerated fibres themselves were very similar to one another and so can be hard to distinguish. The peanut fibre *Aralac* had similar physical and chemical properties to those of the milk fibre *Lanital* (Park and Shore, 1999: 208). Identification is further complicated by the fact that regenerated protein fibres are usually found as blended yarns or in mixed fibre fabrics, which may also be protein fibres, so it is necessary to distinguish and identify the different fibres one from another and sample yarns from both the warp and weft direction. As noted, matters are made more challenging by the fact that there are few – or in some cases no – samples available for testing, and firmly identified comparators are rare.



Techniques used to identify regenerated protein fibres include traditional methods of identification such as burn tests (Carroll-Porczynski, 1961: 43, 45, 47), microscopy, stains or measuring fibre density. Tests such as those described by the Textile Institute (1975) may be useful to establish the presence of protein fibre, although these tests, of course, do not always distinguish a regenerated protein fibre from a natural protein fibre. Some methods do enable this. Moncrieff (1975) noted that casein, peanut, soya bean and zein fibres will all give a yellow-orange colouration with cold Shirlastain A stain. Evans *et al.* (1947) reported that acetylated zein fibre gives a weak colour reaction with Millon's reagent as opposed to the very dark red colouration of non-acetylated zein fibres. Measuring fibre density or specific gravity was the established method of distinguishing azlon fibres in the industry. The peanut fibre *Ardil* (specific gravity 1.31) could thus be distinguished from casein fibres (specific gravity 1.29). Methods such as conventional and polarised Fourier-transform infrared (FT-IR) spectroscopy now offer the possibility of more precise identification of specific types of regenerated protein fibres if comparative spectra of known fibres are available (Fig. 7.1).<sup>1</sup>

### 7.2.5 Characteristics

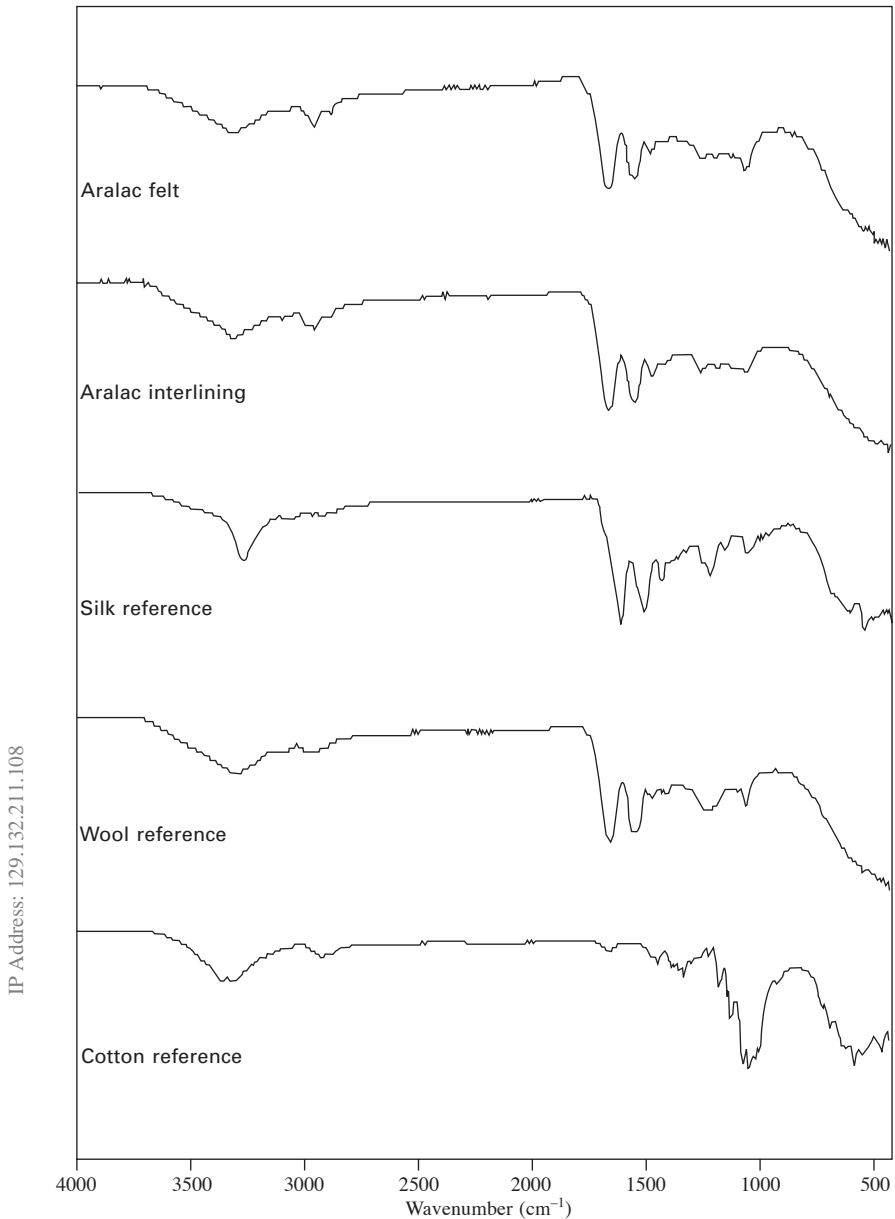
To aid comparison between the different fibres – and to help clarify which fibres are not regenerated protein fibres, although they are made from protein sources – their respective physical structures will be discussed by protein source in alphabetical order. The fibres are generally similar chemically, sharing as they do the goal of mimicking a protein fibre. At a microscopic level, regenerated protein fibres tend, like synthetic fibres, to be smooth, uniform and almost featureless, although they do have some differentiating features such as longitudinal striations. Cross-sections tend to be round, although this depends on the form of the spinnerets used in the extrusion process.

#### *Blood*

Blood as a source for fibres was mentioned in some of the earliest patents for the first generation of regenerated protein fibres and in one patent dating from the second generation. Interestingly the latter foreshadows the third generation fibres in that it seeks to combine protein-based fibres with synthetic materials in an attempt to gain the benefits of both while minimising their disadvantages. However, there is no evidence that any fibres were made commercially from blood or from blood/synthetic fibre mixtures, and blood seemed to have disappeared rapidly from proposed sources. Millar's 1898

---

<sup>1</sup> See the Notes at the end of this chapter.



7.1 ATR FT-IR spectra of *Aralac*, silk, wool and cotton (taken by Paul Garside, Textile Conservation Centre).

patent (BP 6,700 1898) claimed that filaments produced from blood albumen were 'similar in chemical composition to silk, wool, hair and other insoluble animal products'. In order to achieve insolubility in water, Millar treated the

air-spun fibres with a variety of agents including 'formic-aldehyde', alum, chrome alum, 'bichromate of potass' or metallic compounds. Du Pont's 1941 patent (BP 550,022) proposed combining different proteinaceous materials including globin from blood haemoglobin with synthetic linear polyamides or interpolyamides, using them almost as a form of plasticisers to form films or fibres. Little technical data is available on the physical characteristics of either of these blood fibres. Millar claimed his blood albumen fibre had greater flexibility, elasticity and tensile strength than fibres made from gelatine or albumen. Similarly, du Pont reported that their combined blood globin/synthetic fibre had good strength, flexibility and pliability. No data comparing such fibres with other natural or man-made fibres has yet been found and no surviving examples are known.

### *Egg albumen*

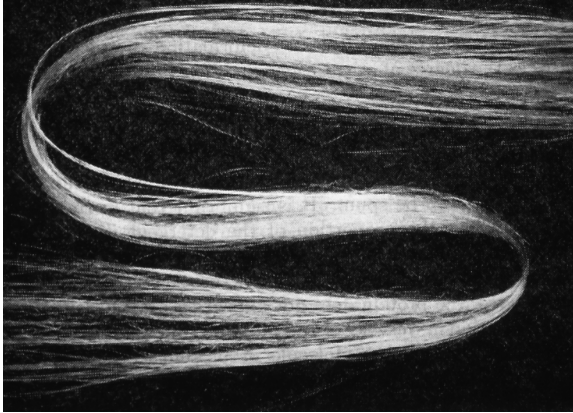
Millar used the same method to produce fibres from egg albumen as he had for fibres from blood albumen but with the addition of aluminium chloride to improve the viscosity of the spinning solution and the strength of the resulting fibre (patent BP 6,700 1898). As with his blood fibre, Millar claimed the resulting egg albumen fibres were similar to the natural protein fibres. No fibres appear to have been produced commercially and no samples are known. In the 1940s Lundgren and his co-workers at the US Department of Agriculture Western Regional Research Laboratory researched the potential of egg albumen for fibres using detergents as a solvent and a salt coagulation bath (Lundgren and O'Connell, 1944: 373). The surviving samples of an egg white fibre named *Zealon* were made by Northern Regional Laboratory (Walsh, 1987) but the fibre does not seem to have been produced commercially. Under microscopic examination these egg white fibres were smooth with some darker flecks (Fig. 7.2).

IP Address: 129.132.211.108

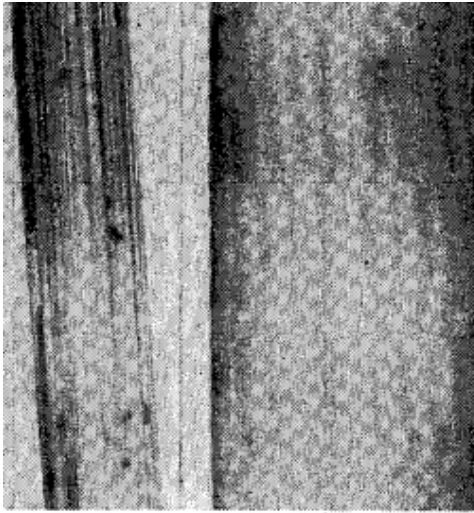
### *Feathers*

Feathers were explored as sources for fibres in the 1940s by researchers in the Western Regional Research Laboratory of the US Department of Agriculture. As with the egg fibres, detergents were used to 'unwind' the protein chains (Traill, 1951: 263) before extrusion into a coagulating salt bath (Lundgren and O'Connell, 1944: 373) and orientation in steam. Experimental fibres were reported to have a feather content of 60–70% (Sherman and Sherman, 1946: 309). Chicken feather fibres were used for blankets by the American military, although their use was discontinued on account of their smell (Anon., 1945). The United States Rubber Company developed a blended fabric using chicken feathers for women's suits and dresses.

Microscopically, feather fibres were similar to other regenerated fibres



(a)



(b)

7.2 (a) Regenerated and stretched technical egg white fibres; (b) left, a polyfilament egg albumin thread, spun mechanically and containing 100 filaments fused together; right, a single egg albumin filament drawn by hand (Lundgren and O'Connell, 1944: 373).

with some striations and flecking, depending on the degree of bleaching. Feather keratin is finer than wool keratin ( $5\ \mu\text{m}$  rather than  $2\text{--}30\ \mu\text{m}$ ). It therefore has a very high surface area, making it an excellent absorbent but also meaning that moisture is retained by the fibre when it is saturated. The fibre was said to be softer, warmer and lighter than wool with a high lustre (Sherman and Sherman, 1946: 309).

*Fish and whale flesh*

Hamor (1941) reported on a Japanese wool substitute made from whale or shark meat protein hardened with formaldehyde, which may have been a regeneration process.<sup>2</sup> Little evidence has yet been found about the physical characteristics of such fibres.

*Gelatine*

Gelatine is a collagen protein derived from animal slaughterhouse waste including hides, hoof and horn. Gérard's 1887 patent (BP 2694) proposed extruding a 'gelatine solution through small orifices, to form threads in a gaseous medium such as ammonia or superheated steam' (Wormell, 1954: xiv) although none was produced commercially (Koch, 1972: 27). Millar's gelatine fibre *Vanduara* was patented in 1894 (BP 15,522) and produced commercially in his factory in Paisley, Scotland (Koch, 1972: 27). *Vanduara* had coarse threads of 40 µm (Koch, 1972: 27) but was said to be a 'beautifully lustrous fibre' (Barker, 1919: 59). By 1919, Barker reported that *Vanduara's* wet strength problems meant that 'it is now little, if at all used' (1919: 60). The Arthur B. Little laboratories of Boston, USA made a purse from gelatine as a laboratory experiment to disprove the proverb that 'You can't make a silk purse from a pig's ear'.<sup>3</sup> This was a promotional project intended to demonstrate the value of research and had no commercial application (Arthur D. Little, 1921). Other fibres were produced from animal sources during the 1940s and 1950s using mechanical treatments rather than regeneration processes.<sup>4</sup>

*Milk casein*

The casein found in milk formed the basis of some of the most successful regenerated protein fibres despite the fact that the globulin protein in milk lacks the straight chain typical of the linear polymers found in most fibres. The production process therefore needed to first straighten the protein and then retain it in an orientated form. Millar's 1890s patents seem to be the first recorded attempt to exploit the fibre-forming potential of milk, although he does not appear to have been successful in producing a viable fibre. In the early twentieth century, the German chemist Todtenhaupt patented a process for making milk casein into fibres. He intended this to be a substitute for artificial silk (itself a regenerated cellulosic fibre imitating a natural fibre) and horsehair. Unfortunately, his production company Deutsche Kunstseidenfabrik failed and little successful research seems to have been carried out until the 1930s when Ferretti, an Italian scientist, modified Todtenhaupt's method to improve the fibre's wet strength. The resulting casein fibre was produced

commercially by the Italian textile conglomerate SNIA Viscosa. By 1940 at least eight countries were producing casein fibres including *Lanital* and *Merinova* in Italy, *Casolana* in Holland, *Polan* in Poland, *Tiolan* and *Thiozell* in Germany, *Cargan* in Belgium and *Fibrolane* in England, as well as Japan, France, Canada and Czechoslovakia. Licensed production of the Italian milk fibre continued in Europe until the 1960s (Koch, 1972: 30).

In America, Atlantic Research Associates, National Dairy's spin-off company, produced and marketed a viable milk fibre trademarked *Aralac*. The interest and involvement of the US government in alternative fibre sources is further demonstrated by the public service patents for milk fibres issued by Earle O. Whittier and Stephen P. Gould, chemists working for the Bureau of Dairy Industry, Department of Agriculture. In England, Courtaulds had the rights to Ferretti's casein fibre process but did not produce *Fibrolane* commercially in any quantity. Milk fibres were used for clothing and domestic textiles in blends with wool, cotton and rayon.

Of the first generation milk fibres, Todtenhaupt's description of his own casein fibre suggested that he had undertaken some systematic analysis. He stated that it 'fairly accurately resemble[d] natural silk, having a percentage of nitrogen from about fifteen to sixteen per cent' (1905/1906 US patent 836,788). The chemical composition of wool, *Fibrolane* and *Aralac* are compared in Table 7.2.

The significantly lower sulphur content in *Fibrolane* and *Aralac* should be noted, as this indicates that the important cystine cross-links found in wool were not present in the casein fibre. In consequence, casein fibres had less strength and resistance to chemical attack. Whittier and Gould noted that their fibre had not been analysed for its sulphur content so 'we do not know how it compares with *Lanital* in this respect' (Whittier and Gould, 1939: 374).

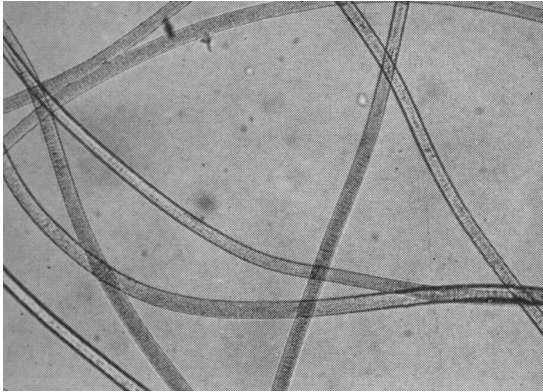
In his 1906 patent (US 836,788), Todtenhaupt asserted that Millar's milk fibre was brittle but his casein fibre was, in turn, criticised for being hard, brittle and having a tendency to stick together. Park and Shore (1999: 208) reported that *Aralac*'s characteristics were closer to chlorinated wool than to natural wool. *Aralac* was produced in fibre widths of 15–30  $\mu\text{m}$

Table 7.2 Chemical composition of wool and casein fibres (Byrne and Johnstone, 1987: 14; Moncrieff, 1970: 296)

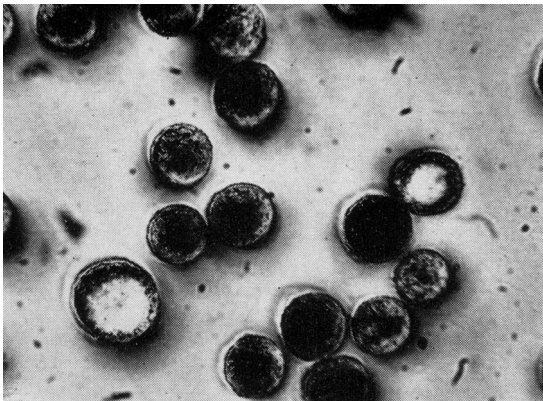
Element	Wool (%)	<i>Fibrolane</i> (%)	<i>Aralac</i> (%)
Carbon	49.2	53.0	53.0
Hydrogen	7.6	7.0	7.5
Oxygen	23.0	23.0	23.0
Nitrogen	15.9	15.5	15.0
Sulphur	3.6	0.7	0.7
Phosphorus	–	–	0.8



and lengths of 0.5 to 6 inches (12.7 to 152.4 mm). Microscopically, the fibres were uniform, smooth and almost featureless, having faint striations and some surface graininess (Fig. 7.3). Moncrieff reported pitting, which enabled these fibres to be easily recognised (1970: 299). In cross-section, they were almost circular. Delustrants showed up as small specks in dulled fibres (Harris, 1954: 81).



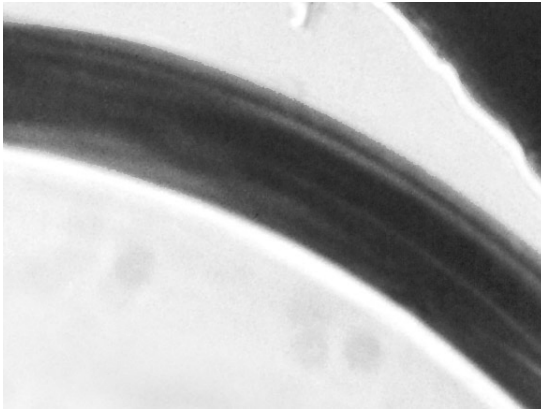
(a)



(b)

7.3 (a) Longitudinal view ( $\times 75$ ) of mid-twentieth century milk protein fibre *Aralac* (Harris, 1954: 81); (b) cross-sections ( $\times 380$ ) of mid-twentieth century milk protein fibre *Aralac* (Harris, 1954: 81); (c) *Aralac*/wool fibres from Merrimac hat (private collection) (copyright of the author); (d) SEM image of *Aralac* fibre. Sample supplied by Dr Kathryn Jakes, Ohio State University, April 2005. SEM image collected at  $300\times$ , with uncoated sample on carbon tape. Copyright: Scientific Research Lab, Museum of Fine Arts, Boston, MA; reproduced by permission.





(c)



(d)

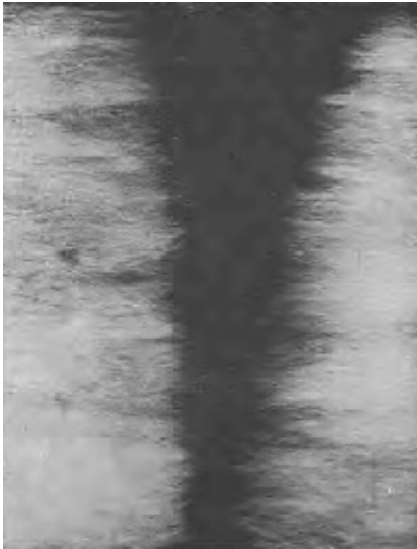
## 7.3 Cont'd

One of the most important characteristics of the second generation of milk casein fibres such as *Aralac* and *Fibrolane*, and in marked contrast to the regenerated cellulose, was their wool-like warmth, softness and good hand. Figure 7.4 shows the close resemblance of *Lanital* and wool fibres at a macro level.

Finer grade fabrics of 100% *Aralac* were said to feel like angora while coarser grades were like sheep's wool (Dirks, 2000: 81). Gould's and Whittier's fibre was said to be like the best quality carded Merino wool.

### *Peanuts (groundnuts)*

Imperial Chemical Industries (ICI) produced the British peanut fibre *Ardil* in 1951, although Astbury and Chiball had patented the original process in 1936



7.4 *Lanital* fibres (left) and wool fibres (right) (Anon., 1939: 33).

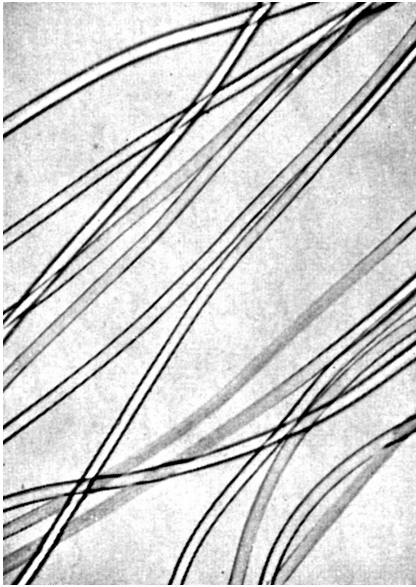
(BP 467,704) and early development work had been undertaken before the war. Intended as an alternative product for ICI's redundant explosives factories, *Ardil* was used for clothing, curtains and carpets. Its poor wet strength and uncompetitive price in comparison to wool meant that production ceased in 1957 (Brooks, 1993). Neither the American peanut fibre *Sarelon* developed by the US Department of Agriculture nor Courtaulds' version *Fibrolane C* seem to have been very successful.

Chemically, *Ardil* was very close to wool and *Fibrolane* although it contained some phosphorus (Table 7.2). Microscopically, peanut fibres are similar to casein and soya bean fibres. They appear translucent and almost featureless. In longitudinal section, they are straight and uniform, although there may be some longitudinal striations and a faint granular pattern on the otherwise smooth surface. The cross-section is generally circular, although some have a small marginal indentation (Harris, 1954: 82). Figure 7.5 shows micrographs of peanut fibres.

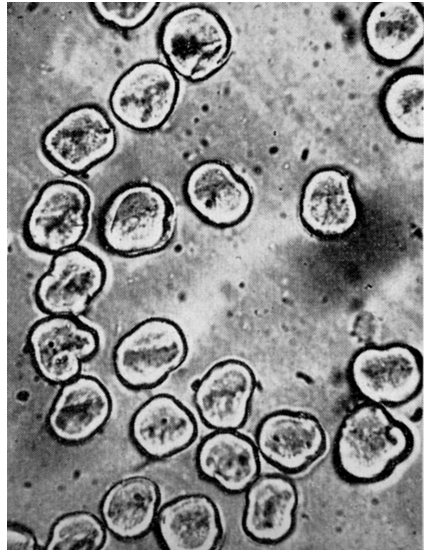
As a staple fibre, peanut fibre had many of the qualities of wool, being warm, soft and resilient. It had a slight lustre and was produced in a variety of cream to buff colours.

#### *Soya bean fibre*

The US Department of Agriculture, Atlantic Research Associates and Ferretti were all interested in soya bean protein as an alternative to milk casein, but Henry Ford emerges as the champion of soya bean fibres (Brooks, 2005). Soya



(a)



(b)



(c)

7.5 (a) Longitudinal view ( $\times 75$ ) of mid-twentieth century peanut fibre (Harris, 1954: 82); (b) cross-sections ( $\times 380$ ) of mid-twentieth century peanut fibres (Harris, 1954: 82); (c) fibre stained with Shirlastain A from *Ardil* blend nightdress, Wallis Archive, York Castle Museum, UK (Museum No. 431.78). This fibre appears to have more striations (York Museums Trust (York Castle Museum)).

beans formed an essential part of his vision of ‘farm chemurgy’, industrial production based on natural materials. His research laboratory explored the industrial potential of soya beans as plastic for car bodywork and as fibres for upholstery fabrics and fillings and produced soya bean fibre between 1939 and 1942 (Sherman and Sherman, 1946: 183). Always a brilliant publicist, Ford paraded in a soya bean and wool fibre suit which was apparently both rather weak and itchy to wear. Unsuccessful in persuading the armed forces to use this fibre, Ford sold the process to the Drackett Company who had supplied his source soya bean protein *alysol* (Sherman and Sherman, 1946: 183). Drackett successfully manufactured soya bean fibre for hat felts, and possibly some yarn, until 1949. The Japanese soya bean fibre *Silkwool* produced in 1938 was not a technical success (Araki *et al.*, 1946).

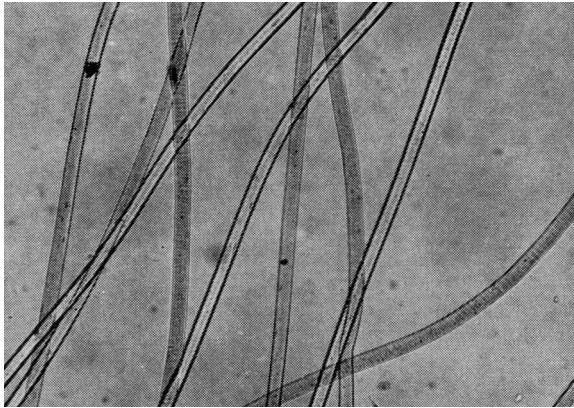
Soya bean fibres were produced as continuous filaments and as staple fibres between 0.25 and 6 inches long (6.35–152.4 mm) with a fibre width of 14–27  $\mu\text{m}$ . Seen under magnification, soya bean fibres were translucent and uniform with a smooth surface, although some granulation and streakiness was often visible. The cross-section was almost circular (Fletcher, 1942: 15; Harris, 1954: 82). Figure 7.6 shows micrographs of soya fibres.

Ford’s process apparently resulted in a white fibre whereas Drackett’s fibre was light tan to white (Wormell, 1954: 168). The staple fibre was described as ‘a loose, fluffy mass with a resemblance to scoured wool’, soft to touch, with a natural crimp and good resiliency (Sherman and Sherman, 1946: 185).

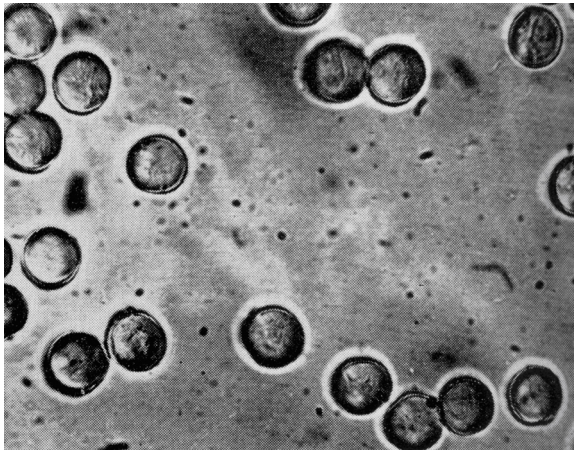
### Corn (*maize*)

Although Ostenberg first patented a process for the production of fibres from zein, the alcohol-soluble protein (prolamin) obtained from corn, in 1919 (US Patent 1,316,854), it was not until Swallen’s 1939 patent (US Patent 2,156,929) that a more commercial process was developed. The zein solution could be either dry or wet spun from a solution containing zein and formaldehyde. The fibres were baked after extrusion to complete the zein formaldehyde cure and to achieve good wet strength (Lawton, 2002: 11). US Department of Agriculture scientists Croston, Evans and Smith undertook research into the production of zein fibres, including hardening methods using formaldehyde methods and acetylation to improve hand and water resistance. The Virginia-Carolina Chemical Corporation, working in cooperation with Evans and Croston, produced zein fibre from 1948 to 1957 (Brooks, 2006). Two versions were produced: *Vicara* for use in wool, cotton and nylon blends, and *Zycon* for hat felts.

Zein fibres were produced in lengths of 0.5 to 6 inches (12.7 to 152.4 mm) and in widths of 12–23  $\mu\text{m}$ . Microscopically, zein fibres were similar to casein and soya bean fibres. They were translucent with relatively smooth



(a)



(b)

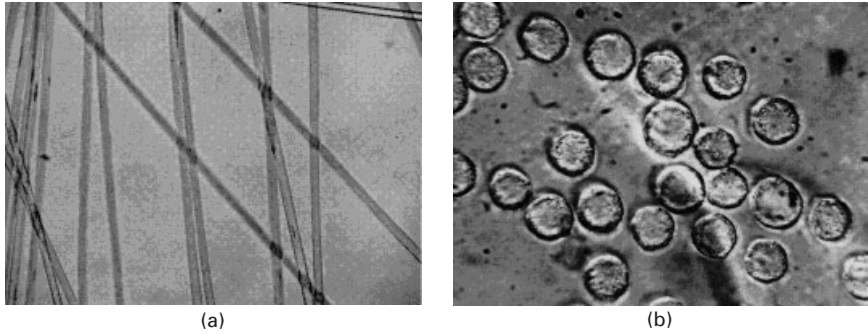
7.6 (a) Longitudinal view ( $\times 75$ ) of mid-twentieth century soya bean fibres (Harris, 1954: 82); (b) cross-sections ( $\times 380$ ) of mid-twentieth century soya bean fibres (Harris, 1954: 82).

surfaces but some granularity and occasional short longitudinal striations. In cross-section, the fibres were round and uniform except for the coarser fibres which tended to be more like flat ribbons and were less uniform (Harris, 1954: 81). Figure 7.7 shows micrographs of zein fibres. *Vicara* was said to be a soft, warm, light-gold and bleachable fibre with a silky lustre and smooth feel which blended well with nylon, cotton and wool.

### 7.2.6 Behaviour

The paucity of surviving artefacts means that finding data with which to corroborate – or contradict – contemporaneous evidence for the behavioural





7.7 (a) Longitudinal view ( $\times 75$ ) of mid-twentieth century zein fibres (Harris, 1954: 81); (b) cross-sections ( $\times 380$ ) of mid-twentieth century zein fibres (Harris, 1954: 81).

properties of the first and second generation fibres is challenging. In some cases, the available documentary evidence may be partial or simply does not exist; the data available is not comprehensive and often uses different measures, making accurate comparison difficult. However, enough contemporary textual evidence exists to enable key qualities to be identified and comparisons made between the different fibre types and those of natural fibres. This section seeks to summarise and compare available evidence for the properties of the main regenerated protein fibres; this is summarised in Table 7.3. Where relevant, comparisons are made with other natural and man-made fibres.

Some aspects of the behaviour of regenerated protein fibres were satisfactory or comparable to wool. For example, like wool, regenerated protein fibres tended to be easily damaged by alkalis. Casein and soya bean protein fibres had similar moisture absorption properties to wool. They do not seem to have been more susceptible to ultraviolet light than other protein fibres, suffering no serious degradation unless exposed to exceptional levels. They were inflammable, although they tended to yellow if heated for short periods at  $100^{\circ}\text{C}$  and rapidly decomposed at  $150^{\circ}\text{C}$ . Second generation azlon fibres were generally stable in organic solvents. Casein fibres were reported to be stable in perchlorethylene and white spirit (Cockett, 1966: 77). The lack of fibre scales meant that azlon fibres such as casein did not felt like wool nor shrink when washed in hot water, although it could be used in combination with wool to make blended felts and seemed to improve felting qualities (Dirks, 2000: 81).

Opinions varied as to the resistance of azlon fibres to pest and microbial activity, a quality which had obvious commercial implications. Some claimed casein fibres were mothproof whereas others stated they could be attacked by moth and suffered from mildew (Cockett, 1966: 77; Byrne and Johnstone, 1987: 14). Whittier and Gould sensibly pointed out that ‘a suit of casein

Table 7.3 Behavioural properties of first and second regenerated protein fibres in comparison to wool (Caroll-Porczyński, 1961: 43, 45, 47; Cockett, 1966: 77; Dirks, 2000: 81; Koch, 1972: 30; Lawton, 2002: 11; Lundgren and O'Connell, 1944: 373; Press, 1959: 110; Sherman and Sherman, 1946: 20, 21, 193)

Behavioural properties	Chicken feather keratin	Egg albumin (USA)	Gelatine: <i>Vanduaara</i> (Scotland)	Milk: Todtenhaupt (Germany)	Milk: <i>Aralac</i> (USA)	Milk: <i>Janital</i> (Italy)	Milk: <i>Merinova</i> (Italy)	Milk: Fibrolane C (USA)	Soyabean 1940s (USA)	Soya: <i>Silkool</i> (Japan)	Peanut: <i>Ardil</i> (UK)	Zein: <i>Vicara</i> (USA)	Wool
Specific gravity					1.29			1.3	1.31		1.3	1.25	1.28–1.33
Density (g/cm <sup>3</sup> )			1.37	1.29		1.30	1.30			1.30	1.30		1.33
Breaking strength (1000 lb/sq.in)	Dry-up to 80	20–70 <sup>1</sup>			Commercial casein up to 10 <sup>1</sup>				Commercial soya bean up to 10				17–25
Moisture regain (%)								Approx. 14			13–15	10.0	
Moisture uptake at 65% RH						13.5–14	13.5–14			11.5	15	13	14.5
Tenacity conditioned (p/den)			0.55	0.64		1.0–1.2	1.0–1.2			0.55		1.1–1.3	1.1–1.8
Breaking strength (thousands lb/sq in)	Up to 80	20–70			Up to 10				Up to 10				17–25
Breaking extension (%) conditioned								50–60			40–60	25–35	
Breaking extension (%) wet								60–70			50–70	30–45	
Extension at break (% orig. length)			4.5	3.8				50–70		5.1	30–35	30–35	28–48



Table 7.3 Cont'd

Behavioural properties	Chicken feather keratin	Egg albumin (USA)	Gelatine: <i>Vanduaara</i> (Scotland)	Milk: Toddenhaupt (Germany)	Milk: <i>Aralac</i> (USA)	Milk: <i>Lanital</i> (Italy)	Milk: <i>Merinova</i> (Italy)	Milk: Fibrolane C (USA)	Soyabean 1940s (USA)	Soya: <i>Silkool</i> (Japan)	Peanut: <i>Ardil</i> (UK)	Zein <i>Vicara</i> (USA)	Wool
Extensibility – dry (elongation at break) (%)					30–50				30–40				30–50
Extensibility – wet (elongation at break) (%)					85–120				60–70				30–60
Elastic recovery					Poor			High			40–60	80% at 5%	
Relative wet tenacity (% of conditioned tenacity)			7.4	18.7		40–55	40–55			44.2	50–70	45–55	76–87
Tensile strength (g/denier) conditioned								1.0–1.1			0.7–0.9	1.2–1.5	
Tensile strength (g/denier) wet	Wet strength significantly lower	Wet strength much less				50–35		0.5–0.6	30		0.4–0.6	0.65–0.8	0.9
Tenacity, dry (g/den)					0.6–0.8				0.6–0.7				1.2–1.7
Tenacity, wet (g/den)									0.35 <sup>5</sup>				
Wet tenacity % of dry tenacity					40%–50%				35%–50%				80%–90%

fibre that had hung in a damp basement through a summer would probably be badly damaged but so would a wool suit' while noting that 'reliable authorities have stated that casein fibre is moth resistant' (Whittier and Gould, 1939: 374). Manufacturers claimed that casein fibres were resistant to moths but Cockett and Dirks both supported Whittier's and Gould's view that these fibres could be severely attacked by mildew and were attractive to moth larvae (Cockett, 1966: 77; Dirks, 2000: 81).

Other aspects of their behaviour were more problematic. Poor abrasion resistance was a persistent problem. Azlon fibres tend to be resistant to cold and hot dilute acids but were susceptible to concentrated acid. Casein, for example, disintegrated and dissolved in concentrated acid. They were also more sensitive to alkali than wool, swelling and disintegrating in alkaline baths. Such behaviour obviously presented problems in dyeing and other after-treatments and in after-care. However, their overwhelming problem was that of poor strength. Dry tenacity tended to be less than wool, itself a fibre which has low tenacity in comparison with other natural and synthetic fibres, but tenacity dramatically worsened when the fibre was wet. This was particularly true of the first generation fibres. Millar's gelatine fibre *Vandua* swelled more in water than any other fibre, showing a 130% increase in thickness (Koch, 1972: 27) and became 'extremely tender' (Barker, 1919: 59).

In his 1905 patent (US 836,788), Todtenhaupt asserted that Millar's casein fibre absorbed water so readily it could not be used but his own casein fibre is reported to have lost 90% of its strength when wet (Fletcher, 1942) and had a tendency to stick together. The problem persisted with the second generation regenerated protein fibres. Casein fibres lost 40–50% of their dry strength when wet with a regain of only 14%, making them 10–20% weaker than rayon. In addition, some claimed that *Aralac* had the unpleasant quality of having 'an odour similar to that of spoiled milk' when wet (Dirks, 2000: 81). Others contested this. Moncrieff argued that wet *Lanital* smelt 'cheesy' but, because *Aralac* had undergone an acetylation process, it did not smell when wet (1970: 297). Soya bean fibres lost 35–50% of their dry strength when wet in comparison with wool which loses about 15% of its dry strength when wet (Sherman and Sherman, 1946: 22, 185). Zein fibres had particularly low tensile strength (Lawton, 2002: 13). Azlon fibres consistently exhibited high elongation (an indication of poor strength) and elasticity, particularly when wet, and performed badly in comparison to wool. The lack of an ordered molecular structure in azlon fibres, tending more to random coiling or folding than to parallel orientation, contributes to their low wet tenacity.

The number of patents filed by researchers and manufacturers seeking to improve the poor wet strength of these fibres indicates that this was a persistent problem. Traill and Simpson's 1947 patent (BP 639,342) for ICI is one such example. This proposed a method for improving the wet strength

of casein, peanut and soya bean fibre using ionisable mercury salt. Atwood's 1944 and 1946 patents (US 234,994; US 2,408,026) described acetylation treatments to improve the performance of casein fibres. Evans *et al.* (1947) also claimed that acetylation improved water and boil resistance, whitened fibres by removal of yellow pigments and slowed dye uptake. Acetylation also moderated reaction with formaldehyde so reducing shrinkage and helping to ensure the fibres remained soft and separated readily. Chemical crosslinking could be used to overcome this to some extent in the case of zein fibres. Alternatively, these physical weaknesses could be addressed by blending with natural or man-made fibres. For example, Picard, Bonnet and du Pont claimed in their 1937 patent (US 2,224,693) that regenerated casein–viscose blend fibre containing 35% casein had better tenacity than most wool fibres and much better than that of 100% casein fibres.

### 7.3 Third generation regenerated protein fibres

#### 7.3.1 Development

Interest in regenerated protein fibres revived in the late twentieth and early twenty-first centuries thanks to innovations in biotechnology, the existence of compatible synthetics and the demand for fibres to have a reduced ecological footprint. Regenerated protein fibres with different structures and different properties are being developed, often with a stress on imitating silk rather than wool (Hudson, 1997). It has taken some time for these fibres to become economically as well as technically viable. The Japanese produced a milk/acrylic fibre called *Chinon* in the 1970s but it is said to have been very expensive and production ceased quickly (Kiplinger, 2003). Interest is focusing primarily on milk and soya beans as protein sources, although chicken feathers are also being researched. These fibres are being promoted as forming luxurious and high-quality niche fabrics. Technically, these fibres usually aim to exploit the soft hand and lustre of the protein element while adding strength and durability through the addition of a synthetic resin. These fibres are also claimed to have ecological benefit. Soya bean fibres may become a substitute for cashmere, reducing the number of grazing cashmere goats and thus helping to minimise desertification in China (Woolmark Company, 2001). Others are said to be biodegradable (BharatTextile, 2001). Chinese milk fibres have passed the Oeko-Tex Standard 100 green certificate for ecological production (Swicofil, n.d.a).

#### 7.3.2 Production

The technical innovations which are enabling the production of a third generation of azlon fibres include the use of biochemistry to modify the structure of the source protein and the incorporation of synthetic materials such

as polyvinyl alcohol (PVA) to improve fibre strength and modulus (Garside and Brooks, 2006). Fibres which seek to be simulations of either wool or silk or to have their own characteristics are being developed. Bicomponent structures are used to create fibres which combine increased strength and durability with lustre and a soft hand, for example a PVA or acrylonitrile (AN) core surrounded by an outer sheath of a protein such as soya or milk (Brooks, 2005; Zhang *et al.*, 1999).

Guanqi Li<sup>5</sup> has led Chinese soya bean fibre research, both establishing commercial companies and undertaking research, the latter with the support of the Chinese government (Fong, 2004). His company, the Shanghai Winshow Soybean Fibre Industry Co. Ltd, is now marketing the Jianghe TianRongSi Fiber soybean protein fibre, sometimes just referred to as 'SPF' (Shanghai Winshow, 2004). American research, much of it undertaken at the Georgia Institute of Technology, has focused on developing bicomponent monofilament fibres with soya bean protein and PVA or polyacrylic acid (Kotliar and Ghasemzadeh, 1994; Zhang *et al.*, 1999). These third generation soya bean fibres are spun using a wet spinning process and stabilised using hydroformylation before standard textile processing (Yi-You, 2004: 8). Soya bean fibre is available as a pure fibre or in blends with cashmere, wool, cotton and synthetic fibres (Brooks, 2005).

Bio-engineering and a wet spinning process are being used to produce the new generation of milk fibres. Grafting has been used to combine casein with acrylonitrile as it is thought to have less effect on fibre strength and mechanical behaviour (Dong and Gu, 2002). Micro-zinc ions incorporated in the fibre enhance durability and give the fibre anti-bacterial properties. Professor Yiqi Yang of the University of Nebraska-Lincoln, USA, is using a regenerated approach to produce chicken feathers but one that differs from Lundgren and O'Connell's work.<sup>6</sup> This research is aiming to produce biodegradable substitutes for wool and synthetic fibres (Hill, n.d.; Hull, 2006: 16).

Ecological concerns are also influencing production methods and selection of source materials such as soya bean, wheat gluten and corn (Huda *et al.*, 2007). Euroflax Industries (n.d.), who market milk fibre in India, report that these third generation fibres are produced in an environmentally friendly way using a graft copolymerisation method which does not require formaldehyde. Investigations are being undertaken at the Institute of Textile Technology, Charlottesville, VA and the University of Illinois into a new formaldehyde-free environmentally friendly zein fibre which would have high resilience, absorbency, elongation and dyeability (Yang *et al.*, 1996). This uses a dry spinning method with polycarboxylic acids as crosslinking agents to avoid the use of environmentally problematic chemicals such as formaldehyde (Lawton, 2002: 13). Although the use of non-toxic citric acid or butane-tetracarboxylic acid did allow the production of a high resiliency experimental fibre with

breaking tenacity of 1 g/d, elongation of 30% and good boiling resistance, the researchers acknowledge that problems remained with low orientation and crystallinity (Yang *et al.*, 1996). Nevertheless, there is sufficient interest in such alternative fibres for companies such as DuPont to have filed a patent for the dry spinning of zein fibres (1997 US Patent 5,750,064).

### 7.3.3 Identification

In addition to the methods discussed above to identify proteins, it is necessary also to establish the nature of any synthetic material present in third generation azlon fibres. ATR FT-IR analysis enables the nature of the co-polymers, such as PVA or polyacrylonitrile, to be identified; see Fig. 7.8 (Brooks and Garside, 2005; Garside and Brooks, 2006).

### 7.3.4 Fibre properties

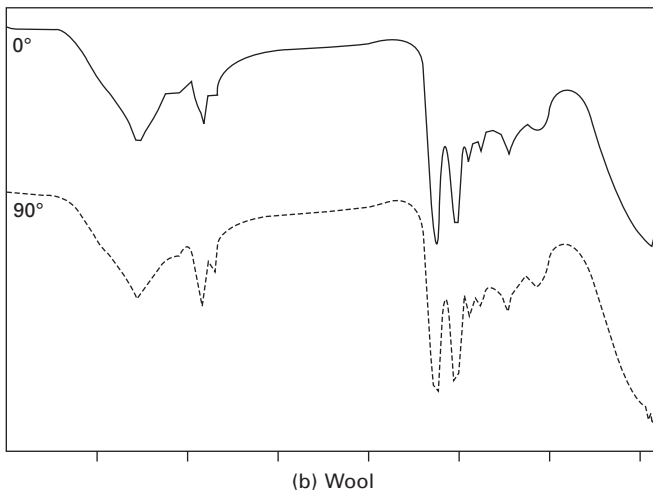
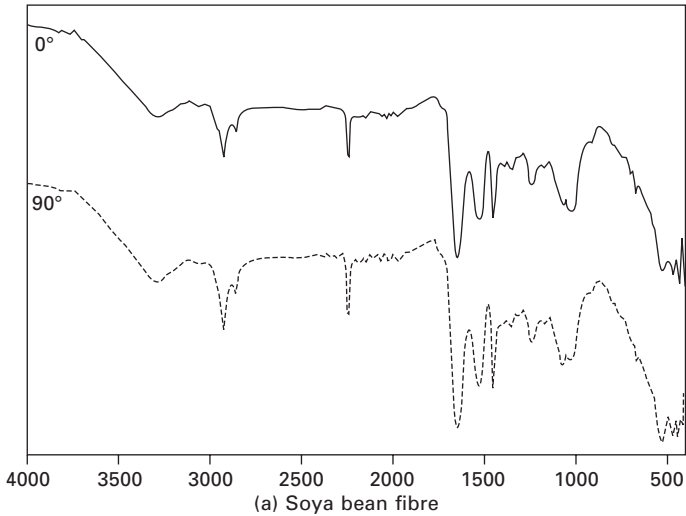
Manufacturers typically claim that these bicomponent regenerated fibres, which naturally have elements of both the chemical and physical qualities of the source proteins and synthetics from which they are made, nevertheless exceed the characteristics of the separate source materials. The excellence of their tactile qualities is repeatedly stressed. SPF yarn is produced in fine deniers and is said to have a soft, smooth handle similar to cashmere, and a silk-like lustre. However, as they have a low crimp ratio, anti-slippage agents are required when spinning (Swicofil, n.d.b).

The health benefits claimed for these fibres appear to be due to the antibacterial agents which are added during the manufacturing process. The Chinese milk protein fibres are promoted as being beneficial to the skin, possessing special humectant qualities (Cyarn, n.d.). The 'amino acid' in soya bean fibres is said to 'activate collagen in the skin' (Euroflax Industries, n.d.) while Yi-You (2004: 9) reports that the addition of Chinese herbal medicines during the spinning process gives the fibre medical benefits which last longer than those of surface finishes as they are bound into the protein.

Their microscopic appearance is very different from the second generation regenerated protein fibres, and generally reflects their bicomponent structure. SPF fibre has an irregular, dumbbell-shaped cross-section and what is described as 'an islands-in-a-sea' structure. This microporous structure makes it air and moisture permeable (Fig. 7.9).

### 7.3.5 Behaviour

The relatively little information that is available on the behaviour of these fibres is generally drawn from manufacturers' data; a summary is given in Table 7.4. They appear to have better tensile properties than their predecessors,

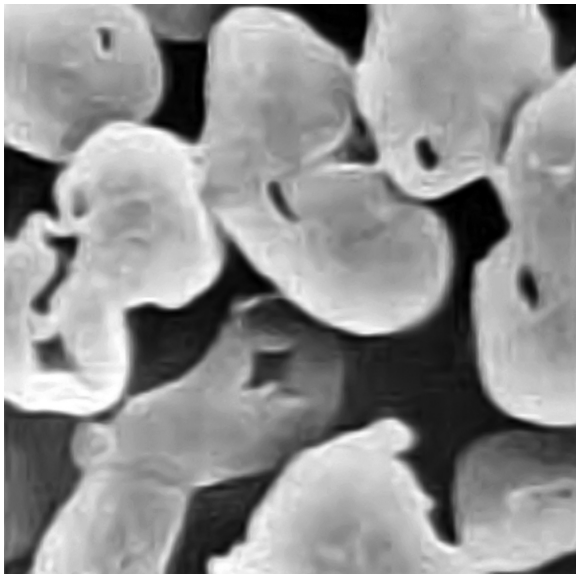


7.8 (a) Polarised ATR FT-IR of third generation soya bean fibre (with fibres aligned parallel ( $0^\circ$ ) and perpendicular ( $90^\circ$ ) to the electric vector of the polarised incident radiation (taken by Paul Garside, Textile Conservation Centre); (b) polarised ATR FT-IR of wool fibre (with fibres aligned parallel ( $0^\circ$ ) and perpendicular ( $90^\circ$ ) to the electric vector of the polarised incident radiation (taken by Paul Garside, Textile Conservation Centre).

as would be expected from the presence of synthetic materials. Some features appear to be better than those of natural fibres. For example, third generation soya bean fibres have improved strength in comparison to the earlier casein fibres and similar moisture absorption, air permeability and heat retention



(a)



(b)

7.9 (a) Longitudinal view of third generation soya bean fibre (©Harvest SPF Textile Co. Ltd, 2002); (b) Cross-section of third generation soya bean fibre (©Harvest SPF Textile Co. Ltd, 2002).

but better UV resistance than cotton (Euroflax Industries, n.d.). SPF fibre has low specific gravity, good elongation and resistance to acid and alkali with a moisture absorption performance which is comparable to cotton (Yi-You, 2004) but its low crimp ratio means that it has poor elastic properties



**Table 7.4** Behavioural properties of third generation regenerated protein fibres in comparison to natural fibres (Cyarn, n.d.; Swicofil, n.d.a, n.d. b; Yi-You, 2004: 8)

Characteristics	Soyabean (SPF)	Chinese milk fibre	Silk	Cotton	Viscose	Wool
Fineness (dtex)	0.9–3.0	1.52	–	1.2–2.0	–	–
Density (g/cm <sup>3</sup> )	1.29	–	1.34–1.38	1.50–1.54	1.34–1.38	–
Tensile strength – dry (cN/dtex)	3.8–4.0	2.8	3.8–4.0	1.9–3.1	1.5–2.0	2.6–3.5
Tensile strength – wet (cN/dtex)	2.5–3.0	2.4	1.9–2.5	2.2–3.1	0.7–1.1	0.8
Dry extension at break (%)	18–21	25–35	14–25	7–10	18–24	–
Initial modulus (cN/dtex)	–	60–80	60–80	60–82	–	44–88
Moisture regain (%)	8.6	5–8	8–9	7–8	13.0	15–17
Behaviour with heat	Yellows and tackifies at approx. 120°C	–	Stable at 148°	–	Loses strength after lengthy processing at 150°	–

(Swicofil, n.d.b). Soya bean fibres are said to be resistant to both mildew and pest attack (Swicofil, n.d.b).

## 7.4 Summary

For different reasons, relatively little is known about the characteristics and behaviour of the three generations of regenerated protein fibres. However, the merging of the qualities of synthetic and natural properties in the latest generation of regenerated protein fibres suggests that this version has a chance of achieving public acceptability. Their chemical and physical characteristics appear to make them an attractive alternative. However, it remains to be seen whether they achieve economic viability and technological longevity.

## 7.5 Notes

1. The ATR spectra presented in this paper were recorded using a *Perkin-Elmer 'Spectrum One'* FT-IR spectrometer, fitted with a '*Universal ATR*' accessory; spectra were recorded over the range 4000–400 cm<sup>-1</sup>, using a resolution of 4 cm<sup>-1</sup> and 32 scans. The spectra were subsequently manipulated using *Galactic 'GRAMS/32'* software. This analysis was undertaken by Dr Paul Garside, Textile Conservation Centre (see Garside and Brooks, 2006).
2. This appears to be different from the Japanese fibre *Cetalon* which was

produced by compressing whale blubber to the point at which a wool-like fibre could be extracted (Loasby, 1952: 145).

3. The Arthur B. Little Laboratory produced two such purses. One is in the Smithsonian Institution, Washington, DC. 'The other was in the company's archive until it was auctioned in 2002; its current whereabouts are unknown (Krasner, 2002).
4. The German fibre *Marena* used for upholstery fillings and brush filaments was made from waste hides and skins produced during leather making (Koch, 1972: 32). It could be used in combination with wool to produce textiles (Jaumann, 1936). *Carnofil* was made from ox or horse muscle and could be used for surgical purposes or for textiles such as suiting (Jaumann, 1936). German researchers also explored the possibility of making fibres from tendons and horsemeat (Hamor, 1941).
5. The Anyang Soybeanfibre Research Centre was set up by Guanqi Li to facilitate collaboration with Chinese scientists and engineers (Textiles & Leather Marketplace 2008).
6. Personal communication, Professor Yiqi Yang, Department of Textiles, Clothing & Design, University of Nebraska-Lincoln, USA, email, 9 March 2008.

## 7.6 Acknowledgements

IP Address: 129.132.211.108 Thanks are extended to the Getty Conservation Institute; Sandy Rosenbaum and Gail Stein, Doris Stein Research Centre, Los Angeles County Museum of Art; Denise Buhr, Research Librarian, Central Soya, Indiana; Patricia Starrett, Archivist, ICI; Katherine Dirks, Smithsonian Institution; the Scientific Research Lab, Museum of Fine Arts, Boston, MA. I would also like thank colleagues at the Textile Conservation Centre, especially Dinah Eastop, Dr Paul Garside for technical analysis, Mike Halliwell for help with images and Nell Hoare MBE, Director, for permission to publish. My thanks also go to Professor Michael Hann, University of Leeds.

## 7.7 References

- Anon. (1939), 'Revue. Le Lanital', *Le Lait*, 19 (181), 29–37.
- Anon. (1945), 'Dresses from chicken', *American Magazine*, 10, 32–33, 94–95.
- Araki S, Tarumi K and Iguchi R (1946), 'Artificial fibers from soybean protein', *Journal of Society of Chemical Industry Japan*, 49 (33); reported in *Chemical Abstracts*, 20 August 1948, 6120d.
- Arthur D. Little Laboratories (1921), *On the Making of Silk Purses from Sows Ears*, Cambridge, MA, Arthur D. Little Laboratories.
- Barker A F (1919), *Textiles*, New York, van Nostrand.
- Bharat Textile (2001), *Soybean Protein Fibre a Reality: China*, <http://www.bharattextile.com> (accessed 26 June 2002).

- Brooks M M (1993), 'Ardil: the disappearing fibre?', in Grattan D W, *Saving the Twentieth Century: The Conservation of Modern Materials*, Ottawa, Canadian Conservation Institute, 81–93.
- Brooks M M (2005), 'Soya bean protein fibres – past, present and future', in Blackburn D, *Biodegradable and Sustainable Fibres*, Cambridge, Woodhead, 398–440.
- Brooks M M (2006), 'Forgotten fibres? Issues in the collecting and conservation of regenerated protein fibres', in Rogerson C and Garside P, *The Future of the Twentieth Century: Collecting, Interpreting and Conserving Modern Materials*, London, Archetype, 33–40.
- Brooks M M (2007), 'Recovering identity: the role of textual evidence in identifying forgotten Azlon fibres from the mid-20th century', in Hayward M and Kramer E, *Textiles and Text*, London, Archetype, 29–33.
- Brooks M M and Garside P (2005), 'Investigating the significance and characteristics of modern regenerated protein fibres', in Parisi C, Buzzanca G and Paradisi A, *Art '05. Proceedings of the 8th International Conference on Non-Destructive Investigations and Microanalysis for the Diagnostics and Conservation of the Cultural and Environmental Heritage. Lecce (Italy), 15–19 May 2005*, Lecce, Italian Society for Non-Destructive Testing Monitoring Diagnostics, Ministry of Cultural Heritage and Activities and Central Institute of Restoration and Department of Materials Science, University of Lecce, 1–14.
- Byrne M S and Johnstone A H (1987), *The Ardil Project. A Discussion Exercise Designed for Use with Tertiary Level Science Students*, London, Royal Society of Chemists, Education Division.
- Carroll-Porzynski C (1961), *Manual of Man-made Fibres. Their Manufacture, Properties and Identification*, New York, Chemical Publishing Co. Inc.
- Cockett S R (1966), *An Introduction to Man-made Fibres*, London, Pitman.
- Cyarn (n.d.), *Milk Protein Fibre*, [http://www.cyarn.com/products/fiber/fiber\\_036.html](http://www.cyarn.com/products/fiber/fiber_036.html) (accessed 23 April 2006).
- Dirks K (2000), 'Aralac: "The cow, the milkmaid and the chemist"', *Ars Textrina*, 33, 75–85.
- Dong Q and Gu L (2002), 'Viscoelastic behavior of AN-g-casein copolymer concentrated solution of sodium thiocyanate', *Journal of Applied Polymer Science*, 84 (9), 1721–1728.
- Euroflax Industries (n.d.), *Euroflax Industries (Imports of Textiles)*, [http://euroflax.com/products\\_imports%20of\\_textiles.htm](http://euroflax.com/products_imports%20of_textiles.htm) (accessed 17 January 2007).
- Evans C D, Croston C B and van Etten C (1947), 'Acetylation of zein fibres', *Textile Research Journal*, XVII (10), 562–567.
- Fletcher H M (1942), *Synthetic Fibres and Textiles*, Agricultural Experiment Station Bulletin 300, Kansas State College of Agriculture and Applied Science.
- Fong M (2004), 'Soy underwear? China targets eco-friendly clothes market', *Wall Street Journal*, 17 December, <http://online.wsj.com/public/article/SB110324276602302867.html> (accessed 23 April 2006).
- Garside P and Brooks M M (2006), 'Probing the microstructures of protein and polyamide fibres', in Rogerson C and Garside P, *The Future of the Twentieth Century: Collecting, Interpreting and Conserving Modern Materials*, London, Archetype, 67–71.
- Hamor W A (1941), 'Industrial research in foreign countries during 1941', *Chemical & Engineering News* 20 (2), 77–109; summarised by V C J [V C Jelinck] (1942), 'Textiles and Clothing', *Journal of Home Economics*, 20 (2), 77–109.
- Harris M (1954), *Handbook of Textile Fibers*, Washington DC, Harris Research Laboratories.

- Harvest SPF Textile Co. Ltd (2002), *The Introduction to Soybean Protein Fiber*. Harvest SPF Textile Co. Ltd, <http://www.spftex.com/product/fibre/character.htm> (accessed 22 February 2008).
- Hill M (n.d.), 'Would you wear a chicken suit?', *American Chemical Society*, 6 November, [http://www.chemistry.org/portal/a/c/s/1/feature\\_ent.html](http://www.chemistry.org/portal/a/c/s/1/feature_ent.html) (accessed 17 January 2007).
- Huda S, Reddy N, Karst D, Xu W, Yang W and Yang Y (2007), 'Non traditional biofibers for a new textile industry', *Journal of Biobased Materials and Bioenergy*, 1 (2), 177–190.
- Hudson S M (1997), 'The spinning of silk-like proteins into fibres', in McGarth K and Kaplan D, *Protein-based Materials. Bioengineering of Materials*, Boston, MA, Birkhäuser, 313–337.
- Hull S (2006), 'Feathers fly but it suits you', *Metro*, 18 September, 16.
- Jaumann A (1936), 'Carnol and Marena fibres', *Kunstseide*, 18, 109–113.
- Kiplinger J (2003), *Meet the Azlons from A to Z: Regenerated and Rejuvenated*, <http://www.fabrics.net/joan103.asp> (accessed 7 November 2002).
- Koch P-A (1972), 'Regenerated protein fibres', *Ciba-Geigy Review*, 1, 25–33.
- Kotliar A M and Ghasemzadeh S (1994), *Novel Silk-like Bicomponent Textile Fibers based on Soybean Protein and Poly(vinyl alcohol)*, USB/ASA Research Report Project Number E-27-663, Georgia Institute of Technology.
- Krasner J (2002), 'Silky profit from sow's ear', *Boston Globe*, 5 November, [http://www.boston.com/dailyglobe2/309/business/Silky\\_profit\\_from\\_sow\\_s\\_ear+.shtml](http://www.boston.com/dailyglobe2/309/business/Silky_profit_from_sow_s_ear+.shtml) (accessed 7 November 2002).
- Lawton J W (2002), 'Zein: a history of processing and use', *Cereal Chemistry*, 79 (1), 1–18.
- Loasby G (1952), 'Regenerated protein fibres – production', *Review of Textile Progress*, 4, 145–149.
- Lundgren H P and O'Connell R A (1944), 'Artificial fibers from corpuscular and fibrous proteins', *Industrial and Engineering Chemistry*, 36 (4), 370–374.
- Moncrieff R W (1970), *Man-made Fibres*, 5th edition, London, Newnes-Butterworths.
- Moncrieff R W (1975), *Man-made Fibres*, 6th edition, London, Newnes-Butterworths.
- Morrison B V and Fletcher H M (1946), 'How the war affected civilian textiles', *Journal of Home Economics*, 38, 21.
- O'Brian R (1942), 'Wartime textile adjustments', *Journal of Home Economics*, 34, 512–514.
- Park J and Shore J (1999), 'Dye and fibre discoveries of the twentieth century. Part 2: Growth of the chemical giants', *Journal for Society of Dyers and Colorists*, 115 (July/August), 207–217.
- Press J J (ed) (1959), *Protein Fibres. Man-made Textiles Encyclopaedia*, New York, Textile Book Publishers.
- Shanghai Winshow (2004), *Shanghai Winshow Soybeanfire Industry Co. Ltd. About Us*, <http://www.soybeanfibre.com> (accessed 22 February 2008).
- Sherman J V and Sherman S L (1946), *The New Fibers*, New York, Van Nostrand.
- Swicofil (n.d.a), *Natural Fibres Milk Fiber*, [http://www.swicofil.com/products/212milk\\_fiber\\_casein.html](http://www.swicofil.com/products/212milk_fiber_casein.html) (accessed 22 February 2008).
- Swicofil (n.d.b), *Soybean Proteins Fibre Properties*, <http://www.swicofil.com/soybeanproteinfiberproperties.html> (accessed 22 February 2008).
- Textile Fiber Products Identification Act. Section 303.7 Generic Names and Definitions for manufactured fibers* (1958), <http://www.ftc.gov/os/statutes/textile/rr-textl.htm#303.6> (accessed 22 February 2008).

- Textile Institute (1975), *Identification of Textile Materials*, 7th edition, Manchester, The Textile Institute.
- Textiles & Leather Marketplace (2008), *Shanghai Winshow Soybean Fibre Industry Co. Ltd.*, <http://www.textiles-leather.cn/suppliers/shanghai-winshow-soybean-fibre-industry-co-ltd-516134e> (accessed 22 February 2008).
- Trill D (1951), 'Some trials by ingenious inquisitive persons: regenerated protein fibres', *Journal of the Society of Dyers and Colourists*, 67, 257–270.
- Walsh A (1987), *Catalogue of the Fibre Museum [University of Leeds International Textile Archive]*, unpublished Final Year Project, University of Leeds.
- Whittier E O and Gould S P (1939), 'Casein fiber' [letter], *Industrial and Engineering Chemistry*, 31 (3), 374.
- Woolmark Company (2001), *China Working on Silk and Cashmere Substitution*, 3 May, <http://melpub.wool.com/enews2.nsf/vwMonthlyWoolmark/efb9350468ce16f141256a400057243c?OpenDocument&Archive> (accessed 26 June 2002).
- Wormell R L (1954), *New Fibre from Proteins*, London, Butterworths Scientific Publications.
- Yang Y, Wang L and Li S (1996), 'Formaldehyde-free zein fiber – preparation and investigation', *Journal of Applied Polymer Science*, 59, 433–441.
- Yi-You L (2004), 'The soybean protein fibre – a healthy and comfortable fibre for the 21st century', *Fibres and Textiles in Eastern Europe*, 12 (2), 8–9.
- Zhang Y, Ghasemzadeh S, Kotliar A M, Kumar S, Presnell S and Williams D L (1999), 'Fibres from soybean protein and poly(vinyl alcohol)', *Journal of Applied Polymer Science*, 71 (1), 11–19.

## The structure of alginate, chitin and chitosan fibres

B NIEKRASZEWICZ, Technical University of Lodz, Poland  
and A NIEKRASZEWICZ, Institute of Biopolymers  
and Chemical Fibres, Poland

**Abstracts:** This chapter discusses the fibres produced from natural polymers such as alginates, chitin and chitosan. The chapter reviews specific properties of these polymers and the fibres obtained from them, together with the methods of producing fibres. The chapter also discusses the influence of polymer structure and spinning conditions on the properties of fibres obtained from these biopolymers. The chapter includes the main fields of applications and the future prospects for alginates, chitin, chitosan and fibres produced from them (composite fibres, nanofibres, nanoporous).

**Key words:** alginate fibres, chitin fibres, chitosan fibres, biopolymers, wound dressings.

### 8.1 Introduction

IP Address: 129.132.211.108  
For years there has been an increasing demand for fibres that are produced from natural polymers such as alginates, chitin and chitosan. These fibres are characterized by such unique properties that it is possible to extend the field of their application. Also, recent and sudden developments in modern technology, such as nanotechnology or composite technologies, add to that. An even greater number of applications are found in producing modern fibre materials from these biopolymers. Owing to their biocompatibility, they are excellent raw materials for creating wound dressings, scaffolds for tissue engineering or resorptive implants or surgical threads.<sup>1</sup>

This chapter will present specific properties of alginates, chitin, chitosan and fibres obtained from them, together with the methods of obtaining fibres. Also the influence of polymer structure and conditions of spinning on the properties of fibres obtained from these polymers will be presented here. An important part will be the future prospects for alginates, chitin, chitosan and fibres produced from them (composite fibres, nanofibres, nanoporous).

### 8.2 Alginate fibres

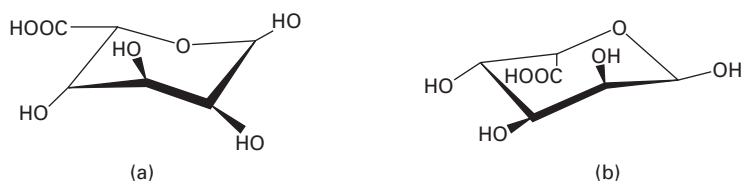
Nowadays, alginate fibres are a subject of increasing interest to both producers and consumers. Alginates are quite common in many kinds of seaweed species: brown seaweeds and alginates are commonly produced worldwide. Owing to

their abundance and low cost, alginates are well-known and commonly used gelling and thickening agents in the textile, food and pharmaceutical industries. For this reason about 50% of alginates are used in the textile industry, 33% in the food and pharmaceutical industry and the rest mainly in the paper and cosmetic industries. Thanks to their properties, such as biocompatibility, high absorption capacity and ion-exchange properties, they are used as medical textiles.<sup>2</sup> Alginate fibres, typically those made of calcium alginate, are able to absorb any exudates and have the unique property of being able to partially change into a gel. This property allows the painless removal of the wound dressing. Nowadays, alginate wound dressings are one of the most modern and universal forms, and their market grows about 40% per year.<sup>3</sup>

### 8.2.1 Structure of alginates

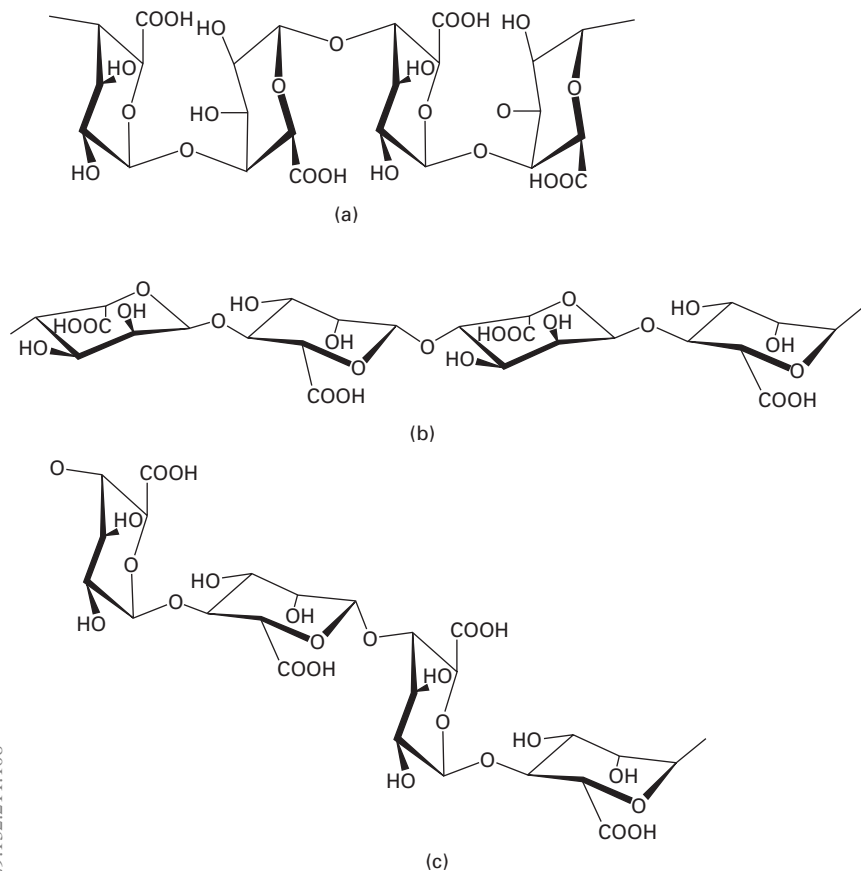
Alginate is a linear polysaccharide derived from brown seaweeds or from soil bacteria. Of most importance, from a commercial point of view, are the genera *Ascophyllum*, *Laminaria* and *Macrocystis*.<sup>4</sup> From a chemical point of view, alginates are linear copolymers based on  $\beta$ -(1 $\rightarrow$ 4)-D-mannuronic acid (M) and  $\alpha$ -(1 $\rightarrow$ 4)-L-guluronic acid (G) units (see Fig. 8.1). In the polymer chain, the units G and M may create three types of blocks, namely GG, MM and MG (see Fig. 8.2). Each of these has a different conformation and therefore physical behaviour. So, alginates can be regarded as true block copolymers, composed of homopolymeric regions of M and G blocks, interspersed with alternating MG blocks. Detailed investigations have shown that alginates have no regular repeating unit and have various distributions of the monomers along the polymer chain. The main difference at the molecular level between algal and bacterial alginates is presence of O-acetyl groups at positions C2 and/or C3 in the bacterial alginates.<sup>5</sup>

Owing to the fact that the  $\beta$ -D-mannuronic acid and  $\alpha$ -L-guluronic acid units are the basic components of the block structure of the polymer, their properties are described by various parameters, e.g. the ratio of the individual units and their distribution (polydispersity), composition and the average molecular weight of the  $\beta$ -D-mannuronic acid,  $\alpha$ -L-guluronic acid blocks and their copolymer blocks. Viscosity data has shown that the stiffness



8.1 Chemical structure: (a)  $\alpha$ -L-guluronic acid (G), (b)  $\beta$ -D-mannuronic acid (M).





8.2 Structure of alginic acid: (a) G-G-G-G blocks, (b) M-M-M-M blocks, (c) G-M-G-M blocks.

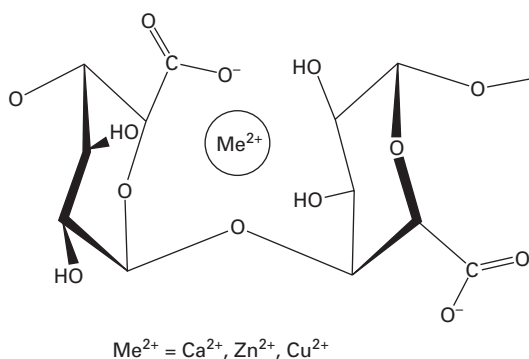
IP Address: 129.132.211.108

of the blocks increases in the order  $MG < MM < GG$ ; so four glycosidic linkages, namely diequatorial (MM), diaxial (GG), equatorial-axial (MG) and axial-equatorial (GM), are possible in alginate.<sup>5</sup> Diaxial linkages in G-blocks cause a large hindered rotation around the glycosidic linkage, which could be the reason for the stiff and extended nature of the alginate chain. Due to the polyelectrolyte character of alginates, the electrostatic repulsion between the charged groups on the polymer chain also increases the chain extension, and hence the intrinsic viscosity.<sup>5,6</sup> The structure of alginates has been widely studied using X-ray diffraction and infrared spectroscopy.<sup>7</sup>

Depending on their source and their growth conditions, alginates differ in composition (proportion of M/G) and sequential structure<sup>8</sup> (see Table 8.1). Alginates derived from seaweed stems are usually characterized by a high content of guluronic blocks (high G), whereas alginates derived from

**Table 8.1** Composition of alginates obtained from alginophytes from various geographical regions (adapted from ref. 8)

Source of alginates	Sources of alginophytes	M content (%)	G content (%)	M/G ratio
<i>Ascophyllum</i>	Norway, Ireland, UK, France	65	35	1.85
<i>Ecklonia</i>	South Africa	62	38	1.60
<i>Macrocystis pyrifera</i>	USA, Mexico, Chile	61	39	1.56
<i>Laminaria digitata</i>	France, Iceland	59	41	1.45
<i>Laminaria hyperborea</i>	Norway, Ireland, UK, France	31	69	0.45



**8.3** The stereochemical structure of the GG block (adapted from ref. 29).

seaweed leaves are characterized by a higher content of mannuronic blocks (high M). The carboxylic group in guluronic acid is situated on the top of the triangle carbon/carbon/oxygen, and is more reactive than in mannuronic acid. In the case of GG blocks, the stereochemical structure of the two repeat units allows the creation of the space and the closing of calcium ions (see Fig. 8.3), thus creating an egg-box-like conformation.<sup>7,9</sup> Alginates have the ability to create a gel through divalent metal ions. Such a structure makes it harder for calcium ions to be exchanged with sodium ions, and therefore these structures are able to retain water. On the other hand, when MM blocks are in the majority water can be absorbed between the polymer chains, and this makes it easier for calcium ions to be exchanged with sodium ions. Alginates with higher content of GG blocks create stronger gels than those with a high content of MM blocks due to their greater ability to bind calcium.<sup>3</sup>

Alginates may be prepared with a wide range of average molecular weights (50 000–100 000 units) to suit the application.<sup>2</sup> They are polydisperse with

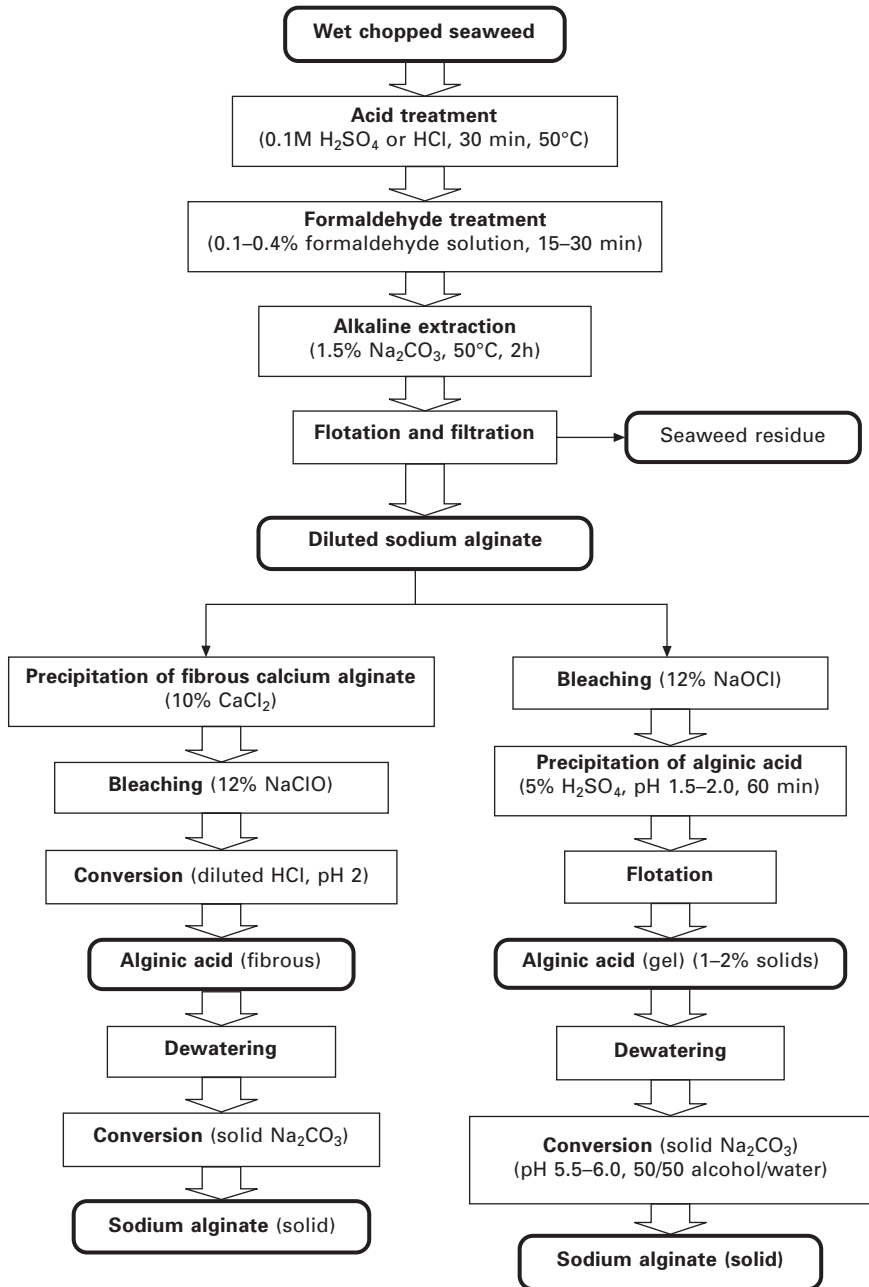
respect to molecular weight. Polydispersity index values are usually between 1.4 and 6.0 and depend on the preparation and purification processes used. Polydispersity can be important for the applications of alginates. Fragments of alginate chains with low molecular weight, which contain only short G-blocks, may not take part in the formation of a gel-network, and as a consequence do not contribute to gel strength. In some high-tech applications, however, the leakage of high mannuronic blocks from gels can cause problems.<sup>4</sup>

## 8.2.2 Alginate production methods

Alginates are present in nature as one of the constituents of brown algae (*Phaeophyceae*), and as capsular polysaccharides in soil bacteria. Despite the fact that studies carried out by various groups have shown that they can be obtained through microbial fermentation and post-polymerization modification of alginate molecules, all of the commercial alginates are currently obtained from algal sources. Alginate is the most abundant marine biopolymer, and occurs in the intercellular mucilage and algal cells of brown seaweeds in the form of calcium, sodium and magnesium salts of alginic acid.

Alginic acid was first discovered by Stanford in 1881, and the first patents concerning obtaining alginates from algae were published in the 1930s.<sup>10,11</sup> More specific descriptions of the process of obtaining alginates from algae have been published by McHugh,<sup>4,12</sup> Moss and Doty,<sup>13</sup> and Hernandez-Carmona *et al.*<sup>14</sup> Some of the biggest producers of alginates are the China Seaweed Industrial Association, Danisco Cultor (Denmark), Degussa Texturant Systems (Germany), FMC BioPolymer (USA), ISP Alginates Ltd (UK), Kimitsu Chemical Industries Co. Ltd (Japan) and Pronova Biomedical A/S (Norway). Nowadays the total capacity of alginate production is about 33 000 tonnes per annum: 16 000 tonnes in Europe, 14 000 tonnes in Asia-Pacific and 3000 tonnes per annum in the Americas.<sup>4,5</sup>

The alginate with the greatest industrial importance is sodium-based salt derivative. The potassium, ammonium and calcium salts have the same applications, as well as alginic acid itself. The sodium salt of alginic acid is soluble in water, whereas the magnesium and calcium salts are insoluble. Obtaining alginates from algae is a multi-stage process. The general process of obtaining alginates is based on converting all alginate salts into sodium salts, dissolving them in water and removing the seaweed residue. To do this, seaweeds are broken into pieces and stirred with a hot solution of alkali, usually sodium carbonate (concentration 1.5%) at temperatures from 50–90°C for 1–2 hours. The dissolved sodium alginate later separates from the alkali-insoluble seaweed residue, mainly comprising cellulose, by flotation and filtration. The next step is the precipitation of the alginate from this diluted filtered solution. This can be done in two ways: as a calcium salt of alginic acid or as alginic acid alone.<sup>4</sup> This process is schematically presented in Fig. 8.4.



IP Address: 129.132.211.108

8.4 Scheme of production of sodium alginate (adapted from ref. 4).

When the first method is used, diluted sodium alginate solution is added into a calcium chloride solution (about 10%) and solid calcium alginate is formed as a fibre. This resulting material is a good form for further treatment. It is easy to separate fibrous calcium alginate, to wash, to dewater and then to bleach by treatment with sodium hypochlorite solution (12%). The next step is conversion of calcium alginate into alginic acid, which is realized by stirring it in dilute HCl (0.5 M) with a pH less than 2. Fibrous alginic acid is dewatered to contain more than 25% solids. Such alginic acid is mixed with sodium carbonate to form a heavy paste, which is then extruded as pellets, dried and then milled.<sup>4</sup> The approach involves initially bleaching with NaClO (12% solution). Sodium alginate extract is then treated with 5% H<sub>2</sub>SO<sub>4</sub> solution in pH 1.5–2.0. After 60 min an alginic acid gel is formed. The next step of this process is the flotation of gel (filtration is not possible). The alginic acid gel obtained from flotation contains only 1–2% solids. The water content of this gel can be removed in three ways; pressing or squeezing and centrifuging or mixing with an alcohol. Pressing and squeezing can increase the solids content to 25–30%, centrifuging to 7–8%, but mixing with alcohol is uneconomical on a large scale. The most popular approach is centrifuging. Conversion of alginic acid into sodium alginate is made by introducing a 50:50 mixture of alcohol (ethanol or isopropanol) and water to 7–8% alginic acid. To obtain a paste of sodium alginate, solid Na<sub>2</sub>CO<sub>3</sub> is added and then this paste is extruded as pellets, dried and milled as for the calcium alginate process.<sup>15</sup>

Both processes have advantages and disadvantages. In comparison to the alginic acid process, the calcium alginate process requires an extra step, but the handling of the fibrous calcium alginate and alginic acid is easier and an expensive alcohol does not have to be used. In the second process, alginic acid forms gelatinous precipitates, which are difficult to separate, and the losses of alginic acid are greater than for the first process. Because of this, alcohol must be used for the conversion to sodium alginate, which makes the process more expensive.<sup>4</sup>

The main properties of alginates, which are particularly important to their application, are:

- Alginates have some unique properties such as non-toxicity, biocompatibility, biodegradability and hydrophilicity and have a relatively low cost.
- Alginates have the ability to create permanent gels as a result of their reactions with calcium salts. This ability is used, for example, in processing into medical materials.
- Alginate fibres are produced mainly for medical use (especially as wound dressings), so the alginates used should be characterized by appropriate properties, such as molecular weight, polydispersity and an appropriate

participation of individual blocks. Taking into consideration demands put in front of fibre-forming polymers and the demands concerning fibre tenacity, it is recommended that they should have a high molecular mass and low polydispersity. To ensure an appropriate functionality of the fibres from the point of view of using them in wound dressings, it is necessary for the presence of a fraction with lower molecular weight to partake.

- Alginates were found useful also as carriers controlling drug release, in tissue engineering and in artificial pancreas construction.

### 8.2.3 Methods of alginate fibre production

Alginate fibres have been known for a long time. Their commercial production was established in England and the USA during the Second World War. Acordis Speciality Fibers, UK (now Speciality Fibres and Materials Ltd) was the first company in the world to develop a commercial process for the manufacture of alginate fibres, and is a world leader in technology today. The fibres are obtained by a wet spinning method, and depending on the technology used, they can be in the form of salts, esters or other alginate acid derivatives.

Fibres are mostly produced from sodium alginate or from calcium-sodium alginate.<sup>15,16</sup> Fibres are usually spun from 4–10% of an aqueous spinning solution into a spinning bath, where an exchange of sodium ions into calcium ions takes place. The content of the bath depends on whether the formed fibre is going to contain alginate acid, calcium alginate or other alginates. In the case of fibres made from calcium alginate, the coagulation bath usually includes calcium chloride, hydrochloric acid and a supporting agent. When spinning fibres made from alginate acid, sulphuric acid and sodium sulphate are present in the coagulation bath. It is also possible to have various combinations of salts in the coagulation bath (salts of zinc, magnesium, copper).<sup>17</sup> Following that stage, the fibres are washed, drawn and dried before they are cut and further processed into nonwoven felt via a conventional textile process.<sup>3,18</sup>

Calcium alginate fibres can also be processed into calcium-sodium alginates fibres by first treating with hydrochloric acid and replacing some of the calcium ions by hydrogen ions. These hydrogen ions are then replaced by sodium ions as a result of treatment with sodium carbonate or sodium hydroxide. Fibres that include both the insoluble calcium alginate and the water-soluble sodium alginate are the effect of such action. These fibres will be characterized by even better absorption properties when more sodium ions introduced into the fibre structure.<sup>3,18</sup> These properties are the key to the wide range of uses of alginate fibres, most importantly for the production of high-tech wound dressings. Alginate fibres have unique gel-

forming characteristics. In the gel state, the dressings provide an ideal moist healing environment for the wound.<sup>3</sup> Some dressings contain calcium alginate fibres (Algisite M, Sorbsan, Tegagen) and others contain sodium-calcium alginate fibres (Melgisorb, Seasorb, Kaltostat). Many clinical examinations have confirmed that alginate wound dressings not only have high absorption capacities, but also have the ability to promote wound healing.<sup>19–21</sup>

Alginate fibers are used in nonwovens, including composite products, and speciality yarns for moist wound dressings on difficult-to-heal chronic wounds such as pressure sores and leg ulcers. The fibres create a rapid gel blocking action, which prevents lateral wicking, reducing the risk of macerating healthy skin around the wound. Alginate fibres have many advantages over other traditional dressings (cotton and viscose fibres), and have now become one of the most important materials for wound management. It has been confirmed that alginate-based dressings are non-toxic, non-carcinogenic, non-allergic, haemostatic, biocompatible, have reasonable strength, are capable of being sterilized, can incorporate medications and are easy to process.<sup>22,23</sup> Calcium alginate fibers can be used for the production of yarns and fabrics for medical applications, and as drug carriers for wound healing.<sup>23–25</sup>

Owing to their ability to dissolve in diluted aqueous alkali solutions and to the fact that they are fire-resistant, alginate fibres were traditionally used to produce upholstery, but nowadays they are replaced by much cheaper speciality chemical fibres.<sup>3</sup>

#### 8.2.4 Influence of structure on properties

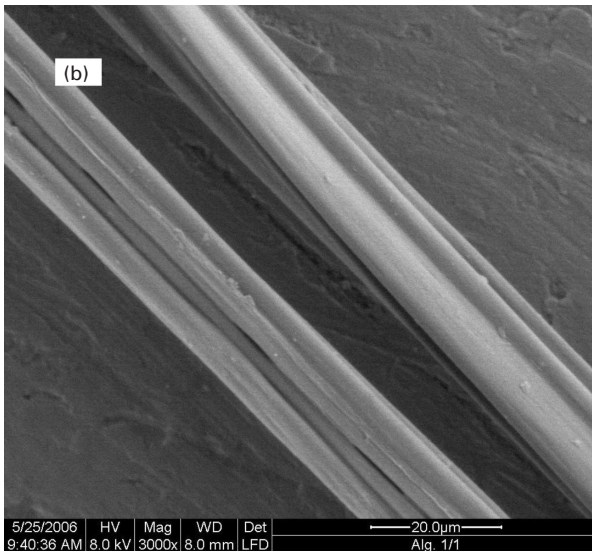
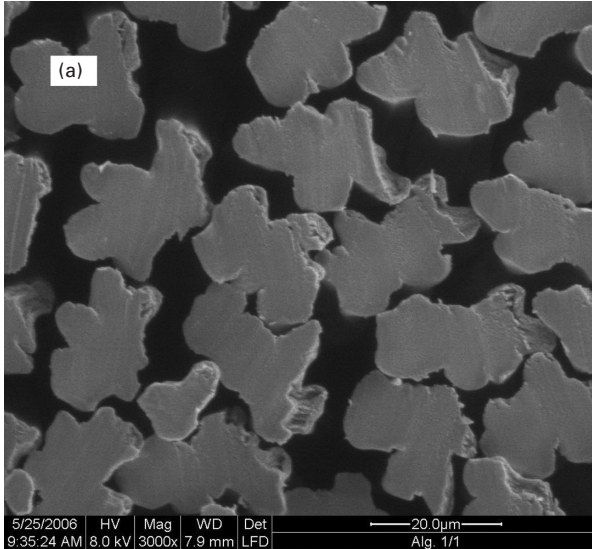
Generally, the properties of alginate fibres are generated by their fibre-forming material structure. Standard calcium alginate fibres are characterized by the following properties:<sup>26</sup>

- Density 1.78 g/cm<sup>3</sup>
- Tenacity (at 21°C and 65% RH) 11–18 cN/tex
- Elongation (at 21°C and 65% RH) 5%
- Typical absorbency (at 0.9% saline) 18 g/100 cm<sup>2</sup>
- Moisture sorption (at 20°C and 65% RH) 20–35%.

Alginate fibres show poor resistance to UV. Fibre solubility depends on the degree and type of crosslinking with multivalent metal ions. The character of the created gel (rigid or elastic gel), its thermomechanical properties and the value of the dynamic module depend on the ratio M/G (mannuronic block/guluronic block). Ion exchange also has relevant influence here.<sup>27</sup> Good absorption properties of alginate fibres are connected to their hydrophilic character as well as their porous structure that is created during the spinning process.<sup>28</sup> In the case of man-made fibres, the fibre structure is strongly dependent on the spinning conditions. In wet spinning, because of



low polymer concentration in the spinning solution there is a large amount of solvent in the as-made fibres. In the case of these fibres, the mechanism of dehydration influences their structure and cross-section. Alginate fibres have irregular cross-sections and a rather rough surface (porous structure), a typical result of wet spinning, as shown in Figs 8.5a and 8.5b.



8.5 SEM micrographs of alginate fibres: (a) cross-sections, (b) surface.

Ion exchange, absorption and gel swelling properties of alginate fibres are very important for using them as wound dressings. Qin *et al.*<sup>29,30</sup> examined the ion exchange of alginate fibres and the wound dressings obtained from them, and confirmed that polymeric acid, which is alginate, can form salts with calcium, sodium, zinc and many other metal ions. Ion exchange in alginate fibres depends on the character of their structure (M/G ratio). In the case of fibres with a high guluronic block content (high G), calcium ions are strongly connected through the fibre structure, and ion exchange does not readily occur. This is caused by the formation of a stable egg-box structure, which does not allow the easy exchange of calcium ion with other ions (see Fig. 8.3). Alginate fibres (high G) swell only a little in the presence of body fluids, and the fibre structure and the wound dressing are not radically violated during the treatment. In the case of alginate fibres with a high mannuric block content (high M), calcium ions are easily exchangeable for sodium ions and they swell, thus becoming an elastic gel. Qin *et al.* have examined the gel swelling properties of alginate fibres.<sup>3,31,32</sup> The swelling properties of fibres with a high guluronic block content can be regulated by introducing sodium ions into the fibres. Water absorption through sodium-calcium alginate fibres (high G) is higher than in the case of fibres formed from calcium alginate, which is a result of the ability to bind water through sodium ions in the fibre. Calcium alginate fibres with a high mannuric block content (high M) are, however, characterized by a much higher absorption of saline than calcium-sodium alginate fibres and alginate fibres (with high guluronic block content). This leads to the excellent ability of alginate fibres with a high mannuric block content (high M) to gel<sup>3,32</sup> (see Table 8.2).

Qin<sup>29</sup> confirmed that calcium alginate fibres can also be treated with ZnCl<sub>2</sub> solutions where calcium/zinc alginate fibres were obtained. These fibres have the ability to deliver zinc ions when placed in contact with body fluids. Zinc is needed for functioning of most enzymes in the body, and is necessary for zinc-deficient patients. Examinations have shown that a high M-type dressing generally has better haemostatic properties than a high G-type alginate dressing. By incorporating silver ions into alginate fibres, highly absorbent alginate wound dressings with antibacterial properties can be made (Silverlon<sup>®</sup> calcium alginate dressing).<sup>29,33</sup> By the release of silver

Table 8.2 Gel swelling properties of various alginate fibres (adapted from ref. 32)

Property	Alginic fibres with various calcium contents		
	~98.2% Ca	~76.6% Ca	~54.3% Ca
Gel swelling ratio in water, g/g	2.68 ± 0.26	24.15 ± 0.86	20.65 ± 2.68
Gel swelling ratio in 0.9% saline, g/g	8.48 ± 0.61	13.43 ± 1.13	18.60 ± 0.95
Gel strength, g	85.1	19.9	7.5

ions from fibres, the bacteria that are trapped within alginate wound dressings are killed.

Fabia *et al.*<sup>34</sup> described investigations into the structure of fibres at their supermolecular level using WAXS (wide angle X-ray diffraction) and SAXS (small angle X-ray diffraction) methods. They examined fibres obtained from high mannuronic sodium alginate (Protanal LF-10/60 LS), which were spun into an aqueous solution of calcium chloride, sodium chloride and/or hydrochloric acid under suitable concentrations. WAXS examinations have shown that the intensity of the peaks from crystalline planes, particularly of guluronian (110), (020) and (200), decreases when the calcium ion content in the alginate fibres increases. SAXS examinations have confirmed the existence of the guluronian and mannuronian blocks' structure.

Mikolajczyk and Wolowska-Czapnik<sup>17</sup> carried out examinations of the production of water-soluble alginate fibres and comparative analysis of the effects of basic fibre spinning parameters on the porous structure, moisture absorption and strength of the fibres from zinc and copper alginates. These fibres were obtained from solutions of sodium alginate (Protanal LF 60/20, FMC Biopolymer AS), which were wet spun into baths containing 3% of ZnCl<sub>2</sub> or 3% of CuCl<sub>2</sub> and 0.3% of HCl. The exchange of sodium ions with zinc or copper ions during the solidification stage allowed the production of zinc alginate or copper alginate fibres with properties suitable for medical applications. The spinning conditions that were used allowed the introduction of about 8.4–8.6 wt% zinc or copper ions into the fibre structure. These fibres were characterized by a strong antibacterial activity, as shown in Table 8.3. Other examinations carried out by the authors have shown that additional protection of wounds against infection by microorganisms and accelerated wound healing can be obtained by introducing antibiotics into the spinning solution.<sup>35</sup> The best and optimal spinning conditions for the production of Cu-alginate fibres have been selected in respect to their strength properties and high values of water retention for Zn-alginate fibres. This optimization is carried out specifically for the fields of uses of obtained fibres. Optimal

IP Address: 129.132.211.108

*Table 8.3* Results of antibacterial tests for various alginate fibres obtained in optimal conditions (adapted with permission from ref. 17)

Sample	Time (h)	Amount of bacteria colony (cfu)	Bacteriostatic activity, log (cfu)	Bacteriocidal activity, log (cfu)	Growth value, log (cfu)
Standard	0	$9.1 \times 10^4$	–	–	–
Standard	24	$6.5 \times 10^7$	–	–	2.8
Zinc alginate fibres	24	47	6.1	3.3	–
Copper alginate fibres	24	<20	6.5	3.7	–

Note: cfu – colony forming unit.

spinning conditions and the main properties of various modified alginate fibres are shown in Table 8.4.<sup>36</sup> Generally, higher values of moisture absorption at 65% RH (over 20%) for fibres substituted  $\text{Ca}^{2+}$ ,  $\text{Zn}^{2+}$ ,  $\text{Cu}^{2+}$  and  $\text{Na}^+$  ions are connected with the hydrophilic character of the fibre-forming material. High values of water retention are connected with the quantitative predominance of large and very large pores in the examined fibres and with the swelling of fibres due to water penetration into their supermolecular structure. The fibre spinning conditions have an influence on the character of the porous structure, as shown in Table 8.5.<sup>36</sup>

As well as the use of alginate fibres for modern wound dressings, Mikolajczyk *et al.* propose to use calcium alginate fibres as precursors to

Table 8.4 Properties of various alginate fibres obtained under the optimal conditions (adapted from refs 36 and 37)

Fibres*	As-spun draw ratio (%)	Total draw ratio (%)	Moisture absorption at 65% RH (%)	Degree of crystallinity (%)	Water retention (%)	Tenacity (cN/tex)
Alg-Ca	70.37	54.65	23.21	8.5	69.68	23.53
Alg-Ca <sub>3%</sub> SiO <sub>2</sub>	60.00	63.66	23.48	11.2	69.44	19.93
Alg-Ca <sub>5%</sub> SiO <sub>2</sub>	90.23	59.03	22.36	10.2	66.35	19.29
Alg-acid	120.00	17.72	15.53	27.0	165.00	16.05
Alg-Na	32.00	25.00	22.65	11.8	177.04 <sup>†</sup>	13.23
Alg-Zn	30.50	64.63	25.00	5.8	101.53	21.24
Alg-Cu	119.90	73.25	21.35	9.5	61.54	21.41

\*Alg-Ca – calcium alginate fibres, Alg-Ca<sub>3%</sub> SiO<sub>2</sub> – calcium alginate fibres with 3% silica nanoparticles per polymer, Alg-Ca<sub>5%</sub> SiO<sub>2</sub> – calcium alginate fibres with 5% silica nanoparticles per polymer, Alg-acid – alginic acid fibres, Alg-Na – sodium alginate fibres, Alg-Zn – zinc alginate fibres, Alg-Cu – copper alginate fibres.

<sup>†</sup> Percentage of water absorbed by sodium alginate fibres from a moist substrate for 1 h.

Table 8.5 Total pore volume, internal surface and percentages of capillary sets of various alginate fibres (adapted from ref. 36)

Fibres	Total pore volume (mm <sup>3</sup> /g)	Internal surface of pores (m <sup>2</sup> /g)	Percentage pore content (%)			
			Small 4–12.3 nm	Medium 12.3–75 nm	Large 75–750 nm	Very large 750–7500 nm
Alg-Ca	54.32	1.80	6.82	0.0	11.36	81.72
Alg-Ca <sub>3%</sub> SiO <sub>2</sub>	91.25	4.53	18.07	8.22	10.96	65.75
Alg-Ca <sub>5%</sub> SiO <sub>2</sub>	90.70	5.53	16.67	11.54	10.26	61.53
Alg-acid	58.73	3.88	18.93	21.62	13.52	45.95
Alg-Zn	47.67	1.60	9.76	0.0	7.2	82.90
Alg-Cu	146.15	4.98	7.89	14.48	15.79	61.84

the preparation of carbon fibres.<sup>28,36,37</sup> Implants obtained from such fibres could support the process of bone reconstruction. This process can also be advantageously affected by presence of silica, one of the main components necessary to rebuild bones. Nanoparticles of SiO<sub>2</sub> have been incorporated into alginate fibres during the preparation of the spinning solution. Optimal spinning conditions, mechanical parameters, hygroscopic parameters and characteristics of the porous structure of alginate fibres with nano-SiO<sub>2</sub> are reported in Tables 8.4 and 8.5. Results showed that the alginate fibres obtained under certain spinning conditions, which give a high total pore volume and an internal surface with a tenacity of 20cN/tex, are suitable for the carbonization process. The incorporation of 5% of SiO<sub>2</sub> nanoparticles does not significantly influence the fibre sorption properties, despite increased fibre porosity. This approach, however, decreases the tenacity of the fibres by 15%.<sup>28</sup> The effect of fibre-forming material structure and content of nanosilica have an influence on the thermal stability of alginate fibres. Examinations of thermal properties showed that the thermal stability indicator  $T_{50}$  (temperature corresponding to a 50% weight loss) for fibre modified using nanosilica achieves values of 440–450°C in comparison with 400°C for Ca-alginate fibres and 330°C for Na-alginate fibres. These parameters for various alginate fibres can be arranged in the following series:<sup>36</sup>

$$T_{50}: \text{Alg-Ca-SiO}_2 > \text{Alg-Ca} > \text{Alg-Zn} > \text{Alg-Cu} > \text{Alg-Na} > \text{Alg. Acid}$$

The fibres made from various types of alginates generate negative static charges in contact with human skin. The fibres obtained from alginates of bivalent metals and those containing nanosilica show a lower level of static charge in comparison with fibres from sodium alginate. The level of the generated charge and its negative polarization can determine the enhancement of the therapeutic effects of alginate fibres. Fibres from alginic acid and sodium alginate show a considerably higher conductivity by three orders of magnitude as compared with that of fibres from Zn, Cu and Ca alginates.<sup>37</sup>

The original technology for manufacturing alginate fibres using a pilot-scale spinning machine was developed at the Institute of Biopolymers and Chemical Fibres (Poland).<sup>38</sup> Commercial sodium alginate (Protanal LF 10/60, FMC Biopolymer) was used for the preparation of alginate fibres. This sodium alginate contained 65–75% of guluronic acid, 25–35% of mannuronic acid, less than 18–24% of ash and less than 20 ppm of heavy metals. The fibres were obtained using an aqueous solution of sodium alginate, which was spun into an aqueous acidic coagulation bath containing calcium chloride and additives to improve the spinning process. As-spun alginate fibres were stretched by 50% into a bath system containing a diluted aqueous solution of calcium chloride, washed in demineralized water and dried at 80°C. They were spun out at a rate of up to 100 m/min. This technology allows the manufacture of alginate fibres with a controlled calcium ion substitution

degree and extremely different properties (see Table 8.6). When the calcium ion substitution was higher than 30%, fibres with tenacity of 15–22 cN/tex, elongation of 12–20% and moisture content of 15–25% were obtained. Clinical tests showed their full conformity with the requirements, including an irritation time  $IT_{50} > 10$  days and no allergic action for human skin. The original technology of the Institute of Biomaterials and Chemical Fibres is based on several advantages:<sup>38</sup>

- The ability to use the modifications at the spinning solution and coagulation bath stages
- A controlled ratio content of  $Ca^{+2}/Na^{+}$  ions
- Controlled structure
- Continuous or staple fibres
- A relatively simple technology.

Alginate fibres obtained by this technology can be used in medicine, as a rope-form filament, for difficult healing wounds, or as staple fibres in the form of nonwovens for wound protecting dressings, or as a component of blended biomaterials.

### 8.2.5 Future prospects

For years there has been increasing demand for fibres produced from alginate. These fibres are characterized by such unique properties as, e.g., non-toxicity, biocompatibility, biodegradability, high absorption, and the ability to create permanent gels. It is possible, therefore, to extend the field of their application. Great progress in such modern technologies as nanotechnology, biotechnology and composite technologies allows alginate fibres to be used for the following purposes:

- New high-tech wound dressings
- Scaffolds for tissue engineering
- Resorptive implants
- Surgical threads
- Carriers controlling drug release
- Nanofibres and nanocomposites for advanced applications.

Alginate fibres are one of the most important materials for wound management.

*Table 8.6* Influence of calcium ion content on properties of alginate fibres (adapted from ref. 38)

Calcium ion content (wt%)	Substitution degree (%)	WRV (%)
3.2	31	561
10.2	99	97

Modern active dressings, besides their function of providing a moist wound environment, should also be adaptable to the stage of wound healing and, on this basis, be capable of stimulating the granulating process or protecting against the damage of a newly formed tissue. Introducing other polymers (chitosan, carboxymethylchitosan, keratin, branched ferulate) or special additives (silver and their salts, antibiotics, deodorizing agent) allows a more functional wound material into alginate material.<sup>39–41</sup> The use of alginate in textile scaffolds that may be knitted, woven, nonwoven, braided, embroidered or combined, has certain specialized applications. Flexibility provides versatility, and that is why alginate fibre systems are ideal for encouraging cells to reconstruct the tissue structure in three dimensions.<sup>22,23</sup> There is also a high potential for nanofibres from this biopolymer<sup>42</sup> to be used in tissue engineering, as a carrier of various drugs to specific sites.

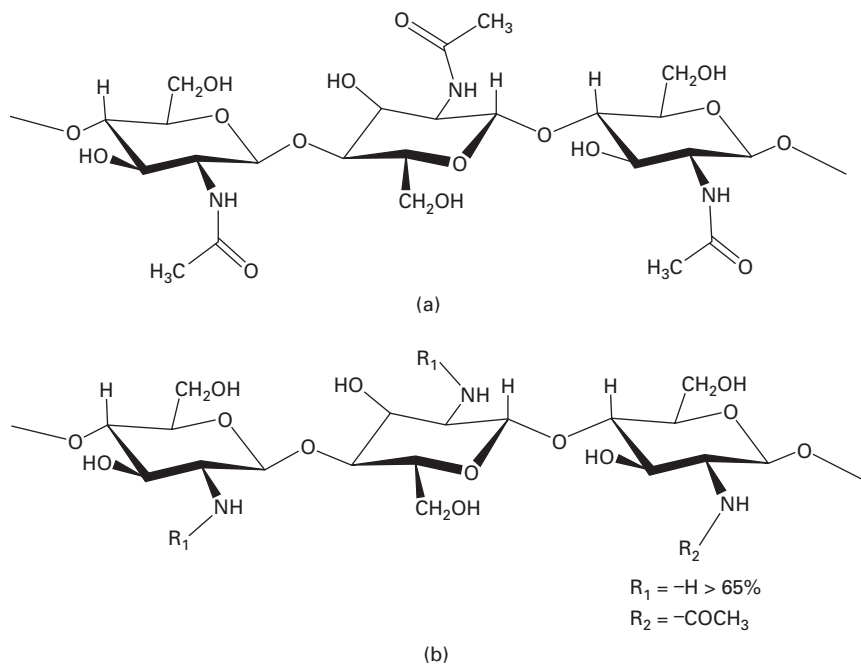
### 8.3 Chitin and chitosan fibres

Chitin is the second most important natural polysaccharide in the world after cellulose. Chitin is present in nature as ordered crystalline microfibrils forming structural components in the exoskeleton of arthropods or in cell walls of fungi and yeast. It is also produced by a number of living organisms in lower plants and animal kingdoms, serving many functions where reinforcement and strength are required.<sup>43</sup> The main commercial sources of chitin are crab and shrimp shells. Chitosan is a partially *N*-deacetylated derivative of chitin. It is the most important derivative of chitin. These polymers are of commercial interest due to their high content of nitrogen (6.89%) compared to synthetically substituted cellulose (1.25%), making them useful chelating agents.<sup>44</sup> Chitin/chitosan fibres and chitosan derivatives are characterized by excellent antibacterial properties and wound healing. They are additionally haemostatic and fungistatic so that they are widely used as wound care products and for other medical uses. Chitin and chitosan are recommended as suitable functional medical materials because of their excellent properties, i.e. biocompatibility, biodegradability, absorption, ability to form film or fibres, and ability to chelate metal ions.<sup>44</sup>

#### 8.3.1 Structure of chitin and chitosan

With regards to their chemical structures (see Fig. 8.6), chitin and chitosan are similar to cellulose, but an acetamide group or amine group replaces the hydroxyl group at the C2 position of the glucosidal ring. Chitin is a polymer of  $\beta$ -(1 $\rightarrow$ 4)-2-acetamido-2-deoxy-D-glucopyranose, while chitosan is a copolymer of  $\beta$ -(1 $\rightarrow$ 4)-2-amino-2-deoxy-D-glucopyranose and 2-acetamido-2-deoxy-D-glucopyranose, obtained by deacetylation of chitin. Because pure chitin with 100% acetylation of the amine groups, and pure chitosan with





8.6 Chemical structure: (a) chitin, (b) chitosan.

IP Address: 129.132.211.108

100% deacetylation, rarely exist, they are often described as copolymers of *N*-acetyl-D-glucosamine and D-glucosamine.<sup>45</sup> The difference between chitin and chitosan is in the acetyl content of the polymer. The degree of deacetylation (DD) is one of the most important structural parameters in chitin and chitosan. When the degree of deacetylation of chitin reaches about 50% (depending on the source of polymer), it becomes soluble in an aqueous acidic media and is called chitosan. For a typical commercial chitosan DD must be 80–85% or higher. It is connected with protonation of the  $-NH_2$  group on the C2 position of the D-glucosamine repeat unit and conversion of the polysaccharide to a polyelectrolyte in acidic media. Chitosan is a pseudonatural cationic polymer<sup>43</sup> with the ability to chemically bind with negatively charged fats, lipids, cholesterol, metal ions, proteins and macromolecules.

Three polymeric crystal structures of chitin ( $\alpha$ ,  $\beta$  and  $\gamma$ ) are known.  $\alpha$ -Chitin is the most crystalline orthorhombic form where the chains are anti-parallel, and can be obtained from the shell of crabs, lobsters and shrimps.  $\beta$ -Chitin has a monoclinic form where chains are parallel, and is obtained from the pen of loligo and squid.  $\gamma$ -Chitin is a mixture of  $\alpha$ - and  $\beta$ -chitins.  $\alpha$ -Chitin is rather resistant to chemical modifications due to the peptide-like hydrogen bonds between chains, and harsh reaction conditions are required to break

it down, whilst  $\beta$ -chitin is less stable, and can be modified under milder conditions. During dissolution or extensive swelling,  $\beta$ -chitin converts to  $\alpha$ -chitin. It is, however, not possible by the reverse approach.<sup>46</sup>

Chitosan is also crystalline and exhibits polymorphism depending on its physical state (various structures for an anhydrous, hydrate or salt form). This has been confirmed by X-ray diffraction analyses.<sup>47</sup> Chitosan is a semicrystalline polymer and its degree of crystallinity is a function of the degree of deacetylation. Crystallinity is maximum for chitin and for fully deacetylated chitosan. Minimum crystallinity is achieved at intermediate degrees of deacetylation. Because of its stable crystalline structure, chitosan is normally insoluble in organic solvents and aqueous solutions at a pH above 7. However, it dissolves readily in most dilute organic acids such as formic, acetic and citric acids because the free amino groups are protonated and the molecule becomes fully soluble below pH 5. Chitosan is soluble to a limited extent in dilute inorganic acids (except phosphoric and sulphuric). The pH-dependent solubility of chitosan is a very useful property.<sup>1</sup> Chitin is insoluble in water and is difficult to isolate without degradation. It is soluble in concentrated mineral acids.

The reactivity of  $-\text{OH}$  and  $-\text{NH}_2$  groups allows various reactions in order to modify the properties of chitin and chitosan, thus obtaining their various derivatives. The basic free amine groups of chitosan can react with many inorganic and organic acids, forming water-soluble salts (mostly). During the acylation of amine groups of chitosan using acyl anhydride, the chitosan in solution slowly loses solubility and a gel is formed. Acetylation of chitosan fibres using acetic anhydride in methanol as a solvent leads to regenerated chitin fibres. During this reaction,  $-\text{NH}_2$  groups with aldehydes or ketone Schiff bases can be formed. So as a result of the modification of chitosan using such compounds, products with excellent chelating properties are obtained. The reaction of chitin and chitosan ( $-\text{OH}$  and  $-\text{NH}_2$  groups) with halogen-substituted compounds allows the modification of the structure of both polymers, and yields various derivatives with a variety of properties. The ability of chitin and chitosan to absorb heavy metal ions is explained by the fact that they form metal ion complexes with many transition metal ions, and this chelating property is mainly as a result of the primary amine groups.<sup>45,48</sup> Chitosan can be hydrolysed by lysozymes. The degradation products of chitosan are amino sugars.<sup>1</sup>

### 8.3.2 Chitin and chitosan production methods

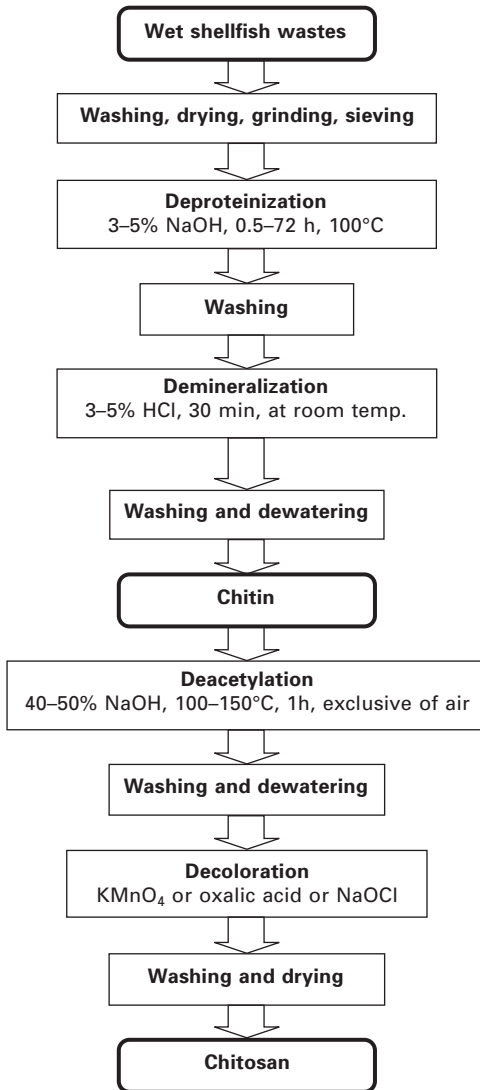
Chitin was first isolated in 1811 by Braconnot, and chitosan in 1859 by Rouget who reported the treatment of chitin using a concentrated potassium hydroxide solution. Hoppe-Seyler in 1894 proposed the name of chitosan for the product.<sup>43</sup> Potential sources for chitin production are shells of crabs,

crustaceans, shrimp and lobster, insects, jellyfish, algae and fungi. A novel method for making a chitin-based fibrous dressing material uses a non-animal source, namely microfungus mycelia, as the raw material. The resulting microfungus fibres are different from the normal spun ones.<sup>23</sup> Commercially, chitin and chitosan are mainly produced from shells of crustaceans such as crabs, shrimps and krill, which are generated by the seafood processing industries as a shell waste. These shells contain three components: proteins (30–40%), calcium carbonate (30–50%) and chitin (20–50%). These various percentage contents depend on the crustacean species and the season in which they are harvested.<sup>47,48</sup>

The methods of chitin and chitosan production are various, generally divided into two groups, chemical and biological, but all of them consist of four main stages: deproteinization, demineralization, decolorization and deacetylation. Chitin and chitosan are commercially manufactured by a chemical method, as schematically shown in Fig. 8.7. Sometimes the sequence of demineralization and deproteinization stages can be reversed. In some procedures demineralization occurs before deproteinization.<sup>49</sup> Technological parameters are different for various methods, but most often the shells are first cleaned, ground and then treated with an aqueous 3–5% NaOH solution at 100°C for a few hours to decompose the proteins. Then, after neutralization the shells are treated with an aqueous 3–5% HCl solution at room temperature to remove calcium carbonate and calcium phosphate. To remove pigments, a bleaching process is performed, and chitin is obtained as an almost colourless to off-white powdery material. Chitosan in nature exists only in a few species of fungi. Commercially, chitosan is produced from chitin by deacetylation with a highly concentrated (40–50%) solution of NaOH at high temperature (100–150°C).<sup>47–49</sup> Chitosan can also be obtained from squid pens. In this case, chitosan is synthesized from  $\beta$ -chitin (amine group aligned with OH and CH<sub>2</sub>OH groups) while crustacean exoskeleton chitosan is synthesized from  $\alpha$ -chitin (anti-parallel chain alignment).

In enzymatic methods proteases can be used for the deproteinization of shells. Microbial synthesis of chitosan is found in various organisms including *Mucor rouxii*, *Phycomyces blakesleeianus* and others. Cell cultures of these organisms have been used for the production of chitosan, and the yields obtained were improved by addition in the culture medium of a chitin source such as *Aspergillus niger*. Thus the mechanism of production was attributed to chitin deacetylation.<sup>50</sup> KitoZyme S.A. (Belgium) produces about 100 tons per year of chitin and chitosan using biological methods, from fungal mycelium.

Chitin, and their derivatives like chitosan, is being produced by about 50 companies, mainly in Asia (China, South Korea, India, Thailand and Japan), North America and Europe. Examples of these companies are Primex Ehf (Iceland), France Chitin (France), Qingdao Hepe Biotechnology Ltd (China/



8.7 Scheme of chitin and chitosan production using chemical method.

IP Address: 129.132.211.108

Germany), FMC BioPolymer (USA), NovaMatrix (Norway), Dalwoo-Chitosan BLS (Korea), Meron Biopolymers (India), Golden-Shell Biochemical Co. Ltd (China) and Vanson Inc. (USA).

Chitosan can be produced:

- at various degrees of purity, which is determined by its use (medical-pharmaceutical grade, industrial grade),

- at various molecular weights (high and low density chitosan, chitosan oligomer),
- at different degrees of deacetylation (50–95%), depending on use,
- at various particle sizes.

Almost all the properties of chitin and chitosan depend on two fundamental parameters: the degree of deacetylation (DD) and the molecular mass distribution (or average molecular weight), although they do have some contrasting properties. The molecular weight of chitin and chitosan can be determined by methods such as chromatography, light scattering and viscometry. There are many methods that are well described in the literature for estimating DD, e.g. IR spectroscopy, UV spectroscopy, gel permeation chromatography, various titration schemes and others. Converting chitin into chitosan lowers the molecular weight and changes the degree of deacetylation, and thereby alters the charge distribution, which turn influences agglomeration. The weight-average molecular weight of chitin<sup>44</sup> is  $1.03\text{--}2.5 \times 10^6$ , but the *N*-deacetylation reaction reduces this to  $1.0\text{--}5.0 \times 10^5$ . Depending on the source and preparation methods, commercial chitosan's average molecular weight ranges from 50 to 1000 kDa. Commercially available preparations have degree of deacetylation in the range 50–90%.

The main properties of chitin and chitosan, which are important in many applications, are:<sup>43,44</sup>

- IP Address: 129.132.211.108
- Highly basic polysaccharides
  - Semicrystalline structures
  - Formation of polyoxysalt
  - Ability to form films, fibres and gels
  - Good complex formation with metals
  - Ability to bind with negatively charged fats, lipids, cholesterol, metal ions, proteins and macromolecules
  - Non-toxicity
  - Biocompatibility
  - Biological activity
  - Possibility of forming derivatives.

Chitin is highly hydrophobic and is insoluble in water and most organic solvents, but is soluble in hexafluoroisopropanol, hexafluoroacetone and chloroalcohols in conjugation with aqueous solutions of mineral acids and dimethylacetamide containing 5% lithium chloride. Chitosan is soluble in dilute acids such as acetic acid, formic acid, etc. Chitosan has a gel-forming ability in *N*-methylmorpholine *N*-oxide.

From the point of view of special properties, particularly biological activity, chitin, chitosan and their derivatives can be used for many applications:<sup>44</sup>

- *Medicine*: wound dressing materials, sponges, artificial blood vessels,

blood cholesterol control, tumour inhibition, membranes, dental/plaque inhibition, skin burns/artificial skin, eye humour fluid, contact lenses, controlled release of drugs, bone disease treatment and tissue engineering.

- *Cosmetics and toiletries*: make-up powder, nail polish, moisturizers, fixtures, bath lotion, face, hand and body creams, toothpaste and foam enhancers.
- *Water treatment*: removal of metal ions and flocculant/coagulant proteins.
- *Food*: removal of dyes, solids, acids and preservatives, colour stabilization, and as an animal feed additive.
- *Agriculture*: seed coating, leaf coating, hydroponics/fertilizer, controlled agrochemical release and as a fertilizer.
- *Biotechnology*: enzyme immobilization, protein separation, chromatography, cell recovery, cell immobilization, glucose electrode and within biosensors.
- *Pulp and paper*: surface treatment, photographic paper and carbonless copy paper.
- *Membranes*: reverse osmosis, permeability control and solvent separation medium.
- *Special purpose*: chitosan can be used in tobacco slice glue.

### 8.3.3 Methods of chitin and chitosan fibre production

Wet spinning is mostly used to produce chitin and chitosan fibres, as they cannot be formed by either melt- or dry spinning methods. The strong inter-chain forces as derived from the hydroxyl, acetamido and amino groups raise the melting point of chitin and chitosan to well above their thermal degradation temperatures. Therefore, melt spinning is typically not possible for chitin and chitosan.<sup>48</sup> Besides that, these two natural polymers can only be dissolved in polar solvents that have high boiling points. As a consequence, dry spinning is also not practical for producing chitin and chitosan fibres. In wet spinning processes, dissolving the polymer in an appropriate solvent first makes a polymer solution. The solution is then filtered and degassed before it is extruded through fine holes into a non-solvent to precipitate the polymer in a filament form.<sup>48</sup> In the case of chitin fibres, a number of solvent-coagulant systems have been tried to form the chitin fibres. Spinnability of the chitin solutions can be improved with increasing the coagulation bath temperature and with the addition of the right type of plasticizer to the spinning solution.<sup>48</sup>

Regenerated chitin fibres can be produced using a viscose method from chitin xanthate. At first chitin is converted into chitin xanthate by treatment with 40% NaOH at room temperature and then after removing the caustic

soda the chitin solution is shaken with carbon disulphide for 4 hours at 25°C. Suitable solutions for the production of fibres are obtained after mixing chitin xanthate with crushed ice, and other additional operations. The chitin xanthate solution in aqueous NaOH is then filtered, degassed at room temperature and spun into a coagulation bath containing 8–10% sulphuric acid, 25% sodium sulphate and 1–3% zinc sulphate. These fibres are characterized by low tenacity at break (about 2.7 cN/tex).<sup>48–53</sup>

Other methods of regenerated chitin fibre production use a halogenated solvent system. In this case, the spinning solutions are obtained using di- or trichloroacetic acid in combination with organic solvents such as formic acid, acetic acid, chloral hydrate and methylene chloride. The chitin solutions are extruded into an acetone coagulation bath.<sup>44,48</sup> Tokura and co-workers used a combination of formic acid, dichloroacetic acid and isopropyl ether as a solvent system. Chitin solutions were obtained by a freezing process. They extruded the spinning solution into various coagulation baths (ethyl acetate and water, isopropyl ether), and at various draw ratios.<sup>48,53</sup> Unitika Co. used trichloroacetic acid/dichloromethane and trichloroacetic acid/chloral hydrate/dichloroethane solvent systems for chitin. All spinning solutions in this system were spun into an acetone bath at various concentrations. Fibres obtained in this way have good mechanical properties, but the solvents used, namely solutions in amide organic solvents with some additives, mostly lithium chloride (LiCl) (amide–lithium systems),<sup>44</sup> are corrosive and degrade the polymer produced. A mixture of *N*-methyl-2-pyrrolidone (NMP) and lithium chloride (LiCl) is often used as a solvent. Chitin solutions are extruded into a coagulation bath, which is usually acetone or alcohol. Fibres obtained in this way are characterized by low tenacity (about 2.5 cN/tex), which results from low concentration of chitin in the solution (about 2%) and a low molecular weight.<sup>49</sup>

Chitin fibres with greater tenacity have been obtained from a 3–3.5% solution of chitin, which consists of *N*-methyl-*N*-pyrrolidone (NMP), dimethylacetamide (DMAc) and LiCl. When solvents containing NMP and DMAc in the ratio 1:1 with 5% additive of LiCl were used, a spinning solution with a relatively low viscosity was obtained. A mixture of DMAc–glycol–ethanol was used in a volumetric ratio of 4:4:2 as a coagulation bath. Under these conditions, fibres with a tenacity of about 12–18 cN/tex were obtained. When drawing fibres in a plastification bath, a glycol and ethanol mix of 50:50 was used. In this approach the tenacity of the chitin fibres increased to 27 cN/tex, with 3% strain at break.<sup>49</sup> The problem with this system is the removal and recovery of lithium from the fibre.<sup>44</sup>

Agboh and Qin described a wet spinning process for chitin fibres using DMAc–LiCl.<sup>48</sup> At first chitin was depolymerized by pre-treatment in *p*-toluene sulphonic acid in *i*-propanol. After this treatment a 5–9% solution of chitin in DMAc–LiCl was prepared. Then this spinning solution of chitin was extruded



into various coagulation baths and fibres were obtained. This spinning solution is suitable for dry-jet spinning. At first the solution was spun into an air gap and then into a non-solvent coagulation bath. They proposed a coagulation bath mixture of DMAc and H<sub>2</sub>O (75:25), at temperatures of 40–75°C, or methanol at room temperature. Chitin fibres obtained using these conditions were 20–80 μm in diameter and had tenacities of 0.7–2.2 cN/tex, an initial modulus of 10–54 cN/tex and an elongation at break of 7–75%.<sup>48</sup>

Wet spinning of chitosan fibres is obtained by extruding the viscous chitosan solutions in a dilute acid into a coagulation bath. In dilute acids, the free amino groups of the glucosamine residues are protonated and the molecule becomes fully soluble below pH 6. To form the spinning dope, chitosan (3%) is thus dissolved in an acidic solution (usually 0.5–4% aqueous acetic acid). Viscous solutions can be transformed into fibres in different coagulation solutions, such as aqueous solutions of NaOH (5%),<sup>53–57</sup> KOH,<sup>58,59</sup> cupric ammonia,<sup>60</sup> alcohol or calcium chloride or acetate,<sup>61</sup> NaOH–Na<sub>2</sub>SO<sub>4</sub> or NaOH–AcONa,<sup>62</sup> NaOH–40% methanol,<sup>63</sup> CuSO<sub>4</sub>–NH<sub>4</sub>OH or CuSO<sub>4</sub>–H<sub>2</sub>SO<sub>4</sub>,<sup>64</sup> etc. The coagulated fibre can be subsequently washed in water to remove the excess of coagulant, dried and collected on a winder. The washing bath usually comprises distilled water,<sup>59</sup> aqueous methanol or ethanol.<sup>60,61</sup> This mixture often plays the role of a pre-drying bath. In order to obtain fibres with good mechanical properties, some physical and chemical treatments, which are called drying treatments, can be used at the end of the process. It has been found that the drying treatments, as well as spinning conditions, have a strong effect on the fibre properties.<sup>58,65</sup>

Special chitosan fibres for medical applications were obtained by a wet method at the Institute of Biopolymers and Chemical Fibres.<sup>38</sup> The acidic spinning solution containing dissolved chitosan and special additives to improve properties was spun into an alkaline coagulation bath at a temperature of 20–30°C. Then fibres were stretched by 35% into a double-bath system containing diluted aqueous alkali, washed in demineralized water, prepared by a Span-20/Tween-20 blended avivage, and dried at a temperature of 70°C. Chitosan fibres were spun out at a rate of 20–25 m/min. Fibres obtained by this method had typical properties for medical uses:<sup>38</sup>

- Titre 1.5–3.0 dtex
- Tenacity in standard conditions 10–15 cN/tex
- Tenacity in wet conditions 3–7 cN/tex
- Elongation in standard conditions > 10%
- Average molecular weight ( $M_v$ ) 150–300 kD
- Polydispersity ( $P_d$ ) 3.5–6.0
- Water retention value (WRV) > 150%
- Crystallinity index (CrI) 35–50%.

The advantages of this method for the preparation of chitosan fibres are:<sup>38</sup>

- Controlled bioactivity and biodegradability of fibres
- Controlled structure
- Ability to utilize most commercial chitosan grades
- Continuous or staple form fibres
- Relatively simple technology
- Fibres are not irritating or allergic to human skin.

Notin *et al.*<sup>66</sup> described a new method to spin polysaccharides in the absence of any aqueous bath after the spinneret. This coagulation method consisted of subjecting the extruded monofilament to gaseous ammonia. They applied this new process to chitosan and studied the role of several parameters to enable optimal spinning conditions.

The pH-dependent solubility of chitosan is a very useful property, which provides a convenient mechanism for processing chitosan under mild conditions. For example, viscous solutions of chitosan can be prepared at low pH and then extruded and gelled in higher pH solutions or baths of non-solvent such as methanol. The gel fibres obtained can be subsequently drawn and dried to form high-strength fibres.

The development of new spinning solvents and coagulating baths as well as new techniques is still important for the production of high quality chitin and chitosan fibres and their derived fibres.

### 8.3.4 Influence of structure on properties

Modification of the structure of chitin and chitosan fibres allows the creation as well as the improvement of their specific properties at the molecular, super-molecular and morphological levels, at different stages of the manufacturing processes,<sup>38</sup> namely whilst:

- preparing the spinning solution
- spinning the fibres
- stretching the fibres
- finishing the fibres.

Some typical properties of chitin and chitosan fibres in comparison with other natural polymer-based fibres are reported in Table 8.7.<sup>48</sup>

It is known that the solvent system and the type of coagulation bath influence the fibre structure and as a consequence, the fibre properties. The surface and cross-section of fibres are strongly affected by the mechanism of dehydration of as-spun fibres during wet spinning. Chitin and chitosan fibres are characterized by a rather round cross-section under most spinning conditions, but their surface depends on the methods used for coagulation and drying. Cross-sections and surfaces of chitosan fibres are shown in Figs 8.8a and 8.8b. Tokura and co-workers<sup>48,53</sup> used a combination of formic acid,

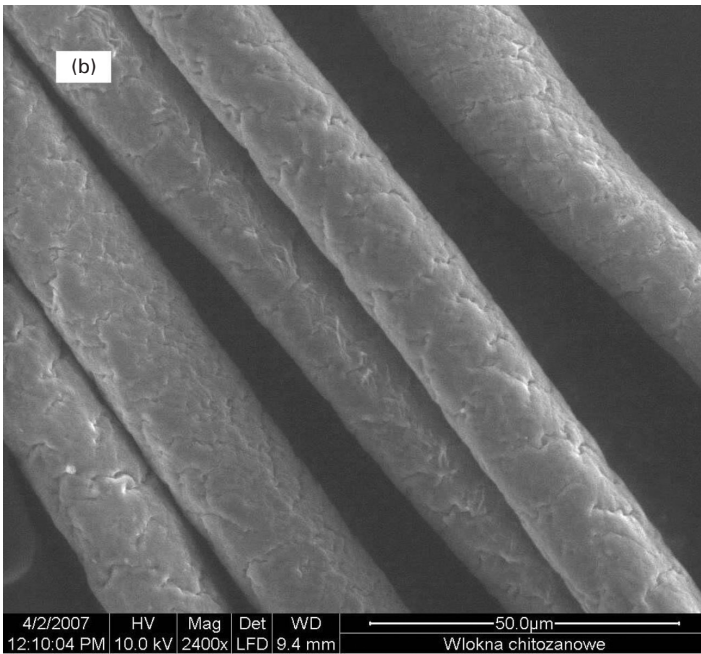
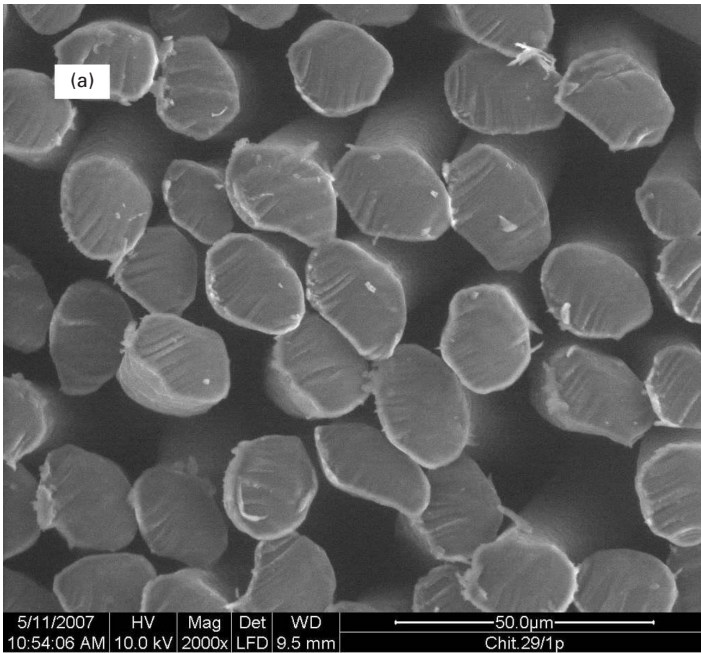
*Table 8.7* Comparison of typical properties of chitin and chitosan fibres with other natural polymer-based fibres (adapted from ref. 48)

Type of fibres	Specific gravity (g/cm <sup>3</sup> )	Moisture (%)	Tenacity (g/tex)	Elongation (%)
Cotton	1.54	7–8.5	2.3–4.5	3–10
Viscose rayon	1.52	12–16	1.5–4.5	9–36
Alginate	1.78	17–23	0.9–1.8	2–14
Chitin	1.39	10–12.5	1.2–2.2	7–33
Chitosan	1.39	16.2	0.61–2.48	5.7–19.3

dichloroacetic acid and isopropyl ether as a solvent system. They extruded spinning solutions into various coagulation baths and with various draw ratios. These examinations showed that the fibres spun into ethyl acetate and water have the best fibre properties. Fibres spun into isopropyl ether had a dull fibre surface and many cracks along the fibre axis, but other fibres had smooth surfaces and lustrous textures.

Chitin fibres with high tenacity (about 27 cN/tex) were obtained from solutions of chitin in a mixture of NMP, DMAc and LiCl, which were spun into a special coagulation system (DMAc–glycol–ethanol) and drawn in a plastification bath containing glycol and ethanol.<sup>49</sup> According to the authors, such high tenacity parameters result from the chain stiffness and highly oriented fibrillar structure of fibres. On the basis of X-ray examinations and electron microscopy, the authors suggested that the spinning solutions of chitin used in the work have a liquid crystal character. Confirmation of this idea is provided by an 80% loss of tenacity of the chitin fibres in the wet state where, at the same time, the elongation at break increases by a factor of 5.<sup>49</sup> The amide–lithium systems showed some of the best dry tenacities, although they still lack adequate wet tenacities. Low wet tenacities are probably due to low crystallinity and poor consolidation of the fibre.<sup>44</sup> High-strength fibres were manufactured using special spinning conditions such as the dry-jet wet spinning technique and special solvent systems to obtain a liquid crystal phase for the chitin and chitosan solutions. Thanks to this technique, fibres can be made into highly oriented structures when they are stretched to a high degree. It is known that chitin and chitosan are semicrystalline polymers, which can form three-dimensionally ordered structures. In the case of chitin, the type of polymorphic form has an influence on the properties of the fibre, e.g.  $\alpha$ -chitin has high hardness, but  $\beta$ - and  $\gamma$ -chitins have high toughness, flexibility and mobility.<sup>48</sup>

Examinations carried out by East and Qin<sup>58</sup> showed that when producing chitosan fibres from solutions in 2% aqueous acetic acid, the spinning conditions such as jet stretch ratio and draw ratio and the composition of the coagulation bath have little effect on the fibre properties, though higher draw ratios are obtained at lower jet stretch ratios and slightly improved fibre tenacities



IP Address: 129.132.211.108

8.8 SEM micrographs of chitosan fibres: (a) cross-sections, (b) surface.

are obtained by using a more dilute NaOH solution as the coagulant. The drying conditions, however, had a big effect on the fibre properties. Fibres obtained by air-drying had much higher extensibilities than those dried by radiant heating. Strong fibres were obtained by using a coagulation bath containing concentrated  $\text{Na}_2\text{SO}_4$  with a small amount of NaOH. East and Qin explained that, when the chitosan fibres are acetylated to produce chitin fibres, the increase of both the dry and wet strengths with the increase in the degree of acetylation is a reflection of the increase in interchain forces and the increase in the degree of crystallinity.<sup>58</sup> This was confirmed by X-ray examinations.<sup>58</sup> During acetylation, at first wet strength decreases, which is caused by the irregularity of the polymer structure. Chitosan is a highly irregular copolymer of glucosamines and acetylglucosamines. The moisture regain of the fibre also has an influence on the strength of chitosan fibres.

The creation of chitosan structure, which is responsible mainly for its bioactivity, is also utilized during the preparation of fibres.<sup>38</sup> The biological significance of chitosan in the human body depends mostly on the biodegradation action of enzymes, such as lysozymes and lipases. The resulting chitooligomers stimulate various cells; the released monomers are phosphorylated and incorporated into hyaluronan, a component of the intracellular matrix and connective tissue.<sup>67</sup> The specific behaviour of chitosan fibres with different properties during the biodegradation test in the presence of lysozyme is reported in Table 8.8. These results confirmed the influence of the structure of chitosan fibres on their biological activity.

Because of the primary amine groups in the structure, chitosan is a natural chelating polymer with excellent absorption capacities for many heavy metal ions, especially silver, copper and zinc. These metals are useful for biomedical applications. Because of their large specific surface area, chitosan fibres are particularly effective in absorbing metal ions. Qin *et al.*<sup>68-70</sup> prepared chitosan fibres containing silver, copper, or zinc. They examined the absorption and release of these metal ions by chitosan fibres. Chitosan fibres can chelate up to 9.0% and 6.2% of their own weight of copper and zinc ions, respectively.<sup>69</sup> Results showed that chitosan fibres containing silver, copper or zinc had

**Table 8.8** The specific behaviour of chitosan fibres with different properties during the biodegradation test in the presence of lysozyme (adapted from ref. 38)

Chitosan fibres	Tenacity (cN/tex)	Crystallinity index (%)	WRV (%)	$M_v$ before test (kD)	$M_v$ (kD)		Oligoamino-saccharide content (mg/cm <sup>3</sup> )	
					after 6 days	after 24 days	after 6 days	after 24 days
1	14.8	48.0	240	252	145	75	0.05	0.15
2	10.9	35.3	290	235	102	34	0.11	0.25

much stronger antimicrobial properties than the original chitosan fibres. Chelation is enhanced for greater degrees of deacetylation of chitin, and it is also related to the degree of polymerization of oligo-chitosans.

### 8.3.5 New fibres based on chitin and chitosan

Pure chitosan fibre processing has rarely been reported in the literature. The formation of chitosan fibres crosslinked by epichlorohydrin<sup>57</sup> has been described. A series of novel human-made fibres (biofibres) based on chitin and chitosan have been prepared by wet spinning, and post-chemical modification of chitosan fibres was recently reviewed by Hirano.<sup>71</sup> He showed the possibility of obtaining monocomponent, bicomponent and tricomponent fibres. Many of his papers have detailed the preparation of composite chitosan fibres such as *N*-acylchitosan–cellulose fibres,<sup>72,73</sup> fragrant chitosan derivatives,<sup>74</sup> chitosan–collagen fibres,<sup>75</sup> chitosan/poly(vinyl alcohol) blend fibres<sup>76</sup> or chitosan–silk fibroin fibres.<sup>77,78</sup> Moreover, post-treatments were performed on chitosan fibres with solutions containing phthalate or phosphate ions,<sup>59</sup> and even aldehydes including vanillin.<sup>62</sup> These biofibres based on chitin, chitosan, chitin–cellulose, chitosan–cellulose–silk fibroin, chitosan–tropocollagen and chitin–cellulose–silk fibroin have been proposed for applications including antithrombogenic, antimicrobial, haemostatic and wound healing. *N*-hexanoyl and *N*-octanoylchitosan fibres are antithrombogenic, blood compatible and resistant to chitanase and lysozyme hydrolyses, and are usable as antithrombogenic biomaterials. *N*-acylchitosan filaments have been used for surgical suture production. The *N*-acylchitosan suture is digested by lysozymes in tissue, and the digestion period is controlled by the chemical structure of *N*-acyl groups and their degree of substitution. It is not necessary to take out the stitches after the operation when using this material.<sup>71</sup>

Novel chitosan–alginate fibres are very promising for wound dressing applications. Chitosan is increasingly being combined with other materials, especially with lower-cost biopolymers, for effective and better wound healing properties. This has the potential of considerably reducing the unit cost of chitosan dressings as well as improving properties.<sup>79</sup> Chitosan and alginate under certain conditions can have opposite charges. Chitosan is a cationic polysaccharide consisting of glucosamine, and alginic acid is anionic. An ionic interaction can be expected between them.<sup>79</sup> So far it has been impossible to obtain composite alginate–chitosan fibres because of the differences in the solubility of both polymers, as chitosan is soluble in aqueous solutions of organic and inorganic acids, whereas sodium alginate is soluble in water and aqueous alkali solutions.<sup>39</sup> The problems of directly manufacturing alginate–chitosan fibres have been solved in different ways, e.g. the alginate and chitosan staple fibres have been obtained separately and then mixed in order to produce a nonwoven. Another method has consisted of introducing

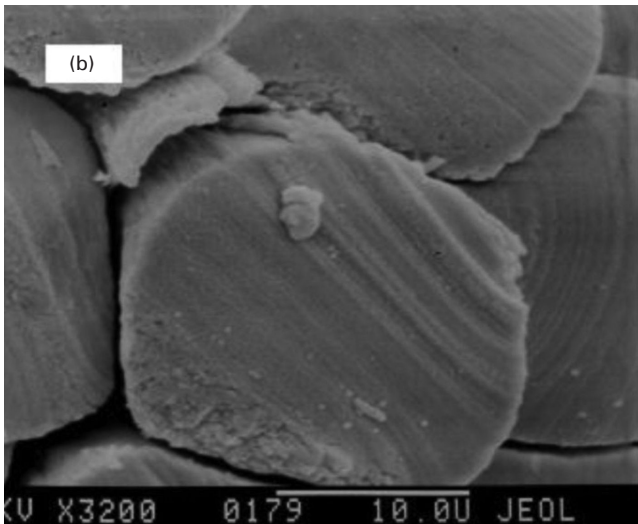
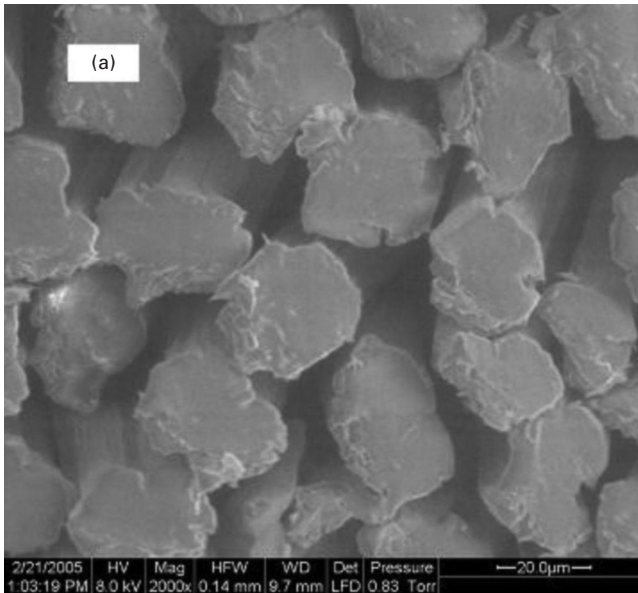


a chitosan solution into a coagulation bath containing an aqueous solution of calcium chloride while spinning alginate fibres. The chitosan concentration was, however, relatively low using this method and the amount of polymer introduced into the fibres was not high enough.

Steplewski *et al.*,<sup>39</sup> from the Institute of Biopolymers and Chemical Fibres, have proposed a manufacturing process for obtaining modern two-component alginate–chitosan fibres of the core–skin types (calcium alginate and chitosan, respectively). Two methods have been developed. The first method (A) of producing fibres, which consists of fibre spinning by feeding chitosan into a coagulation bath, allowed alginate–chitosan fibres to be produced with a maximum chitosan content of about 3.1%. The second method (B) turned out to be more efficient. This method consists of using chitosan in a finishing process and obtained alginate–chitosan fibres with a chitosan content of up to 9.2%. In order to further increase the chitosan content in the alginate–chitosan fibres manufactured by method B, polyvinylpyrrolidone (PVP), in amounts from 4% to 20% in relation to calcium alginate, was introduced into the spinning solution. PVP enables better penetration of the chitosan solution into the alginate fibres, an increase in the total amount of chitosan deposited on the fibres, and better binding of the chitosan shell with the alginate core. Furthermore, the addition of PVP enables the production of two-component fibres with a chitosan content twice that of fibres spun without PVP. The two-component fibres manufactured with the use of PVP, and which included 11.6% of chitosan, were characterized by a tenacity of 22.3 cN/tex and an elongation at break of 19%. Additionally, the alginate–chitosan fibres of this type were characterized by very high water retention values (WRV) of up to 1300%, which make these fibres suitable for use in sanitary and medical products, especially for new generations of dressings.<sup>39</sup> This group examined the molecular, supermolecular and morphological structures of the obtained fibres.<sup>39</sup> It is possible to obtain alginate–chitosan fibres with a chitosan core and an alginate skin. Examinations of these fibres, however, showed the worst mechanical and WRV results. SEM micrographs showed significant differences in the cross-sections which are clearly visible when comparing chitosan–alginate fibres with chitosan shells and alginate cores (see Fig. 8.9a) and chitosan–alginate fibres with alginate shells and chitosan cores (see Fig. 8.9b).<sup>39</sup>

It is known that using chitin for higher technology products, such as fibres for modern wound dressings, is limited because of its lack of solubility in common solvents. Therefore the practical application of chitin in this technology requires suitable methods of modification to increase its reactivity and solubility.<sup>80</sup> Modification of chitin by butyric anhydride treatment produces dibutyrilchitin (DBC), a chitin derivative which is soluble in organic solvents such as dimethyl formamide (DMF), dimethyl sulphoxide (DMSO), *N*-methyl-2-pyrrolidone (MP), ethyl alcohol (EtOH) and others.





8.9 SEM micrographs of cross-sections of chitosan–alginate fibres: (a) chitosan shell, alginate core; (b) alginate shell, chitosan core (adapted with permission from ref. 39).

IP Address: 129.132.211.108

DBC solutions distinguished by high stability and suitable rheological properties can be used for spinning DBC fibres.<sup>80,81</sup> The dry, wet–dry and wet methods can be used for spinning of DBC fibres, depending on the kind of solvent used to obtain the DBC spinning solution. Wawro *et al.*<sup>80</sup> and Binias *et al.*<sup>81</sup> examined dissolution conditions for many solvents and

spinning conditions to obtain DBC fibres with the best properties. When they used solvents such as DMF, MP, DMSO and EtOH to spin DBC fibres, they obtained fibres with different mechanical properties, depending on the type of solvent and spinning conditions.<sup>80</sup> DBC fibres spun from EtOH solution were characterized by low tenacity (8.12 cN/tex), which was probably caused by large porosity. In this case, high-porous DBC fibres were produced.<sup>80,81</sup> These fibres are being considered for the production of knitted materials, namely bandages, dressing gauzes, and nets for supporting and/or isolating internal organs under surgery.<sup>80</sup>

### 8.3.6 Future prospects

The many unique properties of chitin and its derivatives are now attracting more and more scientific and industrial interest from diversified fields such as chemistry, biochemistry, medicine, pharmacology, biotechnology, and food and textile sciences. Properties such as biodegradability, biocompatibility, non-toxicity, wound healing and antimicrobial activity have generated much research work and show promise for the future. Products produced using chitin have been shown to increase wound healing in animals and humans. Chitin has also demonstrated a physiological compatibility with living tissues. Chitin's ability to form sulphate esters, which are non-thrombogenic, appears to make it a promising candidate for prosthetic structural devices of any shape or size. Therefore, chitin could serve as replacements for bone, cartilage, arteries, veins, and musculo-facial replacements. The uses of chitin and chitosan are only limited by the creativity of the biomedical engine. Many unique products have been developed for various applications such as surgical sutures, artificial skin, cosmetics and dietary foods. Hirano<sup>71</sup> and other scientists believe that the following directions will be important for chitin and chitosan fibres in the future:

- Novel methods for preparation of the parallel oriented fibrils
- New composite materials
- New artificial intelligent materials which have mechanical movements, magnetic functions, shape-memory and novel biological functions.

New promising functional fibres from chitin/chitosan derivatives or composite fibres with other polymers, i.e. alginates, branan ferulate, hyaluronian, carbamate<sup>23</sup> and others, are described in Section 8.3.5. Reduced molecular weight and lowered crystallinity by random deacetylation generally improves chitosan solubility in dilute acids and enables processing into various forms, such as beads, membranes and fibres.

Recent attention has been focused on making chitosan fibrous membranes by electrospinning. Pure chitosan fibres have only been electrospun from 7–8% solutions of chitosan at relatively low molecular weights, such as 210

kDa ( $M_v$ ) and 78% degree of deacetylation in trifluoroacetic acid, and 106 kDa and 54% degree of deacetylation in 90% aqueous acetic acid.<sup>82,83</sup> Others have reported fibre generation by electrospinning of chitosan mixtures with other polymers, for example with silk fibroin; polyvinyl alcohol (PVA) and poly(ethylene oxide) (PEO)<sup>82,83</sup> have also been reported. Li and Hsieh<sup>82</sup> prepared chitosan/PVA bicomponent nanofibres, but by using an alkaline treatment of these nanofibres, and removing the PVA phase, new nanoporous structures (nanoporous fibre) were obtained. In parallel, electrospinning experiments using other polysaccharides, especially cellulose, crosslinkable chitosan derivatives and synthetic polypeptides, are in progress.<sup>83</sup> In the literature, chitin nanofibrous matrix (membranes) for wound dressings, for scaffolds in tissue engineering, for sensing applications and for filter applications are reported.<sup>84,85</sup> As future materials for scaffolds in tissue engineering, there are special chitosan<sup>86,87</sup> and alginate–chitosan fibres.<sup>88</sup> New advantages in nanocomposites based on chitosan can be focused and new materials (hydroxyapatite, magnetite, carbon nanotubes, montmorillonite) have been utilized to develop chitosan composites; most of them are expected to be used in medical fields.<sup>89–91</sup>

## 8.4 Conclusions

Chitin/chitosan and alginate fibres are still some of the most interesting constructive biomaterials designed for special applications, especially for medical uses. These biopolymers are ecological and environmentally friendly. The specific properties of alginate, chitin and chitosan polymers and fibres allow them to find more and more uses in chemistry, biochemistry, medicine, pharmacology, biotechnology, food and textile sciences for the production of modern and functional materials. Further development of new technologies of production, for instance micro- and nanofibres based on electrospinning, will allow the construction of special new materials, including wound dressings, drug carriers for controlled release and implants, and scaffolds for tissue regeneration. Fibres that are produced using dibutrylchitin should have high potential because of the more effective technology of spinning them. Mastering the technology of producing composite fibres will allow the production of new multifunctional materials.

## 8.5 Sources of further information and advice

Some details of described polymers and fibres are in the references (Section 8.7) and on producers' websites, which are listed below:

*Alginate producers' websites:*

<http://www.ispcorp.com/products/alginates>

<http://www.fmc.com>, [www.fmcbiopolymer.com](http://www.fmcbiopolymer.com)  
<http://www.texturantsystems.com>  
<http://www.kimica.com>  
<http://www.waila.or.jp/kasei>

*Alginate fibres and wound dressings producers' websites:*

<http://www.sfm-limited.com>  
<http://www.convatec.com>  
<http://wound.smith-nephew.com>  
<http://silverlon.com>

*Chitin/chitosan producers' websites:*

<http://www.france-chitine.com>  
<http://www.primex.is>  
<http://www.fmcbiopolymer.com>  
[http://novamatrix\\_info@fmc.com](mailto:novamatrix_info@fmc.com)  
<http://www.dalwoo.com/chitosan>  
<http://www.meronbiopolymers.com>  
<http://www.golden-shell.com.cn>

*Chitin/chitosan fibres producers' websites:*

<http://www.fujibo.co.jp>  
<http://www.omikenshi.co.jp>  
<http://www.swcofil.com/>  
<http://www.ibwch.lodz.pl>

## 8.6 Acknowledgements

The authors would like to acknowledge John Wiley & Sons Ltd, Fibres and Textiles in Eastern Europe and Akademiai Kiado for giving permission to adapt their copyright materials. The authors also appreciate the contribution of Mrs Agnieszka Wachowska, Dr Piotr Czarnecki and Dr Marcin Rubacha in creating the manuscript for this chapter.

## 8.7 References

1. Shi D., 'Naturally occurring polymer biomaterials', Chapter 10 in *Introduction to Biomaterials*, ed. Shi D., World Scientific Publishing Company, Hackensack, NJ, 2006.
2. Struszczyk H., 'Alginate and chitosan fibers for medical uses', Chapter 7 in *Natural Fibers, Polymers and Composites*, ed. Wallenberger F.T., Weston N.E., Kluwer Academic Publishers, Boston, MA, 2004.
3. Qin Y., Agboh C., Wang X., Gilding D.K., 'Alginate fibers', *Chemical Fibers Int.*, 1996, 46, 272–273.
4. McHugh D.J., 'A guide to the seaweed industry', *FAO Fisheries Technical Paper*, No. 441, FAO, Rome, 2003.

5. Draget K.I., Smidsroed O., Skjaak-Braek G., 'Alginates from algae', Chapter 1 in *Polysaccharides and Polyamides in the Food Industry. Properties, Production and Patents*, ed. Steinbüchel A., Rhee S.K., Wiley-VCH Verlag, Weinheim Germany, 2005.
6. Smidsroed O., Glover R.M., Whittington S.G., 'Relative extension of alginates having different chemical composition', *Carbohydr. Res.*, 1973, 27, 107–118. doi: 10.1016/80008-6215(00)82430-1
7. Atkins E.D.T., Mackie W., Parker K.D., Smolko E.E., 'Crystalline structure of poly-D-mannuronic and poly-L-guluronic acids', *J. Polymer Sci. Part B: Polymer Lett.*, 1971, 9, 311–316.
8. Kelco Inc., 'Alginate products for scientific water control', third edition, San Diego, CA, 1987.
9. Grant G.T., Morris E.R., Rees D.A., Smith P.J.C., Thom D., 'Biological interactions between polysaccharides and divalent cations. The egg-box model', *FEBS Lett.*, 1973, 32, 195–198.
10. Thornley F.C., Walsh M.J., 'Process of preparing alginic acid and compounds thereof', US Patent 1,814,981,1931.
11. Green H.C., 'Process for making alginic acid and product', US Patent 2,036,934, 1936.
12. McHugh D.J., 'Production, properties and uses of alginates', *FAO*, 1987, 58–115.
13. Moss J.R., Doty M.S., 'Establishing a seaweed industry in Hawaii: an initial assessment', Honolulu, Hawaii State Department of Land and Natural Resources, 73, 1987.
14. Hernandez-Carmona G., McHugh D.J., Arvizu-Higuera D.L., Rodrigues-Montesinos Y.E., 'Pilot plant scale extraction of alginate from *Macrocystis pyrifera*. Studies on extraction conditions and methods of separating the alkaline-insoluble residue', *J. Appl. Phycol.*, 1999, 11, 493–502.
15. GB Patent 8002–300, 1980.
16. Japanese Patent 10376, 1957.
17. Mikolajczyk T., Wolowska-Czapnik D., 'Multifunctional alginate fibres with antibacterial properties', *Fibres & Textiles in Eastern Europe*, 2005, 13(3), 35.
18. Qin Y., Hu H., Luo A., 'The conversion of calcium alginate fibers into alginic acid fibers and sodium alginate fibers', *J. Appl. Polym. Sci.*, 2006, 101, 4216–4221. doi:10.1002/app.24524
19. McMullen D., 'Clinical experience with calcium alginate dressing', *Dermatol. Nurs.*, 1991, 3(4), 216–219.
20. Sayag J., Meaume S., Bohbot S., 'Healing properties of calcium alginate dressings', *J. Wound Care*, 1996, 5(8), 357–363.
21. Qin Y., 'The gel swelling properties of alginate fibers and their applications in wound management', *Polym. Adv. Technol.*, 2008, 19, 6–14. doi: 10.1002/pat.960
22. Muri J.M., Brown P.J., 'Alginate fibres', in *Biodegradable and Sustainable Fibres*, ed. Blackburn D., Woodhead Publishing, Cambridge, 2005, 89–109.
23. Petruyte S., 'Advanced textile materials and biopolymers in wound management', *Dan. Med. Bull.*, 2008, 55, 71–75.
24. Chen X., Wells G., Woods D.M., 'Production of yarns and fabrics from alginate fibres for medical applications', in *Medical Textiles*, ed. Anand S.C., Woodhead Publishing, Cambridge, 2001, 20–29.
25. Le Y., Annand S.C., Horrocs A.R., 'Using alginate fibres as a drug carrier for wound healing', in *Medical Textiles 96*, Woodhead Publishing, Cambridge, 1997, 21–26.

26. Fritz S.G., Herlinger K.H., 'Fibers, 1. Survey', in *Ullmann's Fibers*, Wiley-VCH Verlag, Weinheim, Germany, 2008, 1, 3–38.
27. Qin Y., Agboh C., Wang X., Gilding D.K., 'Alginate fibers and dressings', *Med. Dev. Technol.*, 1996, 7(9), 32–41.
28. Mikolajczyk T., Wolowska-Czapnik D., Bogun M., 'Precursor alginate fibres containing nano-particles of SiO<sub>2</sub>', *Fibres & Textiles in Eastern Europe*, 2004, 12(3), 18–23.
29. Qin Y., 'Ion-exchange properties of alginate fibers', *Textile Res. J.*, 2005, 75(2), 165–168. doi: 10.1177/004051750507500214
30. Qin Y., Hu H., Luo A., 'The conversion of calcium alginate fibers into alginic acid fibers and sodium alginate fibers', *J. Appl. Polym. Sci.*, 2006, 101, 4216–4221. doi: 10.1002/app.24524
31. Qin Y., 'The gel swelling properties of alginate fibers and their applications in wound management', *Polym. Adv. Technol.*, 2008, 19, 6–14.
32. Qin Y., 'Gel swelling properties of alginate fibers', *J. Appl. Polym. Sci.*, 2004, 91, 1641–1645. doi: 10.1002/app.13317
33. Qin Y., 'Silver-containing alginate fibers and dressings', *Int. Wound J.*, 2005, 2(2), 172–176.
34. Fabia J., Slusarczyk Cz., Gawlowski A., 'Supermolecular structure of alginate fibres for medical applications studied by means of WAXS and SAXS methods', *Fibres & Textiles in Eastern Europe*, 2005, 13(5), 114–117.
35. Mikolajczyk T., 'Water-soluble alginate fibres for medical applications', *Fibres & Textiles in Eastern Europe*, 2001, 9(3), 20–23.
36. Janowska G., Mikolajczyk T., Wolowska-Czapnik D., Bogun M., 'Effect of the fibre-forming material structure and silica nanoparticles on the thermal properties of alginate fibres', *J. Therm. Anal. Cal.*, 2005, 79, 1–7.
37. Mikolajczyk T., Urbaniak-Domagala W., Wolowska-Czapnik D., 'Effect of the structure of polymer and nanosilica additive on the sorption and electric properties of various alginate fibres', *J. Appl. Polym. Sci.*, 2006, 101, 686–694. doi: 10.1002/app.23892
38. Struszczyk H., 'Some aspects on preparation and properties of alginate and chitosan fibres', *Mat. Res. Soc. Symp. Proc.*, 2002, Vol. 702.
39. Steplewski W., Wawro D., Niekraszewicz A., Ciecchanska D., 'Research into the process of manufacturing alginate–chitosan fibres', *Fibres & Textiles in Eastern Europe*, 2006, 14(4), 25–31.
40. Mirafatab M., Qiao Q., Kennedy J.F., Anand S.C., Grocock M.R., 'Fibres for wound dressings based on mixed carbohydrate polymer fibres', *Carbohydr. Polym.*, 2003, 53, 225–231. doi: 10.1016/S0144-8617(03)00108-5
41. Wrzesniewska-Tosik K., Wawro D., Steplewski W., Szadkowski M., 'Fibrous products with keratin content', *Fibres & Textiles in Eastern Europe*, 2007, 15(2), 30–35.
42. Lu J.W., Zhu Y.L., Guo Z.X., Hu P., Yu J., 'Electrospinning of sodium alginate with poly(ethylene oxide)', *Polymer*, 2006, 47, 8026–8031.
43. Rinaudo M., 'Chitin and chitosan: properties and applications', *Prog. Polym. Sci.*, 2006, 603–632. doi: 10.1016/j.progpolymsci.2006.06.001
44. Ravi Kumar M.N.V., 'A review of chitin and chitosan applications', *Reactive & Functional Polymers*, 2000, 46, 1–27.
45. Roberts G.A.F., *Chitin Chemistry*, Macmillan, London, 1992.
46. Chiellini E., Chiellini F., Cinelli P., 'Polymers from renewable sources', in *Degradable Polymers. Principles and Applications*, 2nd edn, ed Scott C., Kluwer Academic Publishers, Dordrecht, The Netherlands, 2003, 174–178.

47. Kurita K., 'Controlled functionalization of the polysaccharide chitin', *Prog. Polym. Sci.*, 2001, 26, 1921–1971.
48. Agboh O.C., Qin Y., 'Chitin and chitosan fibers', *Polym. Adv. Technol.*, 1997, 8, 355–365.
49. Skryabin K.G., Viknoreva G.A., Varlamov V.P., *Chitin and Chitosan: Production, Properties and Usage*, Nauka, Moscow, 2002.
50. Versali M.F., Clerise F., Bruyere J.M., Gautier S., 'Cell wall derivatives from biomass and preparation thereof', EP 1483299, 2003.
51. Domard A., Domard M., 'Chitosan: structure–properties relationship and biomedical applications', in *Polymeric Biomaterials*, ed. Dimitriu S., Marcel Dekker, New York, 2002, 187–212.
52. Tuzlakoglu K., Reis R.L., 'Processing and biomedical applications of degradable polymeric fibers', Chapter 11 in *Biodegradable Systems in Tissue Engineering and Regenerative Medicine*, CRC Press, Boca Raton, FL, 2005, 163–174.
53. Tokura S., Nishi N., Noguchi J., 'Studies on chitin: preparation of chitin fibres', *Polym. J.*, 1979, 11, 781.
54. Knaul J.Z., Creber C.A.M., 'Coagulation rate studies of spinnable chitosan solutions', *J. Appl. Polym. Sci.*, 1997, 66, 117–127. doi: 10.1002/(SICI)1097-4628(19971003)66: 1
55. Lee S.-H., 'Ripening time and fiber formation of chitosan spinning dope', *J. Appl. Polym. Sci.*, 2003, 90, 2870–2877. doi: 10.1002/app.13070
56. Knaul J.Z., Creber C.A.M., 'Degradable chaff from chitosan fibers', in *Advances in Chitin Sciences*, vol. II, ed. Domard A., Roberts G.A.F., Varum K.M., Jacques André Publisher Lyon France, 1997, 779–784.
57. Lee S.H., Park S.H., Choi J.H., 'Fiber formation and physical properties of chitosan fiber crosslinked by epichlorohydrin in a wet spinning system: the effect of the concentration of the crosslinking agent epichlorohydrin', *J. Appl. Polym. Sci.*, 2004, 92, 2054–2062. doi: 10.1002/app.20160
58. East G.C., Qin Y., 'Wet spinning of chitosan and the acetylation of chitosan fibers', *J. Appl. Polym. Sci.*, 1993, 50, 1773–1779. doi: 10.1002/app.1993.070501013
59. Knaul J.Z., Hudson S.M., Creber K.A.M., 'Improved mechanical properties of chitosan fibers', *J. Appl. Polym. Sci.*, 1999, 72, 1721–1732. doi: 10.1002/(SICI)1097-4628(19990624)72: 13
60. Kulpinski P., Nishimura S.I., 'Preparation and characterization of functionalized chitosan fibers', in: *Advances in Chitin Sciences*, vol. II, ed. Domard A., Roberts G.A.F., Varum K.M., Jacques André Publisher, Lyon France, 1997, 334–338.
61. Tamura H., Tsuruta Y., Itoyama K., Worakitkanchanakul W., Rujiravanit R., Tokura S., 'Preparation of chitosan filament applying new coagulation system', *Carbohydr. Polym.*, 2004, 56, 205–211. doi: 10.1016/j.carbpol.2004.02.003
62. Hirano S., Nagamura K., Zhang M., Kim S.K., Chung B.G., Yoshikawa M. *et al.*, 'Chitosan staple fibers and their chemical modification with some aldehydes', *Carbohydr. Polym.*, 1999, 38, 293–298. doi: 10.1016/S0144-8617(98)00126-X
63. Urbanczyk G.W., 'Fine structure and properties of filaments prepared from chitin derivatives', in *Applications of Chitin and Chitosan*, ed. Goosen M.F.A., Technomic, Lancaster, PA, 1997, 281.
64. Tokura S., Nishimura S., Nishi N., Nakamura K., Hasegawa O., Sashiwa H. *et al.*, 'Preparation and some properties of variously deacetylated chitin fibers', *Sen-i Gakkaishi*, 1987, 43, 288–293.
65. El-Tahlawy K., Hudson S.M., 'Chitosan: aspects of fiber spinnability', *J. Appl. Polym. Sci.*, 2006, 100, 1162–1168. doi: 10.1002/app.2301



66. Notin L., Viton C., Lucas J.M., Domard A., 'Pseudo-dry-spinning of chitosan', *Acta Biomaterialia*, 2006, 2, 297–311. doi: 10.1016/j.actbio.2005.12.005
67. Muzzarelli R.A.A., Mattioli-Belmonte M., Pugnali A., Biagini G., 'Biochemistry, histology and clinical uses of chitins and chitosans in wound healing', in *Chitin and Chitanases* ed. Jolles P., Muzzarelli R.A.A., 1999, Birkhäuser Verlag, Basel, 1999, 251–264.
68. Qin Y., Zhu Ch., Chen J., Liang D., Wo G., 'Absorption and release of zinc and copper ions by chitosan fibers', *J. Appl. Polym. Sci.*, 2007, 105, 527–532. doi: 10.1002/app.26271
69. Qin Y., Zhu Ch., Chen J., Chen Y., Zhang C., 'Absorption and release of silver and zinc ions by chitosan fibers', *J. Appl. Polym. Sci.*, 2006, 101, 766–771. doi: 10.1002/app.23985
70. Qin Y., Zhu Ch., Chen J., Zhong J., 'Preparation and characterization of silver containing chitosan fibers', *J. Appl. Polym. Sci.*, 2007, 104, 3622–3627. doi: 10.1002/app.26083
71. Hirano S., 'Wet-spinning and applications of functional fibers based on chitin and chitosan', *Macromol. Symp.*, 2001, 168, 21–30. doi: 10.1002/1521-3900(200103)168:1
72. Hirano S., Usutani A., Midorikawa T., 'Novel fibers of *N*-acylchitosan and its cellulose composite prepared by spinning their aqueous xanthate solutions', *Carbohydr. Polym.*, 1997, 33, 1–4. doi: 10.1016/S0144-8617(97)00039-8
73. Hirano S., Midorikawa T., 'Novel method for the preparation of *N*-acylchitosan fiber and *N*-acylchitosan-cellulose fiber', *Biomaterials*, 1998, 19, 293–297.
74. Hirano S., Hayashi H., 'Some fragrant fibers and yarns based on chitosan', *Carbohydr. Polym.*, 2003, 54, 131–6. doi: 10.1016/S0144-8617(02)00329-6
75. Hirano S., Zhang M., Nakagawa M., Miyata T., 'Wet spun chitosan-collagen fibers, their chemical *N*-modifications, and blood compatibility', *Biomaterials*, 2000, 21, 997–1003.
76. Zheng H., Du Y., Yu J., Huang R., Zhang L., 'Preparation and characterization of chitosan/poly(vinyl alcohol) blend fibers', *J. Appl. Polym. Sci.*, 2001, 80, 2558–2565. doi: 10.1002/app.1365
77. Strobin G., Ciechanska D., Wawro D., Steplewski W., Jozwicka J., Sobczak S., Haga A., 'Chitosan fibres modified by fibroin', *Fibres & Textiles in Eastern Europe*, 2007, 15(5–6), 146–148.
78. Hirano S., Nakahira T., Nakagawa M., Kim S.K., 'The preparation and applications of functional fibers from crab shell chitin', *Journal of Biotechnology*, 1999, 70, 373–337.
79. Chijioke F.I., 'Novel chitosan–alginate fibres for wound dressing applications', *ANTEC 2006 Plastics*, Annual Technical Conference Proceedings, Society of Plastics Engineers, 2006, 1386–1391.
80. Wawro D., Steplewski W., Wawro D., Ciechanska D., Krucinska I., Wesolowska E., 'The effect of solvent type on mechanical properties of dibutrylchitin (DBC) fibres', *Fibres & Textiles in Eastern Europe*, 2007, 15(3), 14–18.
81. Binias D., Boryniec S., Binias W., Wlochowicz A., 'Alkaline treatment of dibutrylchitin fibres spun from polymer solution in ethyl alcohol', *Fibres & Textiles in Eastern Europe*, 2006, 14(3), 13–18.
82. Li L., Hsieh Y.L., 'Chitosan bicomponent nanofibres and nanoporous fibres', *Carbohydr. Res.*, 2006, 341, 374–381. doi: 10.1016/j.carres.2005.11.028

83. Okhkawa K., Cha D., Kim H., Nishida A., Yamamoto H., 'Electrospinning of chitosan', *Macromol. Rapid Commun.*, 2004, 25, 1600–1605. doi: 10.1002/marc.200400253
84. Min B.M., Lee S.W., Lim J.N., You Y., Lee T.S., Kang P.H., Park W.H., 'Chitin and chitosan nanofibers: electrospinning of chitin and deacetylation of chitin nanofibers', *Polymer*, 2004, 45, 7137–7142. doi: 10.1016/j.polymer.2004.08.048
85. Noh H.K., Lee S.W., Kim J.M., Oh J.E., Kim K.H., Chung Ch. P., Choi S.C., Park W.H., Min B.M., 'Electrospinning of chitin nanofibres: degradation behaviour and cellular response to normal human keratinocytes and fibroblasts', *Biomaterials*, 2006, 27, 3934–3944. doi: 10.1016/j.biomaterials.2006.03.016
86. Phongying S., Aiba S., Chirachanchai S., 'Direct chitosan nanoscaffold formation via chitin whiskers', *Polymer*, 2007, 48, 393–400. doi: 10.1016/j.polymer.2006.10.049
87. Tuzlakoglu K., Alves K.M., Mano J.F., Reis R.L., 'Production and characterization of chitosan fibers and 3-D fiber mesh scaffolds for tissue engineering applications', *Macromol. Biosci.*, 2004, 4, 811–819. doi: 10.1002/mabi.200300100
88. Majima T., Funakosi T., Iwasaki N., Yamane S.T., Harada K., Nonaka S., Minami A., Nishimura A.I., 'Alginate and chitosan polyion complex hybrid fibers for scaffolds in ligament and tendon tissue engineering', *J. Orthop. Sci.*, 2005, 10, 302–307. doi: 10.1007/s00776-005-0891-y
89. Yang K.K., Wang X.L., Wang Y.Z., 'Progress in nanocomposite of biodegradable polymer', *J. Ind. Eng. Chem.*, 2007, 13(4) 485–500.
90. Matsuda A., Ikoma T., Kobayashi H., Tanaka J., 'Preparation and mechanical property of core-shell type chitosan/calcium phosphate composite fiber', *Mater. Sci. Eng.*, 2004, 24, 723–728. doi: 10.1016/j.msec.2004.08.047
91. Spinks G.M., Shin S.R., Wallace G.G., Whitten P.G., Kim S.I., Kim S.J., 'Mechanical properties of chitosan/CNT microfibers obtained with improved dispersion', *Sensors and Actuators*, 2006, 115, 678–684. doi: 10.1016/j.snb.2005.10.047

# The structure and properties of glass fibres

F R JONES, University of Sheffield, UK and  
N T HUFF, Owens Corning Inc., USA

**Abstract:** This chapter describes the structure and properties of the variety of glass fibres manufactured principally for use as reinforcements for composites. Optical glass fibres are considered in Chapter 14. We give a brief history of the glass fibre industry before describing the fundamental thermodynamic and atomistic concepts of glass formation. Sufficient detail is given to enable the manufacture, structure and properties to be described. The role of the different oxide compositions is reviewed, as is a detailed discussion of the strength of fibres. The phenomenon of static fatigue is also considered. For completeness, the role of sizing technologies on protecting glass fibres from damage and for functionalising the surface for compatibility with polymers and resins in composite manufacture is also given. Recent ideas about the structure of silane coupling agents (adhesion promoters) deposited on glass fibres, is also reviewed.

**Key words:** glass fibres, manufacture, structure, strength, static fatigue, sizing technologies, structure of silane coupling agents, interphase formation in composites.

## 9.1 Introduction

On a weight basis, more than 99% of glass fibres (also known as synthetic vitreous fibres or SVCs) in use today are spun from silicate glasses. Therefore, this discussion of glass fibres will be limited to silicate (containing at least 50% SiO<sub>2</sub> on a molar basis) glass fibres. For example, we will not discuss fibres made from chalcogenide glasses which are mainly used in infrared optics. Fibres made from glassy metals will also not be discussed. However, glass optical fibres (almost 100% SiO<sub>2</sub>) are discussed in Chapter 14.

### 9.1.1 Historical perspective

Glass fibres have been known for centuries but there were few utilitarian uses for them until the middle of the nineteenth century. At that time, methods were devised for melting naturally occurring basaltic rocks and producing fine fibres from them. This 'rock wool' (also known as mineral wool or basalt wool) was used as a thermal insulation material. This wool material had a large range of fibre diameters (from one to more than 15 microns in diameter). It also contained a significant amount of shot or partially melted

input raw material. The composition of rock wool varies depending upon the geographic source of the basaltic material. This material is still used in many applications as a high-temperature thermal insulation material throughout the world. However, there are now health concerns associated with its use because of the number of very small (<3 microns) diameter fibres it contains. These fibres have the potential of being inhaled into the deep lung. Since they are not readily soluble in lung fluids, they may cause health issues because they could be a long-term irritant in the lung (European Directive 97/69/EC).

One of the more unusual examples of the early use of glass fibres was in a dress worn by an actress of the day at the Columbian Exposition in Chicago in 1893 to draw attention to a cut glass exhibition (1). The first actual significant commercial use of glass fibres made from 'standard' glass making raw materials where the composition was closely controlled in a glass melting furnace would appear to be as a substitute for steel fibres in air filters. These were produced in the 1920s from a furnace used for making milk bottles in Newark, Ohio, USA (2).

It was recognised by a number of people in the early part of the twentieth century that fine glass fibres made with a controlled glass composition could be a very effective material for thermal insulation. However, it was not until the 1930s that a commercially viable process was developed which could compete with the rock wool processes of the day. The breakthrough occurred in 1932 when a recently graduated engineer, Dale Kliest, working at Owens-Illinois attempted to seal architectural glass blocks together using a metal layer gun. The compressed air metal layer gun was popular at that time in applying a thin layer of bronze to objects. Instead of a bronze rod, the researcher used a glass rod in the device. Instead of a smooth layer of molten glass being laid down on the blocks, fine fibres came out of the gun in a manner totally unacceptable for sealing glass blocks together. An associate researcher, Jack Thomas, involved in the use of fibreglass for air filters saw the fibres and immediately recognized that this could be a method of making fibreglass for thermal insulation applications. Compressed air was replaced with steam and the first commercial fibreglass thermal insulation based on this concept, identified in the 'failed' sealing experiment, was installed in October 1933. Work continued on a commercial process at both Owens-Illinois Glass Company and Corning Glass Works, and at St Gobain in France. In 1935, Owens-Illinois and Corning decided to pool their technical resources and in 1938 they formed a joint venture known as Owens Corning whose main product was fibreglass produced in the former glass milk bottle factory. That factory is still a major producer of fibreglass for thermal insulation applications.

In 1933, the same Owens-Illinois research group utilised a refractory 'bushing' to produce continuous glass filaments. Experiments were performed using these continuous filaments in textile machines, substituting the glass

fibres for natural fibres such as cotton. In 1935, the first polymer–glass fibre composites were produced. That same year, a commercial process for the manufacture of continuous glass fibres was made operational in the same plant in Newark, Ohio, that was now being utilised to produce the glass wool used for thermal insulation and air filters. The first plant dedicated exclusively to the manufacture of continuous filament glass fibres was commissioned in 1941 at Ashton, Rhode Island, USA. This plant showed that it was commercially feasible to produce continuous filament fibreglass for use as a reinforcement material in literally thousands of composite applications.

The three people most responsible for the development of the modern fibreglass business, Dale Kleist, Jack Thomas and Games Slayter, were inducted into the (USA) National Inventors' Hall of Fame in 2006 for their pioneering efforts in this now global industry.

### 9.1.2 Fibreglass for insulation and filtration

The first significant commercial application was in air filtration, especially in forced air furnace systems for buildings. Fibreglass dominated the market for several decades. Although in the last decade, lower-cost organic polymer fibres have replaced fibreglass in most air filtration systems for home and commercial applications, the market for thermal insulation has continued to grow, driven by the desire to provide more energy-efficient buildings. This market is, in fact, the largest (by mass) user of fibreglass of all types. The energy required to produce thermal insulation products from fibreglass compares very favourably with the energy which can be saved in space heating/cooling applications over a few years. This makes fibreglass wool one of the most energy-efficient commodity products on the market today. This is especially important where, in the USA, 40% of the total energy usage is in residential and commercial buildings.

### 9.1.3 Fibreglass for reinforcement

The second largest market (by mass) for fibreglass is in composite materials, where the fibreglass is used as reinforcement for a polymer. The tensile strength and elastic modulus of fibreglass reinforcement are much higher than those for the matrix polymer. However, the glass fibre can serve as a reinforcement only when stress transfer to the polymer matrix can occur. Otherwise, the glass filaments would simply act as a filler reducing the overall cost of the composite. To achieve this, the fibres are coated within milliseconds of exiting the spinnet or bushing with a dilute (typically aqueous) mixture or emulsion of organic molecules called the sizing. The sizing system effectively acts as an adhesive which bonds the polymer to individual glass filaments. The mechanism by which the sizing

system functions has been and rightly continues to be the subject of much investigation (see Section 9.5).

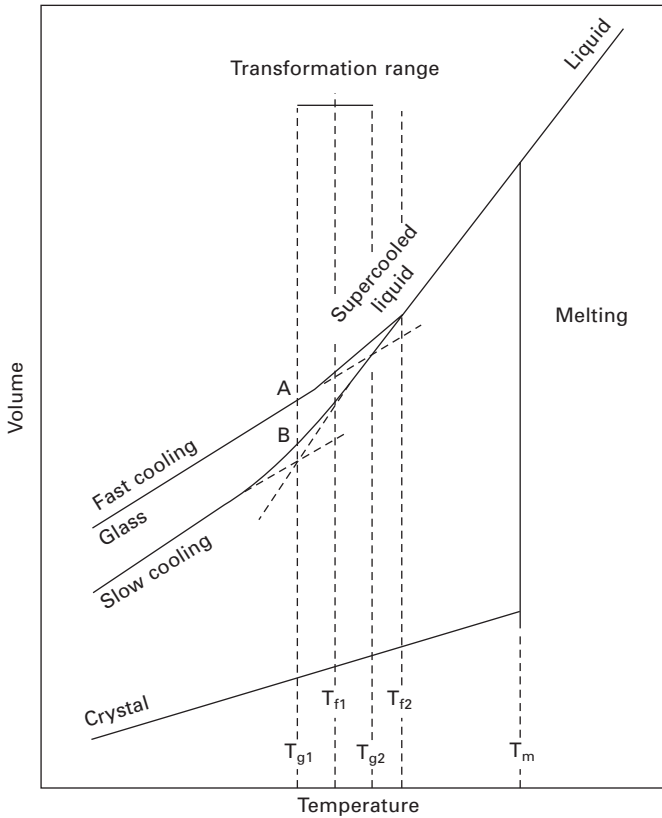
#### 9.1.4 Other glass fibres

Fibres used for optical communications are an order of magnitude larger in diameter ( $>100\ \mu\text{m}$ ) than typical insulation and reinforcement fibres ( $5\text{--}30\ \mu\text{m}$ ). Furthermore, the manufacturing process is very different. A chemical vapour or particulate deposition process is used to produce ‘preforms’ weighing up to a few kilograms which are used in the optical fibre drawing process. This is to be compared with the tons of raw materials which are charged into a fossil fuel-fired or electric furnace to produce fibreglass wool or continuous filament fibreglass for the reinforcement market. The chemical composition is also very different. For optical communication, extremely high purity silica with precisely controlled concentrations of doping ions to adjust the refractive index are utilised. In contrast, a mixture of several oxides with a range of impurities is used for drawing continuous filaments. Glass fibres used for communication will be discussed in Chapter 14. Furthermore, there is a range of glass-ceramic fibres available commercially but these are not considered here. There are also limited uses for non-oxide glasses whose structure will not be discussed in this document.

## 9.2 The nature of glass

### 9.2.1 A thermodynamic viewpoint

In the absence of long-range order within the atomic structure of a glass, the material solidifies in an amorphous arrangement. The polymeric nature of the chain molecules in organic polymers and inorganic silicates means that on cooling the viscous ‘melt’ there is insufficient time for crystallisation to occur and a random structure forms. This leads to the concept of the glass transition (3). This concept of a non-equilibrium structure being ‘frozen in’ implies that the particular structure which is frozen in is a function of the kinetics of the relaxation process. Because of the rapid change in viscosity of glass-forming liquids (especially silicate glasses) with temperature, the structure which is frozen in is dependent upon the cooling rate. Thus, there is a range of temperatures over which the transition from a true liquid to the glassy state occurs. This is called the glass transition temperature range. One can define a glass transition temperature based upon measurements of specific properties of the material. For example, Fig. 9.1 shows how a glass transition temperature can be defined by monitoring the change in volume of the material (or thermal expansion coefficient) as it is cooled. Because of the change in heat capacity of the material in the glass transition region,



9.1 Volume–temperature relationships for glasses, liquids, supercooled liquids and crystals. On fast cooling the supercooled liquid curve follows path A and on slow cooling path B. The temperature at which the structure of the supercooled liquid is ‘frozen in’ is referred to as  $T_f$  or the fictive temperature. The glass transition temperature  $T_g$  can be defined by extrapolating the linear expansion curves above and below the transformation range. After Hutchins and Harrington (3).

one can also define the glass transition temperature  $T_g$  through calorimetric methods. Again, the value of  $T_g$  obtained is dependent upon the measurement conditions and the glass cooling rate.

The concept of the ‘fictive temperature’ as represented in Fig. 9.1 is an attempt to characterise uniquely the structure of the glass. The fictive temperature itself is dependent upon the cooling rate which the material undergoes. However, Agarwal *et al.* (4) have utilised IR measurements in an attempt to measure the fictive temperature of glasses where the measurement technique itself is performed at a constant temperature.



Thermodynamically, there is a difference in heat capacity between the glass and its liquid. It is also seen that the glass which was prepared after fast cooling has a higher  $T_g$  ( $T_{g2}$  in Fig 9.1) and occupies more volume and therefore has a lower density. After slow cooling, the glass which forms has a  $T_g$  at  $T_{g1}$  and a higher density. Thus, the entropy of the glass formed at  $T_{g2}$  must be higher than that of  $T_{g1}$ . As a result, it can be considered that the configurational structure of the glass differs across the transformation range of  $(T_{g2} - T_{g1})$ . Therefore, the glass cannot be considered to be a supercooled liquid. The temperature at which the liquid becomes supercooled is referred to as the fictive or configurational temperature  $T_f$  in Fig. 9.1 (5). In Fig. 9.1, a fast-cooled glass will also have a higher fictive temperature than that prepared after slow cooling. Studies on polymer glasses have attempted to examine whether the glass transition is a thermodynamic quantity. A second-order transition is represented by a discontinuity in a second-order thermodynamic property.

According to the well-known thermodynamics of Ehrenfest, for a glass to exhibit a second-order transition of temperature,  $T_2$ , the following relationships need to be applicable:

$$\frac{dT_2}{dP} = \frac{\partial \Delta V / \partial T}{\partial \Delta S / \partial T} = \frac{V \Delta T_2}{\Delta C_p} \tag{9.1}$$

$$\frac{dT_2}{dP} = \frac{d \Delta V / d p}{\partial \Delta S / d p} = \frac{\Delta k}{\Delta \alpha} \tag{9.2}$$

where  $P$  is pressure,  $\Delta V$  is the change in volume at the transition,  $\Delta S$  is the change in entropy,  $\Delta C_p$  is the change in heat capacity,  $\Delta \alpha$  is the difference between the linear thermal expansion coefficients above and below  $T_2$ , and  $\Delta k$  is the compressibility. The second-order temperature dependence of Gibbs free energy,  $G$ , is given by equation 9.3, and pressure dependence by equations 9.4 and 9.5:

$$\left( \frac{\partial^2 G}{dT^2} \right)_P = - \frac{C_p}{T} \tag{9.3}$$

$$\left( \frac{\partial^2 G}{\partial P^2} \right)_T = - kV \tag{9.4}$$

$$\left[ \frac{\partial}{\partial T} \left( \frac{\partial G}{\partial P} \right)_T \right]_P = \partial V \tag{9.5}$$

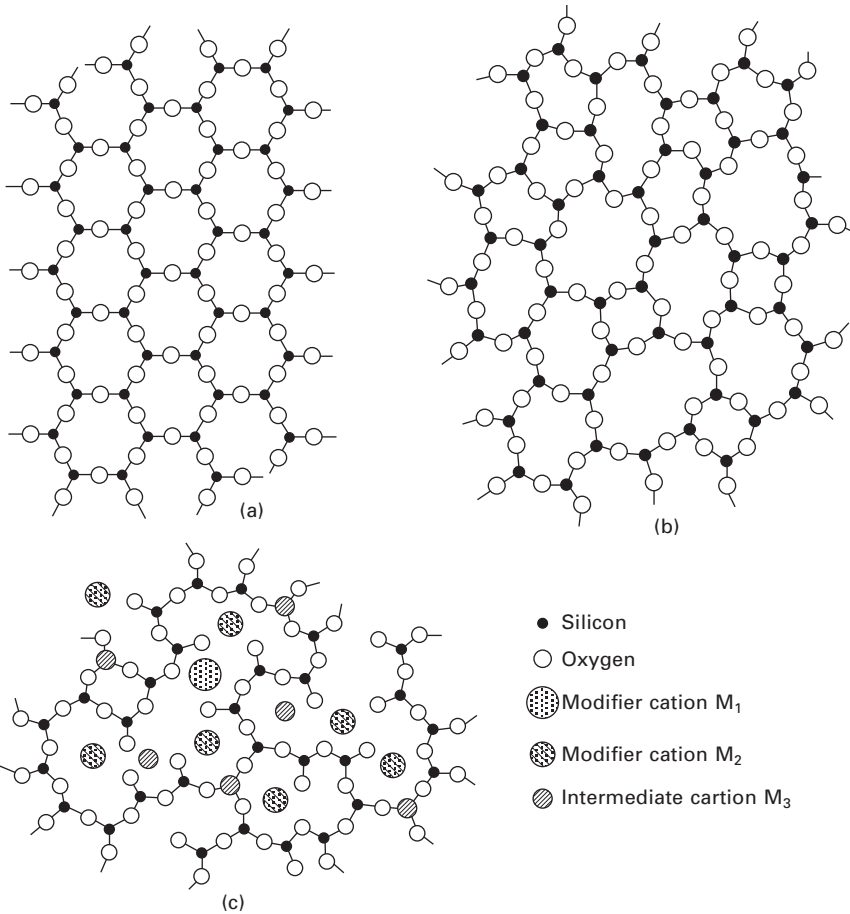
For a detailed discussion of the thermodynamics of second order transitions, the reader is referred to the review by Haward and Young (6). Gibbs and

DiMarzio (7) have argued that  $T_2$  is effectively the lowest value of  $T_g$  which can be achieved. At this temperature, the configurational entropy is considered to be zero and no further reorganisation of the molecular glass structure occurs at temperatures below  $T_2$ . Thus, this model has been applied to inorganic glasses (8) with some success to explain the structure and formation of glasses. In practice, equation 9.1 holds but equation 9.2 does not, so a glass has both kinetic and thermodynamic characteristics. If neither equation 9.1 nor equation 9.2 hold, the glass is considered to be a supercooled liquid. Thus  $T_2$  can be considered the lowest value of  $T_g$  which would be achieved by cooling the glass infinitely slowly.

## 9.2.2 An atomistic viewpoint

The structure of glass on an atomistic level has been the subject of much theoretical speculation and experimental work for nearly a century. Still, however, we do not have a clear atomic-level concept of glass structure. This difficulty comes from the lack of a high degree of long-range (greater than 1 nm) atomic-level order present in the glass structure. Attempts to explain the short-range order but long-range disorder of glasses have revolved mainly around two theories. One explanation, proposed by Lebedev (9), postulated the presence of ‘crystallites’ in glasses. These crystallites were essentially assumed to be very ‘small’ regions consisting of dozens of atoms which were arranged in a crystalline order in the glass. These ‘crystallites’ were joined together in a somewhat random manner. There were a number of variations on this theme proposed from the 1920s for the next 50 or so years. As the sensitivity of experimental techniques has improved the maximum possible size of these ‘crystallites’ has decreased to the point where there is little to distinguish them from the ‘1 to 2 nearest neighbour’ order assumed by Zachariasen (10) in his random network model. Zachariasen’s model suggested that vitreous silica was composed of a random network of  $\text{SiO}_4$  tetrahedra. Early X-ray diffraction work (11, 12) supported Zachariasen’s general picture of short-range order present in silica (<0.3 nm) but little long-range order (>3 nm). Early two-dimensional representations of the differences between (a) a crystal, (b) a  $\text{SiO}_2$  glass, and (c) a glass with ‘modifier cations’ are presented in Fig. 9.2. The short-range order but lack of long-range order in Fig. 9.2b results from  $\text{SiO}_4$  tetrahedra being the basic building block of amorphous silica, but the orientation of the tetrahedra with each other possesses some random character. The O atoms at the corners of the tetrahedra are shared between two tetrahedra. Thus, the overall chemical composition is that of  $\text{SiO}_2$ .

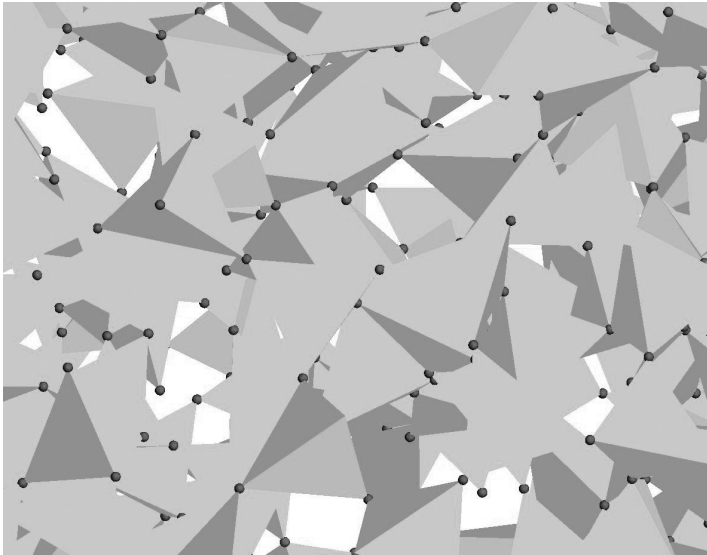
Molecular dynamics (MD) modelling of silica glass using a variety of force fields (13) indicates that the basic building block is a four-coordinated Si atom surrounded by four oxygen atoms as suggested by Zachariasen (10).



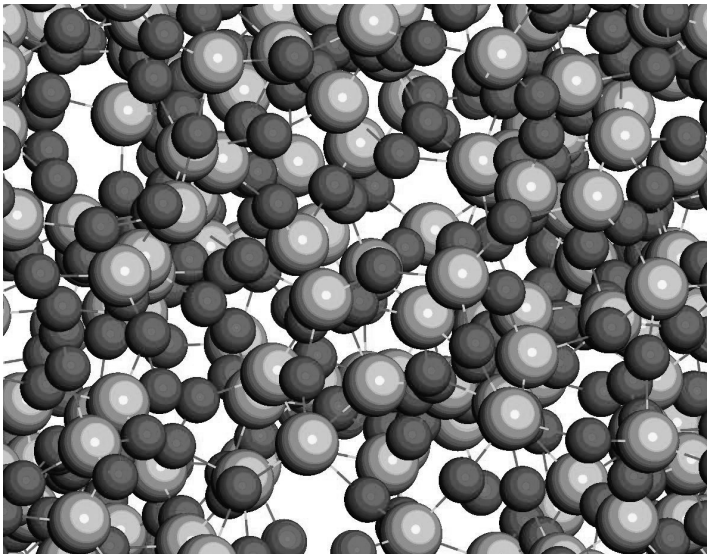
9.2 Two-dimensional schematic representation of (a) a crystalline structure; (b) a simple glass; and (c) a multicomponent glass.

IP Address: 129.132.211.108

MD simulations suggest that the O–Si–O bond angle distribution is centred at about  $108^\circ$  with the bond angle distribution at half the maximum amplitude (full width half maximum or fwhm) of the distribution being about  $15^\circ$ . This implies that the O atoms assume a fourfold tetrahedral arrangement around the Si atoms. Calculations on the MD structure indicate that about 99% of the Si atoms are fourfold coordinated. Thus, some disorder is introduced even at the nearest neighbour inter-atomic distance. These same calculations indicate that there is a much wider distribution of angles between tetrahedra (represented by the Si–O–Si bond angle). The tetrahedron-to-tetrahedron bond angle is about  $155^\circ$  while the fwhm is about  $35^\circ$ . With this wide variation in bond angles, the resulting structure is a three-dimensional joining of the tetrahedra. This is represented in Fig. 9.3a.



(a)



(b)

**9.3** Two different representations of a molecular dynamics-generated structure of silica glass. Figure 9.3(a) emphasizes the tetrahedral configurations of O atoms around Si atoms at the centre of the tetrahedrons. Figure 9.3(b) is a CPK representation of the same atomic arrangement in (a). In this representation, the spheres are proportional to the van der Waals radii of the atoms.

The tetrahedra tend to form non-planar ring structures. The most common ring size contains six Si and six O atoms. (In the inorganic glass community, the size of these rings is commonly referred to by the number of Si atoms contained in the ring. Thus, a ring containing six Si and six O atoms would be called a six-membered ring.) The large variation in the Si–O–Si bond angles is consistent with a three-dimensional structure where there is a rather large distribution of ring sizes, varying from three Si member rings to 10 Si member rings. Smaller rings will produce structures with somewhat strained Si–O bonds. When these are located at the surface of the glass, they are expected to be more reactive than other regions containing six-membered rings. Molecular dynamics and density functional *ab initio* calculations support this view (14).

Because of the irregular distribution of strained bonds, these reaction sites will probably be randomly located on the glass surface. This, of course, greatly complicates our ability to study how the coatings (e.g. sizing systems) on a glass surface are assembled at the molecular level. This, in turn, makes the study of the interphase region between the glass surface and an organic polymer matrix a very complex subject (see Section 9.5).

Because of the somewhat random relative orientation of SiO<sub>4</sub> tetrahedra, significant variation in the density of the glass can occur over distances of 1–2 nm. MD calculations suggest that the density of regions of several hundred atoms can vary by as much as 5%. This is supported by experimental scattering measurements (15).

From a thermodynamic standpoint, this random nature of glass structure suggests that there are many atomic configurations that silica glass can assume which are very nearly of the same energy. The energy barriers between local minima are relatively low. This is consistent with the concept of fictive temperature discussed by Tool (16) that results from the inability of the glass structure to transition from one configuration to another of lower energy, because the rate at which the silica can move over an energy barrier to a lower-energy configuration becomes slower and slower as the thermal energy in the glass (represented by the average glass temperature) is reduced. Moynihan *et al.* (17) and others have expressed the change in fictive temperature as a function of the rate of change in cooling of the glass and a structural relaxation activation energy which is approximated by the shear viscosity activation energy. Again this type of model is consistent with the idea that there are many atomic configurations of nearly the same energy which are separated by low energy barriers.

### 9.2.3 Glass forming systems and composition

The discussion above has focused upon amorphous silica. Commercial glasses, including fibreglasses, contain significant amounts of elements other

than Si. In fact, most large tonnage glasses typically contain between 55 and 75%  $\text{SiO}_2$  on a molar basis. Elements in the first column (e.g. Na, K) and second column (e.g. Mg, Ca, Sr, Ba) of the periodic table typically make up a significant fraction of the compositions used for most fibres. These exist as cations and are generally referred to as network modifiers, which disrupt the corner bonding of tetrahedral  $\text{SiO}_4$  units. This results in significant changes in the physical properties of glasses. The thermal expansion and density increase, while the viscosity decreases. This leads to a decrease in hardness, tensile strength and electrical resistivity (especially for the alkali metal atoms) at a given temperature. Other properties, such as refractive index, can either increase or decrease on addition of network modifiers to the silica glass. Chemical durability can either increase or decrease depending upon the environment. For example, the addition of alkali metals to silica will decrease the chemical durability of the glass in acidic solutions. However, it will tend to increase the chemical durability in alkaline solutions.

Atoms in the third column of the periodic table (e.g. B, Al) can participate in the network structure by assuming either threefold or fourfold coordination with the O atoms. This type of coordination is dependent upon the network modifiers present in the glass. Boron plays a significant role in the thermal conductivity properties of fibreglass used for thermal insulation. Aluminium is a significant component of various types of fibreglass used for reinforcement of organic polymer materials. Boron is also present in many reinforcement fibreglasses (18, 19) but its use is decreasing in order to reduce batch costs and pollution control equipment required in the melting and forming process.

Although pure silica glasses appear to mostly have random arrangements of atoms beyond the nearest neighbours, when network modifiers (e.g. Na, Ca) and alternative network formers (e.g. B and Al) are introduced, some of the randomness of the structure is compromised. For example, in a sodium silicate glass, molecular dynamics simulations indicate that there are regions of relatively higher and lower concentrations of sodium atoms. This sort of phenomenon can result in phase separation in some glasses where, in essence, there are two types of glass compositions present in a glass body. The two phases can separate either in a spinodal manner, where one phase can form channels through the other phase, or in a droplet manner, where one phase separates typically into droplets within the other phase.

The existence of glass lasers also implies that order beyond just the nearest neighbours of the atoms does exist in modified silicate glasses. For example, the phenomenon responsible for laser properties of some glasses implies that there is order in more than just the nearest neighbours of the lasing ions (e.g.  $\text{Nd}^{3+}$ ) in silicate glasses.

## 9.2.4 Fibreglass compositions

Table 9.1 illustrates the range of glass compositions which have been used in fibre spinning operations (18, 19). The applications and some characteristics of these are described below.

### *'A' glass*

Fibreglasses designated as 'A' glasses are essentially a soda-lime-silica glass very similar to the type of glass used to produce bottles and flat glass. It has lower batch costs than the glasses typically used for thermal insulation and reinforcements for plastics. 'A' glasses typically have lower tensile strengths and lower chemical durability, especially in acidic media, than glasses normally used in thermal insulation and reinforcement applications.

### *AF (wool) glass*

AF glasses are typically used in producing fibreglass used as thermal insulators and for sound absorbers in buildings. The name AF (all fibre) was coined to differentiate it from basalt glass wool insulation which contains significant amounts of non-fibrous materials (shot). The composition of AF glasses is similar to that of glass container and flat glasses (basically a soda-lime-silica glass). The main difference is the inclusion of 2–10%  $B_2O_3$ . The addition of boron to the glass batch does significantly increase the batch cost. It also significantly affects the melting characteristics of the glass, its chemical durability, and the effective thermal conduction properties of the glass in its fibrous form.

IP Address: 129.132.211.108

### *AR glass*

AR (alkali resistant) glass fibres were developed as a reinforcement fibre which could be used in alkaline environments. Specifically, AR glass is mainly used as a reinforcement in concrete. It is considered as a speciality glass but it is produced in furnaces using standard fibreglass melting techniques.

### *Basalt glass*

Historically, basalt glasses have been used in thermal insulation applications (often called mineral wool). The method of producing these wool glasses is quite different from the glass melting tank and spinners used in the production of AF glasses for insulation.

Because of the production techniques, the wool pack contains particles of unfibred materials called shot. As the name implies, basalt glass is



*Table 9.1* Compositions (wt%) of typical glasses for fibres (18, 19)

Constituent	E	ECR	Advantex® (20)	C	A	S-2®	R	Cemfil (21)	AR1 (22)	AR2	D
SiO <sub>2</sub>	55.2	58.4	59–62	65	71.8	65.0	60	71	60.7	61.0	75.5
Al <sub>2</sub> O <sub>3</sub>	14.8	11.0	12–15	4	1.0	25.0	25	1	–0.5	0.5	
B <sub>2</sub> O <sub>3</sub>	7.3	0.09	–5	5	–	–	–	–	–20.0		
ZrO <sub>2</sub>	–	–	–	–	–	–	16	21.5	13.0	–	
MgO	3.3	2.2	1–4	3	3.8	10.0	6	–	–0.05	0.5	
CaO	18.7	22.0	20–24	14	8.8	–9	–	–	5.0	0.5	
ZnO	–	3.0	–	–	–	–	–	–	–	–	
TiO <sub>2</sub>	–	21	<1	–	–	–	–	–	5.5	–	
Na <sub>2</sub> O	0.3	–	0.1–2	8.5	13.6	–	11	14.5	–	–	
K <sub>2</sub> O	0.2	0.9	<2	–	0.6	–	–	2.0	14.0	30	
Li <sub>2</sub> O	–	–	–	–	–	–	–	1.3	–	–	
Fe <sub>2</sub> O <sub>3</sub>	0.3	0.26	<0.5	0.3	0.5	trace	–	trace	trace	–	
F <sub>2</sub>	0.3	–	<0.5	–	–	0–	–	–	–	–	

produced using naturally occurring basalt rocks as the main batch ingredient. As a result, the composition of basalt glass varies significantly from one geographical region to another. Recently, there have been some efforts to add other batch materials to basalt rocks in an attempt to have a more consistent glass composition and to alter its chemical durability so that it will dissolve in the lungs and thus not have any long-term health effects if very fine fibres are inhaled into the deep lung. (Fibres need to be less than about 3  $\mu\text{m}$  in diameter to be inhaled into the deep lung.)

Some basalt compositions have also been used in the production of continuous roving for use in reinforcement applications. Because of the high content of FeO in basalt rock and the relatively high tendency of these compositions to form crystals, the production of continuous basalt roving has been limited to rather low throughput and thus labour-intensive production methods. (The presence of relatively large amounts of FeO in these compositions greatly reduces the radiative thermal conductivity of these glasses in melting and forming operations, which results in glass with poor thermal homogeneity. This greatly reduces the efficiency of melting and forming operations.) Up to the present time, this has severely limited the use of continuous basalt fibreglass in reinforcement applications.

### *E-glass*

Table 9.2 illustrates the composition of a range of E-glass fibres (18, 19). Glasses broadly classified as E-glass are primarily used as reinforcements in a wide variety of organic polymers (plastics). The term E-glass came from its early use as a reinforcement in electrical applications. At room temperature, E-glasses have very high electrical resistivity. Thus they are well suited as reinforcement in such applications as printed circuit boards. E-glasses have higher viscosity at a given temperature than most other high-tonnage fibreglasses or glass compositions used in container and flat glass applications. The chemical durability of these glasses in acidic solutions is very good, exceeding the resistance of most stainless steels to acids containing chloride ions. The main oxides used in these glasses are silica, calcia and alumina. Most E-type glasses have contained boron. However, E-type glasses without boron or fluorine are now gaining wide acceptance in the fibreglass industry because of lower batch costs and lower emissions during the melting and forming operations. These glasses have even higher chemical durability to acidic solutions than the boron-containing type of E-glasses but also higher melt viscosities (and thus melting temperatures). Because of the excellent chemical durability, especially in acidic solutions, they belong to the subclass of E-glasses called ECR (chemically resistant) E-glasses.

*Table 9.2* E-glass compositions, 1940–2008 (wt%)

Constituent	Original E-glass (23)	'Improved' E-glass (24)	621 glass (25)	MgO-free glass	816 glass (26)	F-free glass (27)	B- and F-free glass (28)	Advantex®	Low $n_D$ glass (29)
SiO <sub>2</sub>	60	54.3	54.0	54.3	58.0	55.3	59	60	55.8
Al <sub>2</sub> O <sub>3</sub>	9	14.0	14.0	15.1	11.0	13.9	12.1	13.5	14.8
B <sub>2</sub> O <sub>3</sub>	–	10.0	10.0	7.4	–	6.8	–	–	5.2
TiO <sub>2</sub>	–	–	–	–	2.4	0.2	1.5	–	–
MgO	4	4.5	–	0.1	2.6	1.8	3.4	3.0	–
CaO	27	17.5	22.0	22.1	22.5	21.4	22.6	22.5	21.0
ZnO	–	–	–	–	2.6	–	–	–	–
Na <sub>2</sub> O/K <sub>2</sub> O	–	1.0	1.0	0.1	1.0	0.4	0.9	1.0	1.4
Fe <sub>2</sub> O <sub>3</sub>	–	trace	trace	0.2	0.1	0.2	0.2	–	n.d.
F <sub>2</sub>	–	0.5	0.5	0.6	0.01	–	–	–	0.5

#### 9.4.6 High strength glass (R and S glasses)

High strength glasses typically have relatively higher amounts of  $\text{SiO}_2$  than the other types of fibreglass (Table 9.1). Because of this, these glasses have higher melting temperatures than the conventional E-glasses. There are a number of designations of these types of glasses with various degrees of improved tensile strength. R glass is a calcia-magnesia-alumina-silica glass of slightly lower strength than S-2<sup>®</sup> glass. The highest tensile strength glass sold in relatively large tonnages is called S-2<sup>®1</sup> glass. This magnesia–alumina–silica glass has a tensile strength which is about 50% higher than that of standard E-glasses (Table 9.3). It is melted in special small-volume and very high-temperature melters. As a result, it is relatively expensive and is used only in speciality applications where very high thermal durability and strength retention is required. Recently, a magnesia–alumina–silicate glass with significantly higher tensile strength than E-glass has been developed which can be melted in modified conventional E-glass melters. Because of the relatively high throughput achievable for this glass, it holds the potential for greatly increasing the use of glass as a reinforcement material in such applications as ballistics, wind turbine blades and compressed gas tanks. The term high performance glass has been used to characterize these fibre glasses.

#### *D-glass*

For the specific requirements of fast-response electronic circuit boards, dielectric glass (D-glass) with low dielectric constant is available as shown in Table 9.1 where a typical D-glass composition is given.

### 9.3 Fibre manufacture

The manufacture of glass and glass fibres is described in detail by Mohr and Rowe (32) and Loewenstein (18) and only a brief description is given here.

#### 9.3.1 Wool process

The main process used today to produce fibreglass wool for thermal insulation purposes involves draining a stream of molten glass into a spinner (a bowl-shaped base metal container with holes in the walls). The spinner operating temperature is typically 900–1100°C. The spinner typically rotates at 2000 rpm to more than 3000 rpm, ejecting fine streams of glass through the holes

<sup>1</sup>AGY Holding Corp.

Table 9.3 Some typical properties of glass fibres (18, 19, 30, 31)

Property	E	ECR	Advantex®	C	A	S-2®	R	Cemfil (21)	AR1	AR2	D
Liquidus temperature* (°C)	1140	–	–	–	1010	–	–	1201	1172	–	–
Fiberising temperature† (°C)	1200	–	1250	–	1280	–	–	1470	1290	–	–
Single fibre tensile strength at 25°C (GPa)	3.7	3.4	3.8	3.4	3.1	4.7	4.5	2.9	3.24	2.5	2.4
Single fibre tensile modulus (GPa)	76.0	73.0	–	–	72.0	86.0	85.0	–	73.0	80	52
Density (g/cm <sup>3</sup> )	2.53	2.6	2.62	2.49	2.46	2.48	2.55	–	2.74	2.74	2.1
Refractive index $n_o$	1.550	1.58	1.56	–	1.541	1.523	–	–	1.526	1.561	1.465
Coefficient of linear thermal expansion (10 <sup>-6</sup> K <sup>-1</sup> )	5.4	5.9	–	7.1	9	2.85	4.10	–	6.5	–	2.5
Volume resistivity (  cm)	10 <sup>15</sup>	–	–	–	10 <sup>10</sup>	10 <sup>16</sup>	–	–	–	–	–
Dielectric constant at 25°C and 10 <sup>6</sup> Hz	6.6	6.9	–	6.9	6.2	5.3	6.4	–	8.1	–	3.85
Dielectric constant at 25°C and 10 <sup>10</sup> Hz	6.11	7.0	–	–	–	5.2	–	5.21	–	–	4.0
Loss tangent at 25°C and 10 <sup>10</sup> Hz (10 <sup>-3</sup> )	3.9	–	–	–	–	–	1.5 <sup>a</sup>	6.8	–	–	0.5

\*The liquidus temperature is the highest temperature at which a glass, if held there sufficiently long, will develop crystals. The greater the difference between this and fiberising temperature, the more stable the fibre-forming process with respect to process interruptions caused by crystals forming in the glass.

†The temperature at which the viscosity of the glass is 10<sup>3</sup> P.

in the spinner sidewalls. These streams of glass coming out of the sidewalls are attenuated by high velocity air and combustion gases or steam into fine ( $<10\ \mu\text{m}$  diameter) fibres which are several centimetres in length. A binder is applied to the glass fibres just below the spinner and the discontinuous filaments move through the 'forming hood' and are collected on a moving chain belt. The function of the forming hood is to distribute the fibres evenly and in a random alignment across the width and length of the moving chain. The chain continues through an oven which dries and cures the binder. The wool mat is then cut into appropriate lengths and widths and packaged. Because the fibres are thermally quenched at high rates, the density of the glass is less than the density of the same composition which had been cooled slowly (annealed).

### 9.3.2 Continuous filament process

While the wool manufacturing process produces fibres of varying length and diameter, the process used to produce filaments for reinforcement purposes produces fibres with small diameter (most reinforcement fibres have diameters between 9 and 25  $\mu\text{m}$ ) with a relatively narrow diameter distribution (e.g. one standard deviation of the fibre diameter is normally less than 8% of the mean diameter). In addition, the fibres are typically produced in packages with strand lengths up to 10 km. (A strand is a collection of typically 100 to several thousand fibres.)

Figure 9.4 shows a schematic representation of a typical continuous filament fibre glass production process. The continuous fibres are produced using bushings (sometimes called spinnerets) which have a few hundred to several thousand small tubes (or tips) in the bottom (a flat plate) of the bushing. One fibre is produced from each tip. The temperature of the glass exiting the tip is typically in the range of 1150–1300°C, depending upon the composition of the glass. The bushings are typically made from an alloy of platinum and rhodium. The rhodium improves the high-temperature mechanical properties of the bushing. Attempts to utilise ceramic oxides to coat or strengthen the bushing have not been commercially successful for continuous-filament large-tonnage fibreglass compositions.

The glass will normally flow out of the bushing under the force of gravity into fibres on the order of 1 mm diameter. The final diameter of the glass fibre is a strong function of the tension applied to the fibre as it is being drawn. Tension increases with lower glass temperatures (higher glass viscosity) and with higher pull speeds. Both temperature and pull speed are process variables that are adjusted to obtain the desired fibre diameter. Typically, lower pull speeds are utilised for large-diameter fibres and high pull speeds are utilised with small-diameter fibres. In commercial production operations, the pull speed of the fibre is produced by winding the fibres around a rotating tube

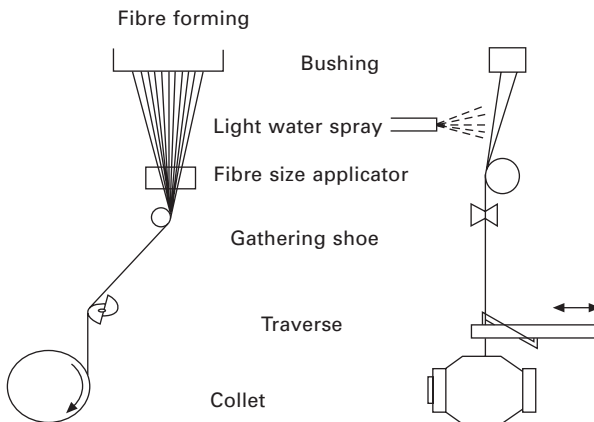
(collet) placed 1–4 metres below the bushing. In addition to collecting long lengths of the strands of fibre glass, the rotation of the tube applies stress to the fibre and stretches the fibres to their final diameter. This force on the fibres also results in the glass moving through the tips at a higher velocity than is attained from gravity only. The linear pull speeds typically range from a few metres per second to more than 30 m/s. This results in the glass fibre velocity increasing from a few millimetres per second through the bushing tip to as high as 30 m/s (108 km/h) over a distance of a few centimetres.

In some processes, the continuous filaments are not collected on a tube but instead are chopped into short lengths (a few millimetres to a few centimetres in length). In this process, a large wheel serves the same function (pulling the filaments) as the collet in Fig. 9.4. The fibres are cut into short lengths while the strand is in contact with the wheel by a smaller rotating wheel which has a series of blades. These blades cut (or more precisely break) the continuous filaments into bundles of the appropriate length.

Clean air and water (a fine mist) are introduced into the area just below the bushing to help remove the heat from the vicinity of the bushing and cool the individual fibres. The thermal quench rates which the fibres undergo are the highest quench rates of any high-volume commercial process. These quench rates are typically in the range of 500 000 to 1 000 000 K s<sup>-1</sup>.

Because of the high quench rates and acceleration of the fibres, the structure of the glass fibres is of a more open nature (lower density) than if the fibres had been cooled slowly. Fine fibres are cooled more quickly than more coarse fibres. As a result, as-formed large-diameter fibres will

IP Address: 129.132.211.108



**9.4** Schematic of a typical continuous filament fibreglass production process. The left side of the figure represents the view from the front of the bushing. The right side of the figure represents the view from the end of the bushing.



typically have a higher density than small-diameter fibres of the same glass composition.

### *Marble process*

In the early days of continuous fibre operations, the glass was made into marbles. The marbles were produced by a machine similar to a bottle-making machine in that the glass stream coming out of the forehearth was cut into individual 'gobs'. These gobs dropped into a marble machine which rolled the gob into a sphere. These marbles would be cooled and shipped to a facility where the marbles were remelted in specially designed bushings and drawn into continuous filaments. Originally, the marble process could produce higher glass quality (good chemical homogeneity, low bubble populations, etc.). Now comparable glass quality can be obtained with large continuous melt furnaces, so the marble process is being phased out. Because of the remelt process, the energy required to produce continuous fibres from marbles is higher. The continuous filament process described above involves a very large furnace and tank in which the mineral batch is continuously melted, refined and homogenised as it flows into the tank immediately above the bushing. However, for smaller specialist fibre drawing, the marble process is still used. One advantage of remelting on a smaller scale is that the fibres exiting the bushing can be quenched rapidly without the need for water spray. More details are given by Mohr and Rowe (32).

## **9.4 Strength of glass fibres**

Table 9.3 gives the typical properties of a range of glass fibres. The modulus of E-glass is very much a function of the chemical forces operating within the amorphous network. As the number and strength of the chemical bonds in the three-dimensional network decrease and/or become weaker, the modulus of the glass will decrease. Thus, the introduction of network modifiers such as alkali or alkaline earth oxides will decrease the moduli of the various glasses. Typical glass formulations used for continuous filament applications will have a Young's modulus on the order of 70–80 GPa. Similarly, the tensile strength of the fibres will vary with the composition of the glass. For typical E-type glasses, the tensile strength of filaments collected without contacting other filaments will have tensile strengths around 3.5 GPa. Pure silica glass filaments collected in the same way will exhibit tensile strengths up to about 7 GPa. The introduction of alkali network modifiers can reduce the tensile strength of the fibres to around 2.5 to 3 GPa. Borate glasses, phosphate glasses and lead silicate glasses typically have strengths of approximately 1–2 GPa.

While tensile strength as typically determined is a function of composition,

it is not a fundamental material property because it depends heavily on the presence of defects and flaws within the structure. Although the actual flaw responsible for the strength of a glass is still uncertain, molecular dynamics simulations are starting to give us insights into the mechanism of brittle fracture (33).

#### 9.4.1 Griffith theory of strength

It has been established by Griffith (34) that the strength of glass is a strong function of the presence of flaws or defects in the material. He used the spinning of glass fibres to validate the theory of strength. Equation 9.6 defines the critical stress before fracture, where  $\gamma$  is the surface free energy of the solid,  $E$  is the modulus and  $c$  is the crack length. If we assume that a micro-crack exists at the surface, we can substitute half the depth of the micro-crack for the crack length  $c$  in equation 9.6 to obtain the maximum technical strength ( $\sigma_m$ ) of the glass (equation 9.7).

$$\sigma_k = 2 \left( \frac{\gamma E}{c\pi} \right)^{1/2} \quad 9.6$$

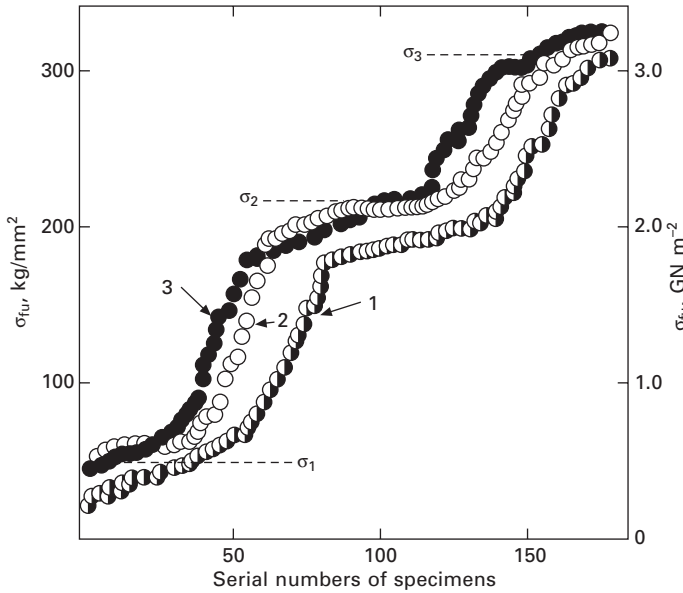
$$\sigma_m = \left( \frac{2\gamma E}{\pi l} \right)^{1/2} \quad 9.7$$

where  $l$  is the depth of a surface crack which is half that of an inner flaw.

Thus the strength is a function of the surface free energy created when the crack propagates. The surface free energy of glass changes from 122 erg/cm<sup>2</sup> to 290 erg/cm<sup>2</sup> in the presence of water, which is the explanation for the observation of static fatigue. Thus, in the presence of flaws the theoretical strength of approximately  $E/10$  is reduced further. Thus a glass with a Young's modulus of 70 GPa would have a theoretical strength of 7 GPa, but its practical strength could be as low as 0.07 GPa (35) for bulk glass. Converting bulk glass into fibres reduces the probability of the presence of a strength-reducing flaw, enabling the actual strength to be nearer to the theoretical. However, to reduce the development of surface flaws, methods have been developed to coat the fibre with a polymer or otherwise hermetically seal the fibre to protect it from damage and attack by moisture. Fibre strengths approaching the theoretical  $E/10$  value can be obtained with such processes.

#### 9.4.2 Theories of fibre strength and structure

The explanation for the distribution of fibre strength is dominated by the ideas of Metcalfe and Schmitz (36) and Bartenev (37), Fig. 9.5 illustrates the observation of three strength levels in fibre populations (38).



9.5 Distribution of strength values for three series of industrial glass-fibre specimens 10  $\mu\text{m}$  in diameter in order of serial number. (1) Average strength 1.48 GPa, specimen length 40 mm ( $\circ$ ). (2) 1.76 GPa and 25 mm ( $\bullet$ ). (3) 1.89 GPa and 25 mm ( $\bullet$ ) (after Bartenev and Izmailova, 37, 40) Reproduced from McCrum (38) with permission of the controller, Her Majesty's Stationery Office, London.

IP Address: 129.132.211.108

*Concepts of Metcalfe and Schmitz (36)*

These authors used a statistical analysis to conclude that the fibres had a distribution of flaws of different severity, which gave rise to the differing populations of strength. The fibres of average strength of 3 GPa could be attributed to severe surface flaws at a separation of 20 mm. The population of average strength of 4.5 GPa could be attributed to flaws spacing of 0.1 mm. The population of average strength of 5 GPa could be attributed to internal defects  $10^{-4}$  mm apart, characteristic of a defect-free filament with an uninterrupted surface layer.

Hand and Seddon (39) have attempted to identify the Griffith flaws responsible for the strength of a glass network and have associated these defects with the random structure of the glass network.

*Concepts of Bartenev (37)*

Figure 9.5 shows the distribution of strengths in 175 specimens of industrial alkaline-free aluminium boro-silicate glass fibre of diameter 10  $\mu\text{m}$ , with

gauge lengths of 25 and 40 mm. As with Metcalfe and Schmitz (36), three levels of strength are apparent in the distribution:  $\sigma_1$  is the lowest strength,  $\sigma_2$  the intermediate strength and  $\sigma_3$  the maximum strength. The population of highest strength, at 3 GPa, is considered to be determined by the presence of a tempered surface layer of 10 nm thickness, because after treatment with hydrogen fluoride, to remove a 10 nm surface layer, the strength decreased to the  $\sigma_2$  level of 2.0 GPa.  $\sigma_2$  was considered characteristic of a flawless glass where the strength was determined by structural heterogeneities within the glass. This was confirmed because heat-treated fibres required 60 nm etching before the strength returned to the magnitude of  $\sigma_2$ .

Furthermore, industrial glass fibres, after prolonged storage, required the removal by etching of 40 nm before the strength returned to  $\sigma_2$ . They also demonstrated that heat-treated fibres have a lower level of strength, to  $\sigma_0$  of 0.821 GPa. In summary, Bartenev and co-workers (37, 38) identified six strength levels within inorganic glasses, ranging from 0.05 GPa to 3 GPa. The maximum strength observed was 10–20 GPa. They also pointed out that the data in Fig. 9.5 would move to the right after heat treatment, indicating a higher population of fibres of  $\sigma_1$  and  $\sigma_2$  strengths. Thus, the strength of these glass fibres was attributed to a tempered surface layer 10 nm thick arising from the cooling of the polymeric inorganic glass and viscoelastic deformation. The tempered layer was considered either to exhibit a compressive thermal stress or to have a more uniform molecular structure.

#### *Fibre strength – summary*

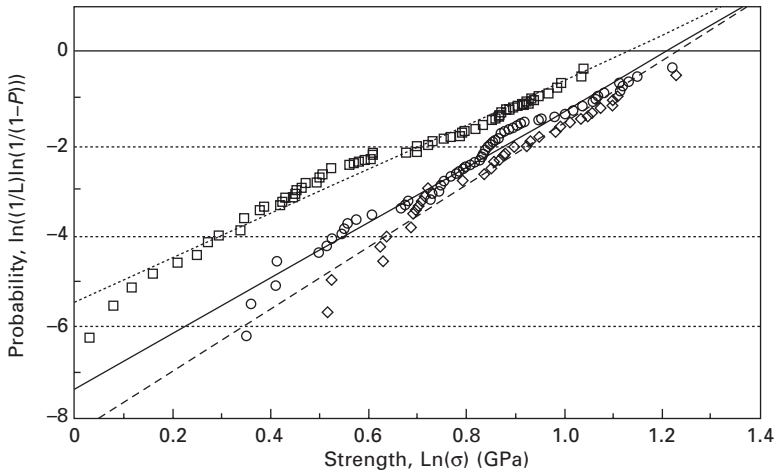
As described above, the theories of fibre strength discuss the population and size of strength-reducing flaws. The role of a tempered surface layer is not generally accepted because for a 10  $\mu\text{m}$  fibre the temperature gradient across the fibre is calculated to be less than 5 K which would be insufficient to set up a tempered layer. Therefore, the drawing of fibres under clean conditions with a very low concentration of surface flaws is probably more important. This can also explain the diameter-dependence of strength (40). Low tensile strength can be attributed to significant flaws, such as partially melted batch material.

#### 9.4.3 Weibull statistics of strength

It is clear from Fig. 9.5 (36, 37) that the distribution of strengths within one continuous fibre or within a bundle of glass fibres can be characterised by a statistical method. The Weibull statistical method is commonly used to describe the distribution of strengths. This can be used to enable the strengths of fibres at different lengths to be analysed. First, the strength is strongly dependent on the gauge length of the fibre under test, and this can lead to

uncertainty about the correct value of strength to be used in any predictive analyses of mechanical properties.

Figure 9.6 shows the typical Weibull plot for the strength of glass fibres with different treatments (19). Marks and Jones (42) have also studied the effect of plasma polymer coatings on the statistics of strengths of glass fibres, and these are summarised in Table 9.4. The role of surface defects on fibre strengths again comes to the fore, since manipulating the fibres for plasma polymer coating reduced the fibre strength from 1.46 GPa to 1.35 GPa and the Weibull modulus ( $m$ ) from 3.10 to 1.65. The latter shows that the distribution of fibre strength was also much broader. It confirms the



9.6 Weibull plots for three laboratory coated E-glass fibres showing differing protective abilities.  $\square$  = Pure  $\gamma$ -APS (Sigma Chemicals);  $\circ$  = commercial  $\gamma$ -APS (A1100);  $\diamond$  = polydimethyl siloxane. The values of the Weibull parameter  $m$  and the characteristic strength  $\sigma_0$  are, respectively, 4.88 and 3.1 GPa; 6.1 and 3.4 GPa; 6.7 and 3.4 GPa.  $L$  = gauge length of fibres tested (= 6.35 mm);  $P$  = probability of failure (19).

Table 9.4 Single filament strength of plasma polymer-coated E-glass fibres (42)

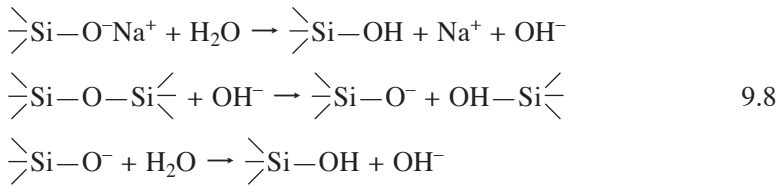
Fibre type/plasma copolymer	Average failure stress (GPa)	Weibull modulus
90% Acrylic acid/10% 1,7-octadiene	1.33 ± 0.56	3.94
0% Acrylic acid/100% 1,7-octadiene	1.58 ± 0.64	3.58
Unsize (as received fibres)	1.46 ± 0.8	3.10
Unsize (after spreading tow, and travelling through the uncharged reactor)	1.35 ± 0.7	1.65

Note: The unsize fibres were water sized and stored before use.

benefit of polymer coatings in protecting strength. Note that the relatively low strengths arise from the fact that as-received fibres were water-sized and not coated with a polymeric size on manufacture.

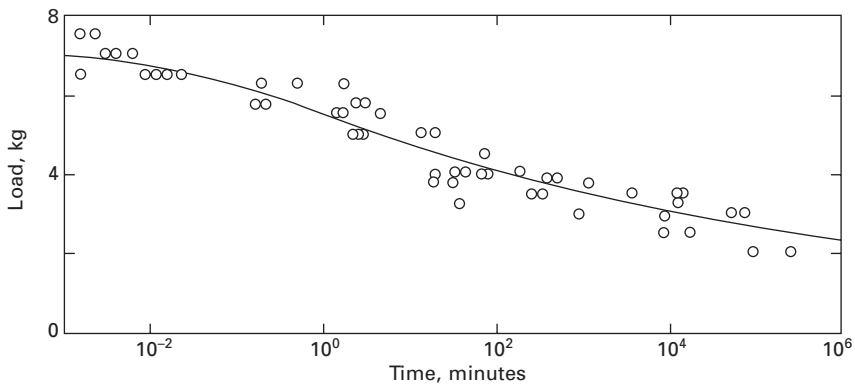
### 9.4.4 Static fatigue of glass fibre

Glass fibres suffer from time-dependent fracture under load. This is referred to as static fatigue (43, 44). This differs from the conventional use of the word fatigue, in that the load is constant. Static fatigue of glass fibres is illustrated in Fig. 9.7 (43, 44). This shows the fibre strength as a function of time at a constant temperature in distilled water. This illustrates that the static fatigue phenomenon is, in effect, a stress corrosion phenomenon. Water is the effective reagent and only in the high vacuum is the time dependence of strength absent. It is worse in alkali glasses because the sodium ion, Na<sup>+</sup>, acts as a catalyst for the hydrolysis of the silica network. The degradation of the silica network is shown below.



Static fatigue occurs in three stages, giving rise to differing time dependence, depending on the load applied. In stage 1, where the fracture behaviour is largely dominated by the mechanics of crack growth, the static fatigue phenomenon is considered to be sodium ion diffusion rate determining. In

IP Address: 129.132.211.108



9.7 Static fatigue of E-glass strands in distilled water. A load of 2 kg caused an applied strain of 0.5%. Redrawn from Aveston *et al.* (43, 44).

stage 2, which is the stress corrosion region, a synergism exists between the applied load and the environment because the rate of crack growth is equal to the rate of corrosion. Thus, the crack always remains sharp and propagates into the weakened material. Stage 3 occurs through stress-assisted corrosion, where the effect of stress on the failure time is much less significant. This is because the rate of hydrolysis of the silica network is higher than the rate of crack growth. According to the theory of Charles (45), the crack tip is blunted by corrosion so that the stress concentration at the crack tip is reduced. The rounding results in a reduction in the radius ( $\rho$ ) of the propagating crack so that in accordance with equation 9.9 a higher load is required for the crack to propagate at the same rate:

$$\sigma_{\max} = 2\sigma_a \left( \frac{x}{\rho} \right)^{1/2} \quad 9.9$$

where  $x$  is the crack length.

Ghosh (46) has studied sub-critical crack growth in *E*-glass and measured the static fatigue limit of the threshold stress intensity factor ( $K_{th}$ ), which had a value of  $0.15 \pm 0.04 \text{ MN m}^{-2/3}$  compared with the critical stress intensity factor ( $K_{Ic}$ ) of  $0.93 \pm 0.03 \text{ MN m}^{-3/2}$  for monotonic mode I loading. In order to predict the time to failure of a filament, the stress corrosion exponent to  $K_{th}$  is required, for the calculation crack growth rate. This can be estimated from the strain rate dependence of fibre strength. For a bundle of fibres (as a model for a composite) this needs to be combined with Weibull statistics (47).

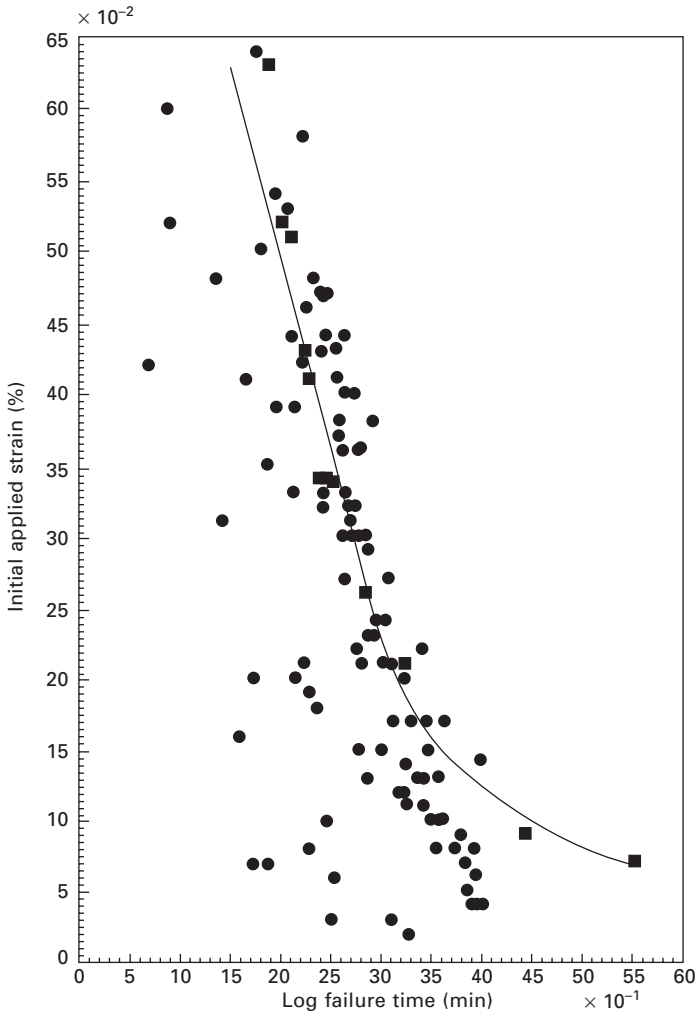
The static fatigue of glass fibres will determine the maximum life of any structural material based on glass fibres. In a composite material, where resin is used to bind the fibres together, the rate of moisture diffusion will be a controlling factor and, as such, the protection given by a well-bonded resin matrix can extend the life of the structure significantly. Under these circumstances diffusion of moisture through the resin becomes an important predictive parameter for the life of the structure. It is also important to ensure that the interfacial bond between the glass fibre and any matrix is maintained in the presence of moisture, otherwise the capillary action associated with a poor interface would dominate the failure process. While interfacial failure may not necessarily lead to brittle fracture, it can reduce the strength of a composite material significantly.

### *Environmental stress corrosion*

In the presence of moisture, *E*-glass fibres have a reduced lifetime under load as indicated by the static fatigue described above. However, in the presence of more severe degrading environments, usually of low pH, brittle fracture can



be initiated (Fig. 9.8). This is referred to as environmental stress corrosion cracking (ESCC). Also included in Fig. 9.8 are comparative failure times for composite materials showing the direct link between time-dependent fracture of glass fibres and the failure of an epoxy composite. As with static fatigue, there is a synergism between the stress and the chemistry as described above for stage 2. Clearly with a more corrosive environment, the load at which the crack propagates at the same rate as the corrosion leads to a brittle fracture



9.8 The stress corrosion failure times of single E-glass filaments (●) and their epoxy resin composites (■) in 0.5M aqueous sulphuric acid. An error of  $\pm 10\%$  on applied strain for 10  $\mu\text{m}$  single filaments (48).

at a lower load than for water alone. In alkaline environments the rate of corrosion is relatively slow so that the phenomenon observed is mostly that of stress-assisted corrosion, rather than environmental stress cracking. In acidic environments corrosion of the glass is highly pH dependent, and at acidities at which the glass modifiers can be readily dissolved, fracture of the glass can occur at strains as low as 0.1%. The network modifiers which are involved in the corrosion process are those associated with  $\text{Ca}^{2+}$ ,  $\text{Al}^{3+}$ ,  $\text{Mg}^{2+}$ ,  $\text{Na}^+$  and  $\text{K}^+$ . This means that glasses which have reduced aluminium concentration and alkaline concentration can have more resistance to environmental stress cracking. ECR glass, or Chemical Resistant E-glass, is an example of these phenomena. High-strength glasses, such as S-2<sup>®</sup> glass, also exhibit good resistance to stress corrosion cracking.

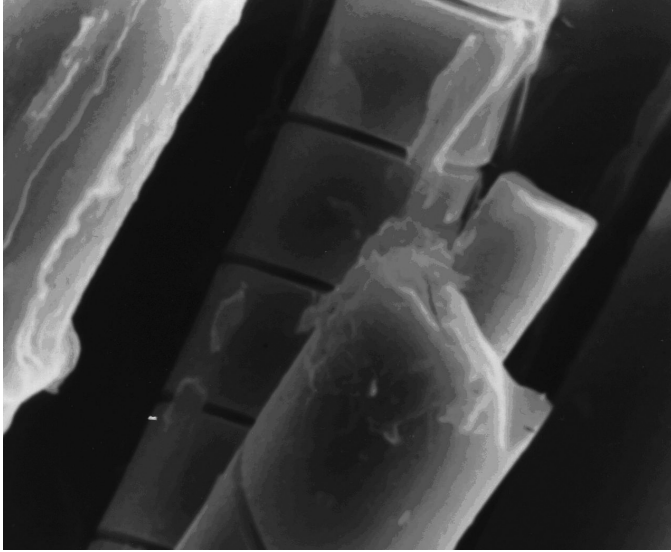
Owens Corning has recently introduced to the market Advantex<sup>®1</sup> glass fibres. These are based on boron-free, fluorine-free E-glass compositions (Table 9.2). As such, they tend to be closer in structure to the ECR glass and have brought a higher chemical resistance to the commercial 'E-glass fibres'.

Of particular relevance to the structure of glass fibres is the phenomenon that the extractions of alkali and other network modifiers from the glass fibre can lead to spiral cracking of unstressed fibres (49) after storage in aqueous acid (Fig 9.9). While it is not clear whether the formation of the spiral crack is the result of drying during electron microscopic examination, one could assume that the formation of a weakened sheath on the fibre surface implies that the structure of the glass is not homogeneous. This is consistent with the Bartenev model (Section 9.4.2). Although there are only limited studies on the effect of annealing on this phenomenon, slight inhomogeneities within the glass fibre structure certainly contribute to the static fatigue and ESCC phenomena.

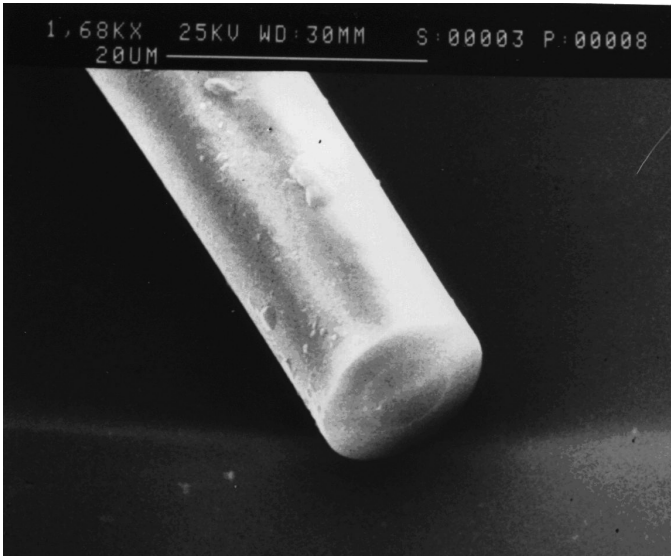
Figure 9.10 demonstrates how the retained strength of unloaded E-glass fibres is affected by the pH of the environment (50). E-glass fibres have the least durability in an acidic pH of 0.5. This can be explained by the thermodynamics of the interaction of aqueous solutions with the glass. Figure 9.11 shows how the solubility of the different glass modifiers varies with pH (44, 51). It can be seen that below pH 9, aluminium is soluble, and similarly above a pH of about 10.5 calcium is insoluble. As a result, in mildly alkaline environments the network modifiers become mobile in the aqueous environment, but can be precipitated at higher pH. At pH above 10, the silica network becomes hydrolysable and the ions then become soluble as various silicate salts. In this way, the corrosion rate in alkali is increased.

IP Address: 129.132.211.108

<sup>1</sup>OCV Intellectual Capital LLC

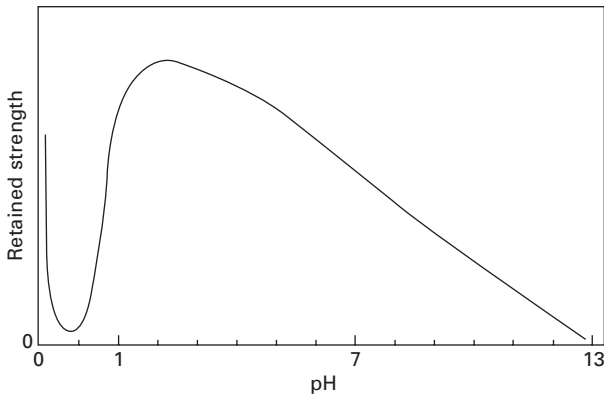


(a)

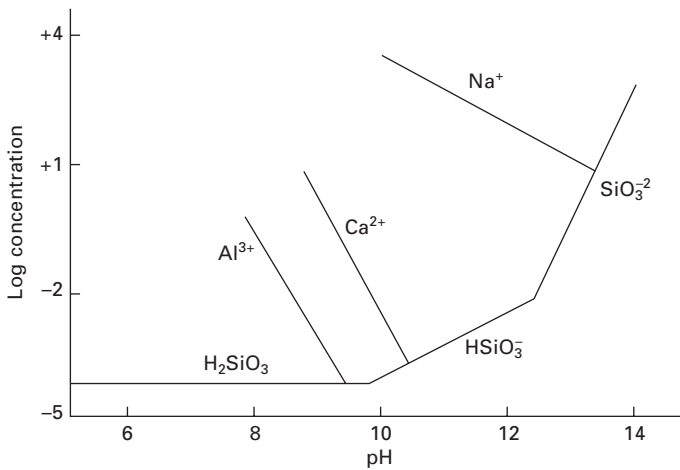


(b)

9.9 (a) E-glass fibres showing 'spiral cracking' after immersion in 0.5M aqueous sulphuric acid. (b) Stress-corroded fracture surface of an E-glass fibre showing core sheath structure (49).



9.10 Schematic of the retained strength of unloaded E-glass fibres in environments of differing acidity and alkalinity (50).



9.11 Thermodynamic calculations of the aqueous solubility of differing glass components at differing pH (after Fox, 51).

IP Address: 129.132.211.108

*Effect of composition*

Following the discussions above, the strength of a glass fibre is generally a function of chemical composition and microstructural features. The microstructural features which are responsible can be induced through the drawing conditions, thermal history, environmental effects and those conditions that can introduce surface defects. Experimental studies show that the highest strength is achieved in melted quartz and S-2<sup>®</sup> glass which has a composition near to MgO, Al<sub>2</sub>O<sub>3</sub>, SiO<sub>2</sub> eutectic (52, 53).

Khazanov *et al.* (52, 54, 55) have classified glass fibres into three groups:

1. Fibres of high strength (5–7 GPa) from quartz or S-2<sup>®</sup> glass composition.
2. Fibres of intermediate strength (2.5–3 GPa) of aluminosilicate composition.
3. Fibres of low strength (1–2 GPa) from borate, phosphate and multi-alkali glasses.

Figure 9.12 shows the range of strengths for a variety of glasses as a function of diameter. The filaments were captured between the bushing and before the fibres were wound up. Fibres from high-temperature low-viscosity melts, structurally non-uniform (e.g. borosilicates) and low-chemical-resistant (e.g. sodium silicate and high boron oxide) glasses had a weak dependence on diameter. Thus, high-performance glass fibres tend to come from compositions where there is strong diameter dependence, which demonstrates that introduced flaws and defects are important. These glasses were mainly those with strong structural bonding and, hence, higher moduli. In the seminal work of Thomas (41), it was demonstrated that under careful control of the fibre-drawing process, the strength–diameter phenomenon was absent for E-glass. Thus, with these glasses fibre-drawing conditions are critical to the production of high-strength fibres (53, 55).

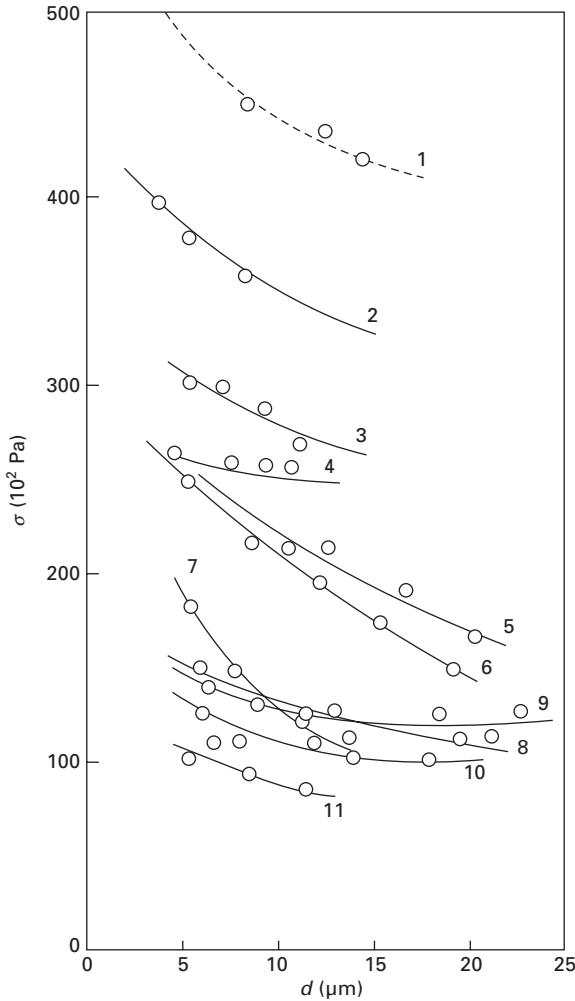
### *Thermal effects*

After heat treatment, glass fibres exhibit a reduced strength. Figure 9.13 shows how fibres of differing composition respond to heat treatment. Quartz fibres are the most resistant, showing an effect only above 600°C, whereas borate glasses appear to show a linear degradation in strength even at temperatures below 200°C. A heating–cooling cycle can induce a reduction in strength through the following mechanisms:

- Network hydrolysis (see above)
- Annealing of compressive tempered layers
- Devitrification of the glass.

The time dependence of glass fibre strength (static fatigue) is independent of temperature as shown in Fig. 9.14, demonstrating that the dominating mechanism is one of network hydrolysis. Nishioka and Schramke (56) have shown how water is lost from the surface at temperatures near 300°C and from the bulk at higher temperatures.

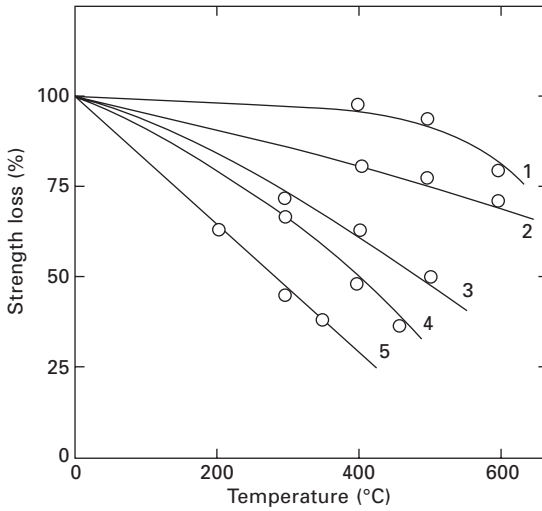
Thus, commercial fibreglasses tend to exhibit degradation in strength as a result of interactions with water. Equation 9.8 shows that sodium and potassium are catalysts for hydrolysis so that more recent commercialised glass fibres which are closer in composition to S-2<sup>®</sup> glass can be expected to have reduced strength sensitivity at high temperatures.



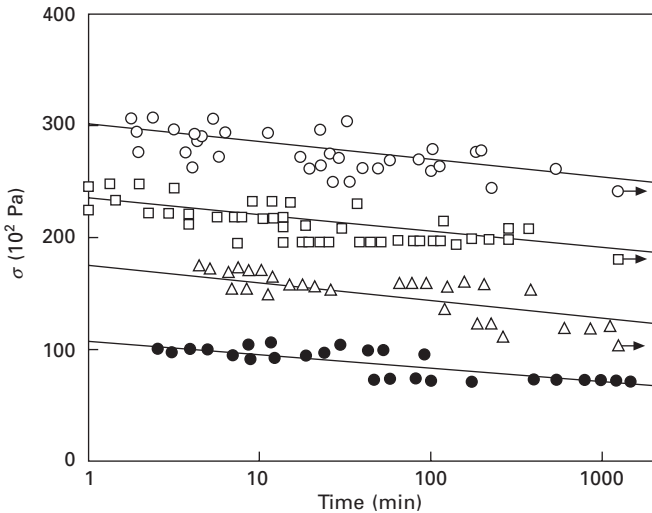
IP Address: 129.132.211.108

9.12 Dependence of strength of glass fibres of various chemical compositions on diameter: 1, 2, magnesium aluminosilicate containing 10 and 20 wt% respectively of MgO; 3 zinc titanium magnesium of aluminosilicate; 4, sodium calcium aluminosilicate; 5, E-type aluminoborosilicate; 6, copper aluminoborosilicate; 7, sodium calcium aluminosilicate; 8, borate; 9, lead; 10, phosphate; 11, sodium silicate (After Khazanov *et al.*, 52).

Most recently, Feih *et al.* (57) have re-examined the temperature dependence of commercial E-glass in the context of the residual strength of glass fibre composites in fire. Fig. 9.15 shows the temperature dependence of sized E-glass bundles of 300 tex. The most important observation is that temperatures in excess of 250°C have a major effect on fibre strength. This data further



9.13 Influence of chemical composition of glass on glass fibre strength after heat treatment: 1, quartz; 2, silica; 3, alkali-free aluminoborosilicate; 4, sodium calcium silicate; 5, borate (After Khazanov *et al.*, 52).

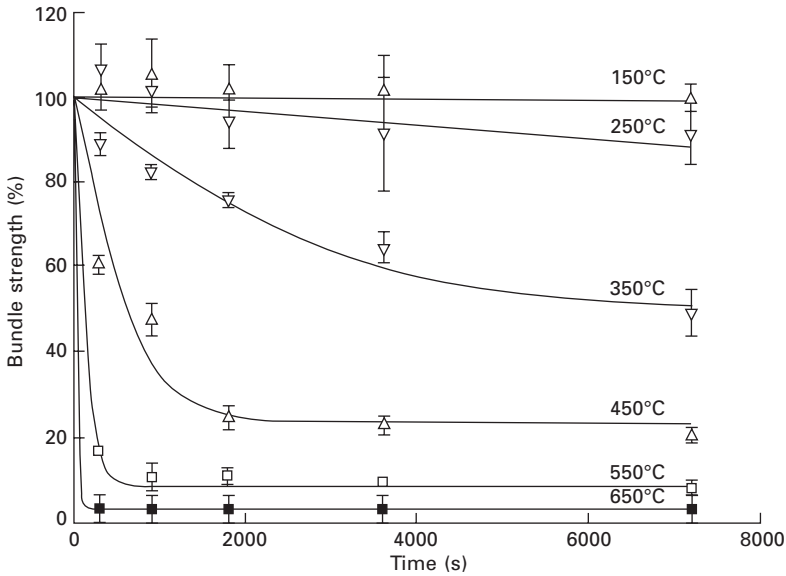


9.14 Time dependence of E-type glass fibre strength at various temperatures:  $\circ$ , 124°C;  $\square$ , 400°C;  $\triangle$ , 500°C;  $\bullet$ , 600°C (After Khazanov, *et al.*, 52).

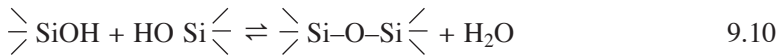
IP Address: 129.132.211.108

supports the silica network hydrolysis mechanism. Below  $\sim 300^\circ\text{C}$  surface silanol groups will tend to condense to siloxane bonds, whereas above this temperature hydrolysis will dominate.





9.15 Effect of time and temperature on E-glass fibre bundle strength (After Feih *et al.*, 57).



IP Address: 129.132.211.108

The clear switch from strength stability below 300°C can be attributed to the thermodynamics of the above reaction. As with any chemical reaction, the rate of hydrolysis is a function of the presence of catalysts. Since the alkali metal glass modifiers (sodium/potassium) catalyse hydrolysis, alkali metal-free glasses are expected to show more resistance to high-temperature excursions.

## 9.5 Protection of fibres for strength retention

### *Sizings and binders*

In production, commercial glass fibres are immediately coated at the bushing with a polymeric sizing. An aqueous-based emulsion is generally used for coating the fibres in contact with a rubber or graphite roller. There are many designs of sizing applicators, but usually they involve the fibres touching a roller which is in contact with the aqueous-based size. One role of the sizing is to provide the fibre surface with protection during handling and transport for the manufacture of artefacts such as woven textiles, preforms or composite materials. In addition, the sizing is chosen to provide strength protection and compatibility with the matrix into which the fibres will be

incorporated. The sizing is also chosen to suit the manufacturing process for the composite material. For example, where the maintenance of strand integrity or slow wet-out is needed in certain manufacturing processes, hard-sized fibres with reduced sizing solubility are used. Where preforms or fibre mats are employed, a secondary binder is used to hold the fibres together during manufacture. Therefore, the finish that is applied to a glass fibre typically consists of (a) an adhesion promoter which is often a silane coupling agent, (b) a protective polymeric film former, (c) lubricants of different composition to aid the flow of the fibres through machinery without damage, (d) differing surfactants used in the emulsification of the polymeric film former, and (e) an optional polymeric binder. A typical emulsion applied to the glass fibre will have a solid content of approximately 10% of which 0.3–0.6% will be the silane coupling agent. The film former will be an appropriate compatible polymer which can be either emulsified or synthesised as a polymer emulsion. A lubricant is usually present in the emulsion at a concentration of 0–0.3%. A surfactant is often added at a level of 0–0.5%, while an antistatic agent may also be used at a loading of 0–0.3%. The term ‘sizing’ may refer to the film former polymer, as well as the compounded finish, sometimes independently of the silane coupling agent, which is used as an adhesion promoter. The generic term ‘finish’ universally refers to the deposited solids on the glass fibre and will include any optional binder in the case of fibre mats and textiles. The film former is used to impart good handleability and control wet-out kinetics for the manufacture of composite materials and is therefore chosen for compatibility with the matrix as well as the choice of fabrication process. For specialist applications such as those requiring environmental resistance, the chemical nature of the film former and/or the binder should be chosen to have excellent compatibility with the resin matrix, otherwise the interface can fail during service, giving rise to a low-durability composite.

The film former needs to satisfy a number of criteria: (a) compatibility with coupling agents and other components of size, (b) a stable emulsion during application at the bushing, (c) good handling characteristics of the roving after the drying of the package, (d) for textile rovings and similar structures the sizing needs to allow the fibres to be unwound for repackaging, (e) the wet-out rate in the resin matrix, and (f) achievement of good hot/wet properties for the composite materials.

Since emulsion technology is used in the preparation of the coating on the fibres, the sizing deposited onto a typical glass fibre has a very complex chemistry. Typical surfactants are polyoxyethylene monophenyl ethers. Typical lubricants are fatty acid amides which are protonated in the presence of the acetic acid used to adjust the pH of the sizing emulsion. The cationic quaternary ammonium sites have an affinity to the negatively charged glass surface, providing the glass with the lubricated structure. The

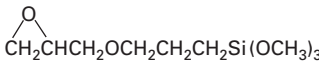
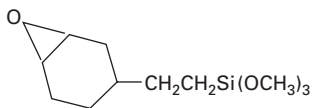
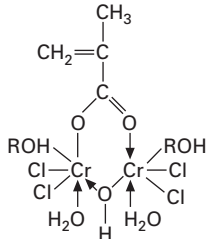
build-up of static electricity during the use of glass fibre rovings can also lead to degradation of the structure of the rovings and other phenomena associated with fabrication breakdown. Therefore, anti-static agents such as alkyltrimethyl ammonium chloride are used to impart surface conductivity to the roving (18, 19).

*Silane coupling agents and the structure of hydrolysed silanes on the glass surface*

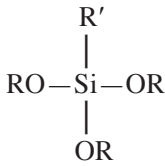
Adhesion promoters are added to the sizing emulsion to provide the glass with compatibility and chemical reactivity to the appropriate matrix. The silane needs to displace adsorbed water from the glass surface to create a hydrophobic surface with the correct thermodynamic characteristics for complete wetting by the matrix resin. This aids the development of a strong interfacial bond between the fibre and the polymeric resin.

Table 9.5 gives details of typical silane coupling agents (19, 58) which

Table 9.5 Typical coupling agents for glass fibre–resin adhesion (19, 58)

Vinyl	$\text{CH}_2=\text{CHSi}(\text{OCH}_3)_3$
Epoxy	
Methacrylate	$\text{CH}_2=\text{C}(\text{CH}_3)\text{COOCH}_2\text{CH}_2\text{CH}_2\text{Si}(\text{OCH}_3)_3$
Primary amine	$\text{H}_2\text{NCH}_2\text{CH}_2\text{CH}_2\text{Si}(\text{OCH}_3)_3$
Diamine	$\text{H}_2\text{NCH}_2\text{CH}_2\text{NHCH}_2\text{CH}_2\text{CH}_2\text{Si}(\text{OCH}_3)_3$
Mercapto	$\text{HSCH}_2\text{CH}_2\text{CH}_2\text{Si}(\text{OCH}_3)_3$
Cationic styryl	$\text{CH}_2=\text{CHC}_6\text{H}_4\text{CH}_2\text{NHCH}_2\text{CH}_2\text{NH}(\text{CH}_2)_3\text{Si}(\text{OCH}_3)_3\text{HCl}$
Cationic methacrylate	$\text{CH}_2=\text{C}(\text{CH}_3)\text{COOCH}_2\text{CH}_2\text{N}^+\text{(Me}_2\text{)CH}_2\text{CH}_2\text{CH}_2\text{Si}(\text{OCH}_3)_3\text{Cl}^-$
Cycloaliphatic epoxide	
Titanate	$[\text{CH}_2=\text{C}(\text{CH}_3)\text{COO}]_3\text{TiOCH}(\text{CH}_3)_2$
Chrome complex	

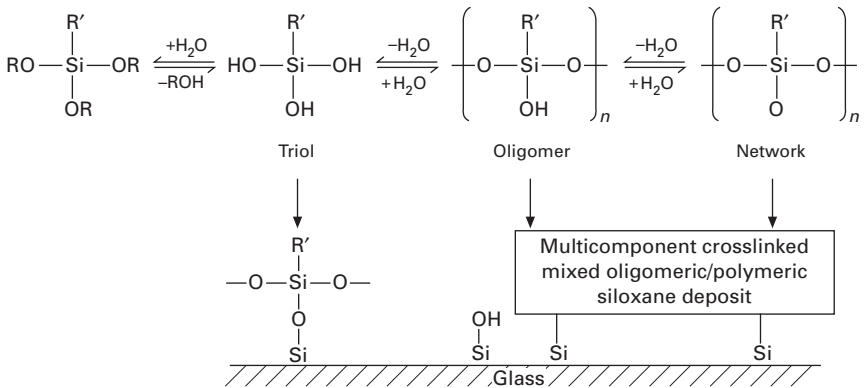
are used to promote adhesion between polymers and the glass fibres. The majority of them are trialkoxy organosilanes with a generic structure as given below:



where R' is a polymer compatible or reactable organic group, and R is either ethyl or methyl.

In the aqueous emulsion, the alkoxy groups are hydrolysed into hydroxyl groups. Depending on the pH of the emulsion, the rate of hydrolysis can vary. The pH is often chosen to be slightly acidic at a pH of 4. Under these conditions, the rates of hydrolysis and polycondensation are such that oligomeric siloxane polymers are formed which are deposited together with oligomers and monomers onto the glass fibre surface. As shown in Fig. 9.16, the deposit on glass fibre is a complex crosslinked polymer containing oligomers of varying degree of polymerisation which depends on the relative rate constants for silanol polycondensation and alkoxy hydrolysis. The polycondensation of the alkoxy groups is an equilibrium polymerisation whose floor concentration is of the order of 0.1%. This means that above this concentration, silanol polymers form in the aqueous solution, whereas below it monomeric trihydroxysilanes are more stable. Therefore, for monomeric-type silane deposits the concentration of silanol in the sizing solution has to be very low. Typically, the concentration of silane in the sizing emulsion is ~0.5%, so that there will always be a mixture of oligomeric silanols of

IP Address: 129.132.211.108



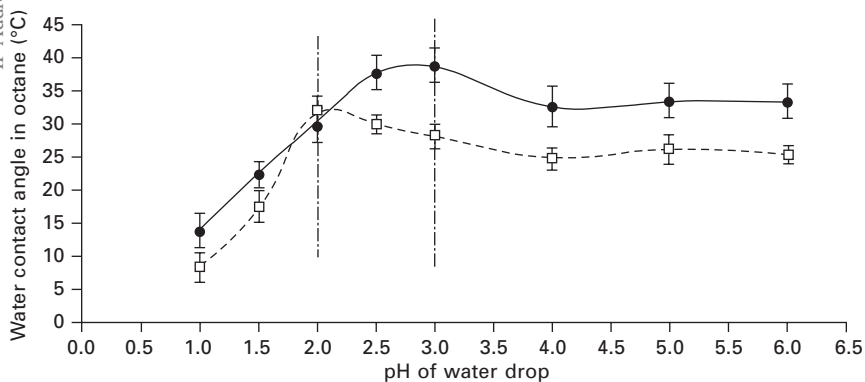
9.16 The chemistry of hydrolysis of a typical organosilane and its adsorption onto a glass fibre surface showing the formation of a complex multi-molecular layer deposit (19).

differing degrees of polycondensation. Since the floor concentrations of the differing hydrolysed silanes vary, their concentration in the sizing emulsion has to be varied to optimise the compatibility and the adhesion of the glass fibres to the matrix.

An E-glass fibre surface has been shown to be largely silica-rich so that after cooling with water it contains hydroxyl groups. The structure of the glass has a major impact on the formation of a strong interface. For example, the presence or absence of boron in the fibreglass composition necessitates a change in the sizing composition to optimise performance. The impact of surface boron atoms upon the interaction of the glass surface with specific molecules has been studied by Pantano *et al.* (59). The very complex chemistry that occurs in the interphase region between a glass surface and the polymer (where the sizing is present) is discussed below. Lui, Thomason and Jones (60) have determined the concentration of surface hydroxyl groups on E-glass and boron-free E-glass from the contact angle with water in an octane environment, using the technique of Carré *et al.* (61). Figure 9.17 shows the contact angle as a function of pH. From the maximum, which is the point of zero charge, the concentration of silanol groups can be estimated. Table 9.6 gives the concentration of silanol groups ( $n_{OH}$ ) per  $\text{nm}^2$ . This shows that an E-glass surface exhibits a lower concentration of silanols compared to a boron-free E-glass.

Silanol groups on the surface of the glass fibre react with those formed during hydrolysis of the alkoxy silane. There is a competition for condensation between the monomeric and oligomeric triols and the glass surface. On drying, the concentration of the silanol groups in the sizing increases, which promotes polycondensation (62, 63). Therefore, in the deposit on the surface

IP Address: 129.132.211.108



9.17 The effect of pH of water on the contact angle of E-glass ( $39 \pm 3^\circ$ ) ( $\blacklozenge$ ) and boron-free E-glass ( $32 \pm 2^\circ$ ) ( $\blacksquare$ ). It is calculated that E-glass surface has  $2.29 \pm 0.04 \text{ nm}^{-2}$  and boron-free E-glass surface has  $2.38 \pm 0.03$  hydroxy groups (OH)  $\text{nm}^{-2}$  (60).

**Table 9.6** Maximum water contact angle ( $CA_{\max}$ ) and calculated concentrations of hydroxyl groups on a variety of E-glass and boron-free E-glass surfaces (60)

	E-glass	B-free E-glass	Dehydrolysed E-glass	Dehydrolysed B-free E-glass	Rehydrolysed E-glass	Rehydrolysed B-free E-glass
$CA_{\max}$	$39 \pm 3$	$32 \pm 2$	$71 \pm 2$	$61 \pm 2$	$52 \pm 3$	$47 \pm 5$
pH	3	2	3	2	3	2
$n_{\text{OH}}(\text{nm}^{-2})$	$2.29 \pm 0.04$	$2.38 \pm 0.03$	$1.71 \pm 0.03$	$1.91 \pm 0.03$	$2.08 \pm 0.05$	$2.16 \pm 0.08$

of E-glass fibres there are typically around 100 molecular layers, of which 90% can be extracted into the matrix on fabrication of the composite. The remaining crosslinked component can then accept the penetration of the matrix resin to form an interpenetrating network.

### *The silane sizing/matrix interphase*

Because of the presence of other matrix-soluble components (64) within the sizing, the interphase region which forms will consist of a semi-interpenetrating network between the silane and the resin, together with dissolved surfactants and monomeric and oligomeric silanols which have diffused over a longer length scale. The interphase region, therefore, has a dimension determined not just by the thickness of the silanol deposit, but also by the diffusional length scale of the other additives, which includes the film former. Figure 9.18 illustrates schematically the structure of the interphase which forms in a composite (65).

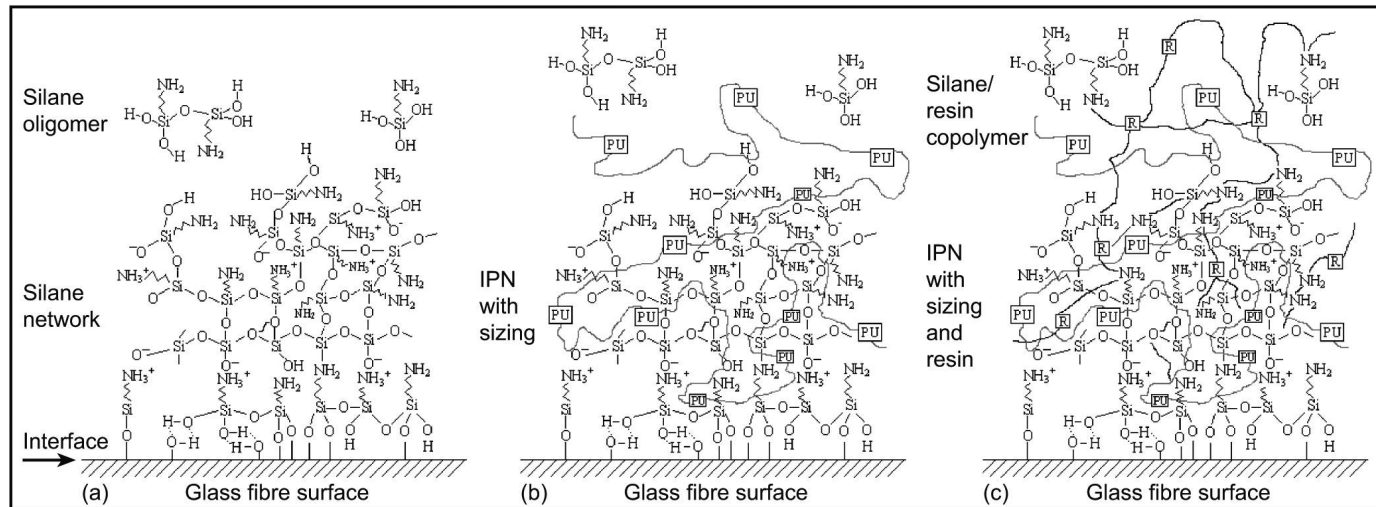
A further complication arises because of the sensitivity of the E-glass to the aqueous environment of the sizing emulsion. It is reported (66, 67) that certain elements of the glass structure are solubilised in the presence of an alkaline or acidic pH. As a result, it is possible to observe the presence of glass elements within the surface coatings on glass fibres. It has been shown by XPS and TOF SIMS analysis that the silanised glass fibre surface has an enriched concentration of aluminium. It appears that aluminium can be extracted from the surface of the E-glass and become copolymerised into the silane deposit. A further consequence of this is that the glass surface becomes denuded of these ions, enabling penetration of the silane into the surface of the glass fibre. Therefore, the interphase region within a glass fibre composite can extend into the subsurface of the glass fibre. The structure of a silanised glass fibre after silanisation with  $\gamma$ -aminopropyltriethoxysilane, shown in Fig. 9.18a, should be modified by the incorporation of  $-\text{O}-\text{Al}-\text{O}-$  bonds in the deposit at the fibre surface. In a previous publication, a revised structure was given (19, 68).

IP Address: 129.132.211.108

### *Silanes – their role in strength retention*

It can be seen in Fig. 9.6 that the silane deposit has a major impact on the strength distributions of individual coated glass fibres. Both the Weibull parameter, which represents the distribution of strengths, and the average strength of the fibres are clear functions of the coating. The purity of the silane used for the silanisation also has a major impact. The reasons for this are unclear, but it demonstrates the need for careful sizing of glass fibres and the choice of appropriate conditions for the silanisation.





9.18 Schematic of the structure of (a) the silane deposit, (b) sizing structure and (c) interphase in a composite (65).

*Silanes – selection for adhesion promotion*

Several mechanisms of adhesion have been identified (19). The most common is that of chemical bonding which is referred to as chemical coupling. In this mechanism it is assumed that monolayer silane deposits are adhered to the glass fibre surface and that the resin-compatible group is reacted directly to the polymer during the curing mechanism. This gives a strong chemical bond between the two components in the formation of an interface. However, as shown above, it is more likely that an interphase region is formed in which an interpenetrating network has been created. Therefore, the deformable layer hypothesis of adhesion can also be invoked, as this can explain many of the phenomena associated with the micromechanics of adhesion of fibres to resins. It has to be recognised that many of the adhesion test methods used for fibre composites measure the stress transfer efficiency between the two components. Since the stress transfer is also a function of the properties of the interphase region, it is clear that the deformable layer hypothesis merely represents this concept. It also explains why the sizing formulations on glass fibres have to be finely tuned to the matrix into which the fibres will be introduced. This is because interphase formation can have a major impact on the micromechanics. It has been shown by finite element analysis and together with experimental validation that for optimum performance the interphase region should have a yield strength which is slightly below that of the matrix, so that the shear stresses at the interface can be accommodated by deformation rather than debonding (69). Ideally, the moduli of the two components should be similar so that the shear stress is confined to the interphase region and the stress transfer efficiency maximised. This observation also explains why the reversible hydrolytic bonding mechanism of Plueddemann (58) may not be applicable. Reversible recovery of dry properties after immersion in water can be accounted for by local reversible plasticisation of the interphase region, so that the concept of reversible hydrolysis of the siloxane bonds is not required.

IP Address: 129.132.211.108

*Adhesion of unsilanised and unsized glass fibres*

It is also observed that under dry conditions, E-glass fibres form an apparently strong bond to epoxy resins (70). It is known that this interfacial bond is lost after immersion in water or humid environments. Therefore, this interfacial response can be attributed to hydrogen bonding between the cured epoxy resins and the glass fibre surface, and radial thermal residual stresses which form on cooling after curing at elevated temperatures. It should be emphasised that silane coupling agents are still essential for durable composites because, in service, residual matrix stresses will relax and interfacial hydrogen bonding will be lost on moisture absorption.

*Plasma polymers as functional sizing for adhesion and protection*

Plasma polymerisation is a technique for depositing molecularly thin conformal polymeric layers onto surfaces. By choosing appropriate conditions, the functional group within the deposit can be retained at a high level. Therefore, this approach is a good sizing technique for achieving a functional adhesive coating at the same time as providing strength protection to the fibres. Table 9.4 shows the strength retention after plasma polymer coating of E-glass fibres. Liu, Zhao and Jones (70) have shown that the interlaminar shear strength of the composites can be increased to above that of the matrix through the formation of an interphase between the plasma polymer and the epoxy resin.

This demonstrates how the interphasal properties of the composite can be optimised for performance. An interphase of thickness 5 nm appeared to provide an optimum mechanical performance of the composite. Plasma polymerisation represents, therefore, an efficient and environmentally friendly technique for creating a functional coating on reinforcing fibres and at the same time producing the appropriate protection that the sizing polymer needs to give to the fibres for use in manufacturing techniques. Swait *et al.* (71) have demonstrated that the combination of controlled interphase and fibre strength retention can change the micromechanics to benefit energy absorption.

## 9.6 Summary

The structure and properties of glass fibres have been discussed. The requirements for fibre drawing have been identified and used to explain their properties. The chemical structure of the glass has been related to the strength properties of drawn filaments. The need for the coating of glass immediately after forming has been addressed. Further, the role of these coatings on the formation of a strong fibre and a durable composite has been discussed.

## 9.7 References

1. *The Evolution of Excellence*, Owens Corning Publication 15-GL-23185 (1998).
2. (Various internal documents of Owens Corning have been utilised in this summary.)
3. J. R. Hutchins III and R. V. Harrington, 'Glass', in *Kirk-Othmer Encyclopedia of Chemical Technology*, 2nd edn, Vol 10, Wiley, New York, 1966, 533–604.
4. A. Agarwal, K. M. Davies and M. Tomozawa, 'A simple IR spectroscopic method for determining fictive temperature of silica glasses', *J. Non-Cryst. Solids*, 185 (1995) 191.
5. A. Q. Tool, *J. Res. Natl. Bur. Stand.*, 37 (1946) 73–90.
6. R. N. Haward and R. J. Young (eds), *The Physics of Glassy Polymers*, 2nd edn, Chapman & Hall, London, 1997, Chapters 1 and 3.

7. J. H. Gibbs and E. A. DiMarzio, *J. Chem. Phys.*, 28 (1958) 373–383.
8. G. W. Scherer, *Relaxation in Glass and Composites*, Krieger, Malabar, FL, 1992, 1–15.
9. A. A. Lebedev, *Trudy Cossud., Opt. Inst.*, 2 (1921) 57.
10. W. H. Zachariasen, ‘The atomic arrangement in glass’, *J. Am. Chem. Soc.*, 54 (1932) 3841.
11. B. E. Warren, *J. Appl. Phys.*, 8 (1937) 645.
12. B. E. Warren, *J. Appl. Phys.*, 13 (1942) 602–610.
13. N. T. Huff, E. Demiralp, T. Çagin and W. A. Goddard III, ‘Factors affecting molecular dynamics simulated vitreous silica structures’, *J. Non-Cryst. Solids*, 253 (1999) 133–142.
14. N. T. Huff, unpublished work (2007).
15. P. H. Gaskell, ‘Medium-range structure in glasses and low Q structure in neutron and X-ray scattering data’, *J. Non-Cryst. Solids*, 351 (2005) 1003–1013.
16. A. Q. Tool, ‘Relation between inelastic deformability and thermal expansion of glass in its annealing range’, *J. Am. Ceram. Soc.*, 29 (1946) 240–253.
17. C. T. Moynihan, A. J. Easteal, M. A. DeBolt and J. Tucker, ‘Dependence of the fictive temperature of glass on cooling rate’, *J. Am. Ceram. Soc.*, 59 (1976) 12–16.
18. K. Loewenstein, *The Manufacturing Technology of Continuous Glass Fibres*, 3rd edn, Elsevier, Amsterdam, 1993.
19. F. R. Jones, ‘Glass fibres’, in *High-Performance Fibres*, ed. J. W. Hearle, Woodhead, Cambridge, 2001, Chapter 6, 191–238.
20. Owens Corning, US Patent 5,789,329 (1998).
21. A. J. Majumdar, GB Patent 1,243,972/1,243,973 (1971).
22. Kanebo Ltd/Nippon Electric Co. Ltd, GB Patent 1,548,776 (1979).
23. GB Patent 520, 247 (1940).
24. R. A. Schoenlaub, US Patent 2, 334, 961 (1943).
25. R. L. Tiede *et al.*, US Patent 2, 571, 074 (1951).
26. W. N. Haggerty, Canadian Patent 1, 067, 230 (1979).
27. S. Yamamoto *et al.*, European Patent 275, 541 (1987).
28. D. E. McWilliams *et al.*, European Patent 275, 541 (1987).
29. J. Sproul, Canadian Patent 1, 248, 555 (1989).
30. D. Hartman, ‘High strength glass fibres’, technical paper, AGY ([http://www.agy.com/technical\\_papers.htm](http://www.agy.com/technical_papers.htm)).
31. D. Hartman, ‘evolution and application of high strength glass fibres’, *The Glass Researcher, Bulletin of Glass Science and Engineering*, 4(2) (1995) 6–13, 5(1) (1995) 10–11.
32. J. G. Mohr and W. P. Rowe, *Fibreglass*, Van Nostrand, New York, 1978.
33. J. H. Simmons, Morey Award Lecture, *J. Non-Cryst. Solids*, 239 (1998) 1–15.
34. A. A. Griffith, ‘The phenomena of rupture and flow in solids’, *Phil. Trans. Roy. Soc., Lond.*, A221 (1920) 163.
35. A. Kelly and N. H. MacMillan, *Strong Solids*, 3rd edn, Clarendon, Oxford, 1990.
36. A. G. Metcalfe and G. K. Schmitz, ‘Mechanism of stress corrosion in E-glass filaments’, *Glass. Tech.*, 13 (1972) 5.
37. G. M. Bartenev, *The Structure and Mechanical Properties of Inorganic Glasses*, Walters-Noordhoff, Groningen, 1970.
38. N. G. McCrum, *Review of the Science of Fibre Reinforced Plastics*, HMSO, London, 1971; and F. R. Jones, ‘Fibre reinforced plastic composites’, in *Aluminium Alloys* –

*Contemporary Research and Applications*, ed. A. K. Vasudevan and R. D. Doherty, Academic Press, New York, 1989.

39. R. J. Hand and A. B. Seddon, 'A hypothesis on the nature of Griffith's cracks in alkali silica glasses', *Phys. Chem. Glasses*, 381 (1997) 11.
40. G. M. Bartenev and L. K. Izmailova, *DAN SSR*, 146 (1962) 1136–1138; and *Soviet Physics Sol. St.*, 6 (1984) 920.
41. W. F. Thomas, 'An investigation of the factors likely to affect the strength and properties of glass fibres', *Phys. Chem. Glass*, 1 (1960) 4–18.
42. D. J. Marks and F. R. Jones, 'Plasma polymerised coatings for engineered interfaces for enhanced composite performance', *Composites A*, 33 (2002) 1293–1302.
43. J. Aveston, A. Kelly and J. M. Sillwood, 'Long-term strength of glass reinforced plastics in wet environments', in *Advances in Composite Materials*, ed. A. R. Bunsell *et al.*, Pergamon, Paris, 1980, 556–568.
44. F. R. Jones, 'The effects of aggressive environments on fatigue in composites', in *Fatigue of Composite Materials*, ed. B. Harris, Woodhead, Cambridge, 2003, Chapter 4, 117–146.
45. R. J. Charles, 'Static fatigue of Glass I and II', *J. Appl. Phys.*, 29 (1958) 1549.
46. S. B. Ghosh, PhD Thesis, University of Sheffield, UK, 2006.
47. A. Kelly and N. McCartney, *Proc. Roy. Soc. Lond.*, A374 (1981) 475–489.
48. F. R. Jones, J. W. Rock and J. E. Bailey, 'The environment stress corrosion cracking of glass fibre-reinforced laminates and single E-glass filaments', *J. Mater. Sci.*, 18 (1983) 1059–1071.
49. F. R. Jones and J. W. Rock, 'On the mechanism of stress corrosion of E-glass fibres', *J. Mater. Sci. Letters*, 2 (1983) 519.
50. D. R. Cockram, *Glass Tech.*, 22 (1981) 211–214.
51. P. G. Fox, 'Mechanisms of environment sensitive cracking in glasses', *Proc. Congress on Mechanisms of Environmental Stress Cracking*, London, Metals Society, 1977, 268–282.
52. V. E. Khazanov, Yu. I. Kolesov and N. N. Trojmov, 'Glass fibres', in *Fibre Science and Technology*, ed. V. I. Kostikov, Chapman & Hall, London, 1995, 15–230.
53. M. S. Aslanova, 'Strength and chemical content of glass', *Steklo i Keramika*, 4 (1967) 1.
54. M. S. Aslanova, 'Les facteurs determinant les propriétés mécaniques des fibres de verre et de quartz et des plastiques par ces fibres', *Verre Textile Plastiques Renforcés*, 1 (1966) 14.
55. M. S. Aslanova, Résistance à la traction des fibres, de silice vitreuse en fonction de l'état de surface et de la microstructure, *Verres et Refractaires*, 22 (1968) 585.
56. G. M. Nishioka and J. A. Schramke, 'Desorption of water from glass fibres in molecular characterisation of composite interfaces', in *Molecular Characterisation of Composite Interfaces*, ed. H. Ishida and G. Kumar, Plenum, New York, 1983.
57. S. Feih, Z. Mathys, A. G. Gibson and A. P. Mouritz, 'Tensile strength modelling of glass fibre-polymer composites in fire', *J. Composite Materials*, 41 (2007) 2387–2410.
58. E. Plueddemann, *Silane Coupling Agents*, 2nd edn, Plenum, New York, 1991.
59. C. G. Pantano, R. A. Fry and K. T. Mueller, *Phys. Chem. Glasses*, 44 (2003) 64–68.
60. X. M. Liu, J. L. Thomason and F. R. Jones, 'The concentration of hydroxyl groups on glass surfaces and their effect on the structure on E-glass surfaces', in *Silanes*

*and Other Coupling Agents*, Vol 5, ed. K. L. Mittal, Brill Academic Publishers, Leiden, The Netherlands and Boston, MA, 2009, 25–38.

61. A. Carré, *J. Coll. Interface Sci.*, 260 (2003) 49.
62. H. Ishida and J. L. Koenig, 'An FTIR spectroscopic study of the hydrolytic stability of silane coupling agents on E-glass fibres', *J. Polym. Sci., Polym. Phys. Ed.*, 18 (1980) 1931.
63. H. Ishida and J. L. Koenig, 'FTIR spectroscopic study of the structure of silane coupling agents on E-glass fibres', *J. Coll. Interface Sci.*, 64 (1978) 565.
64. J. L. Thomason and L. J. Adzima, 'Sizing-up the interphase: an insider's guide to the science of sizing', *Composites A*, 32 (2001) 313.
65. X. M. Liu, J. L. Thomason and F. R. Jones, 'XPS and AFM study of interaction of organosilanes and sizing with E-glass fibre surface', *J. Adhesion*, 84 (2008) 322.
66. D. Wang and F. R. Jones, 'A surface analytical study of the interaction between  $\gamma$ -amino propyltriethoxysilane and E-glass surface, part 11: XPS study', *J. Mater. Sci.*, 28 (1993) 2481.
67. D. Wang, F. R. Jones and P. Denison, 'A TOFSIMS and XPS study of the interaction of hydrolysed  $\gamma$ -aminopropyl triethoxysilane with E-glass surfaces', *J. Adh. Sci. Technol.*, 6 (1992) 79–98.
68. T. Choudhury and F. R. Jones, 'The interaction of Resole and Novolak phenolic resins with  $\gamma$ -aminopropyl triethoxysilane treated E-glass surface: A high resolution XPS and micromechanical study', in *Silanes and Other Coupling Agents*, Vol 2, ed. K. L. Mittal, VSP, Utrecht, 2000, 79–97.
69. R. Lane, S. A. Hayes and F. R. Jones, 'Fibre–matrix stress transfer through a discrete interphase, Part 2, high Volume fraction systems', *Comp. Sci. Technol.*, 61 (2001) 568–578.
70. Z. Liu, F. M. Zhao and F. R. Jones, 'Optimising the interfacial response of high volume fraction glass fibre composites using a function plasma polymer', *Comp. Sci. Technol.*, 28 (2008) 3161–3170.
71. T. Swait, C. Soutis and F. R. Jones, 'Optimisation of interfacial properties for tensile strength by plasma polymerisation', *Comp. Sci. Technol.*, 28 (2008) 2302–2309.

---

O PARIS, University of Leoben, Austria and  
Max Planck Institute of Colloids and Interfaces, Germany and  
H PETERLIK, University of Vienna, Austria

**Abstract:** Carbon fibres are characterised by low weight and very high values of tensile strength and tensile modulus, which are maintained up to temperatures well above 2000°C. These properties make carbon fibres ideal candidates for lightweight composites, in particular for high temperature aerospace applications. The microstructure of carbon fibres is characterised by several peculiar features at different length scales, which are all based on the stacking of graphene sheets and their mutual orientation. This chapter provides an overview about the current knowledge of carbon fibre structure, its manipulation during fibre production and processing, and how the structure determines fibre properties.

**Key words:** graphene sheets, polyacrylonitrile (PAN)-based carbon fibres, mesophase pitch (MPP)-based carbon fibres, mechanical properties, turbostratic structure, preferred orientation.

## 10.1 Introduction

Carbon fibres are based solely on the element carbon and are therefore among the lightest inorganic materials available on earth. The strong covalent bonding between  $sp^2$  hybridised carbon atoms leads to extremely high stiffness which is not surpassed by any other material. Modern high-performance carbon fibres based on mesophase pitch (MPP) precursors, for instance, can have a tensile modulus of almost 1 TPa (1000 GPa), in connection with excellent thermal conductivity. Carbon fibres based on polyacrylonitrile (PAN) polymer precursor exhibit outstanding tensile strength, and fibres with 6.4 GPa strength are currently available on the market. Hence, the specific strength of carbon fibres can surpass typical values for steel by more than an order of magnitude. The vast majority of carbon fibres are therefore used for lightweight structural applications in composites ranging from sporting goods to aerospace materials. PAN-based fibres for ultra-high strength, high temperature applications comprise about 90% of the total carbon fibre production worldwide, while mesophase pitch-based fibres are used for high modulus and thermal management applications. Cellulose-based fibres have almost vanished from the market, and vapour-grown fibres are still awaiting the breakthrough for structural applications.

Besides a short historical overview (Section 10.2) and a brief review



of fibre production (Section 10.3), this chapter provides a comprehensive description of major structural features (Section 10.4) and related mechanical properties (Section 10.5) of high-performance carbon fibres used for structural applications in composite materials. Graphite whiskers as well as vapour grown carbon nanofibres, and in particular carbon nanotubes, may have even superior mechanical properties. These materials as well as activated carbon fibres will, however, not be discussed within this chapter.

## 10.2 Short historical overview

The first carbon fibres were produced already around 1880 by Thomas Edison who made lamp filaments from cotton and bamboo. But it was not until the beginning of the 1960s that high-performance carbon fibre development started. A key experiment stimulating the research on carbon fibres was probably the one by Roger Bacon (Bacon 1960) who produced for the first time graphite whiskers and demonstrated that they exhibit extremely high tensile strength of about 20 GPa and a modulus of at least 700 GPa. First reports on PAN-based (Shindo 1961) and isotropic pitch-based (Otani *et al.* 1965) carbon fibres stem from Japan. A few years later in the UK, the Royal Aircraft Establishment (Moreton *et al.* 1967), as well as Rolls Royce Ltd (Standage and Prescott 1966) also reported on high-strength and high-modulus carbon fibres based on acrylic precursors. Almost in parallel, basic investigations on cellulose based carbon fibres were published by Bacon and Tang (1964), and Union Carbide Corporation in the US began commercial production of carbon fibres from rayon cellulose. The prospect of novel lightweight composites ranging from sporting goods to aircraft and aerospace applications initiated a 'boom' in the investigation of the processing, structure and mechanical properties of carbon fibres based on rayon cellulose and polyacrylonitrile (PAN) (Cahn and Harris 1969; Jeffries 1971; Diefendorf and Tokarsky 1975). About 10 years later in the mid-1970s, carbon fibres from mesophase pitch were first developed and commercialised (Bright and Singer 1977; Otani 1981), after the pioneering work on mesophase by Brooks and Taylor (1965). These fibres very soon became the second important class of high performance carbon fibres beside PAN-based fibres, in particular because of their extremely high tensile modulus (Endo 1988). Finally, vapour grown carbon fibres were first reported in 1976 by Oberlin *et al.* (1976) and, due to the prospect of low-cost production, they very soon became a field of intensive investigation (Dresselhaus and Endo 2001). Though carbon fibre research is now almost 50 years old, there is still quite some effort to improve fibre properties and in particular to decrease production costs in order to open new markets (Edie and McHugh 1999).

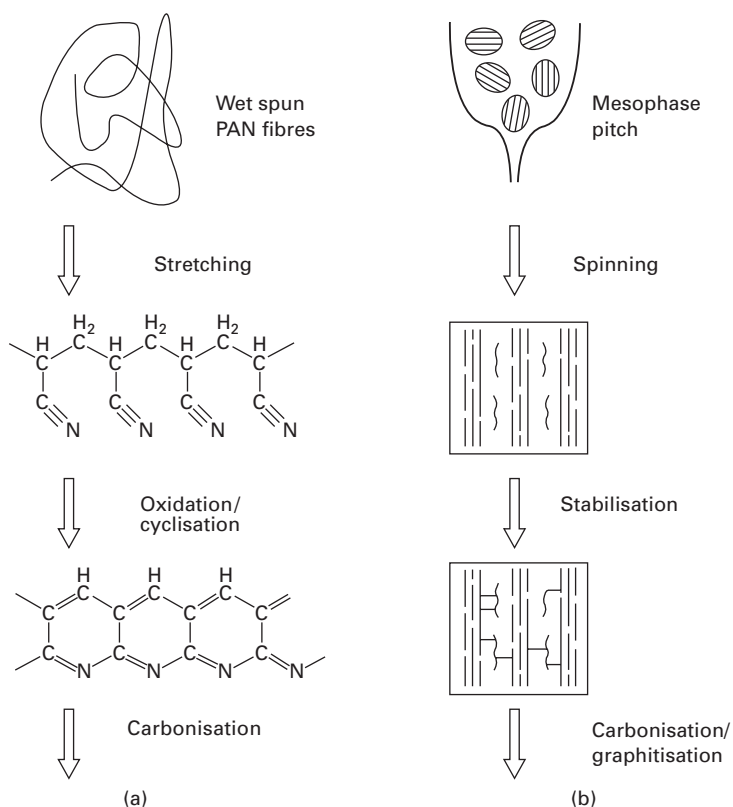
### 10.3 Types and production of carbon fibres

The common step in the production of all carbon fibres is a final high temperature treatment (HTT) of a structurally stabilised and thermally, mechanically and/or chemically pretreated precursor fibre. Concerning HTT, conventions in literature usually speak about carbonisation for temperatures below about 2000°C and about graphitisation above this temperature. This is somewhat misleading, since many carbon fibres do not graphitise even at temperatures above 3000°C, and the term graphitisation should be used only if the final fibre exhibits graphite structure. Besides the HTT, a second important factor concerns the choice of the precursor material and its processing. In the following we recall very briefly the basic processing steps for the four major classes of carbon fibres, namely (i) cellulose based, (ii) PAN based, (iii) mesophase-pitch based, and (iv) vapour grown carbon fibres. More information about the details of fibre production can be found in many textbooks (Fitzer and Manocha 1998; Edie and McHugh 1999; Dresselhaus and Endo 2001) and in numerous overview articles, e.g. Oberlin (1984), Fitzer *et al.* (1986), Jain and Abhiraman (1987), Jain *et al.* (1987) and Edie (1998). It should be mentioned that several other precursors have also been explored for carbon fibres such as, for instance, lignin (Johnson *et al.* 1975) and chitosan (Bengisu and Yilmaz 2002), but they do not play any role in applications.

1. *Cellulose based carbon fibres* are almost exclusively based on regenerated cellulose II fibres (viscose rayon) (see Chapter 6). Natural cellulose I fibres such as cotton and ramie are not suitable as precursors for high performance carbon fibres, since a high defect density limits the strength of the fibres. The basic process of converting rayon into carbon fibres with high preferred orientation consists of a low temperature stabilisation (300–400°) in air followed by slow heating to high temperature (1500–3000°C) in inert atmosphere. The details of the chemical reactions with thermal treatment, and in particular the development of preferred orientation in cellulose based materials, are still not fully clear (Byrne and Nagle 1997; Paris *et al.* 2005), and are mainly based on an early model by Bacon and Tang (1964). Carbonisation of cellulose-based fibres under tension increases the preferred orientation of the graphene sheets with respect to the fibre axis, in particular if hot stretching is applied at temperatures above 2700°C (Walker 1993).
2. The precursors for *polyacrylonitrile (PAN) based fibres* are resins consisting of copolymers with acrylonitrile as the major monomeric component with some other monomers added to control oxidation rate and glass transition temperature. PAN fibres are wet spun from the resin, stabilised in air at temperatures between 200°C and 400°C, and finally carbonised in inert atmosphere to temperatures up to 1500–3000°C.

Rigorous exclusion of impurities in the precursor fibre, as well as detailed control of fibre stabilisation and heating rate, are crucial steps for the final structure and properties of the fibres (Jain and Abhiraman 1987; Walenta and Fink 1990; Schaper and Fink 1990; Edie 1998). The tensile strength is highest for temperatures around 1500°C, the reason being that some high strength PAN-based carbon fibres contain residual nitrogen (Edie and McHugh 1999). The chemical and structural changes during the processing of PAN-based carbon fibres are schematically visualised in Fig. 10.1a.

3. *Mesophase pitch (MPP)-based carbon fibres* are based on discotic nematic liquid crystalline materials which are obtained from the thermal polymerisation of petroleum- or coal tar-based pitches, or from catalytic polymerisation of pure compounds such as naphthalene. Melt spinning is used to convert the mesophase-pitch into fibre form. High shear stresses during flow through the spinneret capillary lead to an orientation of the



10.1 Basic production steps for (a) PAN-based carbon fibres and (b) MPP-based carbon fibres.

disc-shaped molecules, which is further improved by drawing the as-spun fibres (Edie 1998). A stabilisation treatment in air at around 300°C is applied before high temperature carbonisation in inert atmosphere up to 3000°C drives off all non-carbon elements and transforms the fibre into high-strength, high-modulus carbon fibre (Edie 1998; Edie and McHugh 1999). The most important steps and associated structural changes during MPP processing are illustrated schematically in Fig. 10.1b.

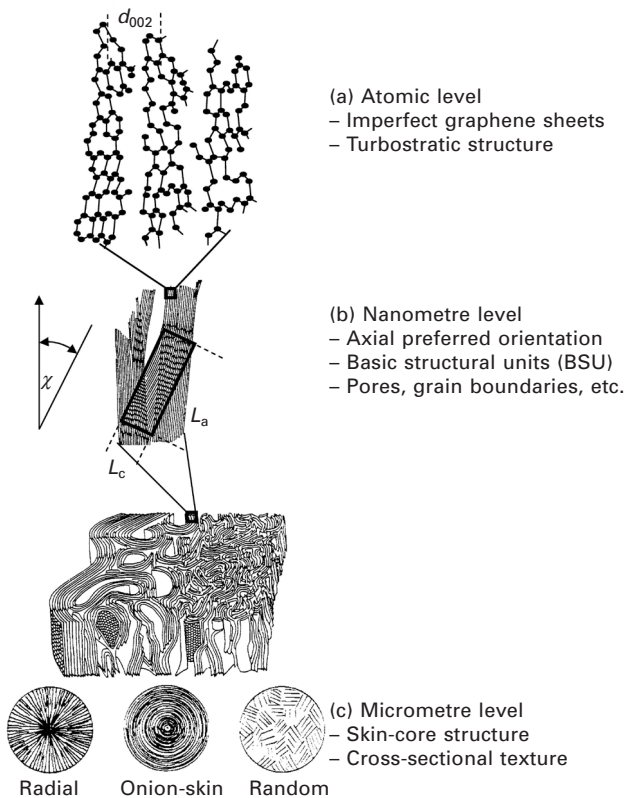
4. The preparation of *vapour grown carbon fibres* is based on the growth of a thin hollow tube by a catalytic process based on ultra-fine particles that have been supersaturated with carbon from the pyrolysis of a hydrocarbon gas at about 1000°C. The fibre thickening occurs through an epitaxial growth process, and subsequent heat treatment at high HTT (~ 2500°C) results in fibres with tree-ring coaxial cylinder morphology. Vapour grown fibres can be produced with a wide range of diameters from 10 nm to more than 100 µm, and all of them have central hollow cores. Vapour grown fibres with diameters up to 100 nm are called nanofibres, and their properties are somewhat between those of carbon fibres and multiwall nanotubes (Dresselhaus and Endo 2001).

## 10.4 Fibre structure

### 10.4.1 General overview

Perfect graphene denotes a two-dimensional (2D) layer of  $sp^2$  bonded carbon atoms that are exclusively positioned on planar hexagonal cells forming a perfect 2D crystal. The most stable carbon polymorph graphite is then obtained by the stacking of these graphene sheets in such a way that a three-dimensional (3D) hexagonal crystal with space group  $P6_3/mmc$  is formed. A major characteristic of the graphite structure is the large difference in bonding strength *within* (covalent) and *between* the graphene layers (van der Waals), which leads to a strong anisotropy in many physical properties parallel and perpendicular to the sheets. This high anisotropy is also a major structural feature common to all high performance carbon fibres, resulting from planar assemblies of graphene sheets oriented more or less parallel to the fibre axis. Carbon fibres should, however, not be seen as homogeneous anisotropic materials similar to fibrous graphite. They are rather a collection of anisotropic nanoscale units linked in such a way that they represent composites in their own right. Figure 10.2 visualises schematically three different levels that are expected to be of major influence for important fibre properties such as stiffness and strength. The structure at each of these levels depends on the precursor material and on the detailed processing conditions. Hence, tailoring individual fibre properties for specific functions is possible in principle by manipulating the structure at the respective level.

1. *Hierarchical Level 1*: The basic unit of carbon fibres is the imperfect graphene sheet. Imperfect means that the layer contains typically a high number of defects such as vacancies that open the six-atom ring structure, interstitials, and/or impurity atoms. As a consequence, the graphene lattice is strongly distorted in-plane and carbon atom positions can also deviate considerably from the perfect planar structure (Fig. 10.2a). Carbon fibres – similar to many other disordered carbons – are based on the stacking of such imperfect graphene sheets. In contrast to graphite, the high density of in-plane defects and a finite lateral extension of the sheets lead usually to a stacking without any orientational and positional order between the sheets, which results in a so-called turbostratic structure. The missing 3D crystalline order was first recognised and correctly interpreted already by Warren (1941), and is one of the most conspicuous structural features of almost all types of carbon fibres.



10.2 Three important structural levels of carbon fibres: the fibre axis is vertical, except for (c) which shows the fibre cross-sections.

2. *Hierarchical Level 2*: Two characteristic length scales determine the structure at the nanometre level. Both the lateral extension of the sheets  $L_a$  and their stacking height  $L_c$  are in the range between one and a few tens of nanometres and define a kind of nanocrystallites, often also termed ‘basic structural units’ (BSU) (Fig. 10.2b). In carbon fibres, these stacks of graphene sheets are preferentially oriented parallel to the fibre axis with some misalignment angle  $\chi$  of the crystallites. The degree of axial preferred orientation is determined by the width of the orientation distribution of the graphene sheet normal vectors with respect to the fibre axis, and primarily determines the tensile stiffness of the fibre. This is easily understood by the fact that any graphene layer slightly misoriented from the fibre axis allows shear to become operative, and thus lowers the tensile modulus of the fibre. The BSU can split, twist, fold and join other BSUs to form micro-domains separated by slit-like or needle-like pores, leading to the famous picture published by Bennett and Johnson (1978) for PAN-based fibres which resembles qualitatively the structure of a crumpled newspaper (Fig. 10.2b).
3. *Hierarchical Level 3*: At the level of about 100 nm and above, many carbon fibres exhibit a pronounced microtexture, which strongly depends on the fibre type and processing conditions (Fig. 10.2c). Moreover, structural heterogeneities such as skin–core structures or production flaws may be present. These structural features together with the fibre diameter, the cross-sectional shape and the surface structure (e.g. roughness) influence in particular the fibre strength.

In the following three subsections we describe these three levels of structural hierarchy in more detail and in Section 10.5 we assess the implications for the mechanical properties of the fibres from different precursors.

Table 10.1 sets out the structural parameters and related physical properties for some typical commercially available carbon fibres based on PAN and MPP precursors. The HTA7 series is from Tenax, K321 and K137 are from Mitsubishi, E35 is from DuPont and FT500 is from Tonen. HTA7 AR is the as-received fibre from the manufacturer; the other PAN based fibres were heat treated at the indicated temperatures of 1800°C, 2100°C and 2400°C. For the pitch-based fibres, no HTT data were provided by the manufacturer. The density  $\rho$  was taken from the producer datasheets, and structural data (fibre diameter  $D$ ,  $d$ -spacing  $d_{002}$ , in-plane lattice parameter  $a$ , X-ray coherence lengths  $L_c$  and  $L_a$ , azimuthal width of the 002 reflection HWHM) as well as the Young’s modulus  $E$  were taken from Loidl *et al.* (2005a, 2005b). The fibre strength (expressed by the scale parameter  $\sigma_0$  ( $L = 200$  mm) of the Weibull distribution) and the Weibull modulus  $m$  were derived from a unimodal Weibull fit of mechanical data obtained from fibre bundle tensile tests with 200 mm test length (unpublished data, courtesy D. Loidl). It should

*Table 10.1* Structural parameters and related physical properties for some commercially available carbon fibres based on PAN and MPP precursors. For explanation and source of information, see text

Fibre (precursor)	$D$ ( $\mu\text{m}$ )	$d_{002}$ (nm)	$a$ (nm)	$L_c$ (nm)	$L_a$ (nm)	HWHM (degree)	$\rho$ ( $\text{g/cm}^3$ )	$E$ (GPa)	$\sigma_0$ (GPa)	$m$
K321 (MPP)	10.5	0.354	0.239	1.67	3.02	17.6	1.90	136	0.99	2.4
E35 (MPP)	9.7	0.348	0.245	3.27	4.93	12.0	2.10	197	1.71	13.5
FT500 (MPP)	10.0	0.343	0.246	10.06	10.22	6.7	2.11	380	2.49	11.2
K137 (MPP)	9.5	0.343	0.246	13.38	11.61	3.4	2.12	500	1.69	4.2
HTA7 AR (PAN)	6.8	0.354	0.238	1.47	2.83	19.0	1.77	198	2.73	4.5
HTA7 1800 (PAN)	7.3	0.350	0.238	2.18	3.60	16.3	1.77	273	2.20	2.8
HTA7 2100 (PAN)	6.4	0.346	0.244	3.78	6.30	11.8	1.71	332	2.20	3.4
HTA7 2400 (PAN)	6.2	0.344	0.244	5.11	7.61	9.6	1.91	349	2.23	3.4

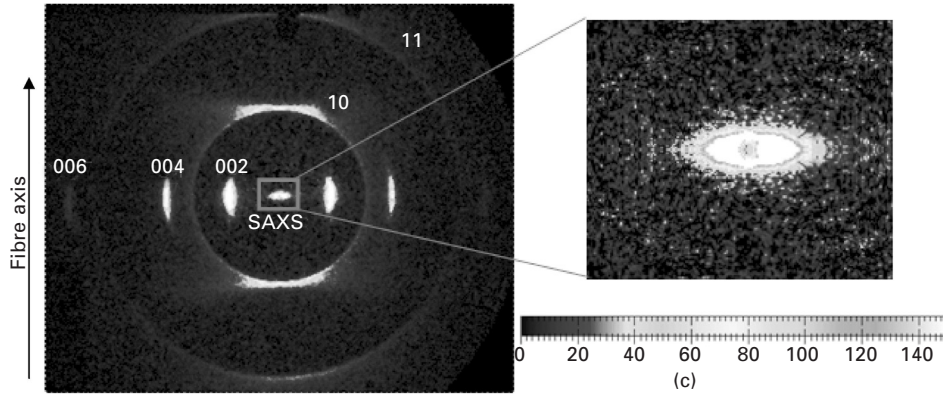
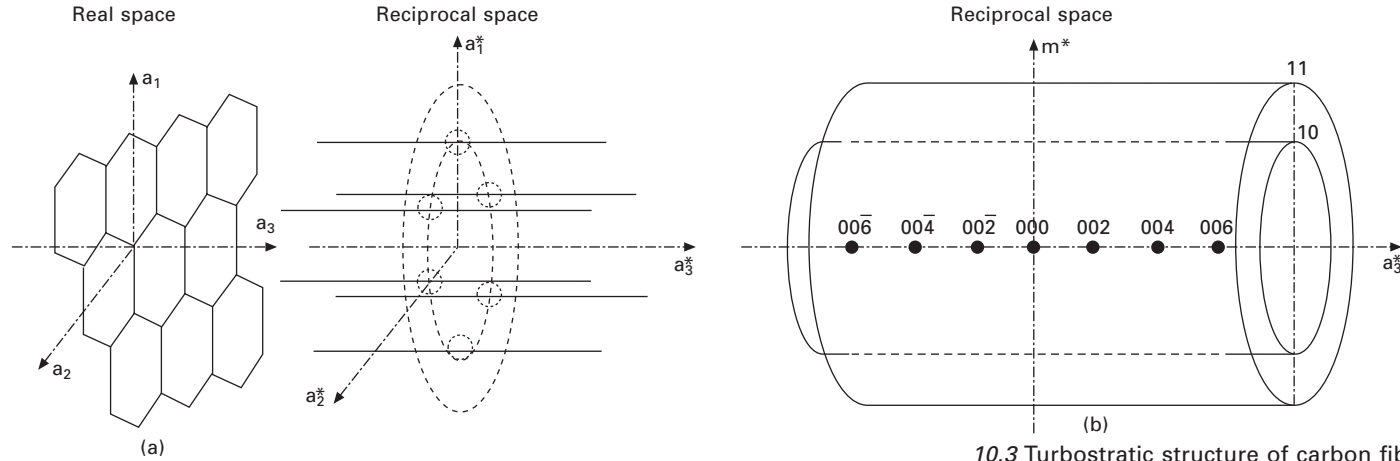
be noted that  $\sigma_0$  increases with decreasing test length,  $\sigma_0(L) = \sigma_0(L_0)(L_0/L)^{(1/m)}$ . Thus, usually higher values are published in producers' data sheets, because experiments are frequently performed at a significantly smaller test length.

#### 10.4.2 Atomic order: turbostratic carbon and the role of covalent crosslinks

The turbostratic structure of carbon is characterised by the one-dimensional (1D) stacking of distorted 2D graphene layers. Owing to the random translational and rotational arrangement of the layers with respect to each other, no ordered 3D crystal structure is formed. As a consequence, only reflections of the type  $hk0$  and  $00l$  are observed in an X-ray or electron diffraction experiment. To underline this fact, only two indices  $hk$  are normally used to describe the graphene reflections, while the reflections along the stacking direction are denoted  $00l$ . As a consequence of the imperfect graphene structure, the average spacing  $d_{002}$  between two layers is always larger than in perfect graphite ( $d_{002} = 0.3355$  nm) (see Table 10.1). The layer spacing becomes smaller with increasing carbonisation temperature, indicating that the disorder decreases with HTT. A transformation into graphite – i.e. the observation of general  $hkl$  reflections with all three indices different from zero – has, however, been observed only for some pitch based fibres at very high HTT. The  $hk$  lines are related to the in-plane lattice constant of the graphene by  $a^2/d_{hk}^2 = 4(h^2 + k^2 + hk)/3$ . The in-plane lattice constant  $a$  in carbon fibres is usually smaller than that of perfect graphene ( $a = 0.2466$  nm), which is due to the non-perfect planar structure and high defect density.  $a$  typically increases with increasing HTT, implying that also the in-plane structure develops towards higher order with HTT (Table 10.1). Generally, the layer spacing  $d$  corresponding to the  $hk$  and the  $00l$  reflections can be obtained from a measured X-ray or electron diffraction pattern by  $d = 2\pi/q$ , with the length of the scattering vector  $q = 4\pi \sin \theta/\lambda$ ,  $\lambda$  being the wavelength of the radiation and  $2\theta$  the scattering angle. The values of  $d_{002}$  and  $d_{10}$  are indicative for the degree of order of the turbostratic structure. They are different for different precursors at a given HTT and typically develop monotonically with HTT. In general, mesophase pitch-based fibres exhibit the highest degree of crystalline order at a given temperature.

The turbostratic structure leads to some peculiar features in the 2D diffraction patterns from carbon fibres, summarised graphically in the sketch in Fig. 10.3. A single graphene layer produces layer lines perpendicular to the layer plane in reciprocal space (Fig. 10.3a). The 'length' of the layer lines is essentially given by the atomic form factor of the carbon atom, and their 'width' is determined by the lateral size of the sheet. Stacking of many layers in a turbostratic manner produces  $hk$  'cylinders' in reciprocal space due to the rotational disorder of the graphene layers within the stack.





10.3 Turbostratic structure of carbon fibres. (a) Single graphene sheets produce layer lines in reciprocal space (only 10 layer lines are drawn for clarity). (b) A turbostratic stack produces  $hk$  cylinders in reciprocal space due to the rotational disorder of the graphene layers within the stack. Additionally, the stacking gives rise to  $00l$  reflections parallel to the direction of a stack. (c) Synchrotron radiation based diffraction pattern from a single MPP-based carbon fibre (FT500, see Table 10.1) with high preferred orientation and random cross-sectional texture. The diffraction pattern can be essentially understood by a rotation of the  $hk$  cylinders around the axis  $m^*$  in (b), and the layer line character of the 10 reflections is clearly seen. The magnification shows the anisotropic SAXS pattern arising from slit-shaped pores.

These so called  $hk$  random-layer lines (Ruland 1967a; Perret and Ruland 1968a) are accompanied by  $00l$  reflections parallel to the direction of a stack which are due to the more or less periodic arrangement of the layers. In a macroscopic carbon fibre, the graphene layers are preferentially parallel to the fibre axis, but their normal vectors are usually randomly oriented in the plane perpendicular to the fibre axis. In reciprocal space, this corresponds to a rotation of the  $hk$  cylinders around the axis denoted by  $m^*$  in Fig. 10.3b, leading to the well-known fibre diffraction pattern of carbon fibres. It is worth noticing explicitly that this pattern has two perpendicular axes of cylindrical symmetry, which is a special feature of the diffraction from carbon fibres. If the orientation is imperfect, this leads to an azimuthal broadening of the  $00l$  reflections into arcs, and the  $hk$  reflections exhibit a characteristic asymmetric shape with a steep flank at the low  $q$  side, and a broad flank at the high  $q$  side. All these features are clearly recognised in the X-ray diffraction pattern from a MPP-based fibre shown in Fig. 10.3c.

An important and still current question in carbon fibre research concerns the role of defects at the atomic level for the bonding strength between graphene sheets. The presence of covalent crosslinks between adjacent layers has been debated for a long time, and such energetically favourable crosslinks have only fairly recently been proposed by *ab-initio* calculations of graphite (Telling *et al.* 2003). They are based on special defect configurations, such as divacancies (i.e. a vacancy in each of the adjacent layers) leading to stable covalent bonds between the two layers. Experimentally, the existence of such bonds has been demonstrated, for instance, by the intertube bridging of carbon nanotubes using electron irradiation to create the respective defects (Kis *et al.* 2004). Since carbon fibres, and in particular those based on long-chain polymeric precursors such as cellulose or PAN, exhibit a large number of in-plane defects, the presence of a large amount of such covalent crosslinks is very probable. A direct proof would require demonstrating the  $sp^3$  character of the bonds using, e.g., UV Raman scattering or electron energy loss spectroscopy (EELS). This has, to our knowledge, not been reported yet for carbon fibres, but would be highly desirable to better understand and to potentially tailor the shear and compression properties of carbon fibres (see Section 10.5).

#### 10.4.3 Mesoscale structure: crystallite size and axial preferred orientation

The basic structural units or crystallites in carbon fibres are defined by two characteristic length scales, the stacking height  $L_c$  and the in-plane size  $L_a$  (Fig. 10.2b). These parameters are in the majority of cases derived from the width of the  $00l$  and  $hk$  reflections by applying the Scherrer equation to measured X-ray diffraction profiles. Explicitly, they are calculated by

$L = 2\pi K/w$ , where  $w$  is the radial peak width (full width at half maximum) and  $K$  is a constant which is usually taken to be  $K = 0.89\text{--}0.91$  for  $L_c$  and  $K = 1.84$  for  $L_a$ . If more than one reflection order can be measured in an experiment, a separation of size and microstrain is possible and is expressed in first approximation by  $w = 2\pi K/L + K_2 \varepsilon^2 q^2$ , where  $K_2$  is a constant,  $q$  is the modulus of the scattering vector and  $\varepsilon$  is related to the microstrain  $\Delta d/d$  (Ergun 1970). More advanced techniques based on detailed structural models have also been proposed (Perret and Ruland 1968a; Shioya and Takaku 1988; Ruland and Smarsly 2002), allowing one to derive more quantitative parameters describing additionally the in-plane and stacking disorder. Values for  $L_c$  have often also been obtained from lattice fringe transmission electron microscopy (TEM) images (Bennett *et al.* 1976; Guigon *et al.* 1984), which usually agree reasonably well with values obtained from X-ray diffraction. The layer-plane length obtained from TEM is, however, typically considerably larger than  $L_a$  determined by X-ray diffraction, since the latter presents a coherence length that is related to the straight portions of the planes (Johnson 1980). The in-plane size  $L_a$  in carbon fibres can also be estimated from Raman scattering according to an empirical relationship between  $L_a$  and the intensity ratio of the Raman D- and G-bands, first reported by Tuinstra and Koenig (1970). Even though this relationship breaks down for very low values of  $L_a$  (Zickler *et al.* 2006), it may give a good working estimate if X-ray diffraction data are not available.

It is clear that different techniques and also the consideration or omission of experimental resolution effects may lead to some differences in  $L_a$  and  $L_c$  when absolute values are compared (Zickler *et al.* 2006). Nonetheless, these two parameters appear to be the most significant measures for structural coherence lengths defining apparent in-plane and stacking sizes of carbon fibres, respectively. Similar to the lattice constants determined by  $d_{002}$  and  $d_{10}$ , there is a distinct dependence of  $L_c$  and  $L_a$  on the final high temperature treatment, with the general tendency to increase with increasing HTT (Table 10.1). The geometrical interpretations of  $L_c$  and  $L_a$  are, however, different for different carbon fibre types. For MPP-based fibres, the basic structural units may, with some caution, be compared with grains in metals or ceramics, exhibiting quite well-defined turbostratic nanocrystallites separated by grain boundaries and/or pores. This is due to the fact that the mesophase discs define already a kind of crystallites that are converted into carbon and grow in size upon HTT. In contrast, cellulose based and PAN-based fibres are characterised by a ribbon structure of undulating graphene sheets, which upon parallel stacking form a kind of microfibrils (Fig. 10.2b) (Perret and Ruland 1970).  $L_a$  and  $L_c$  are in this case rather related to the amplitude and wavelength of the undulations, and the term crystallites may not be adequate or may even be misleading.

The detailed structure at the nanometre scale and the way the BSUs

are connected to build fibrils (cellulose and PAN) or strongly textured crystalline domains (MPP) separated by slit-like or needle-like pores have been investigated intensively over the years. Besides TEM (Johnson 1980; Guigon *et al.* 1984), small-angle X-ray scattering (SAXS) has particularly been used to characterise the porosity in carbon fibres, following the pioneering work of Perret and Ruland (1968b, 1969). The most important structural parameter that can be obtained from SAXS is the mean chord length  $l_p = 4\phi(1 - \phi)/\sigma$ , where  $\phi$  is the pore volume fraction and  $\sigma$  is the total pore surface per unit volume.  $l_p$  is related to the chord length of the pores  $L_p$  by  $L_p = l_p(1 - \phi)$ , which gives a measure for the smallest pore dimension (i.e. the average thickness of slit-like or needle-like pores). It is important to note that besides nanometre-sized pores between the BSU, also density fluctuations resulting from the variation of the stacking distance  $d_{002}$  lead to a small-angle scattering signal (Ruland 1971). The additional diffuse scattering term leads to a deviation from the  $q^{-4}$  dependence of the intensity at large  $q$ . As a consequence, this violation of Porod's law, which is characteristic of the scattering from two-phase systems with sharp interfaces (Glatter and Kratky 1983), has generated speculations about an apparent fractal character of the porosity in carbon fibres (see, e.g., Tang *et al.* 1986). It is nowadays, however, mostly agreed that fractal structures play no role in carbon fibres (Ruland 2001).

The ratio of wavelength to amplitude of the undulations in cellulose-based and PAN-based fibres defines the maximum deviation of the layer planes from the macroscopic fibre axis. Similarly, there is always an orientation distribution of crystallites in MPP-based fibres which deviates from the perfect orientation of graphene layers parallel to the fibre axis. Generally, the degree of preferred orientation of the BSU can be obtained experimentally from the azimuthal spread of the equatorial  $00l$  reflections measured by X-ray diffraction (see Fig. 10.3c). The simplest parameter often used in the literature is the full width (*FWHM*) or half width (*HWHM*) at half maximum of the 002 or 004 azimuthal profiles (Tang *et al.* 1986; Hamada *et al.* 1992; Paris *et al.* 2002; Loidl *et al.* 2003, 2005b). Other authors have used normalised orientation parameters such as  $f = 1 - FWHM/\pi$ , which varies between zero (no preferred orientation) and 1 (perfect alignment of the BSU parallel to the fibre axis) (Takaku and Shioya 1990). Several other authors used an analytical function – the so-called Poisson kernel  $g(\chi) = (1 - s^2)/(1 + s^2 - 2s \cos 2\chi)$  introduced by Ruland (1967b) – to describe the  $00l$  azimuthal intensity profiles. The parameter  $s$  varies between  $s = 1$  (perfect orientation parallel to the fibre axis) and  $s = -1$  (perfect orientation perpendicular to the fibre axis), with  $s = 0$  for fully random orientation. It should be noted that a parameter reflecting the degree of preferred orientation can also be derived from the SAXS signal arising from the slit-like or needle-like pores terminating the BSU. The orientation distribution of the BSU with respect to

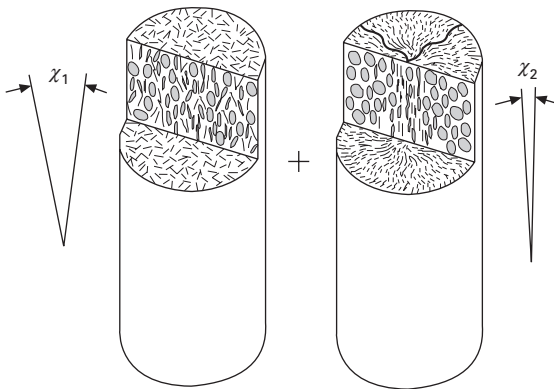
the fibre axis for slit-like pores is directly derived from the azimuthal SAXS profile (see e.g. Fig. 10.3c), and the same parameters as discussed above for the width of the  $00l$  reflections can thus be obtained without difficulty. For needle-like pores, an integral transformation equation has been given by Perret and Ruland (1969) for the derivation of the preferred orientation distribution in real space. Table 10.1 shows the azimuthal width ( $HWHM$ ) of the 002 reflection for some PAN- and MPP-based fibres, demonstrating in particular the strong correlation between the axial preferred orientation and the tensile modulus of the fibres. The degree of orientation is typically controlled by the HTT and by the preferred orientation of the precursor. MPP-based fibres can develop extremely high orientation degrees, which is the main reason for their high tensile stiffness.

#### 10.4.4 Micrometre structure: cross-sectional texture and skin-core structure

Cross-sectional texture in carbon fibres refers to the orientation distribution of the BSU within the fibre cross-section, which is highly oriented along the fibre axis. Cellulose-based and PAN-based fibres exhibit usually a random cross-sectional texture, except perhaps a skin layer with an onion-skin type of layer orientation (Bennett and Johnson 1979). Very pronounced cross-sectional textures with the typical onion skin structure (see Fig. 10.2c) are always found in vapour grown carbon fibres, similar to multiwall carbon nanotubes (Dresselhaus and Endo 2001). MPP-based fibres exhibit a rich variety of cross-sectional textures such as radial (see Fig. 10.2c), radial folded or flat-layer (Edie 1998), as a consequence of the details of the melt spinning process of the (disc-shaped) mesophase. Cross-sectional textures are important factors that can influence the fibre graphitizability (Bright and Singer 1979), and are particularly also believed to affect the fibre strength. It has been reported that fibres with random or radial folded cross-sectional textures tend to have higher tensile strength than fibres with radial structure (Endo 1988; Edie 1998). Cross-sectional texture has typically been investigated with scanning electron microscopy (SEM) examining fractured fibre cross-sections (Barnes *et al.* 1998; Hong *et al.* 1999, 2000; Watanabe *et al.* 2000), and in some cases also by TEM (Bennett and Johnson 1979; Endo 1988). Typically, most carbon fibres exhibit cylindrical symmetry with respect to the fibre axis (e.g. those shown in Fig. 10.2c), even though the orientation distribution of the BSU is not random within the fibre cross-section. Hence, cross-sectional textures cannot be assessed by standard X-ray texture analysis. The use of X-ray microbeams in connection with fibre scanning allows, however, the determination of cross-sectional textures quantitatively (Paris *et al.* 2000, 2001). Detailed modelling of the X-ray diffraction as a function of position across the fibre allows one, for instance, to correlate the cross-

sectional texture with the axial preferred orientation, as shown in Fig. 10.4 for example (Paris *et al.* 2002).

A particular structural feature found in many carbon fibres is a pronounced skin-core structure, with different BSU size, different axial preferred orientation and/or different cross-sectional texture. High axial preferred orientation and large crystallite size in a thin skin layer with otherwise random cross-sectional texture have been identified in some PAN-based fibres by TEM (Bennett and Johnson 1979), and have been considered to be the limiting factor for fibre strength. The origins of these skin-core structures are not always clear and may generally depend in a subtle way on the processing conditions. In PAN-based fibres they have been related to the stabilisation process, where a strong temperature dependence was observed (Yu *et al.* 2007; Hou *et al.* 2008). Another origin for the development of a skin-core structure might be the release of nitrogen during HTT, leading to different nitrogen content, and thus to different crystallite size in the skin and in the core of the fibre (Loidl *et al.* 2007). Besides TEM, X-ray microdiffraction with a beam considerably smaller than the fibre diameter can be used to investigate skin-core structures in carbon fibres (Paris *et al.* 2002; Loidl *et al.* 2005a, 2007). Such data can then be used to test the correlation between the local structure and the mechanical performance. The particular advantage of X-ray microbeam methods is the possibility of performing *in-situ* mechanical deformation of single fibres (Loidl *et al.* 2003, 2005a), which will be discussed in more detail in the next section.



**10.4** Model for the cross-sectional texture in MPP-based carbon fibres derived from a mixture of isotropic pitch and mesophase pitch. The fibres exhibit a composite structure of random and radially folded crystallites with different axial preferred orientation denoted in the sketch by the mean tilt angle  $\chi$  (reprinted from Paris *et al.* (2002), with permission from Elsevier).

## 10.5 Mechanical properties of carbon fibres and their structural origin

### 10.5.1 Tensile stiffness

The two most important arguments for using carbon fibres in aerospace applications are their low density ( $\sim 1.5 \text{ g/cm}^3$  for PAN-based fibres and  $\sim 2.1 \text{ g/cm}^3$  for MPP-based fibres) and their high stiffness (Diefendorf and Tokarsky 1975; Fitzer and Manocha 1998). In high-modulus fibres based on MPP, the Young's modulus can range up to 900 GPa (Edie 1998) and thus approaches the value of diamond. A high Young's modulus is a basic requirement for lightweight structures, as the buckling load of struts in these structures increases linearly with the modulus (Euler buckling). The high stiffness of carbon fibres is a consequence of the preferred arrangement of the graphene sheets as described in the previous section. The drawing process is necessary to achieve a high molecular orientation for the PAN precursor fibres. The preferred orientation – and thus the fibre modulus – in PAN-based fibres increase strongly with HTT (see Table 10.1), requiring thus very high temperatures for high-modulus fibres. On the contrary, PAN fibres develop their highest strength at rather low temperatures (Table 10.1), which is the reason why PAN fibres are optimised for either strength (high-tenacity fibres) or stiffness (high-modulus fibres). In contrast to PAN-based fibres, MPP fibres are already highly oriented due to the spinning process of the mesophase through the capillary, which may be further improved by fibre stretching after the spinning process. Here, research has concentrated more on precursor chemistry and fibre formation than on HTT, since mesophase chemistry offers a variety of fruitful ways to develop fibres with extremely high stiffness values (Edie 1998; Gallego and Edie 2001).

A first quantitative model for the modulus–orientation relationship was developed by Fischer and Ruland (1980), and was successfully applied to experimental data relating the stiffness of carbon fibres to the orientation parameter  $s$  obtained from X-ray diffraction (Section 10.4.3). This 'elastic unwrinkling model' was based on two assumptions: the elongation of the straight parts and the reversible increase of the distorted BSU (Fischer and Ruland 1980). A comparison of this early model with two other models was performed by Northolt *et al.* (1991). In the uniform stress model, the fibre was considered as a parallel array of identical fibrils subjected to a uniform stress along the axis. The uniform strain model assumes that every part of a cross-sectional filament is subjected to the same axial strain. Northolt *et al.* (1991) favoured the uniform stress model, as supported by experimental data for PAN- and MPP-based fibres on the one hand, and by structural arguments, like the arrangement of long wrinkled ribbons separated by elongated voids within the fibres, on the other hand. For a quantitative description of the modulus–orientation relationship, the orientation distribution must be known

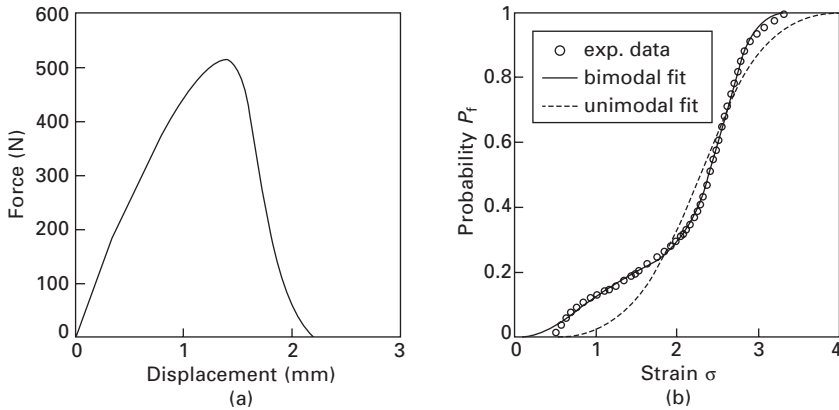


with high accuracy. X-ray diffraction data from fibre bundles suffer from the fact that separating the twist in the fibre bundle from the misorientation of the crystallites within the fibre is not possible. This problem can be overcome by X-ray diffraction on single fibres instead of fibre bundles with X-ray microbeams exhibiting a beam size in the order of 10  $\mu\text{m}$ , utilising the high brilliance of synchrotron radiation (Paris *et al.* 2001, 2002). Synchrotron radiation using X-ray microbeams can also be used for *in-situ* tensile testing of single carbon fibres with accompanying investigations of the structural development during loading. In particular, the shift of the  $hk$  reflections allows obtaining strains at the level of single crystallites, and the change of the azimuthal width of the 002 reflections allows quantifying changes in crystallite orientation upon loading. Using *in-situ* microbeam diffraction, Loidl *et al.* (2003) showed that for MPP based fibres the Young's modulus of the nanosized crystallites exhibited a limiting value of 1140 GPa. The shear modulus estimated from the change in azimuthal width assuming the uniform stress model was 5 GPa for MPP based fibres and 15 GPa for PAN-based fibres, but increased with increasing load (Loidl *et al.* 2003). This increase is reflected in a general non-Hookean behaviour of carbon fibres (Shioya *et al.* 1996; Reder *et al.* 2003), i.e. the Young's modulus increases strongly with increasing load. This non-linearity also limits the determination of precise numerical values for the stiffness of carbon fibres.

### 10.5.2 Tensile strength

Whereas the modulus of carbon fibres is simply dependent on the orientation of crystallites, tensile strength is much more difficult to understand and to control. The most common approach to describe the strength and strength distribution is based on the weakest link theory of brittle materials, where the weakest link – in general the largest flaw within the specimen – controls the strength. For a power law dependence of the frequency of flaws, the strength distribution follows a Weibull distribution, with a scale parameter  $\sigma_0$  for the mean strength and a parameter  $m$  for the width of the distribution, respectively (Weibull 1951). For carbon fibres, this approach has to be seen as a primarily technical approach, because fibre strength is nearly not affected by an increase of the crystallite size by a factor of five (Loidl *et al.* 2007) or an increase of the pore size by a factor of two (Peterlik *et al.* 1994). There seems to be a general agreement that the size of the pores separating extensively folded crystallites (Johnson 1987) or 'crumpled sheets' (Guigon *et al.* 1984) are responsible for the failure of individual carbon fibres, but rather the interlinking and misalignment of crystallites themselves (Reynolds and Sharp 1974; Edie 1998). Therefore, it is very likely that the bimodality in the Weibull strength distribution (see Fig. 10.5) – observed for many types of fibres – is not a consequence of the different effectiveness of





10.5 (a) Force–displacement curve from a fibre bundle test of PAN-based carbon fibres (HTA7, see Table 10.1). (b) Probability distribution of fibre strength (Weibull plot) together with the fits using a unimodal (dashed line) or bimodal defect distribution (reprinted from Loidl *et al.* (2007), with permission from Elsevier).

surface and volume flaws, but rather is induced by a skin–core structure or even by a reversal of the skin–core structure from less to higher orientation as compared to the core (Loidl *et al.* 2007). The disorder induced by the different orientational changes during HTT in PAN-based carbon fibres might lead to a mechanically weaker and a stronger phase, respectively, which are responsible for the bimodality of the Weibull distributions. A HTT in the range of 2400°C leads to a more uniform strength distribution as differences in skin and core are healed due to the enhanced diffusion of carbon atoms.

Interestingly, the tensile strength of carbon fibres increases with increasing test temperature, which is a consequence of the improved alignment and possibly the release of residual shear strains in the fibres (Reynolds and Sharp 1974; Tanabe *et al.* 1991). For the Young’s modulus, either an increase (Tanabe *et al.* 1991) or a decrease (Sauder *et al.* 2004) was reported. An enhancement of the mechanical properties with temperature is a quite unique material property typical for carbonaceous materials. It was demonstrated by Sauder *et al.* (2004) that carbon fibres are not purely elastic for temperatures higher than 1400°C, but show viscoelastic behaviour. For temperatures higher than 1800°C they may even behave in a viscoplastic way. The authors concluded that molecular deformations contribute to a shear strain leading to viscoelasticity. Finally, a critical shear stress leads to local cracking and sliding of the graphene planes, which induces viscoplasticity and subsequent failure.

### 10.5.3 Compression and bending

Compression behaviour of carbon fibres was first investigated by Raman spectroscopy using a cantilever bending beam method (Robinson *et al.* 1987; Melanitis and Galiotis 1990; Melanitis *et al.* 1994), where the Raman frequency shift was correlated to the respective strain in the fibre. The advantage of this method is that the use of a Raman microscope provides a sufficient resolution in the micrometre range, enabling a scanning of the carbon fibre with diameter of 5 to 10 microns. It can thus provide additional information on the local variation of the structure. A number of other compression test methods for carbon fibres were developed and a review may be found in Kozey *et al.* (1995). PAN- and MPP-based fibres reveal significant differences, particularly in compression: while the compressive strength increases significantly with decreasing tensile modulus in PAN fibres, the compressive strength of MPP fibres increases only very moderately to a value about three times smaller than that of PAN fibres (Kozey *et al.* 1995). Also, the occurrence of kink bands with a typical shear angle of  $45^\circ$  was observed in compression failure of MPP fibres. On the contrary, PAN fibres show buckling and kink bands at the innermost surface (Dobb *et al.* 1990). To improve both the compression and tension properties of MPP fibres, the importance of an extensive folding of the graphene planes was pointed out by Endo (1988). This is the reason why radial folded cross-sectional textures in MPP-based fibres (see e.g. Fig. 10.4) are usually beneficial for higher fibre strength.

Bending of carbon fibres occurs generally in carbon fibre reinforced composites due to the crimp angle in different weave patterns (usually either a plane weave or a satin weave). Delamination (Garg 1988; Peterlik *et al.* 1992) as well as tensile and compressive properties (Pollock 1990) of composites have been found to strongly depend on the crimp angle, but this is most probably governed by the interface properties of the composite and not by the fibres themselves. Bending tests of fibres can be realised by the bending beam test, where fibres are bonded by an adhesive on to a beam (which is certainly thick in comparison to the fibre), or by the loop test, where a loop is formed and the radius increasingly diminished up to failure (Kozey *et al.* 1995). Bending via a loop test was used fairly recently to characterise mechanical differences in the tension and compression region by scanning across the fibres with a 100 nm wide X-ray microbeam (Loidl *et al.* 2005a). This allowed calculating the different Young's moduli in tension and compression within the same fibre from the shift of the neutral axis. Whereas the difference in moduli was small in PAN-based fibres, it was found to be huge in MPP-based fibres and local buckling of crystallites at the nanoscale was observed (Loidl *et al.* 2005a). This led to the conclusion that extensive crosslinking of graphene sheets effectively strengthens PAN-based fibres in compression, whereas in MPP-based fibres the crystallites are only weakly

crosslinked. The direct confirmation of the existence of crosslinks and their precise localisation still remains, however, an open question.

## 10.6 Open questions and future directions

From a viewpoint of basic research, the structure of carbon fibres is nowadays quite well understood, and extremely refined production routes have touched the limits in terms of achievable fibre strength and stiffness for structural applications in composites. Open questions from a scientific point of view are particularly related to a deeper understanding and better control of defect-mediated crosslinks between graphene sheets, in order to tune specific properties such as shear and compression properties, as well as thermal and electrical conductivity. Likely future research directions are most probably driven by the need to combine different fibre properties for new functional applications.

There are strong signs for a considerable increase of carbon fibre applications in several industrial fields. In the aerospace industry, for instance, the 'A380' from Airbus or the 'Dreamliner' from Boeing are specifically designed with a large amount of lightweight carbon fibre reinforced composites for the reduction of both weight and energy consumption. Many non-aerospace applications urgently need materials with extremely high modulus – e.g. extremely stiff arms to further increase the velocity and precision of robotic systems. Moreover, the need for materials with excellent optical and haptic properties in automotive industries opens entirely new fields for applications of carbon fibres, and only backing compounds for cars would exceed the today's world production of carbon fibres. Many functional parts involving carbon fibres are currently in development, valve control being one example of many. Finally, safety aspects in automotive industries together with the ecologically necessary future reduction of CO<sub>2</sub> emissions require lightweight components with high fracture toughness. It is therefore not surprising that a significant increase in the world's consumption of carbon fibres is predicted, which demands further improvement of fibre properties and in particular the reduction of production costs.

## 10.7 Sources of further information and advice

Research on carbon fibres has continued now for almost 50 years, and accordingly the number of original papers is huge. Only a very small selection mostly related to carbon fibre structure has been taken into account in the reference list of this chapter. As a starting point for further reading, a comprehensive – although certainly not complete – overview of the field may be obtained by consulting some of the dedicated textbooks on carbon fibres and their composites (Chung 1998; Donnet 1998; Fitzer and Manocha

1998; Burchell 1999; Kelly 2004; Morgan 2005). Moreover, a selection of excellent overview and/or review articles can be recommended for more detailed information on several different aspects of carbon fibre structure and related properties (Diefendorf and Tokarsky 1975; Fitzer 1986; Ruland 1990; Peebles 1994; Edie 1998; Chand 2000; Loidl *et al.* 2005b).

## 10.8 Acknowledgements

The authors would like to thank Dieter Loidl (University of Natural Resources and Applied Life Sciences, Vienna, Austria) and Roland Weiß (Schunk Kohlenstofftechnik, Germany) for many years of constructive collaboration in the field of carbon fibre structure and mechanical properties. Martin Müller (University of Kiel, Germany), as well as Manfred Burghammer and Christian Riekel (ESRF Grenoble, France) are acknowledged for their valuable contributions to microbeam X-ray diffraction experiments on carbon fibres.

## 10.9 References

- Bacon, R. (1960), Growth, structure, and properties of graphite whiskers, *J. Appl. Phys.*, 31(2), 283–290.
- Bacon, R. and Tang, M. M. (1964), Carbonization of cellulose fibers 2. Physical property study, *Carbon*, 2(3), 221–225.
- Barnes, A. B., Dauche, F. M., Gallego, N. C., Fain C. C. and Thies M. C. (1998), As-spun orientation as an indication of graphitized properties of mesophase-based carbon fiber, *Carbon*, 36(7–8), 855–860.
- Bengisu, M. and Yilmaz, E. (2002), Oxidation and pyrolysis of chitosan as a route for carbon fiber derivation, *Carbohydrate Polymers*, 50(2), 165–175.
- Bennett, S. and Johnson, D. (1978), *5th London International Carbon and Graphite Conference*, London, Society of the Chemical Industry.
- Bennett, S. C. and Johnson, D. J. (1979), Electron-microscope studies of structural heterogeneity in PAN-based carbon-fibers, *Carbon*, 17(1), 25–39.
- Bennett, S. C., Johnson, D. J. and Murray, R. (1976), Structural characterization of a high-modulus carbon-fiber by high-resolution electron-microscopy and electron-diffraction, *Carbon*, 14(2), 117–122.
- Bright, A. A. and Singer, L. S. (1977), Electronic and structural characteristics of carbon-fibers from mesophase pitch, *Carbon*, 15(6), 427–427.
- Bright, A. A. and Singer, L. S. (1979), Electronic and structural characteristics of carbon-fibers from mesophase pitch, *Carbon*, 17(1), 59–69.
- Brooks, J. D. and G. H. Taylor (1965), Formation of graphitizing carbons from liquid phase, *Nature*, 206(4985), 697–699.
- Burchell, T. (1999), *Carbon Materials for Advanced Technologies*, Amsterdam, Pergamon.
- Byrne, C. E. and Nagle, D. C. (1997), Carbonized wood monoliths – characterization, *Carbon*, 35(2), 267–273.
- Cahn, R. W. and Harris, B. (1969), Newer forms of carbon and their uses, *Nature*, 221(5176), 132–141.

- Chand, S. (2000), Review: Carbon fibers for composites, *J. Mater. Sci.*, 35, 1303–1313.
- Chung, D. (1998), *Carbon Fiber Composites*, Oxford, Butterworth Heinemann.
- Diefendorf, R. J. and Tokarsky, E. (1975), High-performance carbon-fibers, *Polymer Eng. Sci.*, 15(3), 150–159.
- Dobb, M. G., Johnson D. J. and Park C. R. (1990), Compressional behavior of carbon-fibers, *J. Mater. Sci.*, 25(2A), 829–834.
- Donnet, J. B. (1998), *Carbon Fibers*, New York, Marcel Dekker.
- Dresselhaus, M. and Endo, M. (2001), Relation of carbon nanotubes to other carbon materials, in M. Dresselhaus, G. Dresselhaus and P. Avouris, *Carbon Nanotubes* Springer, Berlin: 11–26.
- Edie, D. D. (1998), The effect of processing on the structure and properties of carbon fibers, *Carbon*, 36(4), 345–362.
- Edie, D. and McHugh, J. (1999), High performance carbon fibers, in T. Burchell, *Carbon Materials for Advanced Technologies*, Amsterdam, Pergamon: 119–138.
- Endo, M. (1988), Structure of mesophase pitch-based carbon-fibers, *J. Mater. Sci.*, 23(2), 598–605.
- Ergun, S. (1970), X-ray scattering by very defective lattices, *Phys. Rev. B*, 1(8), 3371–3380.
- Fischer, L. and Ruland, W. (1980), The influence of graphitization on the mechanical-properties of carbon-fibers, *Coll. Polym. Sci.*, 258(8), 917–922.
- Fitzer, E. (1986), Carbon fibers – the miracle material for temperatures between 5 and 3000 K, *High Temperatures – High Pressures*, 18(5), 479–508.
- Fitzer, E. and Manocha, L. M. (1998), *Carbon Reinforcements and Carbon/Carbon Composites*, Berlin, Springer.
- Fitzer, E., Frohs, W. and Heine, M. (1986), Optimization of stabilization and carbonization treatment of pan fibers and structural characterization of the resulting carbon-fibers, *Carbon*, 24(4), 387–395.
- Gallego, N. C. and Edie, D. D. (2001), Structure–property relationships for high thermal conductivity carbon fibers, *Composites A – Appl. Sci. Manufact.*, 32(8), 1031–1038.
- Garg, A. C. (1988), Delamination – a damage mode in composite structures, *Eng. Fract. Mech.*, 29(5), 557–584.
- Glatter, O. and Kratky, O. (1983), *Small-Angle X-ray Scattering*, New York, Academic Press.
- Guigon, M., Oberlin, A. and Desarmot, G. (1984), Microtexture and structure of some high-tensile strength, PAN-based carbon-fibers, *Fibre Sci. Techn.*, 20(1), 55–72.
- Hamada, T., Furuyama, M., Tomioka, T. and Endo, M. (1992), Preferred orientation of high-performance carbon-fibers, *J. Mater. Res.*, 7(9), 2612–2620.
- Hong, S., Korai, Y. and Mochida, I. (1999), Development of mesoscopic textures in transverse cross-section of mesophase pitch-based carbon fibers, *Carbon*, 37, 917–930.
- Hong, S., Korai, Y. and Mochida, I. (2000), Mesoscopic texture at the skin area of mesophase pitch-based carbon fiber, *Carbon*, 38, 805–815.
- Hou, Y. P., Sun, T. Q., Wang, H. J. and Wu, D. (2008), Effect of heating rate on the chemical reaction during stabilization of polyacrylonitrile fibers, *Text. Res. J.*, 78, 806–811.
- Jain, M. K. and Abhiraman, A. S. (1987), Conversion of acrylonitrile-based precursor fibers to carbon-fibers. I. A review of the physical and morphological aspects, *J. Mater. Sci.*, 22(1), 278–300.
- Jain, M. K., Balasubramanian, M., Desai, P. and Abhiraman, A. S. (1987), Conversion

- of acrylonitrile-based precursors to carbon-fibers. 2. precursor morphology and thermooxidative stabilization, *J. Mater. Sci.*, 22(1), 301–312.
- Jeffries, R. (1971), Prospects for carbon fibres, *Nature*, 232(5309), 304–307.
- Johnson, D. J. (1980), Recent advances in studies of carbon-fiber structure, *Phil. Trans. Roy. Soc. Lond. A – Math. Phys. Eng. Sci.*, 294(1411), 443.
- Johnson, D. J. (1987), Structure property relationships in carbon-fibers, *J. Phys. D – Appl. Phys.*, 20(3), 286–291.
- Johnson, D. J., Tomizuka, I. and Watanabe, O. (1975), Fine-structure of lignin-based carbon-fibers, *Carbon*, 13(4), 321–325.
- Kelly, V. (2004), *Carbon Fiber: Manufacture and Applications*, Oxford, Elsevier.
- Kis, A., Csanyi, G., Salvétat, J. P., Lee, T. N., Couteau, E., Kulik, A. J., Benoit, W., Brugger, J. and Forro, L. (2004), Reinforcement of single-walled carbon nanotube bundles by intertube bridging, *Nature Materials*, 3(3), 153–157.
- Kozey, V. V., Jiang, H., Mehta, V. R. and Kumar, S. (1995), Compressive behavior of materials. 2. High-performance fibers, *J. Mater. Res.*, 10(4), 1044–1061.
- Loidl, D., Peterlik, H., Müller, M., Riekkel, C. and Paris, O. (2003), Elastic moduli of nanocrystallites in carbon fibers measured by in-situ X-ray microbeam diffraction, *Carbon*, 41(3), 563–570.
- Loidl, D., Paris, O., Burghammer, M., Riekkel, C. and Peterlik, H. (2005a), Direct observation of nanocrystallite buckling in carbon fibers under bending load, *Phys. Rev. Lett.*, 95(22), 225501.
- Loidl, D., Peterlik, H., Paris, O., Müller, M., Burghammer, M. and Riekkel, C. (2005b), Structure and mechanical properties of carbon fibers: a review of recent microbeam diffraction studies with synchrotron radiation, *J. Synchrotron Radiation*, 12, 758–764.
- Loidl, D., Paris, O., Renzhofer, M., Müller, M. and Peterlik, H. (2007), Skin–core structure and bimodal Weibull distribution of the strength of carbon fibres, *Carbon*, 45, 2801–2805.
- Melanitis, N. and Galiotis, C. (1990), Compressional behavior of carbon-fibers. 1. A Raman-spectroscopic study, *J. Mater. Sci.*, 25(12), 5081–5090.
- Melanitis, N., Tetlow, P. L., Galiotis, C. and Smith, S. B. (1994), Compressional behavior of carbon-fibers. 2. Modulus softening, *J. Mater. Sci.*, 29(3), 786–799.
- Moreton, R., Watt, W. and Johnson, W. (1967), Carbon fibres of high strength and high breaking strain, *Nature*, 213(5077), 690–691.
- Morgan, P. E. (2005), *Carbon Fibers and their Composites*, Boca Raton, FL, Taylor & Francis.
- Northolt, M. G., Veldhuizen, L. H. and Jansen, H. (1991), Tensile deformation of carbon-fibers and the relationship with the modulus for shear between the basal planes, *Carbon*, 29(8), 1267–1279.
- Oberlin, A. (1984), Carbonization and graphitization, *Carbon*, 22(6), 521–541.
- Oberlin, A., Endo, M. and Koyama, T. (1976), Filamentous growth of carbon through benzene decomposition, *J. Cryst. Growth*, 32(3), 335–349.
- Otani, S. (1981), Carbonaceous mesophase and carbon-fibers, *Molecular Crystals and Liquid Crystals*, 63(1–4), 249–263.
- Otani, S., Yamada, K., Koitabas, T. and Yokoyama, A. (1965), On raw materials of Mp carbon fiber, *Carbon* 4(3), 425.
- Paris, O., Loidl, D., Peterlik, H., Müller, M., Lichtenegger, H. and Fratzl, P. (2000), The internal structure of single carbon fibers determined by simultaneous small- and wide-angle X-ray scattering, *J. Appl. Cryst.*, 33(1), 695–699.

- Paris, O., Loidl, D., Mueller, M., Lichtenegger, H. and Peterlik, H. (2001), Cross-sectional texture of carbon fibres analysed by scanning microbeam x-ray diffraction, *J. Appl. Cryst.*, 34, 473–479.
- Paris, O., Loidl, D. and Peterlik, H. (2002), Texture of PAN- and pitch-based carbon fibers, *Carbon*, 40(4), 551–555.
- Paris, O., Zollfrank, C. and Zickler, G. A. (2005), Decomposition and carbonisation of wood biopolymers – a microstructural study of softwood pyrolysis, *Carbon*, 43(1), 53–66.
- Peebles, L. H. (1994), Carbon-fibers – structure and mechanical properties, *Int. Mater. Reviews*, 39(2), 75–92.
- Perret, R. and Ruland, W. (1968a), Profile analysis of random-layer lines, *J. Appl. Cryst.*, 1, 257–262.
- Perret, R. and Ruland, W. (1968b), X-ray small-angle scattering of non-graphitizable carbons, *J. Appl. Cryst.*, 1, 308–313.
- Perret, R. and Ruland, W. (1969), Single and multiple X-ray small-angle scattering of carbon fibres, *J. Appl. Cryst.*, 2, 209–218.
- Perret, R. and Ruland, W. (1970), Microstructure of PAN-base carbon fibres, *J. Appl. Cryst.*, 3, 525–532.
- Peterlik, H., Domnanovich, A., Kromp, W. and Kromp, K. (1992), Transverse expansion of 2-D carbon–carbon laminates as a consequence of delamination, *Comp. Sci. Techn.*, 45(1), 65–72.
- Peterlik, H., Fratzl, P. and Kromp, K. (1994), Pore structure of carbon–carbon composites studied by small-angle X-ray scattering, *Carbon*, 32(5), 939–945.
- Pollock, P. B. (1990), Tensile failure in 2-D carbon–carbon composites, *Carbon*, 28(5), 717–732.
- Reder, C., Loidl, D., Puchegger, S., Gitschthaler, D., Peterlik, H., Kromp, K., Khatibi, G., Betzwar-Kotas, A., Zimprich, P. and Weiss, B. (2003), Non-contacting strain measurements of ceramic and carbon single fibres by using the laser-speckle method, *Composites A – Appl. Sci. Manufact.*, 34(11), 1029–1033.
- Reynolds, W. N. and Sharp, J. V. (1974), Crystal shear limit to carbon-fiber strength, *Carbon*, 12(2), 103–110.
- Robinson, I. M., Zakikhani, M., Day, R. J., Young, R. J. and Galiotis, C. (1987), Strain dependence of the Raman frequencies for different types of carbon-fibers, *J. Mater. Sci. Lett.*, 6(10), 1212–1214.
- Ruland, W. (1967a), Fourier transform methods for random-layer line profiles, *Acta Cryst.*, 22, 615–623.
- Ruland, W. (1967b), X-ray studies on preferred orientation in carbon fibers, *J. Appl. Phys.*, 38(9), 3585–3589.
- Ruland, W. (1971), Small-angle scattering of 2-phase systems – determination and significance of systematic deviations from Porod's law, *J. Appl. Cryst.*, 4, 70–73.
- Ruland, W. (1990), Carbon-fibers, *Adv. Mater.*, 2(11), 528–536.
- Ruland, W. (2001), Apparent fractal dimensions obtained from small-angle scattering of carbon materials, *Carbon*, 39(2), 323–324.
- Ruland, W. and Smarsly, B. (2002), X-ray scattering of non-graphitic carbon: an improved method of evaluation, *J. Appl. Cryst.*, 35, 624–633.
- Sauder, C., Lamon, J. and Pailler, R. (2004), The tensile behavior of carbon fibers at high temperatures up to 2400 degrees C, *Carbon*, 42(4), 715–725.
- Schaper, A. and Fink, H. P. (1990), High-resolution electron-microscope observations of carbon-fiber structures, *Acta Polymerica*, 41(10), 515–518.



- Shindo, A. (1961), Studies on Graphite Fibre, Rep. 317 (Govt. Indust. Res. Inst., Osaka).
- Shioya, M. and Takaku, A. (1988), Wide-angle X-ray diffraction of materials comprising layer-type molecules, *Acta Cryst.*, 44, 150–157.
- Shioya, M., Hayakawa, E. and Takaku, A. (1996), Non-hookean stress–strain response and changes in crystallite orientation of carbon fibres, *J. Mater. Sci.*, 31(17), 4521–4532.
- Standage, A. E. and Prescott, R. (1966), High elastic modulus carbon fibre, *Nature*, 211(5045), 169.
- Takaku, A. and Shioya, M. (1990), X-ray measurements and the structure of polyacrylonitrile- and pitch-based carbon-fibers, *J. Mater. Sci.*, 25(11), 4873–4879.
- Tanabe, Y., Yasuda, E. Bunsell, A. R. Favry, Y. Inagaki M. and Sakai M. (1991), The strength of pitch-based carbon-fiber at high temperature, *J. Mater. Sci.*, 26(6), 1601–1604.
- Tang, M. Y., Rice, G. G., Fellers, J. F. and Lin, J. S. (1986), X-ray scattering studies of graphite fibers, *J. Appl. Phys.*, 60(2), 803–810.
- Telling, R. H., Ewels, C. P., El-Barbary A. A. and Heggie M. I. (2003), Wigner defects bridge the graphite gap, *Nature Materials*, 2, 333–337.
- Tuinstra, F. and Koenig, J. L. (1970), Raman spectrum of graphite, *J. Chem. Phys.*, 53(3), 1126–1130.
- Walenta, E. and Fink, H. P. (1990), Investigation of the thermal oxidative stabilization of PAN filaments in carbon-fiber processing, *Acta Polymerica*, 41(12), 598–600.
- Walker, E. J. (1993), The importance of fibre type and fibre surface in controlling composite properties, in C. R. Thomas, *Essentials of Carbon–Carbon Composites*, Cambridge, The Royal Society of Chemistry: 37–66.
- Warren, B. E. (1941), X-ray diffraction from random layer lattices, *Phys. Rev.*, 59(9), 693–698.
- Watanabe, F., Korai, Y., Mochida, I. and Nishimura, Y. (2000), Structure of melt-blown mesophase pitch-based carbon fibers, *Carbon*, 38, 741–747.
- Weibull, W. (1951), A statistical distribution function of wide applicability, *J. Appl. Mech. – Trans. ASME*, 18(3), 293–297.
- Yu, M. J., Wang, C. G., Bai, Y. J., Ji, M. X. and Xu Y. (2007), EM and OM study on the microstructure of oxidative stabilized polyacrylonitrile fibers, *Polymer Bulletin*, 58, 933–940.
- Zickler, G. A., Smarsly, B., Gierlinger, N., Peterlik, H. and Paris, O. (2006), A reconsideration of the relationship between the crystallite size  $L_a$  of carbons determined by X-ray diffraction and Raman spectroscopy, *Carbon*, 44(15), 3239–3246.



## Processing, structure and properties of ceramic fibers

---

G MOTZ, University of Bayreuth, Germany and  
R K BORDIA, University of Washington, USA

**Abstract:** This chapter discusses two broad classes of high performance continuous ceramic fibers (non-oxide and oxide). The processing, structure and properties of these fibers are reviewed. For non-oxide fibers, the emphasis is polymer derived ceramic fibers and both commercially available and developmental fibers are discussed. In the case of oxide fibers, the focus is on commercially available fibers. A summary of the current and anticipated applications together with research and development priorities in this evolving field is presented.

**Key words:** oxide fibers, non-oxide fibers, polymer derived ceramics, ceramic matrix composites, metal matrix composites.

### 11.1 Introduction

Ceramic fibers have a very large aspect ratio and a very small cross-sectional area. Commercially available ceramic fibers, for example, have a fiber diameter of approximately 10  $\mu\text{m}$ . Due to their geometry, the properties of the fibers differ significantly from those of bulk forms of the same material. In particular, fibers have much higher strength, higher strain to failure but also greater chemical vulnerability. Fibers can be manufactured as fiber fabrics, flows, and short or long fibers. Fine fibers are generally bundled into so-called 'rowings', which consist of 500–10 000 single filaments. Bundling keeps the fibers flexible, makes them considerably easier to process and handle, and makes it possible for them to be manufactured into various fibrous forms.

This chapter is focused on continuous, fine diameter fibers. Although the term 'ceramic fibers' refers to all inorganic, non-metallic fibers, this chapter will not include fibers made by the solidification of silicate glass melts or carbon or boron fibers. In addition, fibers made from minerals like basalt will also be excluded. Finally, although fibers have been made from functional ceramics (e.g. piezoelectric and superconducting oxides), the focus of this chapter is on ceramic fibers for structural applications.

In the past half-century, there has been significant development in the processing and use of high performance ceramic fibers. Several compositions of fine diameter fibers (less than 20  $\mu\text{m}$ ) are commercially available and others are being developed. Due to the fine diameter, these fibers have very

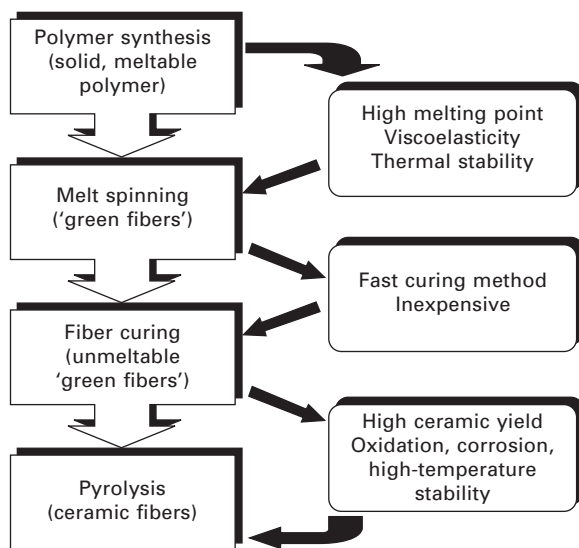
high strength (in the range of 1.5 to 3 GPa) and they can be woven. They maintain the attractive properties of ceramics including high temperature usability, high corrosion resistance and high modulus. A good recent review of high performance ceramic fibers is presented in Ref. 1. The ceramic fibers can be broadly classified as non-oxide and oxide fibers. In Section 11.2, the processing, structure and properties of the non-oxide fibers are summarized. Section 11.3 focuses on oxide fibers. In Section 11.4, composition, structure and properties of selected fibers are compared. Section 11.5 presents examples of current and anticipated applications of these high performance fibers. Section 11.6 outlines the need for further developments. The chapter is summarized in Section 11.7 and sources for additional information are presented in Section 11.8.

## 11.2 Processing, structure and properties of non-oxide fibers

The following sub-sections give an overview of polymer-derived, non-oxide ceramic fibers. Both commercially available products as well as work done on a pilot plant and laboratory scale will be discussed. The fibers are classified with respect to the type of the polymer used in their manufacture (polysilane/polycarbosilane, polysilazane, polycarbosilazane, polyborosilazane and polysiloxane). A generic flow chart for the process used to make non-oxide ceramic fibers from polymers, highlighting the important steps, is shown in Fig. 11.1. Important steps and the most important parameters for each step are presented. Manufacturing methods for specific fiber types not derived from preceramic polymers are briefly mentioned at the end of each section.

### 11.2.1 SiC fibers derived from polysilane/polycarbosilane

As early as the mid-sixties, Fritz *et al.* succeeded in producing a meltable polycarbosilane by means of thermal polymerization of tetramethylsilane at 770°C.<sup>2</sup> The low yield (<7 wt%) did not promise any commercial application for this synthesis; however, this work was the impetus for further research activities with the goal of providing a polycarbosilane with the characteristics and high yields necessary for fiber production on a commercial scale. The development of carbide or nitride fibers became necessary as both carbon fibers as well as oxide fibers are not suitable for many applications due to their low oxidation resistance and low maximum operating temperatures due to creep, respectively.<sup>3</sup>

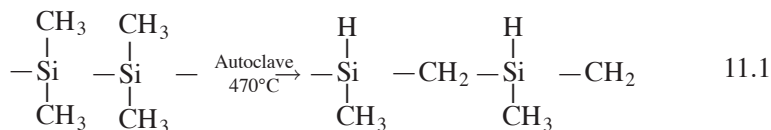


11.1 Flow chart for making polymer-derived ceramic fibers via the melt-spinning process (a representative scheme is shown for illustration). The boxes on the left indicate the important steps and those on the right are the most important parameters that need to be optimized in each step.

### Nicalon fiber types

#### Nicalon<sup>®</sup>

Dodecamethylcyclohexasilane  $[\text{SiMe}_2]_6$  was initially used as the base material for the Nicalon fibers produced by Nippon Carbon Corporation Ltd.<sup>4</sup> Today, polydimethylsilane  $[\text{SiMe}_2]_n$  is used.<sup>5,6</sup> Depending on the reaction process, both precursors can be produced through the synthesis of dichlorodimethylsilane with sodium in a solution. Spinnable polycarbosilanes result from these precursors through the insertion of  $-\text{CH}_2$  groups in the Si-Si bonds at  $470^\circ\text{C}$  in an autoclave (equation 11.1). The following reaction is known as the 'Kumada rearrangement':



Spinning into polymer fibers takes place at  $350^\circ\text{C}$  under nitrogen, and the fibers are hardened by curing in air at  $190^\circ\text{C}$ .<sup>7</sup> The individual polycarbosilane chains are linked through oxidation of the Si-H and Si- $\text{CH}_3$  side chains via Si-O-Si, i.e. Si- $\text{CH}_2$ -O-Si bridges.<sup>8</sup> Due to this reaction, the oxygen

content of the ceramic SiCO fibers can be up to 15 wt%. Okamura sees this development as the start of intensive research in the field of silicon-organic polymers as precursors for ceramic fibers.<sup>9</sup>

To avoid the polymerization step in an autoclave, Hasegawa and colleagues developed a method for the unpressurized production of spinnable polycarbosilanes.<sup>10</sup> In this process, a mixture of conventionally manufactured polydimethylsilane and polyborodiphenylsiloxane is heated in a nitrogen stream for several hours at above 300°C. The spinning temperature of 250°C for the resulting polymer is considerably lower than that of the precursor obtained according to equation 11.1, and curing in air is possible at 110°C.<sup>11</sup> The crosslinked polymer fibers are converted into SiC fibers through pyrolysis in an inert gas atmosphere in the temperature range of 1000–1300°C. However, the use of the polyborodiphenylsiloxane can lead to an oxygen content of up to 20 wt% in the resulting ceramic fibers.

Nippon Carbon introduced a product code for the designation of the various Nicalon variants consisting of the letters NL for 'Nicalon' and a three-digit number. The first digit describes the type of fiber, the second refers to the denier number\*, and the third gives information about the sizing agent used.<sup>12</sup> More information on this coding is given in Table 11.1. In some publications an additional letter is affixed to NL, which designates the type of sizing agent, e.g. NLP-201 for a standard Nicalon fiber with an epoxy sizing agent.

Structural research on Nicalon fibers shows that these fibers are composed of nanocrystalline  $\beta$ -silicon carbide, an amorphous SiOC phase and free carbon.<sup>13</sup> The grain boundary phase, SiOC, links the SiC crystals (diameter <2 nm) to each other and to the <1 nm occlusions of free carbon.<sup>14</sup> The amorphous SiCO phase contained in the Nicalon fibers limits the thermal stability to 1200°C due to the fact that, in addition to the decomposition of this phase into CO and SiO<sub>2</sub>, accelerated SiC crystal growth is observed above this temperature.<sup>15</sup> Thermodynamic calculations also predict the formation of gaseous SiO for the Nicalon system under these conditions,<sup>16,17</sup>

Table 11.1 'NL-XYZ' coding for Nicalon products

X (fiber type)	Y (denier)	Z (type of sizing agent)
2 = Standard	0 = 1800 denier	1 = P sizing agent (epoxy)
4 = High volume resistivity	1 = 900 denier	2 = M sizing agent (polyvinyl acetate)
5 = Low volume resistivity	2 = 1200 denier	6 = C sizing agent (polyimide)
6 = Carbon coated	3 = 600 denier	7 = Polyvinyl alcohol sizing agent

\*'Denier' is an outdated unit of measure for the fineness of a fiber with the unit 1 den = 1 g/9000 m. Today, fineness is usually given in tex with the unit 1 g/1000 m. 1 tex therefore corresponds to 9 den.

which has been experimentally observed using a special mass spectrometer technique.<sup>18</sup> Bouillon and colleagues studied the decomposition mechanism using so-called 'experimental' SiC fibers of a Nicalon type produced in the laboratory, and documented the sharp drop in the tensile strength and Young's modulus values due to the decomposition.<sup>19</sup>

The oxidation behavior is also of considerable importance for the technical application of ceramic fibers. In oxidation tests on Nicalon fibers it was determined that the oxidation rate depends on the diffusion of the oxygen through the passivating SiO<sub>2</sub> layer formed on the fiber surface.<sup>20</sup> This layer inhibits the decomposition of the non-oxidized fiber core. The experimentally discovered parabolic oxidation kinetics up to 1200°C conforms well with the general kinetic relationship for the oxidation of cylindrical fibers.<sup>21</sup>

The findings of these and other studies showed a maximum use temperature limit for Nicalon fibers of 1100 to 1200°C. It became clear that in order to produce SiC fibers with improved thermal stability, the introduction of oxygen in the fibers must be prevented. Since oxygen is introduced in Nicalon fibers in the curing step, this requirement implied the development of alternate cure reactions.

### Hi-Nicalon™

This fiber type represents a further development of the classic Nicalon fibers leading to improved thermal stability. The fibers are produced using the same method as with the Nicalon fibers, the only difference being that the polymer fibers are cured using electron beam or  $\gamma$ -radiation in an inert environment. This results in low oxygen content in the fibers (less than 1 wt%), a level present in the polymer prior to pyrolysis.<sup>22</sup> The content of Si-H groups in the polymer is crucial for this type of curing as the Si-H bond is most easily split into the radicals required for curing by radiation.<sup>23</sup>

The low oxygen content significantly improves the thermal stability under inert conditions. No change in properties has been observed for heat treatment for 10 hours at 1500°C in argon. Observable decrease in tensile strength and Young's modulus is only observed in fibers heat treated above 1500°C. Mass loss due to decomposition does not occur at 1600°C.<sup>24-26</sup> The thermal stability can be further improved with higher pyrolysis temperatures during production (1300 instead of 1000°C).<sup>27</sup> This treatment results in a more stable fiber structure consisting of SiC nanocrystallites and free carbon, which ultimately leads to improved creep behavior.<sup>28</sup> There are primarily two processes responsible for the reduction of the mechanical properties above 1500°C: the incipient SiC crystal growth and the decomposition of trace SiCO phase causing defects in the fiber surface.<sup>29</sup> However, this trace SiCO phase can be nearly completely removed by pyrolysis under reduced pressure (0.13 Pa) at 1300°C. The oxygen is released as carbon monoxide

and active oxidation of the remaining SiC crystals from trace oxygen in the furnace does not occur at this temperature. During a one-hour aging of these fibers in a vacuum oven at 1600°C in argon, the strength now drops only due to the growth of SiC crystals.<sup>30</sup>

The oxidation of Hi-Nicalon fibers in pure oxygen occurs in a manner similar to the Nicalon fibers. For Hi-Nicalon, the parabolic rate law holds up to 1400°C while for Nicalon only up to 1200°C to the decomposition.<sup>31</sup> Oxidation tests with Hi-Nicalon fibers in air with subsequent heat treatment at 1500°C under argon show that a thin, rapidly forming SiO<sub>2</sub> layer of 0.3 to 0.5 μm contributes to the preservation of the non-oxidized fiber core's original tensile strength.<sup>32</sup> In contrast, low partial oxygen pressures prevent the formation of a protective oxide layer, so that it is possible to consume the entire fiber material through active oxidation. These results support the thermodynamic calculations from Vahlas *et al.*<sup>33</sup>

Isostatic pressure treatment at 1500–2000°C in argon also leads to improved thermal stability of Hi-Nicalon fibers.<sup>34</sup> The tensile strength of fibers treated in this manner remains nearly constant up to 1700°C. The smooth, carbon-rich layer that forms on the surface under high pressure is postulated as the reason for the observed improved thermal stability of the fibers.

In summary, Hi-Nicalon fibers exhibit improved high-temperature properties compared to Nicalon fibers, such as in their thermal stability and creep resistance under inert conditions up to 1500°C. In an oxidizing atmosphere or at temperatures above 1500°C, however, their properties do degrade due to their high free carbon content. This limits their widespread use. Another factor preventing large-scale commercial use is the high price of all non-oxide ceramic fibers.

### Hi-Nicalon Type S<sup>TM</sup>

This fiber is derived from the Hi-Nicalon fiber by the reduction of the carbon content to near stoichiometric ratios (C/Si ratio ~1). Mechanical testing on experimental SiC fibers with varying carbon content shows that the samples with a stoichiometric composition exhibit greater thermal stability up to 1500°C and improved oxidation resistance up to 1400°C than samples with a carbon excess or deficiency.<sup>35</sup> The manufacturing method for Hi-Nicalon Type S fibers corresponds to that of the Hi-Nicalon fibers up to the curing process. The C/Si ratio is then adjusted during pyrolysis by adding hydrogen in a set temperature interval or by applying a hydrogen/argon mixture as a process gas during the entire pyrolysis process.<sup>36,37</sup> Elementary silicon formed in this decarbonization step degrades the mechanical properties of the fiber. It is removed via thermal post-treatment in an HCl-containing atmosphere.<sup>38</sup>

Compared to the other Nicalon products, Hi-Nicalon Type S fibers are

characterized by increased thermal stability as well as improved creep and oxidation resistance.<sup>39,40</sup> They also exhibit considerably improved chemical stability to aggressive gaseous compounds such as boron halides and ammonia, which are used in some cases to apply specific coatings to fibers using CVD processes.<sup>41</sup>

The important characteristics and properties of the different Nicalon fiber types are summarized in Table 11.2. In this table, they are also compared to the properties of other non-oxide fibers.

### *Tyranno fiber types*

#### Tyranno (Si–Ti–C–O)

A solid, spinnable polytitanocarborosilane is obtained by the reaction of polydimethylsilane with polyborodiphenylsiloxane and titanium tetraisopropoxide. This precursor can be processed analogously to the manufacturing method for Nicalon fibers into ceramic fibers whose mechanical properties – tensile strength  $\sim 3$  GPa, Young's modulus  $\sim 220$  GPa – are similar to those of the SiC fibers.<sup>42</sup>

These fibers are produced by Ube Industries Ltd. Their high oxygen content (up to 20 wt%) can be reduced to approximately 5 wt% by using electron beam irradiation to cure the fibers (e.g. Tyranno LOX M<sup>43</sup>). Oxidation tests on these fibers between 1000 and 1500°C in pure oxygen show that a dense, titanium-containing oxide layer forms. Here, in contrast to Nicalon fibers, the fiber core is better protected against decomposition, while the high free carbon content prevents the growth of SiC crystals.<sup>44</sup> The price for different types of Tyranno fibers (ZMI, LOX M, S) is in the range of \$1000 up to \$2000 per kilogram. The important characteristics and properties of the different Tyranno fiber types are summarized in Table 11.2. In this table, they are also compared to the properties of other non-oxide fibers.

#### Tyranno SA (Si–Al–C–O)

The reaction of a Yajima-type polycarborosilane with aluminum(III) acetylacetonate at 300°C under nitrogen results in a solid polyaluminocarborosilane from which fibers can be produced via melt spinning.<sup>45</sup> After curing in air and pyrolysis up to 1350°C under inert gas, an amorphous Si–Al–C–(O) fiber is obtained with an oxygen content of approximately 11 wt% and a high free carbon content. A subsequent sintering process at above 1800°C removes excess carbon and oxygen in the form of carbon monoxide, while aluminum acts as a sintering aid in the densification of the residual silicon carbide. With an aluminum content of under 2 wt%, a crystalline, oxygen-poor (0.5 wt%) SiC fiber results with a tensile strength of over 2.5 GPa, a Young's

Table 11.2 Characteristics and properties of selected commercially available continuous non-oxide fibers. The properties (modulus, strength, failure strength and density) are those at room temperature. Reproduced with permission from Ref. 1

Producer <i>Fiber</i>	Composition (wt%)	Diameter ( $\mu\text{m}$ )	Density ( $\text{g}/\text{cm}^3$ )	Tensile strength/ modulus (MPa/GPa)	Production technique/ structure	Approx. price (2007)
Nippon Carbon <i>Hi-Nicalon 'S'</i>	Si: 68.9 C: 30.9 O: 0.2	12	3.10	2600/420	Polycarbosilane/ $\beta$ -SiC	€ 7000/kg > 10 kg
Nippon Carbon <i>Hi-Nicalon</i>	Si: 63.7 C: 35.8 O: 0.5	14	2.74	2800/270	Polycarbosilane/ $\beta$ -SiC+C	€ 3250/kg > 10 kg
Nippon Carbon <i>Nicalon NL-200/201</i>	Si: 56.5 C: 31.2 O: 12.3	14	2.55	3000/220	Polycarbosilane/ $\beta$ -SiC+SiO <sub>2</sub> +C	€ 1000/kg > 10 kg
UBE Industries <i>Tyranno Fiber SA 3</i>	Si: 67.8 C: 31.3 O: 0.3 Al: < 2	10/7.5	3.10	2800/380	Polycarbosilane/ $\beta$ -SiC <sub>cryst.</sub> + ...	€ 6500/kg > 10 kg
UBE Industries <i>Tyranno Fiber ZMI</i>	Si: 56.1 C: 34.2 O: 8.7 Zr: 1.0	11	2.48	3400/200	Polycarbosilane/ $\beta$ -SiC+ ...	€ 1400/kg > 10 kg
UBE Industries <i>Tyranno Fiber LoxM</i>	Si: 55.4 C: 32.4 O: 10.2 Ti: 2.0	11	2.48	3300/187	Polycarbosilane/ $\beta$ -SiC <sub>amorph.</sub> + ...	€ 1200/kg > 10 kg



Table 11.2 Cont'd

Producer <i>Fiber</i>	Composition (wt%)		Diameter ( $\mu\text{m}$ )	Density ( $\text{g/cm}^3$ )	Tensile strength/ modulus (MPa/GPa)	Production technique/ structure	Approx. price (2007)
UBE Industries <i>Tyranno</i> <i>Fiber S</i>	Si:	50.4	8.5/11	2.35	3300/170	Polycarbosilane/ $\beta$ -SiC <sub>amorph.</sub> + ...	€ 1000/kg > 10 kg
	C:	29.7					
	O:	17.9					
	Ti:	2.0					
COI Ceramics <i>Sylramic-iBN</i>	SiC/ BN		10	3.00	3000/400	Precursor-polymer/ SiC/BN and other phases	€ 10 500/kg >10 kg
COI Ceramics <i>Sylramic</i>	SiC:	96.0	10	2.95	2700/310	Precursor-polymer/ SiC and other phases	€ 8500/kg >10 kg
	TiB <sub>2</sub> :	3.0					
	B <sub>4</sub> C:	1.0					
	O:	0.3					
Specialty Materials <i>SCS-Ultra</i>	SiC on C		140 (with carbon fiber core)	3.0	5865/415	CVD on C-filament/ $\beta$ -SiC on C	€ 16 400/kg
Specialty Materials <i>SCS-9A</i>	SiC on C		78 (with carbon fiber core)	2.8	3450/307	CVD on C-filament/ $\beta$ -SiC on C	€ 19 600/kg
Specialty Materials <i>SCS-6</i>	SiC on C		140 (with carbon fiber core)	3.0	3450/380	CVD on C-filament/ $\beta$ -SiC on C	€ 4850/kg
Tisics <i>Sigma</i>	SiC on W		100/140 (with tungsten wire core)	3.4	4000/400	CVD on W-filament SiC on W	Price not available

modulus of over 300 GPa and good high-temperature properties (thermal stability, creep and oxidation resistance).<sup>46</sup> The price of the Tyranno SA fiber is much higher (approx. \$8500 per kilogram) because of the complicated processing.

### *Sylramic fiber types*

The original Sylramic™ SiC fiber was developed by Dow Corning using melt-spinnable silicon-organic polymers and boron as a sintering aid. In the early 1990s, polyorganosiloxanes<sup>47</sup> or polycarbosilanes<sup>48</sup> were used as precursors. The boron was implanted from the gas phase into the fibers during processing. The oxygen was removed during the pyrolysis under argon up to 1800°C as CO. The process using polycarbosilane as a starting material led to the commercial Sylramic fiber product (3.2 GPa tensile strength at room temperature, with a price of approximately \$12 000 per kilogram), whose mechanical properties surpassed those of the Hi-Nicalon fibers.<sup>49</sup> As the implantation of the boron from the gas phase was a complex process, a process to introduce boron compounds, preferably boron tribromide, during polymer synthesis was developed. Other starting compounds were chloromethylsilanes and hexamethylsilazane for the synthesis of the boron-containing methylpolydisilylazanes,<sup>50</sup> chloromethylsilanes and trichloroalkylsilanes for boronized methylpolysilanes,<sup>51</sup> or trichloroalkylsilanes and hexamethylsilazane for polyborosilazanes.<sup>52</sup> It was possible to manufacture polymeric fibers from all of these precursors via melt spinning and subsequent gas phase curing, which resulted in SiC fibers with good mechanical properties after pyrolysis under argon up to 1800°C. Sylramic fiber types were reintroduced as commercially available products in 2004 by COI Ceramics, Inc. The properties of this class of fibers are also presented in Table 11.2.

### *Other SiC fiber developments derived from silicon-containing polymers*

Since the mid-nineties, a group from the University of Osaka has focused its attention on further development of the ‘Yajima polymer’ with the aim of improved spinnability, simplified curing and increased pyrolysis yield. For this purpose, 10–20 wt% of liquid, low-molecular polyvinylsilane ( $[-\text{CH}_2-\text{CH}_2-\text{SiH}_2-]_x[-\text{CH}_2-\text{CH}(\text{SiH}_3)-]_y$ ,  $x \approx y \approx 0.5$ ,  $M_n = 850$  g/mol) is added to the polycarbosilane, which leads to both a reduction of the melting temperature of the mixture, and improved curability of the polymer in air due to the higher number of Si–H groups. The resulting stronger crosslinking of the polymer leads to increased ceramic yield during fiber pyrolysis.<sup>53</sup> In addition, the substantially increased content of Si–H functions enables more effective electron beam curing compared to pure polycarbosilane;

however, high radiation doses are still required.<sup>54</sup> The curing of this advanced polycarbosilane by means of  $\gamma$ -radiation can be achieved with comparably low radiation doses. The increased reactivity to oxygen represents a problem with this method, however, as the curing occurs in air.<sup>55</sup>

Naslain's group at the University of Bordeaux also focused on the optimization of silicon-organic polymers for the production of SiC fibers. In addition to reducing the oxygen content by applying a radiation curing technique, special emphasis was placed on attaining a stoichiometric C/Si ratio. After attempting to retrace the manufacturing process for Hi-Nicalon Type S fibers,<sup>56</sup> a new, multi-stage synthesis route for a polycarbosilane was developed whose pyrolysate exhibited a C/Si ratio of 1.02.<sup>57,58</sup> Here, dichloromethylsilane, methylene chloride and magnesium were initially reacted in tetrahydrofuran under the presence of zinc powder. This was followed by the synthesis of the 2,4-dichloro-2,4-disilapentane and dichloromethylphenylsilane formed in the process at a 2:3 ratio with sodium in toluene at 120°C, which resulted in a phenyl-containing copolymer. In a further processing step it was possible at 70°C to selectively chlorinate this with hydrogen chloride under the separation of benzene and then finally to selectively hydrate this under the influence of  $\text{LiAlH}_4$  in an ethereal solution. The polysilacarbosilane obtained via this route had the chemical structure  $[\text{SiH}(\text{CH}_3)]_{0.6}[\text{SiH}(\text{CH}_3)\text{--CH}_2\text{--SiH}(\text{CH}_3)]_{0.4}$ .

Other studies were carried out on the introduction of boron into Si-C precursors for the production of SiC fibers stable at high temperatures. The triethylamine borane adduct initially proved to be an effective compound for the crosslinking of both polysilanes as well as polycarbosilanes.<sup>59</sup> Furthermore, with the help of this compound derived from polydimethylsilane it was possible to prepare boron-containing polysilacarbosilanes, which were spun into fibers and hardened in two stages via exposure to an ozone-containing oxygen stream as well as a trimethylamineborane-containing argon stream. Pyrolysis of these fibers up to 1800°C under argon resulted in quasi-stoichiometric, oxygen-free SiC fibers with a SiC crystal size of 0.3 to 1  $\mu\text{m}$  and a carbon-rich surface.<sup>60</sup>

Sacks and colleagues at the University of Florida started with an infusible, but soluble polymer. The precursor consists largely of a high-melting Yajima-type polycarbosilane component, which is crosslinked with a vinyl group-containing Si compound, e.g. 1,3,5-trimethyl-1,3,5-trivinylcyclotrisilazane, under exposure to dicumylperoxide in a solution.<sup>61</sup> Infusible polymer fibers are obtained from this solution via the dry spinning method, which are converted to carbon-rich SiC fibers, so-called 'UF fibers', by pyrolysis under nitrogen between 1000 and 1200°C. After the addition of a boron-containing compound to the polymer solution and curing of the fibers at 100–200°C in air, quasi-stoichiometric, microporous SiC fibers result during pyrolysis in argon up to 1600°C through the decomposition of the SiCO phase and the

subsequent reaction of the elementary silicon formed in the process with the free carbon still present. At temperatures above 1750°C, these fibers can be densified with boron acting as a sintering aid (approximately 1 wt%) into so-called 'UF-HM fibers'.<sup>62</sup> The good thermal stability of the fibers up to 1950°C under argon is due to the low oxygen content ( $\leq 0.1$  wt%).<sup>63</sup>

The high-temperature properties of the UF fibers (residual strength after thermal exposure, creep resistance) are comparable to those of the Hi-Nicalon Type S fibers. The properties of the UF-HM fibers are better than those of Hi-Nicalon Type S fibers.<sup>63,64</sup> Sacks also showed that the properties of UF-HM fibers can be further improved if during the sintering process under argon two additional temperature treatments above 1700°C under nitrogen or carbon monoxide/argon are performed.<sup>65</sup> Due to the reaction with carbon monoxide, the boron is extensively removed from the fibers and a thin carbon-rich layer is formed on the fiber surface, which minimizes the surface imperfections usually responsible for fracture.

At the beginning of the seventies, Verbeek and Winter developed a method at Bayer AG by which chlorosilanes can be converted to polychlorocarbosilane resins through pyrolysis between 600 and 800°C.<sup>66</sup> It was possible to produce fibers with these resins using the melt or dry spinning method. In 1995, Müller and Roewer's groups at the TU Bergakademie Freiberg (Freiburg University of Mining and Technology, Germany) again began using polychlorocarbosilanes as precursors for SiC fibers. The disilane fraction by-product arising during the Müller-Rochow synthesis is converted into chlorine-containing silicon polymers by means of heterogeneous catalysis at low temperatures. In order to make it possible to spin the precursor, however, an organic polymer must be added as a spinning additive.<sup>67</sup> The curing of the highly reactive polymer fibers (due to the presence of chlorine atoms) occurs through a gas phase reaction with ammonia.<sup>68</sup> This approach was continued by the ceramic fiber group at Fraunhofer ISC Würzburg, Germany.<sup>69</sup>

Frey *et al.* manufactured spinnable polyorganosiloxanes by means of base-catalyzed co-condensation of linear polysiloxanes as well as alkoxysilanes and alkoxydisilanes.<sup>70</sup> The curing of the spun fibers was successful with UV light, as the polymers contain both Si-H as well as Si-vinyl functions, thus making crosslinking possible through hydrosilylation. After pyrolysis under argon up to 1300°C, the resulting ceramic fibers had a diameter of 10–20  $\mu\text{m}$  and a tensile strength of up to 2.7 GPa.

In the presence of a zirconocene catalyst, it is possible to polymerize methylsilane ( $\text{MeSiH}_3$ ) into a polymethylsilane by undergoing dehydrocoupling. This can then be processed into fibers in a solution and by adding a spinning additive during dry spinning.<sup>71</sup> The addition of 10 wt% of a spinning additive also balances the carbon loss through the separation of methane during pyrolysis, thus enabling a Si/C ratio of nearly 1 in the resulting SiC fibers.<sup>72,73</sup>

The CSA fibers (CSA = Carbon Silicon Alloy) can be produced from a precursor that results from the reaction of polydimethylsilane with the soluble fraction of the petroleum pitch 'Ashland A240'.<sup>74</sup> Fiber curing is achieved in this process by exposure to air at 300–330°C. The mass increase due to the introduction of oxygen must be above 4.5 wt% to ensure complete hardening of the fibers. However, it should not exceed 7.8 wt% as the oxygen content in this case reaches more than 16 wt% which leads to much lower strength fibers.

#### *Other manufacturing methods for SiC fibers*

One method used by DuPont to manufacture SiC fibers uses a polycarbosilane/SiC powder/xylene slurry that is dry spun.<sup>75</sup> The sintering of the dried fibers occurs at 2000°C, with boron carbide added to the spinning mass to act as a sintering aid.

The processing of an organic polymer and SiC powder blend into fibers by means of melt extrusion is based on development at Carborundum.<sup>76</sup> After the extrusion process, the organic additives are extracted from the fibers which are then densified by sintering at 1800–2300°C, with boron carbide added to facilitate the sintering process. In addition to  $\alpha$ -SiC crystals, these fibers have free carbon and boron carbide as additional phases.<sup>77</sup> These fibers are characterized by their high creep resistance.

'CVD-SiC fibers' are manufactured as commercial products at approximately 1300°C by deposition of silicon carbide from a trichloromethylsilane/hydrogen mixture onto a substrate filament. The Sigma™ SiC fiber developed by BP (now supplied by TISICS (UK)) uses a tungsten filament. Speciality Materials, Inc. (USA) developed several SiC fibers with a carbon core.<sup>78</sup> The commercially available products have a large diameter from 78  $\mu\text{m}$  (SCS-9A) up to 140  $\mu\text{m}$  (SCS-Ultra, SCS-6) and are therefore not suitable for applications requiring a high degree of fiber flexibility. Long-term studies at high temperatures show a maximum use temperature of 1100°C for SCS-6 fibers.<sup>79</sup> All fibers of this family are very expensive (SCS-6 fiber approximately \$7000 per kilogram, other types more than \$20 000 per kilogram). Their properties and characteristics are also presented in Table 11.2.

#### 11.2.2 SiN fibers derived from carbon-free polysilazanes

For processing of ceramic SiN fibers a carbon-free polysilazane was used that is obtained from the reaction of dichlorosilane with ammonia in pyridine<sup>80</sup> (TONEN Corporation). However, the polymer can only be spun in a solution and with the addition of an organic spinning additive such as polyethylenoxide or polystyrene.<sup>81</sup> Dry spinning was possible without the use of a spinning additive if the dissolved polymer is post-condensed for several hours at 80°C

under the influence of ammonia in an autoclave.<sup>82</sup> The polysilazane can also be modified by reaction with suitable metal isopropoxides  $M^m[OC(CH_3)_2]_n$  ( $M = Al, Ti, Zr$ ) to increase the stability of the resulting fibers with respect to metal melts.<sup>83</sup>

The mechanical properties of non-doped Si–N fibers are dependent on their composition and degree of crystallinity which is controlled by the pyrolysis temperature. Temperatures above 1400°C lead to increased crystal growth and consequently to reduced strengths. A Si/N ratio of  $>0.75$  enables the formation of elementary silicon, which, at higher temperatures, also leads to a reduction in strength.<sup>84</sup> X-ray diffraction studies show that the Si/N ratio only slightly influences the structural composition of the fibers from  $\alpha$ - and/or  $\beta$ -Si<sub>3</sub>N<sub>4</sub>; a higher oxygen content, however, leads to the formation of Si<sub>2</sub>N<sub>2</sub>O-analogous structures.<sup>85</sup> In an undiluted form, the described perhydropolysilazane is also applied as a matrix precursor for SiC whisker or carbon long-fiber reinforced ceramic composites.<sup>86,87</sup>

Further studies have attempted to shift the crystallization of silicon nitride to higher temperatures by introducing boron into the silazane structure. This has been achieved by the reaction of perhydropolysilazane with trimethylborane. The SiBN precursor obtained exhibits a ceramic yield of 80 wt% after pyrolysis in an ammonia atmosphere up to 1000°C. The pyrolysate remains amorphous in a nitrogen atmosphere up to 1700°C.<sup>88</sup> Solutions of this new polyborosilazane can be processed into polymer fibers via dry spinning without the use of a spinning additive.<sup>89</sup> These deliver amorphous SiBNO fibers after pyrolysis at final temperatures between 200 and 1200°C in an ammonia atmosphere followed by heat treatment under nitrogen at 1300–1800°C. The tensile strength and Young's modulus values of these fibers (maxima for final temperatures of the pyrolysis in ammonia of 800°C and heat treatment in nitrogen of 1600°C) are comparable to those of SiN fibers; however, owing to the improved thermal stability, the properties remain almost constant up to 1600°C (as compared to 1300°C for the SiN fibers).

Aluminum can be incorporated in the perhydropolysilazane by reaction with (ethyl-acetoacetate) aluminum diisopropoxide.<sup>90</sup> The resulting polyaluminosilazane is infusible and soluble in organic solvents and has a ceramic yield of over 60 wt% after pyrolysis up to 1000°C in an ammonia stream. Sorarù *et al.* obtained ceramic SiAlON fibers by the reaction of polycarbosilane with (ethyl-acetoacetate) aluminum di-sec-butoxide (Al/Si ratio 0.25). The polymer fibers were cured in air and pyrolyzed at temperatures up to 1000°C in ammonia.<sup>91</sup> The subsequent annealing of these fibers at temperatures up to 1500°C in a nitrogen stream showed that the incipient crystallization of  $\beta$ -Si<sub>2.5</sub>Al<sub>0.5</sub>O<sub>0.5</sub>N<sub>3.5</sub> at above 1200°C leads to a significant decrease in strength.

### 11.2.3 Ceramic fibers from polyborosilazanes

A carbon-containing polyborosilazane serves as a precursor for a SiBCN fiber manufactured by Bayer AG. It results from the reaction of trichlorosilylaminodichloroborane (TADB) with methylamine in a solution followed by thermal post-treatment of the reaction product under reduced pressure.<sup>92</sup> The fibers obtained from melt spinning can be converted into an infusible state through gas phase curing with amine-borane adducts or dichlorosilane.<sup>93–95</sup> Pyrolysis up to 1500°C in a nitrogen stream results in ceramic fibers that have good mechanical properties and excellent oxidation resistance even at 1500°C.<sup>95,96</sup> The formation of a SiO<sub>2</sub>/BN double layer prevents diffusion of oxygen into the interior of the fiber, leading to exceptionally good oxidation resistance.<sup>97</sup>

A similar way for processing of ceramic SiBCN fibers was developed by research groups at the University of Lyon (France) and the Max-Planck-Institute, Stuttgart (Germany). The measured tensile strength was about 1.3 GPa for ceramic fibers pyrolyzed at 1400°C with a diameter of approximately 23 μm.<sup>98,99</sup> Researchers from China manufactured SiBCNO fibers by first treating polycarbosilane fibers at 400–800°C with ammonia and then at room temperature with boron trichloride.<sup>100</sup> The oxygen content of the fibers can be lowered considerably by sintering above 1500°C in argon.

### 11.2.4 Fibers derived from carbon-containing polysilazanes or from polycarbosilazanes

As early as 1972, Verbeek reacted trichloromethylsilane as well as dichlorodimethylsilane with methylamine and polymerized the resulting methylaminosilanes at 520 and 650°C respectively into carbosilazane resins, which melted at 220°C.<sup>101</sup> The precursors were melt-spun into fibers. After curing in air or with hydrogen sulfide at elevated temperatures, pyrolysis up to 1200°C in a stream of nitrogen led to SiCN fibers with tensile strength values of up to 2.5 GPa. In further research activities the abovementioned chlorosilanes were reacted with ammonia to form infusible polycarbosilazanes. These polymers were mixed with a spinning additive in a solution and spun into fibers via dry-spinning.<sup>102</sup>

In 1982, studies from a research group at NASA were published, which once again focused on the reaction of trichloromethylsilane with methylamine into tris(*N*-methylamino) methylsilane. Here, special emphasis was placed on the characterization of the polycarbosilazane obtained at a very high temperature of 520°C, which was used as a precursor for the production of ceramic fibers.<sup>103</sup>

Intensive research was conducted at Dow Corning to produce fibers in the Si–C–N–(O) system. The starting point for the manufacturing



process of this family of fibers, called MPDZ-PhVi, was the reaction of a mixture of chloromethylsilanes and dichlorophenylvinylsilane with hexamethyldisilazane.<sup>104</sup> However, nitrogen-rich HPZ fibers were the first fibers of commercial importance. The precursor used in the production, a hydridopolysilazane, was formed by the reaction of trichlorosilane with hexamethyldisilazane under the separation of chlorotrimethylsilane, followed by continuous thermal polymerization under partial recovery of the hexamethyldisilazane. The hydridopolysilazane can be spun from this melt. The polymer fibers obtained in this way can be cured with trichlorosilane and converted into ceramic fibers by pyrolysis under nitrogen up to 1200°C.<sup>105</sup> Freeman and colleagues advanced the manufacturing process of HPZ fibers by using hydrogen chloride as a curing agent. In addition, they also attempted to prevent the precursor or the fibers from coming into contact with metallic matter during the process steps to avoid the incorporation of metallic impurities in the fibers.<sup>106,107</sup> In this way it was possible to considerably improve the thermal stability of the HPZ fibers. The development of fibers described in this sub-section up to 1990 was summarized by Cooke in a review article on inorganic fibers.<sup>108</sup>

Based on a patent held by Dow Corning, Wacker Chemie AG developed a SiCN fiber. In this case, the precursors are obtained by reacting a mixture of dichlorodiorganosilanes and dichloromethylsilane with hexamethyldisilazane under continuous heating to 400°C. The polymer fibers spun from the polymer melts can be cured at 100°C in air and pyrolyzed under argon at above 1100°C into ceramic fibers with good yields.<sup>109</sup> Another method starts with polysilazanes formed by the co-aminolysis of chloromethylsilanes and trichlorosilane with methylamine or organylamine mixtures via the corresponding aminodisilanes as an intermediate. The curing of the fiber takes place in air or water vapor which introduces up to 10 wt% oxygen in the final fiber.<sup>110</sup>

Shinetsu Chemical Corporation holds a patent for the production of SiCN hollow fibers, which is also based on the ammonolysis of chlorosilane mixtures. In this case, the formed oligosilazanes are polymerized with potassium hydride or potassium hydroxide into solid, meltable precursors. The curing of the fibers spun from the melt occurs via a two-stage gas phase process. First the fiber surface is made infusible through reaction with a slightly volatile silicon, boron, phosphor or metal halide, then the subsequent treatment with water vapor or ammonia provides for the removal of the halides from the crosslinked polymer structure. The hardened periphery of the fibers remains intact during pyrolysis up to 1200°C under nitrogen, whereas the meltable core completely decomposes.<sup>111</sup>

Rhone Poulenc Chimie synthesized meltable polysilazanes by reacting mixture of trichloromethylsilane and dichlorodimethylsilane with ammonia. The polymer fibers manufactured from these precursors are cured using a



water/ammonia/nitrogen mixture and then pyrolyzed under nitrogen up to 1300°C.<sup>112</sup> It was shown that the tensile strength of the resulting SiCN fibers can be increased from 1 to 1.5 GPa by post-synthesis treatment with 10 vol%-containing hydrofluoric acid.<sup>113</sup> Further development of this method for manufacturing fibers eventually led to a commercially available SiCN fiber with the name Fiberamic<sup>®</sup>, with a nominal tensile strength of 2.2 GPa. These fibers maintain this strength value after heat treatment in air up to a temperature of 1000°C.<sup>114</sup>

The Nippon Carbon Corporation Ltd also conducted experiments for the production of SiCN(O) fibers with the aim of combining the exceptional mechanical properties of SiC fibers with the good electrical insulating properties of SiN(O) fibers. Cured polycarbosilane fibers were initially nitrified with ammonia at a maximum temperature of 600°C followed by a pyrolysis in an HCl/argon mixture up to 1200°C to attain the desired Si/C/N ratio. The specific resistance, depending on the composition of the ceramic fibers ( $10^6$ – $10^8 \Omega \text{ cm}$ ), lies between those of SiC ( $10^3$ – $10^5 \Omega \text{ cm}$ ) and SiN(O) fibers ( $10^{10} \Omega \text{ cm}$ ).<sup>115</sup>

In a synthesis developed at the Laboratoire des Composites Thermostructuraux in Pessac, France, dichlorodimethylsilane and 1,3-dichloro-1,3-dimethyldisilazane reacted with sodium in toluene under dechlorination to form a polysilasilazane (PSSZ). By heating it to between 270 and 470°C, this product can be converted into a meltable polycarbosilazane (PCSZ) by release of molecular hydrogen which is accompanied with an increase in the viscosity.<sup>116,117</sup> Polymer fibers can be spun from the melt and then converted into ceramic fibers after curing in air and by pyrolysis up to 1200°C under argon. Maximum values for the tensile strength of 1.85 GPa and for the Young's modulus of 185 GPa were obtained in fibers cured for 1 h in air at 140°C. This fiber also had 12 atom% oxygen.<sup>118</sup> At pyrolysis temperatures above 1200°C, the amorphous SiCNO matrix begins to decompose, leading to a considerable decrease in the tensile strength values, while the Young's modulus first begins to decrease above 1400°C. However, the decomposition is shifted to temperatures approximately 100°C higher than those for SiCO fibers.<sup>119</sup> Decomposition takes place considerably earlier in argon than in nitrogen as the latter is a decomposition product of the SiCNO phase and a corresponding atmosphere shifts the decomposition reaction to higher temperatures.<sup>120</sup>

The introduction of oxygen into these fibers is prevented if the polymer fibers are cured by means of  $\gamma$ -radiation instead of curing in air. Here, the oxygen content is restricted to below 2 wt%, which also leads to improved thermal stability up to 1400°C. The influence of the heat treatment atmosphere comes into effect above this temperature. On the basis of the abovementioned decomposition of the matrix, a carbon-rich layer forms on the fiber surface in argon, whose thickness grows toward the fiber core with increasing exposure

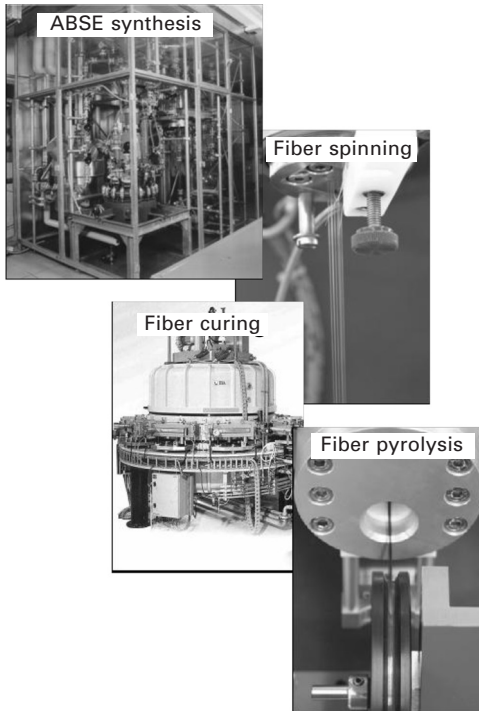
time and temperature. Decomposition in nitrogen occurs quite slowly, so that even at 1600°C the fibers still largely consist of amorphous SiCN material in which small SiC crystallites with a diameter of approximately 6 nm are embedded. The thickness of the carbon-rich layer on the fiber surface is a few nanometers. The tensile strength and Young's modulus values are approximately 25% higher than those of fibers cured in air.<sup>121</sup>

As discussed above, the Si–C–N–(O) system enables two mechanisms that improve the thermal stability of the fibers up to temperatures of 1400°C. Finely distributed free carbon impedes the growth of SiC crystals, thus contributing to the preservation of the residual strength of the fibers, while the homogeneous SiCN matrix remains stable up to its decomposition temperature, i.e. it undergoes almost no continuous structural changes.<sup>122</sup>

In another process, dichloromethylsilane and dichlorodimethylsilane are reacted with ammonia to obtain a meltable polysilazane after a thermally induced polymerization process. A boron trichloride/nitrogen mixture is used for curing of the fibers spun from the melt. The chlorine atoms are removed through post-treatment with ammonia. The remaining boron content in the hardened fibers was more than 0.4 wt%. After pyrolysis the resulting SiCN fibers exhibited considerably better mechanical properties than comparable fibers not containing boron.<sup>123</sup>

At the University of Bayreuth (Germany) in cooperation with ITCF Denkendorf (Germany) a SiCN fiber has been developed by using the self-synthesized ABSE polycarbosilazane and made by sequenced manufacturing on the basis of well-established processing steps (melt-spinning, e-beam curing, pyrolysis). The solid and meltable ABSE-precursor was synthesized by ammonolysis of 1,2-bis(dichloromethylsilyl)ethane on a pilot-plant scale. A picture of the different sections of the pilot plant is shown in Fig. 11.2. The polymer structure consists of very stable five-membered rings connected via linear carbosilazane units. Further crosslinking only takes place via condensation of ammonia at temperatures higher than 220°C. Because of the absence of reactive Si–H and Si–vinyl groups, the most reactive functionality is the N–H group. For this reason the ABSE-polymer shows an astonishing resistance against moisture. The optimization of the rheological properties, specially the viscoelastic behavior, of the polymer melt was crucial for a stable melt-spinning process as well as for good flexibility and tensile strength of the resulting green fibers. In contrast to the Nicalon fiber types, the curing of the polymer fibers was reproducibly accomplished with a very low electron-beam dose of 300 kGy. Continuous pyrolysis at a relatively low temperature of 1100°C led to ceramic SiCN fibers with diameters from 15 up to 120 μm, tensile strength values up to 1.2 GPa and an oxidation stability comparable to that of the Hi-Nicalon fiber.<sup>124–130</sup>

Recently the ABSE precursor was modified by the integration of multi-wall-C-nanotubes (MWCTN) to improve the viscoelasticity of the polymer

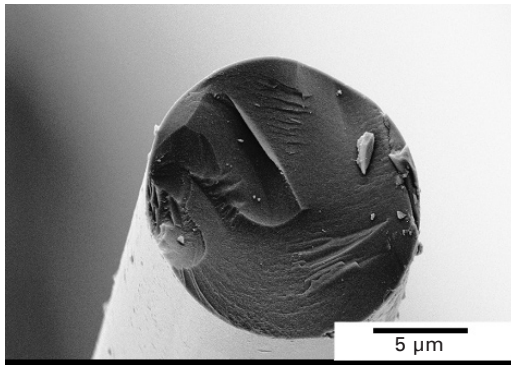


11.2 The different sections of the pilot plant for the processing of polymer derived ceramic SiCN fibers at the University of Bayreuth with the ABSE polycarbosilazane precursor (precursor synthesis, fiber spinning, E-beam curing, fiber pyrolysis).

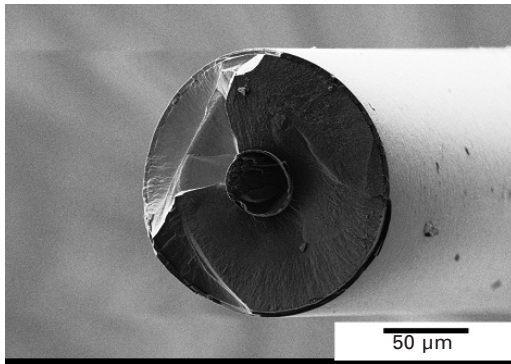
melt by the interaction of the C-nanotubes with the polycarbosilazane. Furthermore, the preferred orientation of the MWCNT along the fiber length during the melt-spinning process leads to reinforced ceramic C/SiCN fibers after pyrolysis.<sup>131,132</sup> Initial investigations demonstrate that only 0.5 wt% MWCNT optimize the rheology of the melt. The melt-spun, MWCNT containing green fibers were cured via e-beam with 300 kGy. These fibers have very attractive properties. For example, the tensile strength of the ceramic C/SiCN fibers after pyrolysis at 1100°C was 50% higher than the values obtained for unreinforced SiCN fibers produced under the same conditions.

Finally, there have been attempts to make SiC short fibers and whiskers from natural sources like rice husk. Dried rice husk contains about 15 wt% SiO<sub>2</sub> and the remainder is primarily carbon.<sup>133</sup> A process has been developed to convert this to SiC short fibers and whiskers by direct pyrolysis.<sup>134</sup> However, since this process does not produce continuous fibers, a detailed discussion of this is outside the scope of this chapter.

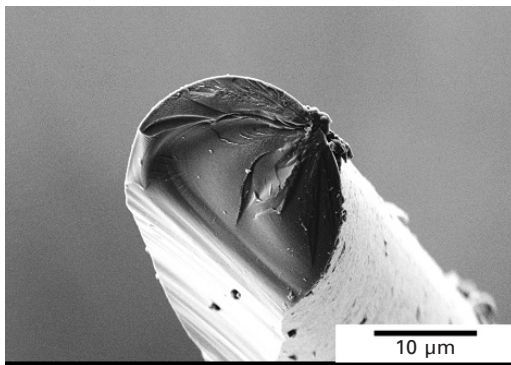
In Fig. 11.3, the fracture surfaces of several commercial and developmental non-oxide fibers are shown. Figure 11.3(a) is for Hi-Nicalon fibers and the glass-like fracture surface typical of the amorphous fibers is clearly evident.



(a)

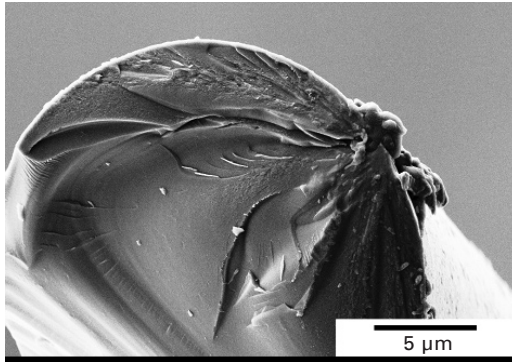


(b)



(c)

11.3 Fracture surface of selected non-oxide fibers: (a) Hi-Nicalon; (b) SCS-6; (c) ABSE precursor derived (lower magnification); (d) ABSE precursor derived (higher magnification).



(d)

11.3 Cont'd

Figure 11.3(b) is for SCS-6 fibers and the carbon core is clearly visible. The fracture origin appears to be at the interface between the carbon core and the SiC cladding. Figure 11.3(c and d) show the fracture surface for ABSE derived fibers, and in this case also, the fracture surface is typical for amorphous fibers with a fracture origin at the surface.

### 11.3 Processing, structure and properties of oxide fibers

The most developed and widely available oxide fibers are composed of  $\text{Al}_2\text{O}_3$  either in the pure form or with other oxides. These fibers are of interest in high temperature applications in an oxidizing environment. Starting from the early 1970s, several oxide fibers have been produced. The earliest developments were in producing alumina fibers with high silica content. The alumina content of these fibers was in the range of 45–60 wt% and they could be melt spun.<sup>108</sup> These silicate glass-like melt-spun fibers are not discussed in this chapter. The demand for high temperature capability led to the development of two broad routes to make high alumina content fibers. These are discussed in detail below.

#### 11.3.1 Slurry spinning process

The first almost pure alumina fiber was produced in 1979 by E.I. du Pont de Nemours and Co. at a commercial scale and was called Fiber FP.<sup>135</sup> It is no longer produced. This fiber was made from spinning slurries of alumina particles into fiber. The major technological accomplishment was to make spinnable slurries of ceramic particles. The green fibers were calcined to a temperature of 800°C and sintered at temperatures up to 1800°C. The fibers

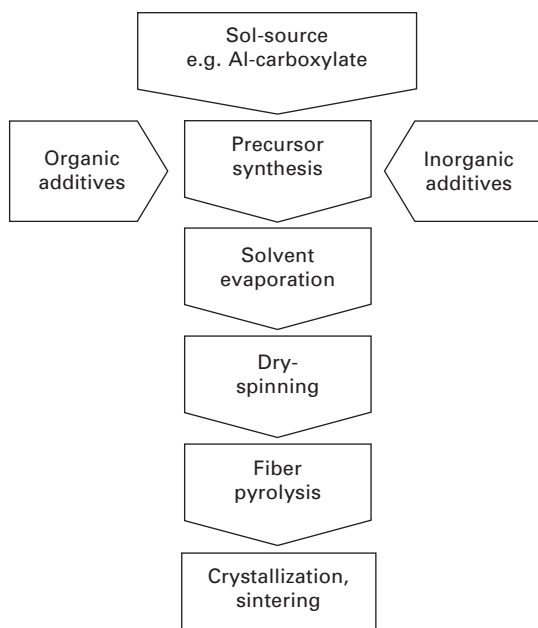
were continuous and had a diameter of approximately 20  $\mu\text{m}$ . The fibers were polycrystalline (>99%  $\alpha$ -alumina), with an average grain size of 0.5  $\mu\text{m}$ , a rough 'cobblestone' type surface and a density of 3.9  $\text{g}/\text{cm}^3$ . The strength of the fibers was approximately 1.55 GPa and the modulus 380 GPa. One of the primary shortcomings of this fiber was its low strain to failure (of the order of 0.4%).<sup>136</sup>

Due to the low strain to failure and large diameter, this fiber was not easily weavable. Another problem was the rapid strength drop above 1300°C due to grain growth and measurable creep deformation above 1000°C due to the fine grain size.<sup>137</sup> DuPont developed another fiber, PRD 166, using the slurry process.<sup>138</sup> This fiber was 80%  $\alpha$ -alumina and 20% tetragonal zirconia. This fiber had somewhat better strength (20–50% higher than FP) and a slightly lower modulus (10% lower). It was also more resistant to high temperature deformation showing linear elastic behavior up to 1100°C (100°C higher than FP) and slightly lower creep rates up to 1300°C. Detailed mechanical and microstructural characterization of these two fibers is reported in Ref. 139. The microstructure of PRD 166 consisted of 0.15  $\mu\text{m}$   $\text{ZrO}_2$  grains at the triple junctions of 0.3  $\mu\text{m}$   $\alpha$ - $\text{Al}_2\text{O}_3$  grains.<sup>140</sup> It was also observed in this study that the microstructure of the PRD-166 was much more stable than that of FP (under heat treatment to 1600°C for 10 minutes). The fine  $\text{ZrO}_2$  grains were postulated to pin the grain growth.

### 11.3.2 Solution or sol-gel process

In this process, either a solution of metal salts (e.g. chlorides or nitrates) or an alkoxide (e.g. aluminum isopropoxide) is used to make a sol. This is then aged to get a gel of the correct rheology that can be drawn as a fiber. The drawn fiber is dried and sintered.<sup>141,142</sup> The generic flow diagram for this process is shown in Fig. 11.4. A significant advantage of this process is that much finer diameter fibers can be made (compared to the slurry process). The primary constituent of the commercial fibers made by this technique is also  $\text{Al}_2\text{O}_3$ . During the heat treatment, the amorphous fiber transforms to  $\alpha$ - $\text{Al}_2\text{O}_3$  via a series of transitional phases.<sup>108</sup> One of the major scientific challenges in these fibers has been the control of the microstructure as it undergoes these phase transitions. In most cases, this has been achieved by adding other oxides ( $\text{SiO}_2$ ,  $\text{B}_2\text{O}_3$  and  $\text{ZrO}_2$  are common additives).

This process has been commercialized by the 3M Corporation to make a series of fibers, with the trade name Nextel™, that are currently available. In 1974, the first of these fibers, Nextel 312, was introduced. This fiber has a chemical composition of 62 wt%  $\text{Al}_2\text{O}_3$ , 24 wt%  $\text{SiO}_2$  and 14 wt%  $\text{B}_2\text{O}_3$ . It has a diameter of 10–12  $\mu\text{m}$  and is amorphous with a smooth surface. At room temperature, its modulus is around 150 GPa and it has a nominal strength of 1.7 GPa. This results in a fairly good strain to failure of around 1.1% which



11.4 Typical flow chart for making oxide fibers from salt solutions or organometallic sols.

coupled with its fine diameter results in a fiber that can be woven.<sup>108,137</sup> This fiber is the least expensive fiber in this family and is widely used. However, due to the volatility of  $B_2O_3$ , it has limited high temperature use. Nextel 440 has much lower  $B_2O_3$  content (70 wt%  $Al_2O_3$ , 28 wt%  $SiO_2$  and 2 wt%  $B_2O_3$ ) and as a result better high temperature performance. It also has a diameter of 10–12  $\mu m$  and has fine  $\gamma$ -alumina precipitates in an amorphous silica matrix with a smooth surface. It has both higher room temperature modulus and strength than Nextel 312 (modulus of 190 GPa and strength of 2.1 GPa). Its strain to failure and weavability are comparable to those of Nextel 312. Due to the low boria content, the fiber is stable to temperatures of 1200°C. However, due to the amorphous matrix, it has quite high creep rates at moderate temperatures.

3M developed a high alumina fiber using this process. Nextel 610 is a high modulus (370 GPa) almost pure  $\alpha$ - $Al_2O_3$  (>99%) fiber. In this sense, it is very similar to fiber FP from DuPont. However, it has much finer diameter (nominally 10–12  $\mu m$ ) and much smaller grain size (0.1  $\mu m$ ), resulting in higher strength (around 3.3 GPa) and much better weaving characteristics.<sup>137,143</sup> However, due to the fine grain size, this fiber is even more susceptible to creep than fiber FP. Creep deformation has been reported at temperatures as low as 900°C. Mitsui also produces a nearly pure  $\alpha$ - $Al_2O_3$  (>99%) fine



fiber (diameter 10  $\mu\text{m}$ ).<sup>144</sup> However, this fiber has residual porosity and hence its strength and modulus are lower than those of Nextel 610 (strength around 1.8 GPa and modulus approximately 330 GPa). Its high temperature properties are similar to those of Nextel 610 (slightly higher creep rates due to porosity).<sup>137</sup>

In order to improve the high temperature performance of these alumina based fibers, composite fibers have been developed using solution and sol-gel based processes. Nextel 720 from 3M has a nominal composition of 85 wt%  $\text{Al}_2\text{O}_3$  and 15 wt %  $\text{SiO}_2$ . Its microstructure consists of 0.5  $\mu\text{m}$  mullite and finer  $\alpha\text{-Al}_2\text{O}_3$  grains. It is also produced with a diameter of 10–12  $\mu\text{m}$ , has strength of approximately 2.1 GPa and modulus of 260 GPa.<sup>137,143</sup> The primary advantage of this fiber is its high temperature performance. For example, in fast fracture, the room temperature strength is retained up to 1150°C, and even at 1300°C 70% of the room temperature strength is retained.<sup>144</sup> The microstructure of this fiber is quite stable up to 1300°C. It also has a much improved creep resistance compared to other alumino-silicate or alumina fibers.<sup>137</sup> This fiber has almost 200 °C higher temperature capability than Nextel 610 and can be used in load-bearing applications up to 1200°C. Sumitomo Chemicals also produces a fine fiber with nominal composition of 85 wt%  $\text{Al}_2\text{O}_3$  and 15 wt%  $\text{SiO}_2$ . The trade name of this fiber is Altex and it is made from polymeric precursors.<sup>145</sup> The microstructure consists of extremely fine  $\gamma$ -alumina grains of a few nanometers in a amorphous silica rich phase.<sup>137</sup> This fiber has a nominal room temperature strength of around 1.8 GPa and a modulus of 210 GPa. Due to the amorphous silica, the fiber demonstrates high creep rates around 1200°C.<sup>146</sup> However, it also undergoes crystallization (formation of mullite and conversion of  $\gamma\text{-Al}_2\text{O}_3$  to  $\alpha\text{-Al}_2\text{O}_3$ ) in the temperature range of 1200–1400°C.<sup>137</sup>

One last fiber to discuss that is commercially available and made by the solution process is Nextel 650 from 3M Corp. This fiber has the nominal composition of 89 wt%  $\text{Al}_2\text{O}_3$ , 10 wt%  $\text{ZrO}_2$  and 1 wt%  $\text{Y}_2\text{O}_3$ . It consists of  $\alpha\text{-Al}_2\text{O}_3$  and cubic  $\text{ZrO}_2$  grains. It is also produced with a diameter of 10–12  $\mu\text{m}$ , has a strength of approximately 2.5 GPa and a modulus of 360 GPa.<sup>137,143</sup> Its creep rate is two orders of magnitude lower than that of Nextel 610 (under the same load and temperature).<sup>147</sup> The properties of this fiber are between those of Nextel 610 and 720. It can be used in load-bearing applications up to 1100°C.

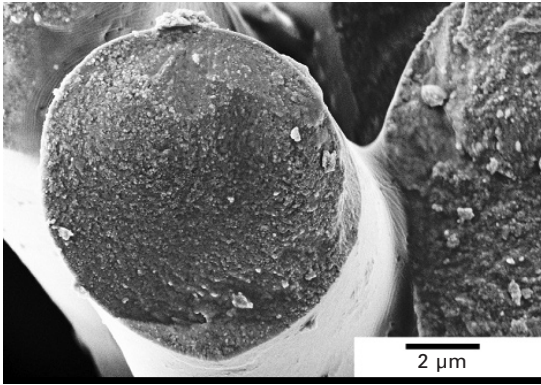
The important characteristics and properties of the many oxide fiber types are summarized and compared in Table 11.3. The fracture surfaces of two commercial oxide fibers are shown in Fig. 11.5. Figure 11.5(a) is for Nextel 610: the fine alumina grains and small amount of residual porosity are clearly visible. Figure 11.5(b and c) are for Nextel 720 and the surface flaw as the fracture origin is clearly visible.

Recently, significant progress has been made in the processing of oxide

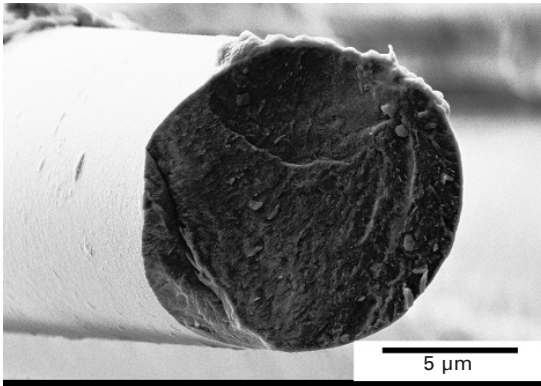


*Table 11.3* Characteristics and properties of selected commercially available continuous oxide fibers. The properties (modulus, strength, failure strength and density) are those at room temperature. Reproduced with permission from Ref. 1

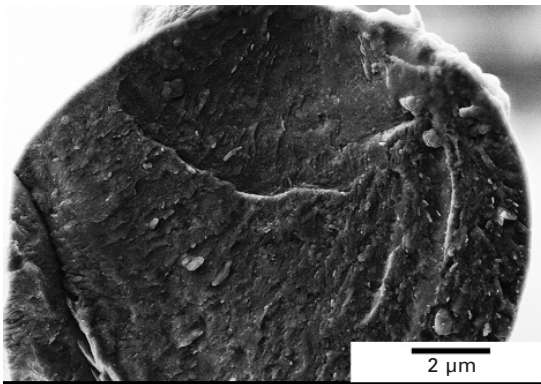
Producer <i>Fiber</i>	Composition (wt%)		Diameter ( $\mu\text{m}$ )	Density ( $\text{g}/\text{cm}^3$ )	Tensile strength/ modulus (MPa/GPa)	Production technique/ structure	Approx. price (2007)
3M <i>Nextel 720</i>	Al <sub>2</sub> O <sub>3</sub> :	85	10–12	3.4	2100/260	Sol-gel/59 vol% $\alpha$ -Al <sub>2</sub> O <sub>3</sub> + 41 vol% mullite	€ 790/kg (1500 den)
	SiO <sub>2</sub> :	15					€ 600/kg (3000 den)
3M <i>Nextel 610</i>	Al <sub>2</sub> O <sub>3</sub> : > 99		10–12	3.9	3100/380	Sol-gel/ $\alpha$ -Al <sub>2</sub> O <sub>3</sub>	€ 790/kg (1500 den) € 600/kg (3000 den) € 440/kg (10000 den)
3M <i>Nextel 550</i>	Al <sub>2</sub> O <sub>3</sub> :	73	10–12	3.03	2000/193	Sol-gel/ $\gamma$ -Al <sub>2</sub> O <sub>3</sub> + SiO <sub>2</sub> amorph.	€ 590/kg (2000 den)
	SiO <sub>2</sub> :	27					
3M <i>Nextel 440</i>	Al <sub>2</sub> O <sub>3</sub> :	70	10–12	3.05	2000/190	Sol-gel/ $\gamma$ -Al <sub>2</sub> O <sub>3</sub> + mullite + SiO <sub>2</sub> amorph.	€ 500/kg (2000 den)
	SiO <sub>2</sub> :	28					
	B <sub>2</sub> O <sub>3</sub> :	2					
3M <i>Nextel 312</i>	Al <sub>2</sub> O <sub>3</sub> :	62.5	10–12	2.7	1700/150	Sol-gel/mullite + amorph. or 100% amorph.	€ 260/kg (1800 den)
	SiO <sub>2</sub> :	24.5					
	B <sub>2</sub> O <sub>3</sub> :	13					
Sumitomo <i>Altex</i>	Al <sub>2</sub> O <sub>3</sub> :	85	10/15	3.3	1800/210	Polyaluminumoxane/ $\gamma$ -Al <sub>2</sub> O <sub>3</sub>	€ 640–720/kg
Nitivy <i>Nitivy ALF</i>	Al <sub>2</sub> O <sub>3</sub> :	72	7	2.9	2000/170	Sol-gel/ $\gamma$ -Al <sub>2</sub> O <sub>3</sub>	€ 390/kg (twisted yarn, twists:10–15)
	SiO <sub>2</sub> :	28					
Mitsui <i>Almax-B</i>	Al <sub>2</sub> O <sub>3</sub> :	60–80	7–10	2.9	Not available	Unknown/ $\delta$ -Al <sub>2</sub> O <sub>3</sub>	Price not available
	SiO <sub>2</sub> :	40–20					



(a)



(b)



(c)

11.5 Fracture surface of selected oxide fibers. (a) Nextel 610; (b) Nextel 720 (lower magnification); and (c) Nextel 720 (higher magnification).

nanofibers by the electrospinning process. A comprehensive discussion of this topic is outside the scope of this chapter. It is a rapidly evolving field and a large variety of oxide fibers are being developed using this process. Interested readers are referred to comprehensive reviews of this topic.<sup>148–150</sup>

## 11.4 Comparison of ceramic fibers

Sawyer and colleagues conducted one of the first comparative studies of several non-oxide fibers including Nicalon NLM-202 and NLP-102 (Si–C–O system) as well as the MPDZ, i.e. HPZ fibers (Si–C–N–O system) from Dow Corning.<sup>151</sup> They determined that the elementary composition has nearly no influence on the tensile strength at room temperature. All of the fibers that were studied displayed the brittle fracture behavior typical of ceramic fibers, with two typical strength-limiting defects: local defects on the fiber surface, and internal defects. Low tensile strengths were generally due to surface defects (i.e. cracks or pores), whereas fibers with greater tensile strength did not exhibit any apparent defects on the surface.

Lipowitz and colleagues also studied the same fibers with regard to their composition and structure.<sup>152</sup> All fibers were shown to be largely amorphous, except for SiC crystallites with diameters in the nanometer range in both Nicalon fibers NLM-202 and NLP-102. Crystallization did not occur until the fibers were exposed to temperatures above their manufacturing temperature, and also only if their composition changed toward the stoichiometry of a thermodynamically stable phase. This was the case for all of the fiber types studied at above 1400°C, as the amorphous phase decomposed above this temperature, releasing CO, SiO and N<sub>2</sub> and leaving only SiC and free carbon. Comprehensive studies of these fibers by means of TEM and EELS showed that curing in argon for 12 hours at 1400°C led to the formation of larger SiC crystallites in all fibers; however, in contrast to the SiCO fibers, both  $\alpha$ -SiC as well as  $\beta$ -SiC were found in the SiCNO fibers.<sup>153</sup>

Langley and colleagues compared the Si–C–O fibers Nicalon SGN, Nicalon CGN and MPS (Dow Corning) to the SiCNO fibers MPDZ-PhVi and HPZ from Dow Corning.<sup>154</sup> Compared to SiC whiskers or CVD-SiC fibers, the fibers that were studied exhibited a loss in strength during aging processes at above 1200°C due to crystallization and the formation of pores. However, the completely amorphous structure of the nitrogen-containing fibers delayed the crystallization of the thermodynamically stable phases to higher temperatures. These fibers were stable up to the decomposition temperature of the SiCNO structure (1400°C).

Lipowitz compared Nicalon, Tyranno and HPZ fibers with regard to their composition, structure and mechanical properties.<sup>155</sup> HPZ fibers proved to have greater thermal stability than Si(Ti)CO fibers both for oxidation over 100 h at 1000°C in air as well as for the two-hour aging process under

argon at 1400°C. Bodet and colleagues also studied the thermal stability of Nicalon and HPZ fibers. It was shown that both fibers had higher thermal stability in air than argon. The SiO<sub>2</sub> layer that formed in air impeded gaseous decomposition products from escaping. Under argon, the loss in strength of the Nicalon fibers was a result of SiC crystal growth and the decomposition of the SiCO phase; for the HPZ fibers, the progressive decomposition of the oxygen-rich surface was the primary factor for the reduction in mechanical properties.<sup>156</sup>

Pysher and colleagues compared the high-temperature tensile strengths of Nicalon and Tyranno fibers to that of selected alumina fibers.<sup>157</sup> Non-oxide fibers exhibit considerably greater strength up to 1400°C; however, at higher temperatures the thermodynamic stability is no longer assured as the fibers decompose. Al<sub>2</sub>O<sub>3</sub> fibers have higher Young's modulus values up to 1100°C and have much greater thermodynamic stability; however, the softening of the glass phase contained in their structure leads to a complete loss in strength at 1300°C. Bunsell and Berger compared commercially available SiC and alumina fibers.<sup>137</sup> The development of SiC fibers to a stoichiometric Si/C ratio enables the application of these reinforcing elements in fiber-reinforced composites up to a temperature of 1400°C. At higher temperatures, application is limited due to surface oxidation. Oxidized fibers are stable, but generally cannot be applied in ceramic composites due to their poor high-temperature creep behavior. Only Nextel-720 fibers have the potential for these extreme applications, provided contamination with alkali metals does not occur.

Almost all of the ceramic fibers obtained from polymeric or solution precursors contain between 5 and 25 vol% nanopores, which develop from the release of gaseous decomposition products during pyrolysis.<sup>158</sup> As the pyrolysis or heat treatment temperature increases, in many cases, pores coarsen and or additional porosity is generated due to decomposition of the amorphous matrix. This results in loss of strength. Villeneuve and colleagues used the SiCN(O) fibers described by Mocaer and colleagues<sup>121</sup> as well as Nicalon NLM-202 fibers for comparative studies of high-temperature tensile strength under reduced pressure (0.1 Pa) in an apparatus designed especially for this purpose.<sup>159</sup> They found that strength values decreased as the test temperature increased, with a very substantial drop occurring at above 1200°C due to the decomposition of the amorphous SiCO and SiCN(O) phases.

Lipowitz and Rabe were able to improve the mechanical properties of polymer-derived SiC, SiCO, SiCNO, and SiCN ceramic fibers by heat treating the fibers for 30 minutes at 1200°C with boron oxide in a carbon rich environment followed by sintering for one hour at 1800°C.<sup>160</sup> The boron is embedded in the fibers at 1200°C via the gas phase and acts as a sintering aid at higher temperatures to remove the porosity formed by the separation of molecular nitrogen and/or carbon monoxide at 1200°C. The fibers treated in this way consist largely of silicon carbide and free carbon.

Pailler and colleagues studied the influence of the curing method on the thermal stability of polycarbosilane and polysilazane-derived ceramic fibers.<sup>161</sup> They determined that the curing method has almost no impact on the mechanical properties up to a pyrolysis temperature of 1200°C. Fibers cured in air and that contain oxygen were less thermally stable at higher temperatures. An interesting and effective variant of SiCN fiber curing was found in the treatment with ozone due to the low levels of oxygen (2–4 atom%). However, the highest strength values have been measured for SiC fibers cured using electron beam irradiation.

Figure 11.6 is a summary of the literature values for room temperature tensile strength for the most significant commercially available non-oxide ceramic fibers that have been annealed, at high temperature, in air (Fig. 11.6(a)) or argon (Fig. 11.6(b)) under different conditions. It is clear that for both annealing treatments, the strength drops; however, annealing in air is more detrimental to fiber properties. As expected, Hi-Nicalon and Tyranno fibers have better performance than Nicalon-S. These results are important because in addition to the room temperature mechanical properties, the oxidation resistance and thermal stability are important properties in the evaluation of ceramic fibers from a technical and applications perspective.

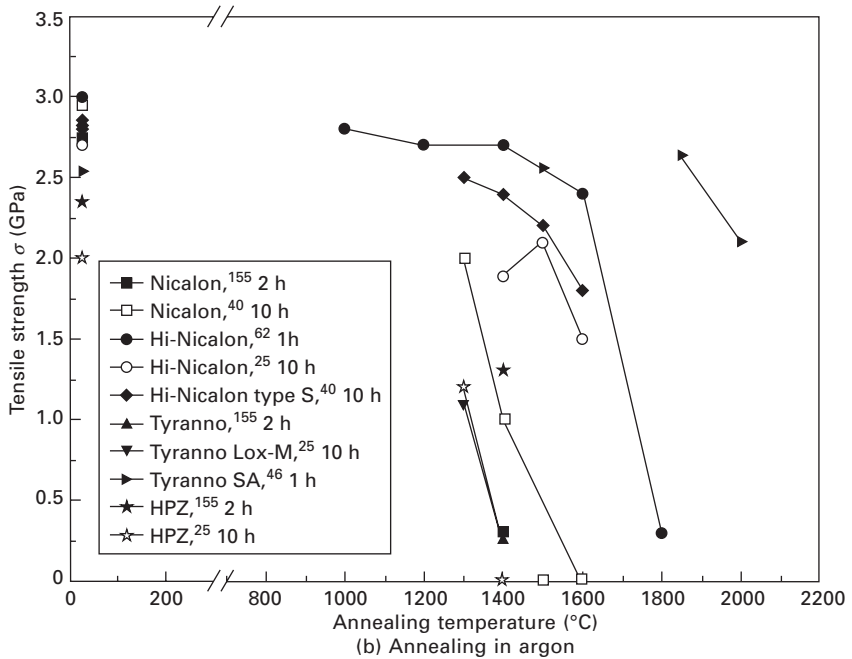
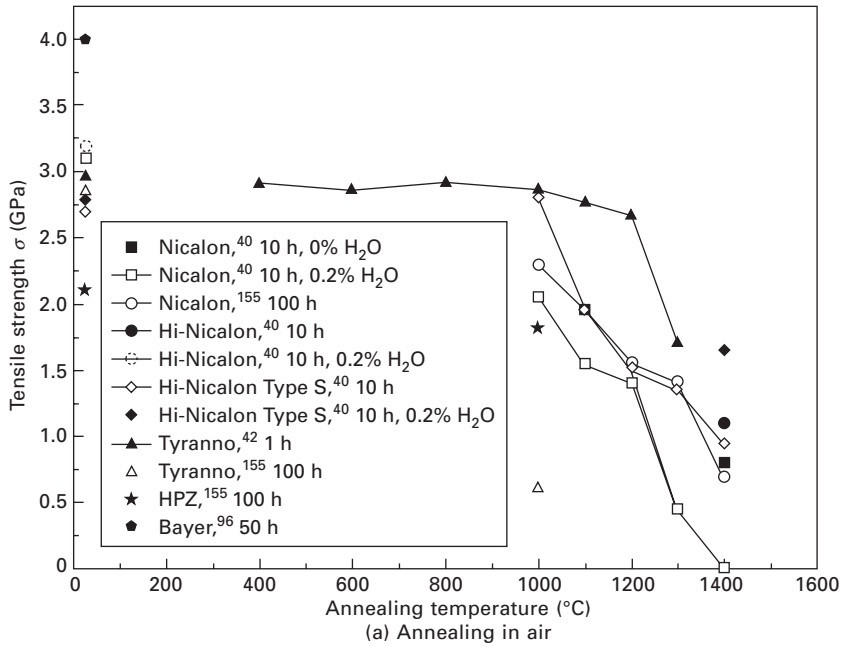
Wilson and Visser have compared the mechanical properties of high performance Nextel fibers.<sup>143</sup> They showed that the room temperature mean strength and Weibull modulus of the three types of fibers (single filament strength tests) were:

- Nextel 610: Mean strength 3.40 GPa, Weibull modulus 10.1
- Nextel 650: Mean strength 2.60 GPa, Weibull modulus 6.8
- Nextel 710: Mean strength 1.98 GPa, Weibull modulus 7.6.

The Weibull modulus obtained from the statistical sample (many filaments) compared well with the Weibull modulus calculated from fibers of different gauge length. High temperature strength was obtained both by measuring the strength of rowings (for six Nextel types of Nextel fibers) and by single filament tests for the high performance Nextel fibers. From the fiber rowing tests, the temperature for 70% of the room temperature strength retention was obtained as:

- Nextel 312: 950°C
- Nextel 440: 1200°C
- Nextel 550: 1300°C
- Nextel 610: 1300°C
- Nextel 650: 1400°C
- Nextel 720: >1400°C

From single filament strength tests, these temperatures (for 70% strength retention) were 1000°C for Nextel 610, 1100°C for Nextel 650 and 1200°C



11.6 Retained room-temperature tensile strength values from the literature for the most significant commercially available non-oxide ceramic fibers that have been annealed at high temperature in (a) air or (b) argon under different conditions.

for Nextel 720. The lower temperature in the single filament tests was attributed to the strain rate being three orders of magnitude lower for these tests compared to the strand tests. Finally, the creep behavior of Nextel 610, 650 and 720 was evaluated in air at 1100°C over a range of stress values. These results clearly show that the strain rates of 650 are one to several orders of magnitude lower than those of 610. The creep resistance of Nextel 720 is the highest (with a one to two orders of magnitude lower creep rate than Nextel 650).

## 11.5 Examples of current and anticipated applications

On account of their properties, ceramic fibers are suitable as an insulating material, e.g. as a refractory, and as reinforcement components in polymer, metallic and ceramic materials. Of particular interest are the ceramic matrix composites (CMCs) in which the fibers are integrated into a ceramic matrix. The aim with this type of composite is to overcome the characteristic brittle fracture behavior of ceramic materials, which can lead to a sudden, complete failure of the component. Embedding the fibers improves the mechanical properties of the matrix material, especially the resistance to cracking. The composite material displays a pseudo-plastic behavior with increased damage tolerance. This is due to a variety of energy absorbing mechanisms ahead and in the wake of cracks. These include crack deflection, crack bridging and fiber pullout. An excellent review of various toughening mechanisms in ceramics is presented in Ref. 162. As shown in this review article and by numerous studies, properly designed continuous fiber reinforced ceramics are extremely damage tolerant with a high toughness. In addition, because of the ceramic matrix, these composites have the other advantages traditionally associated with ceramics (e.g. chemical and oxidation resistance, high temperature capability). For example, in contrast to C/SiC materials SiC<sub>f</sub>/SiC composites offer outstanding oxidation stability at elevated temperatures. These high temperature structural applications are being actively pursued. For example, SiC<sub>f</sub>/SiC composites offer high potential for use in combustion chambers and gas turbines to improve the energy efficiency<sup>163–168</sup> as well as for friction applications like brake discs<sup>169</sup> and friction bearings.<sup>170</sup> These composites suffer from two problems which have limited their widespread use: their lack of long-term durability in a combustion environment, and their high cost. Various approaches to improving their long-term durability and to reduce the cost, of both fibers and composites, are active and important areas of research and development.

Non-oxide ceramic fiber reinforced composites have also found some niche applications. Due to their combination of properties like mechanical strength, oxidation and thermal stability and resistance against irradiation,



$\text{SiC}_f/\text{SiC}$  composites are very interesting for future fusion power reactors.<sup>171-176</sup> Piezoresistive properties of silicon carbide fibers and their applications as sensors (for example, to measure in-service loads in components) are being investigated.<sup>177,178</sup>

There is considerable current interest in developing oxide fiber reinforced oxide matrix composites.<sup>179</sup> This is because these composites are stable for long duration in a combustion environment. This makes them attractive for a range of power generation systems for both land-based and aerospace turbines and rockets. Development of appropriate oxide fiber coatings (with weak bonding either to the matrix or to the fiber) has led to composites with high toughness.<sup>180,181</sup> In addition, the design of porous matrices has also led to the development of damage-tolerant composites.<sup>182</sup> As a result, these composites are being actively developed for a broad range of thermostructural applications. In many respects, these composites may realize the true potential of ceramics (high temperature load-bearing applications in an oxidizing environment).

Metal matrix composites have been and are being developed from both oxide and non-oxide ceramic fibers. The alumina based fibers are ideal reinforcements for aluminum matrix composites.<sup>183</sup> Titanium matrix composites have been made using the large diameter SiC fibers (e.g. SCS-6).<sup>184-186</sup>

## 11.6 Research and development priorities

In contrast to the widely used carbon fibers, applications of ceramic fibers are still limited to a few niche products due to either their high prices and limited commercial availability or their insufficient mechanical (oxide fibers) and oxidation (non-oxide fibers) stability at elevated temperatures. The development of ceramic fibers is one of the most complicated technologies and requires significant patience, resources and experience. To overcome the drawbacks of the current ceramic fibers it is necessary to discuss the different fiber types separately. The use of oxide fibers is limited by their low creep resistance at elevated temperatures. Therefore further research activities should be focused on the improvement of the ceramic micro- and nanostructure, e.g. by adding additives which reduce the creep rate and stabilize the microstructure. Some promising areas that are being currently investigated include the development of spinel and mullite fibers, and the development of large grain (almost single crystal) fibers. Non-oxide ceramic fibers possess good mechanical properties in an inert atmosphere at higher temperatures if the oxygen content of the fiber is low. Depending on their chemical composition, non-oxide ceramic fibers oxidize at elevated temperatures, which leads to a strong decrease in the mechanical properties. To improve the oxidation resistance it is necessary to reduce the oxygen content of the fibers or to develop new precursor systems on the basis of



elements such as, for example, aluminum and hafnium. From a fundamental point of view, a comprehensive review article of the various approaches to designing microstructures of ceramics for high temperature applications is presented in Ref. 187. In the non-oxide fibers, there is an additional trade-off between modulus and strength. Amorphous fibers have high strength but low modulus. Crystallization leads to an increase in the modulus (if porosity is minimized) but a drop in strength.

Regardless of the type of ceramic fiber (oxide or non-oxide), it is very important to reduce the production costs which result from both the fiber manufacturing and the precursor processing. A remarkable cost reduction is only possible if the synthesis of the fiber precursor is cheap and reproducible, and if the subsequent ceramic fiber manufacture is possible in a continuous process. Moreover, a significant cost reduction is achievable by the production of higher quantities. It has been shown that significant cost reduction will lead to the application of ceramic fibers in broad-based applications. Statements from the industry lead to a price barrier of approximately \$750 per kilogram for high performance fibers, to open markets for applications with large volume needs (chemical, automotive, thermo-structural, etc.).

## 11.7 Summary and conclusions

High performance continuous ceramic fibers are needed for a broad range of thermo-structural applications. In particular, the target applications are reinforcements for ceramics and metals matrices. Although there are niche applications (e.g. nuclear fusion), in order for these fibers to be attractive they need to outperform the readily available glass and carbon fibers. As a result, the focus of both the development activities and of this chapter has been on fibers that have higher temperature capability than glass or carbon fibers in an oxidizing environment. Two broad classes of small-diameter fibers are available and are being developed.

Non-oxide fibers are primarily based on the SiC or the SiN system. A broad range of polymeric precursor-derived fibers are commercially available and further improvements and developments are taking place at the pilot plant and lab scale. As a class, the commercially available fibers consist of a small fraction of nanocrystals in an amorphous matrix. They have good strength (2.5 to 3.5 GPa) and intermediate to high modulus (250 to 420 GPa). In an inert environment, these fibers retain their strength to temperatures in the range of 1400–1800°C, while in an oxidizing environment the strength is retained up to a temperature range of 1000–1500°C. Long-term use in structural applications is limited to temperatures less than 1400°C in an oxidizing environment for the best fiber. Another issue is the high temperature stability of these fibers in a water vapor-containing environment (e.g. combustor). The research and development activities are focused on improving the high

temperature performance (specially in an oxidizing moist environment) and on reducing the cost.

The high performance oxide fibers are predominantly based on  $\text{Al}_2\text{O}_3$ . The commercially available small-diameter fibers are made from salt-solution or organometallic sol derived gels. The strength of these fibers is in the range of 1.7 to 3 GPa and the modulus is in the range of 150 to 360 GPa. The main attraction of these fibers (as compared to non-oxide) is similar high temperature performance in both oxidizing and inert environments. These fibers can be broadly classified into three categories. The low temperature fibers consist of nanocrystals of transitional alumina phases in an amorphous matrix. A significant strength drop for these fibers occur in the temperature range of 900–1200°C although, due to creep, their use in long-term applications is limited to temperatures under 800°C. The intermediate temperature fibers are almost pure  $\alpha\text{-Al}_2\text{O}_3$ . These fibers show a strength drop in the range of 1200–1300°C and can be used in long-term applications up to a temperature range of 900–1000°C. The high temperature fibers are composite oxide fibers (alumina with zirconia or mullite). These fibers retain their short-term strength to 1400°C and can be used in long-term applications in the temperature range of 1100–1200°C. For these fibers also, the focus of ongoing research and development activities is in the area of cost reduction and increase in use temperature (while retaining room temperature strength).

## 11.8 Sources of further information and advice

### *Suppliers of ceramic fibers*

Listed below are the contact details for the major suppliers of ceramic fibers. The companies' main websites are also listed and from these pages links are provided to information on the ceramic fibers.

- 3M  
<http://www.3m.com/>  
 3M Corporate Headquarters  
 St Paul, MN 55144-1000, USA  
 Phone: +1-888-3M HELPS (+1-888-364-3577)
- AVCO  
<http://www.avco.at/AVCO.aspx>  
 Austrian Private Equity and Venture Capital Organisation  
 Mariahilfer Straße 54/3/6  
 A-1070 Wien, Austria  
 Phone: +43 1 526 38 05-0 Fax: +43 1 526 38 05-10  
 email: office@avco.at
- COI Ceramics  
<http://www.coiceramics.com/>  
 9617 Distribution Ave

San Diego, CA 92121, USA  
Phone: +1-858-621-5700 Fax: +1-858-621-7451  
E-mail: coiceramics@coiceramics.com

- Carborundum  
<http://www.carborundumabrasives.com/>  
Saint-Gobain Abrasives, Inc.  
8 rue de la Taxe-BP 45  
F28111 Luce Cedex, France  
Phone: +33-237-916413 Fax: +33-237-342855
- Denka  
<http://www.denka.co.jp/eng/product/>  
Nihonbashi Mitsui Tower  
1-1, Nihonbashi-Muromachi 2-chome  
Chuo-ku, Tokyo 103-8338, Japan  
Phone: +81-3-5290-5055 Fax: +81-3-5290-5059
- Nippon Carbon  
[http://www.carbon.co.jp/english/index\\_e.html](http://www.carbon.co.jp/english/index_e.html)  
6-1, Hacchobori 2-chome  
Chuo-ku, Tokyo 104-0032, Japan  
Phone: +81-3-3552-6111 Fax: +81-3-3553-4694
- Nitivy  
<http://www.nitivy.co.jp/english/>  
Katakura Bldg, 1-2, 3-chome  
Kyobashi, Chuo-ku, Tokyo 104-0031, Japan  
Phone : +81-3-3272-6901 Fax : +81-3-3281-2729
- Sumitomo  
<http://www.sumitomocorp.co.jp/english/>  
Sumitomo Corporation Headquarters  
Harumi Island Triton Square Office Tower Y  
1-8-11 Harumi  
Chuo-ku, Tokyo, Japan
- Textron  
<http://www.textron.com/>  
Textron World Headquarters  
40 Westminster Street  
Providence, RI 02903, USA  
Phone: +1-401-421-2800
- UBE Industries  
<http://www.ube-ind.co.jp/english/>  
Seavans North Bldg, 1-2-1, Shibaura  
Minato-Ku,  
Tokyo 105-8449, Japan  
Phone : +81-3-5419-6110 Fax : +81-3-5419-6230

*Selected research groups with active programs in development of new structural ceramic fibers*

- Université Claude Bernard Lyon  
[www.univ-lyon1.fr/](http://www.univ-lyon1.fr/)  
 Laboratoire des Multimatériaux et Interfaces, UMR CNRS  
 43 boulevard du 11 novembre 1918  
 69622 Villeurbanne cedex, France
- University of Bayreuth  
<http://www.ima-keramik.uni-bayreuth.de/>  
 Ceramic Materials Engineering (CME)  
 95440 Bayreuth, Germany
- ITCF Denkendorf  
<http://www.itcf-denkendorf.de/>  
 Körschtalstraße 26  
 73770 Denkendorf, Germany
- Fraunhofer ISC Würzburg  
<http://www.isc.fraunhofer.de/>  
 Neunerplatz 2  
 97082 Würzburg, Germany
- Technical University Darmstadt  
<http://www.tu-darmstadt.de/fb/ms/fg/df/index.html>  
 Institut für Materialwissenschaft  
 Petersenstr. 23  
 64287 Darmstadt, Germany
- University of Trento  
[www.ing.unitn.it/users/soraru/home.html](http://www.ing.unitn.it/users/soraru/home.html)  
 DIMTI  
 Via Mesiano 77  
 38050 Trento, Italy
- Max-Planck-Institut für Metallforschung  
<http://aldix.mpi-stuttgart.mpg.de/>  
 Institut für Nichtmetallische Anorganische Materialien  
 Heisenbergstr. 1  
 70569 Stuttgart, Germany

*Technical reports*

- In 1998, the National Research Council of the United States published a comprehensive study on the status of ceramic fibers and coatings and recommended promising directions for research and development. This report is titled 'Ceramic Fibers and Coatings: Advanced Materials for the Twenty First Century'. It is available from the National Academy Press,

Box 285, 2101 Constitution Ave., N.W., Washington, DC 20055. URL: <http://www.nap.edu>. An executive summary of the report is available at <http://www.nap.edu/html/ceramic/#summ>

- In 2004, SRI Consulting published a report on ‘Speciality Inorganic Fibers’. An abstract of the report together with the Table of Contents is available at <http://www.sriconsulting.com/CEH/Public/Reports/542.6000/>

## 11.9 Acknowledgements

The authors would like to thank Dr Juergen Hacker (POLYNT GmbH, Miehlen, Germany), Tobias Kraus, Franziska Gugel (both University of Bayreuth, Germany), and Dr Bernd Clauss (ITCF Denkendorf, Germany) for their help in the preparation of this chapter. RKB would like to thank the Alexander von Humboldt-Stiftung (Research Award for Senior Scientists to RKB) and the US Department of Energy, Office of Fossil Energy (Grant No. DE-FG26-05NT42528) for partial financial support for this work. RKB would also like to thank the Institute of Glass and Ceramics (WW3), University of Erlangen-Nürnberg, for hosting him as a Guest Professor during the preparation of this chapter.

## 11.10 References

1. B. Clauss, ‘Fibers for ceramic matrix composites’, in *Ceramic Matrix Composites*, ed. W. Krenkel, Wiley-VCH Verlag, Weinheim, Germany, 2008, 1–19.
2. G. Fritz, J. Grobe, D. Kummer, ‘Carbosilanes’, *Adv. Inorg. Chem. Radiochem.*, 1965 **7** 349–418.
3. D. Belitskus, ‘Fibers and whiskers for ceramic reinforcement’, in *Fiber and Whisker Reinforced Ceramics for Structural Applications*, ed. D. Belitskus, Marcel Dekker, New York, 1993, 45–92.
4. S. Yajima, K. Okamura, J. Hayashi, M. Omori, ‘Synthesis of continuous SiC fibers with high tensile strength’, *J. Am. Ceram. Soc.*, 1976 **59** (7/8) 324–327.
5. S. Yajima, Y. Hasegawa, J. Hayashi, M. Imura, ‘Synthesis of continuous silicon carbide fibre with high tensile strength and high Young’s modulus. Part 1. Synthesis of polycarbosilane as precursor’, *J. Mater. Sci.*, 1978 **13** 2569–2576.
6. S. Yajima, J. Hayashi, M. Omori, ‘Silicon carbide fibers having a high strength and a method for producing said fibers’, US Patent 4,100,233, 1978.
7. Y. Hasegawa, M. Imura, S. Yajima, ‘Synthesis of continuous silicon carbide fibre, Part 2: Conversion of polycarbosilane fibre into silicon carbide fibres’, *J. Mater. Sci.*, 1980 **15** 720–728.
8. T. Taki, K. Okamura, M. Sato, ‘A study of the oxidation curing mechanism of polycarbosilane fibre by solid-state high-resolution nuclear magnetic resonance’, *J. Mater. Sci.*, 1989 **24** 1263–1267.
9. K. Okamura, ‘Ceramic fibers from polymer precursors’, *Composites*, 1987 **18** 107–120.
10. Y. Hasegawa, K. Okamura, S. Yajima, ‘Polycarbosilane, process for its production, and its use as material for producing silicon carbide fibers’, US Patent 4,283,376, 1980.

11. S. Yajima, 'Special heat-resisting materials from organometallic polymers', *Am. Ceram. Soc. Bull.*, 1983 **62** (8) 893–898.
12. Produktinformation, 'Nicalon<sup>®</sup>': Thermische Stabilität, mechanische Eigenschaften, Bezeichnungsschlüssel, Nippon Carbon Co. Ltd, Tokyo, October 1986.
13. P. Le Coustumer, M. Monthieux, A. Oberlin, 'Understanding Nicalon<sup>®</sup> fibre', *J. Europ. Ceram. Soc.*, 1993 **11** 95–103.
14. C. Laffon, A.M. Flank, P. Lagarde, M. Laridjani, R. Hagege, P. Olry, J. Cotteret, J. Dixmier, J.L. Miquel, H. Hommel, A.P. Legrand, 'Study of Nicalon-based ceramic fibres and powders by EXAFS spectrometry, X-ray diffractometry and some additional methods', *J. Mater. Sci.*, 1989 **24** 1503–1512.
15. T. Mah, N.L. Hecht, D.E. McCullum, J.R. Hoenigman, H.M. Kim, A.P. Katz, H.A. Lipsitt, 'Thermal stability of SiC fibres (Nicalon<sup>®</sup>)', *J. Mater. Sci.*, 1984 **19** 1191–1201.
16. K.L. Luthra, 'Thermochemical analysis of the stability of continuous SiC fibers', *J. Am. Ceram. Soc.*, 1986 **69** (10) C231–C233.
17. C. Vahlas, P. Rocabois, C. Bernard, 'Thermal degradation mechanisms of nicalon fibre: a thermodynamic simulation', *J. Mater. Sci.*, 1994 **29** 5839–5846.
18. S.M. Johnson, R.D. Brittain, R.H. Lamoreaux, D.J. Rowcliffe, 'Degradation mechanisms of silicon carbide fibers', *J. Am. Ceram. Soc.*, 1988 **71** (3) C132–C135.
19. E. Bouillon, D. Mocaer, J.F. Villeneuve, R. Pailler, R. Naslain, M. Monthieux, A. Oberlin, C. Guimon, G. Pfister, 'Composition–microstructure–property relationships in ceramic monofilaments resulting from the pyrolysis of a polycarbosilane precursor at 800 to 1400°C', *J. Mater. Sci.*, 1991 **26** 1517–1530.
20. T. Shimoo, H. Chen, K. Okamura, 'Mechanism of oxidation of Si–C–O fibers', *J. Ceram. Soc. Jpn., Int. Ed.*, 1992 **100** 918–924.
21. Y.T. Zhu, S.T. Taylor, M.G. Stout, D.P. Butt, T.C. Lowe, 'Kinetics of thermal, passive oxidation of Nicalon fibers', *J. Am. Ceram. Soc.*, 1998 **81** (3) 655–660.
22. T. Seguchi, N. Kasai, K. Okamura, H. Ichikawa, M. Takeda, M. Nishii, 'Super heat-resistant silicon carbide fibers and process for producing the same', US Patent 5,283,044, 1993.
23. T. Taki, K. Okamura, M. Sato, T. Seguchi, S. Kawanishi, 'A study on the electron irradiation curing mechanism of polycarbosilane fibres by solid-state <sup>29</sup>Si high-resolution nuclear magnetic resonance spectroscopy', *J. Mater. Sci. Lett.*, 1988 **7** 209–211.
24. M. Takeda, Y. Imai, H. Ichikawa, T. Ishikawa, T. Seguchi, K. Okamura, 'Properties of the low oxygen content SiC fiber on high temperature heat treatment', *Ceram. Eng. Sci.*, 1991 **12** (7/8) 1007–1018.
25. M. Takeda, Y. Imai, H. Ichikawa, T. Ishikawa, N. Kasai, T. Seguchi, K. Okamura, 'Thermal stability of the low oxygen silicon carbide fibers derived from polycarbosilane', *Ceram. Eng. Sci.*, 1992 **13** 209–217.
26. M. Takeda, Y. Imai, H. Ichikawa, T. Ishikawa, N. Kasai, T. Seguchi, K. Okamura, 'Thermomechanical analysis of the low oxygen silicon carbide fibers derived from polycarbosilane', *Ceram. Eng. Sci.*, 1993 **14** (9/10) 540–547.
27. T. Shimoo, I. Tsukada, T. Seguchi, K. Okamura, 'Effect of firing temperature on the thermal stability of low-oxygen silicon carbide fibers', *J. Am. Ceram. Soc.*, 1998 **81** (8) 2109–2115.
28. G. Chollon, R. Pailler, R. Naslain, P. Olry, 'Correlation between microstructure and mechanical behaviour at high temperatures of a SiC fibre with a low oxygen content (Hi-Nicalon)', *J. Mater. Sci.*, 1997 **32** 1133–1147.

29. G. Chollon, R. Pailler, R. Naslain, F. Laanani, M. Monthieux, P. Olry, 'Thermal stability of a PCS-derived SiC fibre with a low oxygen content (Hi-Nicalon)', *J. Mater. Sci.*, 1997 **32** 327–347.
30. T. Shimoo, M. Ho, K. Okamura, M. Takeda, 'Effect of vacuum heat treatment on electron-beam-irradiation-cured polycarbo-silane fibers', *J. Am. Ceram. Soc.*, 2001 **84** (1) 111–116.
31. G. Chollon, M. Czerniak, R. Pailler, X. Bourrat, R. Naslain, J.P. Pillot, R. Cannet, 'A model SiC-based fibre with a low oxygen content prepared from a polycarbo-silane precursor', *J. Mater. Sci.*, 1997 **32** 893–911.
32. T. Shimoo, F. Toyoda, K. Okamura, 'Thermal stability of low-oxygen silicon carbide fiber (Hi-Nicalon) subjected to selected oxidation treatment', *J. Am. Ceram. Soc.*, 2000 **83** (6) 1450–1456.
33. C. Vahlas, F. Laanani, M. Monthieux, 'Thermodynamic approach to the oxidation of Hi-Nicalon<sup>TM</sup> fiber', *J. Am. Ceram. Soc.*, 1999 **82** (9) 2514–2516.
34. T. Shimoo, I. Tsukada, T. Seguchi, K. Okamura, 'Thermal stability of low-(oxygen) SiC fiber (Hi-Nicalon) treated in a hot isostatic press', *J. Am. Ceram. Soc.*, 1999 **82** (12) 3508–3512.
35. M. Takeda, J. Sakamoto, Y. Imai, H. Ichikawa, T. Ishikawa, 'Properties of stoichiometric silicon carbide fiber derived from polycarbosilane', *Ceram. Eng. Sci.*, 1994 **15** (4) 133–141.
36. M. Takeda, Y. Imai, H. Ichikawa, J. Sakamoto, 'Process for producing silicon carbide fibers', Patent EP 0653391 B1, 1995.
37. M. Takeda, A. Saeki, J. Sakamoto, Y. Imai, H. Ichikawa, 'Effect of hydrogen atmosphere on pyrolysis of cured polycarbosilane fibers', *J. Am. Ceram. Soc.*, 2000 **83** (5) 1063–1069.
38. A. Saeki, M. Takeda, H. Ichikawa, J. Sakamoto, 'Process for producing silicon carbide fibers', Patent EP 0744390 A3 B1, 1996.
39. M. Takeda, J. Sakamoto, A. Saeki, Y. Imai, H. Ichikawa, 'High performance silicon carbide fiber Hi-Nicalon for ceramic matrix composites', *Ceram. Eng. Sci.*, 1995 **16** (4/5) 37–44.
40. M. Takeda, A. Urano, J. Sakamoto, Y. Imai, 'Microstructure and oxidation behaviour of silicon carbide fibers derived from polycarbosilane', *J. Am. Ceram. Soc.*, 2000 **83** (5) 1171–1176.
41. F. Rebillat, A. Guette, L. Espitalier, R. Naslain, 'Chemical and mechanical degradation of Hi-Nicalon and Hi-Nicalon-S fibers under CVD/CVI BN processing conditions', *Key Eng. Mater.*, 1999 **164–165** 31–34.
42. T. Yamamura, T. Ishikawa, M. Shibuya, T. Hisayuki, K. Okamura, 'Development of a new continuous Si–Ti–C–O fibre using an organometallic polymer precursor', *J. Mater. Sci.*, 1988 **23** 2589–2594.
43. M. Kuntz, 'Keramische Faserverbundwerkstoffe', in *Das Keramiker-Jahrbuch 2001*, Ceramic Forum International, Bauverlag, 2001, Kapitel, *Lehrbuch-Technische Keramik* **15**, 54–71.
44. K. Kakimoto, T. Shimoo, K. Okamura, 'Oxidation-induced microstructural change of Si–Ti–C–O fibers', *J. Am. Ceram. Soc.*, 1998 **81** 409–412.
45. T. Ishikawa, S. Kajii, T. Hisayuki, K. Matsunaga, T. Hogami, Y. Kohtoku, 'New type of sintered SiC fiber and its composite material', *Key Eng. Mater.*, 1999 **164–165** 15–18.
46. T. Ishikawa, Y. Kohtoku, K. Kumagawa, T. Yamamura, T. Magasawa, 'High strength alkali-resistant sintered SiC fibre stable to 2200°C', *Nature*, 1998 **391** 773–775.

47. W.H. Atwell, D.R. Bujalski, E.J. Joffre, G.E. LeGrow, J. Lipowitz, J.A. Rabe, 'Preparation of substantially polycrystalline silicon carbide fibers from polyorgano-siloxanes', Patent EP 0435065 B1, 1991.
48. D.C. Deleeuw, J. Lipowitz, P.P.-Y. Lu, 'Preparation of substantially crystalline silicon carbide fibers from polycarbosilane', Patent EP 0438117 B1, 1991.
49. J. Lipowitz, J.A. Rabe, A. Zangvil, Y. Xu, 'Structure and properties of SYLRAMIC<sup>TM</sup> silicon carbide fiber – a polycrystalline, stoichiometric  $\beta$ -SiC composition', *Ceram. Eng. Sci.*, 1997 **18** (3) 147–157.
50. D.C. Deleeuw, J. Lipowitz, J.A. Rabe, 'Preparation of substantially crystalline silicon carbide fibers from methylpoly-disilylazanes', US Patent 5,268,336, 1993.
51. D.C. Deleeuw, J. Lipowitz, P.P.-Y. Lu, J.A. Rabe, 'Preparation of substantially crystalline silicon carbide fibers from methylpoly-silanes', Canadian Patent 2,030,117, 1998.
52. T.D. Barnard, G.A. Zank, D.R. Bujalski, 'Preparation of substantially crystalline silicon carbide fibers from borosilazanes', US Patent 5,863,848, 1999.
53. M. Narisawa, S. Kitano, K. Okamura, M. Itoh, 'Synthesis of silicon carbide fiber from blended precursor of organosilicon polymers', *J. Am. Ceram. Soc.*, 1995 **78** (1) 3405–3408.
54. A. Idesaki, M. Narisawa, K. Okamura, M. Sugimoto, Y. Morita, T. Seguchi, M. Itoh, 'SiC-based fibers synthesized from hybrid polymer of polycarbosilane and polyvinylsilane', *Key Eng. Mater.*, 1999 **164–165** 39–42.
55. M. Narisawa, A. Idesaki, S. Kitano, K. Okamura, M. Sugimoto, T. Seguchi, M. Itoh, 'Use of blended precursors of poly(vinylsilane) in polycarbosilane for silicon carbide fiber synthesis with radiation curing', *J. Am. Ceram. Soc.*, 1999 **82** (4) 1045–1051.
56. A. Tazi Hemida, R. Pailler, R. Naslain, 'Continuous SiC-based model monofilaments with a low free carbon content. Part I: From the pyrolysis of a polycarbosilane precursor under an atmosphere of hydrogen', *J. Mater. Sci.*, 1997 **32** 2359–2366.
57. A. Tazi Hemida, M. Birot, J.P. Pillot, J. Dunogues, R. Pailler, 'Synthesis and characterization of new precursors to nearly stoichiometric SiC ceramics', *J. Mater. Sci.*, 1997 **32** 3475–3483.
58. A. Tazi Hemida, R. Pailler, R. Naslain, J.P. Pillot, M. Birot, J. Dunogues, 'Continuous SiC-based model monofilaments with a low free carbon content. Part II: From the pyrolysis of a novel copolymer precursor', *J. Mater. Sci.*, 1997 **32** 2367–2372.
59. A. Tazi Hemida, R. Pailler, M. Birot, J.P. Pillot, J. Dunogues, 'Modification of SiC precursors with an amine–borane complex', *J. Mater. Sci.*, 1997 **32** 3237–3242.
60. A. Tazi Hemida, H. Tenaillieu, L. Bardeau, R. Pailler, M. Birot, J.P. Pillot, J. Dunogues, 'A quasi-stoichiometric SiC-based experimental fibre obtained from a boron-doped polycarbosilane precursor', *J. Mater. Sci.*, 1997 **32** 5791–5796.
61. W. Toreki, C. Batich, 'SiC fibers having low oxygen content and methods of preparation', Patent WO 9307103, 1992.
62. M.D. Sacks, 'Effect of composition and heat treatment conditions on the tensile strength and creep resistance of SiC-based fibers', *J. Europ. Ceram. Soc.*, 1999 **19** 2305–2315.
63. M.D. Sacks, A.A. Morrone, G.W. Scheiffele, M. Saleem, 'Characterization of polymer-derived silicon carbide fibers with low oxygen content, near-stoichiometric composition and improved thermomechanical stability', *Ceram. Eng. Sci.*, 1995 **16** 25–35.



64. M.D. Sacks, G.W. Scheiffele, L. Zhang, Y. Yang, J.J. Brennan, 'Polymer-derived SiC-based fibers with high tensile strength and improved creep resistance', *Ceram. Eng. Sci.*, 1998 **19** (3) 73–86.
65. M.D. Sacks, 'Creep-resistant, high-strength silicon carbide fibers', US Patent 6,069,102, 2000.
66. W. Verbeek, G. Winter, 'Formkörper aus Siliciumcarbid und Verfahren zu ihrer Herstellung', German Patent 2,236,078, 1974.
67. R. Richter, G. Roewer, E. Brendler, H. Krämer, H.-P. Martin, E. Müller, 'Synthesis and spinning of new polysilanes as SiC fiber precursors', in *Advanced Structural Fiber Composites*, 1995, 53–60.
68. H.-P. Martin, E. Brendler, E. Müller, R. Richter, G. Roewer, 'Conversion of polycarbosilane fibers into SiC fibers', in *Advanced Structural Fiber Composites*, 1995, 45–52.
69. J. Clade, E. Seider, D. Sporn, 'A new type of precursor for fibers in the system Si-C', *J. Europ. Ceram. Soc.*, 2005 **25** 123–127.
70. V. Frey, B. Pachaly, N. Zeller, 'Process for preparing silicon carbide fibers', US Patent 4,824,651, 1989.
71. Z.-F. Zhang, C.S. Scotto, R.M. Laine, 'Pure silicon carbide fibers from polymethylsilane', *Ceram. Eng. Sci.*, 1994 **15** 152–161.
72. R.M. Laine, F. Babonneau, J.A. Rahn, Z.-F. Zhang, K.A. Youngdahl, 'The effect of monomer architecture on selectivity to ceramic products and microstructure, in *Silicon Pre ceramic Polymers*, 37. Sagamore Army Mater. Res. Conf. Proc., ed. D. J. Viechnicki, Publications Department of the Army, 1991, 159–169.
73. R.M. Laine, Z.-F. Zhang, K.W. Chew, M. Kannisto, C. Scotto, 'Synthesis and Processing of silicon carbide fibers: state-of-the-art', *Ceram. Proc. Sci. Tech., Ceram. Trans.*, Friedrichshafen, 1994 **81** 179–185.
74. S. Lu, B. Rand, K.D. Bartle, 'Carbon-silicon alloy fibers: optimizing tensile properties by control of the stabilization stage', *J. Mater. Res.*, 1999 **14** (9) 3604–3613.
75. J.D. Bolt, S.M. Dinh, L.A. Silverman, 'Silicon carbide fibers and a process for preparing them', US Patent 4,942,011, 1989.
76. F.J. Frechette, R.S. Storm, V. Venkatswaren, M.J. Andrejczak, J.J. Kim, 'Process for making silicon carbide ceramic fibers', US Patent 5,354,527, 1994.
77. H. Tenailleau, X. Bourrat, R. Naslain, R.E. Tressler, L.A. Giannuzzi, 'TEM/EELS characterization of a sintered polycrystalline silicon carbide fiber', *J. Am. Ceram. Soc.*, 1998 **81** (8) 2037–2044.
78. K.K. Chawla, 'Ceramic reinforcements', in *Ceramic Matrix Composites*, ed. K. K. Chawla, Chapman & Hall, London, 1993, 45–125.
79. R.T. Bhatt, D.R. Hull, 'Strength-degrading mechanisms for chemically-vapor-deposited SCS-6 silicon carbide fibers in an argon environment', *J. Am. Ceram. Soc.*, 1998 **81** (4) 957–964.
80. M. Arai, S. Sakurada, T. Isoda, T. Tomizawa, 'Pre ceramic polysilazane to silicon nitride', *Polym. Prepr.*, 1987 **28** (1) 407–408.
81. M. Arai, O. Funayama, H. Nishii, T. Isoda, 'High-purity silicon nitride fibers', US Patent 4,818,611, 1989.
82. H. Aoki, T. Suzuki, T. Katahata, M. Haino, G. Nishimura, H. Kaya, K. Tamura, T. Isoda, 'Silicon nitride-based fibers and composite material reinforced with fibers', US Patent 5,151,390, 1992.
83. H. Aoki, T. Suzuki, T. Katahata, M. Haino, G. Nishimura, H. Kaya, T. Isoda, Y. Tashiro, O. Funayama, M. Arai, 'Silicon nitride based ceramic fibers, process of

- preparing same and composite material containing same', Patent EP 0344870 A3, 1989.
84. O. Funayama, M. Arai, Y. Tashiro, H. Aoki, T. Suzuki, K. Tamura, H. Kaya, H. Nishii, T. Isoda, 'Tensile strength of silicon nitride fibers produced from perhydropolysilazane', *J. Ceram. Soc. Jpn, Int. Ed.*, 1990 **98** 107–109.
  85. Y. Yokoyama, T. Nanba, I. Yasui, H. Kaya, T. Maeshima, T. Isoda, 'X-ray diffraction study of the structure of silicon nitride fiber made from perhydropolysilazane', *J. Am. Ceram. Soc.*, 1991 **74** (3) 654–657.
  86. K. Sato, T. Suzuki, O. Funayama, T. Isoda, 'Fabrication of silicon nitride based composites by impregnation with perhydro-polysilazane', *J. Ceram. Soc. Jpn, Int. Ed.*, 1992 **100** (4) 444–447.
  87. K. Sato, T. Suzuki, O. Funayama, T. Isoda, 'Preparation of carbon fiber reinforced composite by impregnation with perhydro-polysilazane followed by pressureless firing', *Ceram. Eng. Sci.*, 1992 **13** 614–621.
  88. O. Funayama, T. Kato, Y. Tashiro, T. Isoda, 'Synthesis of a polyborosilazane and its conversion into inorganic compounds', *J. Am. Ceram. Soc.*, 1993 **76** (3) 717–723.
  89. O. Funayama, H. Nakahara, A. Tezuka, T. Isoda, 'Development of Si–B–O–N fibres from polyborosilazane', *J. Mater. Sci.*, 1994 **29** 2238–2244.
  90. O. Funayama, Y. Tashiro, T. Aoki, T. Isoda, 'Synthesis and pyrolysis of polyaluminosilazane', *J. Ceram. Soc. Jpn*, 1994 **102** 905–909.
  91. G.D. Sorarù, M. Mercadini, R. Dal Maschio, F. Taulelle, F. Babonneau, 'Si–Al–O–N fibers from polymeric precursor: synthesis, structural, and mechanical characterization', *J. Am. Ceram. Soc.*, 1993 **76** (10) 2595–2600.
  92. H.-P. Baldus, O. Wagner, M. Jansen, 'Synthesis of advanced ceramics in the systems Si–B–N and Si–B–N–C employing novel precursor compounds', *Mat. Res. Soc. Symp.*, 1992 **271** 821–826.
  93. N. Perchenek, G. Passing, H.-P. Baldus, 'Infusible polyborosilazanes for production of ceramic powders, fibres and mouldings', German Patent 19,530,390, 1997.
  94. N. Perchenek, R. Herborn, D. Sporn, H.-P. Baldus, A. Thierauf, 'Ceramic fibers in the system silicon–boron–nitrogen–carbon', Patent EP 0759414 A3 B1, 1997.
  95. H.-P. Baldus, A. Thierauf, R. Herborn, N. Perchenek, D. Sporn, 'Ceramic fibers in the system silicon–boron–nitrogen–carbon', US Patent 5,968,859, 1999.
  96. P. Baldus, M. Jansen, D. Sporn, 'Ceramic fibers for matrix composites in high-temperature engine applications', *Science*, 1999 **285** 699–703.
  97. H.-P. Baldus, M. Jansen, 'Moderne Hochleistungskeramik – amorphe anorganische Netzwerke aus molekularen Vorläufern', *Angew. Chem.*, 1997 **109** 338–354.
  98. S. Bernard, M. Weinmann, P. Gerstel, P. Miele, F. Aldinger, 'Boron-modified polysilazane as a novel single-source precursor for SiBCN ceramic fibers: synthesis, melt-spinning, curing and ceramic conversion', *J. Mater. Chem.*, 2005 **15** 289–299.
  99. S. Bernard, S. Duperrier, D. Cornu, P. Miele, M. Weinmann, C. Balan, F. Aldinger, 'Chemical tailoring of single-source molecular and polymeric precursors for the preparation of ceramic fibers', *J. Optoelectr. Adv. Mater.*, 2006 **8** 648–653.
  100. X.-L. Fan, C.-X. Feng, Y.-C. Song, X.-D. Li, 'Preparation of Si–C–O–N–B ceramic fibers from polycarbosilane', *J. Mater. Sci. Lett.*, 1999 **18** 629–630.
  101. W. Verbeek, 'Formkörper aus homogenen Mischungen von Siliciumcarbid und Siliciumnitrid und Verfahren zu ihrer Herstellung', German Patent 2,218,960, 1973.

102. G. Winter, W. Verbeek, M. Mansmann, 'Formkörper aus homogenen Mischungen von Siliciumcarbid und Siliciumnitrid und Verfahren zu ihrer Herstellung', German Patent 2,243,527, 1974.
103. B.G. Penn, F.E. Ledbetter III, J.M. Clemons, J.G. Daniels, 'Preparation of silicon carbide-silicon nitride fibers by the controlled pyrolysis of polycarbosilazane precursors', *J. Appl. Polym. Sci.*, 1982 **27** 3751-3761.
104. J. Lipowitz, H.A. Freeman, H.A. Goldberg, R.T. Chen, E.R. Prack, 'Structure and properties of ceramic fibers prepared from polymeric precursors', *Mat. Res. Soc. Symp.*, 1986 **73** 489-494.
105. G.E. LeGrow, T.F. Lim, J. Lipowitz, R.S. Reaach, 'Ceramics from hydridopolysilazane', *Am. Ceram. Soc. Bull.*, 1987 **66** (2) 363-367.
106. H.A. Freeman, N.R. Langley, J.A. Rabe, C.-T. Li, J. Lipowitz, 'Polymer derived ceramic fibers having improved thermal stability', Patent EP 0438118 B1, 1991.
107. H.A. Freeman, N.R. Langley, C.-T. Li, J. Lipowitz, J.A. Rabe, 'Polymer derived ceramic fibers having improved thermal stability', US Patent 5,238,742, 1993.
108. T.F. Cooke, 'Inorganic fibers - a literature review', *J. Am. Ceram. Soc.*, 1991 **74** (12) 2959-2978.
109. A. Rengstl, 'Method of making ceramic fibres containing silicon carbide', Patent EP 0255132, 1988.
110. W. Kalchauer, G. Geisberger, 'Herstellung und Untersuchung von SiC- und Si<sub>3</sub>N<sub>4</sub>/SiC-Fasern', 2. *Symp. Materialforschung BMFT*, 1991 1391-1413.
111. M. Takamizawa, A. Hayashida, Y. Takeda, 'Infusibilization of organic silazane polymers and preparation of hollow ceramic fibers', Patent EP 0361181 A3 B1, 1990.
112. E. Chassegneux, J.-L. Lepage, 'Wet process for crosslinking polysilazanes for producing ceramic fibres', Patent EP 0412915, 1991.
113. E. Chassegneux, O. Caix, 'Ceramic fibers having improved surface properties/rupture strength', US Patent 5,043,045, 1991.
114. R. Perez, O. Caix, 'Fiberamic<sup>®</sup>, a new silicon carbonitride ceramic fiber with high thermal stability', in *Developments in the Science and Technology of Composite Materials*, ed. J. Füller, G. Grüninger, K. Schulte, A.R. Bunsell and A. Massiah, Elsevier Applied Science, London and New York, 1991, 573-579.
115. T. Ishikawa, H. Teranishi, H. Ichikawa, S. Mitsuno, 'Ceramic fibers and process for their production', Patent WO 8904884, 1993.
116. R. Naslain, 'Silicon carbide and oxycarbide fibers, silicon nitride and boride based fibers, applications of carbon and ceramic fibers', in *Advanced Inorganic Fibers: Processes, Structures, Properties, Applications*, ed. F.T. Wallenberger, Kluwer Academic Publishers, Dordrecht, Boston and London, 2000, Chapters 10-12, 265-329.
117. D. Mocaer, R. Pailler, R. Naslain, C. Richard, J.P. Pillot, J. Dunogues, C. Gerardin, F. Taulelle, 'Si-C-N ceramics with a high microstructural stability elaborated from the pyrolysis of new polycarbosilazane precursors, Part I: the organic/inorganic transition', *J. Mater. Sci.*, 1993 **28** 2615-2631.
118. D. Mocaer, R. Pailler, R. Naslain, C. Richard, J.P. Pillot, J. Dunogues, 'Si-C-N ceramics with a high microstructural stability elaborated from the pyrolysis of new polycarbosilazane precursors, Part II: Effect of oxygen-curing on properties of ex-PCSZ monofilaments', *J. Mater. Sci.*, 1993 **28** 2632-2638.
119. O. Delverdier, M. Monthieux, D. Mocaer, R. Pailler, 'Thermal behaviour of polymer-derived ceramics. IV. Si-C-N-O fibers from an oxygen-cured polycarbosilazane', *J. Europ. Ceram. Soc.*, 1994 **14** 313-325.

120. D. Mocaer, R. Pailler, R. Naslain, C. Richard, J.P. Pillot, J. Dunogues, O. Delverdier, M. Monthieux, 'Si-C-N ceramics with a high microstructural stability elaborated from the pyrolysis of new polycarbosilazane precursors, Part III: Effect of pyrolysis conditions on the nature and properties of oxygen-cured derived monofilaments', *J. Mater. Sci.*, 1993 **28** 2639-2653.
121. D. Mocaer, R. Pailler, R. Naslain, C. Richard, J.P. Pillot, J. Dunogues, C. Darnez, M. Chambon, M. Lahaye, 'Si-C-N ceramics with a high microstructural stability elaborated from the pyrolysis of new polycarbosilazane precursors, Part IV: Oxygen-free model monofilaments', *J. Mater. Sci.*, 1993 **28** 3049-3058.
122. M. Monthieux, O. Delverdier, 'Thermal behaviour of (organosilicon) polymer derived ceramics. V: Main facts and trends', *J. Europ. Ceram. Soc.*, 1996 **16** 721-737.
123. L. Lu, C.X. Feng, Y.C. Song, 'Curing polysilazane fibres by exposure to boron trichloride', *J. Mater. Sci. Lett.*, 1998 **17** 481-484.
124. G. Motz, J. Hacker, G. Ziegler, 'Design of SiCN-precursors for various applications', *Ceramic Materials and Components for Engines*, 2001 581-585.
125. J. Hacker, G. Motz, G. Ziegler, 'Processing of SiCN-fibres prepared from polycarbosilazanes', *Ceramic Materials and Components for Engines*, 2001 653-656.
126. J. Hacker, G. Motz, G. Ziegler, 'Novel ceramic SiCN-fibers from the polycarbosilazane ABSE', in *High Temperature Ceramic Matrix Composites*, ed. W. Krenkel *et al.*, Wiley-VCH, Weinheim, Germany, 2001, 52-55.
127. G. Motz, J. Hacker, G. Ziegler, 'New SiCN fibers from the ABSE polycarbosilazane', *Ceram. Eng. Sci. Proc.*, 2002 **23** (3) 255-260.
128. G. Motz, J. Hacker, G. Ziegler, B. Clauss, D. Schawaller, 'Low-cost ceramic SiCN fibers by an optimized polycarbosilazane and continuous processing', in *Advanced Inorganic Structural Fiber Composites*, 2002, 47-54.
129. G. Motz, 'Synthesis of SiCN-precursors for fibres and matrices', *Advances in Science and Technology* (Advanced Inorganic Fibrous Composites for Structural Applications), 2006 **50** 24-30.
130. S. Kokott, G. Motz, 'Cross-linking via electron beam treatment of a tailored polysilazane (ABSE) for processing of ceramic SiCN-fibers', *Soft Materials*, 2007 **4** (2-4) 165-174.
131. S. Kokott, L. Heymann, G. Motz, 'Rheology and processability of multi-walled carbon nanotubes - ABSE polycarbosilazane composites', *J. Europ. Ceram. Soc.*, 2008 **28** 1015-1021.
132. S. Kokott, G. Motz, 'Modifizierung des ABSE-Polycarbosilazans mit Multi-Walled Carbon Nanotubes zur Herstellung spinnfähiger Massen' ('Modification of the ABSE polycarbosilazane with multi-walled carbon nanotubes for the creation of spinnable masses'), *Materialwissenschaft und Werkstofftechnik*, 2007 **38** (11) 894-900.
133. P. Gorthy, P.G.I. Mukunda, 'Production of silicon carbide from rice husks', *J. Am. Ceram. Soc.*, 1999 **82** (6) 1393-1400.
134. R.V. Krishnarao, M.M. Godkhindi, P.G.I. Mukunda, M. Chakraborty, 'Direct pyrolysis of raw rice husks for maximization of silicon carbide whisker formation.', *J. Am. Ceram. Soc.*, 1991 **74** (11) 2869-2874.
135. A.K. Dhingra, 'Alumina fiber FP', *Phil. Trans. R. Soc.*, 1980 **A294** 411-417.
136. A.K. Dhingra, 'Advances in inorganic fiber developments', in *Contemporary Topics in Polymer Science*, ed. E.J. Vandenberg, Plenum Press, New York, 1982, 227-260.

137. A.R. Bunsell, M.-H. Betger, 'Fine diameter ceramic fibers', *J. Europ. Ceram. Soc.*, 2000 **20** 2249–2260.
138. J.C. Romine, 'New high temperature ceramic fiber', *Ceram. Eng. Sci. Proc.*, 1987 **8** 755–765.
139. V. Lavaste, M.-H. Berger, A.R. Bunsell, J. Besson, 'Microstructure and mechanical characteristics of alpha-alumina-based fibers', *J. Mater. Sci.*, 1995 **30** 4215–4225.
140. S. Nourbakhsh, F.L. Liang, H. Margolin, 'Characterization of a zirconia toughened alumina fiber, PRD-166', *J. Mater. Sci. Lett.*, 1989 **8** 1252–1254.
141. F.D. Birchall, J.A.A. Bradbury, J. Dinwoode, 'Alumina fibers', in *Handbook of Composites*, ed. W. Watt and B.V. Perov, North Holland Press, Amsterdam, Netherlands, 1985, 115–155.
142. Y.H. Chiou, M.T. Tsai, H.C. Shih, 'The preparation of alumina fibers by the sol-gel process', *J. Mater. Sci.*, 1994 **29** 2378–2388.
143. D.M. Wilson, L.R. Visser, 'High performance oxide fibers for metal and ceramic composites', *Composites Part A*, 2001 **32** 1143–1153.
144. Y. Saitow, K. Iwanaga, S. Itou, T. Fukumoto, T. Utsunomiya, 'Preparation of continuous high purity  $\alpha$ -alumina fiber', *Proc. 37th International SAMPE Symposium*, 1992 808–819.
145. Y. Abe, S. Horikiri, K. Fujimura, E. Ichiki, 'High performance alumina fiber and alumina/aluminum composites', in *Progress in Science and Engineering of Composites*, ed. T. Hayashi, K. Kawata and S. Umekawa, *Japan Soc. Comp. Mater.*, 1982, 1427–1434.
146. K. Jakus, V. Tulluri, 'Mechanical behavior of sumitomo alumina fiber at room and high temperature', *Ceram. Eng. Sci. Proc.*, 1989 **10** (9/10) 1338–1349.
147. D.M. Wilson, L.R. Visser, 'Nextel<sup>TM</sup> 650 ceramic oxide fiber: new alumina-base fiber for high temperature composite reinforcement', *Ceram. Eng. Sci. Proc.*, 2000 **21** 363–373.
148. W. Sigmund, J. Yuh, H. Park, V. Maneeratana, G. Pyrgiotakis, A. Daga, J. Taylor, J.C. Nino, 'Processing and structure relationships in electrospinning of ceramic fibers', *J. Am. Ceram. Soc.*, 2006 **89** (2) 395–407.
149. D. Li, J.T. McCann, Y. Xia, M. Marquez, 'Electrospinning: a simple and versatile technique for producing ceramic nanofibers and nanotubes', *J. Am. Ceram. Soc.*, 2006 **89** (6) 1861–1869.
150. W.E. Teo, S. Ramakrishna, 'A review on electrospinning design and nanofiber assemblies', *Nanotechnology*, 2006 **17** R89–R106.
151. L.C. Sawyer, M. Jamieson, D. Brikowski, M.I. Haider, R.T. Chen, 'Strength, structure and fracture properties of ceramic fibers produced from polymeric precursors: I, Base-line studies', *J. Am. Ceram. Soc.*, 1987 **70** (11) 798–810.
152. J. Lipowitz, H.A. Freeman, R.T. Chen, E.R. Prack, 'Composition and structure of ceramic fibers prepared from polymer precursors', *Adv. Ceram. Mater.*, 1987 **2** (2) 121–128.
153. R. Chaim, A.H. Heuer, R.T. Chen, 'Microstructural and microchemical characterization of silicon carbide and silicon carbonitride ceramic fibers produced from polymer precursors', *J. Am. Ceram. Soc.*, 1988 **71** (11) 960–969.
154. N.R. Langley, G.E. LeGrow, J. Lipowitz, 'Synthetic methods for preceramic polymers and ceramic fibers', in *Fiber Reinforced Ceramic Composites*, ed. K.S. Mazdiyasi, Noyes Publications, Park Ridge, NJ, 1990, 63–92.
155. J. Lipowitz, 'Polymer-derived ceramic fibers', *Ceram. Bull.*, 1991 **70** (12) 1888–1894.

156. R. Bodet, N. Jia, R.E. Tressler, 'Microstructural instability and the resultant strength of Si-C-O (Nicalon) and Si-C-N-O (HPZ) fibres', *J. Europ. Ceram. Soc.*, 1996 **16** 653-664.
157. D.J. Pysher, K.C. Goretta, R.S. Hodder, Jr., R.E. Tressler, 'Strengths of ceramic fibers at elevated temperatures', *J. Am. Ceram. Soc.*, 1989 **72** (2) 284-288.
158. J. Lipowitz, J.A. Rabe, L.K. Frevel, R.L. Miller, 'Characterization of nanoporosity in polymer-derived ceramic fibres by X-ray scattering techniques', *J. Mater. Sci.*, 1990 **25** 2118-2124.
159. J.F. Villeneuve, D. Mocaer, R. Pailler, R. Naslain, P. Olry, 'Tensile testing at high temperatures of ex-PCS Si-C-O and ex-Si-C-N single filaments', *J. Mater. Sci.*, 1993 **28** 1227-1236.
160. J. Lipowitz, J.A. Rabe, 'Method for preparation of polycrystalline silicon carbide fibers', Patent EP 0580380 B1, 1994.
161. R. Pailler, G. Chollon, H. Hannache, R. Naslain, J.P. Pillot, J. Dunogues, M. Birot, 'Influence of different curing processes on the thermal stability of ceramic fibers derived from organosilicon precursors', in *Advanced Structural Fiber Composites*, 1995, 69-76.
162. A.G. Evans, 'Perspective on the development of high-toughness ceramics', *J. Am. Ceram. Soc.*, 1990 **73** (2) 187-206.
163. H. Ohnabe, S. Masaki, M. Onozuka, K. Miyahara, T. Sasa, 'Potential application of ceramic matrix composites to aero-engine components', *Composites: Part A*, 1999 **30** 489-496.
164. D. Brewer, 'HSR/EPM combustor materials development program', *Mater. Sci. Eng. A*, 1999 **261** 284-291.
165. R. Jones, A. Szweda, D. Petrak, 'Polymer derived ceramic matrix composites', *Composites: Part A*, 1999 **30** 569-575.
166. L. Cheng, Y. Xu, L. Zhang, X. Yin, 'Oxidation behaviour of three-dimensional SiC/SiC composites in air and combustion environment', *Composites: Part A*, 2002 **31** 1015-1020.
167. F. Christin, 'Design, fabrication, and application of thermostructural composites (TSC) like C/C, C/SiC, and SiC/SiC composites', *Adv. Eng. Mater.*, 2002 **4** (12) 903-912.
168. T. Araki, K. Watanabe, T. Yoshida, S. Nishide, S. Masaki, 'High temperature properties of SiC fiber reinforced SiC matrix composites for turbine rotor application', *Ceram. Eng. Sci. Proc.*, 2002 581-588.
169. J. Rosenlöcher, G. Deinzer, R. Waninger, J. Münchhoff, 'Hochleistungsbremsscheiben aus Faserverbundkeramik', *Mat-wiss. u. Werkstofftech.*, 2007 **38** (11) 922-926.
170. A. Mühlratzer, M. Leuchs, M. Bickel, 'Entwicklung von Gleitlagerkomponenten aus Verbundkeramik für Kryopumpen', in *Verbundwerkstoffe*, ed. H.P. Degischer, Wiley-VCH Verlag, Weinheim, Germany, 2003, 331-336.
171. L.L. Snead, O.J. Schwarz, 'Advanced SiC composites for fusion applications', *J. Nucl. Mater.*, 1995 **219** 3-14.
172. L.L. Snead, R.H. Jones, A. Kohyama, P. Fenici, 'Status of silicon carbide composites for fusion', *J. Nucl. Mater.*, 1996 **233-237** 26-36.
173. R.H. Jones, D. Steiner, H.L. Heinisch, G.A. Newsome, H.M. Kerch, 'Radiation resistant ceramic matrix composites', *J. Nucl. Mater.*, 1997 **245** 87-107.
174. P. Fenici, A.J. Frias Rebelo, R.H. Jones, A. Kohyama, L.L. Snead, 'Current status of SiC/SiC composites R&D', *J. Nucl. Mater.*, 1998 **258-263** 215-225.
175. S. Ueda, S. Nishio, Y. Seki, R. Kurihara, J. Adachi, S. Yamazaki, 'A fusion power

- reactor concept using SiC/SiC composites', *J. Nucl. Mater.*, 1998 **258–263** 1589–1593.
176. A. Hasegawa, A. Kohyama, R.H. Jones, L.L. Snead, B. Riccardi, P. Fenici, 'Critical issues and current status of SiC/SiC composites for fusion', *J. Nucl. Mater.*, 2000 **283–287** 128–137.
177. A. Kishimoto, G. Toyoguchi, 'Piezoresistivity of Hi-Nicalon Type-S silicon carbide-based fiber', *J. Am. Ceram. Soc.*, 2002 **85** (2) 479–480.
178. S. Wang, D.D.L. Chung, 'Piezoresistivity in silicon carbide fibers', *J. Electroceramics*, 2003 **10** 147–152.
179. F.W. Zok, 'Development of oxide fiber composites', *J. Am. Ceram. Soc.*, 2006 **89** (11) 3309–3324.
180. R.J. Kerans, R.S. Hay, T.A. Parthasarathy, M.K. Cinibulk, 'Interface design for oxidation-resistant ceramic composites', *J. Am. Ceram. Soc.*, 2002 **85** (11) 2599–2632.
181. P.E.D. Morgan, D.B. Marshall, 'Ceramic composites of monazite and alumina', *J. Am. Ceram. Soc.*, 1995 **78** (6) 1553–1563.
182. W.C. Tu, F.F. Lange, A.G. Evans, 'Concept for a damage tolerant ceramic composite with strong interfaces', *J. Am. Ceram. Soc.*, 1996 **79** (2) 417–424.
183. H.E. Deve, C. McCullough, 'Continuous fiber reinforced Al composites: a new generation', *J. Met.*, 1995 **47** 33–37.
184. P. Martineau, R. Pailler, M. Lahaye, R. Naslain, M. Couzi, F. Cruege, 'SiC filament/titanium matrix composites regarded as model composites, Part 1', *J. Mater. Sci.*, 1984 **19** 2731–2748.
185. P. Martineau, R. Pailler, M. Lahaye, R. Naslain, 'SiC filament/titanium matrix composites regarded as model composites, Part 2', *J. Mater. Sci.*, 1984 **19** 2749–2770.
186. R. Leucht, H.J. Dudek, G. Ziegler, 'SiC-faserverstärkte Titanlegierung Ti<sub>6</sub>Al<sub>4</sub>V', *Z. Werkstofftechnik*, 1987 **18** 27–32.
187. R. Raj, 'Fundamental research in structural ceramics for service near 2000°C', *J. Am. Ceram. Soc.*, 1993 **76** (9) 2147–2174.



## Structure and properties of asbestos<sup>1</sup>

---

E J W WHITTAKER, formerly of Ferodo Ltd, UK

**Abstract:** Asbestos was once an important commercial fibre but is no longer used for health reasons. Its scientific interest is in the structure of a natural mineral fibre. The chemistry and crystal structure of different types of asbestos are described. The fibrous form of chrysotile results from the crystal lattice being curved. From an initial nucleus, crystals can grow as cylinders up to certain maximum and minimum diameters before the distortion is too great. Additional crystallization can occur in the central voids and between cylinders. The resulting solid form breaks down into fibres by splitting between cylinders.

**Key words:** asbestos types, asbestos crystal structures, curved lattices, cylindrical fibre formation.

For much of the twentieth century, asbestos was an important industrial fibre, which was widely used for fire protection, insulation, brake linings, conveyor belts and reinforcement of cement. It appears in fibre classification charts as the sole entry under *natural fibres of mineral origin*. As late as 1984, J. G. Cook's *Handbook of Textile Fibres* included the statements: *Asbestos is one of the strangest of all the naturally occurring fibres ... Today, asbestos is the raw material of an important industry, with the fibre serving in many invaluable ways*. No longer! The discovery of the carcinogenic effects of asbestos, leading to *mesothelioma*, cancer of the lining of the lungs, means that there is another industry: the removal of asbestos where it had been installed in the past. Despite the fact that asbestos is no longer used as a commercial fibre, this chapter is reprinted from *Fibre Structure* (The Textile Institute, 1963), because it shows how an unusual form of crystallization can lead to a fibre structure. [JWSH]

### 12.1 Introduction

The name asbestos is of Greek origin and means incombustible. That this material should have received its name in this way, despite the fact that the majority of natural substances are incombustible, shows how closely

---

<sup>1</sup> Reprinted from *Fibre Structure*, J.W.S. Hearle and R.H. Peters (eds), 'Asbestos', pp. 594–620. Copyright Butterworth & Co. (Elsevier) and the Textile Institute, 1963.

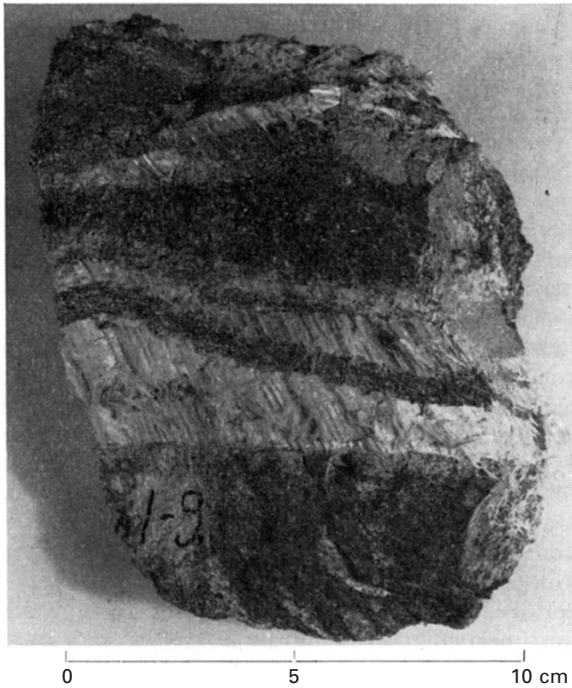


associated in people's minds is inflammability with the idea of a textile. Until the development of glass fibre, however, perhaps the only non-inflammable textile apart from asbestos was cloth of gold. Stories have come down the ages, from Pliny, from the court of Charlemagne, and from Marco Polo, of miraculous pieces of cloth that would not burn. From the scientific point of view, however, the remarkable features about asbestos are quite different from those which inspired the travellers' tales. To a chemist, the incombustibility of asbestos is very natural, since it is an inorganic silicate mineral; the surprising thing is that such a substance should be a textile fibre, and much of this chapter is devoted to explaining this feature.

Although pieces of woven asbestos cloth have been produced from time to time since antiquity, the rise of the asbestos industry is surprisingly recent. The large Canadian deposits began to be exploited for textile uses about 1873: the use of asbestos in insulation had begun in 1866, but its use as a reinforcement in cement sheets began only in 1900 and in brake linings in 1906. The recent growth of the industry is shown by the fact that the quantity of asbestos mined has increased by a factor of about 14 in the last 50 years.

## **12.2 Classification, occurrence, and physical properties of asbestos**

Since the name asbestos has been applied to any incombustible textile that occurs naturally, it is not surprising that material of diverse structure and composition is included under this name. The most important, chrysotile, accounts for about 90% of the total asbestos production, which is substantially over 1 000 000 tons per year. This pre-eminence arises partly from its generally favourable properties and partly from its occurrence in deposits suitable for large-scale exploitation. Chrysotile belongs to the serpentine group of minerals and occurs only in serpentine rocks. These are metamorphic rocks which may be formed under hydrothermal conditions in two ways, either by hydroxylation of olivine or pyroxene rocks or by silicification of dolomite. The former may lead to very large continuous masses of serpentine, whereas the latter gives rise to relatively thin sills, which are less adapted to economic mining. In both cases, the development of chrysotile seams depends on a further hydrothermal recrystallization, which is probably initiated at cracks in the rock. The fibres grow at the expense of the adjacent rock to form the typical cross-fibre seams shown in Fig. 12.1. In economically workable chrysotile deposits, the fibre content of the rock is between about 2% and 10%. The whole rock is mined and the fibre is separated from the rock and graded for length by a series of crushing, screening and air-flotation processes. The proportion of fibres over 1 inch in length is usually very small. The principal sources of chrysotile are Canada, which produces about 70%, and



12.1 Specimen of serpentine rock containing cross-fibre seams of chrysotile.

Southern Rhodesia and Swaziland, which together produce about 10% of the total world output (excluding that from the USSR).

Chrysotile is extremely strong; tensile strengths approaching  $10^6$  lb/in<sup>2</sup> have been recorded. However, its ultimate fibrils are so fine (about 250 Å in diameter) that any handleable fibre contains millions of these fibrils and breakage commonly occurs by a succession of breaks in different fibrils, leading to fraying and thence to complete rupture. Chrysotile is used in virtually all branches of the asbestos industry except when acid-resistance is required.

The other commercially important types of asbestos are grouped together under the heading of amphibole asbestos. Crocidolite is mined in South Africa and to a small extent in Australia and Bolivia, the total output in 1955 being 53 000 tons. It is a blue fibre, which occurs in banded ironstones. Its strength is similar to that of chrysotile and it is sufficiently flexible to be spun and woven. It is much more acid-resistant than chrysotile and has advantages in electrical insulation, but it is more abrasive and loses its strength at a lower temperature. Also of importance is amosite, which occurs in similar geological formations in South Africa, in some places in association with

crocidolite. It quite frequently occurs as very long fibres of up to about 10 inches in length. It is weaker than crocidolite and is not usually sufficiently flexible to be spun and woven. The total output in 1955 was 50 000 tons. The remaining commercial fibres are tremolite, actinolite and anthophyllite. They are widely distributed and are mined to some extent in Canada, Finland and Italy, and to a smaller extent in other countries. They are usually rather weak and not suitable for weaving. Nevertheless, they have some specialized applications, particularly as filtration media and in electrical insulation.

Although asbestos minerals other than chrysotile and the amphiboles do exist (polygorskite and picrolite, for example), they are of no commercial importance and will not be considered here.

It is curious that the two main types of asbestos have presented quite different problems. The amphiboles have a simple structure but their chemical relationships are complex, whereas chrysotile is chemically simple but complex structurally.

## 12.3 Amphibole asbestos

### 12.3.1 Composition and unit cells

The amphibole minerals, besides forming the varieties of asbestos with which we are concerned here, also occur widely in non-fibrous forms and are important rock-forming minerals. They have therefore received considerable attention from mineralogists and petrologists, by whom they were traditionally regarded as meta-silicates, primarily of divalent metals, with the general formula  $M''SiO_3$  (tremolite, for example, was formulated as  $CaMg_3(SiO_3)_4$ ). Such formulae are still rather widely quoted, although it has been established, at least since 1930, that the correct formula is  $M''_7Si_8O_{22}(OH)_2$ , tremolite, for example, being  $Ca_2Mg_5Si_8O_{22}(OH)_2$ . Indeed, this formula had already been proposed by Schaller (1) in 1916 on the basis of the small but consistent amount of firmly bound water found in amphibole analyses. It was fully confirmed by the X-ray structure analysis of tremolite carried out by Warren (2) in 1930.

The range of compositions of the amphiboles is very wide indeed; not only may any of a number of divalent metals (Mg,  $Fe''$  and Ca, and more rarely Mn and Zn) be present but these may also be partially replaced by some monovalent and trivalent metals (Na,  $Fe'''$  and Al, and more rarely Li, K and Cr), provided that electrical neutrality is maintained. The silicon may also be partly replaced by aluminium,  $(OH)^-$  may be partly replaced by  $O^{--}$  ions or by fluorine, and it is even possible to incorporate an additional atom of hydrogen or an alkali metal into the structure without changing it in any fundamental way. However, not all these variants occur in the asbestiform varieties, whose compositions correspond approximately to the following formulae, minor replacements being neglected:

Crocidolite	$\text{Na}_2\text{Mg}_3\text{F}''_2\text{Si}_8\text{O}_{22}(\text{OH})_2$ to $\text{Na}_2\text{Fe}''_3\text{Fe}'''_2\text{Si}_8\text{O}_{22}(\text{OH})_2$ (the higher iron contents are the more usual)
Amosite	$\text{Mg}_2\text{Fe}''_5\text{Si}_8\text{O}_{22}(\text{OH})_2$ to $\text{MgFe}''_6\text{Si}_8\text{O}_{22}(\text{OH})_2$
Tremolite–actinolite	$\text{Ca}_2\text{Mg}_5\text{Si}_8\text{O}_{22}(\text{OH})_2$ to $\text{Ca}_2\text{Fe}''_3\text{Si}_8\text{O}_{22}(\text{OH})_2$ (tremolite and actinolite form a continuous series of solid solutions, the name actinolite usually being applied if there are more than about two Fe atoms in the formula)
Anthophyllite	$\text{Mg}_7\text{Si}_8\text{O}_{22}(\text{OH})_2$ to $\text{Mg}_4\text{Fe}''_3\text{Si}_8\text{O}_{22}(\text{OH})_2$

All these species are monoclinic except for anthophyllite, which is orthorhombic. (Amosite is frequently, but erroneously, stated to be orthorhombic on the basis of its straight extinction in the polarizing microscope.) Their unit cells, subject to small variations as a function of composition, are as given in Table 12.1.

The axial convention used here is that the *c*-axis is parallel to the length of the fibre and the *a*-axis is chosen so that the monoclinic unit cell is body-centred. Some confusion has arisen in the literature because another convention is possible, giving a face-centred cell with values of *a* and *β* which are so similar to the above that the difference in convention may not be obvious.

### 12.3.2 Atomic arrangement

The atomic arrangement in the amphiboles was first determined by Warren (2) in tremolite and by Warren and Modell (3) in anthophyllite. Subsequent, more detailed determinations for crocidolite (4), actinolite (5), tremolite (6), and two non-fibrogenic aluminous varieties (7) have fully confirmed the general lines of Warren's structure, though they have shown that some details must be modified. They have shown, moreover, that the structures of the different species are very similar even in their detailed departures from an idealized regular structure and that there are no appreciable differences between the atomic arrangements in the fibrogenic and non-fibrogenic varieties.

The structure is based on infinite chains of silicon–oxygen tetrahedral running the length of the fibres. Such a chain is shown in an idealized

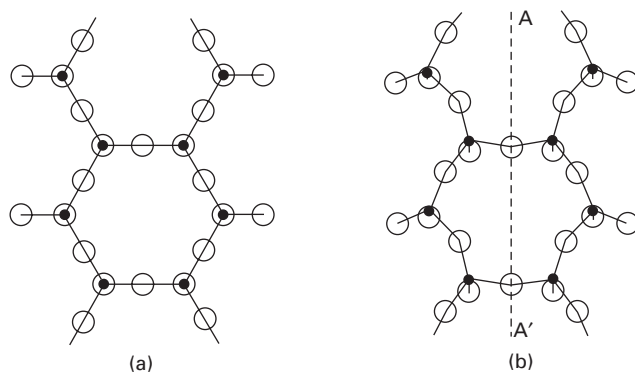
Table 12.1 Crystal lattice values

	<i>a</i> (Å)	<i>b</i> (Å)	<i>c</i> (Å)	<i>β</i>
Crocidolite	9.91	17.99	5.32	107° 39'
Amosite	9.92	18.30	5.30	110° 10'
Tremolite	9.92	18.05	5.28	106° 17'
Actinolite	9.89	18.11	5.34	105° 48'
Anthophyllite	18.54	17.90	5.30	

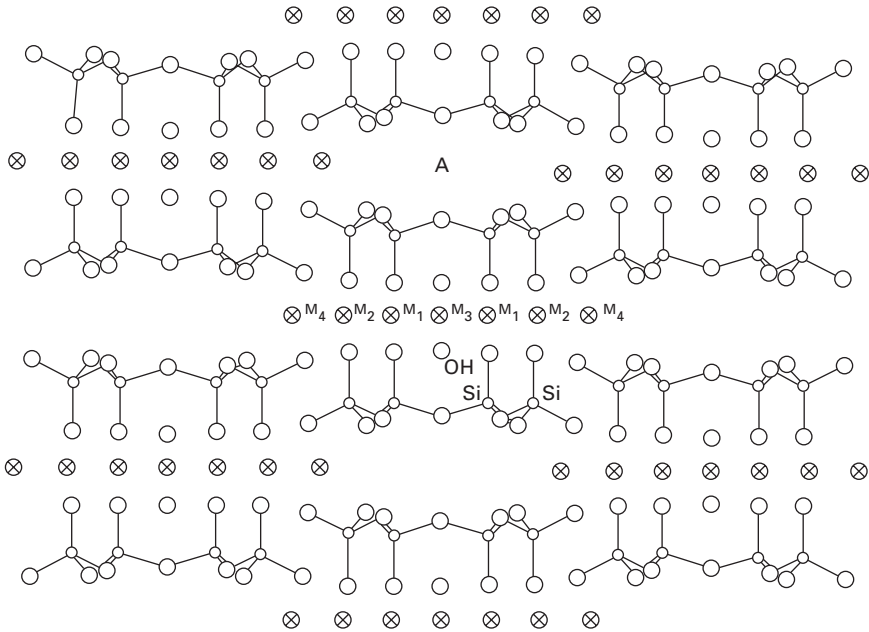
form in Fig. 12.2(a). The oxygen atoms at the vertices of the tetrahedral (superimposed on the silicon atoms in the projection of Fig. 12.2(a) are each attached to one silicon atom only and, together with the hydroxyl ions that lie over the centres of the silicon–oxygen hexagons, they form a narrow strip of hexagonally close-packed oxygen atoms. They serve to co-ordinate the metal ions that lie over one set of the hollows of this close-packed arrangement. A second similar silicate chain and set of hydroxyl ions is then inverted over the layer of metal ions, which thus find themselves in an environment of oxygen co-ordination very similar to that in the hexagonal hydroxides with the brucite structure. The pair of silicate chains with the metal ions sandwiched between them is equivalent to a strip from the structure of the layer silicate talc.

A projection of the structure down the chain is shown in Fig. 12.3. It may be seen that six of the seven metal ions occur symmetrically in pairs, giving a total of four different dispositions for the metal ions in the structural unit.  $M_1$  and  $M_3$  are completely co-ordinated within one chain unit;  $M_2$  and  $M_4$  are only partly co-ordinated by oxygen atoms of their own chain (by four and two respectively), their coordination being completed by oxygen atoms from adjacent chains. There is thus a certain amount of inter-chain bonding, but it is sufficiently weak relative to the internal strength of the chains to account for the prismatic cleavage of macroscopic crystals and the ready separation of the fibres of the fibrous varieties.

The silicate chain is actually distorted from the idealized form shown in Fig. 12.2(a) to that shown in Fig. 12.2(b). Three principal effects are involved. Each silicate tetrahedron is somewhat distorted and is also rotated to some extent about an axis perpendicular to the diagram. This effect is known to occur also in layer silicates and arises from the attraction of the cations for



12.2 A plan of the silicate chain in the amphibole structure: (a) idealized, (b) as found in crocidolite. The open circles denote oxygen atoms and the black dots silicon atoms.



12.3 Projection of the amphibole structure down the fibre-axis.

the nearest basal oxygen atoms. This has the effect of narrowing the chain, but the width of the silicate chain is by nature narrower than that of the strip of brucite-like structure to which it is attached. The narrowing effect is therefore resisted by a straightening of the central Si–O–Si bonds, leading to the form shown in Fig. 12.2(b) and also to a bending (along AA') of the two sides of the silicate chain away from the plane of the cations. This may be seen in Fig. 12.3.

A notable feature of the structure is the presence of a hole at A in Fig. 12.3. This position is not approached more closely than 2.7 Å by any atom and is totally enclosed by the surrounding structure. The hole is thus large enough to accommodate an ion such as sodium and its presence accounts for the existence of amphiboles with up to one extra cation per formula unit when this is required by the charge balance. However, this does not occur in the asbestiform varieties. 'Excess' hydrogen atoms above two do occur in these varieties and the structural explanation of this has not been finally settled. The idea that the extra hydrogen is present in a water molecule in this hole has been disproved (5) and it appears that the excess must either be attached to the peripheral oxygen atoms of the chains, as in afwillite (8), or as (OH)<sub>4</sub> groups replacing SiO<sub>4</sub>, as suggested by McConnell (9) in montmorillonite.

### 12.3.3 Structural basis for the differentiation of the amphibole varieties

The composition ranges occupied by the various amphiboles have been reviewed by Sundius (10) who has shown that, although some substitutions (such as Fe<sup>2+</sup> for Mg in tremolite and actinolite) lead to continuous series of solid solutions, others have only a restricted range. Evidence for this comes either from gaps in the observed ranges of composition or from the existence of mixtures of the two varieties when the overall composition might be expected to lead to an intermediate solution. Such evidence has been extended by Frankel (11) and by the present author to the relations between amosite and crocidolite and by Rabbitt (12) for anthophyllite and amosite. From the evidence that is now available, it appears that the differentiation of the varieties (which manifests itself in the differences of their  $\beta$  angles) depends on the packing of the chains; this is controlled by the size of the ion at M<sub>4</sub> (13). A marked change in the radius of the ion at this position commonly leads to a new variety, whereas replacement of M<sub>1</sub> and M<sub>3</sub> leads to a continuous series of solid solutions. M<sub>2</sub> behaves in an intermediate way, so that, in order to rationalize the seemingly arbitrary divisions between the varieties, it is helpful to divide the cations into three groups instead of the usual two. Thus crocidolite will tolerate either Mg ( $r = 0.78 \text{ \AA}$ ) or Fe<sup>2+</sup> ( $r = 0.83 \text{ \AA}$ ) as M<sub>1</sub> and M<sub>3</sub> but will not tolerate much replacement of the electrostatically balancing Na and Fe<sup>3+</sup> in positions M<sub>4</sub> and M<sub>2</sub> ( $r = 0.98$  and  $0.67 \text{ \AA}$ ) by Mg or Fe<sup>2+</sup>. It is therefore isolated from amosite and anthophyllite. Tremolite will tolerate complete replacement of Mg by Fe<sup>2+</sup> as M<sub>1</sub>, M<sub>2</sub> and M<sub>3</sub> leading to actinolite but not of Ca by Mg or Fe<sup>2+</sup> so that it is isolated from anthophyllite and amosite. In anthophyllite, even the small change of radius from Mg to Fe<sup>2+</sup> in the M<sub>4</sub> position leads to a phase change to amosite. The relationships of the varieties are therefore clarified by writing the approximate formulae as in Table 12.2.

The reason for the non-occurrence of asbestiform varieties of amphiboles outside these composition ranges is not at present clear. It certainly appears that the presence of appreciable proportions of trivalent ions in tetrahedral positions inhibits the formation of asbestos (i.e., in gedrites and aluminous hornblendes).

Table 12.2 Chemical formulae

	M <sub>4</sub>	M <sub>2</sub>	M <sub>1</sub> + M <sub>3</sub>	
Crocidolite	Na <sub>2</sub>	Fe <sup>3+</sup>	(Fe <sup>2+</sup> , Mg <sup>2+</sup> ) <sub>3</sub>	Si <sub>8</sub> O <sub>22</sub> (OH) <sub>2</sub>
Amosite	Fe <sup>2+</sup>	(Mg, Fe <sup>2+</sup> ) <sub>2</sub>	(Mg, Fe <sup>2+</sup> ) <sub>3</sub>	Si <sub>8</sub> O <sub>22</sub> (OH) <sub>2</sub>
Anthophyllite	Mg <sub>2</sub>	Mg <sub>2</sub>	(Mg, Fe <sup>2+</sup> ) <sub>3</sub>	Si <sub>8</sub> O <sub>22</sub> (OH) <sub>2</sub>
Tremolite-Actinolite	Ca <sub>2</sub>	(Mg, Fe <sup>2+</sup> ) <sub>2</sub>	(Mg, Fe <sup>2+</sup> ) <sub>3</sub>	Si <sub>8</sub> O <sub>22</sub> (OH) <sub>2</sub>



### 12.3.4 Texture of amphibole asbestos

Knowledge of the texture and second-order structure effects in the amphiboles is meagre. The fibres usually give quite sharp X-ray diffraction spots and hence the average diameter of a coherently crystalline fibril must be at least  $0.1 \mu$ . On the other hand, the fibre that can be used for X-ray diffraction (approximately  $10 \mu$  thick) usually gives a photograph with full rotational symmetry, so that the individual crystals cannot be much more than  $0.1 \mu$  thick. An exception to this is Bolivian crocidolite, which contains fibrils with cross-sections of up to about  $10 \mu \times 100 \mu$  that are twinned crystals, probably polysynthetic twins with (100) as the twinning plane. The electron microscope reveals lath-like crystals of all ranging from about  $0.3 \mu$  down to about  $300 \text{ \AA}$  in width but the latter may well be artefacts produced by cleavage during the preparation of specimens. The larger laths sometimes show incipient fraying into finer fibres at their ends.

No information seems to be available on the incidence of dislocations in amphiboles, although it would be expected that these would be of major importance in the alternative growth of long fibres or approximately equi-axed crystals. Some disorder effects have been observed in certain anthophyllite and amosite specimens, evidenced by continuous diffraction streaks joining up the sharp reflections along the layer lines. This has not been investigated in detail but probably arises from mistakes in the chain-stacking that would be equivalent to the formation of thin lamellae of anthophyllite in amosite and vice versa. A very weak tremolite fibre from Portugal has also been observed in which there was some curious, partially ordered, disorientation of the *c*-axis with respect to the fibre-axis, but the nature of this is not known.

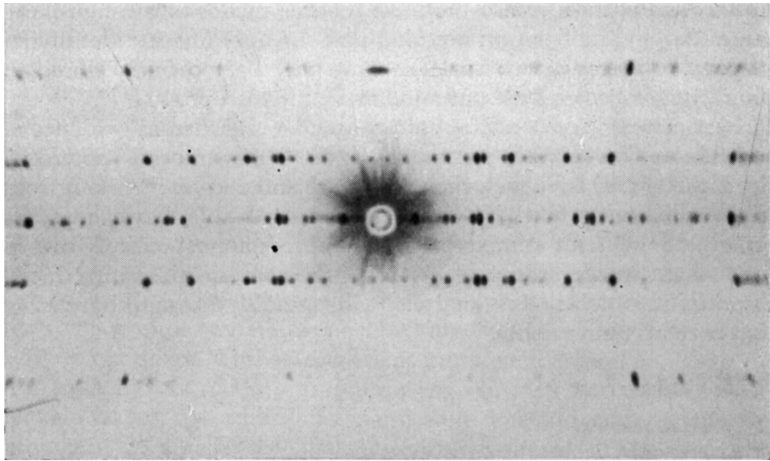
### 12.3.5 Chemical properties and identification

On heating, the amphibole fibres lose their water of constitution in the range  $300^{\circ}$ – $500^{\circ}\text{C}$  and at the same time undergo a decrease in strength. The ferrous iron, which is contained in some varieties, is also oxidized to the ferric state in air in this temperature range. According to Rabbitt (12), there are no well-marked effects in the differential thermal analysis (D.T.A.) curve, at least up to  $1000^{\circ}\text{C}$ , although some authors show D.T.A. curves with appreciable endotherms and exotherms of a surprisingly irregular form. Very little work seems to have been done on the structural changes in amphiboles on heating, but they decompose at  $900^{\circ}$ – $1100^{\circ}\text{C}$  to form pyroxenes and a glassy phase (14).

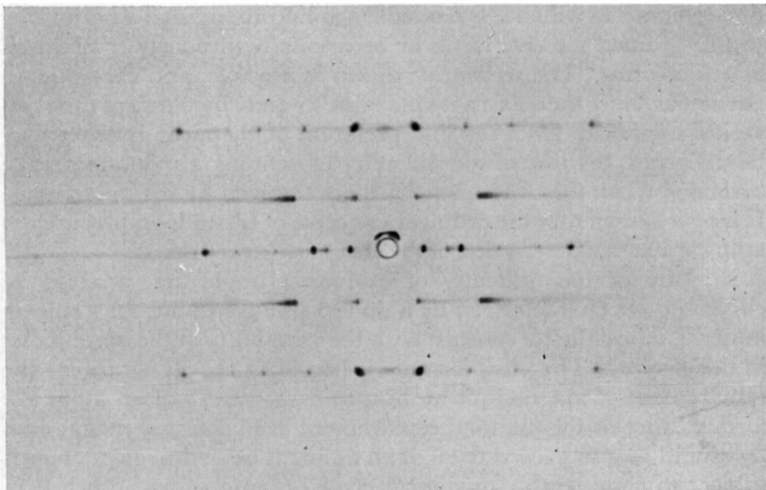
The amphibole fibres may be distinguished as a group from chrysotile by their low water content (2–3%), their higher refractive index ( $>1.60$ ; chrysotile is 1.54–1.56), the fact that they do not stain with a solution of



iodine in glycerol, and their X-ray diffraction pattern. The latter differs so completely from that of chrysotile that the two may be distinguished merely by inspection (Figs 12.4(a) and (b)). More detailed examination of the pattern, most conveniently made by means of a comparison of the particular fibre photograph with similar photographs of standard fibres, also serves to distinguish the amphibole varieties from one another. The X-ray diffraction pattern is also the most reliable means of distinguishing an anthophyllite from an amosite, and the only one for identifying natural mixtures of two



(a)



(b)

12.4 X-ray diffraction photographs of orientated fibre specimens of (a) amosite and (b) chrysotile.

varieties that may be too finely fibred to be distinguished as a mixture under the microscope.

Any appearance of a blue colour may be regarded as evidence of crocidolite or a mixture containing it; the 'blue amosite' described by Frankel (11) is, in fact, such a mixture and derives its colour from its crocidolite content. The converse is less reliable, however; some crocidolite without admixed amosite appears almost entirely brown with slight traces of blue. Apart from the complications introduced by mixtures, chemical analysis will usually distinguish reliably between all the varieties.

## 12.4 Chrysotile

### 12.4.1 Introduction

Unlike the amphibole minerals, chrysotile occurs only in the fibrous form and does not yield macroscopic crystals. Even the other serpentine minerals to which it is related by composition usually occur only in fine-grained massive forms or occasionally in poorly crystallized lamellar forms. The serpentine group as a whole, and chrysotile in particular, were therefore not amenable to study by classical mineralogical methods. Even the interpretation of chemical analyses may be uncertain because of the difficulty of defining a mono-mineralic specimen when the components are not resolved by the microscope. It is now known that the ordinary concepts of crystallography are not appropriate to a description of the chrysotile structure.

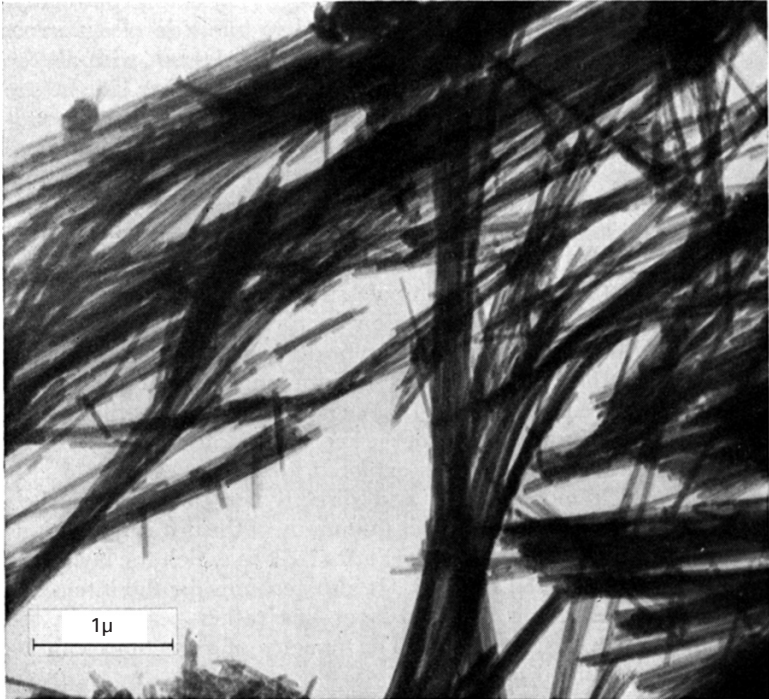
In spite of the difficulty of excluding impurities, analyses of chrysotile are characterized by a remarkable constancy for a silicate mineral, especially by contrast with the variability of the amphiboles in this respect. The ideal formula is  $\text{Mg}_3\text{Si}_2\text{O}_9\text{H}_4$ . It is rare for the replacement of magnesium by iron to exceed 0.13 of an atom per formula unit or for the total replacement of silicon and magnesium by aluminium to exceed 0.08 of an atom. The hydrogen content is subject to considerable analytical error because water adsorbed in micro-pores may be partly retained at temperatures up to 200°C, or even higher, and may therefore be confused with constitutional water. The most common impurities are particles of magnetite and oriented fibrous intergrowths of brucite, but fine-grained particles of calcite and magnesite also occur.

### 12.4.2 Early structural work

An X-ray-diffraction photograph of an oriented bundle of chrysotile fibres is shown in Fig. 12.4, where it is compared with a similar photograph of an amphibole. The latter is identical in appearance with the photograph obtained from a rotating single crystal, whereas the former has a number of

peculiarities, especially the very small number of spots and their division into two kinds, sharp and diffuse. On the other hand, the unit-cell edge parallel to the fibre-axis, which is derived from the spacing of the layer lines, is virtually the same in the two materials and, as early as 1929, Anderson and Clark (15) suggested that this showed a common dependence of the fibrous character on silicon–oxygen chains. Warren and Bragg (16) in 1930 postulated an amphibole-like  $\text{Si}_4\text{O}_{11}$  chain attached to one side of a narrow strip of brucite-like structure as in the amphiboles but with all the hydroxyl groups remaining unsubstituted on the other side of the brucite-like strip. This arrangement has a composition corresponding to  $\text{Mg}_5\text{Si}_4\text{O}_{11}(\text{OH})_6$  and positions between the chains were postulated for the additional magnesium ion and water molecule required to match the chrysotile composition. This structure accounted reasonably well for the intensities of the sharp reflections of the zero layer line but did not explain the peculiarities of the X-ray photograph. Just as the amphibole structure can be described in terms of narrow strips of the talc structure, so that proposed by Warren and Bragg for chrysotile can be described in terms of narrow strips of the then unknown magnesium analogue of the kaolin minerals. Warren and Hering (17) suggested that chrysotile was, in fact, this magnesium analogue of the kaolin minerals and that it had a layer structure. This idea was explored further by Aruja (18). It accounts much more simply and directly for the formula, i.e.,  $\text{Mg}_3\text{Si}_2\text{O}_5(\text{OH})_4$ , and for the fact that many of the diffuse reflections have a shape characteristic of layer structures in which the layers are stacked in a disordered manner. It also accounts for the intensities of sharp reflections on the zero layer line rather better than the Warren and Bragg structure. The paucity of reflections can be associated with the disorder.

It had earlier been suggested by Pauling (19) that the lack of a magnesian kaolin was due to a misfit between the dimensions of brucite and  $\text{Si}_2\text{O}_5$  layers that would lead to a curvature of an unsymmetrically combined layer of this type. Such a tendency to curvature was invoked by Aruja to explain the fibrous nature of chrysotile in terms of a limitation in growth in the direction of curvature, so that the layers would form only very narrow ribbons. However, Turkevitch and Hillier (20) and Bates, Sand and Mink (21) showed that electron micrographs of chrysotile fibres have the appearance of being tubular with an external diameter of 200–300 Å. The reality of this appearance was confirmed by Noll and Kircher (22), especially for synthetic chrysotile, by stereoscopic electron micrographs, which showed the tubular form very clearly. This electron-microscope evidence (Fig. 12.5) therefore provided the perfect link required between the postulated curved layers and the otherwise anomalous association of a layer structure with fibres of such perfection as those of chrysotile. If the layers are bent to such small radii, however, it means that many of the concepts of crystallography, such as that of the unit cell, for instance, cannot justifiably be applied in the investigation

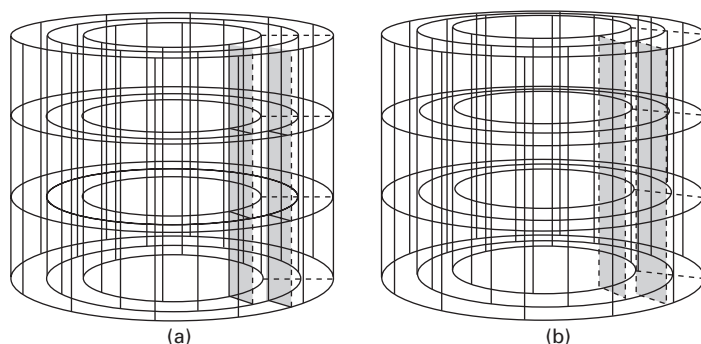


12.5 Electron micrograph of chrysotile fibres. Magnification approximately  $\times 18\,000$ .

of the structure. A theoretical consideration of cylindrical layer structures is therefore necessary to the understanding of the structure of chrysotile.

### 12.4.3 The cylindrical lattice

If a set of identical two-dimensional lattices is stacked together in an ordered way with a regular spacing, an ordinary three-dimensional crystal lattice can be built up. Similarly, if such two-dimensional lattices (which will here be called the generating lattice) are bent into cylinders with radii in arithmetic progression and then stacked coaxially one inside the other with ordered relative translations parallel to the cylinder-axis as shown in Fig. 12.6, then a cylindrical lattice can be built up. Such a lattice does not repeat regularly in three dimensions because the successive layers get out of step with one another in the circumferential direction (and at different rates as one goes from the inside of the lattice to the outside) because of their different radii. A cylindrical lattice therefore has no true unit cell. It is possible, however, to define two projections of a structure based on a cylindrical lattice, each of which has a two-dimensional unit cell. One of these is obviously the radial



12.6 Cylindrical lattices: (a) orthorhombic, (b) monoclinic.

projection through the thickness of any one of the coherent cylindrical layers of which the structure is composed, and the unit cell of this projection is that of the two-dimensional generating lattice (with lattice parameters  $b$ ,  $c$  and  $\gamma$ , say). The other is obtained by projecting the structure circumferentially onto a radial plane through a complete unit of the structure in the circumferential direction (this unit is wedge-shaped in each layer and corresponding points of it from each layer will not lie on the radial plane). This projection will have one axis ( $c$ ) identical with that axis of the generating lattice which is parallel to the cylinder axis; it will have an inter-axial angle  $\beta$ , which depends on the relative translations of the successive layers parallel to the cylinder-axis; and it will have the other axis ( $a$ ) given by

$$a = r \operatorname{cosec} \beta$$

where  $r$  is the radial spacing.

According to whether the two projections are both rectangular, one rectangular and one oblique, or both oblique, the lattice will be analogous to an orthorhombic, monoclinic or anorthic crystal lattice, respectively, and may usefully be described by these terms (23). The theory of diffraction by such a lattice (24) shows that it will give two series of reflections. One series will be sharp and will lie in the positions to be expected for the  $h0l$  reflections from an ordinary crystal with unit-cell parameters  $a$ ,  $c$  and  $\beta$ . The intensities of these reflections will be very nearly proportional to the Fourier components of the projection on the  $a$ ,  $c$  plane (the radial plane in this case), as for an ordinary crystal. The reflections in the other series will be diffuse and will lie near, but not at, the positions to be expected for the  $0kl$  reflections of an ordinary crystal. These diffuse reflections will be fairly similar in form to those from a turbostratic crystal. No  $hk0$  or  $hkl$  reflections occur.

The above descriptions apply to the simplest primitive cylindrical lattices. Non-primitive cylindrical lattices are also possible. In these, either the two-

dimensional generating lattice is centred, or else the adjacent layers may not be equivalent in structure, axial displacement or orientation. If every  $n$ th layer is equivalent, there are  $n$  layers in the unit cell of the  $a, c$  projection. Helical and spiral cylindrical lattices are also possible. In the former, the generating lattice is wrapped round into a cylinder 'on the cross', so that the  $b$ -axes lie on helices instead of circles. In the spiral case, a single layer is wrapped up round itself like a roll of paper. Both these types give diffraction effects closely similar to those already described.

#### 12.4.4 The structure of chrysotile

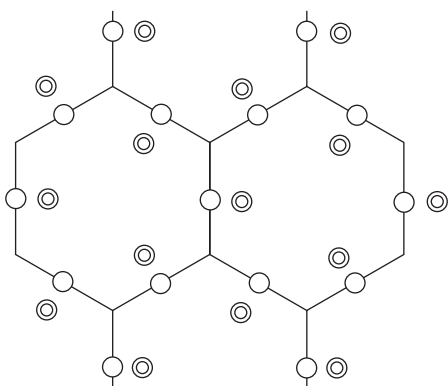
Three crystallographically distinct varieties of chrysotile have been discovered by X-ray diffraction. They usually occur in intimate admixture and all give the diffraction effects to be expected if they are based on a cylindrical lattice with a centred rectangular generating lattice having parameters 9.26 and 5.34 Å and with two layers in the unit cell of the  $a, c$  projection. In ortho-chrysotile  $\beta = 90^\circ$ ; in clino-chrysotile (the commonest variety)  $\beta = 93^\circ 16'$ ; and in para-chrysotile (the rarest)  $\beta = 90^\circ$  again but the 9.26 Å axis is parallel to the fibre-axis, whereas in the other two varieties the 5.34 Å axis is in this orientation. In all three varieties, alternate layers are not in equivalent positions, so that, as stated above, there are two layers in the unit cell of the  $a, c$  projection (25). The  $a$ -parameter is 14.6 Å in clino-chrysotile and within 0.2% of this in the other two varieties. In clino-chrysotile (26), the non-equivalence of alternate layers consists primarily in a relative translation of each layer along the fibre-axis by  $\pm 0.13$  Å with respect to its neighbours. This probably arises from a small distortion of the structure of the individual layers, which is of opposite sign in alternate layers, but the reason for such alternating distortions is obscure. In ortho-chrysotile (27), on the other hand, alternate layers are inverted end to end, with the result that the  $a, c$  projection has the space-group  $pg$ , i.e., a truly orthogonal space group, not merely one in which  $\beta = 90^\circ$ . In para-chrysotile (28), there is a relative displacement along the fibre-axis of  $\pm b/12$  between alternate layers, which can also in this case be expressed as a symmetry operation of the space-group  $pg$ .

The detailed structure of the layers is identical in ortho- and clino-chrysotile within the limits of accuracy of the structure determinations. Less-detailed information is available for para-chrysotile but, so far as it is known, this is also identical. There are some small distortions from the idealized magnesian-kaolin type of layer but these have not so far been interpreted theoretically. The most interesting feature of the structure is the stacking arrangement of the layers, which is fundamentally different from that in the normal clay minerals. In the latter, one layer stacks over another in one or other of a small number of alternative ways which permit the formation of hydrogen bonds between the oxygen atoms in the base of the one layer with the hydroxyl groups

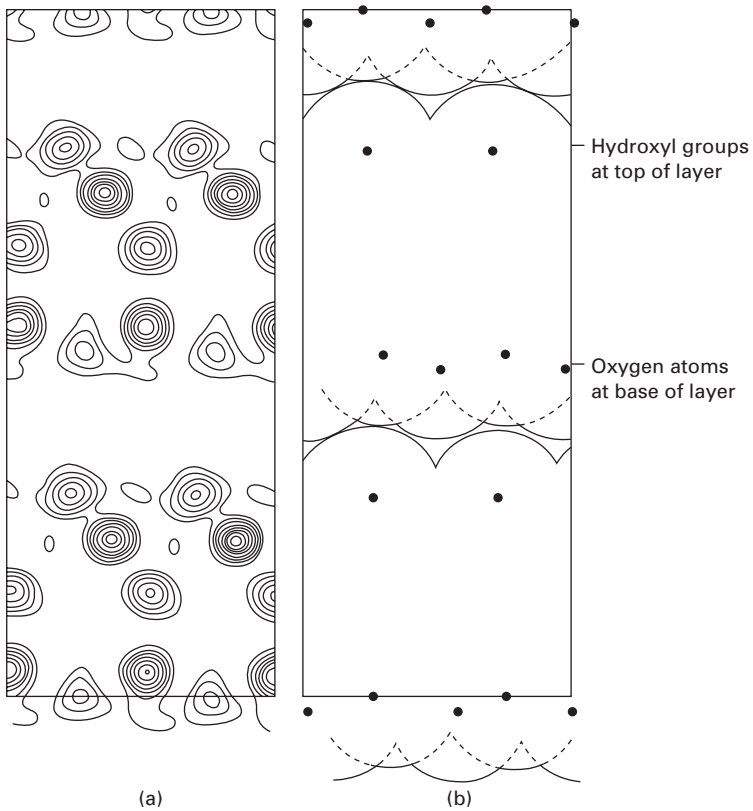


on the top of the layer below. These stacking arrangements, based on the arrangement shown in Fig. 12.7, lead to a small number of permitted values of  $\beta$ . The value adopted by clino-chrysotile is not one of these, however, and the structure analysis shows that in both ortho- and clino-chrysotile the stacking is as shown in Fig. 12.8. This arrangement can be understood when it is remembered that the layers are randomly disordered perpendicular to this projection, not only from layer to layer but from the point of view of any one pair of layers, because, having different cylindrical radii, they get out of step with one another progressively. The hydroxyl groups therefore have no determinate  $y$ -co-ordinates with respect to the next layer above but impose on it the stacking position that would be appropriate if they were smeared out into corrugations parallel to the  $b$ -axis. Since the oxygen atoms at the base of a layer are divided into two sets at slightly different levels, the set at the lower level lies over the grooves between these corrugations, whereas the other set lies over the corrugations. A photograph of a structure model with these corrugations marked by a layer of film is shown in Fig. 12.9. The stacking in para-chrysotile is based on similar principles.

The distribution of the three varieties of chrysotile in nature is very curious. They normally occur in intimate admixture with one another, so intimate that the splitting of a fibre bundle 0.5 mm in diameter down to fibre bundles about 0.05 mm in diameter does not reveal any inequalities in the distribution within the original bundle. Para-chrysotile has never been observed to be present in a proportion greater than about 10%. Even this is rare and it is not unusual for it to be absent altogether. Substantially pure clino-chrysotile seems to occur in all deposits, but deposits differ from one



12.7 The successive layers of kaolin-type minerals are stacked so that the hydroxyl groups (double circles) at the top of one layer are related to the oxygen atoms (single circles) at the base of the next layer, in the way shown here in a projection down an axis perpendicular to the layers.

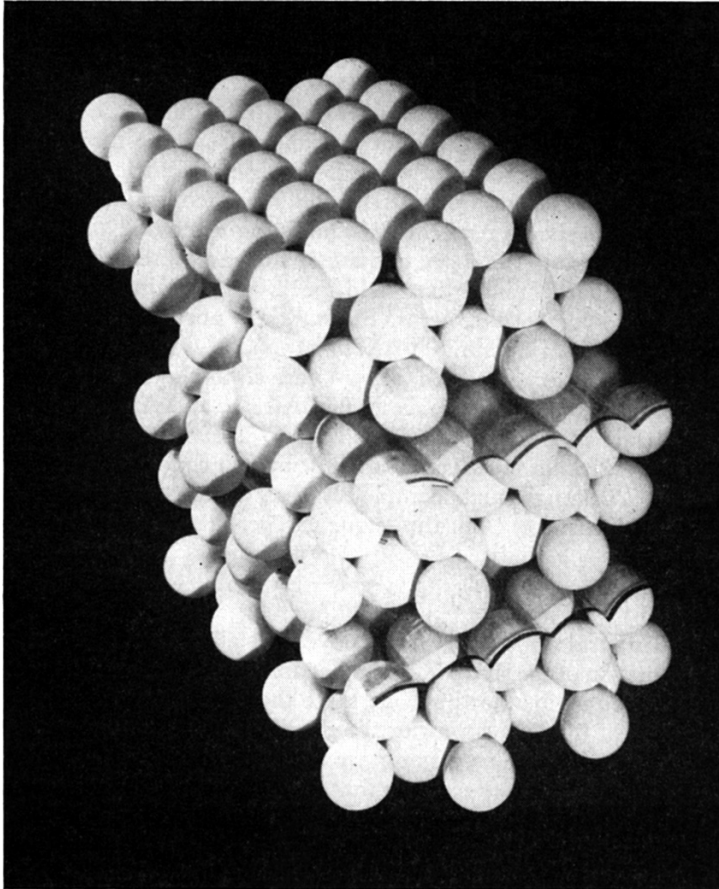


12.8 (a) Electron density map of clino-chrysotile projected down the *b*-axis (circumferential direction in the cylindrical layers); (b) diagram showing the packing of the layers viewed in the same direction as (a).

another in the spread of the values observed for the proportion of ortho-chrysotile in specimens obtained from them. Thus specimens from the major commercial Canadian deposits have not been observed with more than 7% ortho-chrysotile and they usually contain much less, whereas the Rhodesian deposits give specimens containing up to 35%, although the lower the values the more frequently they are observed. This is true also of other localities that yield specimens containing a greater range of ortho-chrysotile content. Substantially pure ortho-chrysotile is known only from Silesia.

The stacking sequences in ortho- and clino-chrysotile may be symbolized by the two sequences ABABAB ... and AAAAAA ..., where A and B stand for layers turned end to end with respect to each other. Fibre from a few deposits is built up in random sequences of A and B. Although such completely disordered stacking is rare, occasional 'mistakes' in the sequence probably occur in most specimens.





129 Packing model of chrysotile, showing a small portion of three layers. The films outline the corrugations simulated by the rows of hydroxyl groups as a result of the relative disordering of the layers round the circumference of the cylinders.

#### 12.4.5 The texture of chrysotile from X-ray evidence

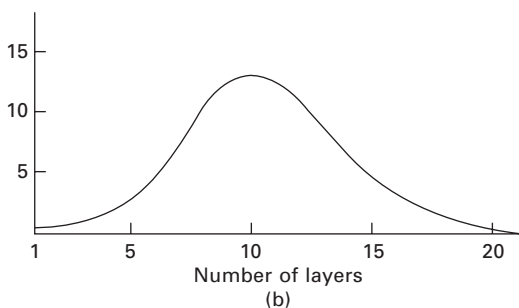
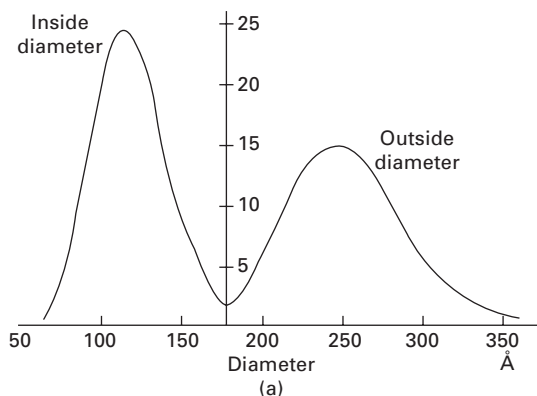
The structural results described above have all been obtained from a consideration of the sharp X-ray reflections. The diffuse reflections are of little value for that purpose, since their form is more sensitive to the sizes of the fibrils than to the details of the atomic positions. They can therefore be used to obtain information about the texture of the material. It can be shown that the form of these reflections is not compatible with the assumption that all the fibrils in a specimen are of the same diameter; if that were the case, many of the diffuse reflections would be split up into rows of resolved spots. Such a situation does, in fact, occur in electron-diffraction photographs of

single fibrils of chrysotile. To explain the smooth profiles of the diffuse X-ray reflections, one must assume that both the inside and outside diameters of the tubular fibrils have a considerable range and that the frequency of occurrence of fibrils falls as both the inside diameter decreases and the outside diameter increases from a preferred value. This is the behaviour that would be expected, since the reason for curvature of the layers is the relief of strain, and this can only be complete for one particular radius of curvature. For radii less than or greater than this, the strain energy will increase progressively and will change more rapidly as the radius falls than as it increases. We may therefore expect that there will be a greater spread of outside diameters than of inside diameters and that their ranges should meet but not overlap. It is possible to set up a mathematical model on this basis containing two arbitrary parameters, one of which is the radius of the strain-free layer and the other a measure of the relationship between strain energy and the frequency with which a layer occurs. These parameters can then be adjusted to give the best possible fit between the observed and calculated shapes of the diffuse reflections. The results obtained for Canadian chrysotile are shown in Fig. 12.10, from which it will be seen that, on this model, the strain-free layer has a radius of about 90 Å and the most frequently occurring fibril has inside and outside diameters of 110 Å and 250 Å and so contains ten layers.

The form of these frequency curves has received confirmation from direct measurements of large numbers of synthetic chrysotile fibres in the electron microscope (29). The radius of the strain-free layer deduced from these measurements is lower than that found above, and so are the fibril sizes, but these values are likely to be affected by the precise composition of the material and the conditions of crystallization. Approximate confirmation of the scale of the results comes from the breadth of the sharp X-ray reflections, which is inversely proportional to an appropriately weighted-mean wall-thickness of the tubes. The value obtained in this way for Canadian chrysotile is 15 layers, whereas the same weighted-mean from the above distributions is about 13 layers.

#### 12.4.6 Helical and spiral structures in chrysotile

It has already been mentioned in Section 12.5.3 that cylindrical lattices may take up both helical and spiral configurations. In the former, the layers are wrapped round into separate coaxial cylinders but the *b*-axis lies on a helix of low pitch instead of on a circle. In the latter, the layer is wrapped up on itself like a roll of paper; a helical characteristic may also be superimposed on such a configuration. Such structures are of interest because they would possess a recurring growth-step like a crystal with a screw dislocation and they might therefore be of importance in the formation and growth of chrysotile fibres. Indeed, Jagodzinski and Kunze (30) have put forward a



12.10 (a) Calculated probability distribution of inside diameters (left-hand curve) and outside diameters (right-hand curve) for a specimen of Canadian chrysotile; (b) probability distribution (obtained from (a)) of the number of layers in the wall of the cylindrical fibres.

theory of chrysotile growth based on the assumption that nucleation of a new layer of material is so improbable that any nucleus which has no helical component will not grow into a fibre at all, while any nucleus which has a helical character but no spiral component will grow into a fibre with a wall-thickness of one layer only. This attractive theory cannot be substantiated in detail. Although there is at present no way in which a spiral form of the layers can be distinguished from a circular cylindrical form, the fact that all the forms of chrysotile have two layers in the radial repeat shows that at least two separate nucleation steps must have occurred. The force of the argument is therefore weakened. Helical structures, on the other hand, can be distinguished from non-helical ones by X-ray diffraction (26), though the differences are virtually confined to reflections lying very close to the origin of the higher-order layer lines. It is found that some specimens consist predominantly of helical fibres, but others consist predominantly of non-helical fibres and yet others are mixtures of the two types. In some specimens of chrysotile that have a helical structure, it is possible that different fibrils may

have their *b*-axes lying on helices with a variety of pitches, but a specimen from the major Canadian deposits has been shown to contain fibrils of one single pitch only, in which the helix advances by one axial repeat unit per turn. This fact is of considerable importance and will be referred to again in the following section.

#### 12.4.7 General considerations on the texture of chrysotile

The foregoing discussion has been based entirely on observations made with the electron microscope and by X-ray- and electron-diffraction techniques. However, in a discussion of chrysotile texture, it is necessary to take account also of results obtained from surface-area and density determinations. Tubular fibres of the size deduced from the electron-microscope and X-ray-diffraction work would be expected to have a total surface area of about  $110 \text{ m}^2/\text{g}$ , of which  $80 \text{ m}^2/\text{g}$  would be due to the external surface of the tube and the remainder to its internal surface. A close-packed parallel array of such tubes would also have a total porosity of about 28%, of which 9% would be due to inter-fibrillar voids and 19% to the cylindrical hollow within each tube. The bulk density of such a close-packed array should therefore be only 72% of that of the material of the tube walls, i.e., about  $1.84 \text{ g/cm}^3$  instead of about  $2.55 \text{ g/cm}^3$ .

Noll, Kircher and Sybertz (29) have shown that synthetic chrysotile (see Section 12.6) does indeed have a surface area (by nitrogen adsorption) of the expected order of magnitude ( $101 \text{ m}^2/\text{g}$ ). Natural chrysotile, however, may give a value as low as only a few  $\text{m}^2/\text{g}$  before it is 'opened' (i.e., subjected to mechanical work to separate the fibres). The measured area increases on opening and hence much of the potential surface area is obviously inaccessible. However, the value has not been observed to rise above about  $40 \text{ m}^2/\text{g}$  and is usually in the range 12–25  $\text{m}^2/\text{g}$ , so that, if the theoretical surface area is present, a considerable part of it must be permanently inaccessible even to nitrogen. It would not be difficult to explain such inaccessibility were it not for the conflicting evidence of density determinations. Careful determinations in a density bottle with either water or carbon tetrachloride yield values of 2.53 to 2.6  $\text{g/cm}^3$  for fibres from various sources, a fact which suggests that all the void spaces are accessible to these liquids. The apparent discrepancy between the experimental results is removed by the work of Pundsack (31), who showed that a block of unopened fibre sealed round with wax had a density (after correction for the wax) near to that of the close-packed material. Thus both surface area and density results indicate that the percentage of voids is small, a result that is a complete contradiction of the electron-microscope and X-ray diffraction results,

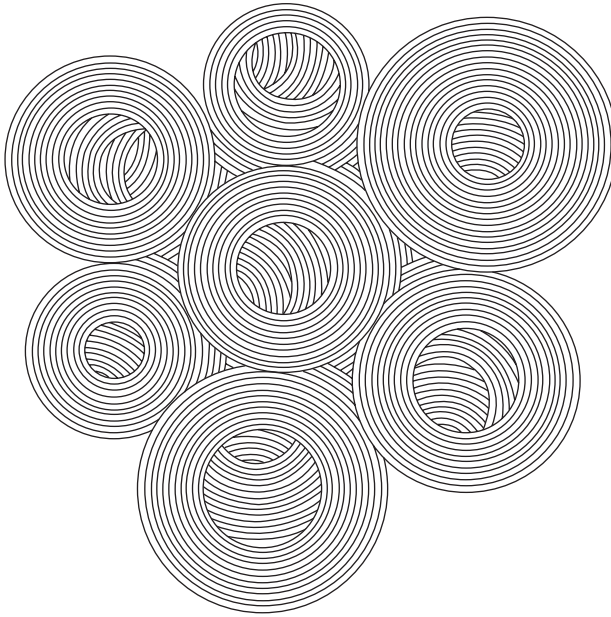
This discovery has led to some revival of belief in a 'ribbon' structure rather than a tube structure for chrysotile. It has been suggested that the tubular appearance in the electron microscope is actually an artefact that is due to the admitted tendency of thin lamellae of this material to curl up when separated from their parent mass. This theory appears to be untenable on the following grounds.

- (a) The tubes observed in the electron microscope are not thin-walled (one-layered) tubes, and the formation of such perfect thick-walled (multi-layered) tubes as artefacts would require the ribbons to have a most improbable trapezoidal cross-section.
- (b) Electron micrographs of replicas of fracture surfaces of blocks of chrysotile show concave cylindrical depressions, whose dimensions support the idea that they fitted the outside of cylinders that have broken away.
- (c) The packing of the layers in chrysotile is comprehensible only in terms of cylindrically curved layers.
- (d) The existence of macroscopic fibre bundles with a helical structure and a unique helix angle is comprehensible only if the cylindrical layers deduced in (c) are wrapped into complete cylinders in the unopened fibre mass.

The only explanation for the density results compatible with the other data is that the spaces between the cylinders are largely filled up with layers in the form of incomplete cylindrical arcs, co-axial with the main parts of the fibrils, and that the tubes themselves are largely stuffed either with similar curved ribbons lying parallel to the tubes but not co-axial with them, or with some more or less amorphous material of the same composition. It must then be assumed also that either there is some selection of the less completely stuffed fibres in the preparation of specimens for the electron microscope or the hollow appearance is enhanced by some diffraction effect. Circumstantial evidence in favour of this explanation is given by the fact that:

- (a) natural chrysotile looks much less hollow in the electron microscope than does synthetic chrysotile;
- (b) some specimens do contain at least a proportion of the expected voids (32); and
- (c) the assumption of the presence of incomplete layers improves the agreement of the calculated and observed profiles of the diffuse X-ray reflections in certain particulars (33).

If the above hypothesis is correct, a cross-section of a group of fibrils will have the form shown in Fig. 12.11.



12.11 Hypothetical cross-section of a group of chrysotile fibrils in which the voids are filled by ribbon-like layers.

#### 12.4.8 Chemical properties and identification

Chrysotile begins to decompose by loss of water from the hydroxyl groups at 550°C. The loss of water is slow and does not go to completion at this temperature. By heating at higher temperatures of up to 500°C, increased water loss, up to that corresponding to the whole content of hydrogen, can be achieved. The crystal structure is unaffected by relatively large losses of water provided that the temperature has not exceeded about 575°C. Presumably the water loss proceeds by migration of hydroxyl groups (and an equal number of protons) from unchanged regions into the vacancies already created and so eventually to a free edge of the layers, from which the water molecule can be lost. At higher temperatures, the structure slowly changes to a forsterite pseudomorph consisting of small crystallites, some with their [010] and some with their [013] axes oriented parallel to the fibre-axis (34). At 600°C, this change takes more than eighteen hours to go to completion. At higher temperatures, the water loss and forsterite formation proceed much more rapidly and, as a result, the main endothermic effect in the D.T.A. curve of chrysotile is at about 700°C. This is about 100°C lower than that of the platy serpentine mineral antigorite but the same as that of the other platy serpentine, lizardite.

A patent is in existence for modifying the properties of chrysotile by heating it for a short time (five seconds) causing it to fall through hot gases from an oil burner (35). This is likely to affect only the outside of fibre bundles. It is claimed that the treated fibre has enhanced drainage properties, which are of value in wet processes.

Chrysotile is attacked by strong acids with removal of the magnesium, leaving a siliceous residue. The residue retains the fine fibrous appearance but is brittle and completely amorphous as judged by X-ray diffraction. The destruction of the chrysotile is completed within one hour in normal HCl at 95°C (36). It is therefore less stable than the other serpentine minerals: lizardite (37) and antigorite are not attacked under these conditions; the former is destroyed in somewhat less dilute acid but antigorite requires concentrated acid for its destruction.

Chrysotile can be distinguished by its X-ray pattern and by its refractive index (1.54–1.56) from amphiboles (>1.60). There is some overlap with the refractive index of glass fibre (1.52–1.55). A staining test using a glycerol solution of iodine has also been proposed (38). This gives a positive reaction with fibrous brucite. The different crystallographic forms of chrysotile can only be distinguished from each other by X-ray or electron diffraction. This, or the electron microscope, is also the only satisfactory method of distinguishing sub-microscopically fibrous chrysotile from the other serpentines, and even then considerable care is needed (25). This is a matter of some importance in the analysis of the dust that often adheres to commercial chrysotile.

## 12.5 Synthetic asbestos

A considerable amount of work has been done in various places on the synthesis of asbestos, but without much success. A so-called synthetic asbestos was produced in Germany during the war but is stated to have been chemically unstable, so its characterization must be regarded as very dubious; it was of very low quality (39). Progress has been made in the synthesis of amphiboles and fluoro-amphiboles (40) from the melt, and acicular growths have been obtained by the use of thermal gradients, but no flexible fibres have been reported. Hydrothermal synthesis of chrysotile has been reported by many authors, and the products have given some of the best electron micrographs of chrysotile, but the fibre length has always been very short, of the order of  $1 \mu$ . Longer fibres of up to 0.2 mm have been reported by Noll (41) as a result of growth by slow diffusion in a gel. Electron-microscopically observable tubular fibres of  $1\text{-}\mu$  length analogous to chrysotile can also be prepared in which magnesium is replaced by nickel (42) or cobalt (43).



## 12.6 References

- 1 W. T. Schaller. *Bull. U.S. Geol. Survey*, 1916, No. 610, 136.
- 2 B. E. Warren. *Z. Krist.*, 1930, 72, 42.
- 3 B. E. Warren and D. I Modell. *Z. Krist.*, 1930, 75, 161.
- 4 E. J. W. Whittaker. *Acta Cryst.*, 1949, 2, 312.
- 5 J. Zussman. *Acta Cryst.*, 1955, 8, 301.
- 6 J. Zussman. *Acta Cryst.*, 1959, 12, 304.
- 7 H. Heritsch, P. Paulitsch and E-M. Walitzi. *Tschermaks min. u. pet. Mitt.*, 1957, 6, 215.
- 8 H. Megaw. *Acta Cryst.*, 1949, 2, 419.
- 9 D. McConnell. *Amer. Min.*, 1950, 35, 166.
- 10 N. Sundius. *Sveriges Geol. Undersökn. Arsbok.*, 1944, 38, No. 2.
- 11 J. J. Frankel. *Mining Mag., London*, 1953, 89, 73.
- 12 J. C. Rabbitt. *Amer. Min.*, 1948, 33, 263.
- 13 E. J. W. Whittaker. *Acta Cryst.*, 1960, 13, 291.
- 14 M. Wittels. *Amer. Min.*, 1952, 7, 28.
- 15 H. V. Anderson and G. L. Clark. *Industr. Engng Chem.*, 1929, 21, 924.
- 16 B. E. Warren and W. L. Bragg. *Z. Krist.*, 1930, 76, 201.
- 17 B. E. Warren and K. W. Hering. *Phys. Rev.*, 1941, 59, 925.
- 18 E. Aruja. Ph.D. Thesis, Cambridge, 1943.
- 19 L. Pauling. *Proc. Nat. Acad. Sci. USA*, 1930, 16, 578.
- 20 J. Turkevitch and J. Hillier. *Anal. Chem.*, 1949, 21, 475.
- 21 T. F. Bates, L. B. Sand and J. F. Mink. *Science*, 1950, 111, 512.
- 22 W. Noll and H. Kircher. *Neues Jb. Mineral Mh.*, 1951, 219.
- 23 E. J. W. Whittaker. *Acta Cryst.*, 1955, 8, 571.
- 24 E. J. W. Whittaker. *Acta Cryst.*, 1954, 7, 827; 1955, 8, 261, 265, 726.
- 25 E. J. W. Whittaker and J. Zussman. *Min. Mag.*, 1956, 1, 107.
- 26 E. J. W. Whittaker. *Acta Cryst.*, 1956, 9, 855.
- 27 E. J. W. Whittaker. *Acta Cryst.*, 1956, 9, 862.
- 28 E. J. W. Whittaker. *Acta Cryst.*, 1956, 9, 865.
- 29 W. Noll, H. Kircher and W. Sybertz. *Kolloid-Z.*, 1958, 157, 1.
- 30 H. Jagodzinski and G. Kunze. *Neues Jb. Mineral Mh.*, 1954, 137.
- 31 F. L. Pundsack. *J. Phys. Chem.*, 1956, 60, 361.
- 32 G. L. Kalousek and L. E. Muttart. *Amer. Min.*, 1957, 42, 1.
- 33 E. J. W. Whittaker. *Acta Cryst.*, 1957, 10, 149.
- 34 G. W. Brindley and J. Zussman. *Amer. Min.*, 1957, 42, 461.
- 35 US Patent 2, 616, 801.
- 36 B. Nagy and G. T. Faust. *Amer. Min.*, 1956, 41, 817.
- 37 E. J. W. Whittaker and J. Zussman. *Amer. Min.*, 1958, 43, 917.
- 38 M. Morton and W. G. Baker. *Trans. Canad. Inst. Mining Met.*, 1941, 44, 515.
- 39 G. M. Bloomfield. F.I.A.T. Final Report 1070, 1947.
- 40 J. E. Comeforo and J. A. Kohn. *Amer. Min.*, 1954, 39, 537.
- 41 W. Noll. F.I.A.T. report, quoted in 1950 Materials Survey—Asbestos. US Bureau of Mines, 1954.
- 42 W. Noll and H. Kircher. *Naturwiss.*, 1952, 39, 233.
- 43 W. Noll, H. Kircher and W. Sybertz. *Naturwiss.*, 1958, 45, 489.

## Thermally and chemically resistant fibres: structure and properties

---

J W S HEARLE, University of Manchester, UK

**Abstract:** Commodity textile fibres, which are described in other chapters, vary in their chemical and thermal resistance. Other resistant fibres are produced specially and described in this chapter. Information on detailed fibre structure is limited. For thermal resistance, the following types are produced: crosslinked, thermoset polymer fibres; *Nomex*, an aromatic polyamide; arimid fibres; the ladder polymer PBI fibre; and partially carbonised fibres. For chemical resistance the types are chlorinated and fluorinated fibres and some other linear polymer fibres.

**Key words:** thermoset fibres, *Nomex*, arimid fibres, PBI fibre, chlorinated and fluorinated fibres.

### 13.1 Introduction

Commodity textile fibres cease to be usable above temperatures of about 200°C or even lower. Nylon 66 and polyester (PET) soften above the glass transition temperature and stick together at about 220°C (lower temperatures for nylon 6 and cellulose acetate). Cotton, rayon, wool and silk char at 180–200°C. Polyethylene naphthalate (PEN) has a higher melting point than PET. The high-modulus fibres, except for HMPE, can be used at higher temperatures: para-aramids and glass, around 500°C, PBO higher; ceramics around 1000°C; and carbon around 3000°C.

The commodity and high-performance fibres vary in their chemical resistance. The olefins, polyethylene and polypropylene have the best chemical resistance, but cannot be used at higher temperatures. The aromatic esters and amides are more resistant than the aliphatic types. Glass, ceramic and carbon fibres have good resistance.

The above fibres are dealt with in other chapters of this book. The present short chapter covers other fibres that are specifically produced for their thermal or chemical resistance. Unfortunately, a comment by Horrocks (2001a) in regard to some fluorinated polymer fibres applies in varying degrees to the fibres included in this chapter: *very little is published about these fibres outside of the technical data sheets provided by manufacturers*. The chemistry is usually well documented but there is little specific information on the physical fine structure. Where the mechanical properties of the linear polymer fibres are similar to those of common textile fibres described in other chapters of

this book, it can be inferred that the physical fine structures will be similar. Their structures will be homogeneous, except for possible skins, and their cross-sections roughly circular or elliptical.

## 13.2 Thermally resistant fibres

### 13.2.1 Thermosets

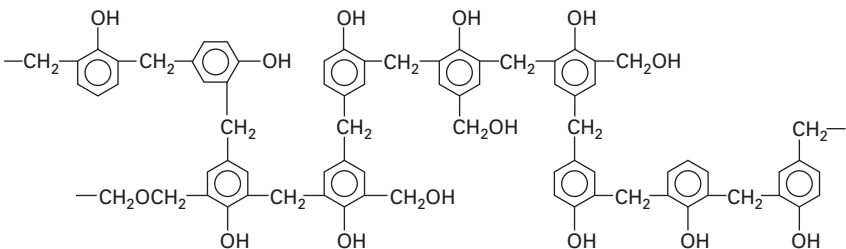
Crosslinked polymers are more familiar as rigid plastics, but both phenol-formaldehyde and melamine-formaldehyde fibres are made by extruding high-viscosity resin and then heat-treating to complete the cure. They have high temperature and chemical resistance, though the phenolic fibre slowly oxidises above 150°C or carbonises above 250°C in the absence of air.

The novoloid fibre *Kynol* has the chemical structure shown in Fig. 13.1, with the formaldehyde,  $\text{CH}_2=\text{O}$ , crosslinking the phenol,  $\text{C}_6\text{H}_5\text{OH}$ . The fibre will have a homogeneous structure and is essentially a single network molecule.

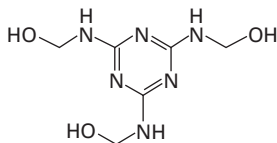
*Basofil*, melamine, shown in Fig. 13.2, is crosslinked by formaldehyde to form the network structure of the fibre. In order to make the fibres suitable for processing on textile machinery, substituted melamines are included in the reaction to act as an internal plasticiser (Eichhorn, 2001).

### 13.2.2 Aromatic polymer fibres

A group of aromatic polymer fibres, which have useful thermal resistance, have been described by Horrocks (2001b).



13.1 Polymer structure of *Kynol* novoloid fibre. From Schwaenke (2001).



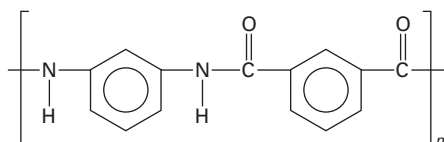
13.2 Formula of melamine.

The meta-aramid fibres, *Nomex* (formula in Fig. 13.3) and others, have good textile properties, which make them suitable for fire-protection clothing. They have thermal resistance in excess of 300°C for short-term exposure, and high inherent flame resistance. In contrast to the relatively straight chains of the para-aramids, such as *Kevlar*, in which opposite positions of the benzene ring are substituted, the meta-aramids are substituted on next-but-one positions. The fibres, which are spun from solution, do not crystallise as readily as the para-aramids and the polymer certainly does not form fully oriented liquid crystals. The fibres will have a partially crystalline, partially oriented, probably micellar structure similar to that of other solution-spun fibres.

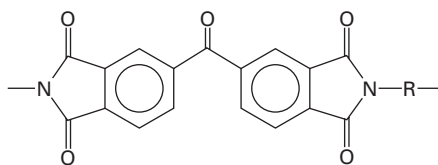
The aramid fibre P84 from *Inspec* is composed of poly(4,4'-diphenylmethane-*co*-tolylene benzophenonetetracarboxylic imide). The formula, shown in Fig. 13.4, has a five-membered ring attached to a benzene ring, but not the relatively straight chain with two five-membered rings found in PBO. It is also solution-spun and would be expected to have a similar fine structure to the meta-aramid fibres. Unlike other fibres mentioned here, it has a multilobal cross-section shown in Fig. 13.5.

Another fibre in this group is the poly (aramide-imide) fibre *Kermel*. Its chemical formula is reported to be that shown in Fig. 13.6.

Superior thermal and chemical resistance is shown by polybenzimidazole (PBI) fibres described by Thomas (2001). PBI is a ladder polymer with the formula shown in Fig. 13.7(a). Flame stability is enhanced by treating with sulphuric acid to give the sulphonated form, Fig. 13.7(b), or with phosphoric acid. Comparing the formulae in Figs. 13.3 to 13.7, it is interesting to note the increasing complexity of the chemical structure. In thermogravimetric tests, there is only a slow loss of weight in PBI fibres heated in air until a sharp drop occurs around 600°C. In nitrogen, the slow loss continues to

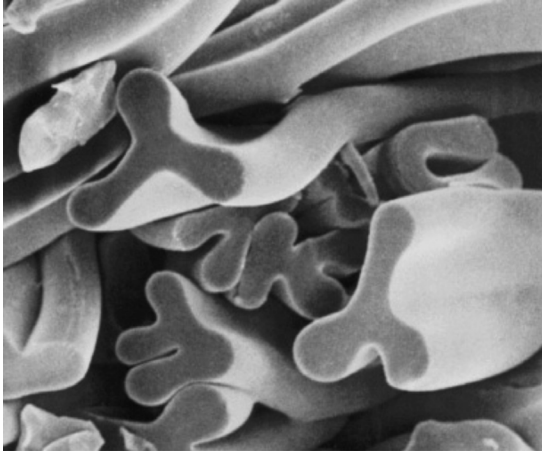


13.3 Formula for meta-aramid fibre, *Nomex*.

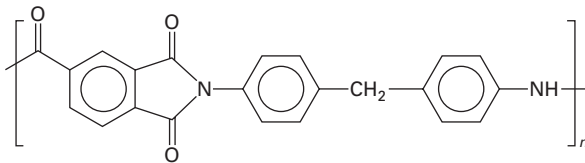


where R = C<sub>6</sub>H<sub>4</sub> · CH<sub>2</sub> or C<sub>6</sub>H<sub>4</sub> · CH<sub>2</sub> · C<sub>6</sub>H<sub>4</sub>

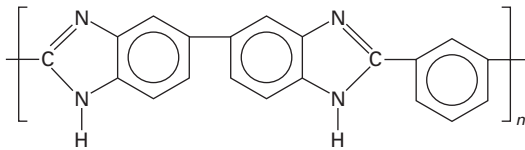
13.4 Formula for P84 arimid fibre. From Horrocks (2001b).



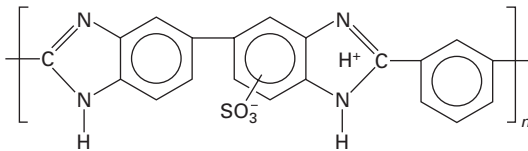
13.5 Cross-sections of P84 fibre. From Evonik Industries, [www.p84.com/products/p84](http://www.p84.com/products/p84).



13.6 Formula for *Kermel*.



(a)



(a)

13.7 Formulae for (a) PBI, and (b) sulphonated PBI.

much higher temperatures. PBI fibres, which are dry-spun from solution, have mechanical properties similar to those of standard viscose rayon. This implies that the fibres have the same partially crystalline, partially oriented structure as other fibres with good textile performance.

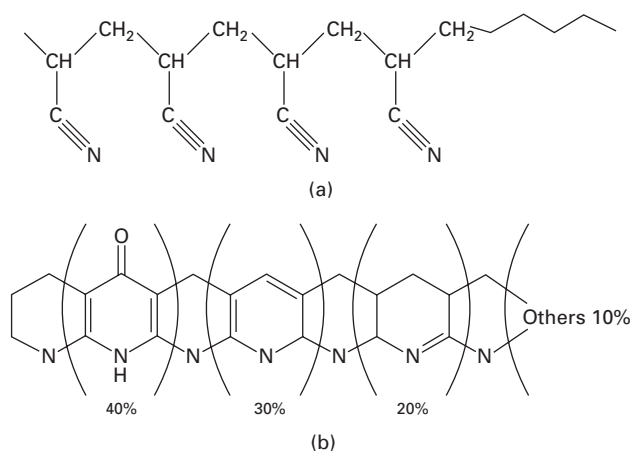
### 13.2.3 Partially carbonised fibres

The first heating stage of converting acrylic fibres into carbon fibres results in a black fibre with good thermal and flame resistance. Similar results can be obtained with cellulose fibres, but acrylics are the usual commercial precursor. These carbonised or semi-carbon fibres are described by Saville (2001). Heating in air of polyacrylonitrile, Fig. 13.8(a), leads to complicated oxidation reactions, which cyclise the polymer into a ladder form. The details of the final fibre composition are uncertain, but, according to Saville, it is thought to be of the general form shown in Fig. 13.8(b). As with other carbon fibres, the particular form of acrylic fibre, including its co-polymerisation and any void structure, will influence the chemical and physical structure of the partially carbonised fibre. The commercial fibre *Panox* uses Courttelle fibres as the precursor. The mechanical properties are similar to those of standard viscose rayon, which indicates that, in addition to the rigid ladder forms, there are other molecular forms, presumably in the 'Others 10%' of Fig. 13.8(b), that give a degree of freedom to the structure.

## 13.3 Chemically resistant fibres

### 13.3.1 Chlorinated and fluorinated fibres

As described by Horrocks (2001a), addition polymers with chlorine or fluorine substitution for hydrogen in  $(-\text{CH}_2-\text{CH}_2)_n$  have improved chemical resistance, which can be combined with better textile properties and thermal stability than polyethylene fibres. The chlorinated fibres are based on the fully



13.8 (a) Polyacrylonitrile precursor; (b) suggested composition of partially carbonised acrylic fibre.

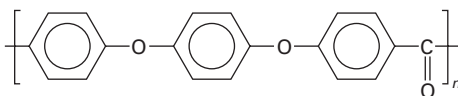
substituted poly(vinylidene chloride) (PVDC),  $(-\text{CCl}_2.\text{CCl}_2-)_n$ , though this may be co-polymerised with polyvinyl chloride (PVC),  $(-\text{CH}_2.\text{CHCl}-)_n$ . *Saran* is the original trade name and is commonly used as thick monofil. The fibre structure will have similarities to PVC fibres described in Chapter 10, Section 10.3 of *Handbook of Textile Fibre Structure, Volume I*.

There is a more diverse range of fluorinated fibres. The best known is poly(tetrafluoroethylene) (PTFE),  $(-\text{CF}_2-\text{CF}_2)_n$ . The similar size of carbon and fluorine atoms gives a compact form to the chain molecules, which can pack closely in locally well-ordered forms with strong intermolecular forces. The consequent chemical inertness is a factor in the low friction of PTFE, but also makes the polymer intractable. In the *DuPont* process for making *Teflon*, filaments are extruded as a suspension of PTFE in a cellulose dope and then sintered at high temperature to give a coherent fibre structure. Alternatively a paste process can be used to make film, which can be slit and drawn to form fibres. This results in a porous fibre structure with low density, which is useful for some purposes. Another process peels off fibres by precision turning of a PTFE rod. *Teflon* can be used up to almost 300°C.

Poly(vinylidene fluoride) (PVDF),  $(-\text{CF}_2.\text{CF}_2-)_n$ , polyvinyl fluoride (PVF),  $(-\text{CH}_2.\text{CHF}-)_n$  and FEP co-polymers have lower melting points and can be melt-spun. Their fibres combine good tensile properties with chemical resistance. FEP fibres consist of various co-polymers of PTFE, designated as PTFE-FEP with hexafluoropolypropylene  $(-\text{CF}(\text{CF}_3).\text{CF}_2-)$ , ECTFE with ethylene  $(-\text{CH}_2.\text{CH}_2-)$  and chlorotrifluoroethylene  $(-\text{CFCl}.\text{CF}_2-)$ , and ETFE with ethylene and trifluoroethylene  $(-\text{CHF}.\text{CF}_2-)$ .

### 13.3.2 Other linear polymer fibres

McIntosh (2001) describes poly(etheretherketone), PEEK, as the foremost member of a family of aromatic thermoplastic polymers, the polyetherketones. Its melting point is 334°C and it can be melt-spun into fibres. The repeat unit of the polymer, shown in Fig. 13.9, consists of three benzene rings linked by two ether groups and one ketone group. Because of the similarity of mechanical properties, it can be assumed that the fine structure of PEEK fibres will be similar to those of nylon and polyester fibres, namely partially oriented and about 50% crystalline. However, this still leaves open the details of the crystalline/amorphous form. The advantage over nylon and polyester is in PEEK's ability to operate in more extreme conditions and over long lifetimes.



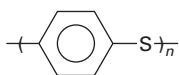
13.9 Formula of poly(etheretherketone), PEEK.



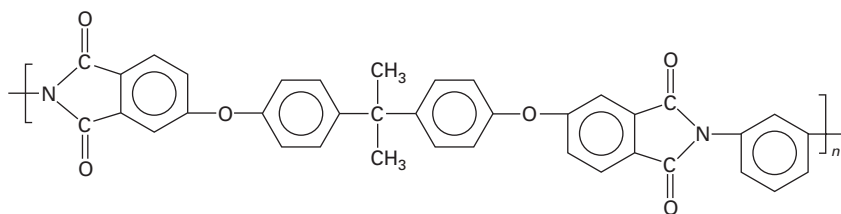
Horrocks (2001c) describes two other linear polymer fibres with good chemical resistance. Poly(phenylene sulphide), PPS, has the formula shown in Fig. 13.10. The melting point is 285°C, so that it can be melt-spun. The fibre has properties similar to nylon, but slightly weaker and with little moisture absorption, and its structure can be assumed to be similar. Poly(ether imide), PEI, is used mainly as an engineering plastic. PEI can be melt-spun into fibres, which have a lower strength and melting point than PEEK or PPS and are more extensible. Fibres based on PEI are reported to have the somewhat irregular chemical formula shown in Fig. 13.11. Consequently, in contrast to the other fibres mentioned here its structure is amorphous.

### 13.4 Conclusion

In conclusion, it is worth quoting a comment by Horrocks (2001d): *An observation that is perhaps worthy of note is the very large number of specialty fibres reported in the literature and often patented since the 1960 period, of which only the fibres [mentioned in this chapter] have survived as commercial examples. Furthermore, not until very recently has the general commercial availability of these fibres increased, as reductions in costs coupled with increasing performance demands have enabled them to displace the more conventional fibres.* The variety of fibre structures provides a range of fibre properties to meet the performance requirements of particular applications. There is a great diversity of uses: filtration of corrosive chemicals or hot gases; packing materials in chemical plants; conveyor belts for aggressive substances; electric cable wrapping for aerospace use; composites for uses in aircraft engines; fire blockers under aeroplane seats; paper machine dryer fabrics; protective clothing; and many more that are described in the various sections of Chapters 8 and 9 of *High-performance Fibres* (Hearle, 2001).



13.10 Formula of poly(phenylene sulphide), PPS.



13.11 Formula of poly(ether imide), PEI.

A primary factor in choosing a fibre is the particular chemical and thermal environment that has to be resisted, but the mechanical and other physical properties also influence the choice. Simple insulation has minimal mechanical requirements, but to replace wire rope by fibre rope in a hot mineshaft, strength and modulus are important. In paper machines, with repetitive bending round rollers, resistance to fibre fatigue is needed. In order to be worn, clothing must be comfortable. For large-volume industrial applications cost is a critical determinant, but for more specialised uses meeting demanding performance requirements may be more important. Continued research is likely to lead to development of fibres having structures with improved performance for current uses and the ability to take fibre-based materials into new demanding environments.

### 13.5 References

- Eichhorn H (2001) in Hearle (2001), 282–288.  
Hearle J W S, editor (2001), *High-performance Fibres*, Cambridge, Woodhead Publishing.  
Horrocks A R (2001a), in Hearle (2001), 260–266.  
Horrocks A R (2001b), in Hearle (2001), 292–300.  
Horrocks A R (2001c), in Hearle (2001), 274–278.  
Horrocks A R (2001d), in Hearle (2001), 321.  
McIntosh B (2001), in Hearle (2001), 267–274.  
Saville N (2001), in Hearle (2001), 301–310.  
Schwaenke H (2001), in Hearle (2001), 288–292.  
Thomas C (2001), in Hearle (2001), 310–322.

## Structure, properties and characteristics of optical fibres

---

A ARGYROS, The University of Sydney, Australia

**Abstract:** This chapter outlines the variety of established and experimental optical fibres, their structure, physical and optical properties and their applications. An initial description of waveguide concepts is followed by an examination of common fibre structures and the influence of the structure and material on the optical properties. This is followed by examining the established technologies of silica and polymer optical fibres and their applications, the emerging technology of microstructured optical fibres and fibres of other materials.

**Key words:** optical fibres, waveguides, microstructured optical fibres, photonic crystal fibres, photonic bandgaps.

### 14.1 Introduction

A variety of optical fibres have been developed, having diverse applications including communications, medicine, astronomy and textiles. Their purpose has been the transmission or manipulation of light from 200 to 6000 nm in wavelength, achieved through the chemical and physical structure of the fibres: the materials the fibre is made of and its refractive index profile. These determine a fibre's transparency, its mechanical properties, manufacturing complexity and cost, which in turn determine the applications of each fibre type. Silica and polymer fibres are the two established platforms, occupying almost exclusive applications. They rely on chemical variations in different parts of their cross-section, achieved through doping or the use of different materials to guide light. Another class of fibre which has emerged with vastly different properties is known as microstructured optical fibres or photonic crystal fibres and consists of a single material with microscopic air channels running the length of the fibre.

This chapter aims to outline the variety of established and experimental fibres, their structure, optical properties and applications. The first section describes various concepts in waveguide theory and the second section looks at common fibre structures, highlighting how the fibre parameters affect their optical properties. The third section is organised on a materials basis and looks at silica, polymer and optical fibres of other materials, discussing their general characteristics and applications. These are followed by the conclusion, sources of further information and references.

## 14.2 Waveguide concepts

The original principle behind optical fibres is total internal reflection of light propagating in a material with high refractive index at an interface with a lower index material (Snyder and Love, 1983; Palais, 1992). The high refractive index material is the fibre core – with index  $n_{co}$  – which is surrounded by the lower-index cladding – with index  $n_{cl} < n_{co}$  – as shown in Fig. 14.1. Light launched into the core can be reflected at the core–cladding interface by total internal reflection and guided along the fibre inside the core. This occurs if the angle of incidence on the core–cladding interface  $\theta_i$  is greater than the critical angle  $\theta_c$ , given by

$$\theta_c = \sin^{-1} \frac{n_{co}}{n_{cl}} \tag{14.1}$$

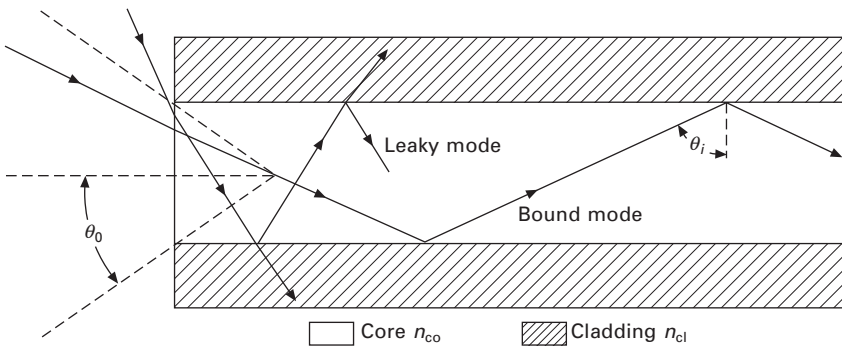
If the angle of incidence is below the critical angle, the light refracts and is only partially reflected at the interface.

### 14.2.1 Modes

As light is guided along the core, the successive reflections from the cladding require the light to interfere with itself. Only discrete angles of incidence result in constructive interference, and each of these corresponds to a guided mode. Each mode is characterised by a mode effective index  $n_{eff}$  which is related to its angle of incidence by

$$n_{eff} = n_{co} \sin \theta_i \tag{14.2}$$

Given their different angles of propagation, every mode travels with a different speed along the fibre, termed the group velocity  $v_g$ . As  $n_{eff}$  increases,



14.1 Schematic of an optical waveguide showing the core and cladding, the trajectories of rays of light in a bound and a leaky mode, and the acceptance cone (NA).

approaching  $n_{co}$ , the light propagates almost parallel to the fibre. Higher  $n_{eff}$  modes travel along shorter paths and so travel faster along the fibre (higher  $v_g$ ). The mode with the highest  $n_{eff}$  will have the highest  $v_g$  and is referred to as the fundamental mode. Fibres that support only the fundamental mode are called single-mode (SM) fibres whilst multi-mode (MM) fibres support many modes.

Modes can also be described as bound or leaky. In bound modes, no light escapes through the side of the fibre and all the light propagates along the core. In leaky modes, where total internal reflection does not occur, some power exits the fibre through the cladding at each reflection. The wavelength for which a mode makes the transition from bound to leaky is called the cut-off wavelength, and corresponds to when its angle of incidence equals the critical angle, giving  $n_{eff} = n_{cl}$ . Bound modes satisfy  $n_{cl} < n_{eff} < n_{co}$ .

### 14.2.2 Numerical aperture

The numerical aperture ( $NA$ ) of a fibre describes the range of angles that can be captured and emitted by the fibre, and depends on the index contrast between the core and cladding:

$$NA = \sqrt{n_{co}^2 - n_{cl}^2} = \sin \theta_o \quad 14.3$$

where  $\theta_o$  is the half-angle of the acceptance cone or the output, as shown in Fig. 14.1. Only light incident on the fibre endface within this cone will be incident on the core-cladding interface at an angle greater than the critical angle and be guided as a bound mode; rays outside the light cone will launch leaky modes. At the output end, as the light travels away from the fibre endface, it spreads out to an approximately Gaussian intensity profile. The edges of the cone are taken to be where the intensity drops to 5% of maximum.

### 14.2.3 Loss

The loss describes the amount of light that exits the fibre  $P_{out}$  as a fraction of the power at the input  $P_{in}$ . This is typically quoted in a logarithmic scale using decibels (dB):

$$\text{loss in dB} = -10 \log_{10}(P_{out}/P_{in}) \quad 14.4$$

Loss may arise through material absorption and/or scattering from inhomogeneity in the material. Rayleigh scattering from features of comparable size to the wavelength of light (hundreds of nanometres) increases at short wavelengths as  $1/\lambda^4$ , whereas scattering from larger features becomes independent of wavelength. Leaky modes will also suffer from confinement loss, which accounts for the fraction of light lost through the cladding. If

this is small, the light may still propagate in these modes for large distances. Large values of confinement loss mean these modes escape immediately and can be ignored.

#### 14.2.4 Dispersion

Dispersion describes the spreading of pulses of light as they propagate along the fibre. It is an important consideration in data transmission as the pulse spreading determines the minimum spacing between pulses, and hence the maximum data transmission rate. Dispersion also becomes important for a variety of nonlinear processes. It is quoted as the amount of pulse spreading per wavelength range used, per distance of propagation (in ps/nm.km).

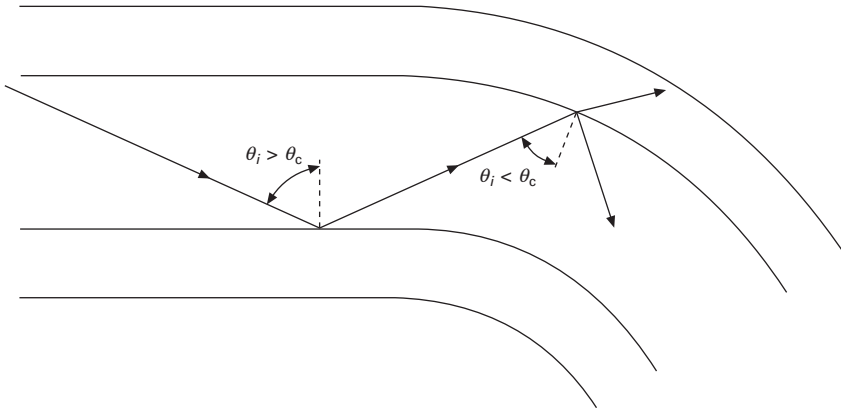
There are three types of dispersion: chromatic, waveguide, and inter-modal dispersion. Chromatic dispersion is a material property and arises from the wavelength dependence of the refractive index of a material. The different wavelength components of a pulse will see a different index and travel at different speeds, causing the pulse to spread. Generally, short wavelengths travel slower than long wavelengths.

Waveguide dispersion arises from the difference in relative size between different wavelengths and the waveguide, causing different wavelengths to travel at a different angle (or  $n_{\text{eff}}$ ) and hence a different speed. This can produce the same effect as chromatic dispersion or the opposite, with shorter wavelengths travelling faster than long wavelengths. The total dispersion is the sum of chromatic and waveguide dispersions. Since chromatic dispersion is determined by the material, the waveguide can be designed to offset it by different amounts.

Inter-modal dispersion arises in multi-mode fibres as the power from a pulse may be distributed amongst many modes, which travel with different group velocities. The pulse spreads by an amount proportional to the difference between the fastest and slowest modes and the propagation length. If the fibre contains defects that cause sufficient power transfer between modes (mode mixing), the pulse spreading is decreased and becomes proportional to the square root of the length. This may come at a cost, however, as the defects may also result in scattering losses. Single-mode fibres do not suffer from inter-modal dispersion, as all the light is in the fundamental mode.

#### 14.2.5 Bending loss

Bends in the fibre can cause leakage of light as a ray that may have otherwise been incident on the core-cladding interface above the critical angle may find itself below in the bent region of the fibre, as shown in Fig. 14.2. The bend loss is reduced for large index contrast (large  $NA$ ) fibres and increases exponentially as the bend radius decreases.



14.2 Leakage of light can be caused by bending a fibre, as the angle of incidence can fall below the critical angle.

## 14.3 Fibre structure and optical properties

### 14.3.1 Conventional fibres

Conventional fibres can be separated into two classes depending on their refractive index profile. Step-index fibres (SI) have a core of a constant, higher refractive index, whereas graded-index (GI) fibres have a gradual decrease of refractive index (Snyder and Love, 1983; Palais, 1992). The fibres can be single-mode or multi-mode, and the effect of this and a schematic of their profiles is shown in Fig. 14.3.

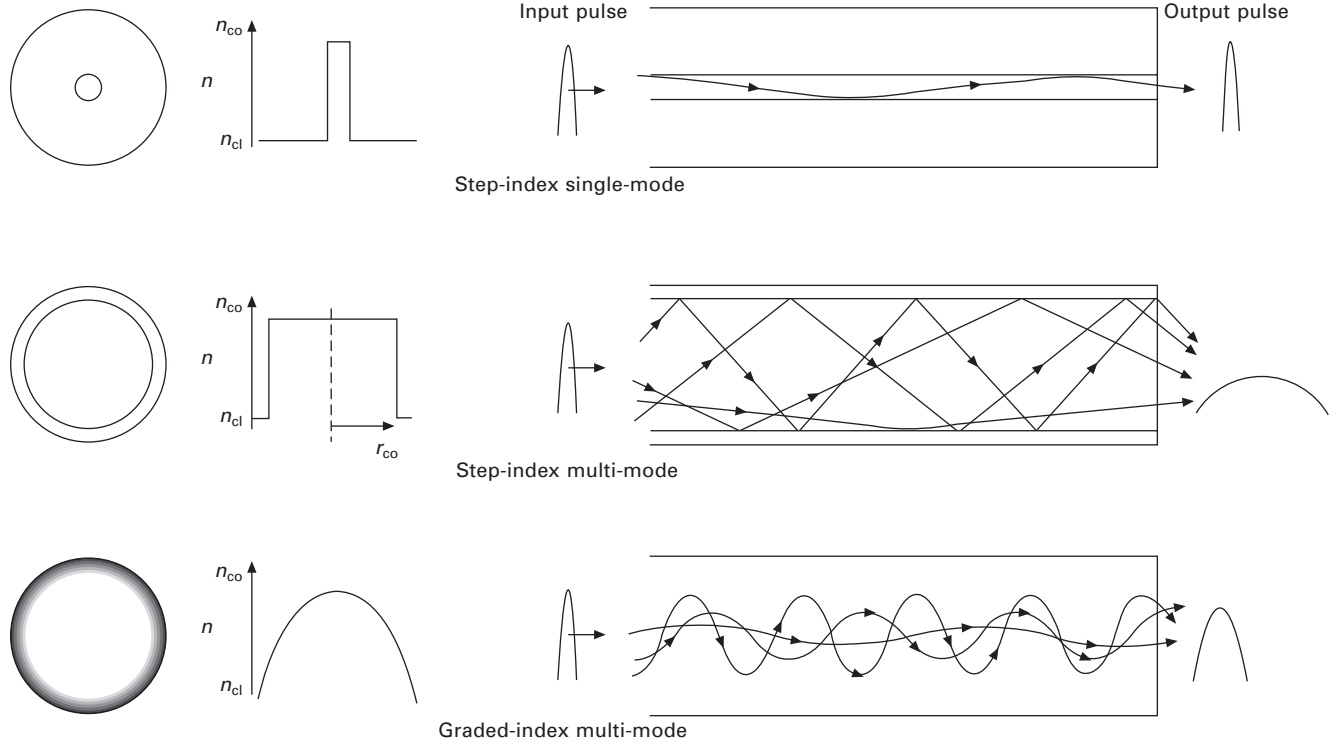
#### *Step-index fibres*

Step-index fibres can be characterised by the normalised frequency parameter  $V$ , given by (Snyder and Love, 1983)

$$V = \frac{2\pi}{\lambda} r_{\text{co}} \sqrt{n_{\text{co}}^2 - n_{\text{cl}}^2} = \frac{2\pi}{\lambda} r_{\text{co}} NA \quad 14.5$$

where  $r_{\text{co}}$  is the radius of the core and  $\lambda$  is the free-space wavelength of light. The number of modes is given by approximately  $V^2/2$ , hence large  $V$  fibres will be multi-mode. If  $V < 2.405$ , fibres are single-mode and this value of  $V$  corresponds to the cut-off of the second mode. Single-mode fibres are desirable for communications and sensing applications as they do not suffer from inter-modal dispersion and the pulse-spreading is minimised. This necessarily limits them to small cores, low  $NA$  and relatively long wavelengths. The fundamental mode has no cut-off but fibres become increasingly unable to confine the light below  $V \sim 1.2$ , becoming sensitive to bend losses and other perturbations. Other variants on the simple SI design are common





14.3 Schematics of step-index single-mode and multi-mode fibres and graded-index fibres, and the degree of pulse spreading resulting from inter-modal dispersion.

and contain further steps after the core, called W-fibres (Samut, 1978) or dispersion compensating fibres (Palais, 1992). This changes the waveguide dispersion, and hence the total dispersion of the fibres.

### *Graded index fibres*

An improvement can be made in terms of data transmission by replacing the step-index structure with a graded-index structure. The grading means the rays refract as they travel across the core (see Fig. 14.3), which equilibrates the group velocities of all the modes and thus minimises pulse spreading due to the intermodal dispersion. In principle, a parabolic profile graded index will approach the pulse spreading of a single-mode fibre, but will bring additional advantages of a larger core size and/or *NA*. In practice however, small deviations from the required profile can be detrimental and the necessary profiles are difficult to achieve.

### 14.3.2 Microstructured fibres

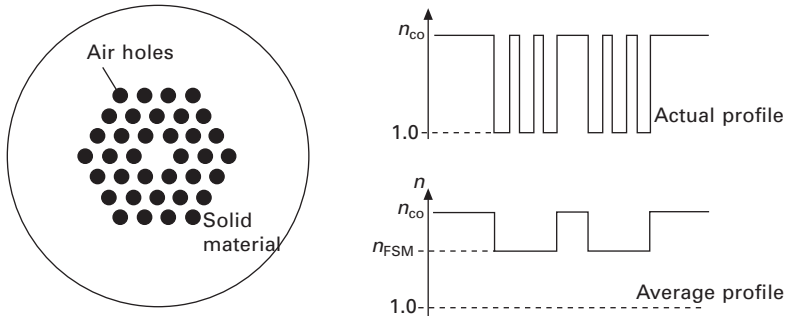
Microstructured optical fibres (MOF), also called photonic crystal fibres (PCF), are made from a single, undoped material and use microscopic air holes running the length of the fibre to guide light (Russell, 2006; Bjarklev *et al.*, 2003; Large *et al.*, 2007). The freedom of hole size and position that microstructured fibres allow gives rise to a wide range of properties not possible with conventional fibres. Microstructured fibres also fall into two categories depending on whether the refractive index of the core is the highest of the entire fibre cross-section, the two cases differing in the way they guide light.

#### *High index core*

If the structure consists of a solid core surrounded by holes, as shown in Fig. 14.4, the guidance mechanism is modified total internal reflection. This is analogous to a step-index fibre with a high index (solid) core and a low index (mixture of solid and air) cladding. In the microstructured cladding the light sees an ‘average’ material with a lower refractive index than the core, often called the effective index of the fundamental space-filling mode  $n_{\text{FSM}} < n_{\text{co}}$  (Birks *et al.*, 1997; Li *et al.*, 2008).

The exact average of air and solid – the value of  $n_{\text{FSM}}$  – is a strong function of wavelength, meaning the cladding has a very large waveguide dispersion which can be controlled through the hole size and spacing. This can be used to change the entire dispersion of a fibre with unprecedented control.

The first novel feature to be demonstrated using microstructured fibres was the ‘endlessly’ single mode fibre (Birks *et al.*, 1997). Given the large



14.4 Schematic of a high index core microstructured fibre. The light sees an average of the air and solid material in the cladding, and hence an average refractive index given by  $n_{FSM}$ .

dispersion of the cladding, in these designs  $V$  can become almost independent of wavelength, and thus the fibres can remain single mode for a much larger wavelength range. A qualitative way to view this is to rewrite Eqn (14.5) as

$$V \propto \frac{1}{\lambda} NA(\lambda) \tag{14.6}$$

with

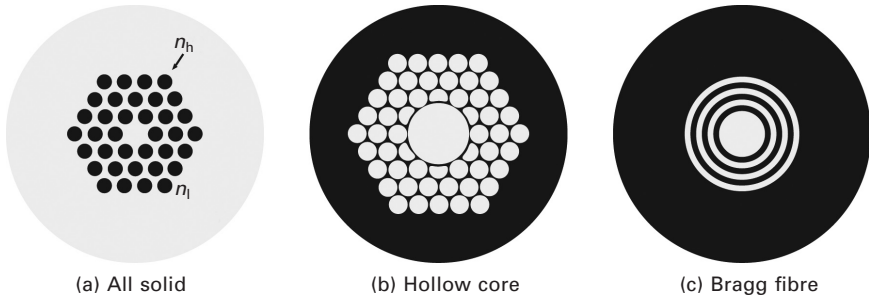
$$NA(\lambda) \propto \lambda$$

As the wavelength decreases,  $V$  is prevented from increasing by an increase in the cladding index  $n_{FSM}$  and hence a reduction of the  $NA$ .

Endlessly single-mode behaviour was demonstrated in structures like Fig. 14.4 when the diameter of the holes in the cladding is less than 40% of the hole spacing (Kuhlmey *et al.*, 2002). Larger holes give lower cladding indices and higher  $NA$  (Issa, 2004), and are multi-mode. Despite the large variety of structures possible, high-index core microstructured fibres operate according to this general principle. The holes must extend significantly beyond the core to reduce the fibre’s confinement loss (White *et al.*, 2001), the amount of light escaping decreasing exponentially with the thickness of the microstructured region.

### Low index core

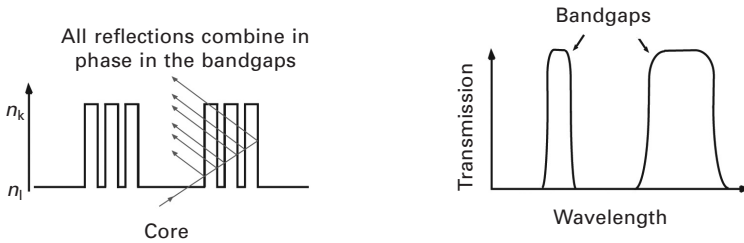
Replacing the high index core with a low index core (Fig. 14.5) means the fibre can no longer guide by total internal reflection, so another mechanism must be employed to reflect the light at the core–cladding interface. This mechanism is coherent reflection by the cladding, possible when the cladding is periodic (Russell, 2006).



(a) All solid

(b) Hollow core

(c) Bragg fibre



14.5 Schematic of different bandgap fibres showing (a) 2D lattice of high index rods in a low index background, (b) a 2D hollow-core example and (c) a 1D Bragg fibre. The light in the core reflects off all the interfaces in the cladding. When these reflections recombine in phase in the core, the resulting strong coherent reflection confines the light. This occurs only for some wavelengths, so transmission occurs only in discrete transmission bands (the bandgaps).

Light incident on a periodic structure will experience many reflections from the interfaces and if these are in phase it results in constructive interference and a strong reflection. This occurs only for specific wavelength ranges. The periodic structures are referred to as photonic crystals and the wavelengths for which strong reflection occurs are called the photonic bandgaps (PBG) (Joannopoulos *et al.*, 1995). Hence these fibres transmit light only in discrete transmission windows – the bandgaps – as shown in Fig. 14.5. Surrounding the low index core with such a material allows the light, if it falls inside the bandgaps, to be reflected at the core–cladding interface and guided along the core. The core can be any lower-index material such as air, so these fibres are often called hollow-core photonic crystal fibres (HC-PCF) or bandgap fibres.

The photonic crystal cladding can be a 1-D or a 2-D crystal. One-dimensional crystals are simply multilayers of alternating high  $n_h$  and low  $n_l$  index materials, rolled into a hollow cylinder, often called Bragg fibres (Yeh *et al.*, 1978) (Fig. 14.5(c)). The simplest 2-D crystals are hexagonal arrangements of high index rods in a low index background (Argyros *et al.*,

2005) (Fig. 14.5(a)). The approximate wavelength position of the photonic bandgaps can be easily calculated and for the 1-D case the bandgaps are in between

$$\lambda = \frac{2\delta\sqrt{n_h^2 - n_l^2}}{m} \quad 14.7$$

where  $\delta$  is the thickness of the high index layer and  $m$  is an integer. For the simple 2-D structure described, they fall between

$$\lambda = \frac{2\pi}{V} r_{co} \sqrt{n_h^2 - n_l^2} \quad 14.8$$

where  $V = 1, 2.405, 3.832, 5.136$  (zeros of Bessel J functions) and  $r_{co}$  is the radius of the high index rods in the cladding. Equations (14.7) and (14.8) assume that the core of the fibre is made of the low index material. This indicates that the uniformity in the high index features is most important, whereas the periodicity is of secondary importance. It also shows how the bandgaps will shift in wavelength with changes to the structure size and the refractive indices. If air is the low index material in the photonic crystal, additional solid struts must be added to the structure to make it self-supporting (Fig. 14.5(b)). These struts will affect the optical properties of the cladding and will result in the closure of most bandgaps (Couny *et al.*, 2007). The typical size of features in the cladding (high/low index layers or high index rods) is hundreds of nanometres to several micrometres depending on the refractive indices of the materials and the wavelength of the bandgaps.

The operation of bandgap fibres ultimately relies on strong coherent reflection by the cladding, but coherent reflection is not achieved by all periodic lattices. Some are less able to reflect light, but do reflect over a much wider wavelength range, giving wider transmission windows but higher confinement loss. This guidance mechanism differs from that in photonic bandgap fibres, and has been called the inhibited coupling mechanism (Argyros and Pla, 2007). Both these types of fibres have the unique property of the low index (hollow) core, but come with the trade-off of narrow transmission windows or higher confinement loss. Both are also extremely sensitive to defects in the structure.

## 14.4 Types of optical fibres, materials and applications

The two broad classes of optical fibre commercially available are silica and polymer optical fibres. The development of fabrication techniques for high purity synthetic silica resulted in the production of highly transparent silica fibre, on which telecommunications systems were developed (Palais, 1992;

Goff, 2002). Polymer fibres, on the other hand, have lower transparency, but can be made significantly thicker while still remaining flexible and provide a lower system cost. The much larger diameters greatly increase the tolerance on connectors, and they operate in the visible range, making them easier to handle. They are thus being taken up in short-distance data communications where the ratio of connections to fibre is high and the transparency is not an issue, and for illumination applications (Ziemann *et al.*, 2008).

An idea of the difference between the most widely used fibres can be gained from the data presented in Tables 14.1 and 14.2, of example specifications of commercially available fibres or deployed data transmission systems. The larger transparency of silica means long-haul links using single-mode fibres can range from inter-city up to intercontinental connections, which require high data rates. At the other extreme, short polymer links would represent connections between individual computers.

#### 14.4.1 Silica optical fibre

##### *General characteristics*

Silica fibres are made of synthetic silica using chemical vapour deposition systems and have very high transparency in the infrared (IR) below 2  $\mu\text{m}$ . As a result, telecommunications systems were developed based on the

*Table 14.1* Physical specifications of some commercially available optical fibres

Fibre	Fibre diameter ( $\mu\text{m}$ )	Core diameter ( $\mu\text{m}$ )	Coating diameter ( $\mu\text{m}$ )	Profile and modes	Temperature range ( $^{\circ}\text{C}$ )	Tensile strength (N)
Silica Corning SMF-28 <sup>1</sup>	125	8.3	245	SI SM	-60 to 85	>33 <sup>5</sup>
Silica Corning InfiniCor CL 1000 <sup>2</sup>	125	62.5	245	GI MM	-60 to 85	>33 <sup>5</sup>
Polymer Mitsubishi ESKA MEGA MH-4001 <sup>3</sup>	1000	980	2200	SI MM	-55 to 85	>70
Fluorinated polymer Asahi Glass Co. Lucina Fibre <sup>4</sup>	120	120	492	GI MM	-10 to 60 <sup>6</sup>	14

Specifications from <sup>1</sup>Corning (2002), <sup>2</sup>Corning (2007), <sup>3</sup>Mitsubishi (2001), <sup>4</sup>AGC (2004).

<sup>5</sup>Quoted as >0.7 GN/m<sup>2</sup>.

<sup>6</sup>For cabled fibre; specifications not available for bare fibre.

Table 14.2 Optical specifications of some commercially available optical fibres

Fibre	NA	Operating wavelength (nm)	Loss (dB/km)	20 dB attenuation length (km)	Typical deployment length (km)	Data rate (GHz)
Silica Corning SMF-28	0.13	1310 1550	0.3 0.2	67 100	50 to >10 000 <sup>1</sup>	>600 <sup>2</sup>
Silica Corning InfiniCor 1000	0.275	850 1310	2.9 0.6	6.9 33	0.5 1.0	0.5 <sup>3</sup>
Polymer Mitsubishi ESKA MEGA MH-4001	0.3	650	160	0.125	0.05	0.2 <sup>4</sup>
Fluorinated polymer Asahi Glass Co. Lucina Fibre	0.17–0.195	850 1300	<25	0.8	0.2	1.25 <sup>5</sup>

<sup>1</sup>50 km is the standard length of fibre commercially available. Longer lengths must be deployed with amplifiers every approximately 80 km.

<sup>2</sup>Demonstrated as 1.28 Tbit/s systems over lengths of 400 km and 9000 km (Leppla *et al.*, 2006; Coleman, 2008). Maximum capacity depends more on encoding systems used and is generally not limited by the fibre. An assumption of non-return to zero encoding was used to convert the bit rate to a frequency: bits/s = 2 × frequency.

<sup>3</sup>Quoted as 1 Gbit/s over the deployment length.

<sup>4</sup>Measured over 50 m at 650 nm using NA = 0.3.

<sup>5</sup>Quoted as 1250 MHz over 200 m at 850 nm, overfill launch.

wavelength of light for which the fibres were most transparent, historically increasing from 850 nm to 1300 nm to 1550 nm. The most widely used silica fibres are based on ITU-T standard G652, these being Corning SMF-28 (see Tables 14.1 and 14.2) and variants thereof tailored for specific dispersion, loss and nonlinear properties. Larger-core graded-index multi-mode silica fibres are also available, providing low loss and high data rates for shorter-distance applications.

### *Chemical structure and fabrication*

The base material of the fibres is amorphous silica SiO<sub>2</sub> fabricated through the oxidation of ultra-pure silicon tetrachloride SiCl<sub>4</sub> in a variety of chemical vapour deposition systems such as modified chemical vapour deposition (MCVD), vapour axial deposition (VAD), outside vapour deposition (OVD)

or plasma chemical vapour deposition (PCVD) (MacChesney and DiGiovanni, 1990; Nagel *et al.*, 1982). In all these systems the (silica) soot particles generated by the oxidation deposit one layer at a time onto a substrate and are sintered to form a solid rod called the optical fibre preform, typically 1–10 cm in diameter, from which the fibre is drawn in a subsequent step at approximately 1900°C.

In order to modify the refractive index profile of the preform, additional materials are incorporated into the silica matrix to produce a variety of doped glasses (see Table 14.3). Common dopants are GeO<sub>2</sub> which increases the refractive index in the core, and P<sub>2</sub>O<sub>5</sub> which lowers it in the cladding. Doping can be achieved through the simultaneous oxidation of precursors like GeCl<sub>4</sub> and the deposition of soot and dopant concentrations can range from a few percent to tens of percent. In addition, active media can be incorporated in the glass with optical gain for the fabrication of fibre lasers and amplifiers (Hewak, 1998). The most common are erbium and ytterbium in the form of Er<sup>3+</sup> and Yb<sup>3+</sup>, added to silica using solution doping – immersing the soot layers into a solution of the dopant prior to drying and sintering.

The chemical structure is important on a microscopic level as the dopants must ideally disperse uniformly and produce a homogeneous material. Crystallisation or agglomeration of any form will result in scattering of the light, and thus increase losses, and may also inhibit certain processes required for active systems. For example, the addition of Al reduces the clustering of Er<sup>3+</sup>, and the addition of P<sub>2</sub>O<sub>5</sub> inhibits Al<sub>2</sub>O<sub>3</sub> from crystallising, thus these are often used in combination to increase the Er<sup>3+</sup> concentration.

Water contamination must be avoided as the Si–OH bond absorbs light near 1380 nm and can decrease the transparency of the fibre for both the 1300 nm and 1550 nm windows. Dopants or glass combinations must be thermally compatible in terms of processing temperatures and thermal expansion coefficients. A difference in thermal expansion can create large

Table 14.3 Common dopants used in silica fibres and their function

Dopant	Function	Doping method
GeO <sub>2</sub>	Increases index	Oxidation of GeCl <sub>4</sub>
P <sub>2</sub> O <sub>5</sub>	Increases index, reduces viscosity and scattering	Oxidation of POCl <sub>3</sub>
Al <sub>2</sub> O <sub>3</sub>	Increases index, reduces clustering of Er <sup>3+</sup>	Solution doping, AlCl <sub>3</sub>
B <sub>2</sub> O <sub>3</sub>	Decreases index and viscosity	Oxidation of BCl <sub>3</sub>
F	Decreases index	Oxidation of SiF <sub>4</sub> , CF <sub>4</sub> or CCl <sub>2</sub> F <sub>2</sub>
Er <sup>3+</sup>	Optical gain at ~1550 nm	Solution doping of ErCl <sub>3</sub>
Yb <sup>3+</sup>	Optical gain at ~1000 nm	Solution doping of YbCl <sub>3</sub>



stresses in the fibres as they cool from the drawing temperature to room temperature. This can be caused intentionally to modify the properties of the glass using stresses and induce birefringence. All these factors contribute to determining the maximum concentrations of the various dopants.

The chemical structure can be modified locally over short lengths in the fibre after it is drawn to inscribe fibre Bragg gratings (FBG) using ultraviolet (UV) light (Kashyap, 1999). The exact mechanism and changes to the chemical structure are unknown, but the exposure results in a change of refractive index at the point of illumination, which is likely to be due to the breaking and reforming of chemical bonds leading to a different atomic arrangement and density. Fibres most sensitive to UV have Ge-doped cores and are hydrogen-loaded (placed under high pressure  $H_2$ , so that it enters the silica matrix) prior to exposure. The fibre is exposed to a fringe pattern created by interfering a UV beam, which inscribes a grating in the core of the fibre. The grating pitch is of the order of 500 nm and reflects one or a variety of wavelengths with extremely high precision.

The chemical structure is also relevant to a fibre's nonlinear properties (Agrawal, 1995). High Ge concentrations tend to increase nonlinearity, and other dopants like P can modify the Raman gain of the glass and be used in fibre amplifiers. The nonlinearity can also be modified post-drawing through the application of a strong electric field whilst heating the fibre (poling). This results in the migration of mobile charges in the glass (like  $Na^+$  impurities and  $H^+$  that enters from the atmosphere), creating a permanent electric field, and the local crystallisation of the amorphous silica into cristobalite (An and Fleming, 2006).

### *Mechanical properties*

The mechanical strength of the fibres can be greatly undermined by small cracks on the surface. To prevent this, a polymer coating is applied while the fibre is in pristine condition, as it is drawn from the preform. The coating can be applied as a UV-curable polymer, cured online during the draw. Examples of coatings are polyvinylidene fluoride (Kynar) and acrylates. The tensile strength of typical fibres is approximately 33 N (Table 14.1) and the elastic limit is approximately 0.5%.

Different levels of cabling are required, depending on the environment in which the fibre will be placed, to provide protection from moisture and to take the tensile load away from the fibres (Palais, 1992). The cables include from one to 200 fibres and beyond their plastic coating a buffer coating is added, followed by strength members and an outer consolidating polymer jacket. If metallic, the strength members can be used to deliver electricity to components (such as amplifiers) along the cable. The strength members can include metal pipes, corrugated metal inclusions, steel wires, aramid yarn or

Kevlar. Modular, loose-tube configurations allow a subset of the fibres to be accessed at a point along the cable without affecting the remaining fibres, the cable acting as a conduit. Tight-buffered cables allow access only at the cable's termination points.

As an example, submarine cables can be up to 69 mm in diameter and composed of eight layers including copper (also for power delivery), aluminium tube and steel wire reinforcements. Their tensile strength can reach 200 kN.

### *Applications and limitations*

The high transparency and small core of silica fibres makes them ideal for telecommunications, where the distances, data transmission rates and fibre-to-connector ratios are large. The ability to incorporate active materials like  $\text{Er}^{3+}$  to make fibre amplifiers has increased the deployment lengths and data rates as optical signals can be re-amplified every  $\sim 80$  km in fibre, without requiring their regeneration by electronic means. The incorporation of gratings has enabled the use of wavelength division multiplexing (WDM) to further increase data rates, where multiple signals are transmitted along the same fibre at slightly different wavelengths, and manipulated independently using sets of fibre Bragg gratings. The combination of these three types of silica fibres has allowed high speed telecommunications to be realised, and resulted in a worldwide network exceeding 100 million kilometres in fibre length.

Other uses of silica fibres (typically with larger cores) include medical applications in the form of illumination and imaging for endoscopes using fibre bundles, in which each fibre corresponds to one pixel, and laser power delivery for surgery and other treatments. Fibre sensors (Udd, 1991) is also a large field and includes using fibre Bragg gratings for temperature and/or strain sensing (although this is limited by the low elastic limit), and using Faraday rotation to measure the strength of magnetic fields, and hence measure currents. Optical fibre lasers (doped with active media) are receiving increased attention as they produce high quality beams and the large surface area to volume ratio of the fibre is ideal for thermal management and high power lasers (Digonnet, 2001).

For short-distance applications, the transparency and large data transmission rates become increasingly irrelevant and the low tolerances on connections (arising from the small core) only add to increasing the cost of an implemented system. The physical properties of silica prevent the core and fibre from being significantly larger, as thicker fibres become rigid. Their operation in the infrared makes them unsuitable for user-installed consumer products as the radiation is invisible, and the ability of silica to shatter makes it unsafe for some *in vivo* applications.

## 14.4.2 Plastic optical fibres

### *General characteristics*

In contrast to silica, polymer optical fibres (POF) remain flexible at large diameters – 1 mm – and operate at visible wavelengths. The large diameter increases the tolerances on connectors, which greatly reduces their cost. Polymer fibres are thus used for short-distance communications and illumination applications where the mechanical properties of the fibre provide an advantage, and the lower transparency (compared to silica) does not pose a significant disadvantage.

### *Chemical structure and fabrication*

The polymers used in optical fibres can be divided into two general categories: ordinary polymers containing hydrogen, and fluorinated polymers in which all the hydrogen atoms are replaced by a fluorine atom (or, less commonly, deuterium). The transparency of polymer materials is affected by resonances of the C–H bond vibrations and scattering that arises from the packing of the polymer molecules. The heavier fluorine or deuterium atoms shift these resonances to longer wavelengths and open up a larger and deeper transparency window (Ziemann *et al.*, 2008). Some examples are presented in Table 14.4.

Apart from the polymer itself, the grade of the polymer can be important. Key properties are the molecular weight and the degree of crosslinking (bonds linking adjacent polymer chains). Crosslinking and/or large molecular weights (leading to very long polymer chains and their physical entanglement) prevent the molecules from sliding past each other and thus prevent the polymer being drawn. The molecular weight also affects the glass transition temperature ( $T_g$ ), at which the backbone of the polymer molecules becomes mobile and the polymer softens; a fibre is generally stable up to 20°C below

Table 14.4 Common polymers used in optical fibres

Polymer	Refractive index	Minimum loss (dB/km)	Wavelength (nm)	$T_g$ (°C)
PMMA	1.49	150	650	115
D-PMMA		20	680	
PS	1.59	114	670	100
PC	1.58	800	770	150
CYTOP	1.34	8	1070	
		15	1300	

Note: The material loss does not equal the fibre loss as fabrication-induced defects and the thermal history of the fibre will affect the loss. PMMA is polymethylmethacrylate, D-PMMA is deuterated PMMA, PS is polystyrene, PC is polycarbonate, CYTOP (cyclic transparent optical polymer) is used in Lucina fibres.

the  $T_g$ . Crystallisation of polymers leads to the formation of many interfaces between the crystals and reduces the transparency through scattering, leading to a white colouration. During polymerisation, various chemicals are added to the monomer to initiate and control the polymerisation and these impurities may also lead to scattering of light. In general, fluorinated polymers are more prone to crystallisation and fluorinated/deuterated polymers are significantly more expensive owing to the cost of the raw materials, the production of hydrofluoric acid during fluorination and the proprietary nature of these materials.

In addition to the grade, the properties of a polymer sample will be influenced by its thermal history. The most relevant example is drawing a fibre from a preform. In a bulk sample the polymer chains will have a random orientation, whereas the tension used when drawing to fibre will align the polymer chains along the longitudinal axis of the fibre. The latter is more homogeneous and will have a lower loss through reduced scattering. Further heating of the fibre near  $T_g$  will result in a relaxation and return to the random chain orientation, increasing the loss and possibly deforming the fibre.

The most common fibres consist of a polymethylmethacrylate (PMMA) core and a fluorinated polymer cladding, operating in the red at 650 nm (see Tables 14.1 and 14.2). PMMA has the highest transparency of the commonly available polymers, while fluorinated polymers have low refractive indices and are typically used only in the cladding. A refractive index profile suitable for waveguiding can be obtained from using combinations of polymers, or modifying one base polymer through doping (dopant dispersed in the polymer matrix) or the use of co-polymers (dopant incorporated into the polymer molecules). This results in relatively large index contrasts and  $NA$ , meaning that single-mode fibres are not available.

Once the materials are selected, the fibre may be drawn from a preform (Ziemann *et al.*, 2008). Step-index preforms can be made by placing the core material inside a tube of the cladding material and fusing together, or by polymerising the cladding onto the core. The materials used must be thermally compatible, e.g. have similar softening temperatures to enable drawing, and similar thermal expansion coefficients to prevent stresses once cooled, which could lead to delamination between the core and cladding and large losses for the fibre.

Graded-index profiles are more complex and are primarily produced using two methods. Interfacial gel polymerisation relies on the different diffusivity of two components in the monomer mixture. A tube filled with the mixture is heated from the outside and polymerises inwards. The lighter species diffuses to the outside and the heavier species remains near the centre as the polymerisation front proceeds, creating a concentration gradient and hence a refractive index gradient. The second method relies on differences

in density between the two species and employs a centrifuge to induce the concentration gradient prior to initiating polymerisation. The preforms are spun at rates of 50 000 rpm, making this approach impractical.

Drawing fibre from preforms is necessarily a batch process, using one preform at a time, and the large diameters of POF mean that the length of fibre produced from each preform is relatively low. A more cost-effective method involves drawing the core from a rod or extruding it from a monomer mixture that polymerises online, followed by coating and curing the cladding onto the core, and the addition of any jacketing layers. This results in a continuous process. Graded-index fibre can be made by the co-extrusion of many layers or the controlled diffusion (by heating) of a dopant in the innermost layer. The thermal stability of a fibre may be increased through UV irradiation to cause crosslinking after it has been drawn.

### *Mechanical properties*

The mechanical properties of plastic fibres differ significantly from those of silica, most notably in that they are more flexible at large diameters and much more elastic. Elastic limits for PMMA and CYTOP fibres fall in the range of 5–10% (Dobb *et al.*, 2006; AGC, 2004).

Given the applications, the extent of cabling used in silica fibres is unnecessary in POF. The fibres may be coated with an additional protective layer that does not alter their properties significantly. Duplex cables are common in data transmission, as sending one signal in one direction per fibre minimises the complexity of the optics and electronics of the transmitter/receiver and connector.

### *Application and limitations*

Given their properties, POF has had the largest uptake in short-distance transmission of light. In data communications, local area networks using polymer fibres are being installed in German-made cars. Home and office local area networks using POF are also available but not widely utilised. The largest opportunity for POF is in the deployment of fibre-to-the-home (FTTH), to provide high speed internet, voice over IP and radio/TV broadcasts over the one fibre connection (so-called triple-play networks), as well as high data rate links within and between consumer electronics like high definition televisions. The easier handling and operation in the visible range make polymers attractive in these applications as they lower installation costs and make user-installation possible. The large cores also make POF suitable for illumination applications in architectural lighting and signage. All these applications typically use lengths of less than 100 m. The second range of applications arises from the mechanical properties, as polymers are

more flexible and more elastic than silica, and do not shatter. This makes them suitable for a variety of sensing applications such as strain sensing (Ziemann *et al.*, 2008).

The major limitations of POF are the transparency and temperature stability. Although the transparency can be improved through fluorination, this is not cost-effective and undermines the 'cheap and easy' solution POF offers. The low operating temperature (see Table 14.4) of POF is also a limitation in many applications and no suitable, sufficiently transparent high-temperature POF has become widely available. The difficulty in making single-mode POF is also inhibiting their use in many sensing applications, such as strain sensing, as single-mode fibres with gratings inscribed are necessary.

### 14.4.3 Microstructured optical fibres

#### *General characteristics*

Microstructured optical fibres have been produced using silica (Knight *et al.*, 1996; Russell, 2006) and polymer (van Eijkelenborg *et al.*, 2001; Large *et al.*, 2007). Given the effectiveness of conventional fibres, microstructured fibres have typically been of interest only when particular properties which are not obtainable in conventional fibres are achieved. Fibres guiding by modified total internal reflection will typically have interesting dispersion, nonlinear properties or *NA* and hollow-core fibres have the unique feature of a hollow core. Although the light travels in air in hollow-core fibres, some fraction of the light (<1%) overlaps with the solid material and thus material absorption and scattering are weakened, but still experienced.

Given the large variety of structures possible, there is no 'general' description of microstructured fibres. Some notable designs are outlined in Table 14.5 and examples of fabricated structures are shown in Fig. 14.6.

#### *Materials and fabrication*

Silica microstructured preforms are made by stacking capillaries and rods in the correct arrangement and inserting the stack in a larger consolidating silica tube prior to drawing (Russell, 2006). Microstructured polymer optical fibres (mPOF), produced using PMMA, can also be made using the stacking method, although drilling, extrusion and casting have all been demonstrated, which allow the fabrication of larger preforms compared to silica (80 mm diameter compared to 30 mm) (Large *et al.*, 2007). The preforms are typically drawn to fibre in two steps via an intermediate cane stage of approximately 10 mm diameter.

During the draw the temperature, surface tension, viscosity and pressure in the holes control the deformation of the structure, e.g. the collapse or relative expansion of the holes. The holes also change shape depending on

Table 14.5 Examples of microstructured fibres

Fibre	Material	Core size ( $\mu\text{m}$ )	Operating wavelength (nm)	Minimum loss (dB/km)	Distinguishing property
Endlessly single mode <sup>1</sup>	Silica	8.5 35	400–2000	25 10	Large core, yet single mode over a wide wavelength range
Hollow core <sup>2</sup>	Silica	4.9 20	440 1570	2000 20	Hollow-core bandgap fibres
Highly nonlinear <sup>3</sup>	Silica	1.5–2.0 2.1	800 1550	80 10	> 100 times higher nonlinearity than SMF-28
High bandwidth mPOF <sup>4</sup>	PMMA	30	650	300	Multimode fibre with inter-modal dispersion that decreases with length – pulses stop spreading after a certain length
Single mode mPOF <sup>5</sup>	PMMA	5–15	400–1600	2000	Single-mode polymer fibre
Hi-NA fibres <sup>6</sup>	Silica	110	700–2000	1.3	$NA > 0.6$ , low bend loss
	PMMA	300	500–1100	1000	
Birefringent <sup>7</sup>	Silica	$3.1 \times 3.5$	1550	1.5	Highly birefringent, large dependence of effective index on polarisation
	PMMA	$3 \times 12$	650 750	2000	

Specifications from <sup>1</sup>Crystal Fibre (2005a), <sup>2</sup>(2004a), <sup>3</sup>(2004b), <sup>6</sup>(2005b), <sup>7</sup>(2004c); polymer fibres from <sup>4,5,6</sup>Large *et al.* (2007).

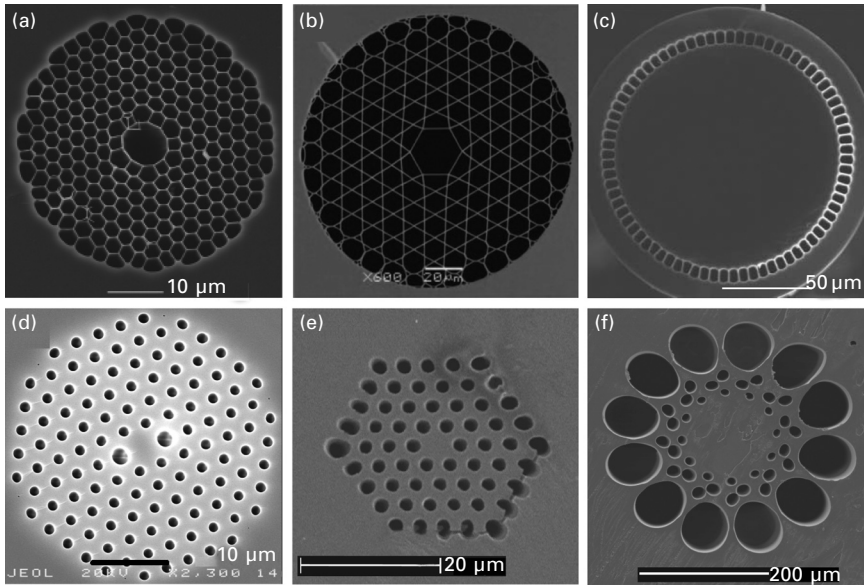
their proximity to other holes – the wall between two adjacent holes will be straightened by the surface tension, and smaller holes will deform to match the curvature of larger holes. Hence, these fibres are difficult to produce as precise control of the draw conditions is necessary.

The lower drawing temperature of PMMA has allowed other material to be incorporated into mPOF such as wires and organic dyes introduced to the polymer through solution doping (Large *et al.*, 2004). Nanoparticles and quantum dots can be added to the polymer in powder form and the powder consolidated into a rod, which is then incorporated into the preform (Yu *et al.*, 2007).

### Applications and limitations

Microstructured fibres are still very much a research fibre. However, the large variety of structures and properties (some outlined in Table 14.5) mean that





14.6 Examples of fabricated microstructured fibres: (a) silica hollow-core photonic bandgap fibre (Humbert *et al.*, 2004); (b) silica hollow-core kagome lattice fibre (Couny *et al.*, 2006) which guides by the inhibited coupling mechanism (Argyros and Pla, 2007); (c) silica hi-NA fibre (Wadsworth *et al.*, 2004b), © IEEE; (d) silica birefringent fibre (Xiong and Wadsworth, 2008); (e) single-mode mPOF; (f) high bandwidth mPOF.

microstructured fibres have potential to satisfy a variety of applications. To date, only a few examples are available commercially and only a subset of those have found niche applications outside research.

As an example, in some microstructured fibres the control over the dispersion can greatly enhance the efficiency and lower the threshold of nonlinear processes, leading to supercontinuum generation: the generation of a wide, flat, continuous spectrum from the visible range to the mid-infrared (e.g. 500–2200 nm), using a low-power low-cost laser (Wadsworth *et al.*, 2004a). These supercontinuum sources have become valuable tools for spectroscopic applications. Placing very large holes with thin strands of material in between can produce a very low index cladding (referred to as ‘air-clad’ fibres) and an *NA* approaching 1 (Issa, 2004). Silica air-clad fibres are used for high power fibre lasers as large amounts of pump light can be launched into the fibre. Endlessly single-mode mPOF provide the only effective method to make single-mode polymer fibres, which have in turn been inscribed with gratings and used as strain sensors (Dobb *et al.*, 2005; Hiscocks *et al.*, 2006).

The potential applications of other microstructured fibres include using



their dispersion properties to shape optical pulses. Multi-mode microstructured polymer optical fibres have been demonstrated with large data rates that become independent of length as the pulses stop spreading after a length of  $\sim 40$  m (Large *et al.*, 2007). Longer fibres could thus be deployed without requiring a reduction in data rates. Similarly, mPOF with negligible bending loss may be suitable for connections which require many turns in a confined space. Both of these may be applicable to FTTH.

Hollow-core microstructured fibres may find applications in high power beam delivery where the powers are above the damage threshold of the material (Humbert *et al.*, 2004). Hollow-core polymer fibres with losses  $100\times$  below the material absorption in the infrared have been demonstrated and may allow the use of lower optical quality polymers that offer other advantages, like temperature stability (Argyros and Pla, 2007). Filling the fibres with a solution can create a high sensitivity sensor as a 1 m interaction length can result from less than 1  $\mu\text{L}$  of a sample solution, demonstrated in the sensing optical activity and for Raman spectroscopy inside fibres (Cox *et al.*, 2007).

Lastly, due to the presence of photonic bandgaps, some optical fibres also display an external colouration and iridescence. They have thus been proposed for use in coloured textiles, with the possibility of acting as a security marker – the exact details of the reflected spectrum providing a unique signature that can be used for identification purposes (Kuriki *et al.*, 2004).

## 14.5 New materials and material combinations in optical fibres

Niche applications that can be fulfilled by neither silica nor polymer fibres are being addressed, at least experimentally, by optical fibres of other materials. Both silica and polymers are opaque to the UV and mid-IR (wavelengths around 2–6  $\mu\text{m}$ ). UV transmission is achieved in silica fibres with undoped silica cores with a high OH content and a fluorine-doped cladding. Additional treatment is used to remove specific defects in the material which result in UV absorption, and hydrogen loading can be used to minimise UV-induced damage to the glass (Polymicro, 2006). Losses of order 1000 dB/km are typical around 200 nm, with the loss decreasing to 10 dB/km at 400 nm.

Transparency in the mid-IR is achieved in fluoride or chalcogenide glasses. Fluoride glasses such as ZBLAN contain  $\text{ZrF}_4$ – $\text{BaF}_2$ – $\text{LaF}_3$ – $\text{AlF}_3$ – $\text{NaF}$  mixtures and are the most common examples (France *et al.*, 1990). Chalcogenide glasses contain Group VI elements, with  $\text{As}_2\text{Se}_3$ ,  $\text{Ga}_2\text{S}_3$ – $\text{La}_2\text{S}_3$  and  $\text{ZnO}$ – $\text{TeO}_2$  as examples (Sanghera *et al.*, 2002). These glasses also provide a more favourable environment for rare-earth ions like  $\text{Er}^{3+}$  (Pollnau and Jackson, 2001), allowing them to produce optical gain over a wider wavelength range.

However, these advantages are offset by the tendency of these materials to crystallise, which results in scattering of the light, and they are also expensive and difficult to handle. Step-index fibres are available in some materials and microstructured fibres have been demonstrated (Monro *et al.*, 2000). Losses in excess of 300 dB/km are typical.

The other favourable property of the chalcogenide glasses is a high nonlinearity, which is also found in  $\text{SiO}_2\text{-Al}_2\text{O}_3\text{-B}_2\text{O}_3$  glasses containing Pb, Bi or La (called 'soft' glasses). The optical nonlinearities are at least an order of magnitude larger than in silica, though the loss of fibres made from these materials is of order 2000 dB/km (Dimitrov and Komatsu, 1999).

One notable material combination is polymer-clad-silica fibres, consisting of a silica core and a (fluorinated) polymer cladding. This combines some of the mechanical and cost advantages of polymer fibres with a high *NA* and the high transparency of a silica core (Polymicro, 2004).

## 14.6 Conclusions

Optical fibres are in one sense an established technology, but are continuing to expand into new applications and markets. The three classes of fibres discussed here are quite different in this respect and present the mature and established (silica), the developing (polymer) and the promising though largely unexplored (microstructured) technologies.

The silica fibre telecommunications infrastructure was the largest driver of the technology for several decades. This began with large infrastructure investments in the deployment of long-distance submarine and terrestrial fibre cables, and was followed with the gratings and multiplexing technology which allowed higher data transmission rates to be obtained from the same cable infrastructure. Its exceptional quality as a product and its ability to supersede demand meant that no drastic changes in silica fibre communications technology have occurred, nor have been necessary, for some time. More cables are being deployed, driven by increases in Internet traffic and the development of China and India. Moves away from telecommunications include fibre lasers, medical and sensing applications, and were driven in part by a need to diversify after the technologies crash in 2002.

Polymer fibres are in contrast much less mature as a technology, reflecting the younger and smaller market. The lack of maturity is evident in the relative lack of standards and supporting technology such as light sources and detectors optimised for wavelengths at which POF operate. The development of the MOST standard by the German automotive industry and incorporation of POF in high-end German cars was the first large uptake in data transmission. The largest upcoming opportunity for POF is the last stage of the optic fibre communication network: FTTH. Japan and South

Korea are the only countries with significant infrastructure investments in FTTH, and POF-FTTH is under consideration in the EU by the POF-ALL project. However, in this market plastic fibres are competing with wireless and silica solutions, as well as among themselves. The constraints differ from the telecommunications world, and include low bend loss and possibly user-installation which have not been thoroughly addressed. Other applications likely to succeed include data transmission within/between appliances and illumination. The outcome of FTTH deployment over the next decade will play the largest role in shaping the technology and deciding its fate. Many sensing applications with material-specific requirements are being addressed, but the lack of single-mode POF and POF-gratings may prove problematic.

Microstructured fibres are yet a younger and less mature technology, barely out of the research phase. Great potential is seen in these fibres' unique properties, but given the quality of available conventional fibre and the corresponding established markets, it is yet unclear as to how much demand there is for these unique properties. Supercontinuum sources for spectroscopy, hollow-core fibres for beam delivery and single-mode mPOF with gratings inscribed for strain sensing stand out as possible successes, but the use of these fibres is still being explored and demand is only beginning to be created.

## 14.7 Sources of further information and advice

Many textbooks are available on optical fibres, addressing different aspects of the technology. Snyder and Love (1983) is the definitive reference on waveguide theory, and Palais (1992) and Goff (2002) present an introduction to silica fibres and telecommunications. Agrawal (1995) is a useful reference for nonlinear optics, Udd (1991) for optical fibre sensors, Dignonnet (2001) for amplifiers and lasers and Kashyap (1999) for fibre Bragg gratings. A comprehensive reference for polymer fibres and associated technology is Ziemann *et al.* (2008). A review of microstructured fibres can be found in Russell (2006) and Bjarklev *et al.* (2003), which cover mainly silica fibres, and in Large *et al.* (2007), which covers microstructured polymer fibres. Countless websites also provide information and tutorials on different aspects of fibre optics.

In terms of sourcing fibres, there are many large-scale manufacturers of conventional fibres, such as Corning, (USA) and Sumitomo, (Japan) for silica, and Mitsubishi Rayon, (Japan) (ESKA product line-step index) and Optimedia, (Korea) (graded index) for polymer. Fluorinated polymer fibres are typically available only as installed systems, from Asahi Glass Company (Japan) (Lucina product line), and lighting applications and installations are available from PolyOptics (Australia). The Plastic Optical Fibre Trade Organisation (POFTO) is a central reference point for POF products and

suppliers. Some products may also be sourced from general optics suppliers such as Thorlabs (USA).

Microstructured silica and polymer fibres have only one supplier each: Crystal Fiber (Denmark), producing silica PCF, and Kiriama (Australia), producing mPOF. More specialised fibres also have few suppliers. UV-guiding fibres are available from Polymicro Technologies (USA) and TransMIT, (Germany), and mid-infrared fibres are available from CorActiv (chalcogenide fibres) and IRPhotonics (fluoride), both in Canada. Polymicro Technologies is the largest supplier of specialised fibres in general and offers a variety of additional specifications above the fibre itself, such as speciality coatings and endface preparation (e.g. addition of diffusers or lenses on the end of the fibre).

## 14.8 References

- AGC (2004), *Lucina duplex cable technical bulletin T012E rev.3*, Asahi Glass Company.
- Agrawal GP (1995), *Nonlinear Fiber Optics*, San Diego, Academic Press.
- An H and Fleming S (2006), 'Nanocrystal formation accompanying the creation of second-order nonlinearity in thermally poled fused silica glass', *IEEE Photon. Technol. Lett.*, 18, 94–96.
- Argyros A and Pla J (2007), 'Hollow-core polymer fibres with a kagome lattice: potential for transmission in the infrared', *Opt. Express*, 15, 7713–7719.
- Argyros A, Birks TA, Leon-Saval SG, Cordeiro CMB, Luan F and Russell PSTJ (2005), 'Photonic bandgap with an index step of one percent', *Opt. Express*, 13, 309–314.
- Birks TA, Knight JC and Russell PSTJ (1997), 'Endlessly single-mode photonic crystal fiber', *Opt. Lett.*, 22, 961–963.
- Bjarklev A, Broeng J and Sanchez Bjarklev A (2003), *Photonic Crystal Fibres*, Norwell, MA, Kluwer.
- Coleman L (2008), 'Telstra US cable landing heralds new Australian bandwidth boom', *Communications Day*, 3248, 2.
- Corning (2002), *Corning SMF-28 optical fiber product information*, Corning.
- Corning (2007), *Corning Infinicor 62.5  $\mu$ m optical fibers product information*, Corning.
- Couny F, Benabid F and Light PS (2006), 'Large-pitch kagome-structured hollow-core photonic crystal fiber', *Opt. Lett.*, 31, 3574–3576.
- Couny F, Benabid F, Roberts PJ, Burnett MT and Maier SA (2007), 'Identification of Bloch-modes in hollow-core photonic crystal fibre cladding', *Opt. Express*, 15, 325–338.
- Cox FM, Argyros A, Large MCJ and Kalluri S (2007), 'Surface enhanced Raman scattering in a hollow core microstructured optical fibre', *Opt. Express*, 15, 13675–13681.
- Crystal Fibre (2004a), 'Blaze photonics hollow-core photonic bandgap fibre HC-x-x', Crystal Fibre.
- Crystal Fibre (2004b), 'Blaze photonics highly nonlinear PCF NL-x-x', Crystal Fibre.
- Crystal Fibre (2004c), 'Blaze photonics polarisation maintaining PCF x-PM-x', Crystal Fibre.
- Crystal Fibre (2005a), 'Large mode area photonic crystal fiber LMA.x', Crystal Fibre.

- Crystal Fibre (2005b), 'Multimode ultra high NA photonic crystal fibre MM.HNA.x', Crystal Fibre.
- Digonnet MJF (2001), *Rare-earth-doped Fiber Lasers and Amplifiers*, New York, CRC Press.
- Dimitrov V and Komatsu T (1999), 'Electronic polarizability, optical basicity and nonlinear optical properties of oxide glasses', *J. Non-Cryst. Sol.*, 249, 160–179.
- Dobb H, Webb DJ, Kalli K, Argyros A, Large MCJ and van Eijkelenborg MA (2005), 'Continuous wave ultraviolet light-induced fibre Bragg gratings in few- and single-mode microstructured polymer optical fibers', *Opt. Lett.*, 30, 3296–3298.
- Dobb H, Carroll K, Webb DJ, Kalli K, Komodromos M, Themistos C, Peng GD, Argyros A, Large MCJ, van Eijkelenborg MA, Fang Q and Boyd IW (2006), 'Grating based devices in polymer optical fibre', *Proceedings of SPIE Photonics Europe Conference*, Strasbourg, France.
- France PW, Drexhage MG, Parker JM, Moore MW, Carter SF and Wright JV (1990), *Fluoride Glass Optical Fibers*, Glasgow, Blackie.
- Goff DR (2002), *Fiber Optic Reference Guide*, St Louis, MO, Focal Press.
- Hewak D (1998), *Properties, Processing and Applications of Glass and Rare-earth Doped Glass for Optical Fibres*, Stevenage, Herts, Institution of Electrical Engineers.
- Hiscocks MP, van Eijkelenborg MA, Argyros A and Large MCJ (2006), 'Permanent imprinting of long period gratings in microstructured polymer optical fibre', *Opt. Express*, 14, 4644–4649.
- Humbert G, Knight JC, Bouwmans G, Russell PStJ, Williams DP, Roberts PJ and Mangan BJ (2004), 'Hollow core photonic crystal fibers for beam delivery', *Opt. Express*, 12, 1477–1484.
- Issa NA (2004), 'High numerical aperture in multimode microstructured optical fibres', *Applied Optics*, 43, 6191–6197.
- Joannopoulos JD, Meade RD and Winn JN (1995), *Photonic Crystals: Molding the Flow of Light*, Singapore, Princeton University Press.
- Kashyap R (1999), *Fiber Bragg Gratings*, San Diego, Academic Press.
- Knight JC, Birks TA, Russell PStJ and Atkin DM (1996), 'All silica single-mode optical fiber with photonic crystal cladding', *Opt. Lett.*, 21, 1547–1549.
- Kuhlmeiy BT, McPhedran RC and de Sterke CM (2002), 'Modal cutoff in microstructured optical fibers', *Opt. Lett.*, 27, 1684–1686.
- Kuriki K, Shapira O, Hart SD, Benoit G, Kuriki Y, Viens JF, Bayindir M, Joannopoulos JD and Fink Y (2004), 'Hollow multilayer photonic bandgap fibers for NIR applications', *Opt. Express*, 12, 1510–1517.
- Large MCJ, Ponrathnam S, Argyros A, Cox F, Pujari NS (2004), 'Solution doping of microstructured polymer optical fibres', *Opt. Express*, 12, 1966–1971.
- Large M, Poladian L, Barton G and van Eijkelenborg MA (2007), *Microstructured Polymer Optical Fibres*, New York, Springer.
- Leppä R, Vorbeck S, Scheinder M, Weierhausen W, Schmidt M, Witte M, Buchali F, Lach E, Le Rouzic E, Salaun S, Papernyi SB and Sanapi K (2006), 'Field trials with channel bit rates of 160 Gbit/s', *Optical Fiber Communications Conference OFC 2006*, Anaheim, CA.
- Li Y, Yao Y, Hu M, Chai L and Wang C (2008), 'Analysis of the fundamental space-filling mode of photonic crystal fibres: a symmetry point of view', *J. Opt. A: Pure Appl. Opt.*, 10, 075302.
- MacChesney JB and DiGiovanni DJ (1990), 'Materials development of optical fiber', *J. Am. Ceram. Soc.*, 73, 3537–3556.

- Mitsubishi (2001), *ESKA MEGA polyethylene jacketed optical fiber cord: MH-4001*, Mitsubishi Rayon.
- Monro TM, West YD, Hewak DW, Broderick NGR and Richardson DJ (2000), 'Chalcogenide holey fibres', *Electron. Lett.*, 36, 1998–1999.
- Nagel SR, MacChesney JB and Walker KL (1982), 'An overview of the modified chemical vapour deposition (MCVD) process and performance', *IEEE Journal of Quantum Electronics*, QE-18, 459–476.
- Palais JC (1992), *Fiber Optic Communications*, Englewood Cliffs, NJ, Prentice Hall.
- Pollnau M and Jackson SD (2001), 'Erbium 3- $\mu$ m fiber lasers', *IEEE J. Sel. Top. Quantum Electron.*, 7, 30–40.
- Polymicro (2004), *Silica/hard polymer clad optical fiber JTFSSH*, Polymicro Technologies.
- Polymicro (2006), *New UV optical Fibers with stable transmission, FD series optical fibers*, Polymicro Technologies.
- Russell PSTJ (2006), 'Photonic crystal fibers', *J. Lightwave Tech.*, 24, 4729–4749.
- Samut RA (1978), 'Range of monomode operation of W-fibers', *Optical and Quantum Electronics*, 10, 509–514.
- Sanghera JS, Shaw LB and Aggarwal ID (2002), 'Applications of chalcogenide glass optical fibers', *Comptes Rendus Chimie*, 5, 873–883.
- Snyder AW and Love JD (1983), *Optical Waveguide Theory*, New York, Chapman and Hall.
- Udd E (1991), *Fiber Optic Sensors*, New York, John Wiley & Sons.
- van Eijkelenborg MA, Large MCJ, Argyros A, Zagari J, Manos S, Issa NA, Bassett I, Fleming S, McPhedran RC, de Sterke CM and Nicorovici NAP (2001), 'Microstructured polymer optical fibre', *Opt. Express*, 9, 319–327.
- Wadsworth WJ, Joly N, Knight JC, Birks TA, Biancalana F and Russell PSTJ (2004a), 'Supercontinuum and four-wave mixing with Q-switched pulses in endlessly single-mode photonic crystal fibers', *Opt. Express*, 12, 299–309.
- Wadsworth WJ, Percival RM, Bouwmans G, Knight JC, Birks TA, Hedley TD and Russell PSTJ (2004b), 'Very high numerical aperture fibers', *IEEE Photon. Technol. Lett.*, 16, 843–845.
- White TP, McPhedran RC, de Sterke CM, Botten LC and Steel MJ (2001), 'Confinement losses in microstructured optical fibers', *Opt. Lett.*, 26, 1660–1662.
- Xiong C and Wadsworth WJ (2008), 'Polarized supercontinuum in birefringent photonic crystal fibre pumped at 1064 nm and application to tuneable visible/UV generation', *Opt. Express*, 16, 2438–2445.
- Yeh P, Yariv A and Marom E (1978), 'Theory of Bragg fibre', *J. Opt. Soc. Am.*, 68, 1196–1201.
- Yu HCY, Argyros A, Barton G, van Eijkelenborg MA, Barbe C, Finnie K, Kong L, Ladoucer F and McNiven S (2007), 'Quantum dot and nanoparticle doped microstructured polymer optical fibre', *Opt. Express*, 15, 9899–9997.
- Ziemann O, Krauser J, Zamzow PE and Daum W (2008), *POF Handbook*, Berlin, Springer.

**Abstract:** This chapter discusses both the advantages and disadvantages of using the hollow fiber configuration in various applications. The application of the technology to the chemical, petrochemical and biotechnology industries is addressed. Definitions of key terms in hollow fiber technology are provided and structure–property relationships of hollow fibers are highlighted. How those relationships are highly dependent on the fiber processing conditions is a focus of the chapter.

**Key words:** hollow fiber, dry process, polyolefin, spinneret, structure–property relationships.

## 15.1 Introduction

Membrane separation processes have become one of the fastest emerging technologies during the past few decades. Membranes used for separation purposes are typically composed of a homogeneous, polymeric composition through which the components to be separated from the mixture are able to travel at different rates under a given set of driving force conditions, e.g. transmembrane pressure and concentration gradients. The separation membranes can be provided in various forms including flat, spiral wound and pleated sheets and tubes.

Among the various possible types of separation membranes, the hollow fiber membrane module is a commercially preferred form because it presents an extremely large transfer area per unit volume and especially per unit module cross-sectional area. The excellent mass transfer properties provided by the hollow fiber configuration have led to numerous commercial applications in various fields such as medicine (blood fractionation), reclaiming of water, through both purification and desalination, and gas and mixture separation using pervaporation techniques. Other applications of hollow fiber modules that are continuing to emerge are related to the biochemical industry for bioseparations and to separation of various hydrocarbon mixtures by pervaporation for the petrochemical industry.

The basic element of a hollow fiber membrane module is a very small diameter hollow fiber made of a selectively permeable material. Usually, hundreds or thousands of hollow fibers are aligned substantially parallel to each other in bundles and positioned within a cylindrical housing to form a



module. The ends of the bundles are 'potted', usually in a polymeric resin, and the fiber ends are kept open. Thus, the module is structured very much like a conventional tube and sheet style fluid heat exchanger. Reference 1 provides a complete and thorough description of various hollow fiber membrane modules.

Due to the high technological interest in these types of materials, there is much development activity presently ongoing in the area of hollow fibers. This chapter will discuss both the advantages and disadvantages of the hollow fiber membrane configuration. Also, the application of the technology to the chemical, petrochemical and biotechnology industries will be discussed. Specifically, the chapter will begin with a definition of the relevant terms for the hollow fiber technology. Following that section will be a discussion of the various application areas in which hollow fibers are currently being used. Then, the various polymers which are typically used and the resultant fiber properties will be discussed. Special attention will be paid to the structure–property relationships of the fibers and how those relationships are dependent on the fiber processing conditions. Finally, the chapter will conclude with some recommendations for areas that need additional investigation, and with sources of further information and references.

## **15.2 Background**

### 15.2.1 Definition of terms

Two basic morphologies are possible with hollow fiber membranes: isotropic and anisotropic morphologies, of which the anisotropic configuration is of particular value. In the early 1960s (2), the development of anisotropic membranes which exhibit a dense, ultrathin skin on a porous fiber provided momentum to the area of membrane separation technology. The concept of the anisotropic membrane is based essentially on the idea of the permeating small molecules exhibiting a higher permeability rate through the fiber wall, so allowing for the selective separation of the various permeants by the membranes. This is possible because the skin is the active separation portion of the fiber.

There are two general categories of technology commonly used for the production of hollow fibers: the dry process and the wet process. In the dry process, a non-porous thermoplastic polymer, typically either polyethylene or polypropylene, is extruded and produced into a fiber from the melt phase. Extrusion conditions are such that a high level of crystallinity, typically at least 60%, is present in the fiber. If necessary, the crystallinity level can be increased through an annealing process. Also, through the use of proper extrusion conditions, the desired morphology for further processing is established. With the desired level of crystallinity and morphology, the



fiber is stretched at a temperature at or below room temperature, in a so-called 'cold stretch' process. This cold stretching allows for the generation of pores in the fiber. Subsequently, the fiber is further stretched at higher temperatures in a 'hot-stretch' and the size and dimensions of the pores are changed and can be controlled. Each polymer used in the dry process has its own optimum cold and hot stretching ratios and temperatures.

The wet process involves dissolving a polymer in a mixture of solvent and non-solvent. In this case, during extrusion, there is a phase separation process which occurs during fiber production and which leads to the creation of pores. Depending on the kinetics of the actual phase separation, different-sized pores can be produced. The wet process is, in general, applicable to more types of polymers than is the dry process because the number of polymers that crystallize to the required level and morphology for utilization of the dry process is severely limited. On the other hand, in order to utilize polymers in the wet process, it is only necessary to define a suitable solvent/non-solvent system and, in theory, any polymer can be processed.

In general, hollow fibers are created by an extrusion process which involves forcing a thick, viscous fluid through the holes of a device called a spinneret to form continuous filaments of a semi-solid polymer. In their initial state, the polymers that form the fibers are solids which must first be converted into a fluid state for the extrusion process. This can be achieved either by melting, if the polymers are thermoplastics, or by dissolving them in a suitable solvent if they are non-thermoplastic in nature. More recently (3), technologies have been developed for certain specialty fibers that are made from polymers that do not melt, dissolve or form suitable derivatives that can be extruded.

The spinnerets used in the production of most manufactured fibers are similar, in principle, to a bathroom shower head. A spinneret may have from one to several hundred holes. As the filaments emerge from the holes in the spinneret, the liquid polymer is converted first to a rubbery state and then it solidifies.

There are three general methods for producing hollow fibers by extrusion: wet spinning, dry spinning and melt spinning. Wet spinning is the oldest process. It is used for fiber-forming substances that have been dissolved in a solvent. The spinnerets are submerged in a chemical bath and as the filaments emerge from the bath they precipitate from solution and solidify.

Dry spinning technology is also used for fiber-forming substances in solution. However, instead of causing precipitation of the polymer by dilution or chemical reaction, solidification of the fiber is achieved by the evaporation of the solvent in a stream of air or inert gas. In the dry spinning process, the filaments do not come in contact with a precipitating liquid, thereby eliminating the need for drying and making solvent recovery easier.

In melt spinning, the fiber-forming polymer is melted for extrusion through

the spinneret and then directly solidified by cooling. Melt spun fibers can be extruded from the spinneret in different cross-sectional shapes (round, trilobal, pentagonal, octagonal and others). Hollow fibers trap air, creating insulation and provide loft characteristics equal to, or better than, down.

### 15.2.2 Advantages and disadvantages of hollow fibers

Many of the advantages and disadvantages of hollow fibres are categorized based on their actual performance in various industrial applications. This summary is possible primarily because hollow fibers are one of the most popular membranes used in several industries at the present time.

#### *Advantages*

- One of the major advantages of hollow fibers is the modest energy requirement that is necessary with their use. In the hollow fiber filtration process, there is no phase change involved, so there is no need for latent heat. This gives hollow fiber membranes excellent potential to eventually replace some operations that consume heat, such as distillation or evaporation columns.
- Another advantage is that no waste products are generated. Since the basic use of hollow fibers is in filtration, no wastes are created from their operation except for any unwanted material from the feed stream itself. This can help to decrease the overall cost of the operation as it eliminates the need for waste handling.
- Hollow fibers have a large surface area per unit volume, that is, large membrane surfaces per volume of a single module. Hence, hollow fibers are smaller than other types of membrane but their overall performance can be higher.
- Hollow fibers are flexible membranes, so they can carry out a filtration process in two different ways, either so-called 'outside-in' or 'inside-out'.
- Hollow fibers have low operating costs compared to other types of operation, so that processes based on hollow fiber technology are generally inexpensive compared to the same processes based on different technologies.

#### *Disadvantages*

- There are also, of course, disadvantages to hollow fiber technology. One of the most significant disadvantages is that, due to the membrane configuration, membrane fouling generally occurs more frequently than

with other processes. Also, if the feedstream which passes through the fiber is somehow contaminated, the fouling level will further increase, especially for hollow fibers.

- The capital cost of hollow fibers is usually higher than that of other membranes, in contrast with their low operating cost (see above). Much of the expense associated with hollow fiber technology is related to the high cost of the fiber itself, which is relatively expensive because of its fabrication method.
- Hollow fiber technology is relatively new, so it has been the subject of less fundamental research compared to other similar technologies. Therefore, potential issues and concerns have not yet been completely documented. On the other hand, the full potential of hollow fibers has yet to be realized. More research is needed to better understand both the pitfalls and the full potential of the use of hollow fibers.

### 15.3 Types of fibers and general features

Various types of membrane processes have been discussed in both the patent literature and the open literature, including both medical and more industrial-type processes, such as filtration. Attention will now be turned to each of these applications and the basic fundamentals of each process will be described.

#### 15.3.1 Medical applications

The biotechnology industry, which originated in the late 1970s, has grown to become an industry of worldwide significance, in part due to the possibility of producing medically important proteins. Hollow fiber technology is important in this regard because of its ability to separate and purify biochemical products.

The manner in which this technology works is depicted in the figure titled 'Basic principle of hollow fiber' in reference 4. Each bioreactor contains thousands of hollow fibers that simulate a living capillary system. Cells which are suspended in the appropriate media are introduced into the area outside the fibers (generally known as 'extra-capillary space' or ESC). With the aid of a recirculating pump, the medium circulates through the center of each fiber (called 'intra-capillary space' or ISC). The circulating media and the features of the hollow fibers regulate the support of the various nutrients and the transport of the products of cell metabolism. Due to the fact that the secreted proteins are larger than the pores of the fibers, they do not cross back into the ICS. Instead, they remain in the ECS in very high concentration.

### 15.3.2 Reverse osmosis

Reverse osmosis (RO) is a liquid-driven membrane process, with the reverse osmosis membranes being capable of allowing water to pass through while rejecting solutes, such as salts or low molecular weight organic materials. A pressure driving force is needed to overcome the force of osmosis that causes the water to flow from the dilute permeate to the concentrated feed. Presently, the principal use of reverse osmosis is desalination, in which the reverse osmosis process has been shown to offer considerable advantages over the conventional method of desalination, which is ion exchange.

Before leaving the discussion of reverse osmosis, a comment needs to be made about its distinction from other filtration processes. In that sense, there is considerable confusion in the open literature between several membrane processes, i.e., microfiltration, ultrafiltration, and reverse osmosis. In order to clearly distinguish these separation processes, Porter (5) presented a useful method which will be adopted here, based on the smallest particles which can be restrained by the various membranes. According to this approach, reverse osmosis has a separation range from 0.0001 to 0.001  $\mu\text{m}$ , or 1 to 10  $\text{\AA}$ .

### 15.3.3 Pervaporation

In this process, liquid mixtures are fed, under pressure, to a non-porous membrane, where components pass through the membrane by solution diffusion at the permeate side of the membrane. Using this technique, it is possible to separate an azeotropic mixture. The current use of pervaporation is well known in the dehydration of organic solvents and mixtures and the removal of organics from an aqueous stream. In the future, pervaporation will have continued applications in the area of hydrocarbon separation, where its main advantage compared to more conventional distillation techniques is the energy required.

### 15.3.4 Gas separation

Two types of gas separation processes have been identified in the literature: gas permeation (GP) and gas diffusion (GD). In industrial applications, gas permeation is used. This is a pressure-driven process where vapor-phase components pass through a non-porous membrane by a solution/diffusion mechanism, similar to reverse osmosis. On the other hand, gas diffusion uses microporous membranes, operating under either a concentration or a partial pressure gradient.

Membranes are used in a variety of gas separation processes, as shown in Table 15.1. The main reasons for their widespread use are advantages in

Table 15.1 Gas membrane separation application areas

Gas separation	Application
O <sub>2</sub> /N <sub>2</sub>	Oxygen enrichment, inert gas generation
H <sub>2</sub> /hydrocarbons	Refinery hydrogen recovery
H <sub>2</sub> /N <sub>2</sub>	Ammonia purge gas
H <sub>2</sub> /CO	Syngas ratio adjustment
CO <sub>2</sub> /hydrocarbons	Acid gas treatment, landfill gas upgrading
H <sub>2</sub> O/hydrocarbons	Natural gas dehydration
H <sub>2</sub> S/hydrocarbons	Sour gas treating
He/hydrocarbons	Helium separation
He/N <sub>2</sub>	Helium recovery
Hydrocarbons/air	Hydrocarbons recovery, pollution control
H <sub>2</sub> O/air	Air dehumidification

the separation process, low capital cost, low energy consumption, ease of operation, cost-effectiveness even at low gas volumes, and good weight and space efficiency. Within these various applications, hollow fibers play a very important role, because of their high separation area and selectivity. Hollow fiber membranes have approximately 30 times the productivity of other oxygen-enriching membranes, plus excellent inertness, which is associated with their chemical composition.

Hollow fibers have been shown to have a stable, high flux with full selectivity in a full-scale system. The high flux is due to the combination of high transfer or separation areas and the thin membrane wall, as well as the fact that hollow fibers, in general, have a low surface energy.

Owing to these characteristics, hollow fibers are widely used in many gas separation industries (6). For example, they are used in O<sub>2</sub>/N<sub>2</sub> separation for oxygen enrichment and inert gas separation, separation of H<sub>2</sub> and hydrocarbons for refinery hydrogen recovery, H<sub>2</sub>/CO separation for adjustment of the gas ratio, H<sub>2</sub>/N<sub>2</sub> separation for ammonia purge gas, separation of CO<sub>2</sub> and hydrocarbons for acid gas treatment and landfill gas upgrading, H<sub>2</sub>O/hydrocarbons separation for natural gas dehydration, H<sub>2</sub>S/hydrocarbons separation for sour gas treatment, helium separation and other processes. In many of these applications, the low capital cost associated with hollow fibers has led to their popularity. The majority of the cost associated with hollow fibers is for compression and not for purification, primarily because the hollow fiber itself already provides a good medium for purification.

### 15.3.5 Ultrafiltration

Hollow fibers are also being used in ultrafiltration applications. Ultrafiltration (7) is a method of filtration using a membrane in which hydrostatic pressure forces a liquid against a semipermeable membrane or hollow fiber. During

the filtration process itself, suspended solids and high molecular weight solutes are retained, while water and low molecular weight solutes pass through the membrane. Ultrafiltration is normally used in research and in industry for purifying and concentrating macromolecules, especially protein solutions. Fundamentally, the process of ultrafiltration is no different from reverse osmosis, already discussed in this chapter, except in terms of the size of the molecules the membrane retains.

## 15.4 Polymers used

### 15.4.1 Polyolefins

As already discussed in this chapter, one of the common methods of producing hollow fibers is through a melt extrusion process, so those polymers that can be easily extruded in the melt are commonly used for the production of hollow fibers. Among these, polyolefin polymers represent a natural class of polymers to use. Owing to their relatively low cost and general availability, polypropylene and polyethylene represent two of the most usual polymers for hollow fiber production.

In early patent literature issued to Celanese Corporation (8), polymers were described for forming microporous articles, such as fibers and films, using a uniaxial stretching technology. For that technology to work effectively, the polymers were described as needing to have a significant level of crystallinity. Various types of polymers, including polyolefins, polyacetals, polyamides and polyesters, among others, were described as being useful in that regard. However, it was also stated that polyolefin resins are most preferred and that a particularly preferred polymer is polypropylene.

In reality, the majority of current commercial activity founded on that earlier work is indeed based on the use of polyolefins, particularly polypropylene. In the described technology, a non-porous, highly crystalline, elastic film or fiber is cold stretched at a temperature that is typically at or below room temperature. In some cases, the required level of crystallinity is achieved through an annealing process. One of the key requirements in the process is the attainment of the proper morphology in the fiber prior to the cold stretching step. The cold stretching operation generates the pores in the fibers, and subsequent stretching at higher temperatures usually changes the dimensions of those pores. This so-called hot stretching step is performed at temperatures that are relatively close to the melting point of the polymer. In practice, the cold and hot stretching temperatures and stretch ratios depend on the type of polymer used. Thus, the optimum stretching conditions for polypropylene are significantly different from those for polyethylene.

There are certain limitations and restrictions on the types of polyolefin

resins that will work effectively in this process. As already mentioned, the polymers must be capable of establishing the correct morphology for the production of pores. However, even with polymers that can yield the correct morphology, there are further restrictions. Some studies (9, 10) have shown that higher crystallinity is more preferred as well as broader molecular weight distribution materials. Also (11), there are certain molecular weight ranges that work most effectively in this process. If the polymers being used fall outside the preferred ranges of properties, it is very difficult to establish the desired porous structure in the final fiber product.

#### 15.4.2 Other polymers

Since the number of polymers that can produce hollow fibers through a melt extrusion process is limited, as discussed above, other fabrication technologies which employ a variety of different polymers have been developed. One of the natural fabrication methods to be employed in this regard is wet spinning of fibers from solution. In this technique, also sometimes called solvent spinning, a polymer dope is created by mixing a polymer, a solvent and other ingredients in a mixer. For example, a polymer with desirable high temperature properties can be used in this technology, assuming that a suitable solvent for the polymer can be found. This means that, in theory, the properties of the resultant hollow fiber can be controlled through the judicious selection of the appropriate polymer/solvent system.

A polymer on which much work has been done in the hollow fiber area is polyethersulfone (PES). In a very important study of that polymer and hollow fibers produced from it (12), Ismail *et al.* studied the effects of dope extrusion rate on the performance of PES hollow fibers in ultrafiltration applications and the relationship to the fiber morphology. The authors used a dope based on dissolving the PES in 1-methyl-2-pyrrolidone (NMP). The experimental results show that the flux measured with the hollow fiber ultrafiltration membrane decreases and the separation performance increases with an increase in dope extrusion rate. The explanation given for these observations is that the outer skin layer of the hollow fibers becomes thicker and denser with increasing dope extrusion rate. However, once the separation performance reaches a maximum critical point, the rejection decreases with an increase in the dope extrusion rate, possibly due to the formation of an outer skin structure at high dope extrusion rate. Fourier transform infrared (FTIR) spectroscopy suggests that higher orientation is responsible for the enhanced separation performance. This study implies that it is possible to control the performance of the hollow fibers through manipulation of their processing features. This will be further discussed in a later section in this chapter.

Recently (13), a new method has been proposed for fabricating hollow

fibers from membrane materials that are not suitable for extrusion or that are difficult to extrude in small diameters. The technique enables precursor materials such as low consistency silicones, highly diluted thermoplastics and two-part liquid systems to be formed into hollow fibers and readily processed into membrane modules. The method involves first providing a hollow fiber from a water-soluble polymer, such as polyvinyl alcohol (PVOH), which is easily extruded. The PVOH fiber is then coated with the membrane precursor material in a continuous coating process through a coating die. The diameter of the PVOH fiber and the thickness of the coating layer are appropriately adjusted to the specified inner and outer diameters of the membrane hollow fiber. The membrane precursor material is then allowed to either cure or flash-off solvent in an oven or other continuous processing chamber. Additional coating layers from the same or different membrane materials may be subsequently applied.

Since the PVOH fiber acts as a rigid core within the membrane hollow fiber, the modulus of the resulting coated fiber is typically at least that of the PVOH even if the membrane material is elastic. This allows for processing of the hollow fiber into membrane modules using similar techniques to those presently used for the fabrication of membrane hollow fiber modules. That is, the coated fiber can be easily woven into fiber bundles, knitted in array fabrics, and potted within module housings.

The next step in the proposed process is to pot both ends of a bundle of coated fibers within a module housing or a temporary mold. A suitable potting material that bonds to the membrane material needs to be used. Once potted, the inner section of the PVOH hollow fiber is exposed by cutting through the potted ends of the fiber bundle. Lastly, hot water is passed through the inner section of the PVOH hollow fibers while infusing at one potted end and draining through the other end. The hot water dissolves the PVOH from the inside out, leaving behind the membrane material configured into hollow fibers neatly potted within the module housing.

This approach was used to fabricate silicone membrane hollow fiber modules for blood–gas exchange applications. In this study, a gas exchange device using silicone membrane hollow fibers was constructed and its oxygen transfer capability was compared to the corresponding capability of a device based on traditional microporous membrane hollow fiber made from polypropylene. The results of the tests were that a comparable oxygen transfer was achieved with the module based on the silicone membrane hollow fibers as was obtained with the more usual microporous membrane hollow fibers. The conclusion of the study, then, is that this new technique can be used to fabricate silicone hollow fibers from resins that are not suitable for extrusion. Further, this new technology enables and simplifies the construction of membrane modules that incorporate hollow fibers. The application of this technology to new materials opens up the possibility of



producing hollow fibers and the corresponding membranes based on materials that had previously not been considered possible. The resultant properties and performance could lead to the use of hollow fiber membranes in previously unforeseen applications.

## 15.5 Structure–property relationships

An increasing number of studies have begun to appear in the literature that relate the structure of hollow fibers to their properties and performance in various applications, largely because advances in polymer science have enabled membrane scientists to utilize engineering plastics to improve the structure–property relationships of membrane products. As discussed earlier in this chapter, no longer are hollow fibers limited to polyolefins, specifically polyethylene and polypropylene. Polyvinylidene difluoride (PVDF), polysulfone (PSF) and polyacrylonitrile (PAN) (14) are examples of polymers presently being used to produce durable hollow fibers. As these different polymers are being employed, it is necessary for polymer science to continue to advance so that an understanding of what these new polymers have to offer can be completely appreciated.

One of the most important features that governs the performance of hollow fibers in many applications is the average pore size and the pore size distribution. In fact, as alluded to earlier, it is the average pore size which distinguishes fibers for use in various filtration applications. The average pore size and its distribution is also important for controlling the rate of migration of species through the fibers as well as allowing for the separation processes discussed earlier in this chapter. The simple idea is that the size of the pores can be controlled to be larger or smaller than the molecules passing through the fiber. This further restricts the passage of the molecules through the fibers.

In the case of the melt extrusion of polyolefins for the production of hollow fibers (15), the molecular weight of the polyolefin polymer itself and its distribution has been shown to be an important factor in determining the pore size distribution in the final fiber. In addition, the stretching temperatures used to perform the cold and hot stretching steps in the process are also important. Further, as would be expected, the stretch ratios used at the various stretching steps can also significantly impact the pore size and distribution.

As already mentioned, as different polymers are being examined in potential hollow fiber applications, an increasing number of structure–property relationship studies are appearing in the literature. One example was discussed in Section 15.4.2, in which it was pointed out that the final morphology that is observed in polyethersulfone fibers is dependent on the dope extrusion rate. A study of a similar kind was recently reported by Wang *et al.* (16) using polybenzimidazole (PBI) hollow fiber membranes. These

workers examined the water permeation flux through PBI membranes during a forward osmosis process by examining magnesium chloride solutions with different concentrations as draw solutions. They concluded that high water permeation flux and excellent salt selectivity were achieved using a PBI hollow fiber membrane which has a narrow pore size distribution. Beyond that conclusion, however, the study is significant because the effect of the membrane morphology and operation conditions on the water transport performance was systematically and thoroughly investigated.

Another area of research that has been attracting a great deal of attention recently in polymer science involves producing mixtures or polymer blends as an approach to tailor the properties of the final product. The production of hollow fibers has also seen activity in this area. Isihara *et al.* (17) have developed unique polysulfone (PSF) hollow fiber membranes by adding 2-methacryloxymethyl phosphorylcholine (MPC) polymer. In that work, an MPC polymer was specifically synthesized to be blended with PSF as a way to improve the hydrophilicity, permeability and nonfouling characteristics of the PSF hollow fiber in a hemodialyzer unit. The MPC polymer was blended into the PSF in the 7–15 wt% range. The resultant membranes had an asymmetric structure with good mechanical strength. Surface characterization showed that the MPC polymer was concentrated at the fiber surface. Further, the permeability of solutes through the PSF/MPC hollow fiber was higher, and the amount of protein adsorbed on the membrane was lower, than with the control PSF membrane. These results show that it is possible to control and tailor the properties of hollow fiber membranes through a polymer blending process.

## 15.6 Conclusions and recommendations

Membrane science and the use of hollow fibers as membrane materials began emerging as an independent technology only in the mid 1970s, and most of the necessary engineering concepts are still being defined. Many of the developments in the field initially arose from fundamental studies that were government sponsored in nature. Some of these developments are now successfully gaining the interest and attention of various industries, as membrane separation, and specifically technology based on the use of hollow fibers, has emerged as a feasible technology.

The use of new membrane materials is still a big unexplored option in this new technological area. Much research work continues to be done to provide improvements in the separator systems. In this regard, membrane-based hybrid systems serve as an excellent example, often serving to combine conventional unit operations with membrane separation processes. This combination often results in separation processes that offer significant advantages over the exclusive use of either component process. A good example of such a

hybrid system is a membrane/vapor-recompression hybrid system that can be used to recover energy in hot, moist dryer exhaust (18).

From the polymer science perspective, membrane science and the use of hollow fibers is an area fertile for additional investigation. As new polymers and new materials are being developed and investigated for use in many of the applications discussed in this chapter, a need to establish structure–property relationships for these new materials becomes increasingly evident. This becomes even more important when new and unique processes for the formation of hollow fibers from both new and existing polymers are considered. Also, as blends or mixtures of different polymers are being considered as a viable approach to tailoring the final properties of the resultant hollow fibers and corresponding membranes, a complete and thorough understanding of the manner in which various processing conditions affect the final properties is required.

Along these same lines of investigation, additional approaches to tailoring the separation performance of hollow fibers for specific applications are constantly being sought. For example, a particular filtration application may require a hollow fiber membrane to have a particular average pore size or pore size distribution. In many cases, an understanding of ways to achieve such a pore size distribution are lacking and the factors that affect it are not well understood. Improved theoretical models which allow for the estimation and prediction of such hollow fiber membrane properties would be of great value. This is especially true as new and unique applications are being developed for these materials.

Continuing that same line of thought, one of the areas experiencing a great deal of growth that will continue to generate much academic and industrial interest is the use of hollow fiber membranes in bioreactor applications. Hollow fibers are rapidly becoming the technology of choice for producing monoclonal antibodies, recombinant proteins and other secreted proteins. This type of activity is expected to increase, mainly because cost-effective hollow fiber bioreactors produce a highly concentrated supernatant that is simple to purify and can be scaled from the discovery stage to commercial production with relative ease. Consequently, many leading healthcare companies around the world are continuing to look into replacing their more traditional equipment with hollow fiber bioreactors to produce their diagnostic and therapeutic products.

## 15.7 Sources of further information and advice

There are several excellent textbooks available that cover many of the fundamental aspects of the separation process and membrane science in general terms (19, 20). Both the *McGraw-Hill Dictionary of Scientific and Technical Terms* (19) and the *Handbook of Separation Technology for*

*Chemical Engineering* (20) tend to be encyclopedic in nature and discuss general information. Neither provides a great deal of detailed information about any one process or particular material system.

As would be expected, in order to obtain that level of detail, it is often necessary to study the original technical literature in the appropriate journals. There are several journals devoted to membrane science and the development of hollow fibers for various applications. For example, the *Journal of Membrane Science* contains articles that range from fundamental studies of the structure–property relationships of new materials, such as the PBI article already discussed, to others that are more oriented to the development of new applications. As such, the journal serves as an excellent reference for the most recent advances in the area of hollow fibers and membranes made from them.

Another excellent source of information is the short course and corresponding notes developed by Fauzi *et al.* (21) and published as ‘A short course of membrane technology’. This serves as an excellent source of definitions and background information in the areas of membrane science and hollow fibers.

In conclusion, then, an increasing number of references and review articles are being generated in the exciting general area of hollow fibers. Up to now, much of this has been in the patent literature, but this trend is beginning to change. As additional discoveries are being made and a better understanding of the fundamentals that govern those discoveries is being sought, more and more journal articles will be published in the open literature.

A very active society in the area of membrane science and hollow fiber research is the North American Membrane Society (NAMS). This organization serves the membrane community by fostering the development and subsequent dissemination of knowledge in the areas of membrane science and technology. The society further promotes the collaborative efforts of researchers, technologists and end-users. Each year, NAMS holds a meeting at which both workshops are held and presentations are given on current research topics in various areas. These meetings serve as excellent sources of updated information on hollow fibers and their uses.

## 15.8 References

1. J.M. Maxwell *et al.*, US Patent 3,339,341, 5 September 1967.
2. D.M. Ruthven, 1997, *Encyclopedia of Separation Technology*, John Wiley & Sons, New York.
3. P. Montoya, 2004, *North America Membrane Society Proceedings*, Hollow Fiber Membranes Session.
4. In Vitro Systems & Services, Product Brochure on Hollow Fiber Technology.
5. M.C. Porter, ed., 1990, *Handbook of Industrial Membrane Technology*, Noyes Publ., Park Ridge, NJ.

6. R.E. Kesting and A.K. Fritzsche, 1993, *Polymeric Gas Separation Membranes*, John Wiley & Sons,
7. K.S. Kamalesh and R.L. Douglas, 1988, *New Membrane Materials and Separation Processes*, AIChE.
8. See, for example, Celanese Corporation, US Patents 4,058,582 (15 November 1977) and 4,138,459 (6 February 1979).
9. J. Xu, M. Johnson and G.L. Wilkes, *Polymer*, Volume 45, Number 15, July 2004, pp. 5327–5340.
10. T.H. Yu and G.L. Wilkes, *Polymer*, Volume 37, Number 21, October 1996, pp. 4675–4687.
11. T.H. Yu, PhD Thesis, Virginia Polytechnic and State University.
12. A.F. Ismail, M.I. Mustaffar, R.M. Illias and M.S. Abdullah, *Separation and Purification Technology*, Volume 49, Number 1, April 2006, pp. 10–19.
13. Y. Wang and A. Aneja, 2006, National Textile Center Annual Report, NTC Project F04-GT02.
14. F. Brady and I. Jaferey, *Water and Wastewater News*, feature article, September 2003.
15. Celanese Corporation, US Patent 4,541,981, 17 September 1985.
16. K.Y. Wang, T.S. Chung and J.J. Qin, *Journal of Membrane Science*, Volume 300, Numbers 1–2, 15 August 2007, pp. 6–12.
17. K. Isihara, T. Hasegawa, J. Watanabe and Y. Iwasaki, *Artificial Organs*, Volume 26, Number 12, December 2002, pp. 1014–1019.
18. R. Reynolds, 1996, *Unit Operations and Processes in Environmental Engineering*, PWS Publishing Company, Boston, MA.
19. S.A. Parker, 1994, *McGraw-Hill Dictionary of Scientific and Technical Terms*, McGraw-Hill, New York.
20. P.A. Schweitzer, 1988, *Handbook of Separation Technology for Chemical Engineering*, 2nd edition, McGraw-Hill, New York.
21. I. Fauzi, N. Ghazali and Y. Rosli, 1998, *A Short Course of Membrane Technology*, CEPP, University Technology Malaysia.

- A380, 372  
 $\alpha$ -chitin, 282, 284  
A glass, 318  
 $\alpha$ -keratin, 109, 132  
ABSE, 395, 396, 397, 398  
acetate fibres, 8  
    generic classification, 9–10  
acetic acid, 283  
*Acetobacter xylinum*, 46, 49  
*Acetobacter xylinus*, 201  
acetylation, 255, 283  
Acordis Speciality Fibers, 273  
acrylates, 471  
acrylonitrile, 257  
actinolite, 428, 429, 432  
Advantex glass fibres, 334  
AF (wool) glass, 318  
air-clad fibres, 478  
akund, 80–1  
alginates, 39–40, 266–81  
    chemical structures  
         $\alpha$ -L-guluronic acid and  
             $\beta$ -D-mannuronic acid, 267  
        alginic acid, 268  
        stereochemical structure of GG  
            block, 269  
    composition of alginates obtained from  
        alginophytes, 269  
    fibre production methods, 273–4  
    fibres cross-sections and surface, 275  
    future prospects, 280–1  
    influence of calcium ion content on  
        properties of alginate fibres,  
        280  
    influence of structure on properties,  
        274–80  
    main properties of alginates, 272  
    production methods, 270–3  
    sodium alginate production scheme,  
        271  
    structure, 267–70  
    various alginate fibres  
        gel swelling properties, 276  
        optimal spinning conditions and  
            modified fibre properties, 278  
        results of antibacterial tests, 277  
        total pore volume, internal surface  
            and capillary set percentages,  
            278  
alginic acid, 270  
alginic acid process, 270, 272  
Algisite M, 274  
alkalicellulose, 19  
alkalisation, 19–20  
alkyltrimethyl ammonium chloride, 342  
Al<sub>2</sub>O<sub>3</sub>, 398, 399  
Altex, 401  
alum, 242  
alumina, 320  
alumina fibre, 398–9, 405  
aluminium, 317  
aluminous hornblendes, 432  
alysol, 250  
amino acids  
    acidic, 112  
    basic, 112  
    with hydroxyl groups, 112  
    sulphur-containing, 112  
    without reactive, non-polar groups,  
        112  
ammonia, 244  
ammonolysis, 395  
amosite, 427, 429, 432, 434  
amphibole asbestos, 428–35

- plan of silicate chain in amphibole structure, 430
- structure projection down the fibre-axis, 431
- angora, 247
- anhydroglucose units, 204
- Antherea* spp., 146
- anthophyllite, 428, 429, 432, 434
- anti-static agents, 342
- antibiotics, 281
- antigorite, 448
- apolar interaction, 112
- AR glass, 318
- Aralac, 236, 239, 245, 247, 255
- Araneus*, 162
- Araneus diadematus*, 161, 188
- Ardil, 236, 240, 247, 248
- argon, 388, 394
- artificial silk, 244
- asbestos
  - amphibole, 428–35
    - atomic arrangement, 429–31
    - chemical properties and identification, 433–5
    - composition and unit cells, 428–9
    - structural basis for differentiation of amphibole varieties, 432
    - texture, 433
  - chemical formulae, 432
  - chrysotile, 435–48
    - chemical properties and identification, 447–8
    - cylindrical lattice, 437–9
    - early structural work, 435–7
    - general considerations on texture, 445–6
    - helical and spiral structures, 443–5
    - introduction, 435
    - structure, 439–41
    - texture from X-ray evidence, 442–3
  - classification, occurrence and physical properties, 426–8
  - crystal lattice values, 429
  - orientated fibre specimens of amosite and chrysotile, 434
  - structure and properties, 425–48
  - synthetic asbestos, 448
- Ascophyllum*, 267
- Ashland A240, 390
- Aspergillus niger*, 20, 34, 284
- ATR FT-IR analysis, 258
- azlons, *see* regenerated protein fibres
- $\beta$ -Chitin, 282, 284
- $\beta$ -glucosidases, 20
- $\beta$ -pleated sheets, 177
- $\beta$ -sheet crystal areas, 163
- $\beta$ -sheets, 98
  - and  $\alpha$ -helix crystal structure, 99
- banana leaf fibre, 87
- Bartenev model, 334
- basalt glass, 318, 320
- basalt wool, 307
- Basofil, 451
- bast fibres, 7, 81–4
- bending beam test, 371
- BHK mammal cell lines, 188
- bichromate of potass, 242
- bioengineering, 257
- birefringence, 163
- blood, 239, 240–2
- blue amosite, 435
- Bolivian crocidolite, 433
- Bombyx* fibres, 173, 176
- Bombyx mori*, 101, 146, 154, 155, 157, 163, 172
- Bombyx* silk, 153
- borate glasses, 326
- boron, 317, 318, 320, 344, 391
- Bragg fibres, 466
- branan ferulate, 281
- brown algae, 270
- brown seaweed, 266, 267
- brucite, 430, 435
- bulk modulus, 181
- butane-tetracarboxylic acid, 257
- C. tentans*, 153
- C-CP/MAS-spectroscopy, 215
- caddis-flies, 153
- calcia, 320
- calcia-magnesia-alumina-silica glass, 322
- calcite, 435
- calcium alginate, 267
- calcium alginate fibres, 273–4
- calcium alginate process, 272
- Canadian chrysotile, 443
- cantilever bending beam method, 371
- Carb1, 217

- Carb6, 217
- CarbaCell, 28, 203
- carbamate–NMMO system, 228
- Carbodundum, 390
- carbohydrates, 173
- carbon fibres, 353–72
  - cross-sectional texture with the axial preferred orientation, 367
  - fibre structure, 357–67
    - atomic order, 361, 363
    - general overview, 357–9, 361
    - mesoscale structure, 363–6
    - micrometre structure, 366–7
  - future directions, 372
  - major classes, 355–7
    - cellulose based, 355
    - mesophase pitch-based, 356–7
    - PAN based, 355–6
    - vapour growth carbon fibres, 357
  - mechanical properties and their structural origin, 368–72
    - compression and bending, 371–2
    - tensile stiffness, 368–9
    - tensile strength, 369–70
  - PAN-based and MPP-based, basic production steps, 356
  - short historical overview, 354
  - structural parameters and related physical properties, 360
  - three important structural levels, 358
  - turbostratic structure, 362
  - types and production, 355–7
  - Weibull strength distribution, 370
- Carbon Silicon Alloy, 390
- carbonised fibre, 454
- carboxymethylchitosan, 281
- Cargan, 245
- casein, 240, 248, 255, 259
- casein curd, 238
- casein fibres, 252, 255
- cashmere, 256, 257, 258
- Casolana, 245
- cell membrane complex, 119–20
- Cellca, 27
- cellulases, 20, 33–4
- cellulose, 3–51, 64–6, 354, 363, 365
  - acetate and triacetate fibres, 8
  - generic classification, 9–10
  - alternative cellulosic fibres, 12–13
  - chemical, physical and biochemical modification, 19–25
    - alkalisation, 19–20
    - enzymatic modification, 20–1
    - hydrothermic activation, 24–5
    - radiation treatment, 21–2
    - steam-explosive treatment, 22–3
  - chemistry, 4
    - chemical formula, 4
  - composite fibres, 36–46
    - blends with other polysaccharide, 36–40
    - blends with proteins, 40–3
    - blends with synthetics, 43–6
  - cupro fibres, 8, 11
  - hydrogen bonding, 65
  - Lyocell fibres, 11
  - manufactured fibres, 8
  - microfibril section, 66
  - modal fibres, 11–12
  - molecular structure, 64
  - natural fibre variety, 7–8
    - textile fibre classification, 7
  - occurrence and formation, 3–4
  - organic and inorganic solvents, 13–19
    - derivatising solvents and corresponding derivatives, 18
    - solvent classification, 15
  - physical structure, 4, 6
    - hydrogen bonding, 6
    - schematic view, 5
  - prospectives - nanocellulosic fibres, 46–9, 51
    - bacterial cellulose/chitosan composite pellicle, 48
    - bacterial cellulose fibrous network, 47
    - biosynthesis of modified bacterial cellulose, 47
    - cellulose nanofibres formation, 50
    - dome loudspeakers, 50
    - parameters of loudspeakers with MBC membranes, 49
  - spinning technologies, 25–36
    - cellulose carbamate process, 27–9
    - Celsol/Biocelsol process, 33–6
    - Lyocell process, 29–32
    - viscose process, 25–7
  - viscose fibres, 12



- cellulose acetate, 203
- cellulose acetate-based fibres, 222–7
  - cross-section, morphology and pore structure, 223
  - crystallinity, crystallite dimensions and orientation, 223–5, 227
  - fibre cross-sections, 223–4
  - fibre cryo-fracture surfaces, 226
  - inner and outer regions of fibre, 225
- cellulose-based composite fibres, 36–46
  - blends with other polysaccharide, 36–40
  - blends with proteins, 40–3
    - influence of silk-fibroin content, 41
    - mechanical properties of cellulose-keratin fibres, 43
    - SEM image of cellulose/silk-fibroin, 42
    - SEM photos of fibre cross-sections and surface, 44–5
  - blends with synthetics, 43–6
- cellulose carbamate process, 27–9
- cellulose fibre properties, 28
  - mechanical properties, 29
  - production scheme, 28
- cellulose fibres
  - cellulose acetate-based fibres, 222–7
  - chemical structure of cellulose chain with atom numbering, 204
  - crystal structure
    - cellulose II, 205–6
    - cellulose triacetate, 208
  - fringed fibrillar model, 209
  - future trends, 228–9
  - introduction and spinning methods, 201–3
    - derivative methods, 202–3
    - direct methods, 203
    - fibre spinning processing principles, 202
  - lyocell-type fibres, 218–22
  - man-made, 201–29
  - mechanical properties and X-ray crystallinities, 210
  - rayon (viscose)-type fibres, 209–18
  - structural levels and general models, 204–8
    - cellulose acetate crystal structures, 207
    - cellulose crystal structures, 204–7
    - partially crystalline structures, 207–8
    - single chain, 204
  - tenacity, lattice distortion parameter, crystallite dimensions, and cross-section, 216
  - total crystalline and amorphous orientation factors, 217
  - WAXS qualitatively assessed chain orientation, 227
- cellulose I, 6
- cellulose II, 6, 205–6
- cellulose solvents, 13–19
  - derivatising solvents and corresponding derivatives, 18
  - solvent classification, 15
- cellulose triacetate, 203, 207, 208
- cellulose xanthogenate, 202
- Celsol, 13
- Celsol/Biocelsol process, 33–6
  - Biocelsol end products, 37
  - fibre manufacture scheme, 33
  - hydrogenated non-woven sheet, 36
  - mechanical properties, 35
  - typical cross-section, 35
- Celsol process, 203
- ceramic fibres
  - classification, 379
  - comparison, 404–8
  - current and anticipated applications, 408–9
  - different sections of pilot plant, 396
  - non-oxide fibres processing, structure and properties, 379–98
    - ceramic fibres from polyborosilazanes, 392
    - characteristics and properties, 385–6
    - fibres derived from carbon-containing polysilazanes or from polycarbosilazanes, 392–8
    - fracture surfaces, 397–8
    - literature values for room temperature tensile strength, 407
    - SiN fibres derived from carbon-free polysilazanes, 390–1
  - oxide fibres processing, structure and properties, 398–404
    - characteristics and properties, 402
    - flow chart for making fibres from

- salt solutions or organometallic sols, 400
  - fracture surface, 403
  - slurry spinning process, 398–9
  - solution or sol-gel process, 399–404
- polymer-derived ceramic fibres from melt-spinning process, 380
- processing, structure and properties, 378–411
- research and development priorities, 409–10
- SiC fibres derived from polysilane/polycarbosilane, 379–90
  - Nicalon fibre types, 380–4
  - other manufacturing methods for SiC fibres, 390
  - other SiC fibre developments
    - derived from silicon-containing polymers, 387–90
    - Sylramic fibre types, 387
    - Tyranno fibre types, 384–7
  - summary and conclusions, 410–11
- ceramic matrix composites, 408
- chalcogenide glasses, 307, 479, 480
- chemical coupling, 348
- chemically resistant E-glasses, *see* ECR glass
- Chinese soya bean fibre, 257
- Chinon, 256
- chironomid midges, 153
- chironomid silk, 153
- chitin and chitosan, 281–98
  - applications, 286–7
    - agriculture, 287
    - biotechnology, 287
    - cosmetics and toiletries, 287
    - food, 287
    - medicine, 286–7
    - membranes, 287
    - pulp and paper, 287
    - special purpose, 287
    - water treatment, 287
  - fibre production methods, 287–90
  - four main stages in production
    - deacetylation, 284
    - decolorisation, 284
    - demineralisation, 284
    - deproteinisation, 284
  - future prospects, 297–8
  - influence of structure on properties, 290–1, 293–4
  - main properties, 286
  - new fibres based on chitin and chitosan, 294–7
  - polymeric crystal structures of chitin
    - $\alpha$ -Chitin, 282
    - $\beta$ -Chitin, 282
    - $\gamma$ -Chitin, 282
  - production methods, 283–7
  - production scheme using chemical method, 285
  - sources of chitin, 283–4
  - structure, 281–3
    - chemical structure, 282
    - vs other natural polymer-based fibres, 291
- chitin xanthate, 287–8
- chitosan, 36–8, *see also* chitin and chitosan
  - behaviour during biodegradation test, 293
  - cross-sections and surface, 292
- chitosan–alginate fibres, 294, 295, 296
- cross-sections, 296
- chrome alum, 242
- chrysotile, 426, 428, 435–48
  - cylindrical lattices, 438
  - electron density map of clino-chrysolite, 441
  - electron micrograph of chrysolite fibres, 437
  - hypothetical cross-section of chrysolite fibrils, 447
  - packing model, 442
  - probability distribution of inside and outside diameters, 444
  - serpentine rock containing cross-fibre seams of chrysolite, 427
  - stacking arrangement of kaolin-type minerals, 440
- citric acid, 257, 283
- clino-chrysotile, 440
- cobalt, 448
- coir fibre, 88
- cold stretch process, 487
- cold stretching operation, 492
- concept of capacity to shrink, 163, 164, 171
- conventional fibres, 462–4
  - graded index fibres, 464

- step-index fibres, 462, 464
- copper alginate fibres, 277
- copper ammonia technology, 203
- Cord, 217
- Cordenka, 17
- corn (maize), 250–1
- Corning SMF-28, 469
- cortex, 119
- cotton, 185, 245, 250, 257, 260, 274, 309
- cotton fibres, 77–9
  - development of fibre morphology, 77–8
  - microstructure based on chemical modification, 78–9
  - source and production, 77
- Courtaulds, 218, 245
- Courtelle fibres, 454
- Crabyon, 38
- crack deflector, 158
- cribellate orb weaver, 158
- crocidolite, 427, 429, 432
- crystallisation, 207
- cuprammonium process, 8, 11
- Cupro, 214
- cupro fibres, 8, 11
- cut-off wavelength, 460
- cuticular cell envelope, 119
- CVD-SiC fibres, 390
- CYTOP fibres, 475
  
- D-glass, 322
- delustrants, 246
- denaturation enthalpy, 135
- deodorising agent, 281
- derivatising solvent, 14
- Diptera*, 153
- dissolving pulp, 201
- disulphide bridge, 113
- dodecamethylcyclohexasilane, 380
- dolomite, 426
- Drackett's fibre, 250
- Dreamliner, 372
- droplet windlass system, 161
- dry-jet wet spinning technique, 291
- DuPont process, 455
  
- E35, 359
- E. coli*, 188
- E-glass, 320, 326
  - compositions, 1940–2008, 321
  - concentration of silanol groups per nm<sup>2</sup>, 345
  - effect of pH of water on contact angle, 344
  - effect of time and temperature on fibre bundle strength, 340
  - retained strength of unloaded fibres in environments of differing pH, 336
  - single filament strength of plasma polymer-coated E-glass fibre, 330
  - spiral cracking after immersion in sulphuric acid, 335
  - static fatigue of strands in distilled water, 331
  - stress corrosion failure times of single filament, 333
  - time dependence of strength at various temperature, 339
- E-glass fibres, 334
- ECR glass, 319, 320, 323, 334
- ecribellate orb weaver, 158, 159
- EELS, 404
- egg albumen, 239, 242
- elastic coil mechanisms, 161
- elastic modulus, 181
- elastic unwrinkling model, 368
- electron beam curing, 382, 387
- electron beam irradiation, 384, 406
- electron diffraction, 361, 448
- electron energy loss spectroscopy, 363
- electron irradiation, 363
- electrospinning, 229, 297–8, 404
- electrostatic forces, 161
- endoglucanases, 20
- energy dissipation mechanisms, 157
- Enka, 17
- environmental stress corrosion, 332–4
- environmental stress corrosion cracking, 333
- enzymatic modification, 20–1
- epichlorohydrin, 294
- epicuticle, 119
- erbium, 470
- Escherichia coli*, 46
- Euler buckling, 368
- exoglucanases, 20
  
- F-layer, 119

- Faraday rotation, 472  
 farm chemurgy, 250  
 feather keratin, 243  
 feathers, 242–3  
 Ferretti's Italian milk fibre, 238  
 Fiber FP, 398, 400  
 Fiberamic, 394  
 fibre Bragg gratings, 471, 472  
 fibres, *see also* specific fibres  
   alginate, 266–81  
     fibre production methods, 273–4  
     future prospects, 280–1  
     influence of structure on properties, 274–80  
     production methods, 270–3  
     structure, 267–70  
   chemically and thermally resistant, 450–7  
   chemically resistant fibres, 454–7  
     chlorinated and fluorinated fibres, 454–5  
     other linear polymer fibres, 455–6  
     PEEK formula, 455  
     PEI formula, 456  
     PPS formula, 456  
   chitin and chitosan, 281–98  
     fibre production methods, 287–90  
     future prospects, 297–8  
     influence of structure on properties, 290–1, 293–4  
     new fibres based on chitin and chitosan, 294–7  
     production methods, 283–7  
     structure, 281–3  
   man-made cellulosic fibres structure, 201–29  
     cellulose acetate-based fibres, 222–7  
     future trends, 228–9  
     introduction and spinning methods, 201–3  
     lyocell-type fibres, 218–22  
     rayon (viscose)-type fibres, 209–18  
     structural levels and general models, 204–8  
   thermally resistant fibres, 451–4  
     aromatic polymer fibres, 451–3  
     Kermel formula, 453  
     melamine formula, 451  
     meta-aramid fibre formula, 452  
     P84 aramid fibre formula, 452  
     partially carbonised acrylic fibre, 454  
     partially carbonised fibres, 454  
     PBI and sulphonated PBI formulae, 453  
     polyacrylonitrile precursor, 454  
     polymer structure of Kynol novoloid fibre, 451  
     thermosets, 451  
   fibroins, 165  
   fibroin–sericin thread, 155  
 Fibrolane, 245, 247, 248  
 Fibrolane C, 248  
 fibrous brucite, 448  
 fictive temperature, 311  
 film former, 341  
 finish, 341  
 flax, 7  
 flax fibre, 83–4  
 Flory-Huggins equation, 130  
 fluoride glasses, 479  
 fluorine, 320  
 FMC Biopolymer, 279  
 FMC Biopolymer AS, 277  
 folding index, 169  
 Ford's process, 250  
 formaldehyde, 244, 250  
 formic acid, 283  
 formic-aldehyde, 242  
 Fortisan, 203, 214, 223, 224  
 Fourier transform infrared spectroscopy, 240, 493  
 Fox equation, 130  
 fringed fibrillar model, 207  
 fruit fibres, 87–9  
   *see also* specific fibres  
 FT500, 359  
 $\gamma$ -aminopropyltriethoxysilane, 346  
 $\gamma$ -Chitin, 282  
 $\gamma$ -radiation, 382, 394  
 garden cross spider, 188  
 gas separation, 490–1  
   gas diffusion, 490  
   gas membrane separation application areas, 491  
   gas permeation, 490  
 Gaussian intensity profile, 460  
 gedrites, 432  
 gelatine, 244

- Gibbs free energy, 312
- glass fibres, 448
- aqueous solubility of differing glass components at differing pH, 336
  - chemistry of hydrolysis of organosilane, 343
  - classification, 336–7
    - aluminosilicate composition, 337
    - borate, phosphate and multi-alkali glasses, 337
    - S-2 glass composition, 337
  - compositions, 318–21
    - AF (wool) glass, 318
    - AR glass, 318
    - basalt glass, 318, 320
    - E-glass, 320
    - A glass, 318
  - compositions of typical glasses for fibres, 319
  - concept of fictive temperature, 311
  - continuous filament fibreglass
    - production process, 325
  - dependence of strength on diameter, 338
  - differences between crystal, SiO<sub>2</sub> glass and multicomponent glass, 314
  - fibre manufacture, 322–6
    - continuous filament process, 324–6
    - wool process, 322, 324
  - historical perspective, 307–9
  - influence of chemical composition of glass on strength after heat treatment, 339
  - insulation and filtration, 309
  - molecular dynamics-generated
    - structure of silica glass, 315
  - nature of glass fibres, 310–22
    - atomistic viewpoint, 313–14, 316
    - glass forming systems and composition, 316–17
    - high strength glass, 322
    - thermodynamic viewpoint, 310–13
  - other glass fibres, 310
  - protection of fibres for strength retention, 340–9
    - adhesion of unsilanised and unsized glass fibres, 348
    - plasma polymers as functional sizing for adhesion and protection, 349
    - silane coupling agents and structure of hydrolysed silanes, 342–4, 346
    - silane sizing/matrix interphase, 346
    - silanes—role in strength retention, 346
    - silanes—selection for adhesion promotion, 348
    - sizings and binders, 340–2
    - reinforcement, 309–10
    - strength of glass fibres, 326–40
      - Griffith theory of strength, 327
      - static fatigue, 331–4, 336–40
      - Weibull statistics of strength, 329–31
    - strength values distribution for industrial glass-fibre specimens, 328
    - structure and properties, 307–49
    - structure of interphase which forms in a composite, 347
    - summary, 349
    - theories of fibre strength and structure, 327–9
      - concepts of Bartenev, 328–9
      - concepts of Metcalfe and Schmitz, 328
      - fibre strength summary, 329
    - typical coupling agents for glass fibre–resin adhesion, 342
    - typical properties, 323
    - Weibull plots for strength of glass fibres with different treatments, 330
  - glass optical fibres, *see* optical fibres
  - glass transition temperature, 163, 181, 310, 473
    - range, 310
  - globular proteins, 98
  - glycerol solution of iodine, 448
  - glycine, 154, 169
  - glycoprotein, 173
  - glycoprotein complex, 161
  - golden silk spider, 188
  - Gould's fibre, 247
  - graded-index fibres, 464, 475
  - grafting, 257

- graphene sheets, 358  
 graphite, 357  
 Griffith theory of strength, 327
- hagfish slime thread, 103–5  
   coiled thread bundle inside the cell wall, 104  
   IF structure, 104
- hair, 239  
   and wool, 101–3  
   levels of structure for mechanical modelling, 103
- hair of angora goat, *see* mohair
- halogenated solvent system, 288
- hemicellulose, 74–5, 201  
    $\beta$  1  $\rightarrow$  4-D-xylan, 75
- hemp fibre, 83
- heptadrule, 122
- Hermans factor, 216
- Hi-Nicalon fibres, 382–3, 397, 406
- Hi-Nicalon Type S fibres, 383–4, 388, 389
- high mannuronic sodium alginate, 277
- high temperature treatment, 355, 368
- high wet modulus, 208
- hk* random-layer lines, 363
- hollow-core fibres, 481
- hollow-core microstructured fibres, 466, 479
- hollow fibres  
   background, 486–9  
   advantages and disadvantages, 488–9  
   definition of terms, 486–8  
   basic morphologies  
     anisotropic, 486  
     isotropic, 486  
   conclusions and recommendations, 496–7  
   general categories of commonly used technology, 486–7  
   dry process, 486–7  
   wet process, 487  
   polymers used, 492–5  
     other polymers, 493–5  
     polyolefins, 492–3  
   production and applications, 485–97  
   production general methods, 487–8  
     dry spinning, 487  
     melt spinning, 487–8  
     wet spinning, 487  
   structure–property relationships, 495–6  
   types of fibres and general features, 489–92  
     gas separation, 490–1  
     medical applications, 489  
     pervaporation, 490  
     reverse osmosis, 490  
     ultrafiltration, 491–2
- hot stretch process, 487
- HPZ, 404–5
- HTA7 AR, 359
- HTA7 series, 359
- hydrofluoric acid, 474
- hydroformylation, 257
- hydrogen bonds, 112, 152, 207
- hydrothermal synthesis, 448
- hydrothermic activation, 24–5
- inhibited coupling mechanism, 467
- Institute of Biomaterials and Chemical Fibres, 280
- interfacial gel polymerisation, 474
- intermediate filaments bundle, *see* microfibrils
- ionisable mercury, 256
- islands-in-a-sea structure, 258
- isodipeptide bridge, 113
- ITU-T standard G652, 469
- Japanese soya bean fibre Silkwool, 250
- JEOL JSM 6330 F, 211
- Jianghe TianRongSi Fibre soybean protein fibre, *see* SPF
- jute fibre, 81–2  
   cross-section, 82
- K137, 359
- K321, 359
- Kaltostat, 274
- kaolin, 436
- KAP, *see* keratin associated proteins
- kapok, 7, 79–80  
   cross-section, 80
- kenaf fibre, 82  
   fibre bundles, 83
- Keratec, 100
- keratin, 102, 281
- keratin associated proteins, 102

- keratin fibres, 109, 111  
 animal fibres, 111
- Kermel, 452
- Kevlar, 185, 452, 472
- Kumada rearrangement, 380
- Kynar, 471
- Kynol, 451
- Laminaria*, 267
- Lanital, 236, 239, 245, 247, 255
- lead silicate glasses, 326
- leaf fibre, 84–7, *see also* specific fibres
- Lenzing AG, 218
- Levenberg-Marquardt method, 137
- lignin, 75–6, 201  
 chemical structure, 75
- lipids, 114–15
- liquid nitrogen, 150
- lizardite, 447, 448
- Loxosceles*, 161–2
- Lyocell fibres, 11, 210, 216, 218–22, 223  
 cross-section, morphology and pore structure, 218–20  
 cryo-fractured surfaces, 220  
 crystallinity, crystallite dimensions and orientation, 220–2  
 fibre cross-sections, 219  
 lyocell fibre after wet abrasion treatment, 221
- Lyocell process, 29–32, 203, 228, 229  
 NMMO process flowsheet, 30  
 phase diagram, 30  
 process parameters comparison, 31  
 SEM images of untreated Lyocell-unwoven, 32  
 trade names produced by NMMO process, 33
- lysozymes, 283, 293, 294
- MAC-T, 188
- Macrocystis*, 267
- magnesite, 435
- magnesium, 448
- magnetic silk-fibre composites, 185
- magnetite, 185, 435
- MaSp2 proteins, 171
- medulla, 120
- melamine, 451
- melamine-formaldehyde fibre, 451
- Melgisorb, 274
- melt extrusion, 390
- Merino, 132
- Merino wool, 247
- Merinova, 245
- mesophase pitch precursors, 353
- mesothelioma, 425
- meta-aramid fibre, 452
- 2-methacryloxymethyl phosphorylcholine, 495
- 1-methyl-2-pyrrolidone, 493
- micro-zinc ions, 257
- microfibrils, 67–72, 120  
 cotton fibre cellular structure, 69  
 earlywood cellular structure, 67  
 fractured earlywood tracheids, 68  
 mechanical properties of plant fibres, 70  
 methods for studying orientation in S<sub>2</sub> layer of plant cell wall, 69  
 physical properties of plant fibres, 70  
 plant fibre ultimate cell, 68  
 Young's modulus vs microfibril angle, 71
- microfungal mycelia, 284
- microstructured optical fibres, 464–7, 476–9  
 applications and limitations, 477–9  
 general characteristics, 476  
 high index core, 464–5  
 low index core, 465–7  
 materials and fabrication, 476–7
- milk/acrylic fibre, 256
- milk casein, 239, 244–7
- milk fibre, 257
- Millon's reagent, 240
- mineral acids, 16–17
- mineral wool, 307, 318
- modal fibres, 11–12
- modified chemical vapour deposition, 469
- mohair, 132
- molecular dynamics modelling, 313–14
- montmorillonite, 431
- MPDZ-PhVi, 393, 404
- Mucor rouxii*, 284
- Müller-Rochow synthesis, 389
- multi-mode fibres, 460
- mygalomorph, 168
- N*-methylmorpholine-*N*-oxide, 17, 24
- nanofibres, 357

- NaOH/thiourea/urea aqueous solution, 16
- Nephila*, 148, 150, 154, 158–9, 161, 162, 177
- Nephila clavipes*, 177
- Nephila dragline*, 174, 182
- Nephila edulis*, 148, 155, 157, 172
- Nephila* fibres, 176
- Nephila madagascariensis*, 188
- network modifiers, 317
- Nextel, 399
- Nextel 312, 399, 400, 406
- Nextel 440, 400, 406
- Nextel 550, 406
- Nextel 610, 400, 401, 406, 408
- Nextel 650, 401, 406, 408
- Nextel 710, 406
- Nextel 720, 401, 405, 406, 408
- Nicalon, 380–2, 404–5
- NL-XYZ coding for Nicalon products, 381
- Nicalon CGN, 404
- Nicalon NLM-202, 404, 405
- Nicalon NLP-102, 404
- Nicalon-S, 406
- Nicalon SGN, 404
- nickel, 448
- nitrogen, 452
- NLP-201, 381
- NMMO, *see* *N*-methylmorpholine-*N*-oxide
- NMMO fibres, 204, 222
- NMMO process, *see* Lyocell process
- Nomex, 452
- non-derivatising solvent, 14
- novoloid fibre, 451
- nylon, 185, 455
- nylon 2.2, 146
- nylon blends, 250
- O-acetyl groups, 267
- Oeko-Tex Standard 100, 256
- oil palm empty fruit bunch fibre, 88–9
- olivine rock, 426
- opisthosoma, 154
- optical fibre preform, 470
- optical fibres
- commercially available optical fibres
    - optical specifications, 469
    - physical specifications, 468
  - common dopants used in silica fibres and their function, 470
  - common polymers used in optical fibres, 473
  - fibre structure and optical properties, 462–7
    - conventional fibres, 462–4
    - microstructured fibres, 464–7
  - general categories of polymers used, 473
  - new materials and material combinations, 479–80
  - structure, properties and characteristics, 458–81
    - different bandgap fibres, 466
    - examples of microstructured fibres, 477
    - fabricated microstructured fibres, 478
    - high index core microstructured fibre, 465
    - leakage of light can be caused by bending a fibre, 462
    - optical waveguide showing the core and cladding, 459
    - step-index single-mode and multi-mode fibres and graded-index fibres, 463
  - types of dispersion
    - chromatic dispersion, 461
    - inter-modal dispersion, 461
    - waveguide dispersion, 461
  - types of optical fibres, materials and applications, 467–79
    - microstructured optical fibres, 476–9
      - plastic optical fibre, 473–6
      - silica optical fibre, 468–72
  - waveguide concepts, 459–61
    - bending loss, 461
    - dispersion, 461
    - loss, 460–1
    - modes, 459–60
    - numerical aperture, 460
- ortho-chrysotile, 440, 441
- OsO<sub>4</sub> staining technique, 218
- outside vapour deposition, 469
- P84 aramid fibre, 452
- cross-sections, 453
  - formula, 452
- Panox, 454



- para-aramid fibre, 452
- para-chrysotile, 440
- parabolic profile graded index, 464
- peanut, 240
- pectins
  - alternating  $\alpha$ - (1 $\rightarrow$ 2)-L-rhamnosyl and  $\alpha$ - (1 $\rightarrow$ 4) D galacturonosyl units, 76
  - poly- $\alpha$ - (1 $\rightarrow$ 4)-galacturonic acid, 76
- PEEK, *see* poly(etheretherketone)
- PEI, *see* poly(ether imide)
- perchloroethylene, 252
- perhydropolysilazane, 391
- pervaporation, 490
- Phaeophyceae*, 270
- phenol-formaldehyde fibre, 451
- Philips TEM CM 200, 208–9
- phosphate glasses, 326
- phosphorus, 248
- photonic bandgaps, 466
- photonic crystal, 466
- photonic crystal fibres, *see* microstructured optical fibres
- Phycomyces blakesleanus*, 284
- Pichia pastoris*, 188
- plant cell wall
  - cellulose deposition, 72–4
  - living plant cell vs differentiated tracheary cell, 73
  - microfibril alignment, 74
- plant fibres
  - structure, 62–89
    - bast fibre bundles, 81–4
    - chemical composition, 64
    - classification and approximate world annual production, 63
    - composition, 63–76
    - fibre categorisation, 63
    - fruit fibres, 87–9
    - leaf fibres, 84–7
    - seed fibres, 77–81
- plasma chemical vapour deposition, 470
- plastic optical fibre, 473–6, *see also* optical fibre
  - application and limitations, 475–6
  - chemical structure and fabrication, 473–5
  - general characteristics, 473
  - mechanical properties, 475
- POF-ALL project, 481
- POF-FTTH, 481
- Poisson kernel, 365
- Poisson ratio, 150
- Polan, 245
- polyacrylonitrile, 258, 354, 363, 365, 495
- polyacrylonitrile polymer precursors, 353
- polyaluminocarbosilane, 384
- poly(aramide-imide) fibre, 452
- polybenzimidazole fibres, 452
- polybenzimidazole hollow fibre, 495
- polyborosilazane, 379
- polycarbosilane/SiC powder/xylene slurry, 390
- polycarbosilazane, 379, 394
- polydimethylsilane, 380
- polydispersity, 267
- polydispersity index values, 270
- polyester fibres, 455
- poly(ether imide), 456
- poly(etheretherketone), 455
- polyethersulfone, 493, 495
- polyethylene, 492
- poly(ethylene oxide), 298
- polymer blending process, 495
- polymer-clad-silica fibres, 480
- polymer repeat, 96
- polymethylmethacrylate, 210, 474, 475, 476
- polyoxyethylene monophenyl ethers, 341
- poly(phenylene sulphide), 456
- polypropylene, 492
- polysilane/polycarbosilane, 379
- polysilasilazane, 394
- polysilazane, 379
- polysiloxane, 379
- polysulfone, 495
- polysulfone hollow fibres, 495
- poly(tetrafluoroethylene), 455
- polytitanocarbosilane, 383, 384
- polyvinyl alcohol, 257, 258, 494
- polyvinyl chloride, 455
- polyvinyl fluoride, 455
- poly(vinylidene chloride), 455
- poly(vinylidene fluoride), 455, 471, 495
- polyvinylpyrrolidone, 295
- polyvinylsilane, 387
- Porod's law, 365
- potassium, 337

- PPS, *see* poly(phenylene sulphide)  
 PRD 166, 399  
 prolamin, 250  
 proline, 169, 170–1  
 Protanal LF 10/60, 279  
 Protanal LF 60/20, 277  
 Protanal LF-10/60 LS, 277  
 protein fibres, 95–106
  - amino acid residue content, 97
  - diversity, 99–105
    - fibre types, 99
    - hagfish slime thread, 103–5
    - regenerated and other manufactured protein fibres, 100
    - silks, 101
    - wool and hair, 101–3
  - structures, 96–8
    - chemistry, 96–8
    - physical forms, 98
- proteins, 112–14, *see also* specific proteins
  - fictive peptide chain structure, 113
  - primary protein fractions in Merino wool, 115
  - wool protein separation by 2D SDS-PAGE, 114
- pyrolysis, 357  
 pyroxene rock, 426
- quartz fibres, 337
- R glass, 322
- radiation curing technique, 388
- radiation treatment, 21–2
- Raman band shifts, 222
- Raman frequency, 371
- Raman scattering, 364
- Raman spectroscopy, 163, 371, 479
- ramie, 7
- ratchet clamp mechanism, 173
- Rayleigh scattering, 460
- rayon, 202, 235, 245, 255
- rayon fibres, 202, 209–18
  - cross-section, morphology and pore structure, 209–11, 213–14
  - cryo-fracture surfaces, 213
  - crystalline and partially ordered fraction from <sup>13</sup>C-CP/MAS-NMR, 215
  - crystallinity, crystallite dimensions and orientation, 214–18
  - fibre cross-sections, 211–12
  - micrograph after wet abrasion treatment, 214
- Rayon-PP composite, 44
- reeling speed, 171, 173, 176, 177
- refractive index gradient, 474
- regenerated cellulose, 235
- regenerated cellulose fibres, *see* modal fibres
- regenerated protein fibres, 100, 234–61
  - Aralac milk protein fibre, 246–7
  - ATR FT-IR spectra of Aralac, silk, wool and cotton, 241
  - chemical composition of wool and casein fibres, 245
  - first and second generation, 235–56
    - behaviour, 251–6
    - characteristics, 240–51
    - development, 235–6
    - five main production stages, 238–9
    - identification, 239–40
    - production, 236–9
    - production dates, trade names, and manufacturers, 237
    - surviving examples, 236
    - vs behavioural properties of wool, 253–4
  - Lanital fibres and wool fibres, 248
  - peanut fibres, 249
  - regenerated and stretched technical egg white fibres, 243
  - soya bean fibres, 251
  - summary, 261
  - third generation, 256–61
    - behaviour, 258–61
    - behavioural properties in comparison to natural fibres, 261
    - development, 256
    - fibre properties, 258
    - identification, 258
    - longitudinal view of soya bean fibre, 260
    - polarised ATR FT-IR of soya bean fibre, 259
    - production, 256–8
    - zein fibres, 252
- regeneration, 185
- reverse osmosis, 490

- rock wool, 307
- Ruland–Vonk method, 223
- S-2 glass, 322, 334, 336, 337
- salt bridge, 112–13
- Sarelon, 236, 248
- scanning electron microscopy, 210, 214, 366
- Scherrer equation, 215, 363
- SCS-6, 386, 390, 397, 398, 409
- SCS-9A, 386, 390
- SCS-Ultra, 386, 390
- Seasorb, 274
- semi-carbon fibre, 454
- shark meat protein, 244
- Shirlastain A stain, 240
- shot, 318
- SiBCN, 392
- SiCN hollow fibres, 393
- SiCN(O) fibres, 405
- Sigma SiC fibre, 390
- silica, 320
- silica optical fibre, 468–72
  - applications and limitations, 472
  - chemical structure and fabrication, 469–71
  - general characteristics, 468–9
  - mechanical properties, 471–2
- silk, 101, 146–89, 239
  - artificial silk, 184–8
    - genetically engineered silk, 187–8
    - regenerated silk, 185–7
  - composition, 152–4
  - description, 146–7
  - detailed calculations of dynamic mechanical properties, 183
  - elastomericity and role of glycine residues, 170
  - evolution of silk glands, proteins and fibres, 168
  - fibre and its model, 175–9
  - fine structure and morphology, 154–63
    - banding pattern vs microvilli, 155, 157–8
    - silkworm silk morphology, 155
    - spider silk morphology, 155
    - supercontraction, 162–3
  - genetic basis for silk structural strength, 153
  - influence of structure on properties, 179–84
    - mechanical predictive and interpretative model, 181–4
    - order–disorder, water and nanostructures, 180–1
  - major types
    - $\beta$ -silk, 176
    - co-l-linear, 176
    - cross- $\beta$  silk, 176
  - mechanical envelope of properties, 184
  - mechanics, 147–52
    - major polymer vs biopolymer fibres, 148
    - summary, 152
    - tensile properties, 147–8, 150
    - torsional properties, 151–2
  - nanofibril string of bead structure, 180
  - orientation and structural models, 178
  - processing variables, 176
  - regenerated silk
    - mechanical properties, 186
    - rheological properties, 187
- silk diversity, 158–62
  - capture silks, 159, 161
  - ribbon silk vs cylindrical silk, 161–2
- spider silk, 164–74
  - beta silks, 164–5
  - processing, 169–74
- spinning the fibres
  - Bombyx mori* silk gland, production and spinning, 174
  - Nephila edulis* silk gland, production and spinning, 175
- structural order and supercontraction, and proline residues, 172
- summary of typical origins, composition and sequences, 166–7
- supercontraction and its relation to orientation in dragline silk, 164
- silk-fibroin, 40–1
- silk proteins, 165
- silkworm silk, 148, 154, 155, 177, 185, 186
  - Bombyx mori* spider silk ultrastructural details, 157
- effect of reeling speed on *Bombyx mori* silk fibres, 177
- morphology, 155

- silkworm silk cocoons, 185  
 silver, 281  
 Silverlon calcium alginate dressing, 276  
 single-line method, 215  
 single-mode fibres, 460  
 sisal fibre, 84–6  
     bundle fractured in tension, 87  
     cross section of bundle fibre, 86  
     section through leaf and mechanical fibre, 85  
     SEM image, 86  
 sizing, 341  
 sizing systems, 316  
 slurry process, 399  
 small angle X-ray diffraction method, 277  
 small-angle X-ray scattering, 218, 365  
 soda-lime–silica glass, 318  
 sodium, 337  
 sodium silicate glass, 317  
 soft glasses, 480  
 solvent spinning, 493  
 Sorbsan, 274  
 soya bean, 240  
 soya bean fibre, 100, 248, 250, 252, 255, 256, 259, 261  
 Span-20/Tween-20, 289  
 SPF, 257, 258, 260  
 spider silk, 100, 164–74, *see also* silk  
     beta silks, 164–5  
     co-evolution of silk spinning and silk dope, 165, 168–9  
     glass transition temperature, 163  
     golden orb spider silk functions and associated mechanical properties, 149  
     mechanical properties across spider species, 150  
     molecular phases  
         amorphous, 163  
         crystalline, 163  
     *Nephila* dragline thread fine structure, 158  
     *Nephila* spider silk ultrastructural details, 156  
     processing, 169–74  
         dope structure, elastomericity and role of glycine residues, 169–70  
         dye geometry and processing variables, 172–3  
         fibre formation and role of proline residues, 170–1  
         other influences, 173–4  
     spider's extrusion spinning device, 162  
     structural diversity, 159–60  
     torsional behaviour, 151  
 spidroin, 165  
 spidroin 1, 153, 174  
 spidroin 2, 153, 174  
 spinnerets, 324  
 stacking method, 476  
*Staphylococcus aureus*, 46  
 staple fibre, 248  
 static fatigue phenomenon, 331–4, 336–40  
     effect of composition, 336–7  
     environmental stress corrosion, 332–4  
     thermal effects, 337–40  
 steam-explosive treatment, 22–3  
 stem fibre, *see* bast fibres  
 step-index fibres, 462, 464  
     preforms, 474  
 strain sensing, 476  
 strength–diameter phenomenon, 337  
 stress corrosion phenomenon, 331  
 string of beads morphology, 180, 181  
 supercontraction, 162–3  
 Swiss Protein Database, 180  
 Sylramic fibre, 387  
 synchrotron radiation, 218, 369  
 synthetic asbestos, 448  
 synthetic vitreous fibres, *see* glass fibres  
  
 tannins, 174  
 Teflon, 455  
 Tegagen, 274  
 Tencel, 11, 218  
 Tencel A100 fibre, 31  
 tensile modulus, 182  
 theory of diffraction, 438  
 thermal expansion coefficient, 310, 312, 474  
 thermal insulation, 308  
 thermal transitions, 128–38  
     denaturation transition, 131–8  
         DSC traces for mohair, 133  
         regression analysis of denaturation temperatures, 134  
         wool denaturation temperatures, 136

- viscoelastic,  $\alpha$ - and  $\beta$ -transitions, 129–31
  - dynamic  $E$ -modulus of horse hair and rhino horn, 129
- thermodynamics of Ehrenfest, 312
- thermogravimetric tests, 452
- Thiozell, 245
- Tiolan, 245
- Todtenhaupt's German fibre, 238
- TOF SIMS analysis, 346
- transmission electron microscopy, 209, 210, 364, 366, 404
- tremolite, 428, 429, 432
- tremolite–actinolite, 429
- triacetate fibres, 8
- trichloromethylsilane/hydrogen mixture, 390
- Trichoderma reesei*, 20, 34
- Trichoptera*, 153
- triple-play networks, 475
- Tufcel, 216
- turbostratic structure, 358, 361
- Twaron, 185
- Tyranno fibres, 384, 404–5, 406
- Tyranno LOX M, 384
- Tyranno SA (Si–Al–C–O), 384, 387
- UF fibres, 388
- UF-HM fibres, 389
- ultra-microtome Leica Ultracat S, 210
- ultrafiltration, 491–2
- ultraviolet light, 471
- unimodal Weibull, 359
- urea, 202–3
- UV Raman scattering, 363
- Valonia ventricosa*, 201
- van der Waals, 357
- van der Waals forces, 216
- van der Waals interactions, 152
- Vanduara, 244, 255
- vapour axial deposition, 469
- vegetable albumen, 239
- Vicara, 236, 250, 251
- viscose, 17, 202, 223
- viscose fibres, 12, 274, *see also* rayon fibres
- viscose process, 25–7, 202, 214, 228, 287–8
  - flowsheet, 26
  - production, 27
- viscose rayon, 202, 453
- Viscostar, 26
- W-fibres, 464
- Warren's structure, 429
- wavelength division multiplexing, 472
- weakest link theory, 369
- Weibull analysis, 329–31, 332, 346, 359, 369, 370, 406
- wet spinning, 257, 287–9
- white spirit, 252
- Whittier's fibre, 247
- wide-angle X-ray diffraction method, 277
- wide-angle X-ray scattering, 214, 215
- windlass silk, 159
- wool, 239, 245, 250, 252, 257
  - and hair, 101–3
    - levels of structure for mechanical modelling, 103
- wool and hair fibres, 108–38
  - $\alpha$  and  $\beta$ -keratinous materials, 110
  - chemical composition, 111–15
  - elemental composition, 111
  - lipids, 114–15
  - proteins, 112–14
  - fibre formation, 115–17
    - morphological components of developing hair, 116
  - keratin fibres, 109, 111
  - mechanical properties and models, 125–8
    - elastic moduli, 127–8
    - swelling and moduli changes, 126
    - two-phase model for  $\alpha$ -keratins, 125–7
  - molecular structures, 121–5
    - $\alpha$ -keratin monomer structure, 122
    - 2-rule hierarchical structure formation, 124
    - amino acid arrangement in the  $\alpha$ -helix, 122
    - IF monomer arrangement, 123
  - morphology, 117, 119–20
    - electron micrograph of porcupine quill tip, 121
    - principal types of composite structure, 118
    - structural principles, 118

- structure of Merino wool fibre, 118
- thermal transitions, 128–38
- wool fibres, 247
- wool keratin, 243
  
- X-ray diffraction, 154, 163, 168, 175, 176, 216, 268, 283, 361, 363, 364, 366, 368, 369, 391, 448
- X-ray microbeam, 366, 367, 369, 371
- X-ray scattering, 180, 204
- XPS analysis, 346
  
- Yajima polymer, 387
  
- Young's modulus, 326, 327, 359, 368, 369, 370, 371, 382, 384, 391, 394, 405
- ytterbium, 470
  
- Zachariasen's model, 313
- ZBLAN, 479
- Zealon, 242
- zein, 250
- zein fibres, 240, 255, 258
- zinc alginate fibres, 277
- zirconocene catalyst, 389
- Zycon, 250